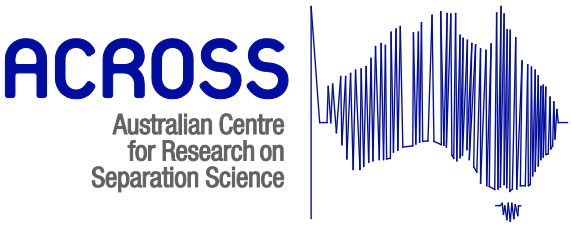

CHARACTERISATION OF CHITOSAN AND ITS FILMS FOR TISSUE ENGINEERING

Presented by:

Joel J. Thevarajah

BSc (Advanced Science - Biochemistry and Molecular Biology)

BSc (Honours - Analytical/Polymer Chemistry)

A thesis submitted in fulfillment of the requirement of

Doctor of Philosophy

Principal Supervisor: Dr Marianne Gaborieau

Co-Supervisors: Dr Patrice Castignolles, Dr Michael O'Connor,

Dr Richard Wuhrer, Dr Catherine Lefay

Western Sydney University, Australia

August 2016

To my amazing wife. Thank you for everything. You are the best. I will love you always

Acknowledgements

I wish to first thank all my supervisors for their guidance over the course of my PhD. Firstly to Patrice and Marion, thank you for everything that you have done for me over the course of my PhD (also including my Honours and Undergraduate degrees). This has truly been a valuable experience and your guidance has allowed me to grow on a professional, personal and intellectual level. Although I wasn't convinced at first to pursue a PhD, your support in providing with me with research assistant and teaching positions to appease my financial situation was a real help. Both of you go above and beyond any expectation of a supervisor and that is why you will both always be the best supervisors anyone could ever ask for. You pushed me to extend myself in areas you knew I wasn't confident in (i.e maths) but I am better for it now. We are all pretty spoilt to have supervisors like you both but I can't imagine a better team to have spent my time with.

To Cathy, Michael and Ric, thank you for your support overall and in proofreading my thesis, providing ideas for the direction of the project overall and allowing me full access to equipment which allowed me to progress. Your contributions to my PhD allowed me to succeed so thank you. Thank you to Tim Murphy for always being available to help and willingness to train me on different instruments and discuss the interpretation of the results. Also to Sarah Chandler,Adam Hale and Greg Fathers, thank you for all your help which made the administrative part of a PhD bearable!

To Hervé Cottet and Robert Graf, thank you again for accepting the Endeavour proposal to come and work with you in your labs. Hervé you worked with me

directly even though you had a number of other students dependant on you. Thank you for taking out the time to explain the different concepts (which I found difficult) and readily reviewing manuscripts and suggesting improvements. To Robert, thank you for the discussions and suggestions of different experiments to try and probe a very difficult question in chitosan characterization.

To the macromolecular characterisation team (both past and present). As the longest standing member it has been an honour working with you all. Johnny! (JBL), Coco, Diksha, J-Lee, Vin Diesel (Kevin Diesel), Tibro, Lucie, Maelie, Melissa, Aaron, Michael Jimmy Bob Stan Lee, Michele Mason (M&M) and Papaya (Pauline). To Aiden (the JOKE), mate you are a massive clown and wasted a lot of my time with computer games, but thanks for your contributions and intellectual discussions. To Mar – Dean – Du – Plessis (not Batman), although you were only my side-kick for a short time you still recognized that I was the best supervisor ever (so you must be pretty smart!) Good luck for your masters and hopefully PhD ☺. To Ke-Vin Diesel, my last official minion, it was great supervising you and being gym buddies, here is some free life advice: always remember you can't out train a bad diet!! To the massive noob team (masters team 2013) Adam, Lizbet and Michelle, you guys will always be the worst team but Matt and Bob (Michael) are getting there pretty quickly! In all seriousness it was great working and travelling with you. The constant banter made for an entertaining time and the vibe definitely changed when you guys left.

To 1.11 (now 1.19), Minion/Midget (Alison), Shaggy Dog (Matt) and Mudblood (Michelle), "see you never" haha "nothing is sacred anymore". Our room

atmosphere was awesome, always filled with awesome music (i.e) drum covers, Alison's ridiculously loud sneezing and our 4 part harmonies when we sang karaoke. It was definitely the "good one" and made getting through my PhD a whole lot easier. Alison, what a struggle these last few years have been aye?! Haha although difficult at times it was great going through the suffering of a PhD with someone else. Thank you for your continual source of cookies, lollies, hot chocolate and all other healthy treats. Your useless facts about "smooth" and long winded stories will unlikely be missed…ever. But PhD team 2013 will always be the best team the macromolecular characterisation team will have ever seen. I know you will be eternally grateful for the constant source of wisdom and insight I was to you (I know I was always right :P) Finally…..We did it! Matt, Shags, Shaggy Dog, you are the worst but still my best bud! Thanks for all your IT help and assistance in the lab. Good luck for your PhD and I can only wish Penny luck in surviving life with you! I know you will always struggle to understand this but I know deep down you know that "I'm the best!" and you will definitely miss me. It has been great going through these last couple of years with you guys, you will be missed.

To my family, this is likely the only part of my thesis that you will ever read…To Appa and Amma, thank you for supporting me in my decision to continue studying and for supporting me ever since I was born. I know you found it difficult to grasp what exactly I was doing in my PhD but now you have this 400+ page document which should finally help! I could never put into words how grateful I am to both of you but thank you. To my sister Sarah, I'm not exactly sure what I should thank you for because more often than not you .other sister like mine and I am glad that is the case (it is unlikely the world

could handle that p.s we look nothing alike). To Dad and Mum, thank you for your generosity and willingness to always help and support Leena and I. Continuing to study was a difficult choice but your continual support after we got married allowed us to go without want. Thank you. To my wonderful grandparents ammamma and ammappa, your amazing influence on my life has been one of a kind just like you both. Thank you for your prayer and support, it has always been felt here in Sydney.

Finally to the best person in the world. My beautiful wife Leena ☺ (you thought I was going to talk about myself didn't you). Although I already dedicated this whole thesis to you I couldn't write the acknowledgements without including you. I know it has been a crazy couple of years and me doing my PhD hasn't exactly made that any easier at any time but you have been incredibly patient and supportive. You are the best and most amazing wife I could ever ask for. I look forward to spending the rest of my life with you always challenging me to grow. Love you always and more than most <3

Statement of Authentication

The work presented in this thesis is, to the best of my knowledge and belief, original except as acknowledged in the text. I hereby declare that I have not submitted this material, either in full or in part, for a degree at this or any other institution.

…

Joel J Thevarajah

August 2016

Research Output

Peer-reviewed Journal Articles:

J.J. Thevarajah, M.E. Mason, T. Murphy, D. Bairamian, R. Graf, M.D. O'Connor, R. Wuhrer, P. Castignolles, M. Gaborieau,' Fabrication and characterization of modified chitosan films – homogeneity of the surface and biocompatability', In preparation

J.J. Thevarajah, M.P. Van Leeuwen, H. Cottet, M. Gaborieau, P. Castignolles, 'Determination of the distribution of degrees of acetylation of chitosan', International Journal of Biological Macromolecules, 95 (2017), 40-48. (IF 5.6, top 20 % of Polymer Science)

http://dx.doi.org/10.1016/j.ijbiomac.2016.10.056**J.J. Thevarajah**, J.C. Bulanadi, M. Wagner, M. Gaborieau, and P. Castignolles, 'Towards a Less Biased Dissolution of Chitosan', Analytica Chimica Acta, 935 (2016) 258-268. (IF 4.7, top 10 % of Analytical Chemistry) http://dx.doi.org/10.1016/j.aca.2016.06.021

J.J. Thevarajah, M.D. O'Connor, P. Castignolles, M. Gaborieau, 'Capillary electrophoresis to monitor peptide grafting onto chitosan films in real time', Journal of Visualized Experiments, (2016), e54549. (IF 1.3, top 30 % of Multidisciplinary Sciences). Invited contribution http://dx.doi.org/10.3791/54549

J.J. Thevarajah, A.T. Sutton, A.R. Maniego, E.G. Whitty, S. Harrisson, H. Cottet, P. Castignolles, and M. Gaborieau, 'Quantifying the Heterogeneity of Chemical Structures in Complex Charged Polymers through the Dispersity of Their Distributions of Electrophoretic Mobilities or of Compositions',

Analytical Chemistry, 88 (2016), 1674-81. (IF 5.9, top 5 % of Analytical Chemistry)
http://dx.doi.org/10.1021/acs.analchem.5b03672

D. L. Taylor*, **J. J. Thevarajah***, D. K. Narayan, P. Murphy, M. M. Mangala, S. Lim, R. Wuhrer, C. Lefay, M. D. O'Connor, M. Gaborieau, and P. Castignolles, 'Real-Time Monitoring of Peptide Grafting onto Chitosan Films Using Capillary Electrophoresis', Analytical and Bioanalytical Chemistry, 407 (2015), 2543-55. (IF 3.1, top 15 % of Analytical Chemistry), **co-first authorship*
http://dx.doi.org/10.1007/s00216-015-8483-y

J.J. Thevarajah, M. Gaborieau, and P. Castignolles, 'Separation and Characterization of Synthetic Polyelectrolytes and Polysaccharides with Capillary Electrophoresis', Advances in Chemistry, 2014 (2014), Article ID 798403. Invited contribution
http://dx.doi.org/10.1155/2014/798503

A.T. Sutton, E. Read, A.R. Maniego, **J.J. Thevarajah**, J.D. Marty, M. Destarac, M. Gaborieau, P. Castignolles, 'Purity of double hydrophilic block copolymers revealed by capillary electrophoresis in the critical conditions', Journal of Chromatography A, 1372 (2014), 187-195 (IF 3.9, top 15 % of Analytical Chemistry). Invited contribution
http://dx.doi.org/10.1016/j.chroma.2014.10.105

Oral presentations as presenter:

J.J. Thevarajah, M.P. Van Leeuwen, A.T. Sutton, A.R. Maniego, E.G. Whitty, S Harrisson, H. Cottet, P. Castignolles, M. Gaborieau, Characterization of complex polymers: Quantifying heterogeneity through dispersity, 2016 Research and Development Topics Conference, Parramatta (Australia), December 2016. – ***Invited talk for the RACI Original Research Publication Award***

J.J. Thevarajah, M.E. Mason, T.D. Murphy, M.D. O'Connor, R. Wuhrer, P. Castignolles, M. Gaborieau, Functionalisation of Chitosan and its Films, Surfaces and Soft Stuff Meeting (SASSY), NSW, Kensington (Australia), June 2016.

J.J. Thevarajah, M.D. O'Connor, M. Wagner, R. Graf, P. Castignolles, M. Gaborieau, Characterisation of chitosan and its derivatives with solid-state NMR spectroscopy, RACI NSW NMR polymer symposium, Kensington (Australia), April 2016 – ***Best Oral Presentation Prize.***

J.J. Thevarajah, A.T. Sutton, A.R. Maniego, E.G. Whitty, H. Cottet, P. Castignolles, M. Gaborieau, Characterization of complex polymers: Quantifying heterogeneity through dispersity, Polymer Research in NSW Symposium, Kensington (Australia), November 2015.

J.J. Thevarajah, H.Cottet, R. Graf, M. Wagner, P. Castignolles, M. Gaborieau. Chitosan: Distributions and Dispersity, Australian Centre for Research on Separation Science (ACROSS) Annual Meeting, Hobart (Australia), July 2015.

J.J. Thevarajah, R. Wuhrer, M.D. O'Connor, P. Castignolles, M. Gaborieau, Characterisation of modified chitosan films, Seventh International

Symposium on the Separation and Characterization of Natural and Synthetic Macromolecules (SCM-7), Amsterdam (Netherlands), February 2015.

P. Castignolles, A.R Maniego, M. Gaborieau, **J.J. Thevarajah**, Smart polymers and polysaccharides: characterisation and functional properties, ENSIACET-Institut National Polytechnique de Toulouse, Toulouse (France), January 2015.

J.J. Thevarajah, H. Cottet, M.D. O'Connor, R. Wuhrer, C. Lefay, P. Castignolles, M. Gaborieau, Characterisation of chitosan for tissue engineering, Université Toulouse III – Paul Sabatier, Toulouse (France), January 2015.

J.J. Thevarajah, H. Cottet, M.D. O'Connor, R. Wuhrer, C. Lefay, P. Castignolles, M. Gaborieau, Characterisation of chitosan for tissue engineering, University of Montpellier II, Montpellier (France), December 2014.

J.J. Thevarajah, M.D. O'Connor, R. Wuhrer, C. Lefay, P. Castignolles, M. Gaborieau, Characterisation of chitosan for tissue engineering, Australian Centre for Research on Separation Science (ACROSS) Annual Meeting, Hobart (Australia), July 2014.

J.J. Thevarajah, M.D. O'Connor, R. Wuhrer, C. Lefay, P. Castignolles, M. Gaborieau. Charaterisation of chitosan for tissue engineering. University of Western Sydney (UWS) Higher Degree of Research Meeting, June 2014.

Posters presentations as presenter:

M.E. Mason, **J.J. Thevarajah**, M.D. O'Connor, P. Castignolles, M. Gaborieau, Monitoring the PEGylation of chitosan films by capillary electrophoresis, Polymer Research in NSW Symposium, Kensington (Australia), November 2015.

M.P. Van Leeuwen, **J.J. Thevarajah**, J.R. Coorssen, M. Gaborieau, P. Castignolles, Characterisation of branching in starch using capillary electrophoresis, Polymer Research in NSW Symposium, Kensington (Australia), November 2015.

J.J. Thevarajah, C. Lefay, M.D. O'Connor, P. Castignolles, M. Gaborieau, Characterisation chitosan and its conjugates for biomedical applications with capillary electrophoresis, Virtual Symposium on Applied Separation Science (VSASS), online, May 2015.

J.J. Thevarajah, P. Castignolles, M. Gaborieau, Neither obvious nor impossible: Chitosan dissolution, Seventh International Symposium on the Separation and Characterization of Natural and Synthetic Macromolecules (SCM-7), January 2015. ***Prize for "top 5" poster presentations.***

J.J. Thevarajah, D. Taylor, C. Lefay, Y Guillaneuf, MD O'Connor, P Castignolles, M Gaborieau, Characterizing chitosan and its conjugates for biomedical applications, RACI NSW Polymer Group workshop on Macromolecular Characterisation, Parramatta (Australia), November 2013.

J.J Thevarajah, D.L. Taylor, C. Lefay, Y. Guillaneuf, M.D. O'Connor, P. Castignolles, M. Gaborieau, Characterizing chitosan and its conjugates for biomedical applications, 34th Australasian Polymer Symposium (34APS), Darwin (Australia), July 2013.

Oral presentations presented by others:

AR Maniego, AT Sutton, **JJ Thevarajah,** J Nicolas, CM Fellows, M Destarac, Y Guillaneuf, P Castignolles, M Gaborieau, Branching Topology and Heterogeneity in Hydrophilic Polyacrylates and the Binding to Anticancer Drugs, Polymer Research in NSW Symposium, Kensington (Australia), November 2015.

JB Lena, AK Goroncy, GT Russell, AR Maniego, **JJ Thevarajah**, P Castignolles, M Gaborieau, Structural Analysis of Poly(Acrylic Acid) by Advanced Techniques, Polymer Research in NSW Symposium, Kensington (Australia), November 2015.

JJ Thevarajah, MR Toutounji, MP Van Leeuwen, J Mata, EP Gilbert, MJ Gidley, HW Spiess, R Graf, P Castignolles, M Gaborieau, Probing molecular dynamics and structure in polysaccharides with spectroscopy in the solid-state, 35th Australasian Polymer Symposium (35APS), Gold Coast (Australia), July 2015.

JJ Thevarajah, AR Maniego, AT Sutton, E Groison, F d'Agosto, B Charleux, Y Guillaneuf, S Harrisson, M Destarac, H Cottet, M Gaborieau, P Castignolles, Characterisation of polymers beyond molecular weight distribution: Distribution of compositions of copolymers and heterogeneity of the branching in poly(acrylic acid), 35th Australasian Polymer Symposium (35APS), Gold Coast (Australia), July 2015. Invited keynote lecture.

JJ Thevarajah, DL Taylor, MD O'Connor, R Wuhrer, R Graf, P Castignolles, M Gaborieau, Molecular characterisation of chitosan for application in cell culture. 5th International Symposium of Surface and Interface of Biomaterials (ISSIB 2015), Sydney (Australia), April 2015.

P Castignolles, A Sutton, **JJ Thevarajah**, D Taylor, E Read, JD Marty, M Destarac, M Gaborieau, Toward the distribution of compositions of charged copolymers: capillary electrophoresis of block copolymers, polysaccharides and more! Seventh International Symposium on the Separation and Characterization of Natural and Synthetic Macromolecules (SCM-7), Amsterdam (Netherlands), February 2015. Invited Keynote lecture.

AT Sutton, E Read, AR Maniego, **JJ Thevarajah**, JD Marty, M Destarac, M Gaborieau, P Castignolles, Assessing copolymer purity by capillary electrophoresis. 22nd Annual RACI Environmental and Analytical Division R&D Topics Conference, Adelaide (Australia), December 2014.

JJ Thevarajah, DL Taylor, DK Narayan, C Lefay, MD O'Connor, M Gaborieau, P Castignolles, Enabling chitosan for biomedical applications: looking closer at dissolution and grafting and … getting surprised! 2014 RACI National Congress, Adelaide (Australia), December 2014.

JJ Thevarajah, DL Taylor, MD O'Connor, R Wuhrer, P Castignolles, M Gaborieau, Chitosan: a smart polymer for (bio)materials. 3rd biennial conference of the Combined Australian Materials Societies (CAMS2014), Sydney (Australia), November 2014.

JJ Thevarajah, MD O'Connor, P Castignolles, M Gaborieau, Molecular characterisation of polysaccharides for applications in cell culture and nutrition. Molecular Medicine Research Group Annual Meeting, Campbelltown (Australia), November 2014.

P Castignolles, AT Sutton, E Groison, A Singh, **JJ Thevarajah**, M Selim, E Read, V Naumovski, K Chan, JD Marty, M Destarac, B Charleux, M Gaborieau, Distribution of "smartness" in copolymers: Composition of block and statistic copolymers by capillary electrophoresis in the critical conditions,

34th Australasian Polymer Symposium (34APS), Darwin (Australia), July 2013.

JJ Thevarajah, DL Taylor, C Lefay, P Castignolles, M Gaborieau, Chitosan and its conjugates for medical applications, 34th Australasian Polymer Symposium (34APS), Darwin (Australia), July 2013.

D Taylor, **JJ Thevarajah**, D Narayan, C Lefay, M O'Connor, P Castignolles, M Gaborieau, Chitosan films grafted with peptides for stem cell culture, 34th Australasian Polymer Symposium (34APS), Darwin (Australia), July 2013.

Posters presented by others:

MP Van Leeuwen, **JJ Thevarajah**, JR Coorssen, M Gaborieau, P Castignolles, Characterisation of branching in starch using capillary electrophoresis. RACI NSW NMR polymer symposium, Kensington (Australia), April 2016.

JJ Thevarajah, C Lefay, MD O'Connor, R Graf, P Castignolles, M Gaborieau, Characterisation of chitosan-based materials with solid-state NMR spectroscopy. Biennial conference of the Australian and New Zealand Society for Magnetic Resonance (ANZMAG2015), Paihia (New Zealand), December 2015.

JJ Thevarajah, C Lefay, MD O'Connor, P Castignolles, M Gaborieau, Characterisation of chitosan-based materials with solid-state NMR. 6th UWS NMR, MRI and Diffusion Symposium, Campbelltown (Australia), March 2015.

AT Sutton, E Read, AR Maniego, **JJ Thevarajah**, JD Marty, M Destarac, M Gaborieau, P Castignolles, Quantification of homopolymers in block copolymers by capillary electrophoresis in the critical conditions (CE-CC). RACI NSW Polymer Workshop on Polymer Nanoparticles, Self-Assembly and Colloids, Kensington (Australia), November 2014.

DK Narayan, **JJ Thevarajah**, DL Taylor, MD O'Connor, M Gaborieau, P Castignolles, Monitoring the grafting of peptides on chitosan films using free solution capillary electrophoresis, RACI NSW Polymer Group workshop on Macromolecular Characterisation, Parramatta (Australia), November 2013.

Awards, Professional Memberships and Meetings

Awards

- 2016 Original Research Publication Award: Royal Australian Chemical Institute – Analytical and Environmental Chemistry Division
- Best Oral presentation prize: (Solid-state) NMR and Polymers Symposium, Kensington. 6th of April 2016
- Top 5 poster (total of 34) presentation prize: Seventh International Symposium on the Separation and Characterization of Natural and Synthetic Macromolecules in Amsterdam, The Netherlands, January 28th-30th 2015
- Endeavour Research Fellowship, $22,500 (November 2014-April 2015) to undertake research at the University of Montpellier 2, Montpellier, France and the Max Planck Institute for Polymer Research, Mainz, Germany
- Royal Australian Chemical Institute Polymer Division Student subsidies for International Polymer Meetings, $1,000 to travel to the Seventh International Symposium on the Separation and Characterization of Natural and Synthetic Macromolecules in Amsterdam, The Netherlands, January 28th-30th 2015

Professional Memberships

- Royal Australian Chemical Institute (Postgraduate student)

- Australian Nanotechnology Network
- Golden Key International Honours Society
- Australian Centre for Research on Separation Science
- Molecular Medicine Research Group
- Treasurer of organising committee of Royal Australian Chemical Institute Research and Development Topics Conference 2016
- Society of Academic Research 2012-2015

Meetings

- Australian Polymer Summer School (APSS) Gold Coast – February 2016
- RACI NSW Analytical and Environmental Chemistry Annual Honours and Masters by Research student presentation evening at Macquarie University – November 2015
- Australian Nuclear Science and Technology Organisation – June 2014
- 15th Australian Polymer Summer School (15APSS) Parramatta – February 2014
- RACI NSW Polymer group workshop on polymer characterisation Parramatta – November 2013

Table of Contents

ACKNOWLEDGEMENTS II

RESEARCH OUTPUT VII

PEER-REVIEWED JOURNAL ARTICLES: VII

ORAL PRESENTATIONS AS PRESENTER: IX

POSTERS PRESENTATIONS AS PRESENTER: XI

ORAL PRESENTATIONS PRESENTED BY OTHERS: XII

POSTERS PRESENTED BY OTHERS: XV

AWARDS, PROFESSIONAL MEMBERSHIPS AND MEETINGS XVI

AWARDS XVI

PROFESSIONAL MEMBERSHIPS XVI

MEETINGS XVII

TABLE OF CONTENTS XVIII

LIST OF TABLES XXIV

LIST OF FIGURES XXVI

ABBREVIATIONS XXXVIII

ABSTRACT XLIII

CHAPTER 1: BACKGROUND 1

1.1. CHITOSAN 2

1.1.1. Chitosan's potential as a biomaterial 3

1.1.2. Need for characterization 5

1.2. CHARACTERIZATION OF POLYMERS IN SOLUTION 7

1.2.1. Introduction to CE and limitations of previous methods..... 7

1.2.2. Theory and application of Free-solution Capillary Electrophoresis 9

1.2.2.1. Robust separation of a mixture of monosaccharides 10

1.2.2.2. Direct detection due to the photo-oxidation of sugars 14

1.2.2.3. Monitoring of chemical reactions 15

1.2.2.4. Oligoelectrolytes 17

1.2.3. CE in the critical conditions 18

1.2.3.1. Explanation of "critical conditions" 18

1.2.3.2. Pectin, carboxymethylcellulose and gellan gum - Separation by composition 20

1.2.3.3. Chitosan – Separation by composition 24

1.2.3.4. Poly(acrylic acid) - Separation by topology (branching) ... 29

1.2.4. Size determination with Taylor Dispersion Analysis 32

1.2.5. Comparison of SEC and CE in the characterization of block copolymers 34

1.2.6. Summary 36

1.3. CHARACTERIZATION OF POLYMERS IN THE SOLID STATE 37

1.3.1. NMR spectroscopy 37

1.3.1.1. Introduction to NMR spectroscopy 37

1.3.1.2. Line broadening in solid-state NMR spectroscopy 38

1.3.1.3. Magic-angle spinning..... 39

1.3.1.4. Recording ^{13}C solid-state NMR spectra 41

1.3.1.5. Solid-State NMR spectroscopy of chitosan..... 43

1.3.2. Surface characterization of chitosan film 45

1.3.2.1. Fourier-transform infrared (FTIR) and Raman spectroscopy 46

1.3.2.2. X-Ray Photoelectron Spectroscopy (XPS) 47

1.3.2.3. Secondary ion mass spectrometry 47

1.3.2.4. Scanning electron microscopy (SEM) 47

1.3.2.5. Atomic force microscopy (AFM)..... 48

1.4. MODIFICATION OF CHITOSAN 48

1.5. PUBLICATION: REAL-TIME MONITORING OF PEPTIDE GRAFTING ONTO CHITOSAN FILMS USING CAPILLARY ELECTROPHORESIS [3] 49

1.6. THESIS AIMS 55

1.7. OVERARCHING STATEMENT 55

1.7.1. Publications overview..... 55

1.7.2. Contribution to personal, professional development and to the field of study 59

1.7.2.1. Separation and Characterization of Synthetic Polyelectrolytes and Polysaccharides with Capillary electrophoresis – Advances in Chemistry [1] (section 1.2) 59

1.7.2.2. Purity of double hydrophilic block copolymers revealed by capillary electrophoresis in the critical conditions – Journal of Chromatography A [2] (section 1.2.5) 60

1.7.2.3. Real-time monitoring of peptide grafting onto chitosan films using capillary electrophoresis – Analytical and Bioanalytical Chemistry [3] (section 1.4) 61

1.7.2.4. Towards a less biased dissolution – Analytica Chimica Acta [125] (chapter 2)..... 63

1.7.2.5. Quantifying the heterogeneity of chemical structures in complex charged polymers through the dispersity of their distributions of electrophoretic mobilities or compositions – Analytical Chemistry [126] (chapter 3)..... 65

1.7.2.6. Determination of the distribution of composition of chitosan – International Journal of Biological Macromolecules [127] 67

(chapter 4) 67

1.7.2.7. Chitosan film – JoVE [128] / in preparation [129] (chapter 5)..... 68

CHAPTER 2: PUBLICATION: TOWARDS A LESS BIASED DISSOLUTION OF CHITOSAN 71

2.1. PUBLICATION [125] 72

2.2. SUPPORTING INFORMATION 117

CHAPTER 3: PUBLICATION: QUANTIFYING THE HETEROGENEITY OF CHEMICAL STRUCTURES IN COMPLEX CHARGED POLYMERS THROUGH THE DISPERSITY OF THEIR DISTRIBUTIONS OF ELECTROPHORETIC MOBILITIES OR COMPOSITIONS 143

3.1. PUBLICATION [126] 144

3.2. PUBLICATION: SUPPORTING INFORMATION 171

CHAPTER 4: DETERMINATION OF THE DISTRIBUTIONS OF THE DEGREES OF ACETYLATION OF CHITOSAN 188

4.1. PUBLICATION [127] 189

4.2. PUBLICATION: SUPPORTING INFORMATION 224

CHAPTER 5: CHITOSAN FILMS 236

A) CAPILLARY ELECTROPHORESIS TO MONITOR PEPTIDE GRAFTING ONTO CHITOSAN FILMS IN REAL TIME 236

B) FABRICATION AND CHARACTERIZATION OF MODIFIED CHITOSAN FILMS- HOMOGENEITY OF THE SURFACE AND BIOCOMPATIBILITY 236

5.1. A) PUBLICATION [128] 237

5.2. B) PUBLICATION (IN PREPARATION)[129] 265

5.3. B) SUPPORTING INFORMATION 292

CHAPTER 6: CONCLUSION AND FUTURE WORK 311

6.1. FULFILLED AIMS 311

6.2. FURTHER METHOD DEVELOPMENT 312

6.3. DESIGN OF MATERIALS BASED ON CHITOSAN 314

CHAPTER 7: REFERENCES 316

CHAPTER 8: APPENDIX 329

List of Tables

TABLE 2-1. VISUAL EVALUATION OF THE DISSOLUTION OF CHITOSAN SAMPLES WITH VARIED *DA*S IN AQUEOUS SOLVENTS: 50 MM HCL, 0.3 % (W/V) TRIFLUOROACETIC ACID (TFA), AS WELL AS 0.3 % (W/V) TFA WITH 0.1 M NACL (ELUENT) 78

TABLE S2-1: VISUAL EVALUATION OF MEDMW2 CHITOSAN DISSOLUTION IN VARIOUS AQUEOUS ACIDS AND SODIUM BORATE BUFFER AT ROOM TEMPERATURE. "YES" INDICATES TRANSPARENCY WITHIN 15 MINUTES 118

TABLE S2-2: VISUAL EVALUATION OF MEDMW2 CHITOSAN DISSOLUTION AT HIGHER TEMPERATURES IN VARIOUS AQUEOUS ACIDS AND SODIUM BORATE BUFFER. "YES" INDICATES TRANSPARENCY AFTER 1 HOUR. 119

TABLE S2-3: PULLULAN-EQUIVALENT M_N AND M_W OF DIFFERENT CHITOSAN SAMPLES INJECTED AT DIFFERENT CONCENTRATIONS AND DISSOLVED IN DIFFERENT AQUEOUS SOLVENTS (ELUENT IS COMPOSED OF 0.3 % (W/V) TFA AND 0.1 M NACL) 121

TABLE S2-4: CHITOSAN SAMPLES NOT MENTIONED IN TABLE 1 126

TABLE S2-4: PUBLISHED EXAMPLES OF CONDITIONS FOR SOLUTION-STATE NMR SPECTROSCOPY OF CHITOSAN 135

TABLE S2-5. CALCULATION OF ERROR CAUSED BY PHASING OF 8 DIFFERENT SOLID-STATE NMR SPECTROSCOPY DATA SETS. THE *DA* WAS MEASURED AFTER PHASING BY 4 DIFFERENT USERS. ... 138

TABLE S3-1. SUMMARY OF THE INTEGRALS AND DISCRETE EXPRESSIONS OF THE MOMENTS RELEVANT TO THIS WORK 172

TABLE S3-2. RSD OF THE ELECTROPHORETIC MOBILITIES OF POLYELECTROLYTES[4] AND SUGARS[5,6] IN THE LITERATURE. 179

TABLE 3-S3. RELATIVE UNCERTAINTY VALUES OF THE DISPERSITY OF THE ELECTROPHORETIC MOBILITY DISTRIBUTION, CALCULATED FOR A SAMPLE OF EACH OF THE EXPERIMENTAL CASES USING EQ S33 TO S35 AND S39 180

TABLE S3-4. RELATIVE UNCERTAINTY VALUES OF THE DISPERSITY OF THE COMPOSITION DISTRIBUTION, FOR BLOCK COPOLYMER SAMPLES (CALCULATED FROM EQUATIONS ANALOGOUS TO S33 TO S35 AND S39, WITH *C* SUBSTITUTED FOR μ) 181

TABLE S3-5. DISPERSITY OF CHITOSAN SAMPLES 182

TABLE S3-6. DISPERSITY VALUES OF P(NAA-*CO*-APA) SAMPLES. THE VALUES ARE FIRST GIVEN AS DETERMINED FROM EQ 5 TO 8; THE VALUE OBTAINED FOR THE LINEAR PNAA (SAMPLE AT TIME 0) WAS THEN SUBTRACTED FROM THESE VALUES. 183

TABLE 3-S7. SUMMARY OF PNAA DISPERSITY VALUES REPRESENTING THE HETEROGENEITY OF SAMPLES WITH DIFFERENT BRANCHING TOPOLOGIES AND SAMPLES PRODUCED FROM DIFFERENT MONOMERS 184

TABLE S3-8. DISPERSITY OF P(AA-*B*-AM) SAMPLES 186

TABLE S4-1: INFORMATION OF CHITOSAN SAMPLES STUDIED IN THE MANUSCRIPT PROVIDED BY SUPPLIER AND MEASURED. *DA* IS THE DEGREE OF ACETYLATION IN % OF MONOMER UNITS (DA_{SUPP} WAS GIVEN BY THE SUPPLIER, DA_{SSNMR} WAS MEASURED BY SOLID-STATE NMR SPECTROSCOPY). THE VISCOSITY IN CPS WAS GIVEN BY THE SUPPLIER IN THE FOLLOWING CONDITIONS: [A] AT 20°C; [B] AT 1% IN 1% ACOH; [C] AT 1 % IN 1 % ACOH, AT 20 °C, ACCORDING TO DIN 45, 100S-1; [D] AT 20°C, [B] AT 1% IN 1% ACOH. 225

TABLE S5.2-1: CHITOSAN FILMS WERE MEASURED USING A DIGIMATIC MICROMETER AT 4 RANDOM POINTS AROUND THE FILM. AVERAGE THICKNESS RESULTS SHOWN ARE MEAN ± SD. 304

List of Figures

Figure 1-1 Potential applications of chitosan A) Tuned release of antibiotics using electrophoretic deposition of chitosan coatings for dental implantations [11] B) Bioplastics out of shrimp shell materials [17] C) pH responsive self-assembly of chitosan for bioelectronics applications [12] 4

Figure 1-2: Chemical structure of chitosan with a degree of acetylation *DA*. Chitin corresponds to *DA*=1. 5

Figure 1-4. Separation by CE at high pH (12.6) and with direct UV detection of a depolymerized plant fiber sample plotted as a function of electrophoretic mobility (A) and of migration time (B). The sample contains (1) cellobiose, (2) galactose, (3) glucose, (4) rhamnose, (5) arabinose, and (6) xylose (the molecular structures are given for the sole purpose of identification, and they are in equilibrium with a number of linear and charged forms) [53]. 12

Figure 1-5. Fermentation of hydrolyzed plant fiber to ethanol. Samples taken (A) 0, (B) 6, and (C) 24 h. Peak assignments: (1) lactose (internal standard), (2) galactose, (3) glucose, (4) mannose, (5) fructose, (6) arabinose, (7) xylose, (8) arabitol, and (9) unknown. [57] See section 1.2.2.2 for detection of sugars through photo-oxidation in the UV detection window. 13

Figure 1-6. Mechanism of direct UV detection in CE of carbohydrates owing to a photo-oxidation reaction [60]. 16

Figure 1-7. Electropherograms in lithium borate for two different oligoAAs, AA5 and AA15, produced by RAFT polymerization, where 5 and 15 correspond to the degree of polymerization obtained at the maximum of the mass spectrum from ESI-MS-ToF (electrospray ionization - mass spectrometry - time of flight) direct infusion (adapted from [64]). AA15 is not separated by molar mass, it is thus in the critical conditions. The bottom electropherogram is of the RAFT agent, i.e., the control agent for the polymerization. 17

FIGURE 1-8. ELECTROPHEROGRAMS OF A LOW-ACYL GELLAN GUM (DOTTED RED LINE), AND A HIGH-ACYL GELLAN GUM (SOLID BLACK LINE) (IN POTASSIUM BORATE, PH 9.2), AFTER A FEW HOURS DISSOLUTION [84]. THE CHEMICAL STRUCTURE OF GELLAN GUM IS DISPLAYED ON THE GRAPH AND THE BLUE AND RED CIRCLES REPRESENT THE DIFFERENT ACYLATED OR NON-ACYLATED MONOMER UNITS OF THE COPOLYMER. 23

FIGURE 1-9. SEPARATION OF CHITOSAN SAMPLES BY THEIR *DA* WITH CE (SODIUM PHOSPHATE, PH 3): ELECTROPHEROGRAM SHOWN AS A FUNCTION OF (A) MIGRATION TIME, AND (B) APPARENT ELECTROPHORETIC MOBILITY. SAMPLES WITH DIFFERENT DEGREES OF ACETYLATION (WEIGHT-AVERAGE *DA* DETERMINED BY NMR SPECTROSCOPY) ARE SHOWN: BLACK SOLID LINE (4 %), GREEN DASHED LINE (4.3 %), BLUE DASHED-DOTTED LINE (16.5 %), RED DASHED LINE (18.7 %), PINK DASHED LINE (19.8 %), BROWN DOTTED LINE (22.4 %) AND BLACK DOTTED LINE (23.6 %) [88]. 26

FIGURE 1-10. CE OF PURE BLOCBUILDER® (BB, BLUE LINE), CHITOSAN WITH ADSORBED BB (RED LINE) AND CHITOSAN WITH GRAFTED BB (RED LINE) IN SODIUM BORATE BUFFER (PH 9.2) [89]. 28

FIGURE 1-11. SEPARATION OF LINEAR (PURPLE LINE), THREE-ARM STAR (BLACK LINE), AND HYPERBRANCHED (RED LINE) POLY(SODIUM ACRYLATE) BY CAPILLARY ELECTROPHORESIS IN SODIUM BORATE BUFFER (PH 9.2) SHOWN AS A FUNCTION OF A) MIGRATION TIME AND B) ELECTROPHORETIC MOBILITY, WHICH IS A MORE REPRODUCIBLE QUANTITY THAN THE FORMER [91] (NOTE THE LINEAR SAMPLE IS OVERLOADED AND HAS BEEN CORRECTED IN CHAPTER 3).....30

FIGURE 1-12. ELECTROPHEROGRAM IN SODIUM BORATE (PH 9.2) OF A PNAA OBTAINED BY NITROXIDE-MEDIATED POLYMERIZATION OF ACRYLIC ACID INITIATED BY THE MONOFUNCTIONAL INITIATOR MONAMS (RED SOLID LINE) FOLLOWED BY CLEAVAGE OF THE SG1 END-GROUP BY TREATMENT WITH THIOPHENOL (BLUE DASHED LINE) [91].....32

FIGURE 1-13. A) SEC CHROMATOGRAM AND B) CE ELECTROPHEROGRAM OF THE HOMOPOLYMER PAA WITH A MOLAR MASS OF 10,000 G.MOL^{-1} (BLUE) OF A BLOCK COPOLYMER WITH A 10,000 G.MOL^{-1} MOLAR MASS PAA BLOCK AND A 10,000 G.MOL^{-1} MOLAR MASS POLYACRYLAMIDE BLOCK (RED) AS WELL AS OF THE BLOCK COPOLYMER SPIKED WITH A 10,000 G.MOL^{-1} PAA HOMOPOLYMER (BLACK) [2]. 35

FIGURE 1-15: A) HOMOGENEOUS, B) INHOMOGENEOUS AND C) HETEROGENEOUS LINE SHAPES; GREY INDICATES COUPLING [103]. 39

FIGURE 1-16: MAGIC-ANGLE SPINNING (MAS) OF A SOLID-STATE NMR SPECTROSCOPY SAMPLE.....40

FIGURE 1-17: COMPARISON OF ^{1}H SOLID-STATE NMR SPECTRA OF A POLYACRYLATE RECORDED UNDER STATIC CONDITIONS (TOP) AND UNDER MAS (BOTTOM) [103]. 41

FIGURE 1-18: SINGLE-PULSE EXCITATION (SPE) PULSE SEQUENCE. 42

FIGURE 1-19: CROSS-POLARIZATION (CP) PULSE SEQUENCE. 43

FIGURE 1-20. MONITORING THE GRAFTING BY CE: SEPARATION OF COUPLING AGENTS, RGDS AND INTERNAL STANDARD AS A FUNCTION OF A) MIGRATION TIME AND B) ELECTROPHORETIC MOBILITY [3] CONDUCTED IN A 43.5 CM (TOTAL LENGTH) 50 μM INTERNAL DIAMETER FUSED SILICA CAPILLARY WITH 75 MM SODIUM BORATE AT PH 9.2 50

FIGURE 1-21: A) ELECTROPHEROGRAMS OF RGDS SIGNAL SHOWING CONSUMPTION OVER REACTION TIME B) REAL-TIME MONITORING OF RGDS PEPTIDE CONSUMPTION DURING THE GRAFTING ONTO CHITOSAN FILMS WITH CE. DIFFERENT SYMBOLS REPRESENT REPEAT EXPERIMENTS. [3] MEASUREMENTS WERE CONDUCTED IN A 43.5 CM (TOTAL LENGTH) 50 μM INTERNAL DIAMETER FUSED SILICA CAPILLARY WITH 75 MM SODIUM BORATE AT PH 9.2.....52

FIGURE 1-22: POLYCONDENSATION OF RGDS MONITORED BY CE. LINEAR (BLACK), OLIGOMERS (RED) AND HIGHLY BRANCHED (BLUE) RGDS WERE IDENTIFIED BY THEIR MOBILITY (2.5, 1 AND 1.5×10^{-8} $M^2.V^{-1}.S^{-1}$ RESPECTIVELY). [3] THE PEAK AREA WAS MEASURED AND THE FRACTION OF EACH OF THE BRANCHING SPECIES WAS QUANTIFIED. 53

FIGURE 1-23: ^{13}C SPE-MAS SWOLLEN-STATE NMR SPECTROSCOPY WAS CONDUCTED ON BLANK CHITOSAN FILMS (BLACK) AND CHITOSAN FILMS GRAFTED WITH RGDS ON THE SURFACE (BLUE). THE ASTERISKS REPRESENT SIGNALS ASSIGNED TO RGDS.....54

FIGURE 2-1: A) RI (SOLID LINES) AND RALS (DASHED LINES) TRACES OF CHITOSAN MEDMW1 (BLACK), LOWMW1 (RED) AND AKBIOD3 (BLUE). B) RI TRACE OF MEDMW1 IN 50 MM HCL AT 1 $G \cdot L^{-1}$ (SOLID LINE) AND DILUTED TO 0.25 $G \cdot L^{-1}$ (NORMALIZED BY CONCENTRATION, DOTTED LINE).....87

FIGURE 2-2: PM (WITH VISCOSITY NORMALIZATION FOR Cl^-) OF 50 MM HCL (RED) AND OF CHITOSAN (MEDMW1) DISSOLVED IN 50 MM HCL (BLACK, 2 REPEAT EXPERIMENTS SHOWN) A) BEFORE AND B) AFTER Cl^- SUBTRACTION 89

FIGURE 2-3: ELECTROPHEROGRAM OF CHITOSAN (MEDMW1) DISSOLVED IN 50 MM HCL (BLACK LINE), ACOH (RED LINE) AND TFA (GREEN LINE) PREPARED AT A) 60 °C FOR 2 H B) 25 °C FOR 2 H.....92

FIGURE 2-4. ELECTROPHEROGRAM OF CHITOSAN (MEDMW1) DISSOLVED IN 50 MM HCL SEPARATED USING CE (DASHED LINE) AND PACE (SOLID LINE) IN A) MIGRATION TIME AND B) ELECTROPHORETIC MOBILITY. THE ELECTROPHORETIC MOBILITY MARKER IS SEEN AT A MOBILITY OF 76.9×10^{-9} $m^2.V^{-1}.s^{-1}$ AND A MIGRATION TIME BETWEEN 6 AND 8 MIN. THE EOF IS SEEN AT A MOBILITY OF 0.....94

FIGURE 2-5: A. ERROR OF SOLID-STATE NMR SPECTROSCOPY MEASUREMENTS ESTIMATED AS *RSD* FROM *SNR* AND AS *RSD* FROM PHASING. THE STRAIGHT LINE REPRESENTS A LINEAR FIT ($y=10x-16$, $R^2=0.79$). B. *DA* VALUES OBTAINED BY SOLUTION- AND SOLID-STATE NMR SPECTROSCOPY FOR THE SAME CHITOSAN SAMPLES. THE STRAIGHT LINE IS THE DIAGONAL. 96

FIGURE 2-6. A. INTEGRATION OF SOLUTION-STATE NMR SIGNALS MEASURED OVER 61 H AT 60 °C: CHITOSAN BACKBONE (BLACK SQUARES), CHITOSAN ACETYL GROUP (BLUE DIAMONDS), FREE ACOH (RED CIRCLES) AND THE SUM OF THE ACETYL GROUP AND FREE ACOH (NG, PURPLE HEXAGONS). THE FULL SYMBOLS CORRESPOND TO MEASUREMENTS IN 0.8 M DCL IN D_2O, THE EMPTY SYMBOLS TO MEASUREMENTS IN 50 MM DCL IN D_2O.. EVOLUTION ON A LOGARITHMIC SCALE OF THE CONSUMPTION OF THE ACETYL GROUPS ON *N*-ACETYL-D-GLUCOSAMINE UNITS, WITH THE *N*-ACETYL-D-GLUCOSAMINE CONCENTRATION TAKEN AS (B) THE TOTAL AVAILABLE INITIAL *N*-ACETYL-D-GLUCOSAMINE UNITS $[NG]_\infty$ (PLATEAU OF NG PURPLE CURVE IN A) OR (C) AS THE DISSOLVED FRACTION OF THE INITIAL *N*-ACETYL GLUCOSAMINE UNITS $[NG]_T$ (REAL TIME VALUE OF NG PURPLE CURVE IN A). RED LINES REPRESENT LINEAR FITS WITH A R^2 OF 0.99 (B) AND 0.77 (C). 99

FIGURE 2-7. A. WEIGHT-AVERAGE MOBILITY μ_W AND B. INTEGRAL OF CHITOSAN PEAK IN KINETICS OF DISSOLUTION MONITORED WITH PACE IN 50 MM HCL IN WATER (BLACK SQUARES) AND DCL IN D_2O (GREEN TRIANGLES). 103

FIGURE 2-8. INTEGRATION OF THE PEAK AREA IN A KINETICS OF DISSOLUTION OF MEDMW1 (BLACK SQUARES), LOWMW1 (MAGENTA CIRCLES) AND HIGHMW (BLUE DIAMONDS) CHITOSAN UNDERTAKEN WITH PACE IN 50 MM HCL (N=2). 107

FIGURE S2-1: CONVENTIONAL CALIBRATION CURVE OF PULLULAN STANDARDS.....120

FIGURE S2-2: PRESSURE MOBILISATION OF MEDMW1 (NO MIXING) DISSOLVED IN 50 MM HCL (BLACK) AND ACOH (RED) WHILE THE REST OF THE CAPILLARY CONTAINS A. PHOSPHATE BUFFER 100 MM PH 3 AND AT 25 °C B. PHOSPHATE BUFFER 100 MM PH 2 AND AT 55 °C 127

FIGURE S2-3: MIXING WITH INVERSION OF VOLTAGE AT THE BEGINNING OF PRESSURE MOBILIZATION EXPERIMENTS.....128

FIGURE S2-4: PRESSURE MOBILISATION (WITH MIXING) OF 50 MM ACOH (PURPLE) AND OF MEDMW1 IN 50 MM ACOH (RED) 129

FIGURE S2-5: PRESSURE MOBILIZATION OF CHITOSAN DISSOLVED IN 50 MM HCL (4 BLACK LINES) AND ACOH (4 RED LINES) AT 55 °C AND RUNNING IN 50 MM HCL AND 50 MM ACOH RESPECTIVELY. 130

FIGURE S2-6. ^{1}H NMR SPECTRUM OF CHITOSAN (MEDMW1) IN D_2O/DCL (50 MM) AT 60 °C AFTER SEVERAL HOURS 133

FIGURE S2-7. ^{1}H NMR SPECTRUM OF CHITOSAN (BLACK LINE) AND CHITOSAN SPIKED WITH 50 MM ACOH (RED LINE) DISSOLVED IN 50 MM DCL IN D_2O.....136

FIGURE S2-8. ^{1}H NMR SPECTRUM OF CHITOSAN (MEDMW1) DISSOLVED IN A) 50 MM DCL IN D_2O B) 50 MM HCL.....137

FIGURE S2-9. TYPICAL ELECTROPHEROGRAMS OF CHITOSAN DISSOLVED IN 50 MM DCL IN D_2O OVER 20 HOURS WITH A DISSOLUTION TIME OF LESS THAN 2 H (RED LINES), 2-10 H (BLUE LINE) AND 10-20 H (BLACK LINE).....139

FIGURE S2-10. TYPICAL ELECTROPHEROGRAMS OF MEDMW1 CHITOSAN DISSOLVED IN 50 MM HCL OVER 20 HOURS WITH A DISSOLUTION TIME OF LESS THAN 2 H (RED LINE), 2-10 H (BLUE LINE) AND 10-20 H (BLACK LINE).....140

FIGURE S2-11. TYPICAL ELECTROPHEROGRAMS OF LOWMW1 CHITOSAN DISSOLVED IN 50 MM HCL OVER 20 HOURS WITH A DISSOLUTION TIME OF LESS THAN 2 H (RED LINE), 2-10 H (BLUE LINE) AND 10-20 H (BLACK LINE).....140

FIGURE S2-12. TYPICAL ELECTROPHEROGRAMS OF HIGHMW PAR1 CHITOSAN DISSOLVED IN 50 MM HCL OVER 20 HOURS WITH A DISSOLUTION TIME OF LESS THAN 2 H (RED LINE), 2-10 H (BLUE LINE) AND 10-20 H (BLACK LINE). 141

FIGURE 3-1. MOBILITY WEIGHT DISTRIBUTIONS OBTAINED BY CE-CC FOR CHITOSAN SAMPLES WITH VARYING DEGREES OF ACETYLATION. 157

FIGURE 3-2. (A) DISPERSITY VALUES SHOWN FOR CHITOSAN SAMPLES AS $D(W(\mu),1,0)$ (RED CIRCLES, EQ 3-5), $D(W(\mu),2,0)$ (BLACK SQUARES, EQ 3-6), $D(W(\mu),3,0)$ (MAGENTA DIAMONDS, EQ 3-7) AND SD (BLUE TRIANGLES, EQ 3-8) AGAINST (A) THEIR NUMBER AVERAGE DEGREE OF ACETYLATION, OR (B) AGAINST THEIR WEIGHT-AVERAGE ELECTROPHORETIC MOBILITY.....158

FIGURE 3-3. ELECTROPHORETIC MOBILITY DISTRIBUTIONS OF P(NAA-*CO*-APA) SAMPLES AT TIME 0 (RED), 5 MIN (BLUE) AND 4 H (BLACK DASH).....159

FIGURE 3-4. DISPERSITY VALUES SHOWN FOR P(NAA-*CO*-APA) SAMPLES AS $D(W(\mu),1,0)$ (BLACK SQUARE, EQ 3-5), $D(W(\mu),2,0)$ (RED CIRCLE, EQ 3-6), $D(W(\mu),3,0)$ (MAGENTA DIAMONDS, EQ 3-7) AND SD (BLUE TRIANGLE, EQ 3-8) AGAINST REACTION TIME. 160

FIGURE 3-5. ELECTROPHORETIC MOBILITY DISTRIBUTIONS OF PNAA SAMPLES. (A) PNAAS WITH DIFFERENT TOPOLOGIES: LINEAR INJECTED AT A LOWER CONCENTRATION THAN PREVIOUSLY[18] (BLACK), 3-ARM STAR (RED) AND HYPERBRANCHED (BLUE). (B) PNAAS SYNTHESIZED BY NMP OF ACRYLIC ACID (BLACK) AND *TERT*-BUTYL ACRYLATE (RED).....162

FIGURE 3-6: DISPERSITY VALUES SHOWN FOR PNAA SAMPLES AS $D(W(\mu),1,0)$ (BLACK SQUARE, EQ 3-5), $D(W(\mu),2,0)$ (RED CIRCLE, EQ 3-6), $D(W(\mu),3,0)$ (MAGENTA DIAMONDS, EQ 3-7) AND SD (BLUE TRIANGLE, EQ 8) AGAINST THEIR WEIGHT-AVERAGE ELECTROPHORETIC MOBILITY. THE SAMPLES IN INCREASING ORDER OF AVERAGE ELECTROPHORETIC MOBILITY ARE 3-ARM STAR (3.45×10^{-8} $M^2\cdot V^{-1}\cdot S^{-1}$), HYPERBRANCHED ($3.53\times10^{-8}$ $M^2\cdot V^{-1}\cdot S^{-1}$), NMP OF *T*-BA ($3.66\times10^{-8}$ $M^2\cdot V^{-1}\cdot S^{-1}$),NMP OF AA ($3.69\times10^{-8}$ $M^2\cdot V^{-1}\cdot S^{-1}$) AND LINEAR ($3.74\times10^{-8}$ $M^2\cdot V^{-1}\cdot S^{-1}$).....163

FIGURE 3-7. (A) ELECTROPHORETIC MOBILITY DISTRIBUTION AND (B) COMPOSITION DISTRIBUTION OF P(NAA-*B*-AM) SAMPLES: PAA2KPAM10K (BLACK) AND PAA10KPAM10K (RED). THE THEORETICAL M_N VALUES WERE LISTED FOR EACH SAMPLE PREVIOUSLY[16].....165

FIGURE S3-1. THE MOLECULAR STRUCTURE OF (A) CHITOSAN WITH *N*-ACETYL-D-GLUCOSAMINE AND D-GLUCOSAMINE UNITS[7] (B) P(NAA-*CO*-APA), (C) PNAA AND (D) P(NAA-*B*-AM).....181

FIGURE 4-1. CHEMICAL STRUCTURE OF CHITOSAN (OF DEGREE OF ACETYLATION *DA*) AND OF CHITIN (FOR *DA*=1). 191

FIGURE 4-2. DISPERSITY $D(W(\mu),1,0)$ (BLACK), $D(W(\mu),2,0)$ (RED) AND $D(W(\mu),3,0)$ (BLUE) OF CHITOSAN MEDMW1 (SQUARES) AND LOWMW1 (CIRCLES) DURING KINETIC MEASUREMENT OF DISSOLUTION IN 50 MM HCL IN H_2O USING CE-CC WITH THE CAROUSEL KEPT AT 60 °C. SEE SUPPORTING INFORMATION EQUATION S4-1 TO S4-3 FOR DISPERSITY CALCULATIONS [24]. 199

FIGURE 4-3: ELECTROPHEROGRAM OF PALAM (BLACK LINES) AND CHITOSAN (RED LINE) SEPARATED IN A PDADMAC/ALGINATE/PDADMAC COATED CAPILLARY (50 CM TOTAL LENGTH) IN LIPB10 AT -30 KV WITH UV (SOLID LINE – LEFT Y AXIS) AND CONTACTLESS CAPACITIVELY-COUPLED CONDUCTIVITY (DASHED LINE – RIGHT Y AXIS) DETECTIONS. WHERE μ IS THE ELECTROPHORETIC MOBILITY AND $W(\mu)$ IS THE WEIGHT FRACTION OF POLYELECTROLYTE CHAINS WITH A GIVEN ELECTROPHORETIC MOBILITY CALCULATED AS THE ABSORBANCE ($S(T)$) MULTIPLIED BY THE MIGRATION TIME. 201

FIGURE 4-4. A. DISTRIBUTION OF ELECTROPHORETIC MOBILITIES, $W(\mu)$, OF CHITOSAN SEPARATED WITH PACE USING NAPB100 FOR SAMPLES WITH AN AVERAGE *DA* (MEASURED BY SSNMR) BELOW 5 % (GREEN LINES), BETWEEN 5 % AND 10 % (BLUE LINE), BETWEEN 10 % AND 15 % (RED LINES), BETWEEN 15 % AND 20 % (BLACK LINES) AND ABOVE 20 % (PURPLE LINE). DISPERSITY VALUES (SEE SUPPORTING INFORMATION FOR EXPRESSIONS) FOR CHITOSAN SAMPLES AS $D(W(\mu),1,0)$ (BLACK SQUARES), $D(W(\mu),2,0)$ (RED CIRCLES) AND $D(W(\mu),3,0)$ (BLUE DIAMONDS) AGAINST THEIR (B) NUMBER-AVERAGE DEGREE OF ACETYLATION OR (C) WEIGHT-AVERAGE ELECTROPHORETIC MOBILITY (μ_W). SEE SUPPORTING INFORMATION EQUATION S4-1 TO S4-3 FOR DISPERSITY CALCULATIONS [24]. 204

FIGURE 4-5. A. DISTRIBUTIONS OF ELECTROPHORETIC MOBILITIES, $W(\mu)$, OF CHITOSAN SEPARATED WITH PACE USING LIPB100 WITH SAMPLES WITH AN AVERAGE *DA* BELOW 5 % (GREEN LINES),

between 5 % and 10 % (blue line), between 10 % and 15 % (red lines), between 15 % and 20 % (black lines) and above 20 % (purple line). Dispersity values for chitosan samples as $D(W(\mu),1,0)$ (black squares), $D(W(\mu),2,0)$ (red circles) and $D(W(\mu),3,0)$ (blue diamonds) against their (B) number-average degree of acetylation or (C) weight-average electrophoretic mobility. See supporting information equation S4-1 to S4-3 for dispersity calculations [24]. 206

Figure 4-6: Calibration curve of the weight-average electrophoretic mobility in A. NaPB100 ($A = 4.58 \times 10^{-9}$, $B = 3447.2$, $R^2 = 0.62$) B. LiPB100 as a function of DA for chitosan with a Bradley function fit first (black line) ($A = 5.44 \times 10^{-9}$, $B = 693.77$, $R^2 = 0.70$) and second iteration (blue line) ($A = 5.93 \times 10^{-9}$, $B = 399.21$, $R^2 = 0.97$), The electrophoretic mobilities were measured in duplicates; both duplicates are shown on the graph and included in the fit (see section 3.4.2).....209

Figure 4-7: Composition distributions of chitosan samples separated in A. NaPB100 and B. LiPB100.....213

Figure 4-8. Dispersity of composition distributions as $D(W(DA),1,0)$ (black squares), $D(W(DA),2,0)$ (red circles), $D(W(DA),3,0)$ (blue diamonds) and standard deviation (pink triangles) for chitosan samples separated in A) NaPB100 and B) LiPB100. See supporting information equation S4-1 to S4-8 for dispersity calculations [24]. 214

Figure 4-9. A. Composition distributions and B. Dispersity of composition distributions as $D(W(DA),1,0)$ (black squares), $D(W(DA),2,0)$ (red circles), $D(W(DA),3,0)$ (blue diamonds) and standard deviation (pink triangles) for chitosan samples separated in LiPB100 and treated with the 2nd iteration. See supporting information equation S4-1 to S4-8 for dispersity calculations [24].....216

Figure S4-1: Dispersity of electrophoretic mobility distributions $D(W(\mu),1,0)$ (black), $D(W(\mu),2,0)$ (red), $D(W(\mu),3,0)$ (blue) of chitosan MedMW1 dissolved in 50 mM HCl in H_2O (diamonds) and 50 mM DCl in D_2O (triangles) during kinetic measurement using CE-CC with the carousel kept at 60 °C.....228

FIGURE S4-2: ELECTROPHEROGRAM OF PALAM (BLACK LINES) AND CHITOSAN (RED LINE) SEPARATED IN A PDADMAC/ALGINATE MULTILAYER COATED CAPILLARY IN NAPB10, DETECTED WITH UV (SOLID LINE – LEFT Y AXIS) OR CONDUCTIVITY (DASHED LINE – RIGHT Y AXIS).....229

FIGURE S4-3 A. CALIBRATION CURVE OF THE WEIGHT-AVERAGE ELECTROPHORETIC MOBILITY (μw) OF CHITOSAN SAMPLES SEPARATED IN A. NAPB100 AND B. LIPB100. RED LINE REPRESENTS LINEAR FIT AND BLACK LINES REPRESENT POSSIBLE POPULATION FITS 230

FIGURE S4-4: CALIBRATION CURVE OF WEIGHT-AVERAGE ELECTROPHORETIC MOBILITY IN NAPB100 AS A FUNCTION OF DA FOR CHITOSAN WITH A LINEAR FIT (RED LINE) ($R^2 = 0.56$) 231

FIGURE S4-5: CALIBRATION CURVE OF THE INVERSE FUNCTION OF WEIGHT-AVERAGE ELECTROPHORETIC MOBILITY IN NAPB100 AS A FUNCTION OF DA FOR CHITOSAN WITH A LINEAR FIT (RED LINE) ($R^2 = 0.57$).....231

FIGURE S4-6: CALIBRATION CURVE OF WEIGHT-AVERAGE ELECTROPHORETIC MOBILITY IN NAPB100 AS A FUNCTION OF DA FOR CHITOSAN WITH ORDER 2 (BLACK LINE), 3 (RED LINE) AND 4 (BLUE LINE) POLYNOMIAL FIT. 232

FIGURE S4-7: CALIBRATION CURVE OF THE LOG FUNCTION OF WEIGHT-AVERAGE ELECTROPHORETIC MOBILITY IN NAPB100 AS A FUNCTION OF DA FOR CHITOSAN WITH A LINEAR FIT (RED LINE) ($R^2 = 0.56$).....232

FIGURE S4-8: X-RAY DIFFRACTOGRAMS OF VARIOUS CHITOSAN SAMPLES NORMALIZED BY THE PEAK MAXIMUM BETWEEN 18 AND 22°. 233

FIGURE S4-9: CALIBRATION CURVE WITH A BRADLEY FUNCTION FIT OF THE WEIGHT-AVERAGE ELECTROPHORETIC MOBILITY IN NAPB100 AS A FUNCTION OF *DA* FROM THE SOLID-STATE NMR SPECTROSCOPY MEASUREMENTS (BLACK) OR THE PEAK APEX OF THE COMPOSITION DISTRIBUTIONS (BLUE). 234

FIGURE 5.1-1: SCHEME OF THE GRAFTING REACTION. CHEMICAL REACTION SCHEME SHOWING THE ACTIVATION BY EDC-HCL AND NHS OF THE CARBOXYLIC ACID FUNCTIONAL GROUP OF RGDS FOLLOWED BY ITS GRAFTING ONTO THE CHITOSAN'S FILM SURFACE. 251

FIGURE 5.1-2: PEAK ASSIGNMENT OF THE SPECIES PRESENT IN THE REACTION MEDIUM. A. SEPARATION AND PEAK ASSIGNMENT FOR SOLUTIONS OF PARTIALLY HYDROLYZED EDC-HCL (PINK), RGDS

(RED), NHS (BLUE), AS WELL AS FOR PBS (PURPLE) AND THE REACTION MEDIUM (BLACK). B. ELECTROPHEROGRAMS OF REACTION MEDIA (BLACK) PRESENTED AS A FUNCTION OF MIGRATION TIME (ELECTROPHORETIC MOBILITY SHOULD BE USED TO OVERCOME POOR REPEATABILITY IN MIGRATION TIMES). 252

FIGURE 5.1-3: CE MONITORING OF RGDS CONSUMPTION. (A) OVERLAID PEPTIDE PEAKS AT REACTION TIME 30 MIN (PURPLE SOLID LINE), 60 MIN (MAGENTA DASH LINE), 90 MIN (BLUE SOLID LINE), 120 MIN (GREEN DASH LINE), 150 MIN (RED SOLID LINE) AND (B) KINETICS OF GRAFTING COMPLETED OVER 18 HR IN REPLICATES (SQUARE AND CIRCLE). 253

FIGURE 5.1-4: OVERLAID PEPTIDE PEAKS IN REACTION MEDIA SHOWING SUBOPTIMAL RESULTS. (A) VARYING (HYDRODYNAMIC) INJECTION TIMES: 5 SEC (BLUE LINE), 10 SEC (BLACK LINE), 20 SEC (RED LINE) AND 30 SEC (MAGENTA LINE). (B) REACTION MEDIA LEFT IN A CE VIAL FOR AN EXTENDED PERIOD OF TIME BEFORE INJECTION: 30 MIN (RED LINE) AND 90 MIN (BLUE LINE).....254

FIGURE 5.1-5: ^{13}C SWOLLEN-STATE NMR SPECTRA OF CHITOSAN FILMS. COMPARISON OF THE FILMS BEFORE (BLACK LINE) AND AFTER (BLUE LINE) PEPTIDE GRAFTING. SIGNALS PRESENT ONLY IN THE SPECTRUM RECORDED AFTER GRAFTING ARE INDICATED BY ASTERISKS....255

FIGURE 5.2-1. PERMEABILITY OF REGULAR AND THIN BLANK CHITOSAN FILMS, EXPERIMENT COMPLETED IN DUPLICATE (RED AND BLACK CROSSES). NEGATIVE CONTROL WAS CHITOSAN FILMS WITHOUT CORDIAL AND THE POSITIVE CONTROL WAS THE EXPERIMENT WITHOUT CHITOSAN FILM.....272

FIGURE 5.2-2.A) WEIGHT-AVERAGE MOBILITY OF RGDS (BLUE AND PINK TRIANGLES) AND PEG-SH (BLACK AND RED CROSSES) AGAINST THE REACTION TIME B) DISPERSITY OF RGDS (BLUE AND PINK TRIANGLES) AND PEG-SH (BLACK AND RED CROSSES) AGAINST THE REACTION TIME. 275

FIGURE 5.2-3. ELECTROPHEROGRAM OF REACTANTS OF GRAFTING REACTION EDC-HC AND PEG-SH, OF THE EOF MARKER, AND PBS SHOWN AS THE WEIGHT DISTRIBUTION $W(\mu)$ OF ELECTROPHORETIC MOBILITIES (μ)....276

FIGURE 5.2-4. A) DISTRIBUTION OF ELECTROPHORETIC MOBILITY OF PEG-SH SIGNAL OF GRAFTING REACTION SOLUTION OVER 0 MIN (BLACK), 60 MIN (RED), 120 MIN (BLUE), 180 MIN (MAGENTA), 240 MIN (GREEN) AND AFTER RINSING THE CHITOSAN FILM FOLLOWING THE END OF THE GRAFTING (GREY). B) QUANTIFICATION OF PEG-SH CONSUMPTION OVER 4 HOURS IN REPLICATES

(BLACK AND RED SQUARES). THE POINT AT 5 HOURS REPRESENTS RINSING OF THE CHITOSAN FILM AT THE COMPLETION OF THE GRAFTING. 278

FIGURE 5.2-5. A. TGA AND B. DSC OF BLANK CHITOSAN FILM (BLACK LINE), CHITOSAN FILM WITH PEG-SH GRAFTED ONTO THE SURFACE (BLUE LINE) AND PEG-SH POWDER (RED LINE). DERIVATIVES OF TGA AND DSC CURVES ARE SHOWN IN THE SUPPORTING INFORMATION FIGURE S5.2-4. 281

FIGURE 5.2-6: NOESY MEASUREMENTS OF CHITOSAN FILMS SWOLLEN IN PBS AT PH 7 WITH VARYING MIXING TIMES A) 5 MS B) 10 MS C) 20 MS D) 50 MS 283

FIGURE 5.2-7: NOESY MEASUREMENTS OF CHITOSAN POWDER CHITPAR1 SWOLLEN IN PBS AT PH 7 WITH VARYING MIXING TIMES A) 5 MS B) 10 MS C) 20 MS D) 50 MS 283

FIGURE 5.2-9: ^{1}H-^{1}H DOUBLE QUANTUM CORRELATION OF CHITOSAN FILM SWOLLEN IN PBS AT PH 7 WITH VARYING SPINNING RATES AND RECOUPLING TIMES A) 2 TR 5 KHZ B) 4 TR 5 KHZ C) 2 TR 25 KHZ D) 4 TR 25 KHZ 285

FIGURE 5.2-10: ^{1}H-^{1}H DOUBLE QUANTUM CORRELATION OF CHITOSAN POWDER CHITPAR1 SWOLLEN IN PBS AT PH 7 WITH VARYING SPINNING RATES AND RECOUPLING TIMES A) 2 TR 5 KHZ B) 4 TR 5 KHZ C) 2 TR 25 KHZ D) 4 TR 25 KHZ 286

FIGURE 5.2-11: ^{1}H-^{1}H DOUBLE QUANTUM CORRELATION OF CHITOSAN POWDER PARRAMEDMW SWOLLEN IN PBS AT PH 7 WITH VARYING SPINNING RATES AND RECOUPLING TIMES A) 2 TR 5 KHZ B) 4 TR 5 KHZ C) 2 TR 25 KHZ D) 4 TR 25 KHZ 287

FIGURE S5.2-1. REACTION SCHEME FOR PEG-SH GRAFTING TO CHITOSAN FILMS, ADAPTED FROM PREVIOUS RESEARCH.[1] 293

FIGURE S5.2-2. CALIBRATION CURVE OF SIGNAL-TO-NOISE RATIO (SNR) AS A FUNCTION OF PEG-SH CONCENTRATION WITH A LINE OF BEST FIT WITH (BLUE) OR WITHOUT (RED) INTERCEPT SET TO 0. 294

FIGURE S5.2-3. CALIBRATION CURVE OF PEAK AREA OF PEG-SH AS A FUNCTION OF CONCENTRATION WITH A LINE OF BEST FIT WITH (THICK RED) OR WITHOUT (THIN RED) THE INTERCEPT SET TO 0..294

FIGURE S5.2-4: A. DERIVATIVE THERMOGRAVIMETRIC (DTG) CURVE B. DERIVATIVE DIFFERENTIAL SCANNING CALORIMETRY (DDSC) CURVE OF BLANK CHITOSAN FILM (BLACK LINE), CHITOSAN FILM GRAFTED WITH PEG-SH (BLUE LINE) AND PEG-SH POWDER (RED LINE). 296

FIGURE S5.2-5. X-RAY SPECTROMETRY OF CHITOSAN GRAFTED WITH PEG-SH (RED), NO SIGNIFICANT COUNTS OF SULFUR (GREEN).....297

FIGURE S5.2-6: ATR FTIR SPECTROSCOPY OF CHITOSAN FILM (BLACK), CHITOSAN FILM GRAFTED WITH PEG-SH (BLUE) AND PEG-SH POWDER (RED). 298

FIGURE S5.2-7: RAMAN SPECTROSCOPY OF CHITOSAN FILM (BLACK) AND CHITOSAN FILM GRAFTED WITH PEG-SH (BLUE). 299

FIGURE S5.2-8: SEM IMAGE OF CHITOSAN FILMS GRAFTED WITH PEG-SH ON THE SURFACE AT A A) 500 μM B) 100 μM C) 50 μM AND D) 10 μM (SEE SCALE BAR OF IMAGES) 300

FIGURE S5.2-9: SEM IMAGE OF NATIVE CHITOSAN FILMS AT A) 500 μM B) 100 μM C) 50 μM AND D) 10 μM (SEE SCALE BAR OF IMAGES).....301

FIGURE S5.2-10. SURFACE ROUGHNESS OF NATIVE CHITOSAN FILM WITH AFM A) 2D IMAGE AND B) 3D IMAGE 302

FIGURE S5.2-11: ^{13}C SPECTRA OF CHITOSAN FILM (RED), GRAFTED WITH PEG-SH SWOLLEN IN PBS (BLACK) AND D_2O (BLUE). 303

FIGURE S5.2-12: PERMEABILITY TEST SETUP FOR 1X, 2X AND 3X CHITOSAN FILM SAMPLES FOR BOTH 1.5 H AND 3 H WAIT TIMES WITH 30μL RED CORDIAL PIPETTED ABOVE. 305

FIGURE S5.2-13: UV-VIS ABSORPTION ACROSS 200-800 NM FOR A 0.15% (V/V) RED CORDIAL SOLUTION. 305

FIGURE S5.2-14: CALIBRATION OF UV ABSORBANCE OF RED CORDIAL SOLUTIONS WITH LINEAR FIT (RED).....306

FIGURE S5.2-15: ^{1}H-^{1}H DOUBLE QUANTUM CORRELATION OF CHITOSAN FILMS SWOLLEN IN D_2O WITH VARYING SPINNING RATES AND RECOUPLING TIMES A) 2 TR 25 KHZ B) 4 TR 25 KHZ.....307

FIGURE S5.2-16: ^{1}H-^{1}H DOUBLE QUANTUM CORRELATION OF CHITPAR1 SWOLLEN IN D_2O WITH VARYING SPINNING RATES AND RECOUPLING TIMES A) 2 TR 25 KHZ B) 4 TR 25 KHZ.....307

FIGURE S5.2-17: ^{1}H-^{1}H DOUBLE QUANTUM CORRELATION OF PARRAMEDMW SWOLLEN IN D_2O WITH VARYING SPINNING RATES AND RECOUPLING TIMES A) 2 TR 25 KHZ B) 4 TR 25 KHZ.....308

FIGURE S5.2-18: ^{13}C (^{1}H) CORRELATION MEASUREMENT OF CHITOSAN FILM SWOLLEN IN A) PBS AT PH 7 AND B) D_2O 309

FIGURE S5.2-19: ^{13}C (^{1}H) CORRELATION MEASUREMENT OF CHITPAR1 SWOLLEN IN A) PBS AT PH 7 AND B) D_2O 309

FIGURE S5.2-20: ^{13}C (^{1}H) CORRELATION MEASUREMENT OF PARRAMEDMW SWOLLEN IN A) PBS AT PH 7 AND B) D_2O 310

Abbreviations

Abbreviation	Definition
γ	Magnetogyric ratio
δ	Chemical shift
δ_x	Chemical shift of nucleus x
μ_{app}	Apparent electrophoretic mobility
μ_{ep}, μ	Electrophoretic mobility
f	Larmor frequency
a	Slope
AcOH	Acetic acid
AFM	Atomic force microscopy
ATR	Attenuated total reflectance
b	Intercept
BGE	Background electrolyte
C	Concentration
CE	Free solution capillary electrophoresis

CE-CC	Free solution capillary electrophoresis in the critical conditions
CP	Cross-polarisation
DA	Degree of acetylation
DDA	Degree of deacetylation
DAD	Diode array detector
DB	Degree of branching
DE	Degree of esterification
DD	Dipolar decoupling
DP	Degree of polymerisation
DS	Degree of substitution
DSC	Differential scanning calorimetry
E	Electric field
ESI-MS-ToF	Electrospray ionization - mass spectrometry - time of flight
EOF	Electroosmotic flow
FFF	Field flow fractionation

FID	Free induction decay
FTIR	Fourier transform infrared
HCl	Hydrochloric acid
HPAEC	High performance anion exchange chromatography
HPLC	High performance liquid chromatography
IC	Ion chromatography
IUPAC	International Union of Pure and Applied Chemistry
L_t	Total capillary length
L_d	Effective capillary length
LC-CC	Liquid chromatography in the critical conditions
LOD	Limit of detection
LOQ	Limit of quantification
MAS	Magic-angle spinning
MS	Mass spectrometry
NMP	Nitroxide-mediated polymerization
NMR	Nuclear magnetic resonance

NS	Number of scans
oligoAA	Oligo(sodium acrylate)
PAA	Poly(acrylic acid)
PEG	Poly(ethylene glycol)
r^2	Correlation coefficient
RAFT	Reversible addition-fragmentation chain-transfer
rf	Radio frequency
RI	Refractive-index
RSD	Relative standard deviation
RT	Room temperature
SD	Standard deviation
SEC	Size-exclusion chromatography
SEM	Scanning electron microscopy
SNR	Signal-to-noise ratio
SPE	Single-pulse excitation
t_{eof}	Migration time of EOF

t_m	Migration time
TDA	Taylor dispersion analysis
TFA	Trifluoroacetic acid
TGA	Thermogravimetric Analysis
ToF-SIMS	Time of flight – secondary ion mass spectrometry
UV	Ultraviolet
UV-Vis	Ultraviolet and visible light
V	Voltage
v	Velocity
XRD	X-ray diffraction

Abstract

Chitosan is a renewable polymer produced from a waste product of the seafood industry. It has been seen as useful for a range of applications due to its inherent properties. It is antifungal, antibacterial, biodegradable, biocompatible and has low immunogenicity which makes it attractive specifically for biomedical applications. Examples of chitosan's possible applications include bioadhesive films, stem cell growth substrates and drug delivery agents. Chitosan is produced from the *N*-deacetylation of chitin. Chitin is the second most abundant polysaccharide in the world (by volume after cellulose) and is synthesized by many organisms which results in it being readily available, inexpensive and abundant. Its natural occurrence includes the shells of arthropods such as shrimps, crabs and the cell walls of yeasts. Unfortunately, due to its natural origin and the variation in processing conditions, chitosan is plagued by batch-to-batch variations which affect its widespread utilization. It thus requires appropriate characterization to allow exploitation of its inherent properties.

The molecular structure of chitosan includes varying proportions of D-glucosamine and *N*-acetyl- D-glucosamine monomer units. The degree of acetylation (*DA*) is defined as the fraction of *N*-acetyl- D-glucosamine and the distribution of *DA*s is defined as its variation between polymer chains in a given sample. Although it has been well documented that a distribution of *DA*s exists (not all chitosan chains have the same *DA*), this is often overlooked. Therefore common characterization of chitosan is often incomplete and only takes into

account one of the average *DA*s and neglects the distributions of *DA*s. The complexity and importance of the distribution of *DA*s had been revealed recently through a coupling of size-exclusion chromatography (SEC) with ^{1}H NMR spectroscopy; however, it had not been measured before the work in this PhD.

To allow an accurate characterization of polymers in solution, a true solution must be obtained. Unfortunately, the dissolution of chitosan is often overlooked. Utilizing capillary electrophoresis in the critical conditions (CE-CC), solution- and solid-state NMR spectroscopy, the dissolution of chitosan was probed. Obtaining a true chitosan solution has been proven to be challenging even with commonly used aqueous solvents. Aqueous AcOH which is most commonly used was seen to dissolve chitosan inefficiently compared to aqueous HCl. However, significant deacetylation was seen in chitosan dissolved in aqueous HCl and kept at high temperatures for prolonged periods of time. The standard for polymer size analysis, SEC, was shown to detect aggregation of the chitosan chains in the SEC eluent. Furthermore, comparisons of the average *DA* obtained with solution-state compared to solid-state NMR spectroscopy gave evidence of a clear bias in the characterization due to incomplete dissolution. This is extremely significant as chitosan is often characterized with solution-state NMR spectroscopy. The dissolution was concluded to be complex and a compromise is necessary in allowing a more complete dissolution and minimal deacetylation. However, for routinely measured average *DA* values, measurements should be undertaken in the solid state.

To allow a more comprehensive characterization of chitosan composition, methods were developed in this PhD using free solution capillary electrophoresis in the critical conditions (CE-CC). CE-CC is a separation method and therefore is able to yield distributions. Complex polymers can have distributions of various parameters including composition, branching, end groups and molar mass. For chitosan, CE-CC separates by composition (or degree of acetylation). Capillary electrophoresis has been proven to be a robust technique for the separation and characterization of both natural and synthetic polymers. A method was developed to calculate dispersities from distributions obtained with CE-CC analogous to the calculation of dispersity from molar mass distributions determined by size-exclusion chromatography (SEC). Using a ratio of moments, the dispersity of electrophoretic mobility and composition distributions were obtained. The dispersity values represented either the heterogeneity of branching or composition of the complex polymers. This resulted in further characterization of complex polymers based on their composition or architecture. The dispersity values allowed the quantification and numerical representation of the heterogeneity. This allowed comparisons and trends to be quantified between samples.

In the further analysis of chitosan, improvements in the separation were sought. This included changing the counter-ion of the buffer during the CE separation from sodium to lithium. Lithium showed trends of greater selectivity and combining these results with previous work in reducing the adsorption (lower pH and higher temperature) allowed a more accurate separation. The dispersity was then calculated for a larger range of chitosan samples and both

distributions of electrophoretic mobilities and composition distributions were obtained. A trend was seen in which the dispersity first increased with the average *DA* and then began to reduce. Using the correlation between composition and mobility allowed composition distributions to be obtained for chitosan for the first time. This was the first determination of composition distributions and of their corresponding dispersity values for a statistical copolymer. The results identified chitosan samples with very similar measured average *DA* values having significantly different dispersity values. These results confirm the inaccuracy of characterizing chitosan by only through its average *DA*.

Finally, to improve the use of chitosan for tissue engineering, regenerative medicine and other biomedical applications it was important to ensure low immunogenicity especially in the application of implantation. Poly(ethylene glycol), PEG, and the peptide RGDS was grafted onto the surface of chitosan and the chemical reaction was monitored using CE. The robustness of CE allows samples to be injected without sample preparation and allows it to be used effectively in the analysis of chemical reactions. The films were then characterized by thermogravimetric analysis (TGA) and differential scanning calorimetry (DSC) and the grafting of PEG onto the surface of the chitosan film was validated. Previous cell attachment studies showed that the proliferation of cells occurred in specific regions. This was likely due to an inherent heterogeneity of the chitosan films which could be caused by incomplete dissolution and aggregation seen in the dissolution studies. To probe this heterogeneity of the chitosan films and powder, advanced solid-state NMR

spectroscopy measurements were undertaken. The analysis compared the mobile and rigid fractions of chitosan. The results suggested similar behavior in both fractions, however, gave evidence of possible orientation of the acetyl group away from the backbone. The permeability of the films to small molecules was also tested and confirmed.

In summary, the dissolution of chitosan was seen to be complex and currently used methods were either deemed inefficient in the dissolution or conversely caused degradation. A new method was developed to numerically represent the heterogeneity of composition or branching and this was tested with various complex polymer samples including chitosan. Further development of this method allowed composition distributions of a statistical copolymer (chitosan) to be obtained for the first time and the heterogeneity of composition to be obtained. New low immunogenicity films were produced by the grafting of poly(ethylene glycol) onto the surface of chitosan films and the grafting process was monitored by CE. The grafting was validated and the permeability and heterogeneity of chitosan films were also probed. Future work should involve probing the dissolution of chitosan with ionic liquids, applying the calculation of dispersity of both distributions of electrophoretic mobility and composition distributions to a broader range of polyelectrolytes, further improving the selectivity of the separation of chitosan and testing the biocompatibility of PEG grafted chitosan films. The methods developed in this thesis will enable chitosan to reach its potential for various applications ranging from tissue regeneration, through bioplastics to drug delivery.

CHAPTER 1: Background

1.1. Chitosan

As the issues of overpopulation and pollution become widespread on our planet, there is an increasing necessity for the use of renewable resources and for greater efficiency in the production and consumption of materials. This motivation has influenced the intelligent design and synthesis of materials to include biodegradability but also the increased consideration of the applications of renewable products. As the design of materials and the use of waste products increases, so do the complexity of the materials and the characterization methods necessary. These developments and requirements are inclusive of polymers. Currently natural and synthetic polymers are used extensively in industries including but not exclusive to: biomedical, food and health, and manufacturing. To allow polymers, especially those produced from waste products or renewable resources, to be used to their potential characterization methods are required to be improved.

The introduction to my thesis is made up of a first authored invited review article on the separation of polyelectrolytes and polysaccharides using CE [1] (section 1.2), part of an article comparing the separation of block copolymers (section 1.2.5) with size-exclusion chromatography (SEC also known as GPC) and capillary electrophoresis (CE) which provided me with training in separation methods [2] and part of an earlier feasibility study of my PhD project which was completed using results from both my BSc Honours degree and PhD, of which I am joint first author [3] (section 1.4).

1.1.1. Chitosan's potential as a biomaterial

The polysaccharide chitosan is derived from the *N*-deacetylation of chitin. Chitin is the second most abundant polysaccharide in the world (by volume after cellulose) and is synthesized by many organisms [4, 5]. Its natural occurrence includes the shells of arthropods such as shrimps, crabs and the cell walls of yeasts [6]. Being a major waste product of the seafood industry, chitosan is a renewable and sustainable polymer. Its most promising derivative is chitosan, for which various biomedical applications have recently been discovered such as bioadhesive chitosan films, [7] stem cell growth substrates [8] microspheres for tissue regeneration [9] and as a drug delivery agent [10]. Further applications include but are not limited to bioremediation, weight-loss supplements, dental applications (Figure 1-1A) [11], bioplastics (Figure 1-1B) and bioelectronics (Figure 1-1C) [12]. Chitosan has several specific properties that allowed it to become a significant area of research for biomedical applications: it is biocompatible, biodegradable, antimicrobial and antifungal [7, 13-15]. Chitosan is formed from the deacetylation of chitin and therefore the average degree of acetylation can be as low as 1-2 % and as high as 50 %. Chitosan's p*K*a depends on its *DA* and is generally between 6 and 6.5. It also has a semi-crystalline structure which is influenced by the *DA* and the process used to produce chitosan from chitin. [6] The molar mass of chitosan is uncertain due to issues with solubility. Lack of dissolution and aggregation prevent accurate molar mass determinations. Chitosan is often modified to improve its mechanical and surface properties, especially in biomedical applications. These properties are generally described as average. The sensitivity of mechanical and surface properties to pH is a significant drawback in some cases. [16]

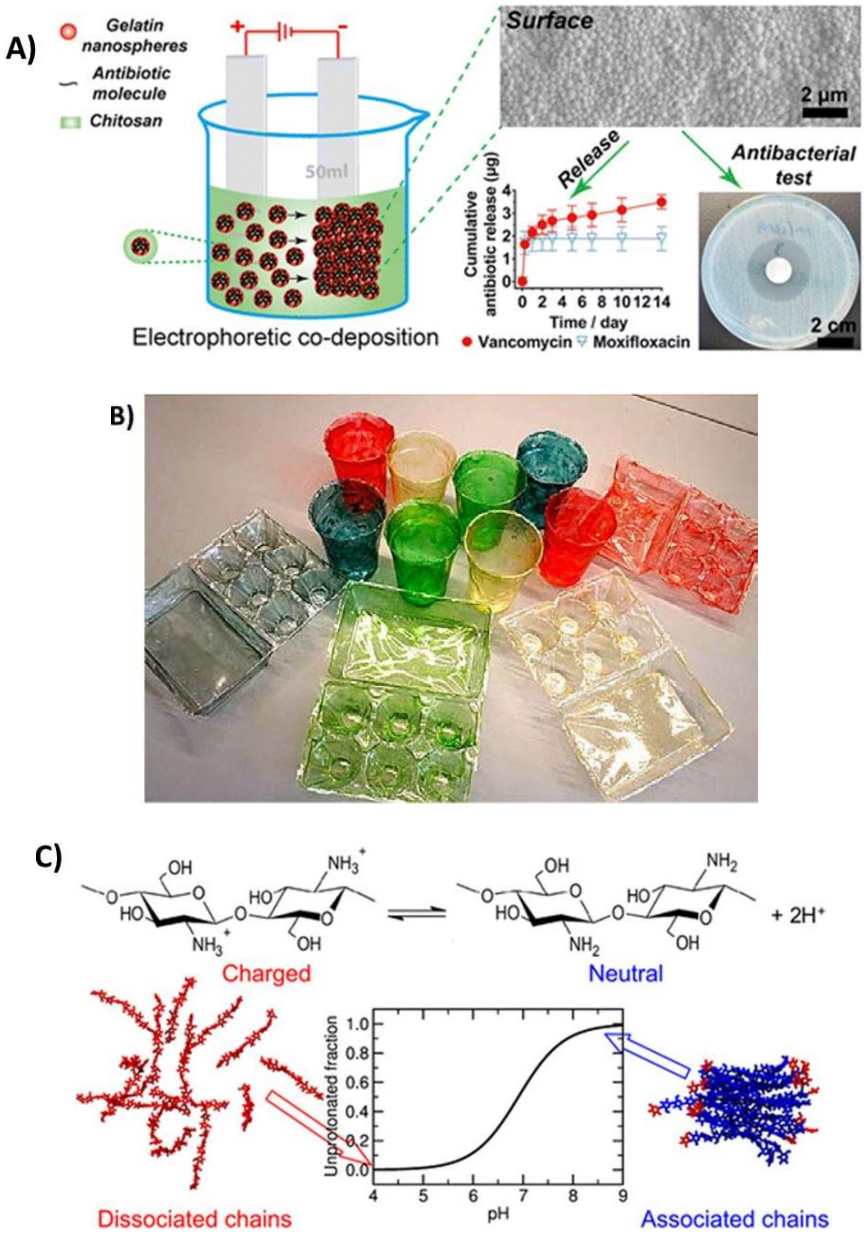

Figure 1-1 Potential applications of chitosan A) Tuned release of antibiotics using electrophoretic deposition of chitosan coatings for dental implantations [11] B) Bioplastics out of shrimp shell materials [17] C) pH responsive self-assembly of chitosan for bioelectronics applications [12]

1.1.2. Need for characterization

The molecular structure of the polysaccharide chitosan includes varying proportions of D-glucosamine and *N*-acetyl- D-glucosamine (Figure 1-2). The degree of acetylation (*DA*) is defined as the fraction of *N*-acetyl- D-glucosamine and the distribution of *DA*s is defined as its variation between polymer chains in a given sample. Although it has been well documented that a distribution of *DA*s exists (not all chitosan chains have the same *DA*) [6, 18, 19], this is often overlooked. The *DA* of chitosan is extremely important as it influences the majority of chitosan's properties including solubility, mechanical/surface properties, film formation and ability to graft onto or modify chitosan [16].

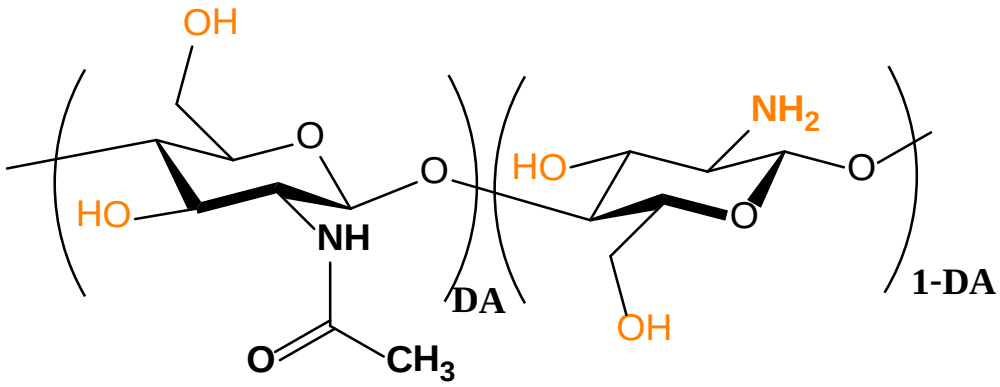

Figure 1-2: Chemical structure of chitosan with a degree of acetylation *DA*. Chitin corresponds to *DA*=1.

Due to its natural origin and the variation in processing conditions, chitosan can have a broad distribution of *DA*s. The complexity and importance of the distribution of *DA*s has been revealed recently through a coupling of SEC with ^{1}H NMR spectroscopy (Figure 1-3); however, it still has not been measured [18].

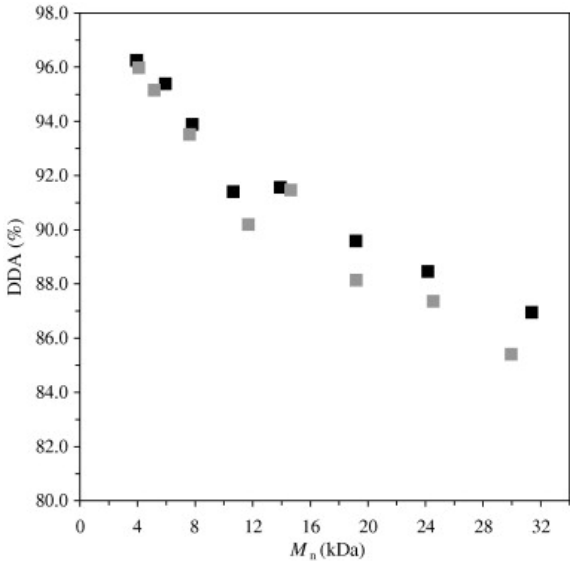

Figure 1-3: Degree of deacetylation, *DDA* (%) (*DDA* = 1-*DA*), of SEC fractions of the low molar mass chitosan N-86-10 as a function of M_n, for duplicate 1 (black) and duplicate 2 (grey) [18].

^{1}H NMR spectroscopy is often used to characterize chitosan by its average *DA*. However, this characterization is only by one of chitosan's average *DA*s and therefore alternate characterization methods are sought. Due to an incomplete understanding of chitosan's complex structure, several limitations exist in its characterization. Unlike proteins, chitosan does not fold into a complex regular conformation. Additionally, analysis in the solid state is hampered by residual water between the polymer chains which affect its chemical and physical properties [20]. It is however important to characterize chitosan in the solid state and allow a benchmark of solution-state analysis (see section 1.3). Further, this is increasingly important in the formation and analysis of chitosan films. To allow a more complete characterization of chitosan, the dissolution needed to be analyzed. Previous results suggested dissolution varied in different aqueous

conditions and not all aqueous acidic solvents were able to produce clear transparent solutions [21]. Therefore an appropriate technique to analyze complex polymers in solution was required.

1.2. Characterization of Polymers in Solution

This section covers mostly separation methods used for the characterization of complex polymers. Other important methods in polymer characterization such as NMR spectroscopy are covered in section 1.3.

1.2.1. Introduction to CE and limitations of previous methods

Free solution capillary electrophoresis (CE), or capillary zone electrophoresis, is a robust polymer separation technique. CE differs from the commonly known slab electrophoresis or capillary gel electrophoresis as the capillary does not contain any stationary phase: it is just filled with a buffer (also named background electrolyte). CE does not require tedious sample preparation, not even filtration (see later in section 1.2.3.2 for example). It has several advantages over traditional separation techniques for the characterization of polyelectrolytes which will be outlined in this literature review. The most commonly used method for the separation and characterization of polymers is SEC. SEC is relatively quick and affordable in obtaining data regarding the size or molar mass of a polymer with good repeatability [22]. Among SEC's main limitations is its poor reproducibility in terms of molar mass analysis: round-robin tests often show poor accuracy of the values of the determined molar mass [23, 24]. This is detailed in Berek's recent critical review [25]. The review linked

the common accuracy issue to the difficulties in obtaining a pure size-exclusion separation: secondary retention mechanisms (such as ion exclusion), side processes, parasitic processes, osmotic effects, secondary exclusion, concentration effects, preferential interactions and SEC band broadening. For ultrahigh molar masses, the sample is generally thought to be degraded by shear [26], although a change of conformation of the polymer chains may also take place, leading to a new separation mechanism [27]. In addition, even in ideal conditions (pure size-exclusion mechanism, no degradation), SEC separates by hydrodynamic volume not by molar mass [28]. Apparent molar masses determined by SEC (e.g. polystyrene-equivalent molar masses) thus have a variable and sometimes limited accuracy [29, 30]. Different topologies (branching) or compositions of the polymer sample influence the hydrodynamic volume and the separation is then incomplete in terms of molar mass when a range of branching structures or of compositions is present in a sample [31-33]. This can render the simple determination of molar mass using Mark-Houwink-Sakurada parameters inaccurate, like in the case of most poly(alkyl acrylates) [34, 35]. Up to 100 % error in the determination of the molar mass of branched polymers has been measured using multiple detection SEC (light scattering and viscometry) [36, 37].

The SEC of branched polymers and polysaccharides was recently discussed in a review [38]. Composition of copolymers, branching and purity are often overlooked in polymer characterization, since SEC has a quasi-monopoly and is not suited for these types of characterization. However, alternative methods are being developed, especially alternative liquid chromatography methods [39].

Liquid chromatography in critical conditions (or at the critical conditions) [40] is one of the most prominent: the critical conditions for one homopolymer correspond to the absence of separation by molar mass for this homopolymer, allowing for separation solely by its topology if branched [41] or solely by its composition if copolymerized [42]. These critical conditions are, however, tedious to establish and low recoveries have been observed [43, 44]. CE offers an alternative and the objective of this review is to present and discuss the potential of CE for synthetic polymers and polysaccharides.

1.2.2. Theory and application of Free-solution Capillary Electrophoresis

CE (defined here as free solution capillary electrophoresis) involves separation in a capillary filled with only buffer (no stationary phase) under high voltage [45]. The use of only a buffer and no stationary phase prevents the common problems of adsorption onto the stationary phase (and of degradation or deformation of the ultra-high molar mass chains) as well as of band broadening commonly faced in SEC. The velocity of different analytes is proportional to the electric field: the proportionality constant is named the electrophoretic mobility, μ_{ep}. The selectivity of a CE separation relates to the difference in electrophoretic mobility of the analytes (see Figure 1-4 for the experimental determination of μ_{ep}). The electroosmotic flow (EOF) is created by the movement of the ions of the background electrolyte through the capillary under electric field and it is contributing to migration for all molecules, even neutral ones. At a high pH the silanol groups of the fused silica layer of the capillary are completely ionized. This generates a strong zeta potential and an electrical double layer of

silanolates groups and positive ions from the background electrolyte. The higher the pH, the higher the density of the electrical double layer which increases the EOF [45].

Successful applications of CE to polymer characterization have been the object of a number of publications, especially by Cottet's group and the earliest works have been reviewed [46]. CE has also successfully been used in the analysis of strongly basic proteins [47]. Building on these advances, using CE, several natural and synthetic polymers, especially polysaccharides and poly(acrylic acid) were characterized reliably as described below.

Characterization of polymers by CE can be divided into at least four categories: separation of monomer units after depolymerization (see section 1.2.2.1 and 1.2.2.2), separation of oligoelectrolytes (see section 1.2.2.4) and separation of longer polyelectrolytes (see section 1.2.3). The fourth category discusses the separation of polymers bearing a single charge or no charge. For the fourth category, the reader is referred to the pioneering work of the groups of Cottet [48, 49] and Cifuentes [50].

1.2.2.1. Robust separation of a mixture of monosaccharides

A number of polysaccharides, such as hemicellulose [51, 52], have highly complex chemical structures: they are composed of different monomer units, mainly monosaccharides. The analysis of these polysaccharides is extremely difficult. The average composition can be determined after depolymerization

(hydrolysis) and quantification of the different resulting monosaccharides. Currently high performance liquid chromatography (HPLC) is used to separate carbohydrates using different modes; however, this technique and the different modes used have limitations in regards to co-elution [53], tedious sample preparation and short column life. [54] The detection of monosaccharides is another difficulty. CE is most easily and classically applied to analytes that are charged and possess chromophores. The p*K*a of most mono- and disaccharides is around 12 [55, 56] and separation in CE was obtained at high pH [57] but initially indirect UV detection, conductivity detection, complexation with borate or derivatization were required for detection. Complexation with borate can also induce a charge as discussed later (see section 5.1). Rovio et al. showed that different hemicelluloses can be characterized not only with CE but also with direct UV detection. [55, 56] This method was applied to plant fiber samples without any derivatization: CE achieved a high resolution separation of the depolymerized fiber samples (Figure 1-4) and was compared to the various common HPLC methods and ion chromatography (IC) methods such as high performance anion exchange chromatography(HPAEC) [53, 57]. The CE separation can be optimized at minimal cost by changing the capillary length, buffer counter-ion and/or the buffer concentration [58]. The main advantage of CE is the robustness of the method, especially the minimum sample preparation that is required. The precision of the peak identification and the quantification were greatly improved with the use of an electroosmotic flow (EOF) marker and an internal standard [53]. Figure 1-4 shows the electropherograms when UV absorbance is plotted as a function of migration time is compared to UV absorbance plotted as a function of electrophoretic mobility. Figure 1-4 also gives the equation used to perform this transformation. In the equation, μ_{ep} is

electrophoretic mobility, V is voltage, L_d is the capillary length to the detector, L_t is the total capillary length, t_m is the migration time and t_{eo} is the migration of a neutral species. Using electrophoretic mobility (thus correcting for EOF variations) allows easy visual comparison of results, for example to allow identification of trace sugars in ethanol fermentation [57].

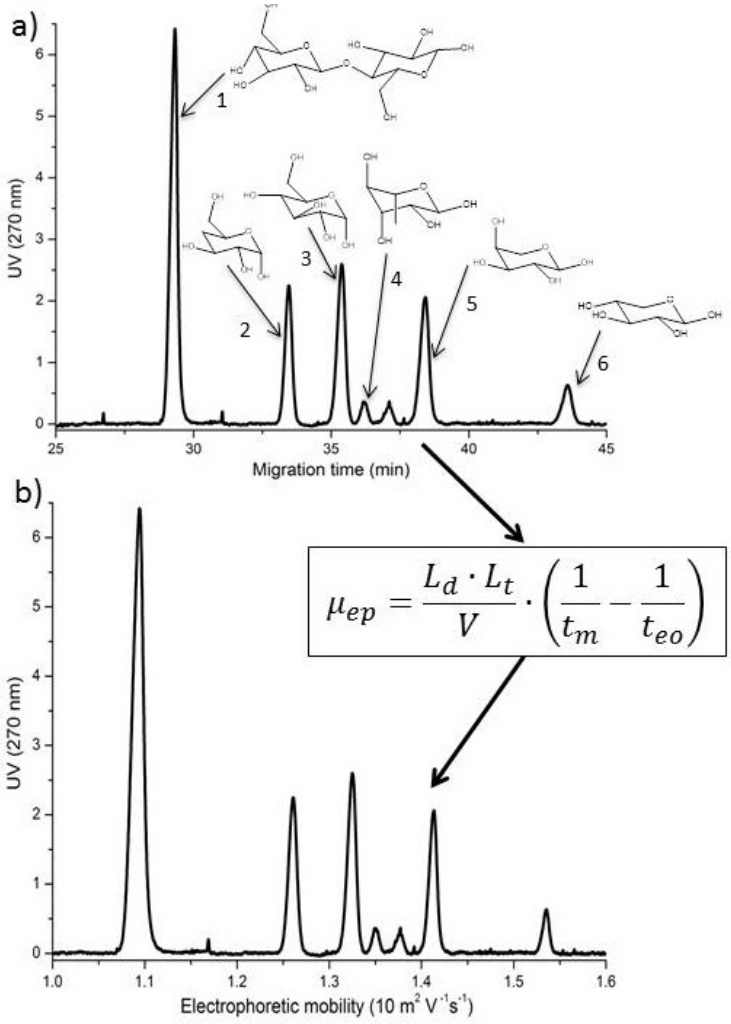

Figure 1-4. Separation by CE at high pH (12.6) and with direct UV detection of a depolymerized plant fiber sample plotted as a function of electrophoretic mobility (a) and of migration time (b). The sample contains (1) cellobiose, (2) galactose, (3) glucose, (4) rhamnose, (5) arabinose, and (6) xylose (the

molecular structures are given for the sole purpose of identification, and they are in equilibrium with a number of linear and charged forms) [53].

CE was able to resolve and quantify mannose, galactose and xylose. The CE quantification of these sugars results in larger amounts when compared to the HPLC results (Figure 1-5).

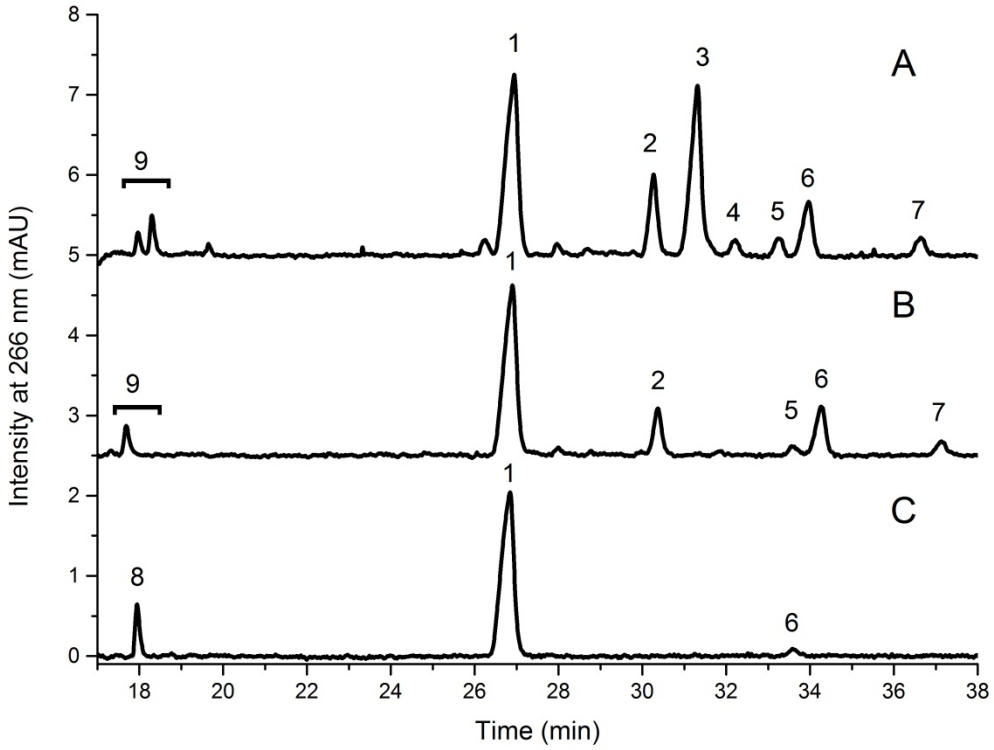

Figure 1-5. Fermentation of hydrolyzed plant fiber to ethanol. Samples taken (A) 0, (B) 6, and (C) 24 h. Peak assignments: (1) lactose (internal standard), (2) galactose, (3) glucose, (4) mannose, (5) fructose, (6) arabinose, (7) xylose, (8) arabitol, and (9) unknown. [57] See section 1.2.2.2 for detection of sugars through photo-oxidation in the UV detection window.

This might indicate incomplete recovery in HPLC possibly due to adsorption onto the stationary phase, which is a common problem associated with the

HPLC of samples in complex matrices. There were weaknesses in the direct UV detection in CE which have been addressed recently.

1.2.2.2. Direct detection due to the photo-oxidation of sugars

Rovio et al. [55] showed that the detection of monosaccharides was possible at 270 nm at pH 12.6. Sarazin et al. [59] suggested the method of detection was due to a photo-oxidation reaction occurring at the detection window. It was confirmed that the detection is by photo-oxidation using a combination of simulation, multi-dimensional CE migration and NMR spectroscopy analysis.[53, 60] The detection occurs without the electric field (i.e., in pressure mobilization instead of CE) but the electric field enhances the sensitivity of the detection. The photo-oxidation is initiated either by hydroxyl radicals formed by minimal but sufficient water decomposition or by direct decomposition of the carbohydrates under UV irradiation [58]. The diode-array detector (DAD) emits down to 190 nm. These wavelengths are not leading to any known sample degradation, except for the photo-oxidation of carbohydrates at high pH. The photo-oxidation is a type of *in situ* derivatization. If one wishes to avoid the photo-oxidation reaction taking place, then the lowest wavelengths need to be filtered out: on commercial equipment this simply means using UV detection and not a DAD. Even using a DAD, most of the sugar molecules are not photo-oxidized (in the timeframe of the detection). The UV-absorbing species are intermediates in the photo-oxidation process: simulations indicate that they might be radical species [60]. These intermediates are present at very low concentration but have a high UV absorption coefficient. The main intermediate was identified as malonenolate by CE-MS [61]. The final products do not absorb UV and are likely obtained after reacting with oxygen. NMR spectroscopy used as an offline detection after CE

migration allowed for the identification of a number of carboxylated compounds in the final products. This CE method is ideally suited for the separation of mono- and disaccharides in complex matrices. Direct detection has the advantage of simplicity and of using the most common detector in CE (DAD). The detection of the CE was found to have a limit of detection 10 to 100 times better than HPLC and a better selectivity of detection. Direct detection in CE is not as sensitive as more convoluted methods based on derivatization or pulsed-amperometric detection in ion-chromatography [53]. The method will thus need further improvement to be used for trace detection. Preliminary results showed that using a radical photoinitiator can increase the sensitivity of the direct UV detection. [60]

1.2.2.3. Monitoring of chemical reactions

The CE method (Figure 1-6) is not only useful to determine the average composition of complex polysaccharides, but also to monitor carbohydrates - for example, in a fermentation process. The latest developments showed that fermentation products, such as ethanol, can also be determined. [58] Ethanol is inhibiting the photo-oxidation process and this leads to indirect detection of ethanol in the presence of a sugar, such as sucrose. This indirect detection was successfully applied to monitoring a lignocellulosic fiber fermentation both in terms of ethanol and sugars alcohols [58].

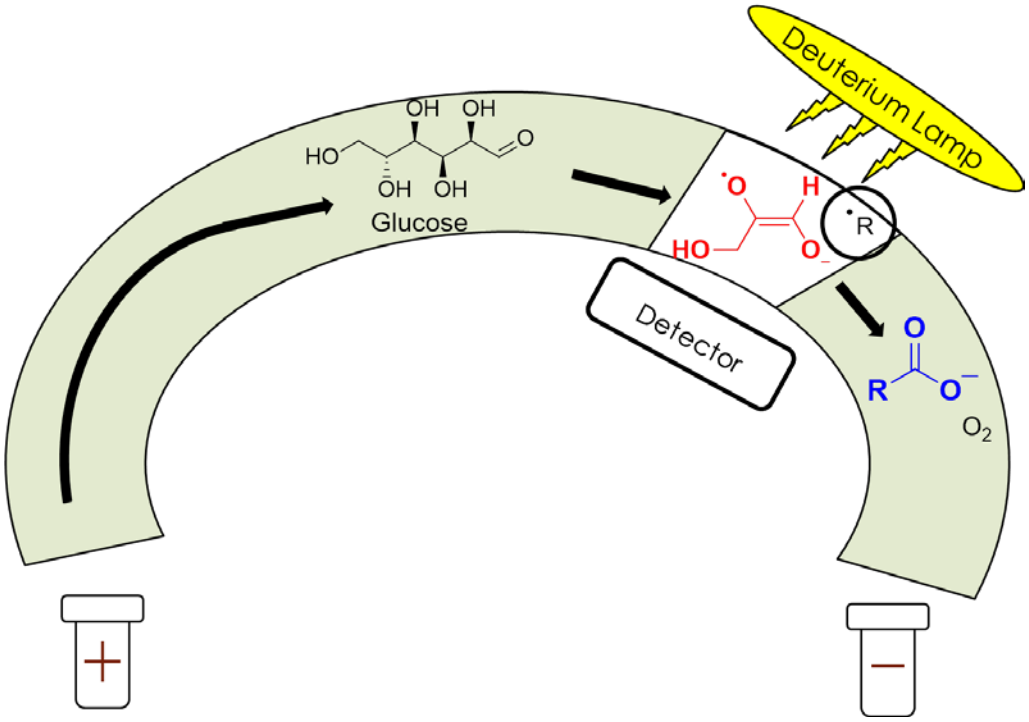

Figure 1-6. Mechanism of direct UV detection in CE of carbohydrates owing to a photo-oxidation reaction [60].

CE has also proven its use in the monitoring of chemical reactions such as the fermentation of hydrolyzed plant fiber to produce ethanol [57]. The CE method was able to detect the sugars galactose, glucose, mannose, fructose, arabinose, xylose and arabitol produced from the fermentation as well the main product ethanol. Through the CE analysis the fermentation process in the production of ethanol could be optimized. The advantage of the CE method is its ability to detect and resolve each of the sugars and ethanol which allows further information on the fermentation process to be revealed as it takes place over time.

1.2.2.4. Oligoelectrolytes

Cottet and Gareil have shown that oligo(styrene sulfonate)s can be separated by their molar mass up to a degree of polymerization of 9 [62]. Oligo(sodium acrylates) - oligoAAs - are used in the paint and coating industries to stabilize emulsions [63]. Controlled polymerization methods such as reversible addition-fragmentation chain transfer (RAFT) allow the controlled synthesis of oligoAA. CE can separate oligoAAs (Figure 1-7) at a higher resolution than that ever obtained with SEC (for oligomers) [64] even using optimal SEC conditions [65, 66].

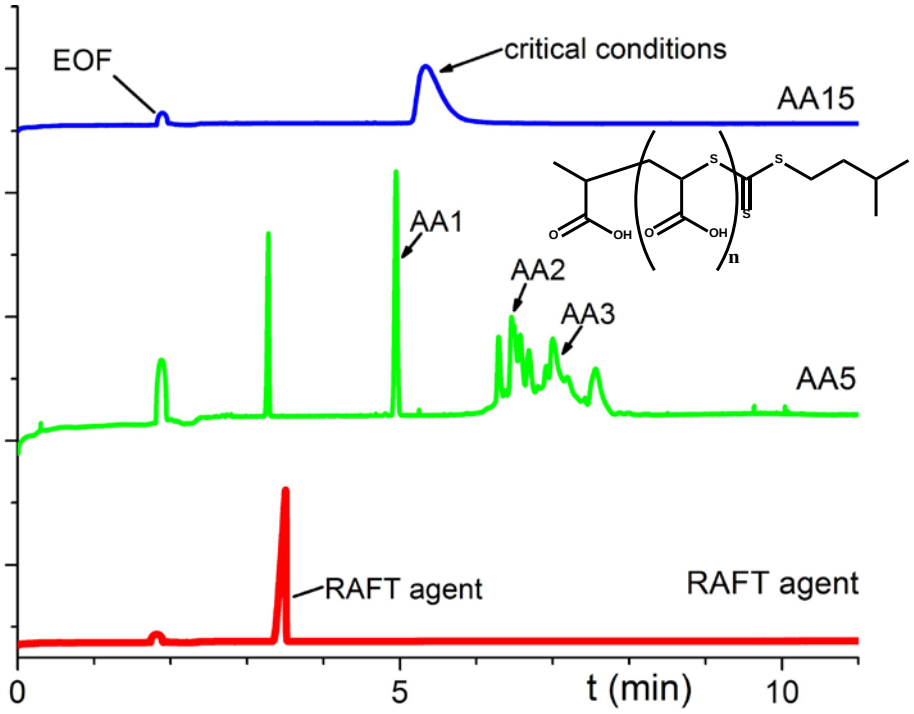

Figure 1-7. Electropherograms in lithium borate for two different oligoAAs, AA5 and AA15, produced by RAFT polymerization, where 5 and 15 correspond to the degree of polymerization obtained at the maximum of the mass spectrum from ESI-MS-ToF (electrospray ionization - mass spectrometry - time of flight) direct infusion (adapted from [64]). AA15 is not separated by molar mass, it is thus in the critical conditions. The bottom electropherogram is of the RAFT agent, i.e., the control agent for the polymerization.

CE was able to separate and quantify the residual RAFT agent used to obtain the oligoAAs, as well as the species of degrees of polymerization (DP) of one, two and three. The identification of these peaks was obtained by the online coupling of CE with ESI-MS-ToF (electrospray ionization - mass spectrometry - time of flight). [67] MS analysis showed that the oligomers are not only separated according to their degree of polymerization and end-group, but also according to their tacticity. The shortest oligoAAs were shown to contain 50 % of unreacted RAFT agent, while the direct infusion in ESI-MS estimated that the sample contained only 2 % of unreacted RAFT agent. This large discrepancy is due to the known issue of the bias of the ionization towards low degrees of polymerization and hydrophilic species in MS analysis. [68] CE was shown to be a relevant and fast method in the study of kinetics of polymerization of RAFT. It has also been used to shed light on the kinetics and mechanism of ring-opening polymerization of either 2-oxazoline [69] or *N*-carboxyanhydrides [49].

Most importantly, the high-resolution separation of CE by molar mass is limited to oligoelectrolytes, with degrees of polymerization below about 10. For large polyelectrolytes, no separation by molar mass is obtained, which corresponds to the "critical conditions" described below.

1.2.3. CE in the critical conditions

1.2.3.1. Explanation of "critical conditions"

The first example of analysis of synthetic polyelectrolytes by electrophoresis dealt with poly(4-vinyl-*N*-*n*-butylpyridinium bromide) more than half a century

ago [70]. The authors concluded that "the electrophoretic behavior of polyvinylbutylpyridinium is not very sensitive to molecular weight". CE in the "critical conditions" differs from the CE undertaken in the separation and characterization of oligoelectrolytes such as oligoAA. Critical conditions refer to the conditions sought in liquid chromatography (LC) in which a homopolymer is not separated by molar mass (see section 1.2). While these critical conditions are of no use to characterize simple (homo)polymers, most, if not all, polymers are not simple in the sense that they possess a distribution of molar masses as well as different end-groups, distribution(s) of compositions for copolymers, distribution of branch molar masses and of positions of branching points for branched polymers, etc. Polymeric samples are multidimensional: the critical conditions allow separating by one (or only a few) dimensions at one time (since the distribution of molar masses does not influence the separation any more). The critical conditions thus enable the characterization of complex polymers through the simplification of a multi-dimensional problem. While a lot of research has been devoted to LC and critical conditions, the method remains tedious and plagued with low accuracy and recovery. [43, 71] Applications to hydrophilic and/or charged polymers are very limited. CE is an alternative to LC in this specific, but important, case of complex polyelectrolytes. The molecular reasons behind critical conditions in LC and CE are completely different and are not widely accepted in any case. The electrophoretic mobility always depends on the charge-to-friction ratio. In the case of polyelectrolytes, it does not depend on the charge-to-size ratio since the friction is not only hydrodynamic. The critical conditions do not correspond to the free draining model as proposed by Flory, in which the solvent penetrates the polymer chains freely [72]. Electrostatic friction, however, screens the hydrodynamic friction [73, 74]

and leads to the electrophoretic mobility having a very weak dependence on molar mass for degrees of polymerization generally above 15-20 [62, 75, 76]. Thus, CE leads to migration independent from molar mass for polyelectrolytes and this corresponds to the critical conditions sought in LC-CC. CE has also been used in the critical conditions in the separation of pectins [77] and carboxymethylcellulose [78] according to their composition. CE in the critical conditions (CE-CC) has allowed the investigation of the composition of natural polymers as well as of synthetic polymers. Further, degree of branching of synthetic polymers was also looked at.

1.2.3.2. Pectin, carboxymethylcellulose and gellan gum - Separation by composition

CE-CC effectively separates the polysaccharide pectin by composition. Several studies reported the separation of pectin by its degree of substitution (DS, which may include esterification) [77, 79-82]. Within one sample, pectins macromolecules with different degrees of esterification could be separated. It was later hypothesized that the shape of the peaks could additionally be used to indicate a distribution of methyl esters of pectin within samples [80]. Guillotin et al. [82] established a protocol in which pectin's degree of amidification, degree of methyl-esterification and subsequently the degree of substitution could be determined.

Other research involved the use of capillary electrophoresis to determine the DS of caboxymethylcellulose [78]. The study showed the possibility of not only

determining the average DS but also the heterogeneity/distribution of the compositions of caboxymethylcellulose.

Gellan gum is a natural polymer which is widely distributed in the environment. Due to its rheological properties it is viewed as a possible stabilizing agent in various industries.[83] Gellan gum's monomer unit structure contains D-glucuronic acid, D-glucose either with or without acyl substituents, and L-rhamnose. The proportion of acyl chains attached to the glucose and the distribution of these acyl chains along the polysaccharide vary from sample to sample. Gellan gum is often characterized by its degree of acylation, which affects its desired properties. CE allowed some separation of gellan gum oligomers according to their degree of polymerization and separation of polymers by their degree of acylation (composition) [84]. It also gave a unique separation of gellan gums that could not be attained with any other existing separation methods. It could characterize not only a low acyl gellan gum but also a high acyl gellan gum (Figure 1-8). The latter sample was a turbid dispersion: while obtaining a true solution was not possible, the characterization of this dispersion is relevant for its applications such as the stabilization of carbon nanotubes [85]. Characterization of the high acyl gellan gum showed the presence of aggregates forming during the dissolution of the gellan gum samples and appearing as very narrow peaks due to their very low diffusion coefficients. This illustrates the robustness of the method as it did not require sample filtration (while the background electrolyte still requires filtration). Filtration would have changed the nature of this colloidal sample and should thus not be performed for a meaningful characterization.

Complementing the CE separation with a simple pressure mobilization analysis (a qualitative version of Taylor dispersion analysis [86], see section 1.2.4), the presence of oligomers, which had never been identified previously in these gellan gum samples, was confirmed. Pressure mobilization can also be used to probe the interaction of samples with the capillary wall, as completed with proteins [87]. In CE the peak shape can be informative about interactions with the wall when a single type of molecule is detected, but with polysaccharides and most polymers the peak shape also depends on the shape of the distribution of composition or other molecular features. Through the CE separation, the oligomers could be separated and quantified. Separation and characterization of this dispersion could only be obtained by CE or field flow fractionation (FFF). In the most common form of FFF, flow FFF, the oligomers would have been lost through the membrane. The low acyl samples contained more oligomers than the high acyl samples suggesting the occurrence of some degradation during the deacylation process. The electrophoretic mobility is also sensitive to the conformation of gellan gum and complementary to light scattering characterization. A high mobility peak, present in the high acyl sample and becoming more intense in the presence of potassium borate ions suggests the possibility of a double-helix conformation. This peak differs in mobility and thus, also suggests the rest of the macromolecules are in a random coil conformation.

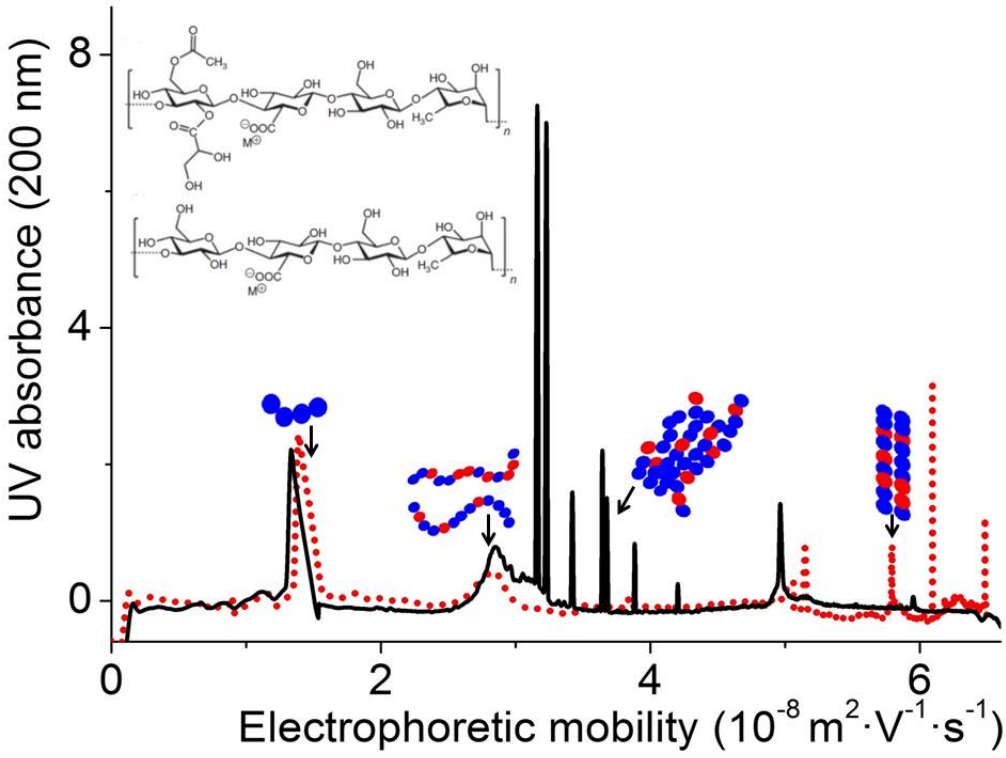

Figure 1-8. Electropherograms of a low-acyl gellan gum (dotted red line), and a high-acyl gellan gum (solid black line) (in potassium borate, pH 9.2), after a few hours dissolution [84]. The chemical structure of gellan gum is displayed on the graph and the blue and red circles represent the different acylated or non-acylated monomer units of the copolymer.

In order of increasing mobility, the electropherograms show the presence of gellan gum oligomers (1.5×10^{-8} $m^2.V^{-1}.s^{-1}$), then gellan gum polymer chains containing different degrees of acylation (random coil conformation at 3×10^{-8} $m^2.V^{-1}.s^{-1}$), then aggregates of gellan gum chains (3.8×10^{-8} $m^2.V^{-1}.s^{-1}$) and finally gellan gum polymer chains in a helix conformation (5.9×10^{-8} $m^2.V^{-1}.s^{-1}$). The gellan gums studied in this work are copolymers containing both repeating units (not necessarily forming blocks). The top molecular structure represents fully acylated gellan gum, and the bottom one represents fully deacylated gellan

gum. The acylated monomer unit is constituted from left to right of one D-glucose with two acyl substituents (one acetyl and one glycerate bearing a diol or glycol), one D-glucuronic acid, one D-glucose without substituents, and one L-rhamnose.

The study undertaken on gellan gum is an example of the robustness of the CE technique. Whilst allowing the successful separation of complex samples by composition it also provides information on the conformation of the polymer chains and the presence of aggregates.

1.2.3.3. Chitosan – Separation by composition

There is currently a limitation in chitosan's use due to its incomplete characterization. Chitosan is often only characterized by its average *DA* [88]. Chitosan samples are, however, not composed of polymer chains with all the same *DA* but they contain a distribution of *DAs*. The complexity and importance of the distribution of *DAs* has been revealed recently through a coupling of SEC with ^{1}H NMR spectroscopy; however, it still has not been measured [18]. ^{1}H NMR spectroscopy can determine number-average as well as weight-average *DAs* [88]. The measurements are accurate, but experiments to obtain precise results are hindered by dissolution and alternative methods are often considered (see chapter 2). Chitosan is usually characterized by only one of its average *DAs*, which is implicitly and incorrectly assuming the sample is homogeneous in terms of *DA*, i.e., does not have a distribution of *DAs*.

CE-CC separates chitosan by its *DA* (Figure 1-9). [88] Chitosan macromolecules with a lower *DA* have a higher mobility (at low pH below the glucosamine monomer unit's p*K*a at ~6.5) since they have a higher number of free amino groups which increases their charge and therefore their electrophoretic mobility. Another important attribute revealed in the CE separation is the broadness and shape of the peaks of the chitosan samples. The peak shape and broadness corresponds to the distribution of *DA*s and some samples have broader distributions than others (Figure 1-9). These differences in distributions will likely affect functional properties such as adhesion, biodegradability and bacteriostaticity [18]. With proper calibration, the CE separation will allow the determination of the distribution of *DA*s (see chapter 4).

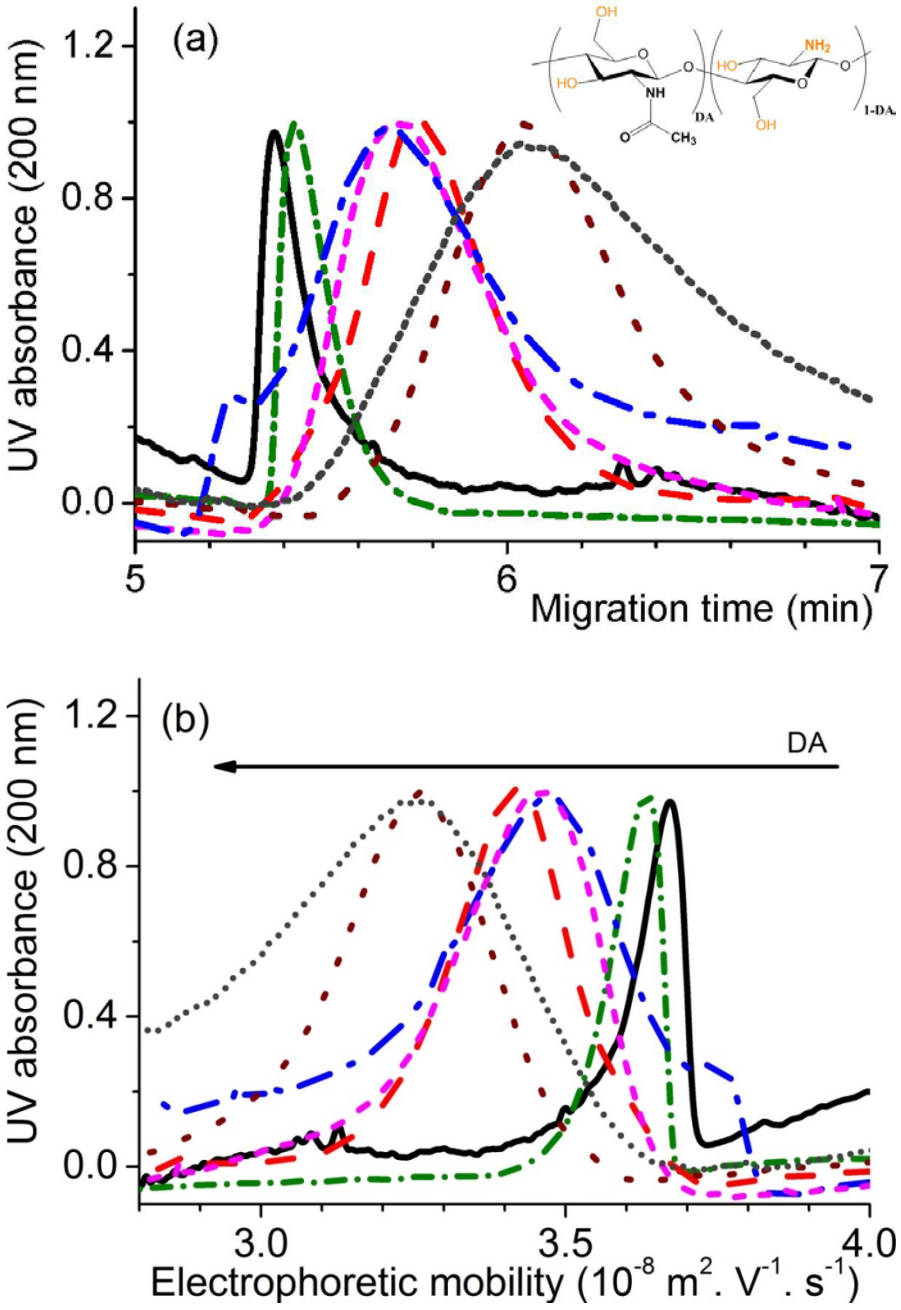

Figure 1-9. Separation of chitosan samples by their *DA* with CE (sodium phosphate, pH 3): electropherogram shown as a function of (a) migration time, and (b) apparent electrophoretic mobility. Samples with different degrees of acetylation (weight-average *DA* determined by NMR spectroscopy) are shown: black solid line (4 %), green dashed line (4.3 %), blue dashed-dotted line (16.5 %), red dashed line (18.7 %), pink dashed line (19.8 %), brown dotted line (22.4 %) and black dotted line (23.6 %) [88].

CE was also used to assist in the grafting of synthetic polymers, poly(sodium styrene sulfonate) and poly(methyl methacrylate-*co*-acrylonitrile), onto a chitosan backbone [89] to address the variability of the mechanical properties of chitosan films [20]. CE could analyze samples produced along the synthetic pathway. This allowed the validation of the grafting process. Chitosan was first functionalized with the introduction of an acrylamide and/or acrylate function. This was followed by a radical addition of BlocBuilder® (BB) alkoxyamine to allow a controlled (nitroxide-mediated) polymerization [90] of the grafted monomers. The limited solubility of chitosan added to the hydrophobicity of the grafted compound made the complete solubilization of the samples impossible. Despite incomplete dissolution, the robustness of CE allowed the analysis of these samples: chitosan functionalized with BlocBuilder® was separated from pure BlocBuilder® (Figure 1-10). This experiment was undertaken in a high pH buffer and therefore the negative charge expressed by BB results in a non-zero mobility in the CE electropherogram whilst the neutral chitosan has no mobility. Pure BB, chitosan covalently functionalized with BB and chitosan physically mixed with BB (control) were then injected at the same pH. The chitosan grafted with BB encounters more hydrodynamic friction than BB alone which reduces the electrophoretic mobility of the chitosan grafted with BB in comparison to the pure BB. The method even allows the discrimination of covalently grafted BB from BB adsorbed to chitosan since the latter has a lower electrophoretic mobility in comparison to the grafted sample. This type of separation of a neutral polymer chain from a slightly modified polymer chain,

was also used by the group of Schoenmakers with non-aqueous CE to prove the presence of charged end-groups in part of their poly(2-oxazoline) samples [69].

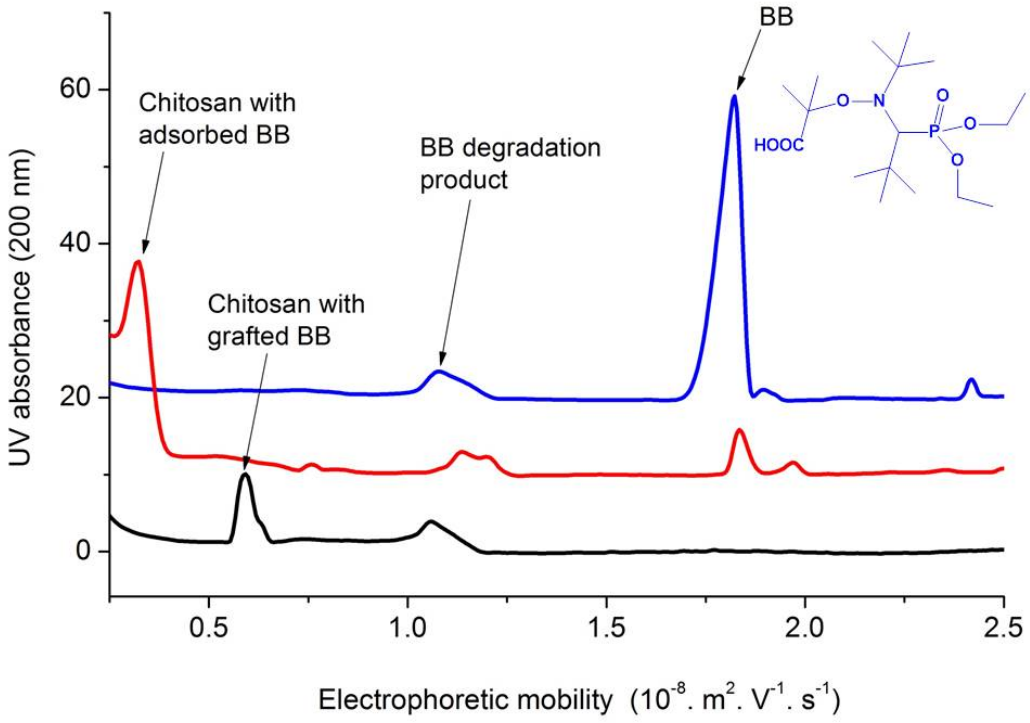

Figure 1-10. CE of pure BlocBuilder® (BB, blue line), chitosan with adsorbed BB (red line) and chitosan with grafted BB (red line) in sodium borate buffer (pH 9.2) [89].

Using both CE and CE-CC a more thorough analysis can be completed on both pure and modified chitosan samples. There is also a possibility of extending the research on chitosan with CE in terms of the determination of the distribution of the degrees of acetylation [88] (see chapter 3 and 4).

1.2.3.4. Poly(acrylic acid) - Separation by topology (branching)

There is a large interest in the characterization of water-soluble polyacrylates as their use has increased to include a range of applications from industrial protective coatings to food packaging. The poly(sodium acrylate)s, PNaA, studied were produced by nitroxide-mediated polymerization (NMP) [90]. The aim of the study was to characterize the branching in PAA using CE-CC. Different topologies of the PAA samples, linear, hyperbranched and three-arm star, were separated within 15 min [91]. Figure 1-11 presents the CE results both as raw data, as a function of migration time, and as EOF corrected data, as a function of electrophoretic mobility. This highlights the importance of converting the results to electrophoretic mobility plots as a trend is not seen in the migration time results due to variation in EOF between experiments. When the EOF correction is made it can be seen that the hyperbranched polymer exhibits the lowest electrophoretic mobility followed by three-arm star and finally the linear ones. The differences in electrophoretic mobility can be explained by a decrease in the effective charge of the branched samples when compared to the linear samples. The results obtained were highly repeatable and reproducible with relative standard deviations (RSD) values below 1.6 %. The separations were also successfully reproduced in a different buffer and whilst they produced different electrophoretic mobility values (as expected, due to different counter-ions), the electrophoretic mobility remained lower for the more branched structures. This study highlights also the accuracy (related to the reproducibility of the separation) of the technique.

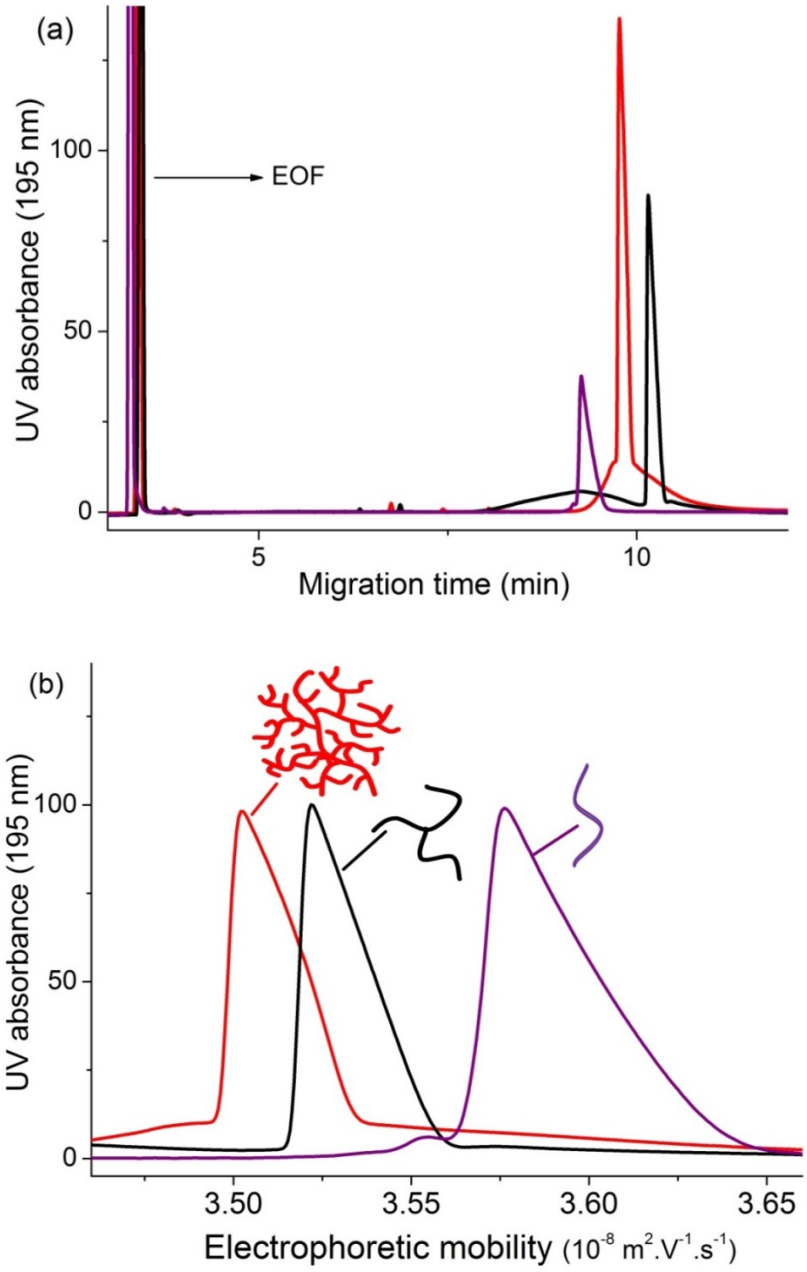

Figure 1-11. Separation of linear (purple line), three-arm star (black line), and hyperbranched (red line) poly(sodium acrylate) by capillary electrophoresis in sodium borate buffer (pH 9.2) shown as a function of a) migration time and b) electrophoretic mobility, which is a more reproducible quantity than the former [91] (note the linear sample is overloaded and has been corrected in chapter 3).

The CE results obtained also provided information regarding the homogeneity of the branching topology. These samples are expected to have a controlled molar mass owing to the reversible termination with the nitroxide but the broadness of the peaks obtained suggests some heterogeneity in the branching structure. The broad range of electrophoretic mobilities is attributed to a broad range of branching topologies produced during the polymerization.

The CE-CC separation was also shown to be influenced by end groups. In figure 1-12 the red solid line represents PAA with a SG1 [*N*-*tert*-butyl-*N*-(1-diethylphosphono-2,2-dimethylpropyl) nitroxide] moiety as the end-group. There is a marked difference between this sample and the sample that has been heated in the presence of thiophenol to replace the SG1 end-groups by hydrogens. The electrophoretic mobility increases with the removal of the SG1 end group, as expected since the bulky SG1 molecule would contribute to the hydrodynamic friction of the PAA chains more than hydrogen (and neither contributes to its charge). The result also suggests heterogeneity of the sample in terms of branching. The thiophenol treatment was also applied to a PAA sample obtained from the hydrolysis of poly(*t*-butyl acrylate) and CE-CC showed that the hydrolysis of poly(*t*-butyl acrylate) did not just cleave the targeted *t*-butyl groups, but also likely led to some degradation of the SG1 end group. This led to a greater heterogeneity of the sample and is expressed in the broadness of the peak.

Through CE-CC, the polymers were separated by their topology (branching) as well as by their end groups. The ability of CE-CC to separate based on the

presence of SG1 (control agent used for nitroxide-mediated polymerization) reveals information regarding the "livingness" of the obtained sample (allowing it to continue reacting through NMP) [91, 92]. This allows the optimization of the method used to produce the sample and provides information regarding further functionalization of the PAA.

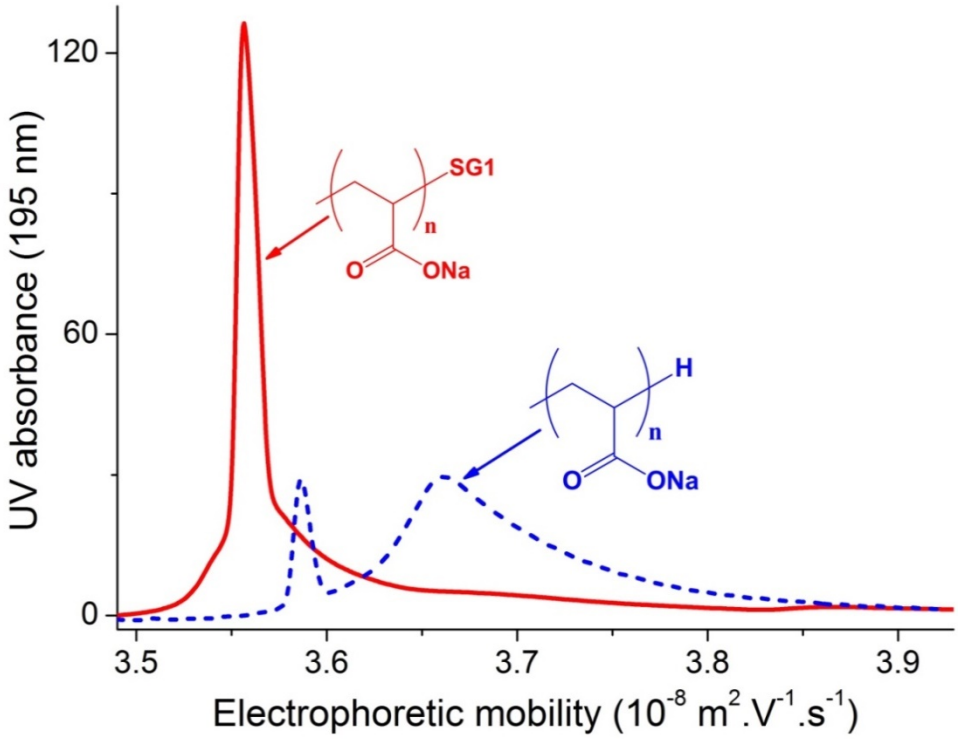

Figure 1-12. Electropherogram in sodium borate (pH 9.2) of a PNaA obtained by nitroxide-mediated polymerization of acrylic acid initiated by the monofunctional initiator MONAMS (red solid line) followed by cleavage of the SG1 end-group by treatment with thiophenol (blue dashed line) [91].

1.2.4. Size determination with Taylor Dispersion Analysis

One limitation of CE for polymer characterization, compared to multiple detection SEC [38], is the limited number of detectors, especially the lack of molar mass sensitive detectors. The group of Cottet is, however, bridging this gap

rapidly by demonstrating that the CE separation can be coupled to Taylor Dispersion Analysis (TDA). TDA is a method that does not involve separation but allows the determination of the diffusion coefficient and hydrodynamic radius of a sample. TDA has been looked at previously to obtain diffusion coefficients in liquid systems. [93, 94] Further it has proven to be practical in the size characterization of macromolecules and particles of virtually any molar mass.[86] [95] TDA has several advantages including that it is an absolute method, meaning that no calibration is required. The group of Cottet has shown that a CE instrument is particularly well suited to carry out TDA. [96, 97] Le Saux and Cottet [98] coupled CE and TDA. A copolymer mixture of 2-acrylamido-2-methylpropanesulfonate/acrylamide and DNA was injected into a fused silica capillary. The mixture was separated in CE conditions (with an electric field) and then pressure was used to push the samples to the detection window where the analysis took place. The experiment proved that the coupling of CE and TDA allowed not only a complete separation of the copolymer from the DNA in the mixture, but also the successful determination of the diffusion coefficient of both the copolymer and DNA. A successful coupling of CE with TDA allowed a combination of a high performance and throughput method with an absolute method of the determination of diffusion coefficients. [99] The diffusion coefficient can then be related to the hydrodynamic volume of the macromolecule as it is classically done in light scattering by the following equation:

$$D = kT\,6\pi\,\eta\,r \qquad \textbf{1-1}$$

where k is the Boltzmann constant (J. K^{-1}), T is the temperature (K), η is the viscosity of the solvent (Pa.s) and *r* is the hydrodynamic radius of the macromolecule (Å) [100].

The relation of the hydrodynamic radius to the molar mass is complex and is influenced by branching and copolymer composition as discussed in section 1.2.1 for SEC [38].

1.2.5. Comparison of SEC and CE in the characterization of block copolymers

Block copolymers are polymers that are composed of two different monomer units in a block formation. The advantage of block copolymers is that they allow the properties of two different polymers to be included in one material. To allow further development of these materials appropriate characterization techniques need to be employed to ensure accuracy in the molar mass, purity, branching and the nature of chain ends. As previously mentioned, SEC is the most common tool for the characterization of polymers in solution and was therefore tested and compared to CE-CC in the analysis of poly(acrylic acid-*b*-acrylamide)[2]. SEC was deemed insufficient to separate homopolymer and block copolymers (Figure 1-13A).

CE-CC was able to fully separate the block copolymers and the homopolymer (Figure 1-13B). This allowed the quantification of the remaining homopolymer in the block copolymer sample. Thus CE-CC was able to assess the purity of the block copolymer synthesized.

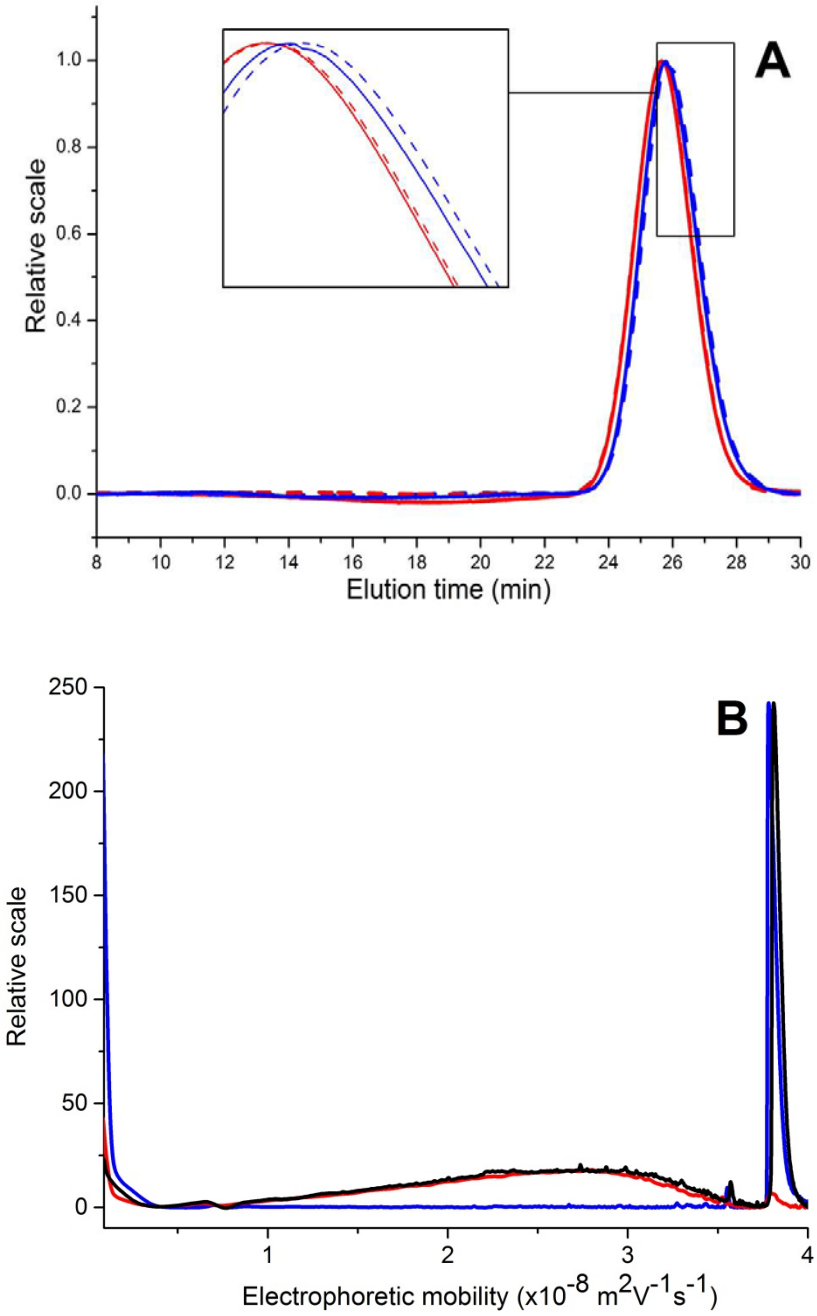

Figure 1-13. A) SEC chromatogram and B) CE electropherogram of the homopolymer PAA with a molar mass of 10,000 g.mol^{-1} (blue) of a block copolymer with a 10,000 g.mol^{-1} molar mass PAA block and a 10,000 g.mol^{-1} molar mass polyacrylamide block (red) as well as of the block copolymer spiked with a 10,000 g.mol^{-1} PAA homopolymer (black) [2].

1.2.6. Summary

Overall, analysis by capillary electrophoresis allows the characterization of complex polyelectrolytes. This is significant for various industries including food, biomedical, energy/fuel and materials (such as paint, bioplastics) industries. The robustness of the method, especially the minimal sample preparation, is one of the main strengths of the method (shared with field flow fractionation). This is seen in chapter 5 with the real-time monitoring of a chemical grafting reaction. The continual development of the CE method and its coupling with other techniques such as TDA widens the scope and depth of the possible characterization and meets the ever-growing needs of progressively increasing complex macromolecular structures for increasingly advanced applications. CE-CC has the most potential and can be applied to a wide variety of charged polymers to characterize their topology, composition or end-groups. This was explored further in chapter 2, 3 and 4 in the analysis of chitosan and various other complex polyelectrolytes. The CE method is also complementary to SEC.

CE coupled with TDA is a very useful and simple technique that will definitely be examined further as it is able to provide extremely valuable information regarding the size and shape of sample molecules by the calculation of their diffusion coefficient. Its simplicity and being an absolute method means it can be applied to the variety of samples.

Overall, the importance of understanding a polymers behavior in solution has been outlined. However, to obtain complete characterization, solid state methods are required as discussed below.

1.3. Characterization of polymers in the solid state

The characterization of chitosan in solution is important; however for various applications analysis of chitosan films is required. Although the characterization of chitosan films is complex, solid-state NMR spectroscopy is a robust method which can be used for the analysis of chitosan. [20]

1.3.1. NMR spectroscopy

1.3.1.1. Introduction to NMR spectroscopy

Nuclear Magnetic Resonance (NMR) spectroscopy has the ability to identify chemical structures through the chemical shifts (shift of the resonance frequency of the nuclei of a compound). NMR spectroscopy is able to identify functional groups depending on their chemical nature and indicate the locations of particular chemical bonds. When all the bonds of the compound have been established the structure of the molecule can be defined [101].

NMR spectroscopy is based on the observation of the nuclear spin of a particular nuclide. Most nuclides exhibit a nuclear spin except those with equal atomic mass and atomic number such as carbon-12. These are unable to be detected by NMR spectroscopy. However, these atoms often have an isotope that does have a nuclear spin.

In the process of NMR spectroscopy, the nucleus is placed in a large magnetic field to induce different spin states. The nucleus then changes its spin state by

the adsorption of energy from electromagnetic radiation. The resonance frequency *f* of the nuclide, also called Larmor frequency is given by:

$$f = -\gamma B_0 \qquad \textbf{1-2}$$

where γ is the magnetogyric ratio (rad.s^{-1}.T^{-1}) and B_0 denotes the static magnetic field (T), γ is constant for each nuclide and describes how magnetic this nuclide is. As it can be seen from the equation 1-2, the measurement of the value *f* is directly proportional to the magnetogyric ratio γ. Therefore, the analysis of different compounds depends on what is being identified (^{1}H, ^{13}C, ^{15}N) and requires the use of different electromagnetic radiation frequencies [101].

1.3.1.2. Line broadening in solid-state NMR spectroscopy

NMR spectroscopy is also able to yield diverse information about solid samples. It is able to reveal not only structure but molecular dynamics of compounds [20, 102]. Solid-state NMR spectroscopy is required in this study due to the insoluble nature of the modified chitosan film samples and to characterize packing and motion of molecules in the solid state [102]. Solid-state NMR spectroscopy differs from solution-state NMR spectroscopy in regards to resonance line width due to dipolar coupling and motion. Resonant lines observed in solid-state NMR spectroscopy are generally much broader and this can be due to homogeneous, inhomogeneous or heterogeneous broadening (Figure 1-15). A homogeneous line is the sum of lines exhibiting the same broadening but no chemical shift difference. This is due to strong dipole-dipole couplings, the majority of which are ^{1}H-^{1}H couplings. An inhomogenous line is the sum of non-overlapping lines with limited broadening. This can be produced by differences in local packing

of the molecules in different parts of the sample. Finally heterogeneous broadening involves the sum of lines with different shifts which are coupled.

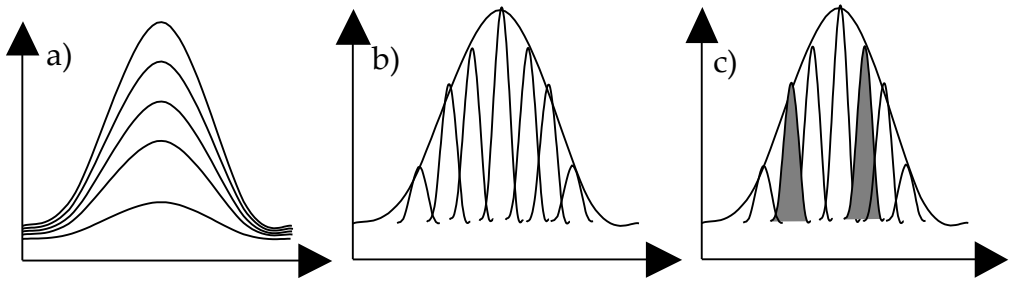

Figure 1-15: a) Homogeneous, b) inhomogeneous and c) heterogeneous line shapes; grey indicates coupling [103].

The width of the broadened line reveals information regarding the molecular motion in the sample. Broadening can be assigned to dipolar coupling (Figure 1-15a) and/or heterogeneity of local packing (Figure 1-15b). Both of these factors can be attributed to the lack of motion of the molecules with respect to the overall timescale of the experiment. Conversely the samples in which the molecules are constantly moving partially overcome these factors, which results in a reduced line width. Thus it is stated that the faster the molecular motion, the narrower the resulting line, which is particularly true in ^{1}H NMR spectroscopy.

1.3.1.3. Magic-angle spinning

As previously mentioned, solid-state NMR spectroscopy produces very broad spectra in static conditions. To allow a higher resolution the technique known as magic-angle spinning (MAS) is used [104]. This technique involves spinning the rotor containing the sample very fast at a specific angle to the static magnetic field during measurement (Figure 1-16). This technique aims at artificially

introducing movement to the molecules to assist in overcoming the previously mentioned causes of dipolar coupling. Currently samples can be spun from 1-2 kHz up to 110 kHz in commercially available equipment [105]. The magic angle is calculated mathematically from the perturbation theory, which introduces a factor of $3\cos^2\theta - 1$ to describe the evolution of the dipolar coupling. The equation for the magic angle is $3\cos^2\theta - 1 = 0$ and under these conditions the effects of the dipolar coupling are reduced. Even though this technique minimizes the broadening of the peaks in solid-state NMR spectroscopy, they are still broader than in solution-state NMR spectroscopy (Figure 1-17). This is due to instrumental factors, residual interactions and motional effects [103, 104].

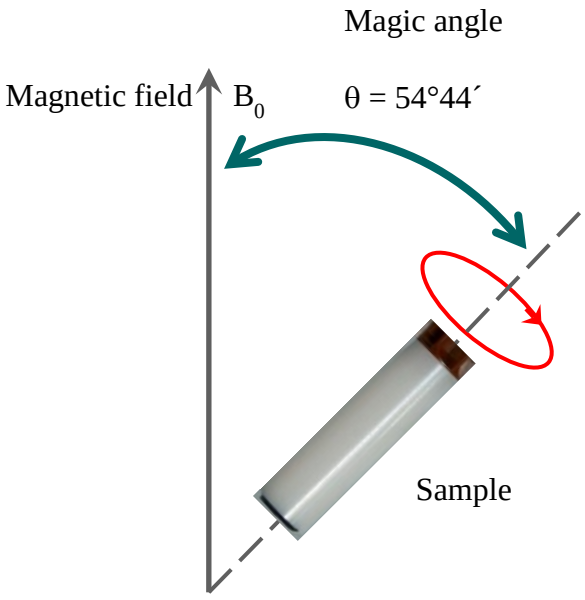

Figure 1-16: Magic-angle spinning (MAS) of a solid-state NMR spectroscopy sample.

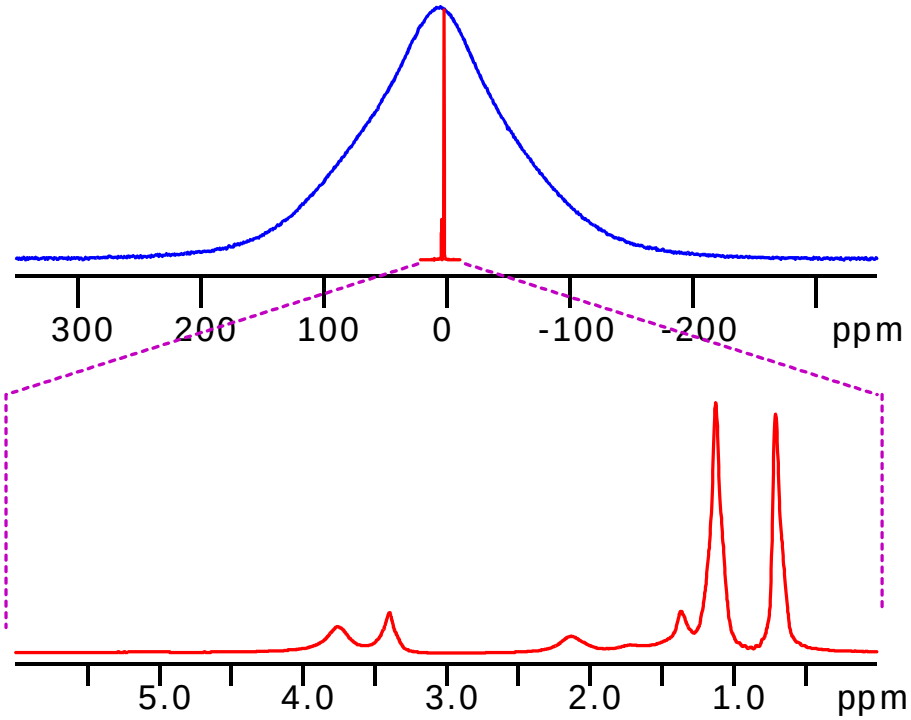

Figure 1-17: Comparison of ^{1}H solid-state NMR spectra of a polyacrylate recorded under static conditions (top) and under MAS (bottom) [103].

1.3.1.4. Recording ^{13}C solid-state NMR spectra

An important factor to consider when recording ^{13}C solid-state NMR spectra is the use of either single-pulse excitation (SPE) or cross-polarization (CP) methods. SPE is most widely used (especially in 1D solution state experiment) and involves one 90^{0} pulse in the carbon channel to irradiate the ^{13}C nuclei immediately before recording their signal (Figure 1-18). Since in natural abundance only 1 % of carbons are ^{13}C nuclei (which are NMR-sensitive) the signal recorded in ^{13}C SPE NMR spectra is very low compared to typical ^{1}H NMR spectra. The free induction decay (FID), represented in the Figure 1-18, is the observable signal generated by the excited nuclear spin magnetization of the sample as it returns to equilibrium. Dipolar decoupling (DD) is the decoupling

of ^{1}H from ^{13}C during FID acquisition. This is necessary to prevent the splitting of observed ^{13}C signals into multiplets which may impair resolution [101].

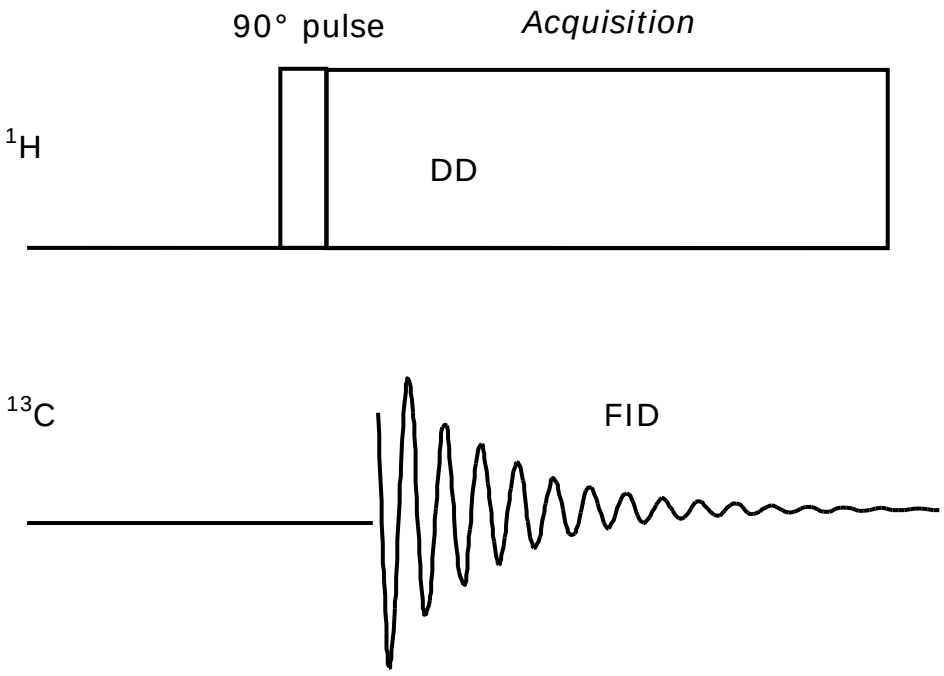

Figure 1-18: Single-pulse excitation (SPE) pulse sequence.

The principle of CP involves obtaining ^{13}C magnetization indirectly via ^{1}H magnetization (Figure 1-19). This involves producing a measurable magnetization of the ^{1}H nuclei and then irradiating both the ^{1}H and ^{13}C nuclei simultaneously in specific conditions. This allows the exchange of magnetization between the ^{1}H and ^{13}C nuclei during the contact time. After this takes place the ^{13}C signal is recorded and analyzed.

^{13}C CP-MAS NMR exhibits a higher sensitivity than ^{13}C SPE-MAS NMR for rigid samples due to two factors. Firstly, ^{1}H nuclei are all NMR-active, unlike carbon for which only 1 % of carbon nuclei is ^{13}C which is NMR-active. Therefore the

irradiation is much higher than when ^{13}C nuclei are directly irradiated with a 90^0 pulse. Secondly, due to the faster relaxation time of ^{1}H nuclei in comparison with ^{13}C nuclei, a higher number of repeat scans can be recorded in a shorter time.

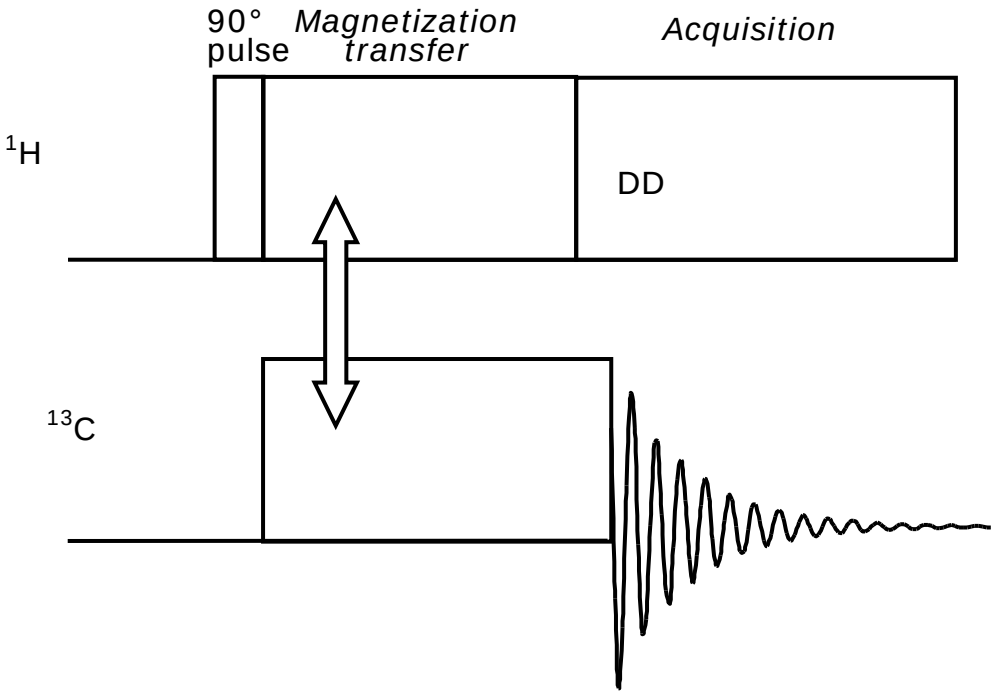

Figure 1-19: Cross-polarization (CP) pulse sequence.

1.3.1.5. Solid-State NMR spectroscopy of chitosan

Chitosan films have been analyzed through ^{1}H, ^{15}N and ^{13}C solid-state NMR spectroscopy [20, 106]. Heux et al. [106] measured the average *DA* of chitin and chitosan samples using ^{1}H solution-state as well as ^{13}C and ^{15}N CP-MAS solid-state NMR spectroscopy, and were able to establish a good agreement between the results of the methods. In another study the molecular origin of several properties of chitosan films was established by modern NMR spectroscopy

techniques and X-ray diffraction. Through CP-MAS, Gartner et al. [20] were able to compare the effect of strong and weak acids on the molecular structure of chitosan and comment on their influence on mechanical strength. ^{15}N solid-state NMR spectroscopy was used to discriminate between the charged and neutral amine groups. Results obtained supported the initial hypothesis that films cast from hydrochloric acid and acetic acid solutions were charged and films rinsed with sodium hydroxide were neutral. ^{13}C solid-state NMR spectroscopy revealed shifts of some signals in the acidic films. This is assigned to rotational distortion around the main chain in which the presence of the charge introduces strong electrostatic interactions which could hinder the chain following the usual hydrogen bonding pattern for packing. This shift is stronger for films prepared with the strong hydrochloric acid than with the weak acetic acid. ^{1}H NMR solid-state spectroscopy was used to investigate the effect of temperature on the films and powder in terms of the molecular motions and chemical exchange of protons. Two dimensional ^{1}H solid-state NMR spectroscopy was also undertaken in which the chemical stability of the films at room temperature and powders was probed. It was noted that due to the rigidity of the film cast from HCl, it was significantly different to the other films and powders. ^{1}H and ^{13}C solid-state NMR spectroscopy measurement were also conducted to probe the dipolar interaction between the ^{1}H and ^{13}C nuclei. Overall, it was concluded that the charges created in acidic films induced strong electrostatic interactions and therefore allowed the films' long-range structure to be better defined. In the case of hydrochloric acid, due to the Cl^- counter-ion causing a strong immobilization of water, the molecular motions in the film became very restricted which caused stiffness and brittleness. Conversely, the acetate counter-ion acted as a charged plasticizer which increased film flexibility. This

information is important to consider in the preparation of biomedical products as the physical characteristics of the film may affect the chemical modification and the application properties.

NMR spectroscopy has demonstrated its ability to accurately and precisely measure the average *DA* of chitosan [107]. If parameters are appropriately set up, quantitative analysis of the *DA* is possible with both solid and solution-state NMR spectroscopy measurements of chitosan samples. For the analysis of chitosan and chitosan conjugates ^{1}H and ^{13}C NMR spectroscopy will be used in this work (see chapters 2 and 5).

1.3.2. Surface characterization of chitosan film

Considering the use of chitosan films in cell culture a thorough characterization of the films surface is necessary. Various factors may affect cell growth including the surface topology and the heterogeneity of the surface. Spectroscopy methods such as Fourier transform infrared (FTIR), Raman and X-ray photoelectron spectroscopy and time of flight-secondary ion mass spectrometry (ToF-SIMS) are able to analyze the chemical nature of the surface. Through the use of microscopy techniques such as scanning electron microscopy (SEM) and atomic force microscopy (AFM) information regarding the surface roughness of the films can be obtained. Each of these surface techniques have varying measuring depths which depend on the conditions of the experiment and the sample. Approximate measuring depths are 1 μm for

FTIR, Raman spectroscopy and SEM, 8 to 10 nm for XPS, less than 1 nm for ToF-SIMS and 0.3 nm for AFM.

1.3.2.1. Fourier-transform infrared (FTIR) and Raman spectroscopy

FTIR spectroscopy allows the chemical nature of polymeric material to be analyzed through the analysis of its infrared (IR) spectral bands. Raman spectroscopy is a complementary method which analyses Raman scattering of monochromatic light produced from a laser. Both FTIR and Raman are vibrational spectroscopic techniques, however, they differ. Whilst FTIR looks at the light absorbed, Raman focuses on the light scattered. Whilst FTIR, Raman and NMR are spectroscopy methods, they focus on different spectra. Each technique involves irradiating the sample with a frequency, radio frequency in the case of NMR, monochromatic light in the case of Raman and infrared in the case of FTIR. The resulting time domain signal is transformed using a Fourier transformation. FTIR and Raman are quicker methods and are useful in identifying functional groups. An advantage of FTIR is that it can be specifically used in the analysis of the surface of a material through attenuated total reflectance (ATR). It has been used in the analysis of both chitosan and its precursor chitin [108]. Characterization includes monitoring the change of crystallinity of chitin during chitosan production [109], analysis of the impurities produced in chitosan production [110] and finally measurement of the *DA* [107]. FTIR is advantageous over NMR spectroscopy as it is a high-throughput method; however, it is limited in its resolution.

1.3.2.2. X-Ray Photoelectron Spectroscopy (XPS)

XPS is a quantitative spectroscopic technique which allows elemental information to be obtained of the surface of a sample. X-ray interaction with the sample causes photoelectrons to be ejected. The analysis of the kinetic energy of the photoelectrons is the basis of XPS. The binding energy is an intrinsic property of the material and does not change. This allows XPS to be a powerful tool in surface analysis. [111] XPS has been used in the analysis of chitosan powder and chitosan films cast from HCl previously [112]. XPS allowed the analysis of the protonated amines and amides, which provided information regarding the acetylation. It was also used to analyse two component films, which contained both chitosan and alginate.

1.3.2.3. Secondary ion mass spectrometry

Time of flight-secondary ion mass spectrometry (ToF-SIMS) allows an accurate analysis of the chemical composition of the films surface. ToF-SIMS has been used previously in the analysis of peptides on a functionalized silane surface in which it was used to provide evidence that the peptide was immobilized, and recognize modified peptides [113]. ToF-SIMS has a measurement depth of less than 1 nm.

1.3.2.4. Scanning electron microscopy (SEM)

SEM has been used previously to analyze both the surface morphology and cross sections of chitosan films [114, 115]. Composite films were analyzed for both their structural integrity and the homogeneity of the composite [115-117]. SEM was

also used to identify and compare the intricate structure of chitosan nanofibres and chitosan film during cell attachment [118]. Another study using SEM was able to identify morphological, physical and mechanical attributes, and degradation products of chitosan [119].

1.3.2.5. Atomic force microscopy (AFM)

AFM as a technique allows the analysis of the surface of polymeric material with a high spatial resolution. It has been used previously in the analysis of chitosan films. Films were mapped and their morphological parameters/surface roughness was analyzed. Pure films and derivatives were compared and the effect of the addition of dansyl derivatives on the surface was investigated [120]. Another study looked into the effects of the surface topology with different treatment of the surface including argon and nitrogen bombardment [121].

1.4. Modification of chitosan

Chitosan is often tailored for specific applications. Chitosan itself already has numerous beneficial properties which allow it to be considered for biomedical applications. However, specific applications require an improvement in the biocompatibility, surface or mechanical properties of chitosan materials. Therefore, chitosan is often modified or functionalized. Non-chemical modifications include the addition of carbon nanotubes to increase tensile strength. Chemical modification often involves reactions with the primary amine or the hydroxyl groups to introduce a different functional group. [16] Other modifications include the formation of a complex with another

polyelectrolyte such as alginate [112], the chemical grafting with a polymer such as poly(ethylene glycol) [122, 123], or short functional groups such as alkyl groups [6]. These materials are generally characterized with methods as described in section 1.3.2.

1.5. Publication: Real-time monitoring of peptide grafting onto chitosan films using capillary electrophoresis [3]

Since CE does not require tedious sample preparation it can be optimized and used for the analysis of chemical reactions. One instance is the grafting of peptides onto the surface of chitosan films. As mentioned previously, chitosan has various properties which allow it to be a promising material for biomedical applications. An example of this includes cell substrates. To enhance cell attachment onto the chitosan films, the peptide RGDS was grafted onto the surface of chitosan films using the coupling agents 1-ethyl-3-(3-dimethylaminopropyl)carbodiimide (EDC-HCl) and *N*-hydroxysuccinimide (NHS). The peptides arginine-glycine-aspartic acid (RGD) and arginine-glycine-aspartic acid-serine (RGDS) are fibronectin mimetic and have been used in cell attachment studies [124].

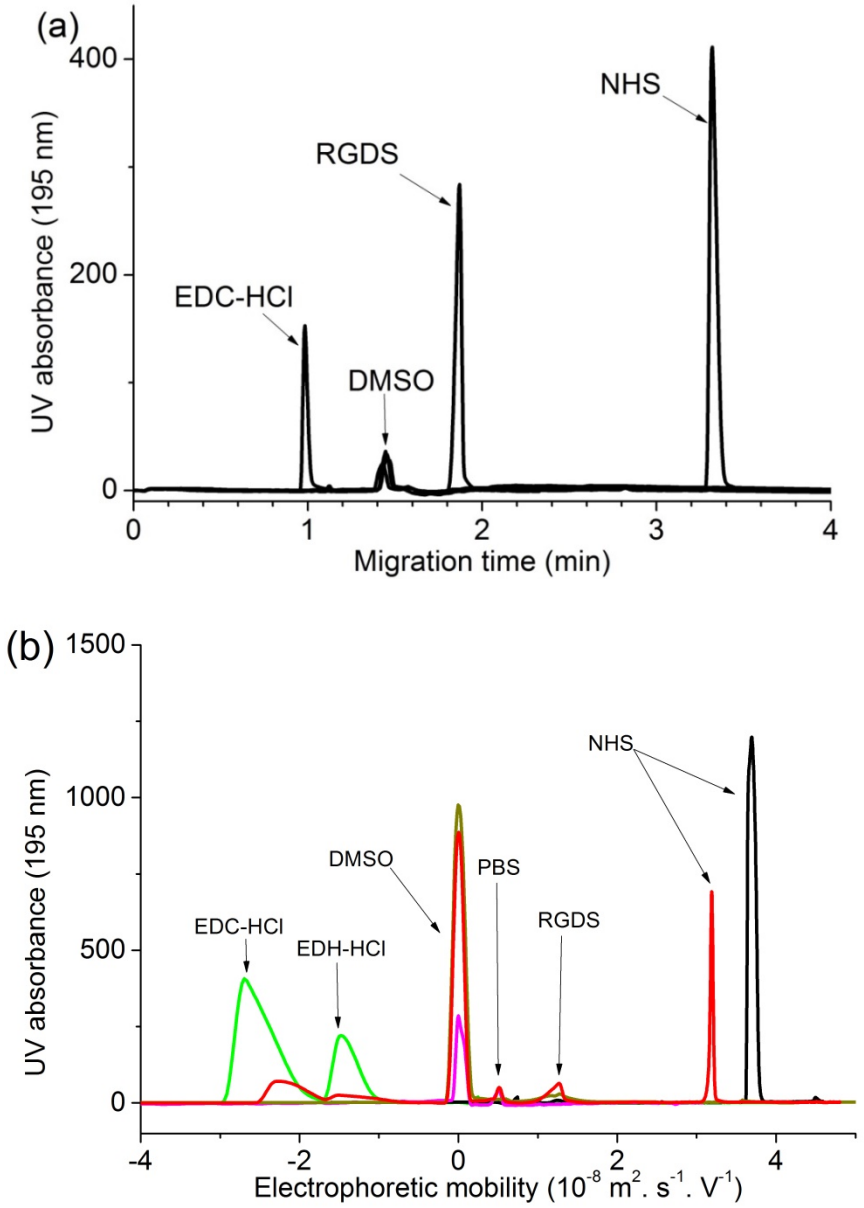

Figure 1-20. Monitoring the grafting by CE: separation of coupling agents, RGDS and internal standard as a function of a) migration time and b) electrophoretic mobility [3] conducted in a 43.5 cm (total length) 50 μm internal diameter fused silica capillary with 75 mM sodium borate at pH 9.2

The grafting of RGDS through of EDC-HCl and NHS took place in a Petri dish containing chitosan film and phosphate buffered saline (PBS). CE was able to separate all reactants in less than 4 min with good resolution with no sample preparation required and each reactant was identified (Figure 1-20). Real-time analysis took place with aliquots of the reaction medium injected at regular time intervals. The grafting of the RGDS was indirectly quantified through the integration of the peptide peak over the reaction time (Figure 1-21). Peptide consumption was seen to plateau after 4 hours and therefore the grafting reaction was able to be optimized.

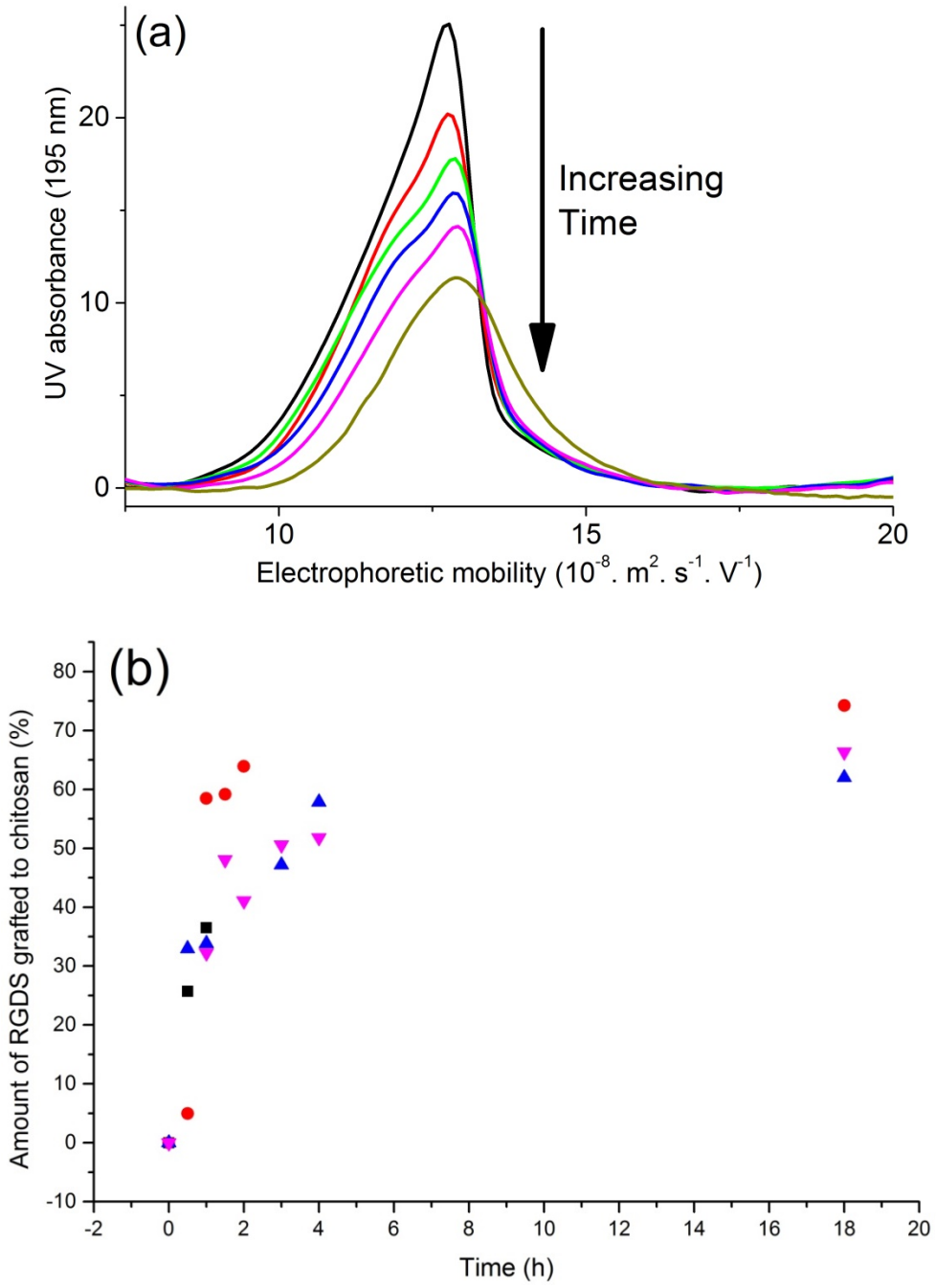

Figure 1-21: a) Electropherograms of RGDS signal showing consumption over reaction time b) Real-time monitoring of RGDS peptide consumption during the grafting onto chitosan films with CE. Different symbols represent repeat experiments. [3] Measurements were conducted in a 43.5 cm (total length) 50 μm internal diameter fused silica capillary with 75 mM sodium borate at pH 9.2

CE was also able to detect the polycondensation of RGDS (which was not protected) which resulted in oligomers of RGDS as well as highly branched polyRGDS. Each species was detected with a shift in the electrophoretic mobility. This shift in the electrophoretic mobility of RGDS demonstrated its branching structure which was indicative of polycondensation. The peak area of the different species were measured and normalized to calculate the fraction of RGDS with a specific branching structure. CE was thus able to monitor the polycondensation of RGDS and quantify the change (Figure 1-22).

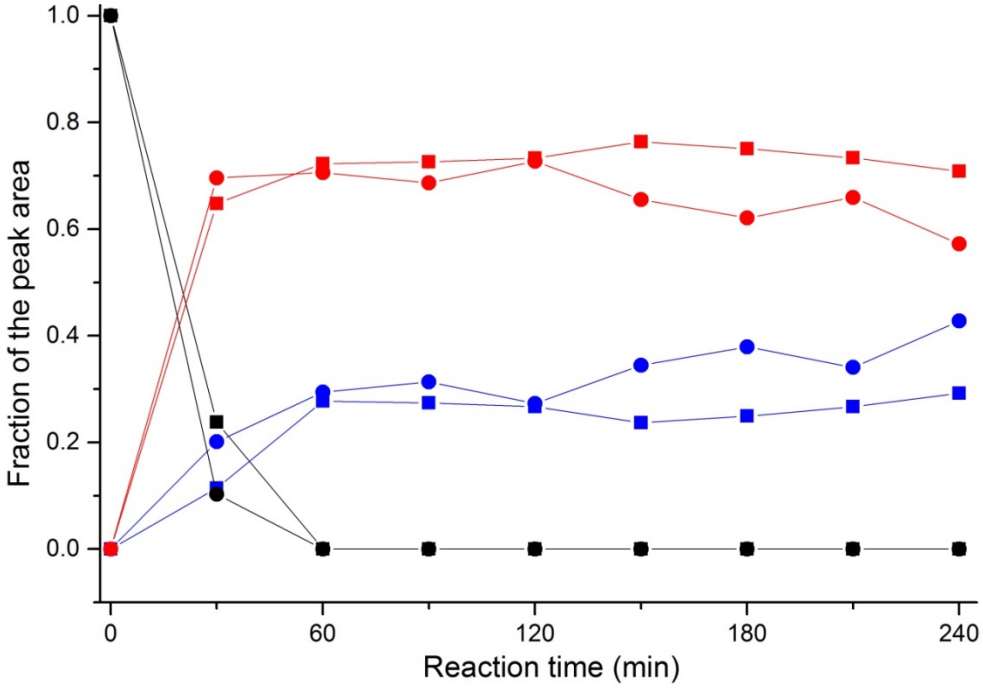

Figure 1-22: Polycondensation of RGDS monitored by CE. Linear (black), oligomers (red) and highly branched (blue) RGDS were identified by their mobility (2.5, 1 and 1.5 $\times 10^{-8}$ $m^2.V^{-1}.s^{-1}$ respectively). [3] The peak area was measured and the fraction of each of the branching species was quantified.

To directly validate the grafting of RGDS onto the surface of chitosan films ^{13}C SPE-MAS swollen-state NMR spectroscopy was used. The swelling of the films in PBS allowed the RGDS to become more mobile and detected even in its small quantity (compared to the bulk of chitosan film). Unfortunately due to swelling the measurements were not quantitative, however, validation of the grafting method and evidence of RGDS on the surface of the chitosan was obtained.

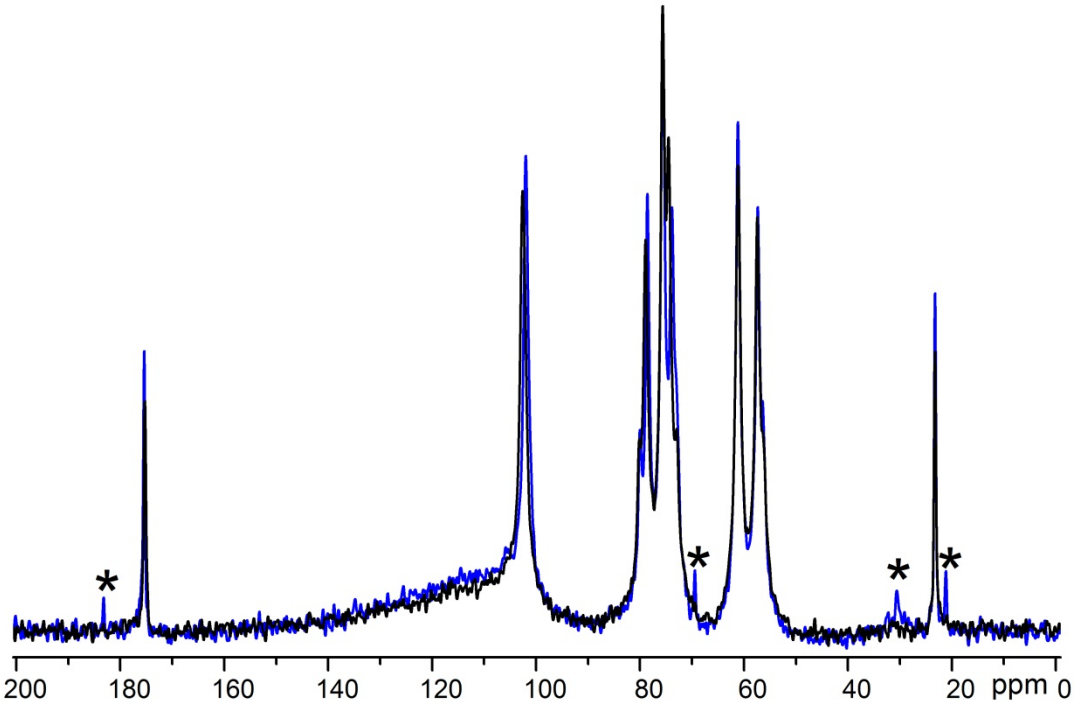

Figure 1-23: ^{13}C SPE-MAS swollen-state NMR spectroscopy was conducted on blank chitosan films (black) and chitosan films grafted with RGDS on the surface (blue). The asterisks represent signals assigned to RGDS.

1.6. Thesis Aims

As mentioned above, current literature is incomplete in the analysis of chitosan. The current standard in polymer analysis in solution is unable to allow a complete characterization. With further developments in functionality of chitosan more analysis needs to take place with more advanced solid-state methods. This thesis aims at filling the gaps in the understanding and development of methods in the characterization of complex polyelectrolytes. The specific aims of this thesis were to:

- Develop simple but effective methods in allowing a more comprehensive characterization of complex polyelectrolytes
- Probing and understanding the dissolution of chitosan to allow an improvement in its application and characterization
- Improving chitosan films functionality through the modification of their surface for regenerative medicine

1.7. Overarching statement

1.7.1. Publications overview

As identified in the background, there was a large gap in understanding of polymers due to their poor characterization. This is especially the case for natural polymers which suffer from batch to batch variations. The following publications allowed a deeper understanding in the area of research.

The published invited review [1] (see section 1.2) presented a background of the CE technique in the analysis of complex samples including polysaccharides, natural and synthetic polymers. Further, the explanation of critical conditions in which the separation takes place without an influence of molar mass was outlined and examples of its application were summarized. The separation in the critical conditions discussed in the review allowed the basis of the separation method to be discussed and further verified in later publications. The knowledge of CE and CE-CC was applied to all results chapters in this thesis.

The most common method in polymer characterization is SEC and therefore a comparison of CE and SEC in the analysis of polymers was needed. This was undertaken with the separation of block copolymers which allowed a significant area of research to be explored (see section 1.2.5) [2]. SEC was deemed inappropriate in the analysis of the double hydrophilic block copolymer as it was unable to detect a difference between the homopolymer and the block copolymer. The training in SEC was used in chapter 2 for the analysis of chitosan. Conversely, CE was able to detect a significant difference between both and was also able to detect residual homopolymer in the block copolymer which allowed the determination of purity. This research paper allowed the significance of CE and its advantages in the analysis of complex polymers to be clearly outlined.

The pioneering paper in the application of chitosan for biomedical applications involved the grafting of peptides onto the surface of chitosan films and testing them with cell attachment (see section 1.4) [3]. For the first time real-time

monitoring of the grafting process was completed with CE which allowed an indirect quantification of the amount of peptide grafted to the surface of the film. Swollen-state NMR spectroscopy measurements allowed the grafting to be validated and initial cell tests on the surface of the film were positive. CE was also able to analyze the branching structures of the peptide due to polycondensation. This paper was significant as it allowed the test of chitosan films for cell culture. Further, advancement in the techniques of CE and solid/swollen-state NMR spectroscopy was possible (see chapter 5.2).

Based on the cell culture results, an important hypothesis in the paper on chitosan films grafted with peptides was the possible heterogeneity of the films. Therefore the possibility of heterogeneity arising from the film preparation i.e the dissolution of chitosan, was identified as an important parameter to understand (see chapter 2) [125]. Visual observations, SEC, time-resolved solution- and solid-state NMR spectroscopy were used to monitor and quantify chitosan dissolution.

Polymers are often studied in solution and their size analyzed. However, with complex polyelectrolytes there are several other parameters of interest including composition or branching. These complex samples could be further characterized using the established "critical conditions" (CE-CC). The data analysis developed was analogous to the commonly used calculation of the dispersity of molar mass distributions with SEC, however, the dispersity values obtained were of electrophoretic mobility distributions relating to either the heterogeneity of composition or heterogeneity of branching. This method was successfully tested with various complex polymers (see chapter 3) [126].

The newly developed method of calculation of dispersity from electrophoretic mobility distributions was then tested with a large number of chitosan samples (see chapter 4) [127]. This required improvement in the separation of chitosan with CE. Different coatings and background electrolytes were tested to optimize the separation and limit adsorption of the polymer to the capillary surface. Calculations of the electrophoretic mobility distributions and determining a correlation between weight-average mobility and composition also allowed composition distributions for statistical copolymers to be obtained for the first time. Although chitosan is a challenging polymer, the research proved that this method could be used with various other polymers or polysaccharides.

Finally the application of chitosan films for tissue engineering was studied. Following feedback from the previous research article on the grafting of peptides onto chitosan films, the grafting process and real-time monitoring method itself was published in the Journal of Visualized Experiments (JoVE) (see section 5.1) [128]. This article was focused on the method itself so that it could be more widespread and utilized for different applications in different research teams.

To further test the use of chitosan films for biomedical applications, in this case for implantation, poly(ethylene glycol) was grafted onto the surface to further improve biocompatibility (see chapter 5.2) [129]. The grafting reaction was monitored using CE and the grafting was quantified indirectly. To confirm

grafting, TGA, DSC and NMR spectroscopy measurements were undertaken on bare chitosan films and PEG grafted films. The permeability of the films was also tested as it was noted to be an important parameter especially in the case of implantation. Advanced NMR spectroscopy techniques were employed to assess the heterogeneity of chitosan.

1.7.2. Contribution to personal, professional development and to the field of study

1.7.2.1. Separation and Characterization of Synthetic Polyelectrolytes and Polysaccharides with Capillary electrophoresis – Advances in Chemistry [1] (section 1.2)

The experience of writing an invited open access review was beneficial in a number of ways. It allowed for the work of the Macromolecular Characterization team at Western Sydney University and developments in the CE of polyelectrolytes to be summarized and published. Further to this, in having the article peer reviewed before submission, I was heavily involved with responding to the reviewers and implementing changes as required. Overall, I completed the first draft of the manuscript and the first draft of the answer to the reviewers.

This experience contributed to my professional development in allowing me to publish an article in which all the writing was undertaken in collaboration with Dr Patrice Castignolles and Dr Marianne Gaborieau. Working together we were able to significantly contribute to the area of research with this review as CE is

often not recognized in the analysis of polymers. The work completed is innovative and an accumulation of all the relevant work was necessary.

1.7.2.2. Purity of double hydrophilic block copolymers revealed by capillary electrophoresis in the critical conditions – Journal of Chromatography A [2] (section 1.2.5)

This publication gave me the opportunity to collaborate extensively with a large group of students and international /Australian academics (Paul Sabatier University, Toulouse, France and Western Sydney University). Not only did this enable personal and professional growth, it allowed me to contribute to an interesting and important research topic while advancing my own understanding of the characterization of polymers. During this project I was also trained in multiple-detection SEC. This was significant as it allowed me to apply this "gold standard" method in the analysis of chitosan (see chapter 2).

The work involved enhanced my communication and written skills, but also broadened my way of thinking and scope of understanding. Another requirement of this piece of work was to generate insightful ideas to further develop the project, as well as to ensure the information was articulated clearly.

Moving forward, I now have a practical knowledge of a widely used analytical technique in my field of study (SEC). This technique was used as a comparison and enabled us to outline the relevance of using CE in the analysis of polymers.

Once more, significant in the area of research as it was innovative in nature and had not been completed before.

The article had 8 authors in total. The first author Adam Sutton wrote the first draft and performed most of the CE data analysis. My role was to obtain the SEC analysis of the block copolymers, prepare 1 manuscript figure and contribute 1 supporting information figure of the SEC elution profile to represent the data and proof-read the manuscript along with the other coauthors.

1.7.2.3. Real-time monitoring of peptide grafting onto chitosan films using capillary electrophoresis – Analytical and Bioanalytical Chemistry [3] (section 1.4)

This article was the preface of the application of my PhD. It was a proof of concept article that outlined chitosan's use in the biomedical field. Further, it was the first article I was a part of that I had a major contribution to. I was able to incorporate ideas from my PhD into the article and be involved with the reviewing process.

For my professional development, once again the project allowed advancement of new techniques in the laboratory. Further this also enabled another research publication.

This article was significant in the field of study as it went further than previous articles in the proof of grafting as well as tests with cells. It was significant as instead of suggesting possible applications of the material, these were tested for the first time. This article played a "proof of concept" role. The results from this publication were presented a number of times during my PhD including at an international conferences (SCM-7) and national meetings (SASSY-UNSW, ACROSS gathering) (see oral presentations in the research output section).

This publication has a total of 11 authors. The first author Danielle Taylor and 2nd author (myself) had equal major contributions to the article. This included carrying out experiments, the collection and analysis of data and writing the results of the CE and NMR experiments. I participated in the initial design of the project during Dr Catherine Lefays' visit to WSU during my BSc(Honours) degree. The initial experiments conducted for this publication occurred during my BSc(Honours) and the first draft of the manuscript included results from my BSc(Honours) thesis. The final experiments from the publication, however, were conducted during my PhD and I wrote the first draft of the answer to the reviewers and completed all extra experiments requested by the reviewers during this time. The 3rd author Diksha Narayan also completed some CE experiments although her contribution focused mainly on the cell attachment studies on the chitosan films which were assisted and supervised by the 4th, 5th and 6th authors. The last 5 authors included academics who guided the project and had the initial ideas.

1.7.2.4. Towards a less biased dissolution – Analytica Chimica Acta [125] (chapter 2)

This work began at the start of my PhD and was a lesson in fortitude. It was a challenging topic which allowed my training and development in the use of advanced techniques including NMR spectroscopy, CE and SEC. Further, the results from this study allowed me to give an oral presentation at the 7th International Symposium on the Separation and Characterization of Natural and Synthetic Macromolecules (SCM-7 in Amsterdam, the Netherlands), Australian Centre for Research on Separation Science (ACROSS) Annual Meeting (Tasmania), University of Montpellier II, (Montpellier, France), Université Toulouse III Paul Sabatier (Toulouse, France) and poster presentations at the Virtual symposium on applied separation science (VSASS), the RACI NSW Polymer Group workshop on Macromolecular Characterisation and SCM-7 (see presentations in the research output section). Thanks to a successful competitive Endeavour application, I was able to meet and discuss this project with Dr Manfred Wagner (Max Planck Institute for Polymer Research, Mainz, Germany) and further develop my understanding of solution-state NMR spectroscopy while setting up international collaborations.

Professional development included train in a laboratory at the Max Planck Institute for Polymer Research (Mainz, Germany). More experience was gained in the analytical techniques of solution-state NMR spectroscopy, SEC and CE.

This publication contributed to the field of study as it proved that the dissolution of polymers in general is an important topic of study. The various methods used in this study showed that the problem which is often not acknowledged is very complex and can cause bias in results which has flow on effects. This affects the overall understanding of any material produced.

The publication has a total of 5 authors. The last author, Dr Patrice Castignolles and the corresponding author Dr Marianne Gaborieau provided the direction of the paper and helped formulate the experiments. Dr Marianne Gaborieau provided training on the solid-state NMR spectroscopy measurements and Dr Patrice Castignolles provided training on the CE and multiple-detection SEC instruments. Dr Manfred Wagner (3rd author) assisted with kinetic measurements using time-resolved solution-state NMR spectroscopy completed during my stay at the Max Planck Institute for Polymer Research. Jerikho Bulanadi (2nd author) provided some initial work (visual observations and their interpretation) completed in his undergraduate degree which helped assist the direction of the publication.

My contribution included the data acquisition for the solid-state NMR experiments, CE, SEC and pressure mobilization. This included method development which was guided by Dr Marianne Gaborieau and Dr Patrice Castignolles. I wrote the first full draft of the publication which was reviewed by Dr Patrice Castignolles and Dr Marianne Gaborieau and then sent to the other co-authors for comments and feedback. After submission I wrote the first full draft of the answer to the reviewer's comments and this was then addressed by Dr Patrice Castignolles and Dr Marianne Gaborieau before resubmission.

1.7.2.5. Quantifying the heterogeneity of chemical structures in complex charged polymers through the dispersity of their distributions of electrophoretic mobilities or compositions – Analytical Chemistry [126] (chapter 3)

This publication was the most challenging and allowed great personal development and was once again a lesson in fortitude. It gave me the opportunity to expand my development into analytical chemistry, physical chemistry and polymer science theory. This involved learning new concepts and theories which allowed an expansion of my knowledge. Thanks to my successful Endeavour Research Fellowship I was able to undergo training with Professor Hervé Cottet (University of Montpellier 2, Montpellier, France) who taught me various concepts. Thanks to the results from this publication I was able to present these findings in an oral presentation at the Polymer Research in NSW Symposium, Kensington (Australia) and Australian Centre for Research on Separation Science (ACROSS) Annual Meeting (see oral presentations in the research output section).

Again I was able to develop by working in a different research group at the University of Montpellier 2. Data treatment was initially carried out with Professor Hervé Cottet and on my return to Sydney I was able to develop a template to allow the calculations to be completed in a more straightforward manner. So far the template has been used by 9 postgraduate students and 2 undergraduate students.

This publication contributed to the field of study by creating for the first time the basis of dispersity calculations based on a parameter other than size for polymers. This theory paper was the first of its kind to outline calculations of dispersity similar to those established with other separation methods.

This publication has a total of 9 authors. The last author, Dr Marianne Gaborieau, corresponding author, Dr Patrice Castignolles and 6th author, Professor Hervé Cottet provided the direction of the paper. Dr Simon Harrison (5th author) had valuable contributions during a revision of the full draft of the manuscript. Alison Maniego and Elizabeth Whitty (3rd and 4th authors) supplied experimental data and 2nd author Adam Sutton had data as well as preliminary work completed in his MSc(Honours) thesis.

Using the template developed, I re-treated and compiled the previously obtained data provided by Alison, Elizabeth, Adam and myself. Using the guidance of Dr Patrice Castignolles and Dr Marianne Gaborieau and the previous work completed by Adam, I was able to write a full draft of the manuscript. This was reviewed by all co-authors before submission. The first full draft of the answer to the reviewers was completed by myself and then reviewed by Dr Patrice Castignolles and Dr Marianne Gaborieau.

1.7.2.6. Determination of the distribution of composition of chitosan – International Journal of Biological Macromolecules [127]

(chapter 4)

This manuscript built on the theory developed in the previous study on the calculation of dispersity. It influenced my personal development as it allowed me to further develop the skills learnt previously. It gave me the opportunity to expand my knowledge in the field of analytical chemistry.

Professional development included once again collaboration with Professor Hervé Cottet at the University of Montpellier 2. Further development in the data treatment and adaptations to the software used for the template allowed an expansion of knowledge and understanding.

This publication contributed to the field of study by expanding on previously published methods on the characterization of chitosan. The dispersity calculations developed in my last publication were tested with a larger range of samples and composition distributions of chitosan were obtained for the first time.

This manuscript has 5 authors in total. The corresponding author Dr Patrice Castignolles and last author Dr Marianne Gaborieau provided the direction of this publication. Professor Hervé Cottet assisted with discussion and added insightful ideas. The 2nd author Matthew Van Leeuwen assisted in data collection and analysis.

The data acquisition, data treatment and the first full draft of the manuscript were completed by me. This was then reviewed a number of times by the co-authors before submission. The development of the data treatment was directed by Dr Patrice Castignolles and Dr Marianne Gaborieau.

1.7.2.7. Chitosan film – JoVE [128] / in preparation [129] (chapter 5)

The chapter on chitosan films included a publication on the real-time monitoring of RGDS onto chitosan films published in the Journal of Visualized Experiments and a manuscript written for publication in Biomacromolecules. A range of characterization techniques were learnt to enable a better understanding of the produced chitosan films. Following on from previous research and also using the developed method of calculating dispersity, a better understanding of the grafting reaction of RGDS was obtained (see section 1.4). Thanks to my successful Endeavour Research Fellowship I was able to undergo training with Dr Robert Graf at the Max Planck Institute for Polymer Research (Mainz, Germany) who assisted with the development of the experiments and taught me advanced NMR spectroscopy methods.

For my professional development, once again learning new skills and techniques in the laboratory allowed further broadening of my technical expertise. I learnt to use the TGA and DSC instruments. Further I was able to collaborate with members of the Advanced Materials Characterisation Facility (AMCF) (Dr Timothy Murphy and Dr Richard Wuhrer), undergraduate students and academics. The invited publication of the JoVE article also gave me experience in editing video scripts and screen shot selections as well instructional manuscript writing.

This study is important as it progresses from the grafting of peptides onto chitosan film. Firstly it allows the visualization of the reaction monitoring which can then be utilized for various applications. It also allows other characterization methods to be utilized in testing a complex samples and answers important questions regarding the permeability, heterogeneity and successfulness of grafting poly(ethylene glycol) onto chitosan films.

The JoVE publication has 4 authors. Dr Marianne Gaborieau, Dr Patrice Castignolles and Dr Michael O'Connor contributed to the ideas and direction of the manuscript. Dr Patrice Castignolles and Dr Marianne Gaborieau also had specific input on the editing of the video script. The manuscript on chitosan film has 10 authors. The last 3 authors Dr Patrice Castignolles, Dr Marianne Gaborieau and Dr Michael O'Connor contributed ideas for the direction of the manuscript. The 4^{th}, 5^{th}, and 6^{th} authors (Dr Timothy Murphy, Dr Richard Wuhrer, and Dr Robert Graf) helped with experiments and trained me in the use of advanced characterization instrumentation. Dr Robert Graf also contributed ideas regarding the direction of solid-state NMR experiments. Michele Mason and Daniel Bairamian contributed experiments of PEG grafting and permeability tests respectively, as a part of their undergraduate program.

For both the publication and manuscript I completed the first full draft. For the JoVE article, I also completed the first draft of the answer to the editor and also to the reviewers. Additionally, I completed the first draft of related video script

questionnaire, video script, screenshot capture and shot list. For the manuscript on chitosan film I completed the first full draft and contributed to the data treatment and compilation of results.

CHAPTER 2: Publication: Towards a less biased dissolution of chitosan

2.1. Publication [125]

Towards a less biased dissolution of chitosan

Joel J. Thevarajah [a,b,c], Jerikho C. Bulanadi [a], Manfred Wagner [c], Marianne Gaborieau [a,b]*, Patrice Castignolles [a]

[a] Western Sydney University, School of Science and Health, Australian Centre for Research on Separation Sciences (ACROSS), Parramatta, 2150, Australia

[b] Western Sydney University, Molecular Medicine Research Group (MMRG), School of Science and Health, Parramatta, 2150, Australia

[c] Max Planck Institute for Polymer Research, Ackermannweg 10, 55128 Mainz, Germany

*Corresponding author : Marianne Gaborieau, m.gaborieau@westernsydney.edu.au, Western Sydney University, Molecular Medicine Research Group (MMRG), School of Science and Health, Parramatta, 2150

ABSTRACT: The dissolution of polysaccharides is notoriously challenging, especially when one needs a "true" solution. Factors influencing chitosan's solubility include composition, also known as degree of acetylation (*DA*). The dissolution of chitosan was investigated by visual observation, size-exclusion chromatography (SEC), pressure mobilization (PM), free-solution capillary electrophoresis (CE) and real-time solution-state NMR spectroscopy. Aqueous

HCl dissolves around 15 % more chitosan than the commonly used aqueous acetic acid (AcOH), however aggregates were detected in SEC suggesting incomplete dissolution. Significant deacetylation of chitosan over the period needed for dissolution at high temperature was observed by NMR spectroscopy in DCl by about 20 % of the initial *DA* value. Accurate *DA* determination by NMR spectroscopy may thus be possible only in the solid state (with a precision within 1 % on the *DA* % scale above a *DA* of 10 %). Overall a compromise between maximum solubilization and minimum degradation is required in attempting to obtain a "true" solution of chitosan. The completeness of the dissolution may be more influenced by the average *DA* than by molar mass.

KEYWORDS: Chitosan, dissolution, solid-state NMR spectroscopy, solution-state NMR spectroscopy. capillary electrophoresis, size-exclusion chromatography (SEC)

1. INTRODUCTION

Chitosan is a polysaccharide derived from the *N*-deacetylation of chitin. Chitin is the second most abundant polysaccharide in the world (by volume after cellulose) and is synthesized by many organisms.[1] Its natural occurrence includes the exoskeletons of arthropods such as shrimps, crabs and the cell walls of yeasts.[2] It is a major waste product of the seafood industry. Its most promising derivative, chitosan, was shown to be biocompatible, biodegradable and antimicrobial, which make it an appropriate material for biomedical applications such as stem cell growth substrate.[3, 4] Chitosan's structure

contains varying proportions of D-glucosamine and *N*-acetyl D-glucosamine units. The degree of acetylation (*DA*) of chitosan refers to the proportion of the *N*-acetyl D-glucosamine monomer units. It is often characterized only by its average *DA* which does not take into account the complex arrangement of monomer units along the polymer chain.[5] The *DA* and the distribution of the acetyl groups along chitosan chains affect the dissolution or hydrolysis of chitosan.[6, 7]

A significant factor that hinders a meaningful characterization of chitosan is the difficulty to fully dissolve it without degrading it. To allow for the proper separation and characterization of a polysaccharide (by chromatography, light scattering, etc.), true solutions are required as in the case of starch.[8] A true (dilute) solution is defined in this work as a solution where all macromolecules (chitosan chains) are surrounded by solvent molecules [9]. True solutions are also necessary to allow the homogenous chemical modification of chitosan.[10] The dissolution of polysaccharides is generally complex, and various techniques have been used to assess it in different ways. A dissolved sample will visually appear as a clear and transparent liquid; however, obtaining a clear and transparent liquid does not always mean that the sample is completely dissolved. In the case of starch, quantitative ^{1}H NMR spectroscopy of a transparent liquid proved it to contain undissolved starch (up to 15 % of the initial starch) for some starches, possibly due to the presence of aggregates which were invisible to the naked eye.[8] Unlike chitin, which is largely insoluble in aqueous and organic solvents, chitosan is partially soluble owing to the amine group of its D-glucosamine monomer. However, the actual extent of dissolution of chitosan is often overlooked and is dependent on structural

characteristics including the distributions of the degrees of acetylation and environmental conditions such as pH, ionic strength, temperature, time and the dielectric constant of the solvent.[3, 11] UV spectrophotometry at 600 nm has been used to analyze the dissolution by analysis of the turbidity, however this overlooks the presence of aggregates or non-dissolved parts of the chitosan small enough to produce minimal scattering of visible light.[12] A range of methods has been used to monitor the dissolution of macromolecules [9], but a number of these methods do not discriminate between true solution and dispersion (aggregation) such as viscometry,[13] FTIR spectroscopy [14], or pyrolysis gas chromatography [15, 16].

Light scattering (static and dynamic) was used to analyze the dissolution of chitosan, unfortunately, there were several limitations. Chitosan dissolution is often complicated by the presence of (concentration dependent) aggregation. Common methods to remove aggregates are ultracentrifugation and filtration. However, in the case of chitosan, these methods were shown to remove high molar mass chains and caused the light scattering results to be strongly influenced by the filttration procedure undertaken.[17] Size-exclusion chromatography (SEC) coupled to multi-angle light scattering (MALS) identified aggregation in chitosan samples and heterogeneity of the solution [18]. It was further identified that the aggregates are stable in solution and thus light scattering cannot accurately characterize chitosan.[17, 18] The extent of the aggregation did not correlate with the average *DA* in this work.

SEC is a commonly used method in the characterization of polysaccharides.[19] It has been used in an attempt to obtain molar mass distributions of chitosan.[2] Unfortunately, as identified previously, chitosan's poor solubility and

aggregation causes difficulty in choosing an appropriate solvent. Solvents such as 0.1 M acetic acid/0.2 M sodium chloride were shown to cause an overestimation of molar mass due to the promotion of aggregation. It was also noted that light scattering was sensitive to the aggregation of highly acetylated chitosan samples.[20]

Beyond light scattering, Taylor dispersion analysis (TDA) can be used to determine the diffusion coefficient of macromolecules, but has never been applied to chitosan. The diffusion coefficient is related to the size of the macromolecules and thus TDA can provide information regarding the presence of aggregates or dissolved molecules. The detection of narrow and broad peaks allows a clear distinction between the dissolved sample and aggregate formation.[21] Free-solution capillary electrophoresis (CE) or capillary zone electrophoresis has been applied in a limited but successful fashion to the characterization of polysaccharides, including the separation of chitosan samples by their *DA*.[5, 22] CE proved to separate the samples by their *DA* with no sample preparation required, not even sample filtration. The area of the peaks on the CE electropherograms could thus be used to analyze the dissolution of chitosan, with no bias due to sample preparation. It is important to note that aggregates, as long as their diffusion coefficient is much lower than that of the macromolecules of interest, lead to very sharp peaks in CE. These sharp peaks are easily distinguished from the polymer peak as in the case of gellan gum [23].

In this paper the dissolution of chitosan samples is investigated with various techniques: capillary electrophoresis and pressure mobilization, multiple-detection SEC, as well as solution-state and solid-state NMR spectroscopy.

Aggregation, extent of dissolution and possible chemical degradation are assessed.

2. EXPERIMENTAL

2.1. MATERIALS

Chitosan powders were purchased from Aldrich, Castle Hill, Australia and from AK Biotech, Jinan, China (Table 1). Samples were prepared at 1 $g \cdot L^{-1}$. Orthophosphoric acid (85 %) was purchased from BDH AnalR, Merck Pty Ltd. Acetic acid (AcOH, glacial, 99 %) and hydrochloric acid (32 %) were purchased from Unilab. Sodium hydroxide pellets, sodium chloride, trifluoroacetic acid (TFA, 99 %), hexaamminecobalt(III) chloride (≥99.5 %), dimethyl sulfoxide (DMSO, 99 %) and adamantane (99 %) were purchased from Sigma-Aldrich. Deuterium chloride (35 %) was purchased from Cambridge Isotope Laboratories. All water used in this study was of Milli-Q quality. The SEC eluent was prepared from TFA at 0.3% (w/v) with 0.1 M NaCl. The eluent was filtered with 0.22 μm nylon 6,6 filter. Nine pullulan standards (with weight-average molar masses between 342 and 805,000 $g \cdot mol^{-1}$ and dispersity values between 1.00 and 1.27) were purchased from Polymer Standard Service, Mainz, Germany. Sodium borate buffer (75 mM) was prepared from 0.5 M boric acid in Milli-Q water, titrated to pH 9.20 with 10 M sodium hydroxide, and diluted with Milli-Q water. Sodium phosphate buffer (100 mM) was prepared from 0.5 M sodium dihydrogen phosphate, titrated with phosphoric acid, and diluted with Milli-Q water. Sodium borate and phosphate buffers were sonicated for 5 min and filtered with a Whatman (0.2 μm) or Millex GP PES syringe filter (0.22 μm) before use.

Table 2-1. Visual evaluation of the dissolution of chitosan samples with varied *DA*s in aqueous solvents: 50 mM HCl, 0.3 % (w/v) trifluoroacetic acid (TFA), as well as 0.3 % (w/v) TFA with 0.1 M NaCl (Eluent)

Sample	Supplier	Batch (Catalogue)	$DA_n^{SS\text{-}NMR}$ (%) [a]	DA_n^{NMR} (%)[b]	HCl	TFA	Eluent
LowMW1	Sigma	MKBG3334V (448869)	17.1 ± 0.3		2h[c]	2h	2h
MedMW1	Sigma	MKBH1108V (448877)	22.3 ± 0.3		2h	2h	1n [d]
MedMW2	Sigma	03318AJ(448877)	20.2 ± 0.3	15.5 ± 1.6	1n	1n	
HighMW	Sigma	MKBD7240V (419419)	11.8 ± 0.3		1n	1n	
Sig	Sigma	120M0028V (C3646)	10.1 ± 0.3		1n	1n	
AKbioV1	AK Biotech	090426V1	10.1 ± 0.3		1n	1n	
AKbioV2	AK Biotech	090423V2	16.5 ± 0.3	18.7 ± 1.9	1n	1n	
AKbioV3	AK Biotech	090426V3	14.8 ± 0.3	16.5 ± 1.7	1n	1n	

AKbioD1	AK Biotech	090422D1	12.5 ± 0.3	19.8 ± 2.0	1n	1n	
AKbioD2	AK Biotech	090422D2	11.1 ± 0.3	13.6 ± 1.4	1n	1n	
AKbioD3	AK Biotech	090422D3	3.8 ± 0.3	3.5 ± 0.4	1n	1n	
AKbioC	AK Biotech	090430C			2w[e)]	2w	
ChitAl	[5]		4.0 ± 0.3	2.5 ± 0.3	2h		

[a)] Number-average *DA* obtained by solid-state NMR spectroscopy in this work for which the *SD* was determined as the error caused by phasing (see section 3.5.)

[b)] Number-average *DA* obtained by solution-state NMR spectroscopy [5]

[c)] sample was visually dissolved after 2 h at 60 °C

[d)] sample was visually dissolved after 2 h at 60 °C and an overnight shaking at room temperature

[e)] sample was visually dissolved after 2 h at 60 °C followed by overnight shaking at room temperature followed by 2 weeks without shaking at room temperature

2.2. CAPILLARY ELECTROPHORESIS AND PRESSURE MOBILIZATION

Free-solution capillary electrophoresis (CE) and pressure mobilization (PM) experiments were carried out using an Agilent 7100 CE (Agilent Technologies, Waldbronn, Germany) instrument equipped with a diode array detector and external circulating bath with MX temperature controller (Polyscience, USA). Polyimide-coated fused silica high sensitivity capillaries (50 μm internal diameter) were purchased from Agilent. The capillary (104 cm total length, 95.5 cm effective length) was initially pretreated by flushing with 1 M NaOH for 10 min, then with 0.1 M NaOH, Milli-Q water and sodium borate buffer for 5 min each at the start of the series of experiments. An oligo(sodium acrylate) was separated [24] in sodium borate (75 mM, pH 9.3) to validate the capillary and the instrument before each session. The electrolyte for chitosan analysis was sodium phosphate (100 mM, pH 2 or 3). Before each experiment the capillary was rinsed with HCl (50 mM) and sodium phosphate (100 mM, pH 2 or 3) for 5 min, respectively. Hydrodynamic injections for PM were carried out with 75 mbar for 10 s and for capillary electrophoresis with 40 mbar for 20 s (both corresponding to injection volumes of 0.14 % of the total capillary volume, see Eq. S2-1 in supporting information). CE was undertaken by applying 30 kV at 25 or 55 °C. PM was undertaken at a pressure of 72 or 63 mbar (without electric field). For PM the sample was mixed with the background electrolyte with the electric field. This involved the ramping voltage up to 30 kV and then down to -30 kV and back up to 0 kV over the first 4 min of separation (Fig S2-3). The mixing of the chitosan with the carrier liquid is due to the electroneutrality of the solution needing to be maintained at all times, even during the ramping process. This is possible due to the reservoirs of buffer which represent an

infinite source of the liquid carrier's ions compared to the capillary volume. As the anions and cations of the buffer migrate with the electric field, the counter-ions migrate as well to maintain electroneutrality which results in mixing. When the electric field is off, the sample is allowed to migrate through the capillary within the carrier liquid. Pressure-assisted capillary electrophoresis (PACE) was undertaken with both an electric field (30 kV) and pressure (50 mbar) at 55 °C. For kinetic measurements undertaken using PACE, the CE carousel was kept at 60 °C using an external circulating bath. Detection was set at 195 nm. All CE and PM data were treated with the software Origin 9 and the x and y axes were normalized based on previous studies [25, 26], converting the y axis into a time-corrected y axis $h(t)$, or a weight distribution of electrophoretic mobilities $W(\mu)$ (see supporting information).

2.3. MULTIPLE-DETECTION SIZE-EXCLUSION CHROMATOGRAPHY

The analysis of chitosan was undertaken with a Malvern Viscotek triple-detector size-exclusion chromatography instrument triple detector array consisting of an online degasser, pump, automatic sample injector, one precolumn and three NOVEMA columns (one low molar mass column: 30 Å and two medium molar mass columns: 1 000 Å, both with particle sizes of 10 μm) from Polymer Standards Service, Mainz, Germany. The triple detector array included in series RALS (right-angle light scattering, 670 nm), refractometer (660 nm) and viscometer thermostated at 50 °C, controlled by the software OmniSEC. The flow rate was 0.85 $mL \cdot min^{-1}$. Ethylene glycol was used as a flow rate marker and the injection volume was set at 100 μL. The eluent

was regularly injected to check for the absence of system peaks on all the detectors' signals and the absence of bleeding from the columns.

2.4. SOLID-STATE NMR SPECTROSCOPY

Solid-state ^{1}H and ^{13}C NMR spectra were recorded on a Bruker Avance DPX200 spectrometer operating at Larmor frequencies of 200 MHz and 50 MHz, respectively. A commercial double resonance probe supporting zirconia MAS rotors with a 4 mm outer diameter and a 3 mm inner diameter was used, and samples were spun at 10 kHz at the magic-angle. ^{1}H experiments were recorded using a 90° pulse, a 3 s repetition delay with at least 64 scans accumulated. ^{13}C CP-MAS NMR experiments were adapted from quantitative measurements found in the literature [27, 28]. They were recorded with a 1 ms contact time and a 4 s repetition delay, and 21,586 to 104,924 scans. For ^{1}H experiments the 90° pulse was optimized using adamantane and power levels for the ^{13}C CP-MAS experiments were optimized using a mixture of three ^{13}C singly labeled alanines. The ^{1}H and ^{13}C chemical shifts scales were externally referenced using adamantane by setting the CH resonance to 1.64 and 38.48 ppm, respectively [29]. The degree of acetylation was measured through Eq. 2-1 [27]:

$$DA_n^{SSNMR}(\%) = \frac{I_{CH_3}}{(I_1+I_2+I_3+I_4+I_5+I_6)/6} \quad \textbf{2-1}$$

Where I_{CH3} is the integral of the methyl group of the acetyl group and I_1 to I_6 are the integrals of the signals assigned to the chitosan backbone.

To measure the deacetylation by solid-state NMR spectroscopy 250 mg chitosan (MedMW1) was dissolved at 1 gL^{-1} in 50 mM HCl in Milli-Q water or in 50 mM DCl in D_2O. Each sample was then kept in an oven at 60 °C for 55 h. After

removing the sample from the oven the dispersion was neutralized with excess 1M NaOH. The dispersion was then filtered and rinsed with 500 mL of Milli-Q water, freeze-dried and measured by solid-state NMR spectroscopy.

2.5. SOLUTION-STATE NMR SPECTROSCOPY

The kinetic measurements were recorded on a Bruker 500 MHz Avance III system operating at a Larmor frequency of 500 MHz, equipped with a 5 mm z-gradient BBFO 1H/X probe with z-gradient using TopSpin 3.2 (Bruker). The ^{1}H NMR spectra were measured in deuterium oxide at 333 K. The accuracy of the temperature was controlled with a methanol sample. The sample was prepared at 1 $g \cdot L^{-1}$ in approximately 0.8 M DCl in D_2O. A standard kinetic ^{1}H NMR experiment was started immediately after the chitosan was mixed with solvent, and recorded with 32 transients per spectrum with a 10.6 μs 90° pulse, a spectral width of 11,000 Hz and a repetition delay of 8.6 s (3.6 s acquisition time and 5 s relaxation delay). A total of 800 successive spectra were recorded over 61 h. The relaxation rate (T_1) of the protons was measured before and after the kinetic run with the inversion recovery method and the T_1 values for the acetyl peak and the peak associated to the backbone were determined to be 1.2 s and 943 ms, respectively. Therefore the kinetic experiment conducted was quantitative. Repeat monitoring experiments were conducted on a Bruker DRX300 spectrometer operating at a Larmor frequency of 300.13 MHz equipped with a 5-mm dual $^{1}H/^{13}C$ probe at 333 K. The temperature was calibrated with 80 % glycol in DMSO. The measurements were undertaken with 64 transients per spectrum with a 1.7 μs 30° pulse and a repetition delay of 18.3 s (4.3 s acquisition time and 14 s relaxation delay).

The solution-state NMR measurements for quantifying *DA* conditions were as previously [5].

3. RESULTS AND DISCUSSION

3.1. VISUAL OBSERVATION OF DISSOLUTION

Pillai [11] suggested that the dissolution of chitosan does not occur in inorganic solvents and therefore the first qualitative measurement of the dissolution of chitosan was through visual observation in aqueous solvents (also more suitable for biomedical applications). Chitosan can be soluble only at a pH below 6.[11] Aqueous solvents (Table S2-1) were used at different acid concentrations, limiting them to low concentrations to prevent chitosan degradation. No dissolution took place at 5 mM or 10 mM hydrochloric, acetic, trifluoroacetic, phosphoric, and boric acid. 50 mM concentration of hydrochloric, trifluoroacetic or acetic acid produced clear transparent suspensions after 15 min at room temperature. Trifluoracetic acid has been suggested to be more effective at dissolving chitosan but also samples with a higher *DA*.[30] Phosphoric and boric acid even at higher concentrations were unable to produce a visually clear sample. The acids that were unable to produce a clear solution at room temperature were tested at higher temperatures (Table S2-2 and Table 2-1). It was observed that only phosphoric acid was able to produce a clear solution if it was left at 60 °C for 1 h. Using the conditions previously established other chitosan samples with a range of different average *DA*s were also evaluated visually for dissolution in HCl 50 mM, TFA 0.3 % and SEC eluent at 60 °C for 2 h. Samples that were not visually dissolved were left overnight on a shaker at room temperature (Table 2-1). It was concluded from the visual observations

that different samples varied in the time needed to produce a clear suspension. This confirmed that the dissolution process was complex and further analysis was required.

3.2. SIZE-EXCLUSION CHROMATOGRAPHY AND AGGREGATION

SEC is the gold standard for the characterization of polymers especially for the determination of molar mass distributions. This, as well as the degradation and oligomers of chitosan, was characterized using a SEC instrument equipped with PSS NOVEMA columns [31-33]. Aqueous HCl was not chosen to prevent the corrosion of the SEC instrument. A TFA-based eluent was indicated as an appropriate running buffer for the PSS NOVEMA columns for chitosan by PSS in an application note [34]. In this study SEC was used to analyze chitosan samples with different *DA*s. Pullulans were used as standards to generate a conventional calibration curve (Figure S2-1). Pullulan-equivalent molar masses of the chitosan samples (Table S2-3) were repeatable, but not reproducible, as commonly observed in SEC.[35] The reproducibility was investigated only by varying the injection concentration, but this already led to significant variations as observed for other polysaccharides.[36] Importantly, the determined apparent molar masses were 7 orders of magnitude larger than that of the largest pullulan standard. The values obtained are physically impossible, well beyond the experimental error associated to pullulan-equivalent (or any apparent) molar masses [37]. This is likely explained by aggregation in these conditions as observed also with other SEC conditions.[18] Analysis of the refractive index and right angle light scattering detector traces (Fig. 2-1)

revealed that all chitosan samples were bimodal. The different samples exhibited 2 different populations and bimodal peaks: a peak at a lower elution time and a peak at a higher elution time. The peak at a low elution time infers a large molar mass and is assigned to the aggregates and the peak at a higher elution time is inferred to be the dissolved chitosan. The large molar mass values obtained and the intensity of the LS signal which is sensitive to large molar masses [38] were in good agreement of the existence of aggregation.

Samples that exhibited a separation of aggregates and dissolved polymer (analysis of elution profile) were then diluted (up to 1/100) to assist in breaking apart the aggregates. However, the aggregation remained in the diluted sample suggesting a high stability (Fig. 2-1B) as suggested in the case of starch.[39]

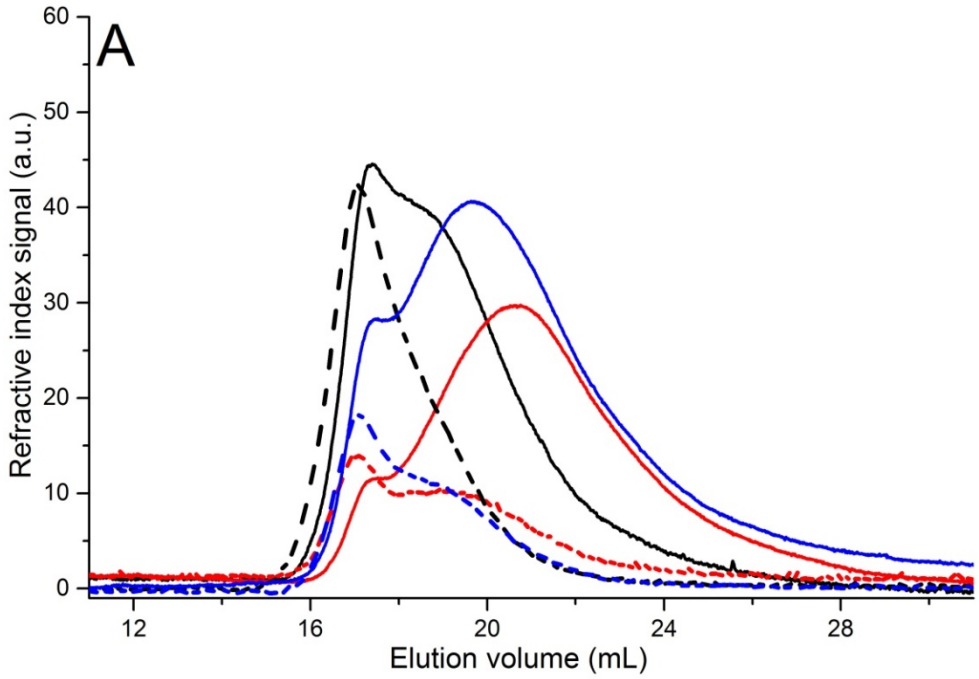

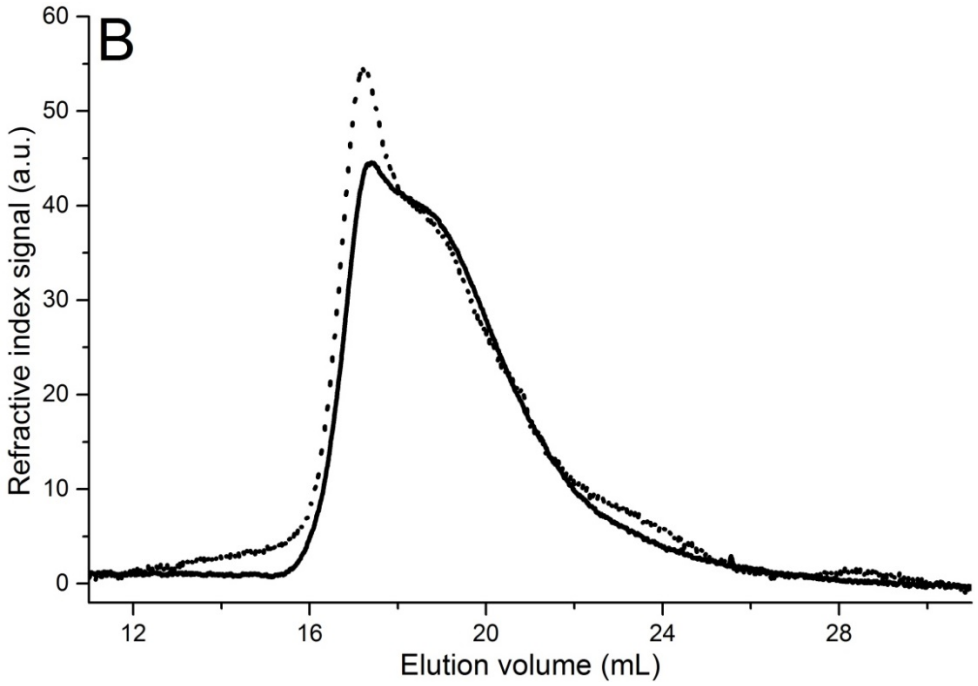

Figure 2-1: A) RI (solid lines) and RALS (dashed lines) traces of chitosan MedMW1 (black), LowMW1 (red) and AKbioD3 (blue). B) RI trace of MedMW1 in 50 mM HCl at 1 $g \cdot L^{-1}$ (solid line) and diluted to 0.25 $g \cdot L^{-1}$ (normalized by concentration, dotted line).

3.3. EVALUATION OF DISSOLUTION BY PRESSURE MOBILIZATION

Chitosan MedMW1 dissolved in aqueous HCl and AcOH was chosen to be analyzed by pressure mobilization (PM) based on initial visual observations. The sample was heated for 2 h at 60 °C to ensure a clear liquid was obtained. PM was used for the first time to analyze the dissolution of chitosan. It was initially performed with phosphate buffer at pH 3 at 25 °C as the carrier liquid without mixing of the chitosan suspension with the phosphate buffer. A large peak with considerable tailing was observed for chitosan dissolved in aqueous HCl and a small peak with tailing for the chitosan dissolved in aqueous AcOH (Fig. S2-2). The large UV absorbance of the sample dissolved in HCl is

uncharacteristic of chitosan; however, the presence of tailing suggests adsorption onto the capillary surface [40]. Repeatable results were obtained with the sample dissolved in HCl; however, samples dissolved in AcOH exhibited adsorption and poor repeatability. Therefore conditions were adapted and PM experiments were carried out with a slightly different carrier liquid of pH 2 phosphate buffer (100 mM) with mixing (Fig. 2-2) at 55 °C. The mixing involved the adjustment of the electric field between 30 kV and -30 kV (Fig. S2-3) immediately after the injection and the addition of pressure (which was reduced from 72 mbar to 63 mbar). Chitosan dissolved in HCl produced 2 signals slightly separated from each other and the blank (no chitosan) produced a large signal from HCl 50 mM (Fig. 2-2A). The large signal was assigned to the Cl^- from HCl [41]. To analyze the chitosan signal the intensity of the Cl^- signal was normalized based on the viscosity difference between the solutions (Eq. S2-2). The peak of Cl^- has a similar migration to blanks with injection of the carrier liquid spiked with DMSO. The injection of 50 mM HCl was then superimposed and subtracted from the chitosan dissolved in 50 mM HCl (Fig. 2-2B). The remaining peak is identified as chitosan. The unexpected separation of chitosan and Cl^- may be due to the occurrence of ion exclusion of the Cl^- and the adsorption of the chitosan. Tailing toward high elution times, indicative of slight adsorption [40] could still be seen; however, this was less pronounced than for chitosan dissolved in 50 mM AcOH.

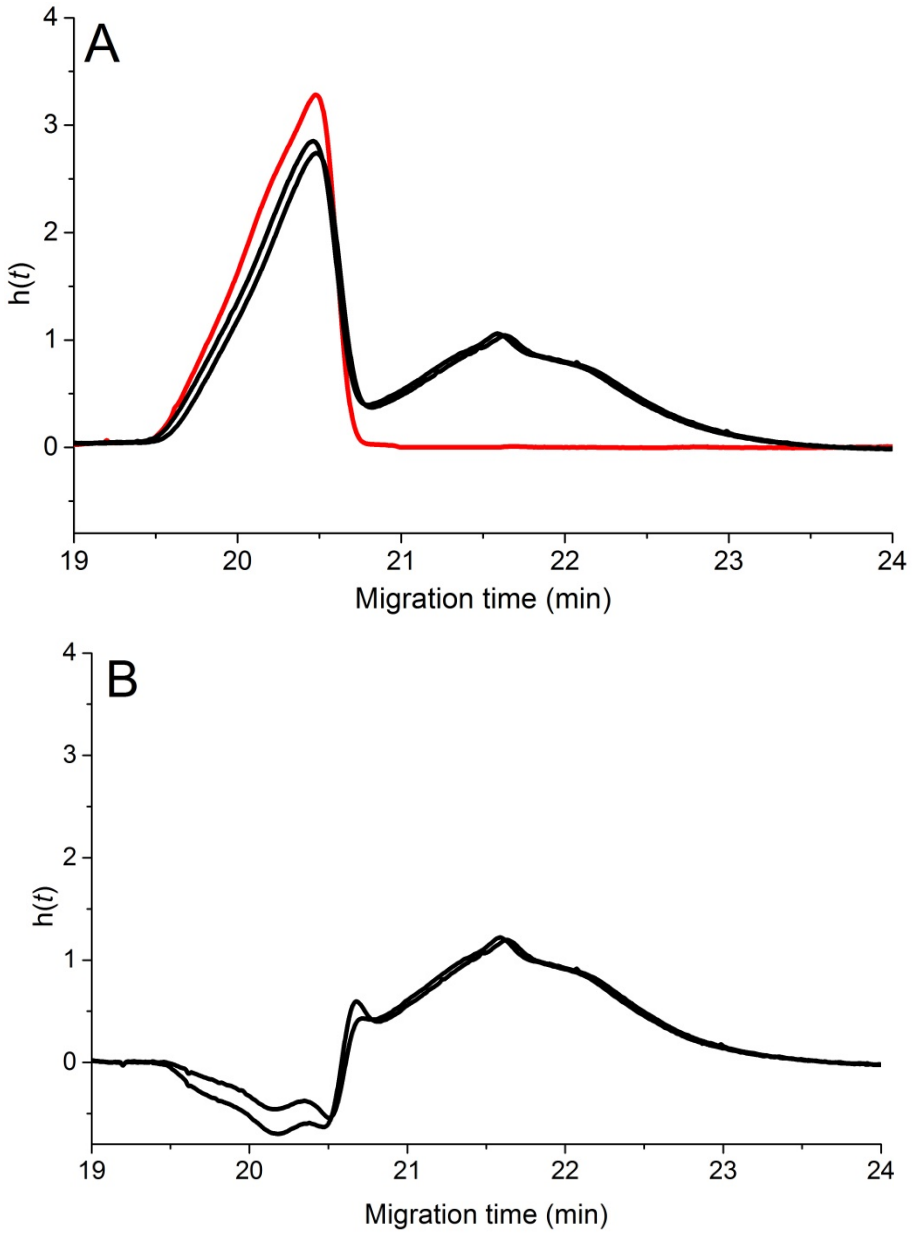

Figure 2-2: PM (with viscosity normalization for Cl^-) of 50 mM HCl (red) and of chitosan (MedMW1) dissolved in 50 mM HCl (black, 2 repeat experiments shown) A) before and B) after Cl^- subtraction

Chitosan dissolved in aqueous AcOH exhibited a sharp peak (also present in the blank) coeluting with a broad peak. The sharp peak is thus assigned to acetate.

The area of the chitosan dissolved in AcOH was calculated by integrating the chitosan with the acetate peak superimposed and subtracting the peak area of the acetate peak (Fig. S2-4). The peak area of chitosan dissolved in aqueous HCl was determined to be 17 % greater than that dissolved in aqueous AcOH (n=2). This is consistent with the CE results (see section 3.4.). PM experiments were also conducted with the solvent as the background electrolyte as is used for TDA (Fig. S2-5). Chitosan in aqueous HCl had the Cl^- peak superimposed on top of the chitosan peak in these conditions, while it was not the case of the chitosan in aqueous AcOH with the AcO^- migrating earlier. From the PM results it was concluded that aqueous HCl was able to dissolve chitosan to a greater extent than aqueous AcOH.

3.4. EVALUATION OF DISSOLUTION BY CAPILLARY ELECTROPHORESIS AND PRESSURE-ASSISTED CAPILLARY ELECTROPHORESIS

CE is growing in use for the characterization of macromolecules such as chitosan [22]. CE in the critical conditions has previously been studied to separate polylysine with a degree of polymerization below 10 [42] and chitosan samples by their *DA* [5]. CE in the critical conditions was used in this work to analyze the dissolution of chitosan in different solvents (Fig. 2-3). All separations were repeatable, but chitosan dissolved in aqueous HCl systematically led to higher recovery in CE. The dissolution of chitosan in aqueous HCl is seen to be more effective than in aqueous AcOH, both at room temperature and at 60 °C. The integration of the chitosan peak showed that the chitosan dissolved in aqueous HCl had at least a 13 % greater peak area compared to that dissolved in aqueous AcOH (n=3). The dissolution in aqueous

TFA is as effective as in aqueous HCl at room temperature but at 60 °C it is not (being then comparable to dissolution in aqueous AcOH). These results are consistent with the initial results obtained from the pressure mobilization and it shows that aqueous AcOH is less efficient as a solvent for chitosan than aqueous HCl even though clear suspensions are produced in both cases.

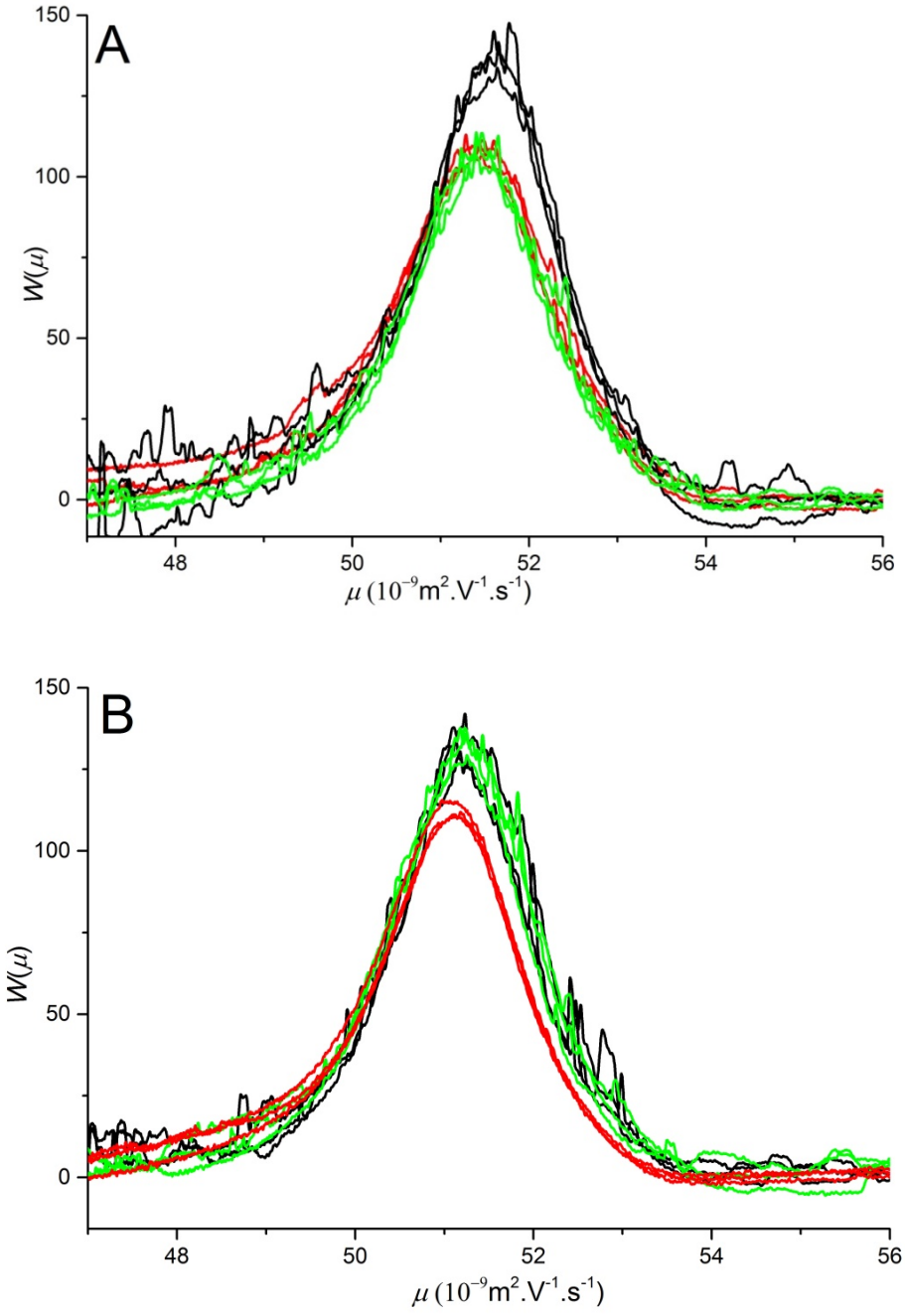

Figure 2-3: Electropherogram of chitosan (MedMW1) dissolved in 50 mM HCl (black line), AcOH (red line) and TFA (green line) prepared at A) 60 °C for 2 h B) 25 °C for 2 h

To increase the precision of the determination of the mobility, PACE was undertaken. PACE is CE with an added pressure during the separation. This is beneficial as the separation of chitosan takes place in a shorter time and the electroosmotic flow (EOF) is detected. The detection of the EOF allows a more precise determination of the electrophoretic mobilities of chitosan through a double correction with the use of an EOF marker and an electrophoretic mobility marker (Fig. 2-4). Further, it allows the correction of the area of the chitosan by the hexaamminecobalt(III) chloride internal standard area (to compensate for variations in injection volumes) and the detection of any neutral impurities that could not be seen in CE of chitosan without very long measuring times. The increase in precision is extremely important as any shifts in mobility caused by possible deacetylation (loss of charge) would be noticed during PACE measurements and be more accurately measured. Therefore, experiments monitoring the kinetics of dissolution (see sections 3.6. and 3.7) with CE were undertaken using PACE.

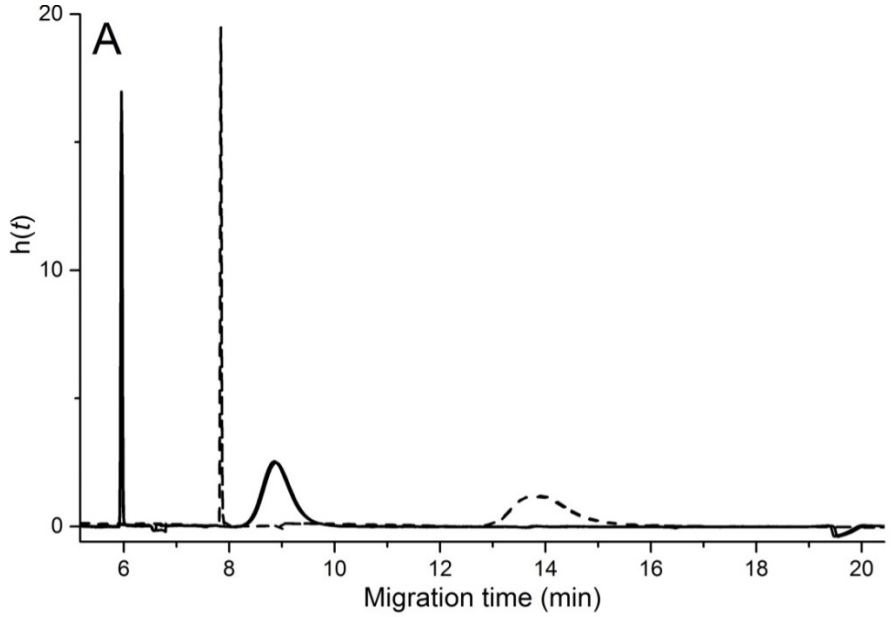

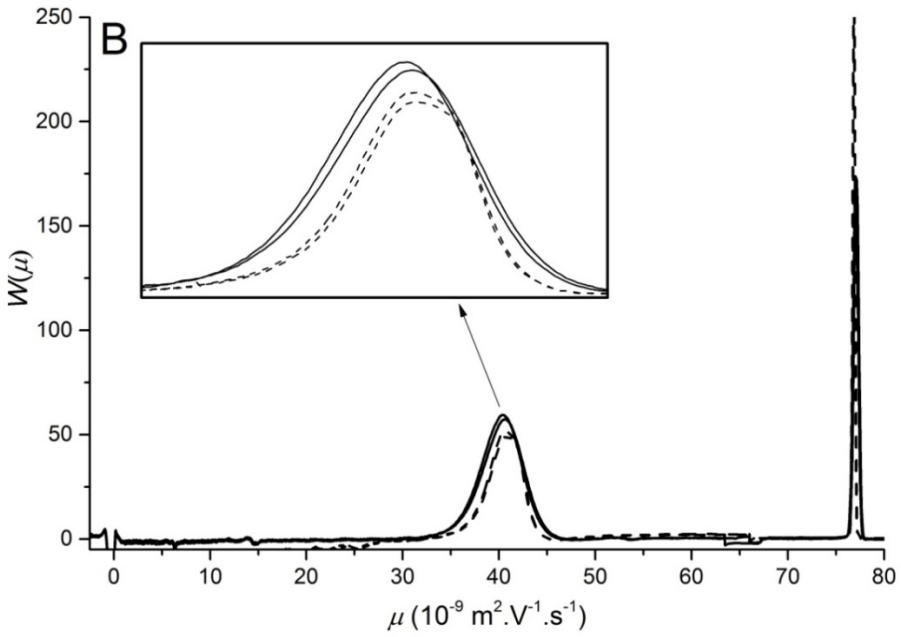

Figure 2-4. Electropherogram of chitosan (MedMW1) dissolved in 50 mM HCl separated using CE (dashed line) and PACE (solid line) in a) migration time and b) electrophoretic mobility. The electrophoretic mobility marker is seen at a mobility of 76.9 × 10^{-9} $m^2.V^{-1}.s^{-1}$ and a migration time between 6 and 8 min. The EOF is seen at a mobility of 0.

3.5. BIAS IN DISSOLUTION EVALUATED WITH NMR SPECTROSCOPY

The measurement of the average degree of acetylation of chitosan is routine in its characterization. Solid-state NMR spectroscopy measurements allow the analysis of the whole sample and an accurate degree of acetylation to be attained. This is further significant taking into account the aforementioned difficulties in obtaining a true solution. A comparison of results from solid-state and solution-state NMR spectroscopy further identifies this bias. The error bars for the solution-state NMR spectroscopy results are based on the relative

standard deviation *RSD* estimated from the signal-to-noise ratio *SNR* (Eq. 2-2 [43]).

$$RSD(\%) = \frac{238}{SNR^{1.28}} \quad \textbf{2-2}$$

The error bars for the solid-state NMR spectroscopy results are based on error caused by phasing and *SNR*. Limited *SNR* may not only result in a limited precision but it can also affect the way the user will phase the spectrum. This is especially true in the case of solid-state NMR spectroscopy in which the signals are generally quite broad. Therefore the error caused by phasing was tested (Table S2-5). It was measured by having 4 different users phase 8 different experimental data sets. The *DA* was measured and a *RSD* value was obtained for each data set. The *RSD* from phasing was observed to correlate with the *RSD* from *SNR* (Fig. 2-5A). Therefore, when the *SNR* was less than 50 the *RSD* of *DA* was estimated as a sum of the error from phasing and the error from *SNR* (Eq. 2-3). The *RSD* was estimated from the *SNR* (Eq. 2-2) for measurements with a *SNR* greater than 50, for which it was deemed that the error from phasing would be negligible.

$$RSD(\%) = 11 \times \frac{238}{SNR^{1.28}} - 16 \quad \textbf{2-3}$$

The MedMW2 sample (Table 2-1 and Fig. 2-5B) has a significantly higher *DA* value when measured with solid-state NMR spectroscopy compared to solution-state NMR spectroscopy which is not the case for the rest of the samples. The error on the average *DA* obtained by solution-state NMR may thus not be systematic. Solution-state NMR measurements can therefore not be calibrated, for example with chitosan samples standardized by solid-state NMR spectroscopy.

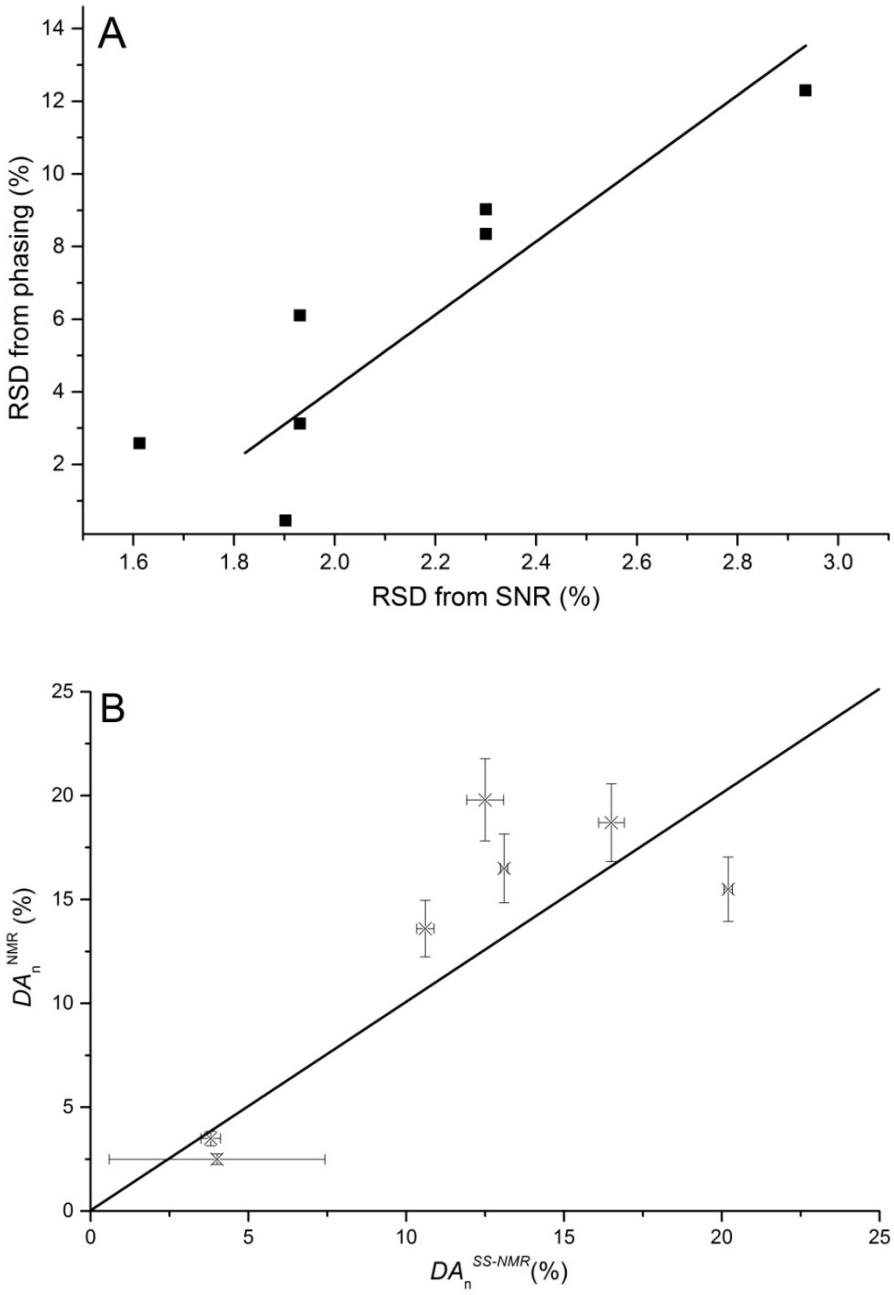

Figure 2-5: A. Error of solid-state NMR spectroscopy measurements estimated as *RSD* from *SNR* and as *RSD* from phasing. The straight line represents a linear fit (y=10x-16, r^2=0.79). B. *DA* values obtained by solution- and solid-state NMR spectroscopy for the same chitosan samples. The straight line is the diagonal.

The analysis undertaken in solution state shows only the *DA* of the dissolved fraction of the partially dissolved sample which introduces a bias in the determination of the *DA* of the whole sample. The solid-state NMR spectroscopy measurements considered more accurate due to the fact that they measure the whole sample and not just its soluble fraction. For the solution-state NMR spectroscopy the difficulty in dissolving chains with many acetyl groups was previously noted [2] and therefore it is likely chitosan chains with a large *DA* may remain undissolved and influence the determination of *DA*. The influence may also cause variance in the total amount of D-glucosamine units in solution as a chain with a block of *N*-acetyl-D-glucosamine units that remain out of solution may cause the rest of the chain to remain out of solution. Such an occurrence would be explained by chitosan's precursor chitin, as chitin has a semi-crystalline structure with extended hydrogen bonding [11]. The deacetylation of chitin may cause some chains to have a tendency towards blocks of *N*-acetyl-D-glucosamine [3]. These blocks depending on their size may cause these chitosan chains to remain out of solution and cause an incomplete dissolution. This would explain the overestimation (AKBioD2, AKBioD3) of the *DA* values by solution-state NMR spectroscopy. The solution-state measurements may also be influenced by the use of deuterated HCl (DCl) as explored below (see section 3.6).

3.6. KINETICS OF DISSOLUTION MONITORED BY SOLUTION-STATE NMR SPECTROSCOPY AND PACE

The kinetics of the dissolution was monitored using solution-state NMR spectroscopy, as previously achieved in the case of starch.[44] Before the kinetics measurement, T_1 relaxation time of the chitosan was measured to allow a quantitative measurement. The T_1 relaxation time of the acetyl peak was 1.2 s which was very similar to that of the backbone signal. Chitosan was suspended in 0.8 M DCl in D_2O. Measurements were taken over a 61 h period with a total of 800 measurements and the probe's temperature was controlled at 60 °C during the experiment. From the second measurement the signals assigned to the backbone between 3 and 5 ppm start to be seen (Fig. S2-6). A signal in the region of the acetyl signal (1.8-2 ppm) is also seen. However, as the measurements progress a second signal is seen in the same region slightly shifted downfield (Fig. S2-6).

As the kinetics measurement continues this new signal becomes more intense. An integration of this peak shows a steady increase even after the plateau of the chitosan backbone signal intensity is reached (Fig. 2-6); this signal is therefore assigned to a product of the deacetylation of chitosan [45]. The sharp signal is indicative of a small/mobile group which supports the hypothesis of deacetylation. The intensity of the signal at 2.2 ppm reduces over time (after 15 h); this signal is thus assigned to the acetyl group of the chitosan. To check the assignment of the signals, chitosan and chitosan spiked with 50 mM AcOH dissolved in 50 mM DCl in D_2O were measured at 60 °C. The signal of the

deacetylation product of chitosan was assigned to free AcOH confirming the occurrence of deacetylation (Fig. S2-7).

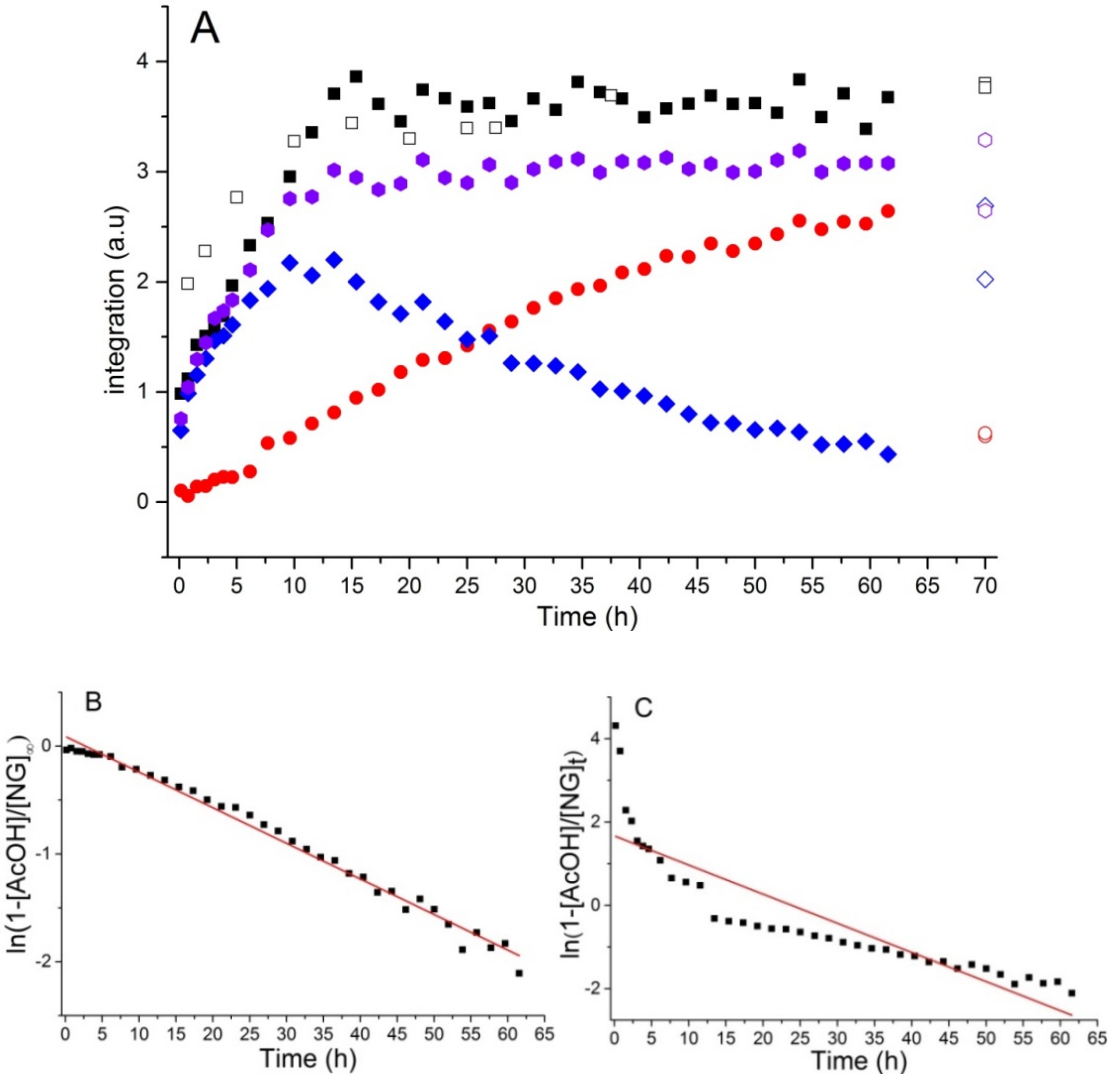

Figure 2-6. A. Integration of solution-state NMR signals measured over 61 h at 60 °C: chitosan backbone (black squares), chitosan acetyl group (blue diamonds), free AcOH (red circles) and the sum of the acetyl group and free AcOH (NG, purple hexagons). The full symbols correspond to measurements in 0.8 M DCl in D_2O, the empty symbols to measurements in 50 mM DCl in D_2O.. Evolution on a logarithmic scale of the consumption of the acetyl groups on *N*-acetyl-D-glucosamine units, with the *N*-acetyl-D-glucosamine concentration taken as (B) the total available initial *N*-acetyl-D-glucosamine

units $[NG]_\infty$ (plateau of NG purple curve in A) or (C) as the dissolved fraction of the initial *N*-acetyl glucosamine units $[NG]_t$ (real time value of NG purple curve in A). Red lines represent linear fits with a r^2 of 0.99 (B) and 0.77 (C).

The intensity of the chitosan backbone signal is stable after 10 h (Fig. 2-6A) however, the signal associated with the acetyl peak and the peak associated to the deacetylation increase and decrease over time, respectively. The detection and quantification of the free AcOH allowed the monitoring of the kinetics of the deacetylation (which is not possible using the acetyl group on the chitosan backbone since it is affected by both dissolution and deacetylation simultaneously). The deacetylation was assumed to follow a 2nd order kinetics:[46] S_N2 reaction with a first order in *N*-acetyl-D-glucosamine units (see Equation S2-10). This hypothesis was tested using the acetyl peak of the free AcOH (see Fig. 2-6B and 2-6C). A linear correlation is observed when the concentration of the *N*-acetyl-D-glucosamine units is determined as the sum of the integrals of the free AcOH and *N*-acetyl-D-glucosamine signals (NG) on the plateau (Fig. 2-6B). This NG concentration at the plateau $[NG]_\infty$ corresponds to the total concentration of *N*-acetyl-D-glucosamine units that can be dissolved, regardless of whether they are deacetylated or not in solution. When the total concentration of *N*-acetyl-D-glucosamine units is taken as the dissolved fraction of the initial *N*-acetyl-D-glucosamine units (real time value of [NG] on Fig. 2-6A), a non-linear relationship is seen (Fig. 2-6C). This result suggests that deacetylation is able to take place as soon as the chitosan is in contact with the solvent. The use of DCl for the dissolution over HCl may cause the dissolution to be slower since the hydrogen bonding that would normally occur in aqueous

HCl is stronger than deuterium bonding. Studies have looked into the deacetylation and hydrolysis of chitin and chitosan in concentrated hydrochloric acid [47, 48] with temperatures of 25 and 30 °C. It was seen that the concentration of the HCl or DCl used and the composition influenced the rate of hydrolysis and deacetylation [7]. In these conditions, the concentration of HCl (high concentrations) was shown to play a significant role over temperature (only tested 25 and 35 °C). However, deacetylation was 4 times faster at 35 °C compared to 25 °C and 6 M HCl was shown to be the most efficient in hydrolysis [47]. It was further suggested that the formation of a glucofuranosyl oxazolinium ion occurs in concentrated DCl, however this was not noted in our spectra as there was an absence of the corresponding 3 ^{1}H NMR signals at 7 and between 5 and 4.7 ppm. A lower concentration of acid (0.8 M) was used in this work than in previous research and the glucofuranosyl oxazolinium, if present, is below its limit of detection. Further, the low concentration of DCl used in this work would not support hydrolysis over deacetylation as seen previously.

The monitoring was then repeated with 16 times lower concentration of DCl in D_2O (50 mM) to see if the deacetylation still occurred. The rate of dissolution was surprisingly comparable. Deacetylation was once again detected and confirmed, but more limited. Deacetylation was seen to be between 18 and 24 % of the initial *DA* value (±3.5 on the *DA* scale). A dissolution experiment was also undertaken with chitosan dissolved for 55 h in 50 mM HCl and DCl in D_2O. The 2 chitosan samples were precipitated and measured with solid-state NMR spectroscopy. Between 14 and 16 % of the initial *DA* value (± 1.5 on the *DA* scale) deacetylation was determined after dissolution. The results suggest that

the deacetylation and dissolution of chitosan is complex however occurs even at low concentrations of DCl.

This NMR method is not a high-throughput method to monitor dissolution. Measurements of chitosan in 50 mM DCl and HCl were also undertaken on a Magritek Spinsolve benchtop NMR spectrometer to try and detect the deacetylation of chitosan in aqueous HCl. However, the signals of chitosan were unable to be distinctly resolved at the low concentration (1 $g \cdot L^{-1}$) chosen for minimal aggregation (Fig. S2-8).

To compare the effects of HCl and DCl on the deacetylation of chitosan, PACE was used to run a kinetic measurement at 60 °C. CE has an advantage over ^{1}H NMR spectroscopy in its ability to test both DCl and HCl and a shift in the mobility would be an indication of the deacetylation of chitosan. Samples were kept in the sample tray (set at 60 °C) during the course of the kinetic experiment. The PACE results show an insignificant difference in the extent of chitosan dissolution between 50 mM HCl in water and 50 mM DCl in D_2O (Fig. 2-7, S2-9). Further, the peak area of both samples does not significantly change over the course of the kinetics after reaching a plateau at 7 h (within experimental error). This is quicker than the 10 h needed for the plateau to be observed in NMR spectroscopy. This might be due to strong intramolecular interactions persisting in the chitosan macromolecules between 7 and 10 h dissolution (this might be related to the tendency towards blocks of *N*-acetyl-D-glucosamine units).

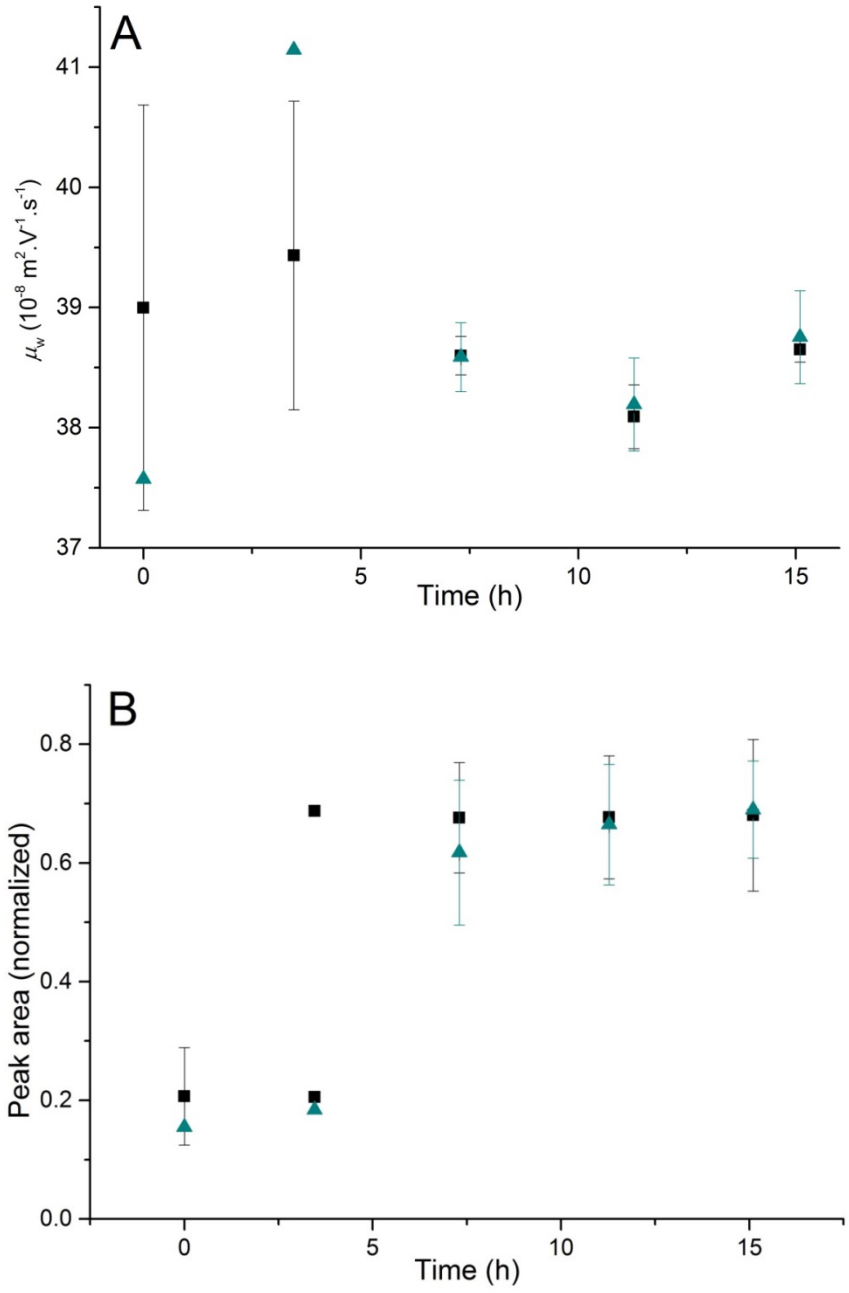

Figure 2-7. A. Weight-average mobility μ_w and B. Integral of chitosan peak in kinetics of dissolution monitored with PACE in 50 mM HCl in water (black squares) and DCl in D_2O (green triangles).

The deacetylation of chitosan at 60 °C in 50 mM DCl in D2O was detected in solution-state NMR spectroscopy and it was observed to occur almost immediately. This should correspond in PACE to a shift to higher electrophoretic mobility because of the higher charge [5] as well as a decrease in peak area since the main chromophore of the chitosan should be the acetamide functional group. However, the evidence of deacetylation was not detected in the PACE results: the electrophoretic mobility remains constant throughout the dissolution apart from the first 5 h in which aggregation affects the dissolution and the peak area of the chitosan dissolved in both aqueous solvents remained constant after reaching a plateau after 7 h (Fig. 2-7). In both cases, the dissolution as well as the deacetylation contribute: some low DA chitosan chains may dissolve a lot quicker than the high DA ones (before the first measurement). The dissolution may thus lead to a shift to lower mobility during the dissolution and this may counterbalance the shift to higher mobility due to deacetylation. A similar effect would be observed on peak area. The absence of mixing of the sample in PACE compared to the rotation of the NMR tube might lead to a lower difference in rate of deacetylation in both systems, but this was not observed in the case of the dissolution. It can be hypothesized through the comparison of the NMR and CE results that higher *DA* chitosan chains dissolve quicker and that, at least in DCl, deacetylation of chitosan takes place at a similar rate as the dissolution.

This finding is extremely significant as solution-state NMR spectroscopy is used routinely for the molecular characterization of chitosan especially for *DA* measurements (Table S2-4). These measurements often use DCl as the methyl from any residual CHD_2COOD in CD_3COOD is likely to overlap with that of the

chitosan. DCl causes degradation and therefore inaccurate measurements are obtained. Conditions used for the solution-state NMR results obtained previously [5] are unlikely to have caused a strong deacetylation due to the short period at higher temperatures; however, the sample would not have been completely dissolved during the measurement and therefore a bias on the measurement of *DA* is clear. Further research is required on obtaining of a "true solution", however it can be concluded that solution-state NMR spectroscopy using 50 mM DCl in D_2O as a solvent yields inaccurate *DA* values.

The effect of acid on the hydrodynamic volume of chitosan was also investigated and compared in the literature [49]. It was concluded that AcOH caused acid hydrolysis when compared to malic acid through a measurement of intrinsic viscosity. This may, however, also be due to a more complete dissolution taking place when compared to malic acid as results undertaken in this study express that chitosan is complicated to dissolve even in aqueous solvents.

3.7. COMPARISON OF THE KINETICS OF DISSOLUTION OF DIFFERENT CHITOSAN SAMPLES

The dissolution of 3 different chitosan samples (MedMW1, LowMW1, HighMW) in 50 mM HCl was analyzed with PACE to compare the effect of molar mass and of *DA* on dissolution. The samples were prepared after the preconditioning of the capillary to obtain an accurate data point at the beginning of the kinetics (t_0). It was seen that the area of the peak for LowMW1, MedMW1 and HighMW reached a plateau (within experimental error) after 7.5

h (from the 3rd measurement, Fig. 2-8, S2-9 to S2-11). The peak area was corrected by the average *DA* obtained from the solid-state NMR spectroscopy measurements. The t_0 measurement of HighMW and LowMW1 had a very large signal at the same electrophoretic mobility as chitosan (Fig. S2-12). This was due to non-repeatable aggregates causing light scattering which would explain the immense absorbance. The dissolution of all 3 samples followed a similar kinetics reaching a plateau after 5 h. The samples dissolution seems to behave similarly with the exception of the t_0 of the HighMW and the LowMW1 which undergoes aggregation. The LowMW1 and MedMW1 are notably less soluble in aqueous HCl than the HighMW with approximately 35 % difference in the peak area (n=2). Low or medium molar masses are expected to lead to faster and potentially more complete dissolution than higher molar masses. It should be noted that the molar masses are of limited accuracy notably due to aggregation (as see with SEC in this work) and incomplete dissolution or deacetylation. Therefore the molar mass supplied may not be representative of the sample. More importantly, HighMW has the lowest average *DA*. A lower *DA* is known to lead to faster and more complete dissolution. Assuming the relative difference of molar mass of the three chitosan samples is true, the results signify *DA* has a greater role in dissolution than molar mass.

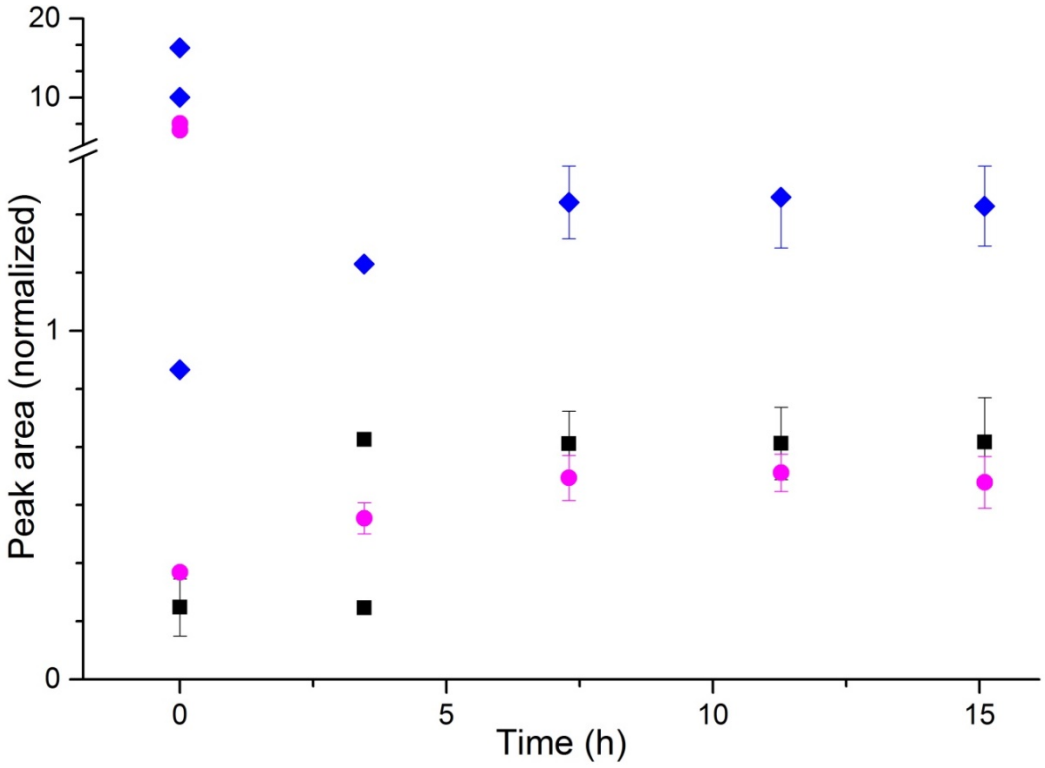

Figure 2-8. Integration of the peak area in a kinetics of dissolution of MedMW1 (black squares), LowMW1 (magenta circles) and HighMW (blue diamonds) chitosan undertaken with PACE in 50 mM HCl (n=2).

4. CONCLUSIONS

Through this study we have showed that the dissolution of chitosan is quite challenging and often overlooked. The presence of aggregates even at low concentrations of chitosan complicates the dissolution and prevents from obtaining a true solution. However, this study was able to show that aqueous AcOH was less efficient at dissolving chitosan when compared to aqueous HCl and the dissolution in aqueous TFA is as efficient only at room temperature. This information is significant due to the prominent use of AcOH in the

dissolution of chitosan for various applications, as well as characterization methods such as SEC for molar mass calculations or CE for the separation of chitosan by its *DA*. Several studies characterize the average *DA* or the molar mass of chitosan on the assumption that all the chains of chitosan are dissolved and the result obtained is representative of the whole sample [11]. A study undertaken to analyze the *DA* of chitosan and its distribution by SEC concluded that the characterization in solution may have been impeded by artifacts [50]. These artifacts could, however, have been the presence of aggregates due to the use of AcOH as a solvent as identified in a later study [18]. Due to the presence of aggregates and the inability to remove them from the solution, it was concluded that characterization was only possible for a small number of samples. The SEC results obtained in our study further supports the presence of aggregation through the extremely large molar mass values determined. The kinetics measurements gave further information regarding the behavior of chitosan in solution and showed the increase in deacetylation caused by long periods at high temperature as well as partial deacetylation in shorter time periods. Samples with different *DA*s measured by NMR spectroscopy were successfully studied and the effects of *DA* on the dissolution were compared by PACE. The average *DA* may play a more important role in the completeness of dissolution than the molar mass. Further, time-resolved NMR spectroscopy and PACE showed that 50 mM DCl is an inappropriate solvent for chitosan due to deacetylation. Following these results, previous measurements of the average *DA* of chitosan in 50 mM DCl using solution-state NMR spectroscopy (Table S2-4), including from our team [5] should be considered very carefully and rather replaced with values obtained by solid-state NMR spectroscopy as published by others [27, 28] and as obtained in this work. Future work should focus on

improving the solubility while minimizing the degradation and this may involve the use of salts as a hydrogen bond disruptor as in the cases of cellulose [51] and starch [8] or the use of ionic liquids [52]. The stability of chitosan in simulated gastric fluid (SGF) and simulated intestinal fluid (SIF) could also be analyzed to help assess the use of chitosan as a drug delivery agent.

ACKNOWLEDGEMENTS

JJT thanks Matthew Van Leeuwen (WSU) for assistance in the laboratory, Alison Maniego (WSU), Michelle Toutounji (WSU) and Lucie Seiler (University Paul Sabatier, Toulouse, France) for assistance with NMR spectroscopy data treatment, and the Australian Government for the Endeavour Research Fellowship to travel to the Max Planck Institute for Polymer Research, Mainz, Germany. MG and PC thank the Molecular Medicine Research Group at WSU for Research Seed Funding. We thank Robert Graf (MPIP), Michael O'Connor (WSU) and Richard Wuhrer (AMCF, WSU) for insightful discussions, Malvern Instruments and ATA Scientific, especially Bryn McDonagh, for the loan of a Triple Detector Array SEC, as well as and Magritek, especially Mitchell Goshert, Peter Hulmston and Andrew Coy, for the loan of a benchtop NMR spectrometer.

REFERENCES

[1] S. Trombotto, C. Ladaviere, F. Delolme, A. Domard, Chemical preparation and structural characterization of a homogeneous series of chitin/chitosan oligomers, Biomacromolecules, 9 (2008) 1731-1738.

[2] M. Rinaudo, Chitin and chitosan: Properties and applications, Prog. Polym. Sci., 31 (2006) 603-632.

[3] A. Domard, A perspective on 30 years research on chitin and chitosan, Carbohydr. Polym., 84 (2011) 696-703.

[4] Z. Li, M. Leung, R. Hopper, R. Ellenbogen, M. Zhang, Feeder-free self-renewal of human embryonic stem cells in 3D porous natural polymer scaffolds, Biomaterials, 31 (2010) 404-412.

[5] M. Mnatsakanyan, J.J. Thevarajah, R.S. Roi, A. Lauto, M. Gaborieau, P. Castignolles, Separation of chitosan by degree of acetylation using simple free solution capillary electrophoresis, Anal. Bioanal. Chem., 405 (2013) 6873-6877.

[6] G. Lamarque, C. Viton, A. Domard, Comparative study of the first heterogeneous deacetylation of alpha- and beta-chitins in a multistep process, Biomacromolecules, 5 (2004) 992-1001.

[7] A. Einbu, K.M. Varum, Characterization of chitin and its hydrolysis to GlcNAc and GlcN, Biomacromolecules, 9 (2008) 1870-1875.

[8] S. Schmitz, A.C. Dona, P. Castignolles, R.G. Gilbert, M. Gaborieau, Assessment of the Extent of Starch Dissolution in Dimethyl Sulfoxide by 1H NMR Spectroscopy, Macromol. Biosci., 9 (2009) 506-514.

[9] B.A. Miller-Chou, J.L. Koenig, A review of polymer dissolution, Prog. Polym. Sci., 28 (2003) 1223-1270.

[10] C. Lefay, Y. Guillaneuf, G. Moreira, J.J. Thevarajah, P. Castignolles, F. Ziarelli, E. Bloch, M. Major, L. Charles, M. Gaborieau, D. Bertin, D. Gigmes, Heterogeneous modification of chitosan via nitroxide-mediated polymerization, 4 (2013) 322-328.

[11] C.K.S. Pillai, W. Paul, C.P. Sharma, Chitin and chitosan polymers: Chemistry, solubility and fiber formation, Prog. Polym. Sci., 34 (2009) 641-678.

[12] Y.I. Jeong, D.G. Kim, M.K. Jang, J.W. Nah, Preparation and spectroscopic characterization of methoxy poly(ethylene glycol)-grafted water-soluble chitosan, Carbohydr. Res., 343 (2008) 282-289.

[13] T.P. Kravtchenko, J. Renoir, A. Parker, G. Brigand, A novel method for determining the dissolution kinetics of hydrocolloid powders, 13 (1999) 219-225.

[14] Y. Zhang, S.K. Mallapragada, B. Narasimhan, A Novel High Throughput Method to Investigate Polymer Dissolution, 31 (2010) 385-390.

[15] A. Chojnacka, H.G. Janssen, P. Schoenmakers, Detailed study of polystyrene solubility using pyrolysis-gas chromatography-mass spectrometry and combination with size-exclusion chromatography, Anal. Bioanal. Chem., 406 (2014) 459-465.

[16] A. Chojnacka, A. Ghaffar, A. Feilden, K. Treacher, H.G. Janssen, P. Schoenmakers, Pyrolysis-gas chromatography-mass spectrometry for studying N-vinyl-2-pyrrolidone-co-vinyl acetate copolymers and their dissolution behaviour, Anal. Chim. Acta, 706 (2011) 305-311.

[17] M.W. Anthonsen, K.M. Varum, A.M. Hermansson, O. Smidsrod, D.A. Brant, Aggregates in Acidic Solutions of Chitosans detected by static Laser-Light Scattering, Carbohydr Polym., 25 (1994) 13-23.

[18] M. Yanagisawa, Y. Kato, Y. Yoshida, A. Isogai, SEC-MALS study on aggregates of chitosan molecules in aqueous solvents: Influence of residual N-acetyl groups, Carbohydr. Polym., 66 (2006) 192-198.

[19] M. Gaborieau, P. Castignolles, Size-exclusion chromatography (SEC) of branched polymers and polysaccharides, Anal. Bioanal. Chem., 399 (2011) 1413-1423.

[20] M.H. Ottoy, K.M. Varum, B.E. Christensen, M.W. Anthonsen, O. Smidsrod, Preparative and analytical size-exclusion chromatography of chitosans, Carbohydr. Polym., 31 (1996) 253-261.

[21] T. Le Saux, H. Cottet, Size-based characterization by the coupling of capillary electrophoresis to Taylor dispersion analysis, Anal. Chem., 80 (2008) 1829-1832.

[22] J.J. Thevarajah, M. Gaborieau, P. Castignolles, Separation and characterization of synthetic polyelectrolytes and polysaccharides with capillary electrophoresis, 2014 (2014) Article ID 798403.

[23] D.L. Taylor, C.J. Ferris, A.R. Maniego, P. Castignolles, M. in het Panhuis, M. Gaborieau, Characterization of Gellan Gum by Capillary Electrophoresis, 65 (2012) 1156-1164.

[24] M. Gaborieau, T. Causon, Y. Guillaneuf, E.F. Hilder, P. Castignolles, Molecular weight and tacticty of oligoacrylates by capillary electrophoresis - mass spectrometry, Aus. J. Chem., 63 (2010) 1219-1226.

[25] J.J. Thevarajah, A.T. Sutton, A.R. Maniego, E.G. Whitty, S. Harrisson, H. Cottet, P. Castignolles, M. Gaborieau, Quantifying the Heterogeneity of Chemical Structures in Complex Charged Polymers through the Dispersity of Their Distributions of Electrophoretic Mobilities or of Compositions, Anal. Chem., 88 (2016) 1674-1681.

[26] J. Chamieh, M. Martin, H. Cottet, Quantitative Analysis in Capillary Electrophoresis: Transformation of Raw Electropherograms into Continuous Distributions, Anal. Chem., 87 (2015) 1050-1057.

[27] M.H. Ottoy, K.M. Varum, O. Smidsrod, Compositional heterogeneity of heterogeneously deacetylated chitosans, Carbohydr. Polym., 29 (1996) 17-24.

[28] L. Heux, J. Brugnerotto, J. Desbrieres, M.F. Versali, M. Rinaudo, Solid state NMR for determination of degree of acetylation of chitin and chitosan, Biomacromolecules, 1 (2000) 746-751.

[29] C.R. Morcombe, K.W. Zilm, Chemical shift referencing in MAS solid state NMR, J. Magn. Reson., 162 (2003) 479-486.

[30] R. Novoa-Carballal, E. Fernandez-Megia, R. Riguera, Dynamics of Chitosan by H-1 NMR Relaxation, Biomacromolecules, 11 (2010) 2079-2086.

[31] C. Prego, D. Torres, E. Fernandez-Megia, R. Novoa-Carballal, E. Quinoa, M.J. Alonso, Chitosan-PEG nanocapsules as new carriers for oral peptide delivery - Effect of chitosan pegylation degree, J. Control. Release, 111 (2006) 299-308.

[32] E. Fernandez-Megia, R. Novoa-Carballal, E. Quiñoá, R. Riguera, Optimal routine conditions for the determination of the degree of acetylation of chitosan by 1H-NMR, Carbohydr. Polym., 61 (2005) 155-161.

[33] M. de la Fuente, B. Seijo, M.J. Alonso, Bioadhesive hyaluronan-chitosan nanoparticles can transport genes across the ocular mucosa and transfect ocular tissue, Gene Ther., 15 (2008) 668-676.

[34] Polymer Standards Service, Characterization of Chitin/Chitosan, GPC/SEC application note 10280.

[35] D. Berek, Size exclusion chromatography - A blessing and a curse of science and technology of synthetic polymers, J. Sep. Sci., 33 (2010) 315-335.

[36] D. Muller, M. Ndoumenze, J. Jozefonvicz, High-pressure size-exclusion chromatography of anticoagulant materials, J. Chromatogr., 297 (1984) 351-358.

[37] Y. Guillaneuf, P. Castignolles, Using apparent Molecular Weight from SEC in controlled/living polymerization and kinetics of polymerization, J. Polym. Sci. A Polym. Chem., 46 (2008) 897-911.

[38] M. Gaborieau, J. Nicolas, M. Save, B. Charleux, J.-P. Vairon, R.G. Gilbert, P. Castignolles, Multiple-detection size-exclusion chromatography of complex branched polyacrylates, J. Chromatogr. A, 1190 (2008) 215-233.

[39] W. Praznik, A. Huber, De facto molecular weight distributions of glucans by size-exclusion chromatography combined with mass/molar-detection of fluorescence labeled terminal hemiacetals, J. Chromatogr. B, 824 (2005) 295-307.

[40] L.T. Cherney, A.P. Petrov, S.N. Krylov, One-Dimensional Approach to Study Kinetics of Reversible Binding of Protein on Capillary Walls, Anal. Chem., 87 (2015) 1219-1225.

[41] N. Higashi, Y. Ozaki, Potential of far-ultraviolet absorption spectroscopy as a highly sensitive quantitative and qualitative analysis method for aqueous solutions, Part I: Determination of hydrogen chloride in aqueous solutions, Appl. Spectrosc., 58 (2004) 910-916.

[42] H.F. Wu, S.A. Allison, C. Perrin, H. Cottet, Modeling the electrophoresis of highly charged peptides: Application to oligolysines, J. Sep. Sci., 35 (2012) 556-562.

[43] P. Castignolles, R. Graf, M. Parkinson, M. Wilhelm, M. Gaborieau, Detection and quantification of branching in polyacrylates by size-exclusion

chromatography (SEC) and melt-state 13C NMR spectroscopy, Polymer, 50 (2009) 2373-2383.

[44] A. Dona, C.-W.W. Yuen, J. Peate, R.G. Gilbert, P. Castignolles, M. Gaborieau, A new NMR method for directly monitoring and quantifying the dissolution kinetics of starch in DMSO, Carbohydr. Res., 342 (2007) 2604-2610.

[45] M. Lavertu, Z. Xia, A.N. Serreqi, M. Berrada, A. Rodrigues, D. Wang, M.D. Buschmann, A. Gupta, A validated 1H NMR method for the determination of the degree of deacetylation of chitosan, J. Pharma. Biomed. Anal., 32 (2003) 1149-1158.

[46] K.M. Varum, M.H. Ottoy, O. Smidsrod, Acid hydrolysis of chitosans, Carbohydr. Polym., 46 (2001) 89-98.

[47] A. Einbu, K.M. Varum, Depolymerization and de-N-acetylation of chitin oligomers in hydrochloric acid, Biomacromolecules, 8 (2007) 309-314.

[48] A. Einbu, H. Grasdalen, K.M. Varum, Kinetics of hydrolysis of chitin/chitosan oligomers in concentrated hydrochloric acid, Carbohydr. Res., 342 (2007) 1055-1062.

[49] R.H. Chen, W.Y. Chen, S.T. Wang, C.H. Hsu, M.L. Tsai, Changes in the Mark-Houwink hydrodynamic volume of chitosan molecules in solutions of different organic acids, at different temperatures and ionic strengths, Carbohydr. Polym., 78 (2009) 902-907.

[50] G. Berth, H. Dautzenberg, The degree of acetylation of chitosans and its effect on the chain conformation in aqueous solution, Carbohydr. Polym., 47 (2002) 39-51.

[51] M. Kostag, T. Liebert, T. Heinze, Acetone-Based Cellulose Solvent, Macromol. Rapid Commun., 35 (2014) 1419-1422.

[52] M. Gericke, P. Fardim, T. Heinze, Ionic Liquids - Promising but Challenging Solvents for Homogeneous Derivatization of Cellulose, Molecules, 17 (2012) 7458-7502.

2.2. Supporting information

Supporting information

For

Towards a less biased dissolution of chitosan

Joel J. Thevarajah [a,b,c], *Jerikho C. Bulanadi* [a], *Manfred Wagner* [c], *Marianne Gaborieau* [a,b]*, *Patrice Castignolles* [a]

[a] Western Sydney University, School of Science and Health, Australian Centre for Research on Separation Sciences (ACROSS), Parramatta, 2150, Australia

[b] Western Sydney University, Molecular Medicine Research Group (MMRG), School of Science and Health, Parramatta, 2150, Australia

[c] Max Planck Institute for Polymer Research, 55128 Mainz, Ackermannweg 10, Germany

*Corresponding author : Marianne Gaborieau, m.gaborieau@westernsydney.edu.au

VISUAL OBSERVATION OF DISSOLUTION

A range of aqueous acids were chosen at different concentrations to assess the dissolution of chitosan at room temperature, 40 °C and 60 °C (see Tables S2-1 and S2-2).

Table S2-1: Visual evaluation of MedMW2 chitosan dissolution in various aqueous acids and sodium borate buffer at room temperature. "Yes" indicates transparency within 15 minutes.

	Concentration				
Acid	5 mM	10 mM	50 mM	1 % [a)]	5 % [a)]
Hydrochloric	No	No	Yes	Yes	-
Acetic	No	No	Yes	Yes	-
Trifluoroacetic	No	No	Yes	Yes	-
Phosphoric	-	-	No	No	No
Boric	-	-	No	No	No
Borate Buffer	-	-	No	-	-
Trifluoroacetic acid (0.3%) [a)]	-	-	No	-	-

- indicates that the experiment was not conducted

[a)] Unit was % w/v for boric acid and % v/v for the others

Table S2-2: Visual evaluation of MedMW2 chitosan dissolution at higher temperatures in various aqueous acids and sodium borate buffer. "Yes" indicates transparency after 1 hour.

Temperature	40 °C		60 °C	
Concentration	50 mM	1 %	50 mM	1 %
Phosphoric acid	Partial	Partial	Yes	Yes
Boric acid	No	No	No	No
Borate Buffer	No	-	No	-
Trifluoroacetic acid eluent	No	-	No	-

SEC OF CHITOSAN

Aqueous SEC of different chitosan samples dissolved with 3 different solvents was conducted. The pullulan-equivalent number-average and weight-average molar masses M_w and M_n were calculated.

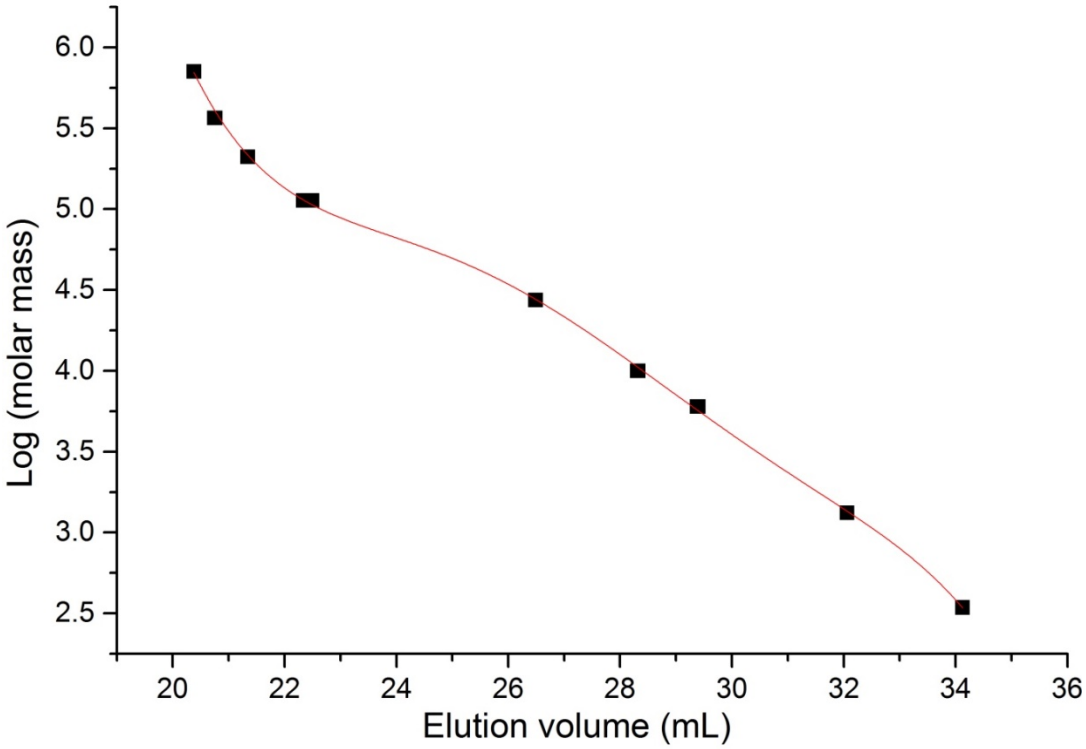

Figure S2-1: Conventional calibration curve of pullulan standards

Table S2-3: Pullulan-equivalent M_n and M_w of different chitosan samples injected at different concentrations and dissolved in different aqueous solvents (eluent is composed of 0.3 % (w/v) TFA and 0.1 M NaCl)

Sample	Solvent	Injection concentration ($g \cdot L^{-1}$)	M_n ($g \cdot mol^{-1}$)	M_w ($g \cdot mol^{-1}$)
LowMW1	50 mM HCl	1	830,000	$16{,}000 \times 10^{10}$
		1	1,100,000	$98{,}000 \times 10^{10}$
		1	960,000	$39{,}000 \times 10^{11}$
		1	950,000	$42{,}000 \times 10^{10}$
		0.5	700,000	$77{,}000 \times 10^{12}$
		0.25	950,000	$59{,}000 \times 10^{10}$
	0.3% (w/v) TFA	1	840,000	$55{,}000 \times 10^{10}$
		1	1,100,000	$76{,}000 \times 10^{10}$
		0.5	860,000	$70{,}000 \times 10^{10}$
		0.25	910,000	$17{,}000 \times 10^{10}$
	eluent	1	1,000,000	$91{,}000 \times 10^{10}$

		1	990,000	$76{,}000 \times 10^{10}$
		0.5	1,300,000	$36{,}000 \times 10^{11}$
		0.25	820,000	$17{,}000 \times 10^{11}$
LowMW2	50mM HCl	1	1,400,000	$15{,}000 \times 10^{12}$
		1	1,600,000	$32{,}000 \times 10^{11}$
		0.5	1,600,000	$91{,}000 \times 10^{14}$
		0.25	1,700,000	$90{,}000 \times 10^{10}$
MedMW1	50mM HCl	1	2,100,000	$73{,}000 \times 10^{12}$
		1	3,300,000	$65{,}000 \times 10^{11}$
		0.5	1,600,000	$57{,}000 \times 10^{12}$
		0.25	5,300,000	$62{,}000 \times 10^{13}$
	0.3% (w/v) TFA	1	1,400,000	$41{,}000 \times 10^{12}$
		1	1,600,000	$10{,}000 \times 10^{13}$
		0.5	2,100,000	$90{,}000 \times 10^{11}$

		0.25	4,200,000	57,000 × 10^{11}
	eluent	1	1,900,000	12,000 × 10^{12}
		1	1,400,000	85,000 × 10^{12}
		0.5	1,500,000	84,000 × 10^{11}
		0.25	2,300,000	19,000 × 10^{12}
MedMW4	50mM HCl	1	1,900,000	23,000 × 10^{10}
		1	2,100,000	51,000 × 10^{12}
		0.5	1,400,000	35,000 × 10^{12}
		0.25	2,000,000	37,000 × 10^{13}
MedMW2	50mM HCl	1	1,300,000	90,000 × 10^{10}
		0.5	1,900,000	13,000 × 10^{12}
		0.25	950,000	41,000 × 10^{12}
MedMW3	50mM HCl	1	3,900,000	38,000 × 10^{14}
		0.5	1,300,000	47,000 × 10^{15}

		0.25	5,400,000	$80,000 \times 10^{13}$
Fluk	50mM HCl	1	4,400,000	$65,000 \times 10^{13}$
		0.5	5,500,000	$21,000 \times 10^{12}$
		0.25	1,300,000	$66,000 \times 10^{12}$
Sig	50mM HCl	1	2,900,000	$99,000 \times 10^{11}$
		0.5	1,500,000	$48,000 \times 10^{12}$
		0.25	3,800,000	$12,000 \times 10^{12}$
HighMW	50mM HCl	1	3,600,000	$74,000 \times 10^{13}$
		0.5	3,500,000	$31,000 \times 10^{12}$
		0.25	1,600,000	$35,000 \times 10^{13}$
AKbioD1	50mM HCl	1	930,000	$25,000 \times 10^{11}$
		1	920,000	$75,000 \times 10^{12}$
		1	940,000	$51,000 \times 10^{11}$
		1	910,000	$52,000 \times 10^{11}$

		0.5	910,000	$78,000 \times 10^{10}$
		0.25	750000	$13,000 \times 10^{11}$
AKbioD2	50mM HCl	1	1,500,000	$14,000 \times 10^{11}$
		0.5	980,000	$14,000 \times 10^{11}$
		0.25	860,000	$50,000 \times 10^{11}$
AKbioD3	50mM HCl	1	1,400,000	$70,000 \times 10^{10}$
		0.5	1,000,000	$13,000 \times 10^{11}$
		0.25	2,300,000	$34,000 \times 10^{11}$
AKbioV1	50mM HCl	1	910,000	$54,000 \times 10^{10}$
		1	870,000	$40,000 \times 10^{10}$
		1	510,000	$97,000 \times 10^{10}$
		0.5	730,000	$40,000 \times 10^{9}$
		0.25	720,000	$18,000 \times 10^{11}$
AKbioV2	50mM HCl	1	2,400,000	$45,000 \times 10^{11}$

		0.5	1,900,000	$88{,}000 \times 10^{18}$
		0.25	2,900,000	$11{,}000 \times 10^{13}$
AKbioV3	50mM HCl	1	1,600,000	$12{,}000 \times 10^{13}$
		0.5	2,600,000	$29{,}000 \times 10^{12}$
		0.25	910,000	$57{,}000 \times 10^{12}$

Table S2-4: Chitosan samples not mentioned in Table 1

Sample	Supplier	Batch number	Catalogue number
HighMW2	Sigma	12913CJ	419419
MedMW3	Sigma	MKBF1336V	448877
MedMW4	Sigma	09303PE	448877
LowMW2	Sigma	06714DJ	448869
Fluk	Sigma (Fluka)	440698/1	28191

OPTIMIZATION OF PRESSURE MOBILIZATION OF CHITOSAN

Pressure mobilisation was used to assess the dissolution between samples dissolved in 50 mM HCl and AcOH. A number of optimisation steps, mainly of the background electrolyte, were required to analyse the samples.

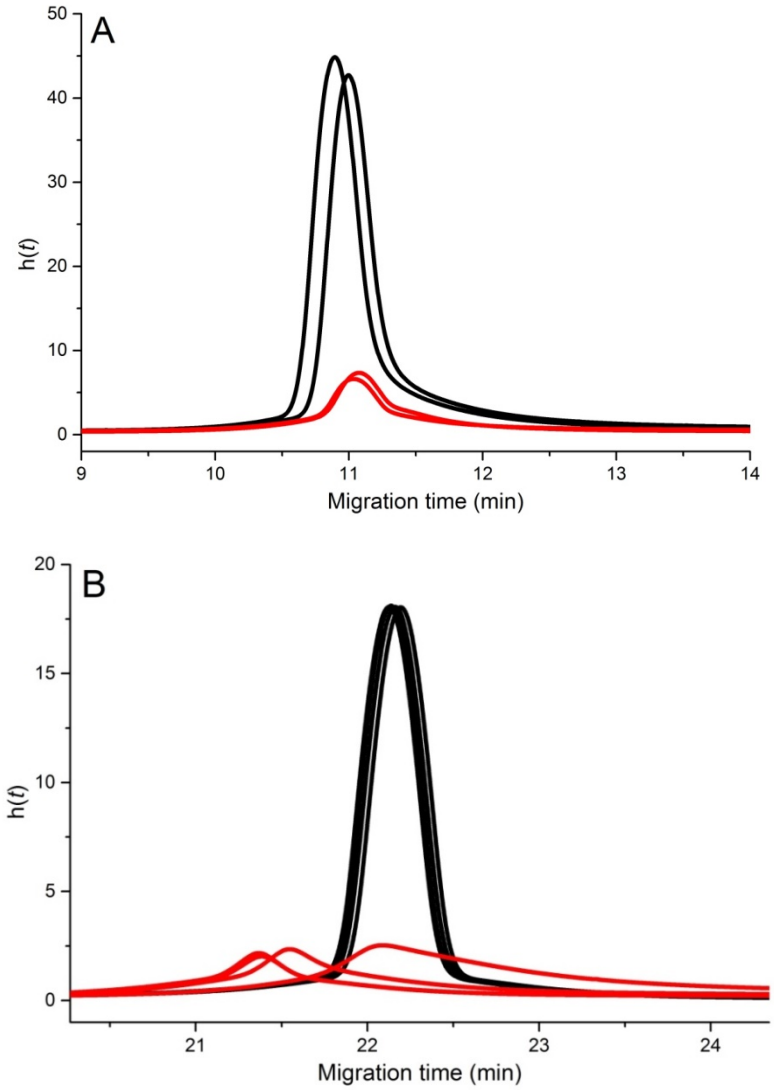

Figure S2-2: Pressure mobilisation of MedMW1 (no mixing) dissolved in 50 mM HCl (black) and AcOH (red) while the rest of the capillary contains A. phosphate buffer 100 mM pH 3 and at 25 °C B. phosphate buffer 100 mM pH 2 and at 55 °C

MIXING USING VOLTAGE

Pressure mobilization experiments used an inversion of voltage at the start of the experiment to mix the sample with the background electrolyte.

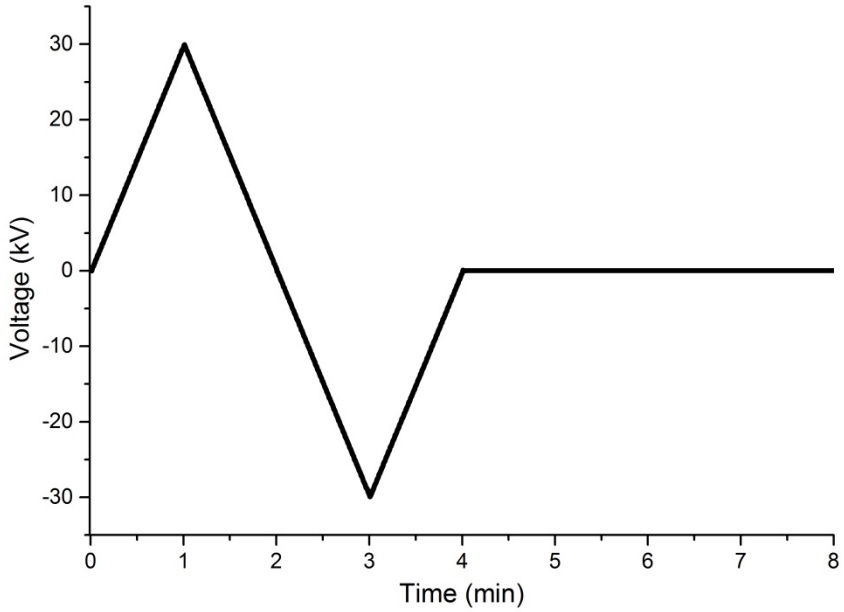

Figure S2-3: Mixing with inversion of voltage at the beginning of pressure mobilization experiments

PRESSURE MOBILIZATION OF CHITOSAN DISSOLVED IN AQUEOUS ACOH

A comparison of chitosan dissolved in AcOH using the same conditions as for chitosan dissolved in 50 mM HCl (Fig. 2) produced a narrow peak superimposed on a broader peak. Using the premixing with the electric field as described above did not separate the peak of the chitosan from that of the AcOH solution. Subtracting the peak of AcOH would introduce a large error. It was interesting to note the behavioral differences and interaction of the chitosan with the capillary in different solvents, however, the lack of separation of the narrow peak superimposed onto the chitosan peak prevents an accurate analysis of the dissolution of chitosan in AcOH. (Fig. S4).

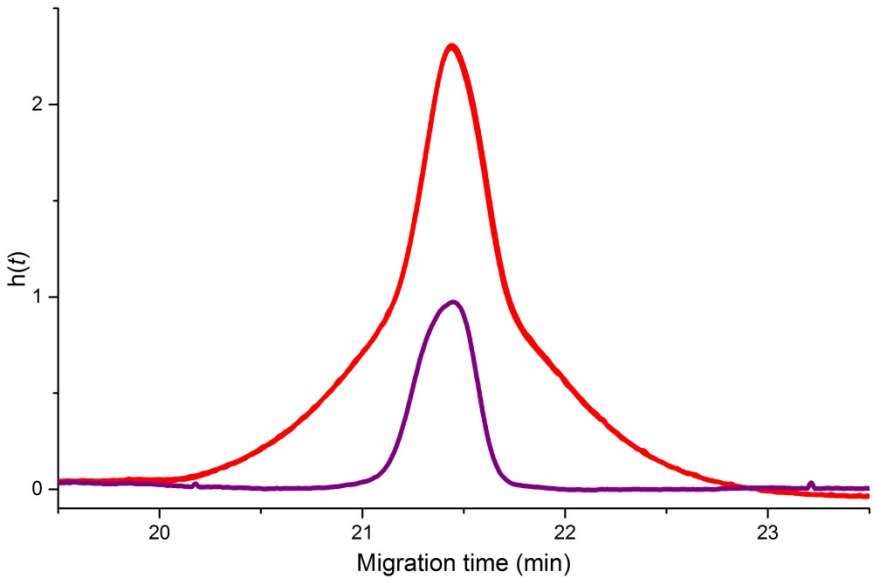

Figure S2-4: Pressure mobilisation (with mixing) of 50 mM AcOH (purple) and of MedMW1 in 50 mM AcOH (red)

NORMALIZATION BASED ON VISCOSITY

To subtract the peak assigned to Cl^-, area normalization was required. The viscosity difference between the chitosan solution and the aqueous HCl (50 mM) was taken into account. The difference between the migration of the apex of the Cl^- peak in the aqueous HCl and the Cl^- peak in the CS solution was measured and used to normalize the y-axis intensity of the Cl^- elugram based on the viscosity difference. The Cl^- peak was then subtracted from the CS elugram.

$$Normalized\ absorbance\ of\ Cl^- = \text{Absorbance of } Cl^- \times \frac{t_2}{t_1} \qquad \textbf{S2-1}$$

Where t_1 is the time at the peak apex of chitosan and t_2 is the time at the peak apex of Cl^-.

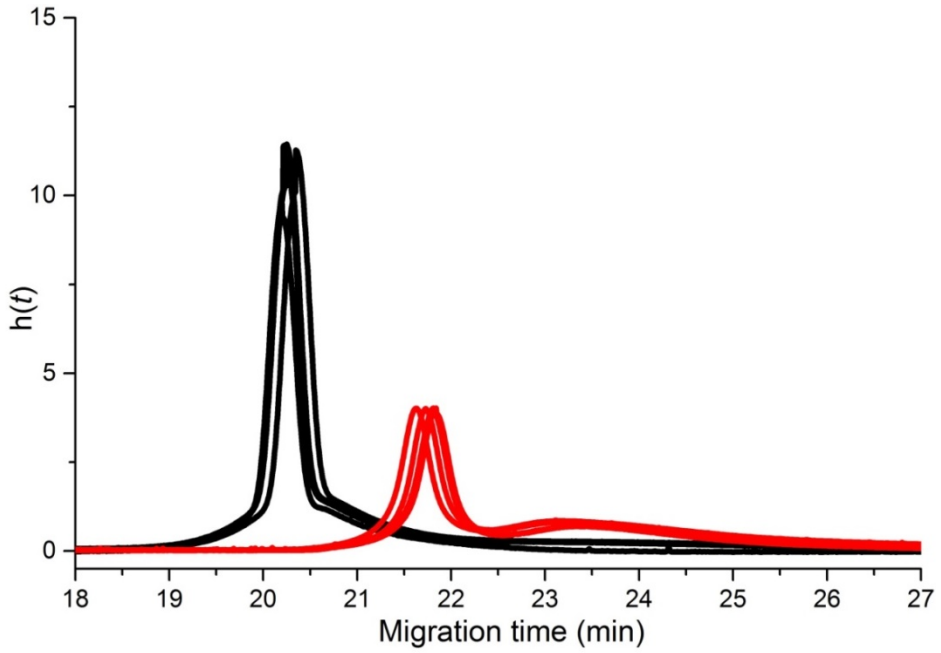

Figure S2-5: Pressure mobilization of chitosan dissolved in 50 mM HCl (4 black lines) and AcOH (4 red lines) at 55 °C and running in 50 mM HCl and 50 mM AcOH respectively.

CALCULATION OF INJECTION VOLUME FOR CE AND PM EXPERIMENTS

The injection volume V is calculated using a rearranged Poiseuille equation as follows:[1, 2]

$$V_t = \frac{\Delta P D^4 \pi}{128 \eta L} \quad \textbf{S2-2}$$

Where η is the viscosity (1.00 x 10^{-3} kg·m^{-1}·s^{-1}), L is the length of the capillary (104 cm total and effective length respectively), D is the diameter of the capillary (50 μm), ΔP is the pressure (72 mbar) and t is the injection time (10 s).

CORRECTION OF RAW DATA

For PM experiments, the y axes of the raw data needs to be time corrected with the following equation:

$$h(t) = \frac{absorbance}{time} \quad \textbf{S2-3}$$

where absorbance is the raw UV signal obtained from the CE instrument and the time is the x axes obtained from the raw data

For CE experiments both the x and y axes need to be converted to electrophoretic mobility and a weight distribution of electrophoretic mobilities respectively with the following equations:

$$\mu = \frac{l_t l_d}{V}\left(\frac{1}{t_m} - \frac{1}{t_{eof}}\right) \quad \textbf{S2-4}$$

$$W(\mu) = time \times absorbance \quad \textbf{S2-5}$$

where l_t and l_d are the length of the capillary and the length to the detector, respectively, V is the voltage, t_m is the migration time and t_{eof} is the migration time of a neutral species (electroosmotic flow).

SOLUTION-STATE NMR SPECTROSCOPY

Solution-state NMR spectroscopy measurements were conducted over 61 hours to analyze the behavior of chitosan kept at 60 °C for an extended period of time.

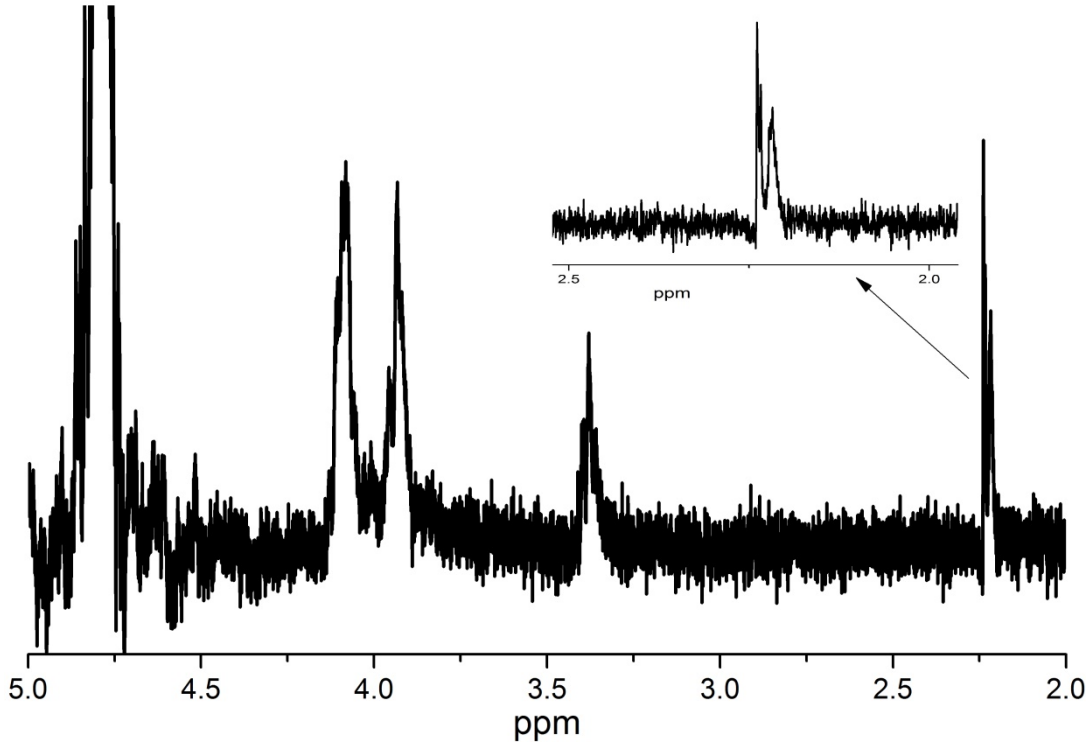

Figure S2-6. ^{1}H NMR spectrum of chitosan (MedMW1) in D_2O/DCl (50 mM) at 60 °C after several hours

KINETICS OF DEACETYLATION

If it obeyed a first order kinetics, the deacetylation of the *N*-acetyl-D-glucosamine unit would follow Eq. S2-6:

$$\frac{-d[NG]}{dt} = k[NG] \qquad \textbf{S2-6}$$

where NG is the *N*-acetyl-D-glucosamine and *t* is the time.

Eq. S2-6 can be rearranged into

$$\frac{-d[NG]}{[NG]} = k \cdot dt \qquad \textbf{S2-7}$$

which integrates into a typical first order kinetics:

$$\ln[NG] - \ln([NG]_\infty) = -kt \qquad \textbf{S2-8}$$

Since free AcOH is only created by the deacetylation of NG:

$$[AcOH] = [NG]_\infty - [NG] \qquad \textbf{S2-9}$$

Combining Eq. S2-8 and S2-9 leads to Eq. S2-10

$$\ln\left(\frac{[NG]}{[NG]_\infty}\right) = \ln\left(1 - \frac{[AcOH]}{[NG]_\infty}\right) = -\mathrm{kt} \qquad \textbf{S2-10}$$

PREVIOUS SOLUTION-STATE NMR SPECTROSCOPY EXPERIMENTS OF CHITOSAN

There are several examples of the analysis of chitosan using solution-state NMR spectroscopy. Tabulated below are the various conditions including temperature, solvent and dissolution time.

Table S2-4: Published examples of conditions for solution-state NMR spectroscopy of chitosan

Year Published, First Author	Solvent	Dissolution Time	Temperature	Reference
1996 Ottoy	1 % v/v AcOH	Overnight	Not specified	[3]
2000 Heux	DCl in D_2O (pH 4)	Not specified	Not specified	[4]
2003 Lavertu	D_2O 1.96 mL + DCl 0.04 mL	30 min	Room temperature	[5]
2014 Dahmane	2 % DCl in D_2O	1 hour	70 °C	[6]
2014 Lago	1 % CD_3COOD in D_2O	Not specified	not specified	[7]

SIGNAL ASSIGNMENT FOR ^{1}H NMR SPECTRA OF CHITOSAN

To assign the signals of the ^{1}H NMR spectroscopy kinetics, chitosan was dissolved in 50 mM DCl in D_2O for 65 h at 60 °C. The sample was measured and then spiked with 50 mM AcOH and re-measured (Fig. S2-7). The chemical shift scales were calibrated with the signal of water at 4.717 ppm at 60 °C [8].

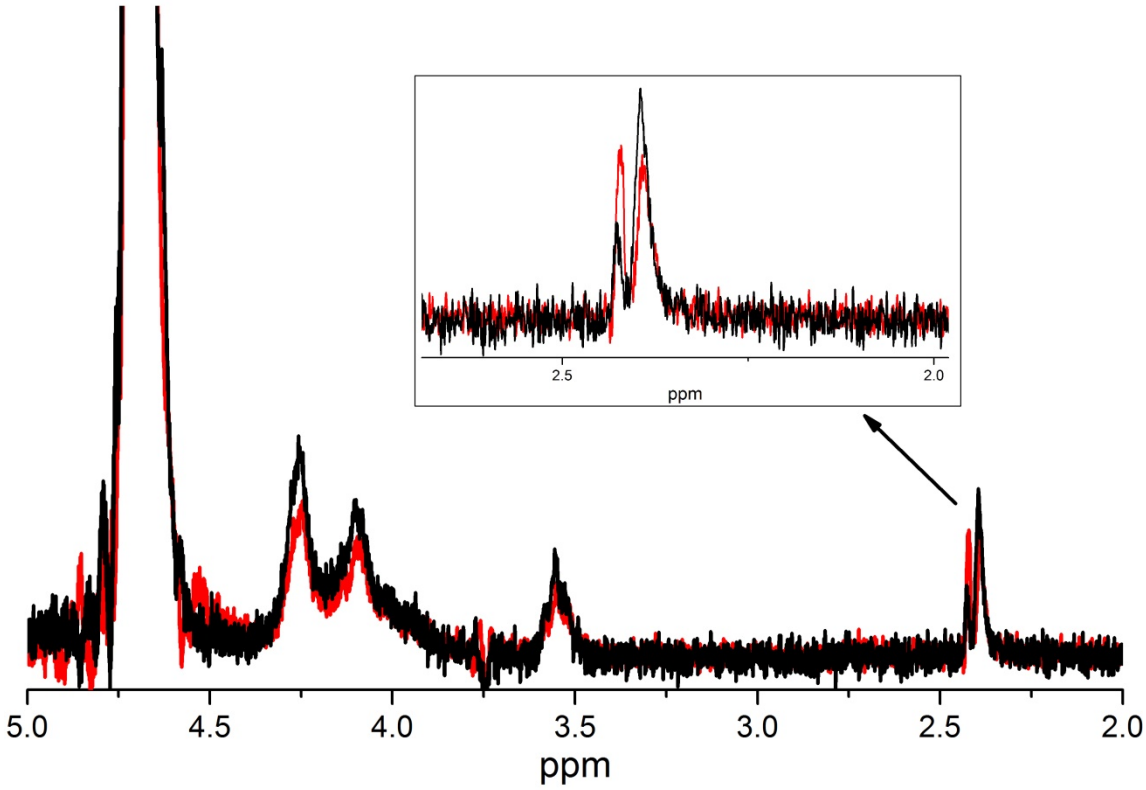

Figure S2-7. ^{1}H NMR spectrum of chitosan (black line) and chitosan spiked with 50 mM AcOH (red line) dissolved in 50 mM DCl in D_2O

MAGRITEK SPINSOLVE BENCHTOP NMR

Solution-state NMR spectra were recorded of chitosan (1 g·L^{-1}) prepared in 50 mM DCl in D_2O and 50 mM HCl.

a)

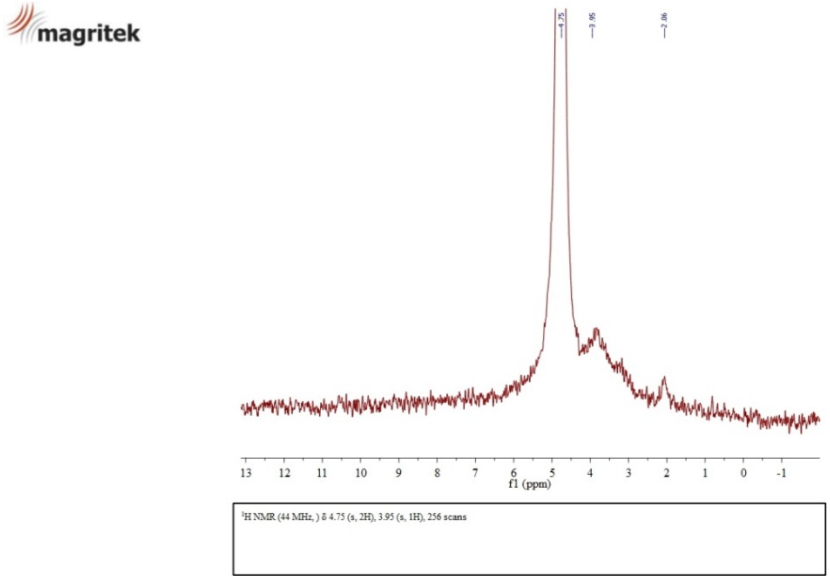

b)

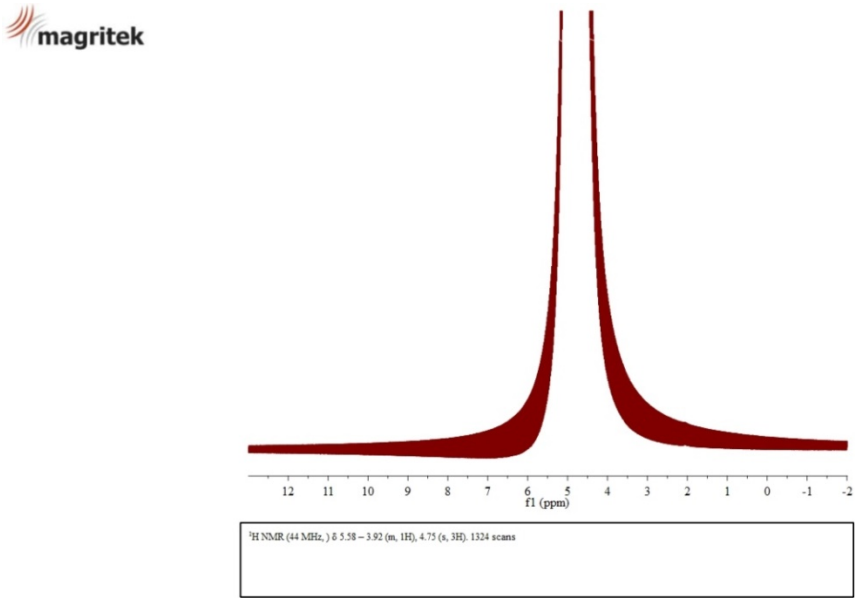

Figure S2-8. ^{1}H NMR spectrum of chitosan (MedMW1) dissolved in a) 50 mM DCl in D_2O b) 50 mM HCl

CALCULATION OF PHASING ERROR ON SOLID-STATE NMR MEASUREMENTS

The error from phasing was measured by having 4 different users phase 8 different experimental data sets. The results are presented in Table S5.

Table S2-5. Calculation of error caused by phasing of 8 different solid-state NMR spectroscopy data sets. The *DA* was measured after phasing by 4 different users.

	User - Calculated *DA* (%)						
	1	2	3	4	Average *DA*	SD	*RSD* (%)
1	9.53	10.44	8.29	8.30	9.14	1.04	11.41
2	12.09	13.21	11.34	10.56	11.80	1.13	9.56
3	6.85	6.04	6.43	6.44	6.44	0.33	5.14
4	10.27	11.65	10.37	11.07	10.84	0.65	5.97
5	3.48	2.51	2.85	3.43	3.07	0.47	15.23
6	16.34	16.47	16.43	16.51	16.44	0.07	0.45
7	14.24	1.12	1.25	14.87	14.37	0.34	2.35
8	10.73	10.50	10.56	12.36	11.04	0.89	8.05

KINETICS OF CHITOSAN DISSOLUTION USING PACE

The dissolution of chitosan (MedMW1) over time in either 50 mM HCl or 50 mM DCl in D_2O at 60 °C was compared using PACE. The dissolution of different chitosan samples prepared in 50 mM HCl was also compared. The electrophoretic mobility was corrected with both the electroosmotic flow and an additional internal standard. The area was corrected through the integral of the internal standard.

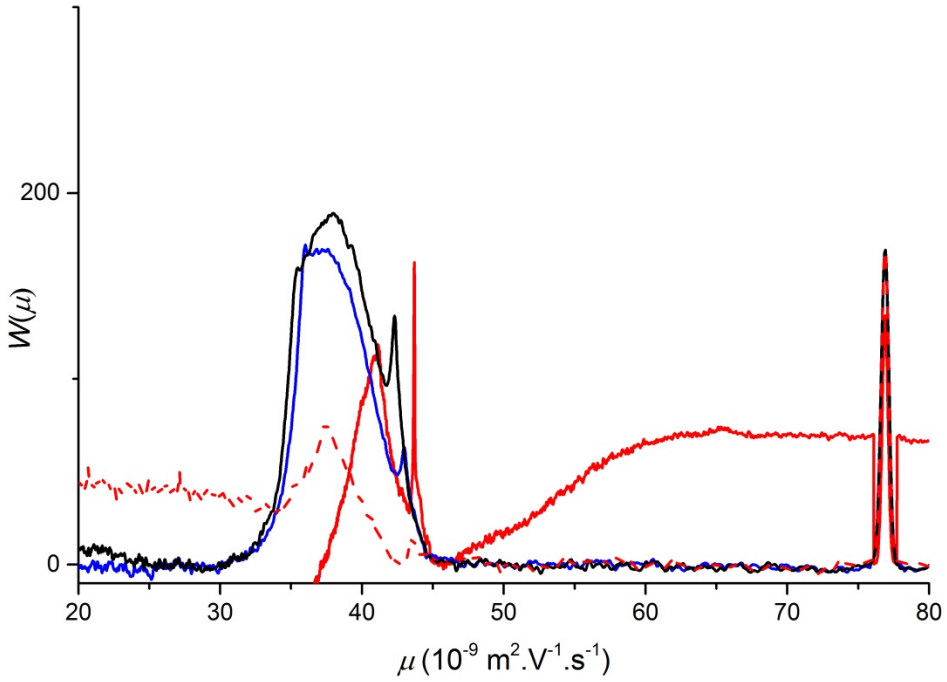

Figure S2-9. Typical electropherograms of chitosan dissolved in 50 mM DCl in D_2O over 20 hours with a dissolution time of less than 2 h (red lines), 2-10 h (blue line) and 10-20 h (black line).

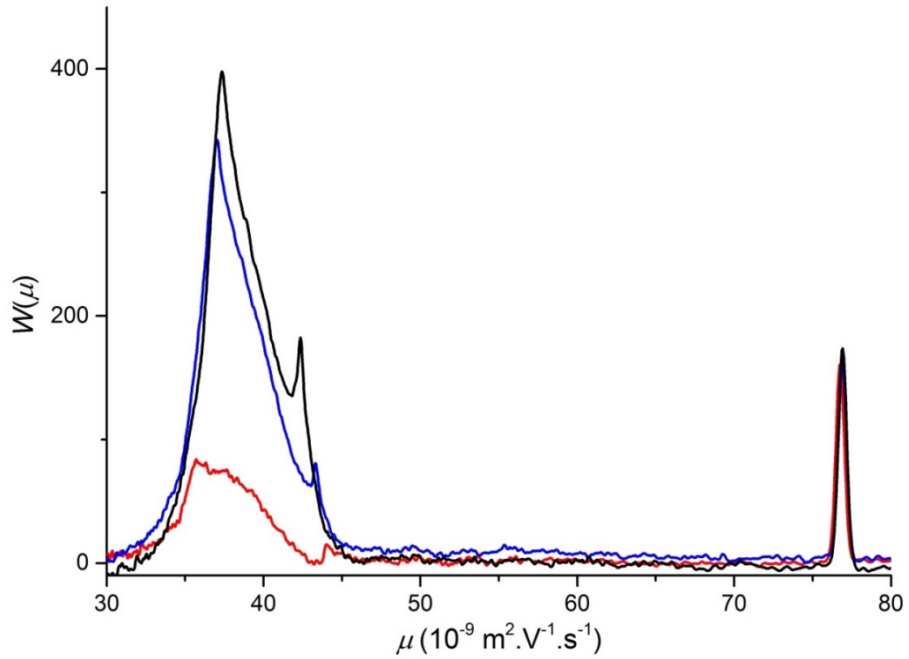

Figure S2-10. Typical electropherograms of MedMW1 chitosan dissolved in 50 mM HCl over 20 hours with a dissolution time of less than 2 h (red line), 2-10 h (blue line) and 10-20 h (black line).

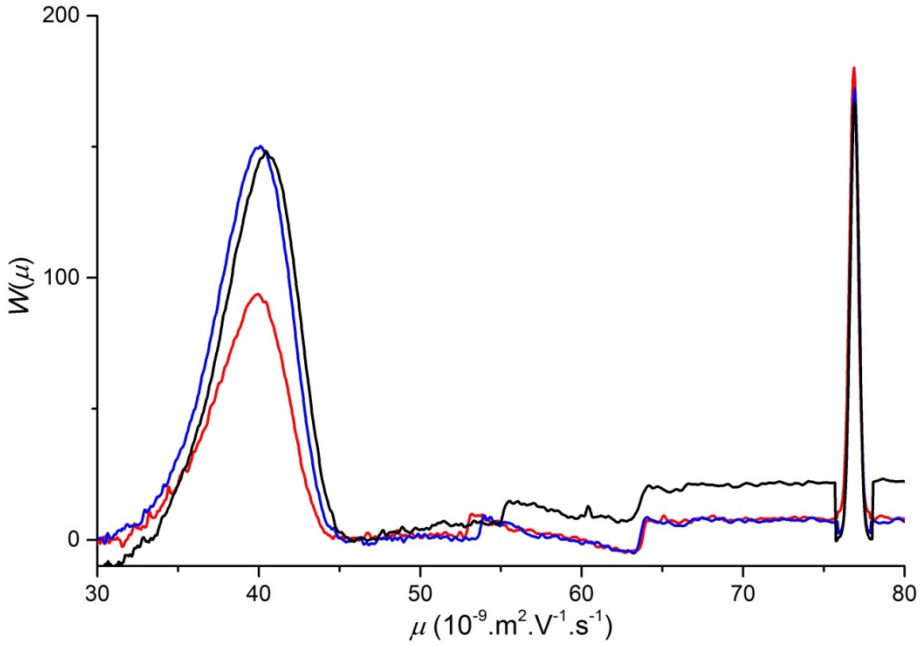

Figure S2-11. Typical electropherograms of LowMW1 chitosan dissolved in 50 mM HCl over 20 hours with a dissolution time of less than 2 h (red line), 2-10 h (blue line) and 10-20 h (black line).

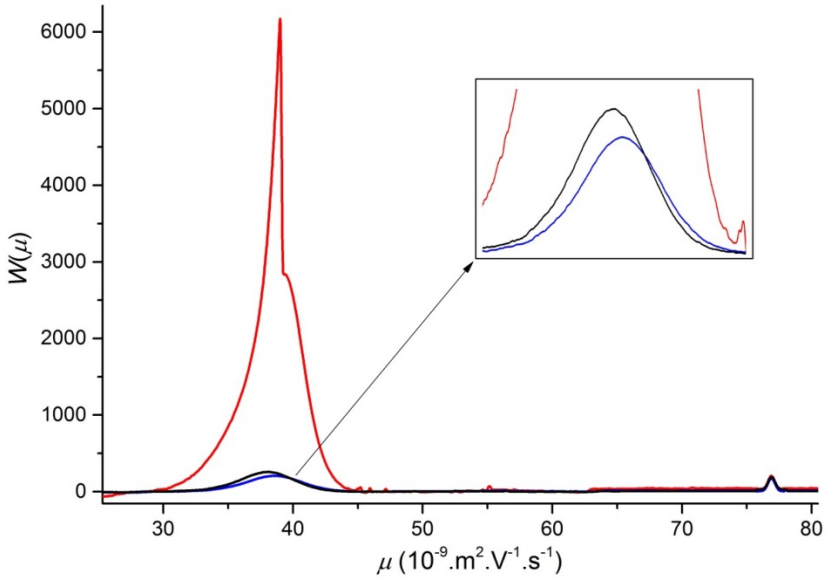

Figure S2-12. Typical electropherograms of HighMW Par1 chitosan dissolved in 50 mM HCl over 20 hours with a dissolution time of less than 2 h (red line), 2-10 h (blue line) and 10-20 h (black line).

REFERENCES

[1] G. Taylor, Dispersion of Soluble Matter in Solvent Flowing Slowly through a Tube, Proc. Royal Soc. London A Math. Phys. Sci., 219 (1953) 186-203.

[2] R. Aris, On the Dispersion of a Solute in a Fluid flowing through a Tube, Proceedings of the Royal Society of London Series a-Mathematical and Physical Sciences, 235 (1956) 67-77.

[3] M.H. Ottoy, K.M. Varum, O. Smidsrod, Compositional heterogeneity of heterogeneously deacetylated chitosans, Carbohydr. Polym., 29 (1996) 17-24.

[4] L. Heux, J. Brugnerotto, J. Desbrieres, M.F. Versali, M. Rinaudo, Solid state NMR for determination of degree of acetylation of chitin and chitosan, Biomacromolecules, 1 (2000) 746-751.

[5] M. Lavertu, Z. Xia, A.N. Serreqi, M. Berrada, A. Rodrigues, D. Wang, M.D. Buschmann, A. Gupta, A validated 1H NMR method for the determination of the

degree of deacetylation of chitosan, J. Pharma. Biomed. Anal., 32 (2003) 1149-1158.

[6] E.M. Dahmane, M. Taourirte, N. Eladlani, M. Rhazi, Extraction and Characterization of Chitin and Chitosan from Parapenaeus longirostris from Moroccan Local Sources, Int. J. Polym. Anal. Charact., 19 (2014) 342-351.

[7] M.A. Lago, R. Sendon, A.R.B. de Quiros, A. Sanches-Silva, H.S. Costa, D.I. Sanchez-Machado, H.S. Valdez, I. Angulo, G.P. Aurrekoetxea, E. Torrieri, J. Lopez-Cervantes, P. Paseiro, Preparation and Characterization of Antimicrobial Films Based on Chitosan for Active Food Packaging Applications, Food and Bioprocess Technology, 7 (2014) 2932-2941.

[8] R.E. Hoffman, Standardization of chemical shifts of TMS and solvent signals in NMR solvents, Magn. Reson. Chem., 44 (2006) 606-616.

CHAPTER 3: Publication: Quantifying the heterogeneity of chemical structures in complex charged polymers through the dispersity of their distributions of electrophoretic mobilities or compositions

3.1. Publication [126]

Quantifying the heterogeneity of chemical structures in complex charged polymers through the dispersity of their distributions of electrophoretic mobilities or of compositions

Joel J. Thevarajah[1,2], Adam T. Sutton[1,2], Alison R. Maniego[1,2], Elizabeth G. Whitty[1,2], Simon Harrisson[3], Hervé Cottet[4], Patrice Castignolles[1]*, Marianne Gaborieau[1,2]

[1]Western Sydney University, School of Science and Health, Australian Centre for Research of Separation Science (ACROSS), Parramatta NSW 2150, Australia

[2]Western Sydney University, Molecular Medicine Research Group, School of Science and Health, Parramatta NSW 2150, Australia

[3]IMRCP, UMR 5623, Université de Toulouse, 118 route de Narbonne, F-31062 Toulouse Cedex 9, France

[4]Institut des Biomolécules Max Mousseron (IBMM, UMR 5247 CNRS, Université de Montpellier, Ecole Nationale Supérieure de Chimie de Montpellier), Place Eugène Bataillon CC 1706, 34095 Montpellier Cedex 5, France

* Corresponding author : Patrice Castignolles,

p.castignolles@westernsydney.edu.au, Fax: +61 2 9685 9915

ABSTRACT: The complexity of synthetic and natural polymers used in industrial and medical applications is expanding, thus it becomes increasingly important to improve and develop methods for their molecular characterization. Free-solution capillary electrophoresis is a robust technique for the separation and characterization of both natural and synthetic complex charged polymers. In the case of polyelectrolytes free-solution capillary electrophoresis is in the "critical conditions" (CE-CC): it allows their separation by factors other than molar mass for molar masses typically higher than 20,000 g/mol. This method is thus complementary to size-exclusion chromatography (SEC). SEC is widely used to determine molar mass distributions and their dispersities. Utilizing CE-CC, an analogous calculation of dispersity based on the distributions of electrophoretic mobilities was derived and the heterogeneity of composition or branching in different polysaccharides or synthetic polymers was obtained in a number of experimental cases. Calculations are based on a ratio of moments and could thus be compared to simulations of polymerization processes, in analogy to the work performed on molar mass distributions. Among five possible types of dispersity, the most precise values were obtained with the calculation analogous with the dispersity of molar mass distribution

M_w/M_n. In addition, the dispersity value allows conclusions based on a single value: the closer the dispersity is to 1, the more homogenous the polymer is in terms of composition or branching. This approach allows the analysis of dispersity of important molecular attributes of polymers other than molar mass and aims at improving the overall molecular characterization of both synthetic and natural polymers. The dispersity can also be monitored online while performing a chemical reaction within the CE instrument.

INTRODUCTION

The accurate molecular characterization of polymers is a necessity as their production and development expands in both industry and research. This requires rigorous method development for the characterization of more complex polymers. Complex polymers can vary in a range of molecular attributes including molar mass, composition, type of copolymer, branching, charge, chain-ends. Each of these attributes exists as distribution(s) in a given sample. These distributions can vary further and be for example broad, narrow, uni- or bi-modal[1]. Therefore, the distributions of particular molecular attributes should be characterized.

Currently, the commonly assessed molecular attribute of polymers is molar mass. The heterogeneity of molar mass in a polymer sample can be assessed through determination of its dispersity typically by size-exclusion chromatography (SEC, also known as GPC)[2]. The dispersity is calculated as the weight-average molar mass divided by the number-average molar mass and most, if not all, commercial software operating SEC instruments is routinely

performing this calculation for the users. The average molar masses and the dispersity are also predicted using simulations of polymerization processes by the method of the moments.[3]

Heterogeneity is not often quantified for the other molecular attributes of polymers such as composition (of copolymers) or branching. A number of methods for separating by composition or branching exist[4]. Following the SEC separation of copolymers of methyl methacrylate and styrene a quadruple detection was implemented which included heavy reliance on the differential UV absorbance of each monomer unit[5]. It was further shown that a relation between sequence length heterogeneity and the molar mass distribution could be achieved, however, a number of conditions were required including: the intrachain interaction of the different monomers to be different to the monomers of the same type, appropriate solvation conditions for the chemical functionalities and the architecture of the copolymer should remain the same as a function of the molar mass[6]. SEC gradient was shown to be able to determine the chemical composition distribution of statistical copolymers.[7] The coupling of SEC and gradient elution liquid chromatography [8,9] was shown to be required for the analysis of both synthetic and artificial copolymers since both dimensions suffered from coelution when performed individually. The dispersity of the distribution of compositions is not determined in the literature. This may result from the absence of straightforward separation and characterization method for the composition or branching of polymers especially for hydrophilic ones, as well as from the absence of a recognized method to calculate their dispersity. SEC separates by hydrodynamic volume, which depends on molar mass as well as on composition or branching. A local

dispersity at a given hydrodynamic volume can be determined using multiple-detection SEC, which assesses the accuracy of the determined molar mass or the local heterogeneity at a given hydrodynamic volume; however, it does not directly assess the heterogeneity of the branching or composition distributions.[1,10] Various forms of liquid chromatography[11] as well as thermal field flow fractionation[12] have been shown to separate polymers according to composition or branching.

Capillary electrophoresis (CE) has been proven to be an appropriate technique for the separation of polyelectrolytes[13] and specifically the analysis of copolymers (natural[14,15] and synthetic[16,17]) and branched polymers[18,19]. Free-solution capillary zone electrophoresis of evenly charged polyelectrolytes (with regularly distributed charges along the polymer backbone) leads to analogous separations to liquid chromatography in the critical conditions (with different separation mechanisms) in which separation is not dependent on molar mass[20]. The technique free-solution capillary electrophoresis (CE) is thus defined here as the method CE in the critical conditions (CE-CC). This method allows the separation and analysis of polymers according to composition or branching as will be discussed. It further allows the distributions of these attributes to be obtained. Importantly, the determination of mass-relative distributions of electrophoretic mobilities, or of any other characteristic parameter such as chemical composition, has been recently addressed by Chamieh et al.[21]. Theoretical background required to convert the electropherogram into a distribution of electrophoretic mobilities was described with an emphasis on the fact that both x and y axes should be converted. Estimation of sample dispersity

was performed via the determination of the standard deviation (or RSD) of the samples chemical composition distribution.

We propose different expressions of the dispersity based on different moments of the distributions. In this work, they were used to estimate the dispersity of distributions obtained through CE-CC (distributions of electrophoretic mobilities and of compositions). The different types of dispersity were then compared by applying them to various natural and synthetic (co)polymers.

THEORY

DISPERSITIES OF MOLAR MASS DISTRIBUTIONS. The expressions of dispersity obtained in this paper are analogous to expressions of dispersity of molar mass distributions. Shortt[22] demonstrated that the number-, weight- and z-average molar mass, M_n, M_w and M_z, can be obtained from the ratio of moments of molar mass distributions from SEC. To calculate the dispersity of molar mass distributions, the ratio M_w/M_n is quasi-exclusively used nowadays, but the ratio M_z/M_w has also been used for example to establish relations between the radius of gyration and M_w. The dispersity calculated as M_w/M_n (eq S1) is related to the standard deviation σ through a simple expression[23]:

$$Đ - 1 = \frac{M_w}{M_n} - 1 = \frac{\sigma^2}{M_n^2} \qquad \textbf{3-1}$$

DISPERSITIES OF ELECTROPHORETIC MOBILITY DISTRIBUTIONS. In this work, weight distributions of electrophoretic mobilities (and of compositions) are considered. $W(\mu)$, the weight fraction of polyelectrolyte chains with electrophoretic mobility μ, can be obtained from a mass-sensitive detection such as UV detection of the monomer units. The number distribution

is usually not straightforward to obtain except in the case of end-labeled polymers (derivatization may be required)[24]. The number-average electrophoretic mobility is thus generally not accessible by CE and it is not possible to access it by single detection contrary to the case of molar mass averages in SEC where M_n and M_w are both determined with single-detection. In this work, ratios of moments were used to express the dispersity of electrophoretic mobility distributions (see Table S3-1 for the expression of the individual moments).

Let D($W(A)$,b,c) be the dispersity of the weight distribution of the variable A (which can be either mobility or composition), as a function of the (b-2)th, (b-1)th and bth order moments, with respect to the reference c. The general expression of the moment, $\overline{A_c^b}$, (eq 3-2) and dispersity, $D(W(A),b,c)$, (eq 3-3) is given by:

$$\overline{A_c^b} = \frac{\int_0^\infty W(A)(A-c)^b dA}{\int_0^\infty W(A) dA} \quad \textbf{3-2}$$

$$D(W(A),b,c) = \frac{\overline{A_c^b} \times \overline{A_c^{b-2}}}{[A_c^{b-1}]^2} \quad \textbf{3-3}$$

It is noted that the number-average mobility could be mathematically defined as the ratio of the 0th and the -1st order moments in analogy to molar mass distribution dispersity[22] but this does not correspond to the definition of the number-average electrophoretic mobility based on the number distribution (see supporting information, eq S3-28 and S3-29). Two reference values were used for the calculation of the moments of the distributions: either c = 0 as in the Shortt equations[22], or the weight-average mobility, c = μ_w, as for the standard deviation (SD). μ_w is determined as the ratio of the 1st and the 0th order moments of the mobility distributions:

$$\mu_w = \frac{\overline{\mu_0^1}}{\overline{\mu_0^0}} = \frac{\int W(\mu)\mu d\mu}{\int W(\mu) d\mu} \quad \textbf{3-4}$$

In the first approach, an analogy with M_w/M_n is used, and the dispersity is calculated as the ratio of 1st and 0th order moments divided by the ratio of 0th and -1st order moments. Eq 3-5 shows this dispersity with the reference (c) taken as 0:

$$D(W(\mu),1,0) = \frac{\overline{\mu_0^1} \times \overline{\mu_0^{-1}}}{[\overline{\mu_0^0}]^2} \quad \textbf{3-5}$$

In the second approach, an analogy with M_z/M_w is used, and the dispersity is calculated as the ratio of 2nd and 1st order moments (or z-average) divided by the ratio of 1st and 0th order moments (eq 3-6):

$$D(W(\mu),2,0) = \frac{\overline{\mu_0^2} \times \overline{\mu_0^0}}{[\overline{\mu_0^1}]^2} \quad \textbf{3-6}$$

In the third approach, dispersity is calculated as a ratio of 3rd and 2nd order moments divided by the ratio of 2nd and 1st order moments (eq3-7).

$$D(W(\mu),3,0) = \frac{\overline{\mu_0^3} \times \overline{\mu_0^1}}{[\overline{\mu_0^2}]^2} \quad \textbf{3-7}$$

The SD of the weight distribution of electrophoretic mobilities, taking μ_w as reference, is represented by eq 3-8:

$$D_\sigma = \left[\frac{\overline{\mu_{\mu_w}^2}}{\overline{\mu_{\mu_w}^0}}\right]^{0.5} \quad \textbf{3-8}$$

The integral expression of eq 3-3 to eq 3-8 are given as eq S3-6 to S3-13.

μ_w can be used as a reference instead of 0 similarly to the calculation for SD. However, for eq S3-3 to S3-5 never gives a finite value different from 0 (see supporting information).

Dispersities of composition distributions for copolymers. The determination of distributions of compositions from electrophoretic mobility distributions first requires establishing a correlation between the electrophoretic mobility and the composition. This can be completed using the weight-average mobility of standard samples and a complementary method to measure their average composition such as NMR spectroscopy[14]; for synthetic polymers the composition may also be estimated from the monomer concentrations used in the synthesis. The challenge faced with establishing a correlation is the requirement of having appropriate samples to cover the whole range of compositions (as for any calibration curve). Samples with particularly broad distributions such as the natural samples studied in this paper could not be studied through composition distributions without acknowledgement of the possibility of significant error caused by the calibration curve.

The (weight-average) composition C is defined as the weight of one type of monomer unit over the weight of all monomer units. Assuming a linear correlation between the electrophoretic mobility and composition[14,25,26], the weight fraction $W(C)$ of the polyelectrolyte chains with the composition C is calculated as:

$$W(C) = \frac{W(\mu)}{\mathrm{d}C/\mathrm{d}\mu} = \frac{W(\mu)}{m} \qquad \textbf{3-9}$$

where m is the slope of the calibration curve of the composition versus mobility. Linear correlation between mobility and composition is generally observed for evenly charged polyelectrolytes when charge densities are either below or above the Manning condensation threshold with a breaking slope at the condensation threshold[27,28]. The weight-average composition C_w is calculated as:

$$C_{\mathrm{w}} = \frac{\overline{C_0^1}}{\overline{C_0^0}} = \frac{\int W(C) C \mathrm{d}C}{\int W(C) \mathrm{d}C} \qquad \textbf{3-10}$$

In analogy with the dispersities of the mobility distributions, the dispersities of the composition distributions are calculated as ratios of moments using 0 as a references (eq S3-20 to S3-23).

Note that in the calculation of dispersity values for experimental cases for both mobility and composition distributions, the discrete forms were used in the software Origin for the moments (eq S3-14 to S3-17 and S3-24 to S3-27).

ESTIMATING THE UNCERTAINTY ON THE DISPERSITY VALUES. In order to compare the calculated dispersity values on different samples it is necessary to estimate the precision of their determination. The error on the dispersity values caused by the uncertainty on the electrophoretic mobility values was calculated for each type of dispersity in eq 3-5 to 3-7 (eq S3-30 to S3-32 for the derivation) using experimental data. This resulted in eq 3-11 to 3-13 for electrophoretic mobility dispersities.

$$\frac{\mathrm{d}D(W(\mu),1,0)}{D(W(\mu),1,0)} = \frac{d\mu}{\mu}\sqrt{\left(\frac{W(\mu)\mu^2}{\int W(\mu)\mu d\mu}\right)^2 + \left(\frac{W(\mu)}{\int W(\mu)\mu^{-1} d\mu}\right)^2 + 2\left(\frac{W(\mu)\mu}{\int W(\mu) d\mu}\right)^2} \qquad \textbf{3-11}$$

$$\frac{dD(W(\mu),2,0)}{D(W(\mu),2,0)} = \frac{\mathrm{d}\mu}{\mu}\sqrt{\left(\frac{W(\mu)\mu}{\int W(\mu) d\mu}\right)^2 + \left(\frac{W(\mu)\mu^3}{\int W(\mu)\mu^2 d\mu}\right)^2 + 2\left(\frac{W(\mu)\mu^2}{\int W(\mu)\mu d\mu}\right)^2} \qquad \textbf{3-12}$$

$$\frac{dD(W(\mu),3,0)}{D(W(\mu),3,0)} = \frac{\mathrm{d}\mu}{\mu}\sqrt{\left(\frac{W(\mu)\mu^2}{\int W(\mu)\mu d\mu}\right)^2 + \left(\frac{W(\mu)\mu^4}{\int W(\mu)\mu^3 d\mu}\right)^2 + 2\left(\frac{W(\mu)\mu^3}{\int W(\mu)\mu^2 d\mu}\right)^2} \qquad \textbf{3-13}$$

For the uncertainty of the dispersity of the distribution of compositions, the same expressions apply and only require the substitution of μ In addition, the error due to the calibration may play an important additional role.

The derivation of the uncertainty of the electrophoretic dispersity expressed as a SD (eq 3-8) is shown in supporting information (eq S3-36 to S3-38) and yields eq 3-14:

$$\frac{\mathrm{d}D_\sigma}{D_\sigma} = \frac{\mathrm{d}\mu}{\mu}\sqrt{0.5\left(\frac{W(\mu)(\mu-\mu_\mathrm{w})^2\,\mu}{\int W(\mu)(\mu-\mu_\mathrm{w})^2}d\mu\right)^2 + 0.5\left(\frac{W(\mu)\mu}{\int W(\mu)}d\mu\right)^2} \qquad \textbf{3-14}$$

The relative uncertainty of the electrophoretic mobility $\mathrm{d}\mu/\mu$ was taken as 1 % corresponding to the order of magnitude of the relative SD of the electrophoretic mobility for free-solution CE of polyelectrolytes[18] and sugars[29,30] (Table S3-2). The calculated relative uncertainties were shown to be lower than 4 x 10^{-6} (sometimes by orders of magnitude) which shows that the error caused by the mobility is negligible for the dispersity values calculated (Table S3-3). Although there does not seem to be a correlation between the samples and the uncertainty, it is noted that D(W(μ),1,0) seems to have the lowest uncertainty. The major contributor of the uncertainty on the dispersity value is thus not the error on the determination of μ but likely other factors such as the error in setting the baselines and the start/end limits of the integration. Therefore, six significant digits (corresponding to 5 decimal places) were considered for the dispersity values. In the case of composition distributions, a higher order of magnitude (10^{-1}-10^{-6}) for the relative uncertainty of the dispersity and of SD (10^{-6}) were calculated (Table S3-4). As mentioned previously, a significant error can be introduced through the imperfect correlation between mobility and composition for the dispersity on composition.

EXPERIMENTAL

Separation conditions were as previously described for chitosan[14], poly(sodium acrylate)/poly(sodium acrylate-*co*-*N*-antipyrine acylamide)[18] and poly(acrylic acid-*b*-acrylamide)[16].

RESULTS AND DISCUSSION

DISPERSITY OF ELECTROPHORETIC MOBILITY DISTRIBUTIONS.

The treatment of CE-CC data allows the calculation of dispersity values based on electrophoretic mobility distributions. As mentioned previously, CE-CC separates evenly charged polymers based on molecular attributes other than molar mass, provided the polyelectrolyte degree of polymerization is typically higher than 10 $g.mol^{-1}$.[20,31] Three experimental cases are presented, two based on the heterogeneity of composition and one on the heterogeneity of branching.

Chitosan. Chitosan is a polysaccharide derived from the deacetylation of chitin. It is a copolymer of *N*-acetyl-D-glucosamine and D-glucosamine in varying proportions (Figure S3-1A). Its composition is generally referred to as degree of acetylation, *DA* (the fraction of *N*-acetyl-D-glucosamine units). Being a natural product, chitosan varies in a range of molecular attributes including molar mass and composition (including the distribution of units along the chain being rather in blocks or statistical). Using CE-CC, different chitosan samples had been separated based on their *DA* and through appropriate data treatment[21] the weight distributions of the mobilities have been obtained (Figure 3-1)[14]. The heterogeneity of *DA*, which is the distribution of the compositions of different

chains within a chitosan sample, is represented by the distribution of electrophoretic mobilities.

Using eq 3-5 to 3-8 dispersity values were obtained for the different chitosan samples (Table S3-5). Dispersity values calculated as $D(W(\mu),1,0)$, $D(W(\mu),2,0)$, $D(W(\mu),3,0)$ and SD were in good agreement in terms of the trend observed (Figure 3-2). They showed an overall decreasing trend in which the chitosan samples with higher average electrophoretic mobilities (lower average *DA*s) have more narrow distributions of compositions (lower *D* values). Thus the calculation of the dispersity values provided a valid numerical demonstration of the data which was represented graphically. The lower selectivity above counter-ion condensation, at the lowest *DA*, may contribute to this trend. The trend of the dispersity with *DA* might also be due to the rate of deacetylation varying for different parts of the chitosan sample which can lead to heterogeneity and may also explain the variation in dispersity of samples between the weight-average electrophoretic mobility of 3.3 and 3.4×10^{-8} $m^2 \cdot V^{-1} \cdot s^{-1}$. This effect would be weaker at low *DA*, since the *DA* cannot (physically) go below 0. It shows the importance of the chemical treatment to which many polysaccharides are subjected in their preparation. This overall trend may not extend to other families of polymers, as seen below.

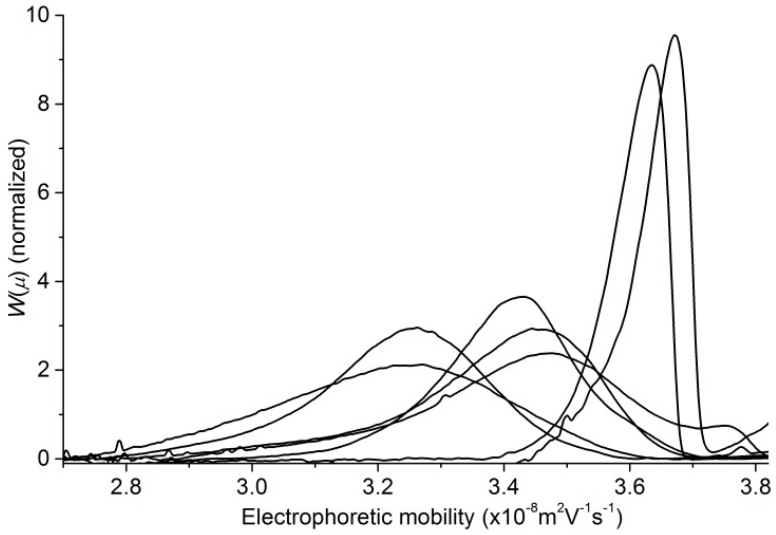

Figure 3-1. Mobility weight distributions obtained by CE-CC for chitosan samples with varying degrees of acetylation.

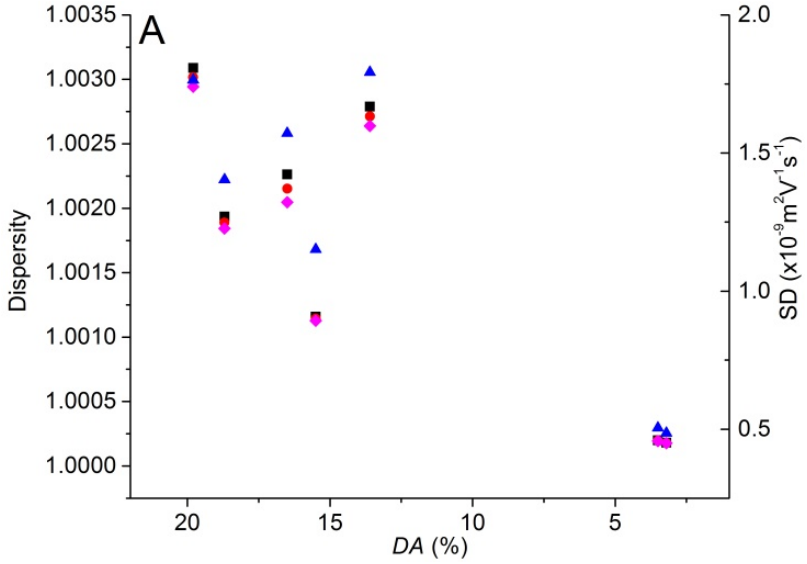

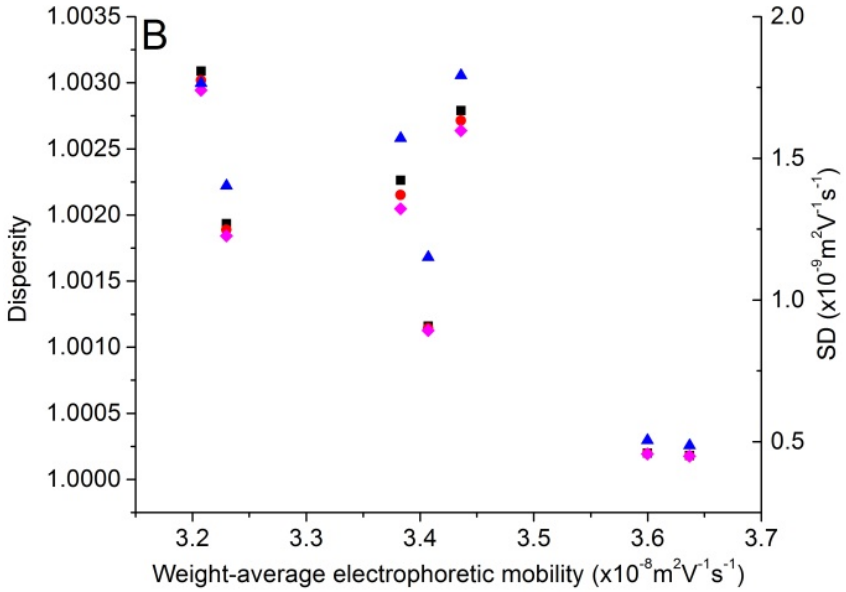

Figure 3-2. (A) Dispersity values shown for chitosan samples as $D(W(\mu),1,0)$ (red circles, eq 3-5), $D(W(\mu),2,0)$ (black squares, eq 3-6), $D(W(\mu),3,0)$ (magenta diamonds, eq 3-7) and SD (blue triangles, eq 3-8) against (A) their number average degree of acetylation, or (B) against their weight-average electrophoretic mobility.

Despite the relatively low selectivity of the separation, dispersity values calculated on the mobility distributions still allows information regarding the sample heterogeneity to be obtained.

Poly(sodium acrylate-*co*-*N*-antipyrine acrylamide), P(NaA-*co*-APA). This copolymer is synthesized using a known coupling reaction[32] between the amine of the 4-aminoantipyrine, AAP, and the carboxylate of the PNaA (Figure S3-1B). The grafting reaction was performed within a CE vial and monitored in real time using capillary electrophoresis in previously established conditions[33,34] (Figure 3-3). The increase of the copolymer peak area with reaction time is consistent with the much larger UV absorption (Beer-Lambert coefficient) for

AAP than PNaA which was calculated to be greater by a factor of almost 20 (see supporting information). The decrease of the electrophoretic mobility with grafting is consistent with both the reduced charge (loss of carboxylate units) and the increased hydrodynamic friction (increased size). As the reaction time increases the P(NaA-*co*-APA) peak becomes broader, indicating a larger heterogeneity of composition.

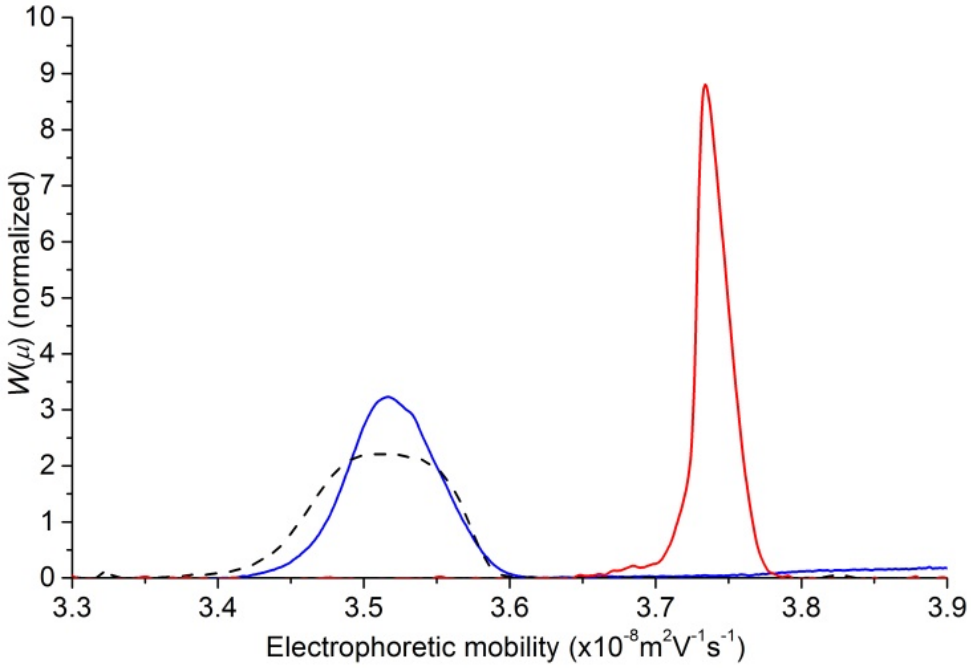

Figure 3-3. Electrophoretic mobility distributions of P(NaA-*co*-APA) samples at time 0 (red), 5 min (blue) and 4 h (black dash).

The dispersity of electrophoretic mobility of the copolymer was obtained from eq 3-5 to 3-8 (Table S3-6). The linear PNaA homopolymer was used as a reference and its dispersity subtracted from the P(NaA-*co*-APA) dispersity values. This enabled to monitor the grafting reaction and assess the heterogeneity of composition of the P(NaA-*co*-APA). The values of D($W(\mu)$,1,0),

D($W(\mu)$,2,0), $D(W(\mu),3,0)$ and SD are in good agreement in terms of the trend observed (Figure 3-4). They increase reaching a maximum at approximately 4 h. The dispersity allows a numerical representation of the change in composition. The heterogeneity of the copolymer increases during the first 4 h, as most of the grafting proceeds. The reaction then slows down and it might lead to a more homogenous copolymer.

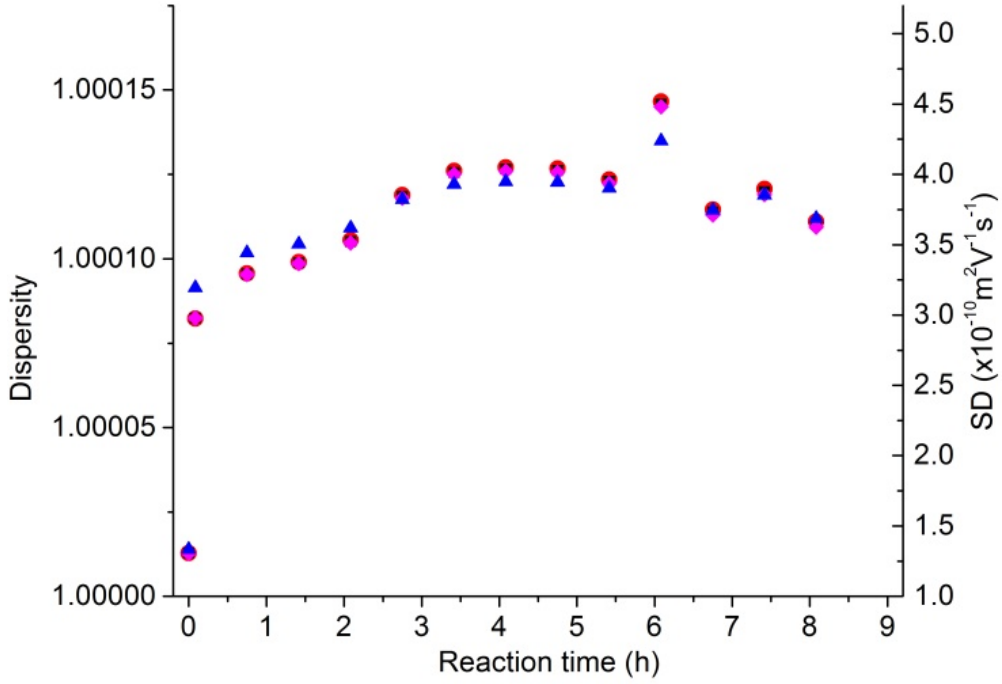

Figure 3-4. Dispersity values shown for P(NaA-*co*-APA) samples as $D(W(\mu),1,0)$ (black square, eq 3-5), $D(W(\mu),2,0)$ (red circle, eq 3-6), $D(W(\mu),3,0)$ (magenta diamonds, eq 3-7) and SD (blue triangle, eq 3-8) against reaction time.

Branched poly(sodium acrylate), PNaA. This synthetic polymer (Figure S3-1C) is industrially produced using conventional polymerization; in this study it was synthesized using a controlled radical polymerization: nitroxide-mediated polymerization (NMP)[35]. The occurrence of branching in PNaA has been noted[36]

and it is an important factor which can be overlooked in PNaA characterization. The branching of PNaA can be used to tailor polymers for specific applications through the choice of an appropriate polymerization technique. CE-CC was shown to separate different PNaA samples based on their branching (Figure 3-5)[18].

Dispersity values were obtained for the 3 samples (Figure 3-6, Table S3-7). It is to be noted that the linear sample does not have any branching since it has been obtained by anionic polymerization[18] and thus the broadness of the peak results from intrinsic experimental factors. Considering the dispersity values are representative of the heterogeneity of branching, the linear (which had the lowest dispersity value and the highest mobility) and the hyperbranched (at a weight-average mobility of 3.53×10^{-8} $m^2 \cdot V^{-1} \cdot s^{-1}$) samples have dispersity values which are quite close (and low). As expected due to its branching architecture, 3-arm star had the highest dispersity and the lowest mobility. This is because although the hyperbranched sample is more branched than 3-arm star it was designed to have a homogenous branching through the use of an inimer for its synthesis.

Similar samples synthesized from different monomers were analyzed with the same method (Figure 3-5b). PNaA samples synthesized by the NMP of acrylic acid and of *tert*-butyl acrylate (*t*BA) had different distributions and dispersities. It is to be noted that different end-groups[18] can also contribute to the heterogeneity of the electrophoretic mobility distribution.

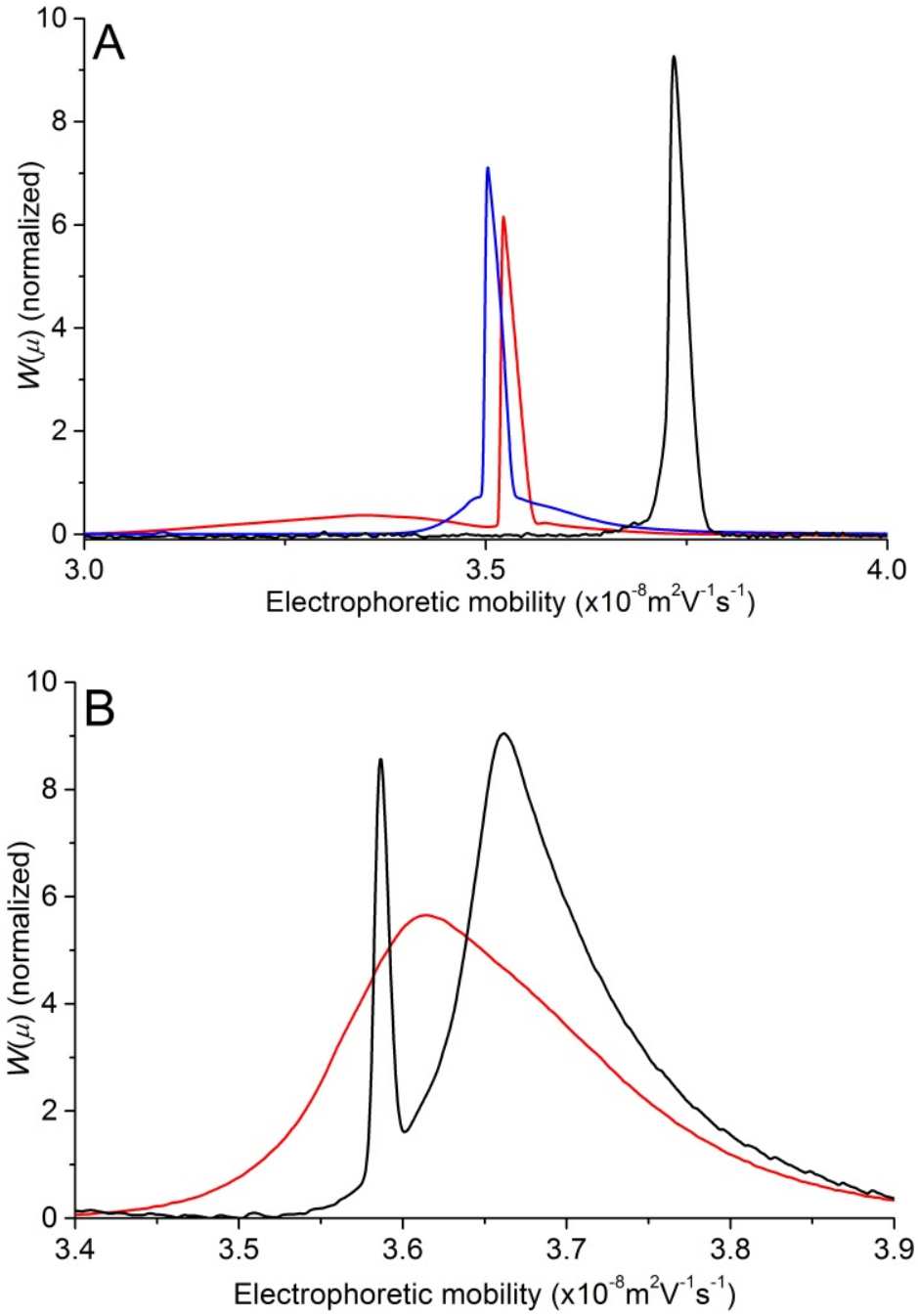

Figure 3-5. Electrophoretic mobility distributions of PNaA samples. (A) PNaAs with different topologies: linear injected at a lower concentration than previously[18] (black), 3-arm star (red) and hyperbranched (blue). (B) PNaAs synthesized by NMP of acrylic acid (black) and *tert*-butyl acrylate (red).

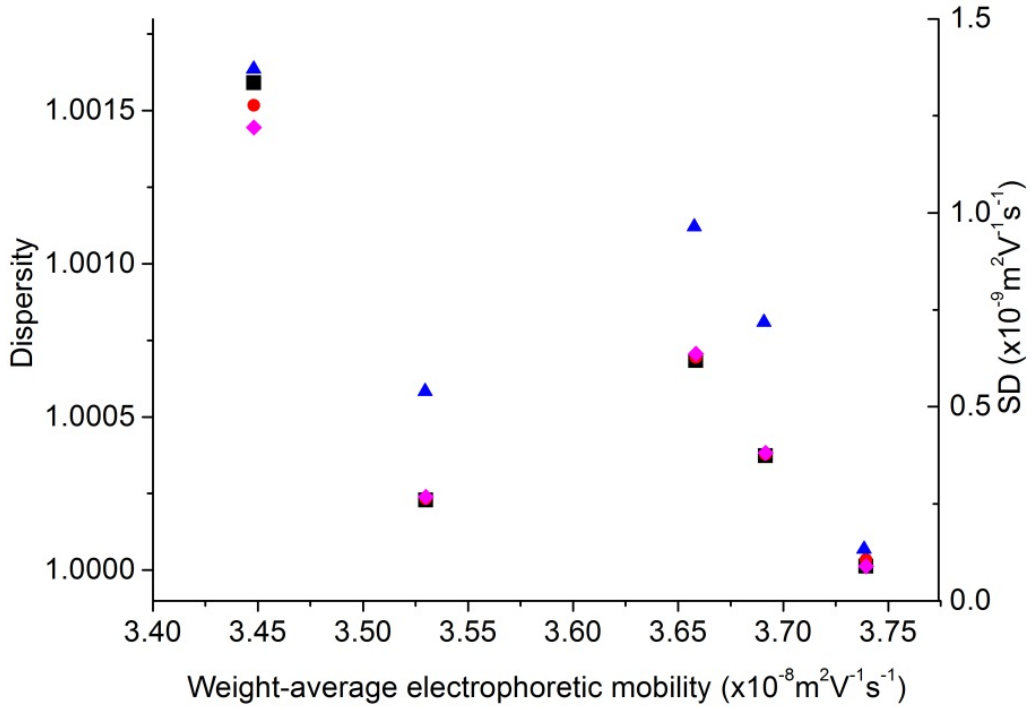

Figure 3-6: Dispersity values shown for PNaA samples as $D(W(\mu),1,0)$ (black square, eq 3-5), $D(W(\mu),2,0)$ (red circle, eq 3-6), $D(W(\mu),3,0)$ (magenta diamonds, eq 3-7) and SD (blue triangle, eq 8) against their weight-average electrophoretic mobility. The samples in increasing order of average electrophoretic mobility are 3-arm star (3.45×10^{-8} $m^2\cdot V^{-1}\cdot s^{-1}$), hyperbranched ($3.53\times10^{-8}$ $m^2\cdot V^{-1}\cdot s^{-1}$), NMP of *t*-BA ($3.66\times10^{-8}$ $m^2\cdot V^{-1}\cdot s^{-1}$),NMP of AA ($3.69\times10^{-8}$ $m^2\cdot V^{-1}\cdot s^{-1}$) and linear ($3.74\times10^{-8}$ $m^2\cdot V^{-1}\cdot s^{-1}$).

Dispersity of composition distributions

Poly(acrylic acid-*b*-acrylamide), P(AA-*b*-AM) block copolymers were synthesized by Reversible-Addition Fragmentation chain Transfer/Macromolecular Design via Interchange of Xantates (RAFT/MADIX) polymerization. Using CE-CC the block copolymers could be separated (Figure 3-7)[16]. The P(AA-*b*-AM) was synthesized with different ratios of the monomers (2K and 10K in the sample name refer to 2,000 and 10,000 $g.mol^{-1}$ theoretical molar mass of the corresponding block). The electrophoretic mobility

distributions were simple to obtain as shown previously, extra treatment was required to obtain composition distributions.

The separation of P(NaA-*b*-AM) using CE-CC is dependent on both the charge of the PNaA monomer units and the hydrodynamic friction of the charged PNaA and uncharged PAM blocks. Therefore, to obtain meaningful composition distributions, both the charged and uncharged blocks of the block copolymer need to be taken into account (eq S3-38, S3-39). However, the necessary rescaling factor α is challenging to obtain (see supporting information). The weight average composition of both samples was determined from the theoretical values of the uncharged and charged block lengths. Dispersity values were obtained for the distributions of both mobilities and compositions (Table S3-8).

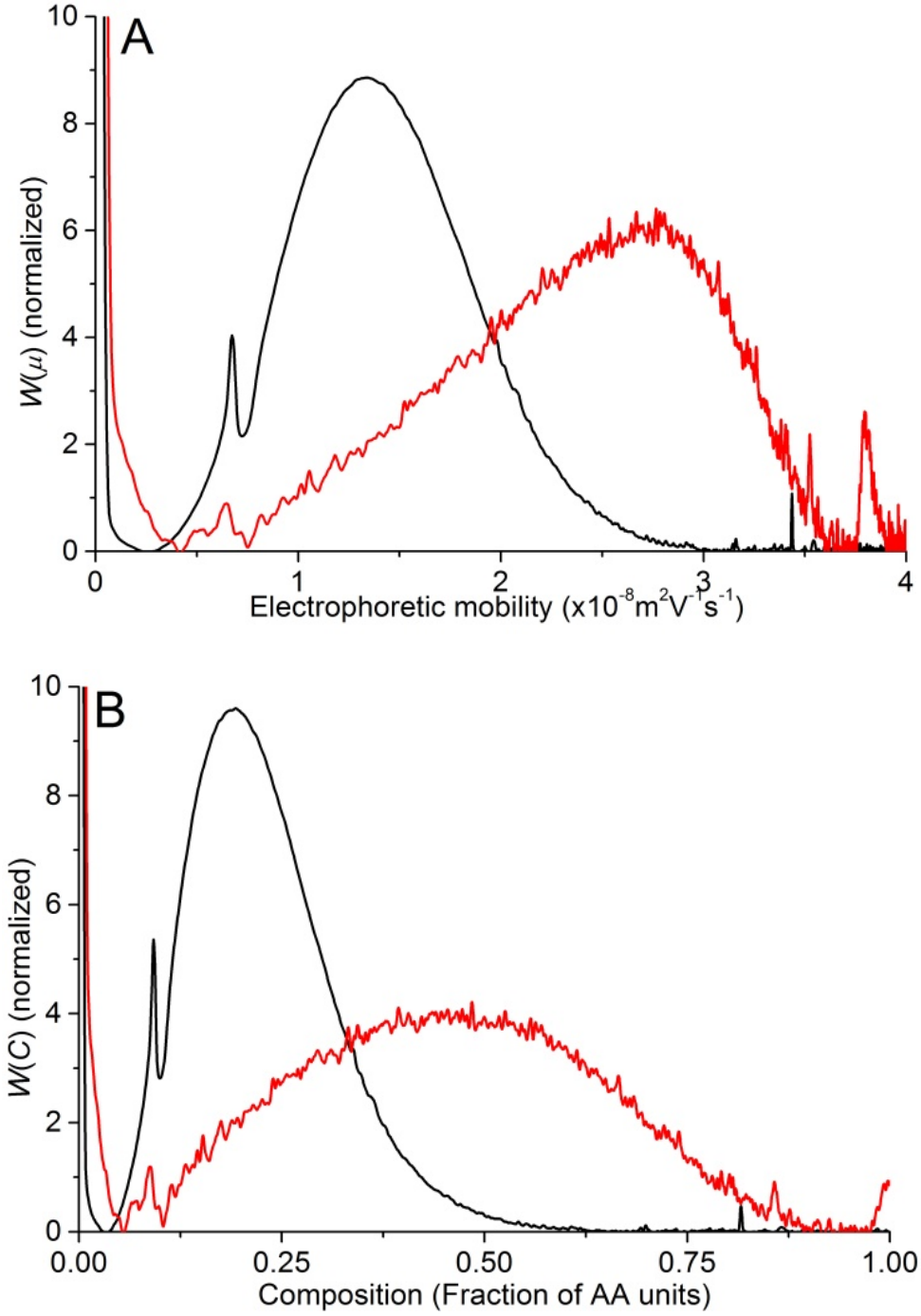

Figure 3-7. (A) Electrophoretic mobility distribution and (B) composition distribution of P(NaA-*b*-AM) samples: PAA2kPAM10k (black) and PAA10kPAM10k (red). The theoretical M_n values were listed for each sample previously[16].

The accuracy of the composition distributions of P(AA-*b*-AM) and of their dispersity depends on the accuracy of α[16] (eq S3-39) and of the correlation between electrophoretic mobility and composition. In the case of statistical copolymers α would not need to be calculated and therefore the accuracy of the composition distribution would depend only on the correlation mobility and composition. The larger uncertainty obtained for dispersities of composition distributions (Table S3-4) compared to that of electrophoretic mobility distributions (Table S3-3) is likely due to a weak correlation between mobility and composition (despite the high selectivity in this case). In some cases a complementary method such as NMR spectroscopy could be used to obtain the average composition of specific samples, thus allowing a more accurate α to be obtained.

CONCLUSIONS

In this study both synthetic and natural polymers were characterized. The distributions of compositions and the heterogeneity of branching were analyzed using the dispersity of the distributions. Using the correct treatment of CE-CC data, the dispersity was quantified, including the monitoring of grafting on polymers. Further, using the dispersity values a numerical representation of the mobility and composition distributions were calculated and allowed comparisons between samples. Dispersity values using 0 as a reference were in good agreement with SD calculations in terms of trends observed. With further research dispersity values obtained through CE-CC can be used as commonly as molar mass dispersity values. Dispersity values calculated using D_σ and $D(W(\mu),1,0)$ were in good agreement. The dispersity values obtained in this

work are closer to unity than typical values obtained on molar mass dispersity by SEC. It is however, to be noted that SEC overestimates $Đ$ and this largely due to band broadening[37,38]. Temperature gradient interaction chromatography[39] and molecular radius analysis with multi-angle light scattering combined with SEC[40] were shown to reduce this effect. In analogy to SEC characterization of molar mass distributions of polymers, we recommend $D(W(\mu),1,0)$ to quantify the heterogeneity due to either composition (copolymers) or branching. However, the three different types of quantification of the dispersity should be further compared, especially in the cases of non-symmetric distributions (with a tail) or bimodal distributions. It would also be very interesting to compare the CE method established in obtaining composition distributions with other methods, typically based on liquid chromatography[41]; however, this has been noted as tedious[42] or was not attempted yet for hydrophilic polymers. Field-flow fractionation, especially thermal[12] may provide very interesting comparisons. In addition, simulation of polymerization processes should allow the prediction of $D(W(\mu),1,0)$ and the results can be compared with the values determined by CE-CC.

ACKNOWLEDGEMENTS

The authors would like to thank Matthew Van Leeuwen, Michelle Toutounji (Western Sydney University) and Aidan Grosas (Australian National University) for insightful discussions. JJT thanks the Australian Government for the Endeavour Research Fellowship to visit the University of Montpellier.

SUPPORTING INFORMATION. Derivation and expressions of moments, dispersity, and uncertainty; dispersity values for experimental; molar absorptivity and rescaling factor determination.

REFERENCES

(1) Berek, D. *J. Sep. Sci.* 2010, *33*, 315-335.
(2) Gilbert, R. G.; Hess, M.; Jenkins, A. D.; Jones, R. G.; Kratochvil, R.; Stepto, R. F. T. *Pure Appl. Chem.* 2009, *81*, 779-779.
(3) Zabisky, R. C. M.; Chan, W. M.; Gloor, P. E.; Hamielec, A. E. *Polymer* 1992, *33*, 2243-2262.
(4) Philipsen, H. J. A. *J. Chromatogr. A* 2004, *1037*, 329-350.
(5) Haidar Ahmad, I. A.; Striegel, A. M. *Anal. Bioanal. Chem.* 2010, *396*, 1589-1598.
(6) Haidar Ahmad, I. A.; Striegel, D. A.; Striegel, A. M. *Polymer* 2011, *52*, 1268-1277.
(7) Maier, H.; Malz, F.; Radke, W. *Macromol. Chem. Phys.* 2015, *216*, 228-234.
(8) Reingruber, E. M.; Chojnacka, A.; Jellema, E.; de Bruin, B.; Buchberger, W.; Schoenmakers, P. J. *J. Chromatogr. A* 2012, *1255*, 259-266.
(9) Shakun, M.; Heinze, T.; Radke, W. *Carbohydr. Polym.* 2015, *130*, 77-86.
(10) Gaborieau, M.; Castignolles, P. *Anal. Bioanal. Chem.* 2011, *399*, 1413-1423.
(11) Radke, W. *J. Chromatogr. A* 2014, *1335*, 62-79.
(12) Ponyik, C. A.; Wu, D. T.; Williams, S. K. R. *Anal. Bioanal. Chem.* 2013, *405*, 9033-9040.
(13) Cottet, H.; Gareil, P. In *Capillary Electrophoresis*, Schmitt-Kopplin, P., Ed.; Humana Press Inc.: Totowa, NJ, United States, 2008, pp 541-567.
(14) Mnatsakanyan, M.; Thevarajah, J. J.; Roi, R. S.; Lauto, A.; Gaborieau, M.; Castignolles, P. *Anal. Bioanal. Chem.* 2013, *405*, 6873-6877.
(15) Taylor, D. L.; Ferris, C. J.; Maniego, A. R.; Castignolles, P.; in het Panhuis, M.; Gaborieau, M. *Aust. J. Chem.* 2012, *65*, 1156-1164.
(16) Sutton, A. T.; Read, E.; Maniego, A. R.; Thevarajah, J. J.; Marty, J. D.; Destarac, M.; Gaborieau, M.; Castignolles, P. *J. Chromatogr. A* 2014, *1372*, 187-195.
(17) Oukacine, F.; Bernard, S.; Bobe, I.; Cottet, H. *J. Control. Release* 2014, *196*, 139-145.

(18) Maniego, A. R.; Ang, D.; Guillaneuf, Y.; Lefay, C.; Gigmes, D.; Aldrich-Wright, J. R.; Gaborieau, M.; Castignolles, P. *Anal. Bioanal. Chem.* 2013, *405*, 9009-9020.
(19) Sisavath, N.; Le Saux, T.; Leclercq, L.; Cottet, H. *Langmuir* 2014, *30*, 4450-4457.
(20) Thevarajah, J. J.; Gaborieau, M.; Castignolles, P. *Adv. Chem.* 2014, *2014*, ArticleID 798503.
(21) Chamieh, J.; Martin, M.; Cottet, H. *Anal. Chem.* 2015, *87*, 1050-1057.
(22) Shortt, D. W. *J. Liq. Chromatogr.* 1993, *16*, 3371-3391.
(23) Burchard, W. *Adv. Polym. Sci.* 1999, *143*, 113-194.
(24) Yao, Y.; Guiltinan, M. J.; Thompson, D. B. *Carbohydr. Res.* 2005, *340*, 701-710.
(25) Zhong, H. J.; Williams, M. A. K.; Keenan, R. D.; Goodall, D. M.; Rolin, C. *Carbohydr. Polym.* 1997, *32*, 27-32.
(26) Guillotin, S. E.; Bakx, E. J.; Boulenguer, P.; Schols, H. A.; Voragen, A. G. J. *Food Hydrocoll.* 2007, *21*, 444-451.
(27) Hoagland, D. A.; Smisek, D. L.; Chen, D. Y. *Electrophoresis* 1996, *17*, 1151-1160.
(28) Cottet, H.; Biron, J. P. *Macromol. Chem. Phys.* 2005, *206*, 628-634.
(29) Oliver, J. D.; Gaborieau, M.; Hilder, E. F.; Castignolles, P. *J. Chromatogr. A* 2013, *1291*, 179-186.
(30) Oliver, J. D.; Sutton, A. T.; Karu, N.; Phillips, M.; Markham, J.; Peiris, P.; Hilder, E. F.; Castignolles, P. *Biotechnol. Appl. Biochem.* 2015, *62*, 329-342.
(31) Cottet, H.; Gareil, P.; Theodoly, O.; Williams, C. E. *Electrophoresis* 2000, *21*, 3529-3540.
(32) Taylor, D. L.; Thevarajah, J. J.; Narayan, D. K.; Murphy, P.; Mangala, M. M.; Lim, S.; Wuhrer, R.; Lefay, C.; O'Connor, M. D.; Gaborieau, M.; Castignolles, P. *Anal. Bioanal. Chem.* 2015, *407*, 2543-2555.
(33) Castignolles, P.; Gaborieau, M.; Hilder, E. F.; Sprong, E.; Ferguson, C. J.; Gilbert, R. G. *Macromol. Rapid Commun.* 2006, *27*, 42-46.
(34) Gaborieau, M.; Causon, T.; Guillaneuf, Y.; Hilder, E. F.; Castignolles, P. *Aust. J. Chem.* 2010, *63*, 1219-1226.
(35) Couvreur, L.; Lefay, C.; Belleney, J.; Charleux, B.; Guerret, O.; Magnet, S. *Macromolecules* 2003, *36*, 8260-8267.
(36) Lacik, I.; Stach, M.; Kasak, P.; Semak, V.; Uhelska, L.; Chovancova, A.; Reinhold, G.; Kilz, P.; Delaittre, G.; Charleux, B.; Chaduc, I.; D'Agosto, F.; Lansalot, M.; Gaborieau, M.; Castignolles, P.; Gilbert, R. G.; Szablan, Z.; Barner-Kowollik, C.; Hesse, P.; Buback, M. *Macromol. Chem. Phys.* 2015, *216*, 23-37.

(37) Vander Heyden, Y.; Popovici, S. T.; Staal, B. B. P.; Schoenmakers, P. J. *J. Chromatogr. A* 2003, *986*, 1-15.
(38) Popovici, S. T.; Kok, W. T.; Schoenmakers, P. J. *J. Chromatogr. A* 2004, *1060*, 237-252.
(39) Park, S.; Chang, T. *Macromolecules* 2006, *39*, 3466-3468.
(40) Shortt, D. W. *J. Chromatogr. A* 1994, *686*, 11-20.
(41) Rollet, M.; Pelletier, B.; Altounian, A.; Berek, D.; Maria, S.; Beaudoin, E.; Gigmes, D. *Anal. Chem.* 2014, *86*, 2694-2702.
(42) Beaudoin, E.; Favier, A.; Galindo, C.; Lapp, A.; Petit, C.; Gigmes, D.; Marque, S.; Bertin, D. *Eur.Polym. J.* 2008, *44*, 514-522.

3.2. Publication: Supporting Information

Supporting Information

for

Quantifying the heterogeneity of chemical structures in complex charged polymers through the dispersity of their distributions of electrophoretic mobilities or of compositions

Joel J. Thevarajah[1,2], Adam T. Sutton[1,2], Alison R. Maniego[1,2], Elizabeth G. Whitty[1,2], Simon Harrisson[3], Hervé Cottet[4], Patrice Castignolles[1]*, Marianne Gaborieau[1,2]

[1]Western Sydney University, School of Science and Health, Australian Centre for Research of Separation Science (ACROSS), Parramatta NSW 2150, Australia

[2]Western Sydney University, Molecular Medicine Research Group, School of Science and Health, Parramatta NSW 2150, Australia

[3]IMRCP, UMR 5623, Université de Toulouse, 118 route de Narbonne, F-31062 Toulouse Cedex 9, France

[4]Institut des Biomolécules Max Mousseron (IBMM, UMR 5247 CNRS, Université de Montpellier, Ecole Nationale Supérieure de Chimie de Montpellier), Place Eugène Bataillon CC 1706, 34095 Montpellier Cedex France

* Corresponding author : Patrice Castignolles, p.castignolles@westernsydney.edu.au, Fax: +61 2 9685 9915

Dispersity calculated through M_w and M_n

Integral expression of the dispersity using M_w and M_n

$$\frac{M_w}{M_n} = \frac{[\int W(M) M \mathrm{d}M][\int W(M) M^{-1} \mathrm{d}M]}{[\int W(M) \mathrm{d}M]^2} \qquad \textbf{S3-1}$$

Moments and dispersity of electrophoretic mobility distributions

The moments are defined as in Table S3-1[1].

Table S3-1. Summary of the integrals and discrete expressions of the moments relevant to this work

Moment order	Integral form	Discrete form
-1	$\int W(\mu)\, \mu^{-1}\, d\mu$	$\sum_z W(\mu_z)\, \mu_z^{-1}\, (\mu_{z+1} - \mu_z)$
0	$\int W(\mu)\ d\mu$	$\sum_z W(\mu_z)\, (\mu_{z+1} - \mu_z)$
1	$\int W(\mu)\, \mu\, d\mu$	$\sum_z W(\mu_z)\, \mu_z\, (\mu_{z+1} - \mu_z)$
2	$\int W(\mu)\, \mu^2\, d\mu$	$\sum_z W(\mu_z)\, \mu_z^2\, (\mu_{z+1} - \mu_z)$
3	$\int W(\mu)\, \mu^3\, d\mu$	$\sum_z W(\mu_z)\, \mu_z\ \ (\mu_{z+1} - \mu_z)$

$$\mu_w = \frac{[\sum_z W(\mu_z) \mu_z\, (\mu_{z+1} - \mu_z)]}{[\sum_z W(\mu_z)\, (\mu_{z+1} - \mu_z)]} \qquad \textbf{S3-2}$$

The general expressions for the equations taking μ_w as a reference are as follows:

$$D(W(\mu),1,\mu_w)=\frac{\overline{\mu^{1}_{\mu_w}}\times\overline{\mu^{-1}_{\mu_w}}}{[\overline{\mu^{0}_{\mu_w}}]^2} \quad \textbf{S3-3}$$

$$D(W(\mu),2,\mu_w)=\frac{\overline{\mu^{2}_{\mu_w}}\times\overline{\mu^{0}_{\mu_w}}}{[\overline{\mu^{1}_{\mu_w}}]^2} \quad \textbf{S3-4}$$

$$D(W(\mu),3,\mu_w)=\frac{\overline{\mu^{3}_{\mu_w}}\times\overline{\mu^{1}_{\mu_w}}}{[\overline{\mu^{2}_{\mu_w}}]^2} \quad \textbf{S3-5}$$

The integral forms of the general equations (eq 3-3, 3-5 to 3-8 and S3-3 to S3-4) are defined as:

$$\mathrm{D(W}(A),b,c)=\frac{\left[\int W(A)(A-c)^{b}\mathrm{d}A\right]\left[\int W(A)(A-c)^{b-2}\mathrm{d}A\right]}{[\int W(A)(A-c)^{b-1}\mathrm{d}A]^2} \quad \textbf{S3-6}$$

$$D(W(\mu),1,0)=\frac{[\int W(\mu)\mu\mathrm{d}\mu][\int W(\mu)\mu^{-1}\mathrm{d}\mu]}{[\int W(\mu)\mathrm{d}\mu]^2} \quad \textbf{S3-7}$$

$$D(W(\mu),1,\mu_w)=\frac{[\int W(\mu)(\mu-\mu_w)\mathrm{d}\mu]\left[\int W(\mu)(\mu-\mu_w)^{-1}\mathrm{d}\mu\right]}{[\int W(\mu)\mathrm{d}\mu]^2} \quad \textbf{S3-8}$$

$$D(W(\mu),2,0)=\frac{\left[\int W(\mu)\mu^{2}\mathrm{d}\mu\right][\int W(\mu)\mathrm{d}\mu)]}{[\int W(\mu)\mu\mathrm{d}\mu]^2} \quad \textbf{S3-9}$$

$$D(W(\mu),2,\mu_w)=\frac{[\int W(\mu)(\mu-\mu_w)^{2}\,\mathrm{d}\mu][\int W(\mu)\mathrm{d}\mu]}{[\int W(\mu)(\mu-\mu_w)\mathrm{d}\mu]^2} \quad \textbf{S3-10}$$

$$D(W(\mu),3,0)=\frac{\left[\int W(\mu)\mu^{3}\mathrm{d}\mu\right][\int W(\mu)\mu\mathrm{d}\mu)]}{[\int W(\mu)\mu^{2}\mathrm{d}\mu]^2} \quad \textbf{S3-11}$$

$$D(W(\mu),3,\mu_w)=\frac{[\int W(\mu)(\mu-\mu_w)^{2}\,\mathrm{d}\mu][\int W(\mu)(\mu-\mu_w)\mathrm{d}\mu]}{[\int W(\mu)(\mu-\mu_w)^{2}\mathrm{d}\mu]^2} \quad \textbf{S3-12}$$

$$D_\sigma=\left[\frac{[\int W(\mu)(\mu-\mu_w)^{2}\mathrm{d}\mu]}{[\int W(\mu)\mathrm{d}\mu]}\right]^{0.5} \quad \textbf{S3-13}$$

In the calculation of dispersity values for the experimental cases in the article, the discrete forms were used for the moments. Eq S3-5, S3-7 and S3-9 thus became:

$$D(W(\mu),1,0) = \frac{[\sum_z W(\mu_z)\mu_z\,(\mu_{z+1}-\mu_z)][\sum_z W(\mu_z)\mu_z{}^{-1}(\mu_{z+1}-\mu_z)]}{[\sum_z W(\mu_z)\,(\mu_{z+1}-\mu_z)]^2} \quad \textbf{S3-14}$$

$$D(W(\mu),2,0) = \frac{[\sum_z W(\mu_z)\,\mu_z{}^2(\mu_{z+1}-\mu_z)][\sum_z W(\mu_z)\,(\mu_{z+1}-\mu_z)]}{[\sum_z W(\mu_z)\,\mu_z(\mu_{z+1}-\mu_z)]^2} \quad \textbf{S3-15}$$

$$D(W(\mu),3,0) = \frac{[\sum_z W(\mu_z)\,\mu_z{}^3(\mu_{z+1}-\mu_z)][\sum_z W(\mu_z)\,\mu_z(\mu_{z+1}-\mu_z)]}{[\sum_z W(\mu_z)\,\mu_z{}^2(\mu_{z+1}-\mu_z)]^2} \quad \textbf{S3-16}$$

$$D_\sigma = \left[\frac{[\sum_z W(\mu_z)\,(\mu_z-\mu_w)^2(\mu_{z+1}-\mu_z)}{[\sum_z W(\mu_z)\,(\mu_{z+1}-\mu_z)]}\right]^{0.5} \quad \textbf{S3-17}$$

μ_w as a reference

In eq S3-7, S3-9 and S3-11 the term $W(\mu)(\mu-\mu_w)d\mu$, can be split. According to eq 3-4 the 2 resulting terms in eq S3-18 are equal and therefore the 1st order moment remains undefined. As this term is undefined it explains why the results using μ_w as a reference do not produce the same trend as $D(W(\mu),1,0)$, $D(W(\mu),2,0)$ and $D(W(\mu),3,0)$.

$$\int W(\mu)(\mu-\mu_w)d\mu = \int W(\mu)\mu d\mu - \mu_w \int W(\mu)d\mu = 0 \quad \textbf{S3-18}$$

Dispersity of composition distributions

The discrete form used in the calculation derived from eq 10 is defined as:

$$C_w = \frac{[\sum_z W(C_z)C_z\,(C_{z+1}-C_z)]}{[\sum_z W(C_z)\,(C_{z+1}-C_z)]} \quad \textbf{S3-19}$$

The integral forms of the general equations (eq 3-5 to 3-8) for composition are defined as:

$$D(W(C)1,0) \quad = \frac{[\int W(C)CdC][\int W(C)C^{-1}dC]]}{[\int W(C)dC]^2} \quad \textbf{S3-20}$$

$$D(W(C),2,0) \quad = \frac{[\int W(C)c^2\mathrm{d}C][\int W(C)\mathrm{d}C]}{[\int W(C)c\mathrm{d}C]^2} \qquad \textbf{S3-21}$$

$$D(W(C),3,0) \quad = \frac{[\int W(C)c^3\mathrm{d}C][\int W(C)c\mathrm{d}C]}{[\int W(C)c^2\mathrm{d}C]^2} \qquad \textbf{S3-22}$$

$$D(W(C),\sigma,C_{\mathrm{W}}) = \left[\frac{[\int W(C)(C-C_w)^2\ \mathrm{d}C]}{[\int W(C)dC]}\right]^{0.5} \qquad \textbf{S3-23}$$

In the calculation of dispersity values for the experimental cases in the article, the discrete forms were used for the moments. Eq S3-20 to S3-23 thus became:

$$D(W(C)1,0) \quad = \frac{[\sum_z W(C_z)\ C_z\ (C_{z+1}-C_z)][\sum_z W(C_z)\ C_z^{-1}\ (C_{z+1}-C_z)]}{[\sum_z W(C_z)\ (C_{z+1}-C_z)]^2} \qquad \textbf{S3-24}$$

$$D(W(C),2,0) = \frac{[\sum_z W(C_z)\ {C_z}^2(C_{z+1}-C_z)][\sum_z W(C_z)\ (C_{z+1}-C_z)]}{[\sum_z W(C_z)\ C_z(C_{z+1}-C_z)]^2} \qquad \textbf{S3-25}$$

$$D(W(C),3,0) = \frac{[\sum_z W(C_z)\ {C_z}^3(C_{z+1}-C_z)][\sum_z W(C_z)C\ (C_{z+1}-C_z)]}{[\sum_z W(C_z)\ {C_z}^2(C_{z+1}-C_z)]^2} \qquad \textbf{S3-26}$$

$$D(W(C),\sigma,C_{\mathrm{W}}) = \left[\frac{[\sum_z W(C_z)\ (C_z-C_{\mathrm{W}})^2(C_{z+1}-C_z)]}{[\sum_z W(C_z)(C_{z+1}-C_z)]}\right]^{0.5} \qquad \textbf{S3-27}$$

Number average electrophoretic mobility

By definition the number-average electrophoretic mobility can be expressed as:

$$\mu_n = \frac{\int N(\mu)\mu d\mu}{\int N(\mu) d\mu} \qquad \textbf{S3-28}$$

Where $N(\mu)$ is the number distribution of electrophoretic mobility (which could be obtained by the detection of end-groups of the polymer after derivatization and use of a fluorescence detector). The ratio between the weight distribution and the number distribution of chains at a given electrophoretic mobility is the number-average molar mass of all polymer chains having the same electrophoretic mobility μ, $M_n(\mu)$. $M_n(\mu)$ has never been determined experimentally. Its determination by coupling the CE separation to a SEC second dimension is highly unlikely due to the injected volume in the CE being several orders of magnitudes smaller than in SEC. The number distribution of electrophoretic mobility is thus not considered further in this work.

In this work, the dispersity of the electrophoretic mobility (or composition) distributions are calculated using the ratio of the 0^{th} to the -1^{st} order moments of the relevant distribution. In the case of M_n, the ratio of the 0^{th} to the -1^{st} order moments of the molar mass distribution leads to a different but corresponding expression to the definition of M_n[2,3]. In the case of μ_n the ratio of the 0^{th} to the -1^{st} order moments of the electrophoretic mobility distribution does not correspond to the definition above:

$$\frac{\int W(\mu)d\mu}{\int \frac{W(\mu)}{\mu} d\mu} = \frac{\int \frac{N(\mu)}{M_n(\mu)} d\mu}{\int \frac{N(\mu)}{\mu M_n(\mu)} d\mu} \neq \mu_n \qquad \textbf{S3-29}$$

Estimation of the uncertainty on the electrophoretic mobility dispersity

To estimate the uncertainty of the dispersity due to the experimental error of the electrophoretic mobility, each of the dispersity equations was derived as follows. Each of the electrophoretic mobility dispersities expressed in eq 3-5 to 3-7 as a function of μ (except the standard deviation) can be expressed as a combination of other functions of μ: *f*, *g* and *h* (each of them being a moment). The fractional uncertainties add in quadrature.

$$D = \frac{f \cdot g}{h^2} \qquad \textbf{S3-30}$$

The differentiation of eq S30 results in:

$$\frac{dD}{D} = \sqrt{\left(\frac{df}{f}\right)^2 + \left(\frac{dg}{g}\right)^2 + 2\left(\frac{dh}{h}\right)^2} \qquad \textbf{S3-31}$$

Eq S31 can be rearranged in:

$$\frac{dD}{D} = \frac{d\mu}{\mu}\sqrt{\left(\frac{\mu \cdot f'}{f}\right)^2 + \left(\frac{\mu \cdot g'}{g}\right)^2 + 2\left(\frac{\mu \cdot h'}{h}\right)^2} \qquad \textbf{S3-32}$$

For example for eq 3-5 with D(W(μ)1,0), $f = \int W(\mu)\mu d\mu;\ g = \int W(\mu)\mu^{-1}d\mu\,;$ and $h = \int W(\mu)\, d\mu$

Therefore $f' = W(\mu)\mu\,;\ g' = W(\mu)\mu^{-1}\,;$ and $h' = W(\mu)\mu$

The expression of eq S3-32 in the case of the derivation of eq 3-5 to 3-7 are given in eq 11 to 13.

To calculate the relative uncertainty of the dispersity values based on eq 3-11 to 3-13, the discrete forms below were used (eq S3-33 to S3-35). Peak areas of the appropriate functions were used for sums, and peak heights for μ_z values outside of sums.

$$\frac{dD(W(\mu),1,0)}{D(W(\mu),1,0)} =$$

$$\frac{d\mu}{\mu}\sqrt{\left(\frac{W(\mu)\mu^2}{\sum_z W(\mu)\mu_z(\mu_{z+1}-\mu_z)}\right)^2+\left(\frac{W(\mu)}{\sum_z W(\mu)\mu_z{}^{-1}(\mu_{z+1}-\mu_z)}\right)^2+2\left(\frac{W(\mu)\mu_z}{\sum_z W(\mu)(\mu_{z+1}-\mu_z)}\right)^2} \quad \textbf{S3-33}$$

$$\frac{dD(W(\mu),2,0)}{D(W(\mu),2,0)} =$$

$$\frac{d\mu}{\mu}\sqrt{\left(\frac{W(\mu)\mu^3}{\sum_z W(\mu)\mu_z{}^2(\mu_{z+1}-\mu_z)}\right)^2+\left(\frac{W(\mu)\mu}{\sum_z W(\mu)(\mu_{z+1}-\mu_z)}\right)^2+2\left(\frac{W(\mu)\mu^2}{\sum_z W(\mu)\mu_z(\mu_{z+1}-\mu_z)}\right)^2} \quad \textbf{S3-34}$$

$$\frac{dD(W(\mu),3,0)}{D(W(\mu),3,0)} =$$

$$\frac{d\mu}{\mu}\sqrt{\left(\frac{W(\mu)\mu^4}{\sum_z W(\mu)\mu_z{}^3(\mu_{z+1}-\mu_z)}\right)^2+\left(\frac{W(\mu)\mu^2}{\sum_z W(\mu)\mu(\mu_{z+1}-\mu_z)}\right)^2+2\left(\frac{W(\mu)\mu^3}{\sum_z W(\mu)\mu_z{}^2(\mu_{z+1}-\mu_z)}\right)^2} \quad \textbf{S3-35}$$

The differentiation of the electrophoretic mobility dispersity expressed in eq 3-8 as a standard deviation follows a different path, as this dispersity can be expressed as a combination of functions f and g of μ (each of them being a moment):

$$D = \left(\frac{f}{g}\right)^{0.5} \quad \textbf{S3-36}$$

The differentiation of eq S3-36 results in:

$$\frac{dD}{d\mu} = \sqrt[0.5]{\left(\frac{df'}{f}\right)^2+0.5\left(\frac{\mu g'}{g}\right)^2} \quad \textbf{S3-37}$$

Eq S37 can be rearranged in:

$$\frac{dD}{d\mu} = \frac{d\mu}{\mu}\sqrt{0.5\left(\frac{\mu f'}{f}\right)^2+0.5\left(\frac{\mu g'}{g}\right)^2} \quad \textbf{S3-38}$$

In eq 8 with D_σ, $f = \int W(\mu)(\mu-\mu_w)^2 d\mu$ and $g = \int W(\mu)d\mu$,

Therefore $f' = W(\mu)(\mu-\mu_w)^2$ and $g' = W(\mu)$

Substituting *f*, *g*, *f'*, *g'* in eq S38 yields eq 3-14. To calculate the uncertainty of the dispersity values based on eq 3-8, the discrete form below was used (eq S3-39).

Peak areas of the appropriate functions were used for sums, and peak heights for μ values outside of sums.

$$\frac{dD_\sigma}{D_\sigma} = \frac{d\mu}{\mu}\sqrt{\left(\frac{W(\mu)(\mu-\mu_w)^2\mu}{2\sum_z W(\mu)(\mu_z-\mu_w)^2(\mu_{z+1}-\mu_z)}\right)^2 + \left(\frac{W(\mu)\mu}{2\sum_z W(\mu)(\mu_{z+1}-\mu_z)}\right)^2} \qquad \textbf{S3-39}$$

The value of the dispersity uncertainty was calculated for a sample of each of the experimental cases through eq S3-33 to S3-35 and S3-39, using 1 % for $\frac{d\mu}{\mu}$ as an estimate of the published RSDs of the electrophoretic mobilities (Table S3-2). Results are listed in Table S3-3.

Table S3-2. RSD of the electrophoretic mobilities of polyelectrolytes[4] and sugars[5,6] in the literature.

Sample	RSD (%)		
Linear PNaA	1.63		
3-arm star PNaA	1.34		
Hyperbranched	1.15		
Cellobiose	0.39		
Galactose	0.41	0.53	0.17
Glucose	0.45	0.63	0.06
Rhamnose	0.63	0.76	
Mannose	0.40	0.77	0.71
Arabinose	0.57	0.60	0.46
Xylose	0.40	0.54	0.29
Arabitol	0.74	1.33	

Table 3-S3. Relative uncertainty values of the dispersity of the electrophoretic mobility distribution, calculated for a sample of each of the experimental cases using eq S33 to S35 and S39. The chitosan sample with a DA of 19.8, P(NaA-*co*-APA) at 5 minutes reaction time, PNaA 3 arm star and PAAkPAM10k were chosen. The uncertainty is given in $m^2V^{-1}s^{-1}$.

Sample	$\frac{dD(W(\mu),1,0)}{D(W(\mu),1,0)}$	$\frac{dD(W(\mu),2,0)}{D(W(\mu),2,0)}$	$\frac{dD(W(\mu),3,0)}{D(W(\mu),3,0)}$	$\frac{dD(W(\mu),\sigma,\mu_w)}{D(W(\mu),\sigma,\mu_w)}$
Chitosan	3.6×10^{-17}	1.3×10^{-12}	4.3×10^{-9}	1.3×10^{-12}
P(NaA-	4.4×10^{-17}	1.1×10^{-12}	4.8×10^{-10}	1.3×10^{-12}
PNaA	9.3×10^{-18}	2.8×10^{-14}	1.4×10^{-13}	9.5×10^{-14}
PAA2k PAM10k	8.0×10^{-18}	5.5×10^{-14}	2.3×10^{-12}	2.0×10^{-13}

Estimation of the uncertainty on the composition dispersity

The differentiation of the composition dispersity follows the same approach as detailed above for the electrophoretic mobility dispersity. The resulting equations are similar to eq S3-33 to S3-35 and S3-39, except that *C* must be substituted for μ. The values of the dispersity uncertainty were calculated for block copolymer samples (Table S3-4).

Table S3-4. Relative uncertainty values of the dispersity of the composition distribution, for block copolymer samples (calculated from equations analogous to S33 to S35 and S39, with *C* substituted for μ)

Sample	$\frac{dD(W(C),1,0)}{D(W(C),1,0)}$	$\frac{dD(W(C),2,0)}{D(W(C),2,0)}$	$\frac{dD(W(C),3,0)}{D(W(C),3,0)}$	$\frac{dD(W(C),\sigma,C_w}{D(W(C),\sigma,C_w)}$
PAA2kPAM10k	2.3×10^{-3}	5.4×10^{-7}	1.2×10^{-6}	3.1×10^{-6}
PAA10kPAM10k	5.6×10^{-3}	2.2×10^{-6}	2.7×10^{-6}	2.8×10^{-6}

Experimental samples

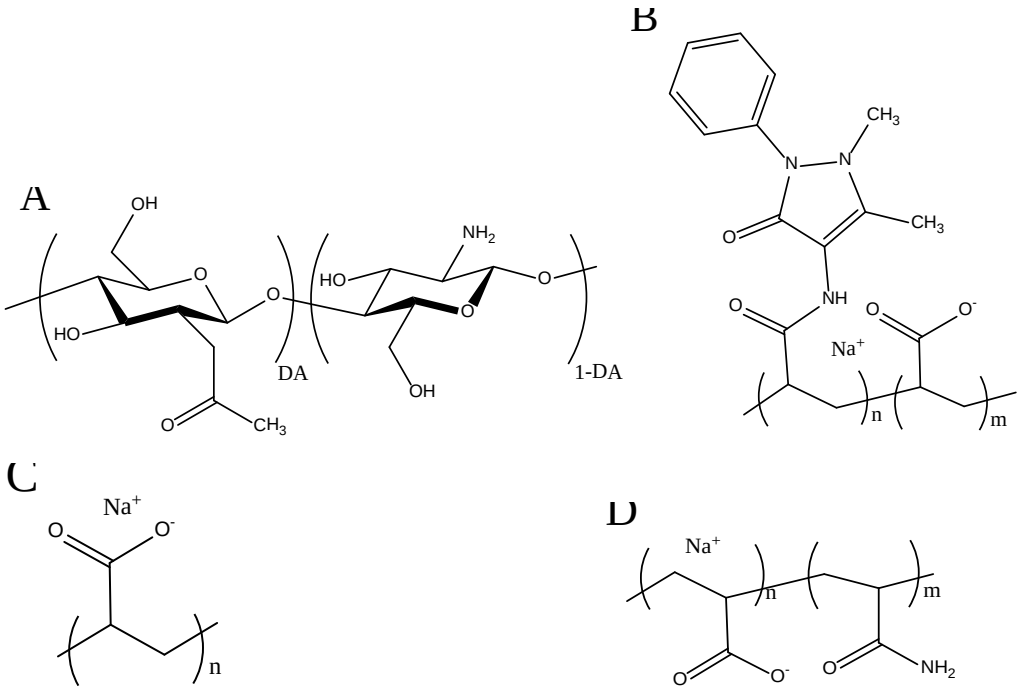

Figure S3-1. The molecular structure of (A) chitosan with *N*-acetyl-D-glucosamine and D-glucosamine units[7] (B) P(NaA-*co*-APA), (C) PNaA and (D) P(NaA-*b*-AM).

Table S3-5. Dispersity of chitosan samples

DA[a]	μ_w[b]	SD[c] (10^{-10})	D($W(\mu)$,1,0)-1 (10^{-4})	$D(W(\mu)$,2,0)-1 (10^{-4})	$D(W(\mu)$,3,0)-1 (10^{-4})
19.8	3.21	17.6	30.9	30.2	29.4
13.6	3.44	17.9	27.9	27.1	26.4
3.5	3.60	5.05	2.00	1.97	1.94
18.7	3.23	14.0	19.4	18.9	18.4
16.5	3.38	15.7	22.6	21.5	20.5
3.2	3.64	4.86	1.81	17.9	1.77
15.5	3.41	11.5	11.6	11.4	11.3

[a] number-average *DA* measured using quantitative ^{1}H NMR spectroscopy at 90 °C[8]

[b] the weight-average electrophoretic mobility is given in $10^{-8}.m^2V^{-1}s^{-1}$

[c] the standard deviation is given in $m^2V^{-1}s^{-1}$

Molar absorptivity P(NaA-*co*-APA)

The UV absorbance of PNaA and AAP were calculated using the absorbance obtained experimentally in the conditions of the separation (195 nm wavelength, sodium borate buffer 110 mM at 25 °C).

Linear PNaA: $1.7 \cdot 10^{-6}$ a.u.·V·s·m^{-2}

AAP: $3.4 \cdot 10^{-5}$ a.u.·V·s·m^{-2}

.

Table S3-6. Dispersity values of P(NaA-*co*-APA) samples. The values are first given as determined from eq 5 to 8; the value obtained for the linear PNaA (sample at time 0) was then subtracted from these values.

					After subtracting value for Linear PNaA			
Time (min)	$D(W(\mu),1,0)$ -1 (10^{-4})	$D(W(\mu),2,0)$ -1 (10^{-4})	$D(W(\mu),3,0)$ -1 (10^{-4})	SD[a] (10^{-10})	$D(W(\mu),1,0)$ -1 (10^{-4})	$D(W(\mu),2,0)$ -1 (10^{-4})	$D(W(\mu),3,0)$ -1 (10^{-4})	SD[a] (10^{-10})
0	0.13	0.13	0.13	1.33	0	0	0	0
5	0.82	0.82	0.825	3.20	0.696	0.696	0.697	1.86
45	0.96	0.96	0.954	3.44	0.830	0.828	0.826	2.11
85	0.99	0.99	0.986	3.51	0.863	0.861	0.859	2.17
125	1.05	1.05	1.05	3.62	0.927	0.923	0.92	2.28
165	1.19	1.18	1.18	3.82	1.06	1.06	1.05	2.49
205	1.26	1.26	1.25	3.93	1.13	1.13	1.12	2.60
245	1.27	1.27	1.26	3.95	1.14	1.14	1.13	2.61
285	1.27	1.26	1.26	3.94	1.14	1.13	1.13	2.61
325	1.24	1.23	1.22	3.90	1.11	1.10	1.1	2.57
365	1.47	1.46	1.45	4.24	1.34	1.33	1.32	2.90
405	1.15	1.14	1.13	3.75	1.02	1.01	1	2.41
445	1.21	1.2	1.19	3.85	1.08	1.07	1.06	2.52
485	1.11	1.1	1.09	3.69	0.983	0.97	0.967	2.35

[a] the standard deviation is given in $m^2V^1s^{-1}$

Branched PNaA

Table 3-S7. Summary of PNaA dispersity values representing the heterogeneity of samples with different branching topologies and samples produced from different monomers

Sample	$\mu_w 10^{-8}$.$m^2V^1s^{-1}$	SD (10^{-10}) $m^2V^1s^{-1}$	$D(W(\mu),1,0)$-1 (10^{-4})	$D(W(\mu),2,0)$-1 (10^{-4})	$D(W(\mu),3,0)$-1 (10^{-4})
3-Arm star	3.45	13.7	15.9	15.2	14.4
Hyperbranched	3.53	5.4	2.28	2.34	2.39
Linear	3.74	1.33	0.10	0.10	0.13
PNaA-AA	3.69	7.18	3.73	3.78	3.83
PNaA-tBA	3.66	9.64	6.84	6.95	7.06

P(AA-*b*-AM) composition calculation

The composition C taken as the molar fraction of acrylic acid monomer units in the copolymer is linked to the electrophoretic mobility μ of the copolymer through eq S40[9]:

$$C = \frac{\alpha\mu}{\mu(\alpha-1)+\mu_0} \qquad \textbf{S3-40}$$

where α is a rescaling factor, and μ_o is the electrophoretic mobility of the charged homopolymer. α depends on the chemical nature of both homopolymers, on the background electrolyte, and on the temperature[10]. Combining eq S40 with eq 9 leads to:

$$W(C) = W(\mu)\frac{[\mu(\alpha-1)+\mu_0]^2}{\alpha\mu_0} \quad \textbf{S3-41}$$

Any error in the determination of the rescaling factor α would thus result in an error in the calculated composition distribution, $W(C)$.

Determining alpha

For a block copolymer consisting of one charged block and one neutral block the number of effective monomer units can be related to its electrophoretic mobility in the following equation[11]:

$$\mu = \mu_0 \frac{n_c}{n_c+\alpha n_u} \quad \textbf{S3-42}$$

Where n_c is the number of charged monomer units in the copolymer and n_u is the number of uncharged monomer units in the copolymer.

Eq S3-42 can be rearranged into eq S3-43 so that a plot of μ_0/μ - 1 vs n_u/n_c will yield α as the slope.

$$\frac{\mu_0}{\mu} - 1 = \alpha\frac{n_u}{n_c} \quad \textbf{S3-43}$$

Since synthetic block copolymers contain a distribution of n_u and n_c values, which then produce multiple μ values, careful selection of n_u and n_c values is required to accurately represent the sample. The values for n_u and n_c were calculated from the theoretical M_n of the block copolymer (previously listed in [12] as well as in the caption of Figure 3-3 to 3-7).

Table S3-8. Dispersity of P(AA-*b*-AM) samples

Sample	PAA2KPAM10K		PAA2KPAM10K	
	A is μ	A is C	A is μ	A is C
D(W(A),1,0)	1.12	1.19	1.12	1.25
D(W(A),2,0)	1.10	1.16	1.08	1.15
D(W(A),3,0)	1.08	1.36	1.05	1.10
SD ($x10^{-9}$)	4.46[a]	0.090	6.56[a]	0.178

[a] the standard deviation is given in $m^2V^1s^{-1}$

REFERENCES

(1) Zabisky, R. C. M.; Chan, W. M.; Gloor, P. E.; Hamielec, A. E. *Polymer* **1992**, *33*, 2243-2262.

(2) Hamielec, A. E.; Ouano, A. C. *J. Liq. Chromatogr.* **1978**, *1*, 111-120.

(3) Gaborieau, M.; Gilbert, R. G.; Gray-Weale, A.; Hernandez, J. M.; Castignolles, P. *Macromol. Theory Simul.* **2007**, *16*, 13-28.

(4) Maniego, A. R.; Ang, D.; Guillaneuf, Y.; Lefay, C.; Gigmes, D.; Aldrich-Wright, J. R.; Gaborieau, M.; Castignolles, P. *Anal. Bioanal. Chem.* **2013**, *405*, 9009-9020.

(5) Oliver, J. D.; Gaborieau, M.; Hilder, E. F.; Castignolles, P. *J. Chromatogr. A* **2013**, *1291*, 179-186.

(6) Oliver, J. D.; Sutton, A. T.; Karu, N.; Phillips, M.; Markham, J.; Peiris, P.; Hilder, E. F.; Castignolles, P. *Biotechnol. Appl. Biochem.* **2015**, *62*, 329-342.

(7) Domard, A. *Carbohydr. Polym.* **2011**, *84*, 696-703.

(8) Mnatsakanyan, M.; Thevarajah, J. J.; Roi, R. S.; Lauto, A.; Gaborieau, M.; Castignolles, P. *Anal. Bioanal. Chem.* **2013**, *405*, 6873-6877.

(9) Vreeland, W. N.; Desruisseaux, C.; Karger, A. E.; Drouin, G.; Slater, G. W.; Barron, A. E. *Anal. Chem.* **2001**, *73*, 1795-1803.

(10) Nedelcu, S.; Slater, G. W. *Electrophoresis* **2005**, *26*, 4003-4015.

(11) Vreeland, W. N.; Desruisseaux, C.; Karger, A. E.; Drouin, G.; Slater, G. W.; Barron, A. E. *Anal. Chem.* **2001**, *73*, 1795-1803.

(12) Sutton, A. T.; Read, E.; Maniego, A. R.; Thevarajah, J. J.; Marty, J. D.; Destarac, M.; Gaborieau, M.; Castignolles, P. *J. Chromatogr. A* **2014**, *1372*, 187-195.

CHAPTER 4: Determination of the Distributions of the Degrees of Acetylation of Chitosan

4.1. Publication [127]

Determination of the Distributions of the Degrees of Acetylation of Chitosan

Joel J Thevarajah[1,2], Matthew P Van Leeuwen[1,3], Herve Cottet[4], Patrice Castignolles[2*], Marianne Gaborieau[1,2]

Corresponding author: p.castignolles@westernsydney.edu.au

[1]Western Sydney University, Molecular Medicine Research Group (MMRG), Parramatta, 2150, Australia

[2]Western Sydney University, Australian Centre for Research on Separation Sciences (ACROSS), School of Science and Health, Parramatta, 2150, Australia

[3]Western Sydney University, School of Medicine, Parramatta, 2150, Australia

[4]Institut des Biomolécules Max Mousseron (IBMM, UMR 5247 CNRS-Université de Montpellier-Ecole Nationale Supérieure de Chimie de Montpellier), Place Eugène Bataillon CC 1706, 34095 Montpellier Cedex 5, France

KEYWORDS: Chitosan, distribution, degree of acetylation, dispersity, solid-state NMR spectroscopy, capillary electrophoresis

ABSTRACT: Chitosan is often characterized by its average degree of acetylation. To increase chitosan's use in various industries, a more thorough

characterization is necessary as the acetylation of chitosan affects properties such as dissolution and mechanical properties of chitosan films. Despite the poor solubility of chitosan, free solution capillary electrophoresis (CE) allows a robust separation of chitosan by the degree of acetylation. The distribution of the degrees of acetylation on chitosan's polymer chains was characterized through the distributions of electrophoretic mobilities. These distributions can be obtained easily and with high precision. The heterogeneity of the chitosan chains in terms of acetylation was characterized through the dispersity of the electrophoretic mobility distributions obtained. The relationship between the number-average degree of acetylation obtained by solid-state NMR spectroscopy and the weight-average electrophoretic mobilities was established. The distribution of degrees of acetylation was determined using capillary electrophoresis in the critical conditions (CE-CC).

1. INTRODUCTION

Chitosan is a polysaccharide derived from the *N*-deacetylation of chitin. Chitin is an abundant polysaccharide and it naturally occurs in the shells of arthropods such as shrimps, crabs and the cell walls of yeasts [1]. The molecular structure of the polysaccharide chitosan includes varying proportions of D-glucosamine and *N*-acetyl-D-glucosamine units (Figure 4-1).

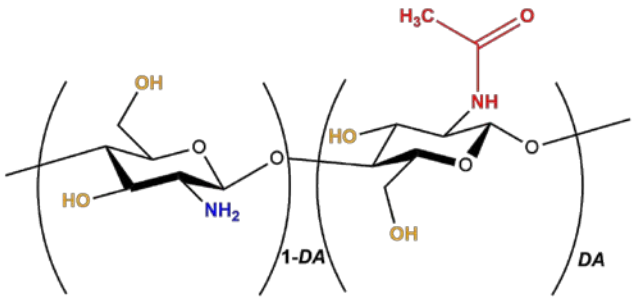

Figure 4-1. Chemical structure of chitosan (of degree of acetylation *DA*) and of chitin (for *DA*=1).

Chitosan has several desirable properties that allowed it to become a significant area of research: it is biocompatible, biodegradable, antimicrobial and antifungal [2]. In characterizing chitosan samples, a properly established structure-property relationship is required to assist in tailoring individual samples for specific uses [3, 4]. Therefore, accurately characterizing the supramolecular structure of chitosan is essential to understanding its properties. However, due to an incomplete understanding of chitosan's complex structure, several limitations exist in its characterization.

The degree of acetylation (*DA*) is defined as the fraction of *N*-acetyl-D-glucosamine units. The distributions of *DA*s correspond to the relative amount of chitosan macromolecules having a given *DA* plotted against *DA*. The existence of this distribution means that chitosan chains having different degrees of acetylation are present in a given sample. Although it has been well documented that a distribution of *DA*s exists (not all chitosan chains have the same *DA*), this is often overlooked [5, 6]. Due to its natural origin and the variation in processing conditions, chitosan can have broad distributions of *DA*s. The existence and importance of the distributions of the *DA*s has been revealed through a coupling of size-exclusion chromatography (SEC) separation with ^{1}H NMR spectroscopy detection; however, the distributions still have not been

determined [5]. SEC [7], gradient SEC [8] and gradient liquid adsorption chromatography [9] have been used to determine chemical composition against molar mass (named "chemical composition distribution"), as well as distributions of composition in some cases [10, 11] for various copolymers, but not for chitosan. In addition, the distribution of compositions (or distribution of *DA*s for chitosan) have never been determined. The presence of a distribution of *DA*s can be attributed to the production of chitosan from chitin. Chitin exists in 3 forms, α, β and γ [12]. The α and β forms vary in reactivity due to their structure. The α form is strongly stabilized by intra- and inter-sheet hydrogen bonds conversely to the β form which does not exhibit hydrogen bonding between successive chains. This results in β chitin being more soluble [13] as well as reactive [14]; however, the α form is more industrially available due to its natural abundance. Thus, heterogeneity is influenced by the structure of the chitin used in the production of chitosan.

The treatment of chitin to produce chitosan can also be a homogeneous or a heterogeneous process. The heterogeneous method has shown to be more effective in the deacetylation and is therefore more researched and used. A study in the heterogeneous deacetylation of both α and β chitin showed that in the deacetylation process two domains of deacetylation existed. There was also differences between α and β chitin which could be attributed to the structure of the α form preventing the accessibility of certain sites [15]. It was also identified that homogeneous deacetylation would increase the chance of a random distribution whereas heterogeneous deacetylation could cause blocks of acetylated/deacetylated units [16]. Block deacetylation is then attributed to the starting materials crystallinity in which the more amorphous region had the

reactive acetylated sites more readily available and allowed a random distribution of acetylation [15].

Methods used to characterize chitosan by its average degree of acetylation/deacetylation previously include FTIR [17], Raman [18] and NMR spectroscopy [7, 19-21]. To determine the distribution of *DA*s, we require a method to identify the average degree of acetylation and a separation technique to identify the distribution of *DA*s. The most widely used method to separate polymers, especially polysaccharides, is size-exclusion chromatography (SEC) [22]. SEC separates polymers by their size (hydrodynamic volume) [23]. For chitosan this depends on both the molar mass and the degree of acetylation of the chitosan. Further, SEC analysis of chitosan has been plagued with aggregation [19]. Separation by composition is possible using liquid chromatography in the critical conditions [24] however, this can be extremely tedious and problematic [25] and is quasi-exclusively applied to organic system, and not aqueous system as used for chitosan. For this reason we propose to use free solution capillary electrophoresis (CE) for the analysis of chitosan by its degree of acetylation and its distributions [26, 27].

CE has been proven to effectively separate the polysaccharide pectin by composition. Several studies reported the separation of pectin by its degree of substitution (*DS*, which may include esterification) [28]. Other research involved the use of capillary electrophoresis to determine the *DS* of caboxymethylcellulose [29]. Further, CE was proven to be a robust, reproducible method in the detection of impurities in the negatively charged biomolecule heparin [30]. The conditions of separation fall above the Manning condensation; however, separation is still possible although with a low selectivity. The

separation of heparin is therefore very similar to that of chitosan. The ability to separate polymers by their composition independently from their molar mass is what differentiates CE from the aforementioned methods and makes it particularly appropriate for our study. It has been proven in the study of polylysine in which the electrophoretic mobility did not vary for a degree of polymerization above 4 [31]. This method is described as "in the critical conditions" (not referring to the separation mechanism but to the absence of separation by molar mass) and has been reviewed recently [26]. CE has previously been used in chitosan analysis including both native [7, 32] and modified chitosan [33].

To allow meaningful distributions to be obtained, the raw data, UV absorption against migration time, first needs to be converted into a distribution of electrophoretic mobilities, [34] and finally into chemical composition distributions. Different expressions of the dispersity of this distribution have recently been developed [27]. The dispersities determined from these different expressions are compared in this work in the case of chitosan. Analysis of the distributions of electrophoretic mobilities of cationic copolymers reveals information regarding their heterogeneity of composition. Understanding the heterogeneity of composition allows for property-structure relationships to be established. Expressions for the composition distributions were also established and tested for some block copolymers [27]. In this study, composition distributions for chitosan (under the form of distribution of *DA*s), or any statistical copolymer, are obtained for the first time.

2. EXPERIMENTAL SECTION

2.1. MATERIALS

Chitosan powders were purchased from Sigma-Aldrich, Castle Hill, Australia and from AK Biotech LTD, Jinan, China (Table S1). Samples were prepared at 1 $g \cdot L^{-1}$. Orthophosphoric acid (85 %) and boric acid were purchased from BDH AnalR, Merck Pty Ltd. Acetic acid (AcOH, glacial, 99 %) and hydrochloric acid (32 %) were purchased from Unilab. Poly(diallyldimethyl ammonium chloride) (PDADMAC 20 % in H_2O), alginic acid sodium salt, poly(allylamine hydrochloride) (PAlAm), sodium hydroxide pellets, lithium hydroxide, sodium chloride, hexaamminecobalt(III) chloride (≥99.5 %), dimethyl sulfoxide (DMSO, ≥99.5 %) and adamantane (99 %) were purchased from Sigma-Aldrich. Sodium dihydrogen orthophosphate was purchased from Univar. Three ^{13}C singly labeled alanines were purchased from Cambridge isotope laboratories. All water used in this study was of Milli-Q quality. Sodium borate buffer (75 mM) was prepared from 0.5 M boric acid in Milli-Q water, titrated to pH 9.20 with 10 M sodium hydroxide, and diluted with Milli-Q water. Sodium phosphate buffer (100 mM) was prepared from 0.5 M sodium dihydrogen phosphate, titrated with phosphoric acid, and diluted with Milli-Q water. Lithium phosphate buffer (100 mM) was prepared from 85 % orthophosphoric acid, titrated to pH 2 with 10 M LiOH and diluted with Milli-Q water. Lithium phosphate, sodium borate and sodium phosphate buffers were sonicated for 5 min and filtered with a Millex GP polyethersulfone (PES) syringe filter (0.22 μm) before use.

2.2. METHODS

2.2.1. CAPILLARY ELECTROPHORESIS

Free solution capillary electrophoresis (CE) was carried out using an Agilent 7100 CE (Agilent Technologies, Waldbronn, Germany) instrument equipped with a diode array detector, contactless conductivity detector (TraceDeC, Innovative Sensor Technologies GmbH, Austria) and external circulating bath with MX temperature controller (Polyscience, USA). Polyimide-coated fused silica high sensitivity (HS) capillaries (50 μm internal diameter, bubble factor 3) were purchased from Agilent (Australia). Fused silica capillaries used for multilayer PDADMAC and alginate coatings with 50 μm internal diameter were purchased from Polymicro (USA). The HS capillary (112.5 cm total length, 104 cm effective length) was initially pretreated by flushing for 10 min with 1 M NaOH, then 5 min with 0.1 M NaOH, Milli-Q water, and sodium borate, respectively at the start of a series of separations. The NaOH 1 M was prepared less than 24 h before use. In conditions of sodium borate (75 mM, pH 9.3) an oligoacrylate with a known separation [35] and a broad range of electrophoretic mobilities was injected to validate the capillary and the instrument before each session. After the standard separation and before the series of chitosan separations, the sodium borate was removed with a rinse method which included flushes for 5 min with 1M NaOH, 0.1M NaOH, and Milli-Q water, respectively, then a 10 min with 50 mM HCl and finally 5 min with either sodium or lithium phosphate. Before each injection the capillary was rinsed with HCl (50 mM) and the background electrolyte (either sodium or lithium phosphate, 100 mM, pH 2) for 5 min each. Separation was obtained by applying 30 kV and 50 mbar pressure at 55 °C.

The fused silica capillary used for multilayer coatings was first treated for 45 min with 1 M NaOH and rinsed for 5 min with Milli-Q water. The coating process adapted from literature [36] included 45 min flushes with 2 % w/v

PDADMAC in H_2O, then with 1 % w/v alginate in H_2O and finally 2 % w/v PDADMAC in H_2O. Following the coating process, the capillary was rinsed for 5 min with Milli-Q water and preconditioned before each injection for 10 min with 0.1 M NaOH and for 10 min with sodium phosphate (10 mM, pH 3). The separation was obtained by applying -30 kV at 25 °C.

The detection was set at 195 nm with a bandwidth of 10 nm.

2.2.2. SOLID-STATE NMR SPECTROSCOPY

Solid-state ^{1}H and ^{13}C NMR spectra were recorded on a Bruker Avance DPX 200 spectrometer operating at Larmor frequencies of 200 MHz and 50 MHz, respectively. A commercial double resonance probe supporting zirconia MAS rotors with a 4 mm outer diameter and a 3 mm inner diameter was used, and samples were spun at 10 kHz at the magic angle. ^{1}H NMR spectra were recorded using a 5.73 μs 90° pulse, a 3 s repetition delay and at least 64 scans. ^{13}C CP-MAS NMR experiments were adapted from published quantitative measurements [19]. They were recorded with a 1 ms contact time and a 4 s repetition delay, and 21,586 to 104,924 scans. For ^{1}H experiments the 90° pulse was optimized using adamantane and power levels for the ^{13}C CP-MAS experiments were optimized using a mixture of three ^{13}C singly labeled alanines. The ^{1}H and ^{13}C chemical shifts scales were externally referenced using adamantane by setting the CH resonance to 1.64 and 38.48 ppm, respectively [37]. The degree of acetylation was measured through Eq. 1 [20]:

$$DA_n^{SSNMR}(\%) = \frac{I_{CH_3}}{(I_1+I_2+I_3+I_4+I_5+I_6)/6} \quad \textbf{4-1}$$

Where I_{CH3} is the integral of the methyl group of the acetyl group and I_1 to I_6 are the integrals of the signals assigned to the chitosan backbone.

RESULTS AND DISCUSSIONS

3.1. CHITOSAN DISSOLUTION

Analyzing a fully dissolved sample of chitosan in solution allows a complete characterization; however, obtaining a true solution of chitosan is quite difficult. In a previous study [19] the dissolution of chitosan was analyzed in a range of conditions with CE including the use of deuterated and aqueous solvents. Our new methodology to determine the distribution of electrophoretic mobilities and their dispersity [27] was applied to monitoring chitosan dissolution in aqueous solvent [19]. This allows further characterization of the dissolution. Initial CE separations of chitosan were based on apparent or electrophoretic mobility [7]. Pressure-assisted capillary electrophoresis (PACE) was used to analyze chitosan samples to obtain more precise electrophoretic mobility values [19]. This was necessary as deacetylation during the dissolution process is suspected and it could be detected only with sufficient precision in the measurement of electrophoretic mobility. PACE allowed the detection of both an internal standard and an electroosmotic flow marker (a neutral marker). It was noted previously that the weight-average electrophoretic mobility did not significantly vary with time of dissolution apart from the first 5 h in which incomplete dissolution led to high variations in electrophoretic mobility due to aggregation. In this work, the dispersity of the electrophoretic mobility distributions obtained were calculated and on the time scale exhibited similar behaviors for the different samples with the exception of LowMW1. MedMW samples were

seen to have a similar dispersity over the period of dissolution with a slight increase in dispersity after the first 5 h suggesting that there was not a significant bias in dissolution (Figure 4-2). The LowMW1 sample exhibited a very different dispersity with a large increase in dispersity after the initial 5 h. This suggests a bias in the dissolution with certain polymer chains with similar compositions dissolving first followed by the rest of the polymer chains. Therefore it is important to study the distributions of composition for chitosan as the *DA* may play a more important role than molar mass in the dissolution [27].

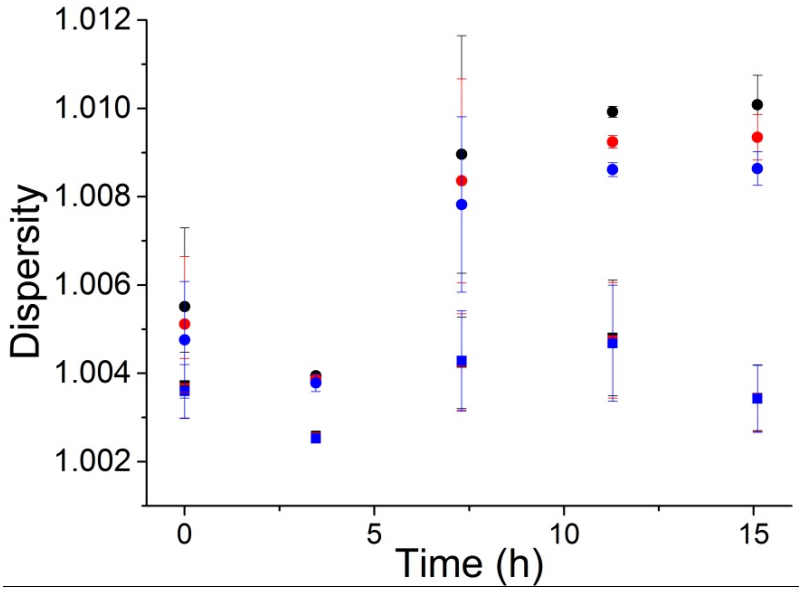

Figure 4-2. Dispersity $D(W(\mu),1,0)$ (black), $D(W(\mu),2,0)$ (red) and $D(W(\mu),3,0)$ (blue) of chitosan MedMW1 (squares) and LowMW1 (circles) during kinetic measurement of dissolution in 50 mM HCl in H_2O using CE-CC with the carousel kept at 60 °C. See supporting information equation S4-1 to S4-3 for dispersity calculations [24].

The kinetics of dissolution of MedMW in 50 mM HCl in H_2O was also compared to that in 50 mM DCl in D_2O (Figure S4-1). No significant variation of

dispersities of the $W(\mu)$ was observed. Following the dissolution study [19] 50 mM HCl at 60 °C for 2 hours was chosen in this work as the dissolution conditions for the range of commercially available chitosan samples with different viscosities, degrees of acetylation (supplied and measured), molar masses and suppliers. This was to ensure minimal deacetylation during the dissolution.

3.2. SEPARATION

3.2.1 ADSORPTION ONTO THE CAPILLARY SURFACE

It is important to optimize the conditions of separation to prevent unwanted broadening especially in the analysis of distributions. A factor that may negatively affect CE-CC separations is the adsorption of the polymer onto the surface of the capillary. To prevent adsorption a number of steps were taken including an increased cassette temperature and a lower pH buffer [19]. Multilayer coatings have been previously used to prevent the adsorption of proteins and plasma [36]. A cationic/anionic multilayer coating of PDADMAC and alginate was successfully tested with a model polyamine sample of poly(allylamine hydrochloride) (PAlAm). PAlAm was separated successfully (Figure 4-3) in lithium phosphate 10 mM at pH 3 (LiPB10). A lower concentration of lithium phosphate buffer was used to prevent interaction with the multilayer coating. Detection of PAlAm was with UV at 195 nm as well as with a conductivity detector. The separation was also tested with sodium phosphate 10 mM at pH 3 (NaPB10); however, low sensitivity was experienced (Figure S4-2). However, in the separation of chitosan with this coating, no chitosan peak was detected, assumingly because chitosan strongly adsorbs onto the coating, the signals detected at very high electrophoretic mobilities may correspond to either

coating displaced by the chitosan or chitosan aggregates. It is assumed that chitosan has a higher affinity at pH 2 with alginate than PAlAm or PDADMAC. This prevented further use of the coating for chitosan characterization.

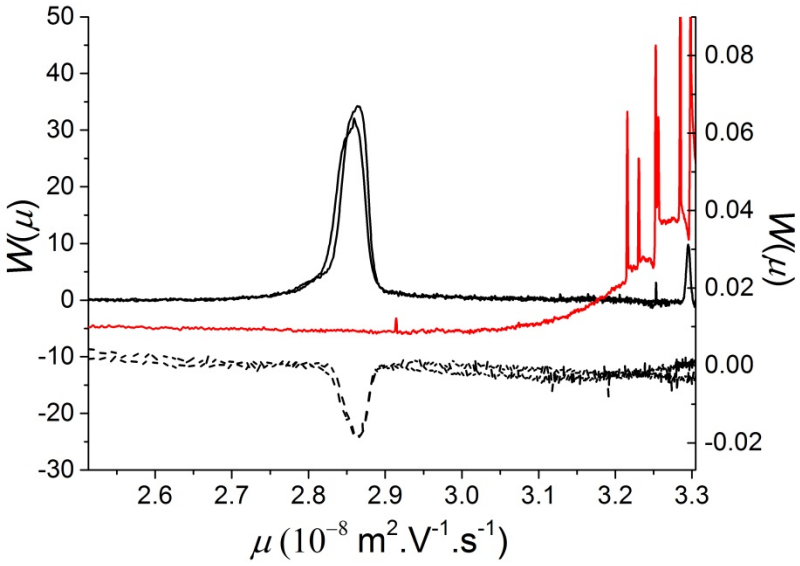

Figure 4-3: Electropherogram of PAlAm (black lines) and chitosan (red line) separated in a PDADMAC/alginate/PDADMAC coated capillary (50 cm total length) in LiPB10 at -30 kV with UV (solid line – left y axis) and contactless capacitively-coupled conductivity (dashed line – right y axis) detections. Where μ is the electrophoretic mobility and $W(\mu)$ is the weight fraction of polyelectrolyte chains with a given electrophoretic mobility calculated as the absorbance ($S(t)$) multiplied by the migration time.

Although the multilayer coating was unable to be used to analyze chitosan, it has successfully been used in the separation of another cationic polymer. The methodology developed below could thus apply to a number of cationic polymers, even if they adsorbed onto standard fused silica capillaries.

3.2.2. SELECTIVITY

To enhance the selectivity of the separation of chitosan in CE-CC compared to previous results [7, 19] various parameters were tested. This included the use of the surfactant Brij™ 35 as a complexation reagent to adjust the selectivity [38]. However, chitosan did not dissolve in the presence of Brij™ 35 and remained as particulates. Brij™ 35 also caused the precipitation of chitosan in solution, which prevented its analysis using CE (the use of an anionic surfactant would lead to water-insoluble complexes [39] and this was not attempted). Different counter-ions for the background electrolyte were also compared.

Chitosan was separated in sodium phosphate and lithium phosphate and the resulting electropherograms were analyzed (section 3.3). It was noted that chitosan was separated with a greater selectivity in lithium phosphate compared to sodium phosphate. The range of electrophoretic mobilities and dispersity values were determined as 3.0 to 4.8 (10^{-8} $m^2.V^{-1}.s^{-1}$) and 1.000 to 1.006 in sodium phosphate, as well as 2.7 to 4.8 (10^{-8} $m^2.V^{-1}.s^{-1}$) and 1.000 to 1.008 in lithium phosphate.

3.3 ELECTROPHORETIC MOBILITY DISTRIBUTIONS

3.3.1 CHITOSAN IN SODIUM PHOSPHATE

Appropriate treatment of the raw electropherograms [34] allowed meaningful mobility distributions to be obtained (Figure 4-4A). The different chitosan samples were each seen to have a broad range of distributions of electrophoretic mobilities. The dispersity of the mobility distributions was calculated based on a ratio of moments [27] and plotted against the average *DA* measured by solid-state NMR spectroscopy (Figure 4-4B). The dispersity was also plotted against the weight-average mobility (Figure 4-4C). The general trend seen is that

samples with a low average *DA* have a lower dispersity. This is expected as the heterogeneity of the composition is likely to increase as the *DA* increases (or decreases) until the composition becomes more homogeneous. The dispersity is seen to first increase and then decrease as the average *DA* increases. This trend is dissimilar to that which is seen for the dispersity against the weight-average electrophoretic mobility. As the weight-average electrophoretic mobility of the chitosan samples increases, their dispersity decreases.

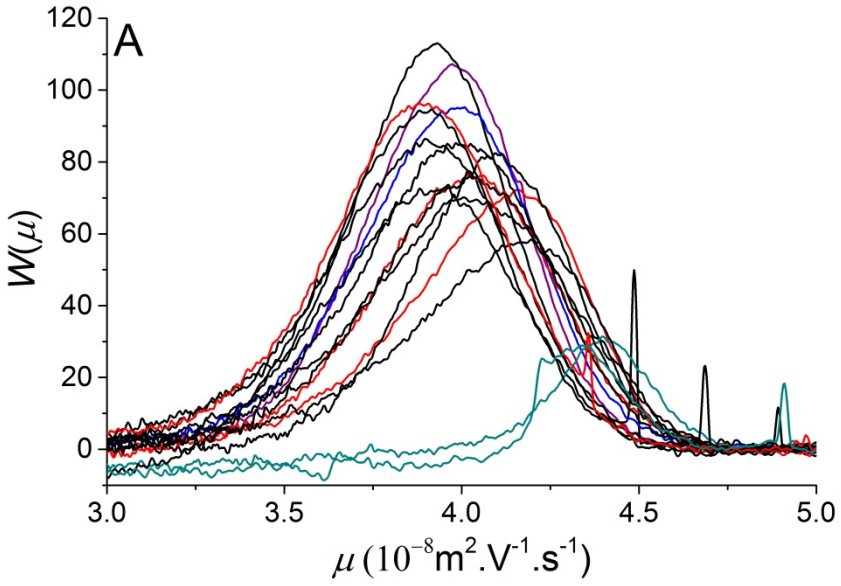

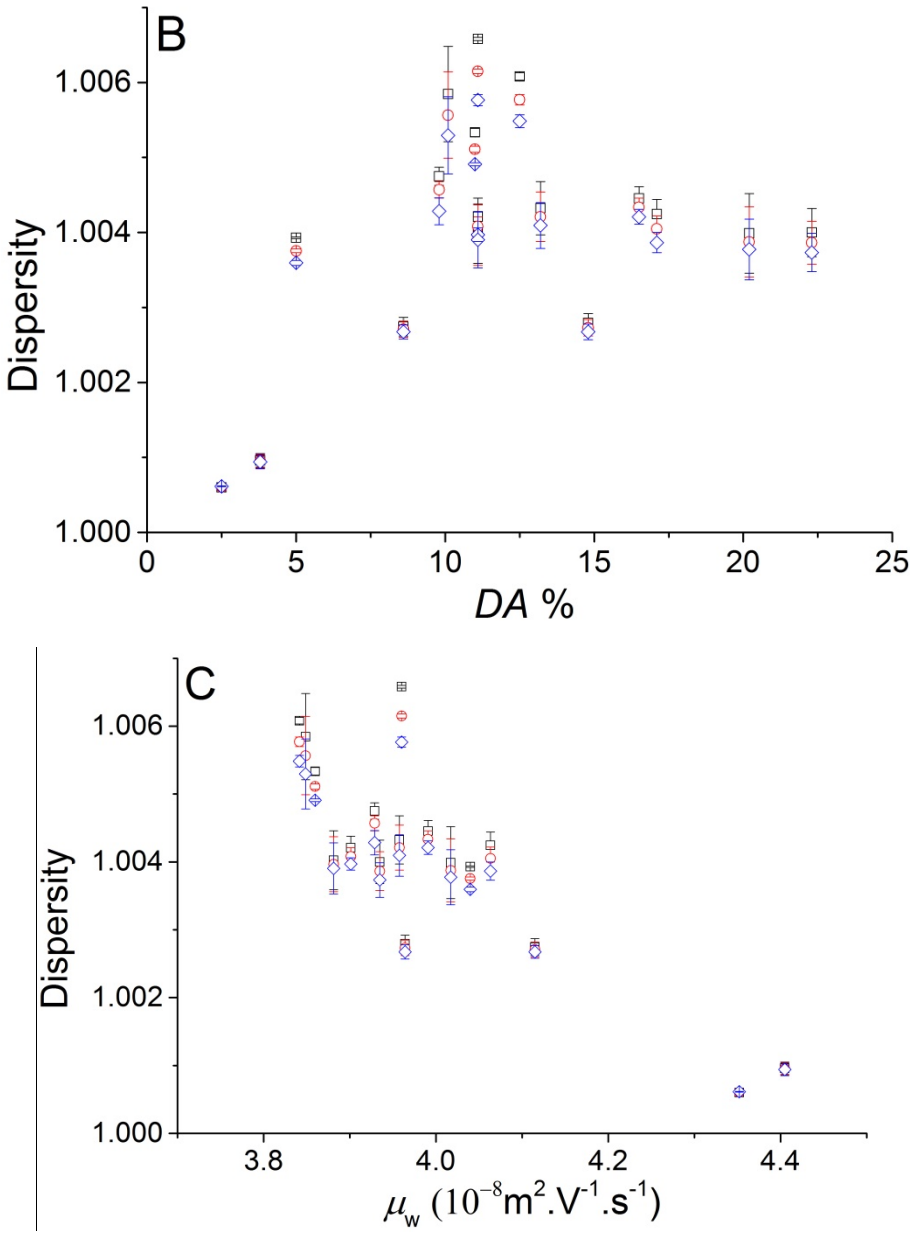

Figure 4-4. A. Distribution of electrophoretic mobilities, $W(\mu)$, of chitosan separated with PACE using NaPB100 for samples with an average *DA* (measured by SSNMR) below 5 % (green lines), between 5 % and 10 % (blue line), between 10 % and 15 % (red lines), between 15 % and 20 % (black lines) and above 20 % (purple line). Dispersity values (see supporting information for expressions) for chitosan samples as $D(W(\mu),1,0)$ (black squares), $D(W(\mu),2,0)$ (red circles) and $D(W(\mu),3,0)$ (blue diamonds) against their (B) number-average degree of acetylation or (C) weight-average electrophoretic

mobility (μ_w). See supporting information equation S4-1 to S4-3 for dispersity calculations [24].

3.3.2 CHITOSAN IN LITHIUM PHOSPHATE

In an effort to improve the selectivity of the chitosan separation, migration was also undertaken using LiPB100 as the background electrolyte (Figure 4-5A). Lithium has a mobility (3.9 x 10^{-8} $m^2.V^{-1}.s^{-1}$) more similar to that of chitosan than sodium (5.2 x 10^{-8} $m^2.V^{-1}.s^{-1}$) [40]. This prevents the occurrence of electrodispersion which may cause unwanted focusing and reduce selectivity further.

The distributions and dispersity values obtained of chitosan in LiPB100 showed similar trends to that in NaPB100. However, a greater repeatability was noted in the dispersity values of each of the samples.

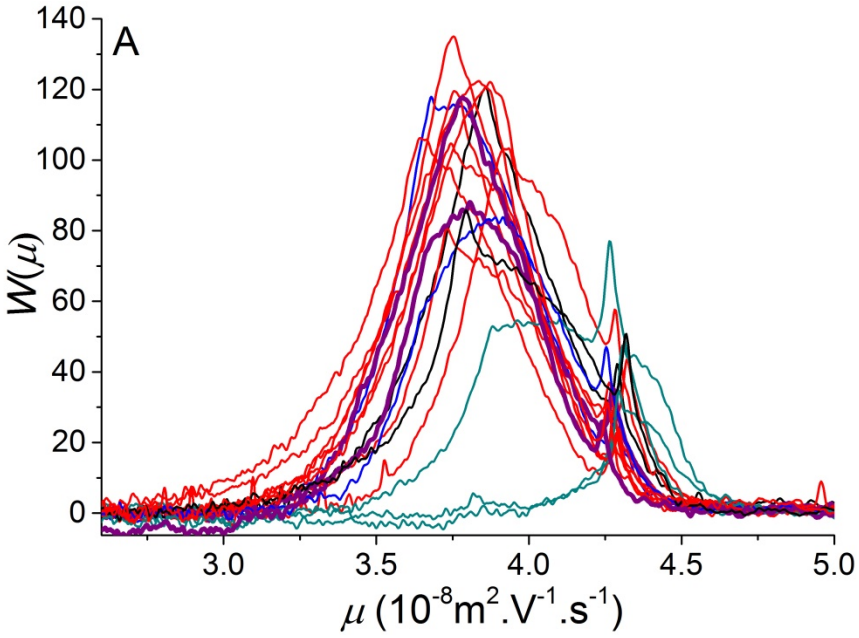

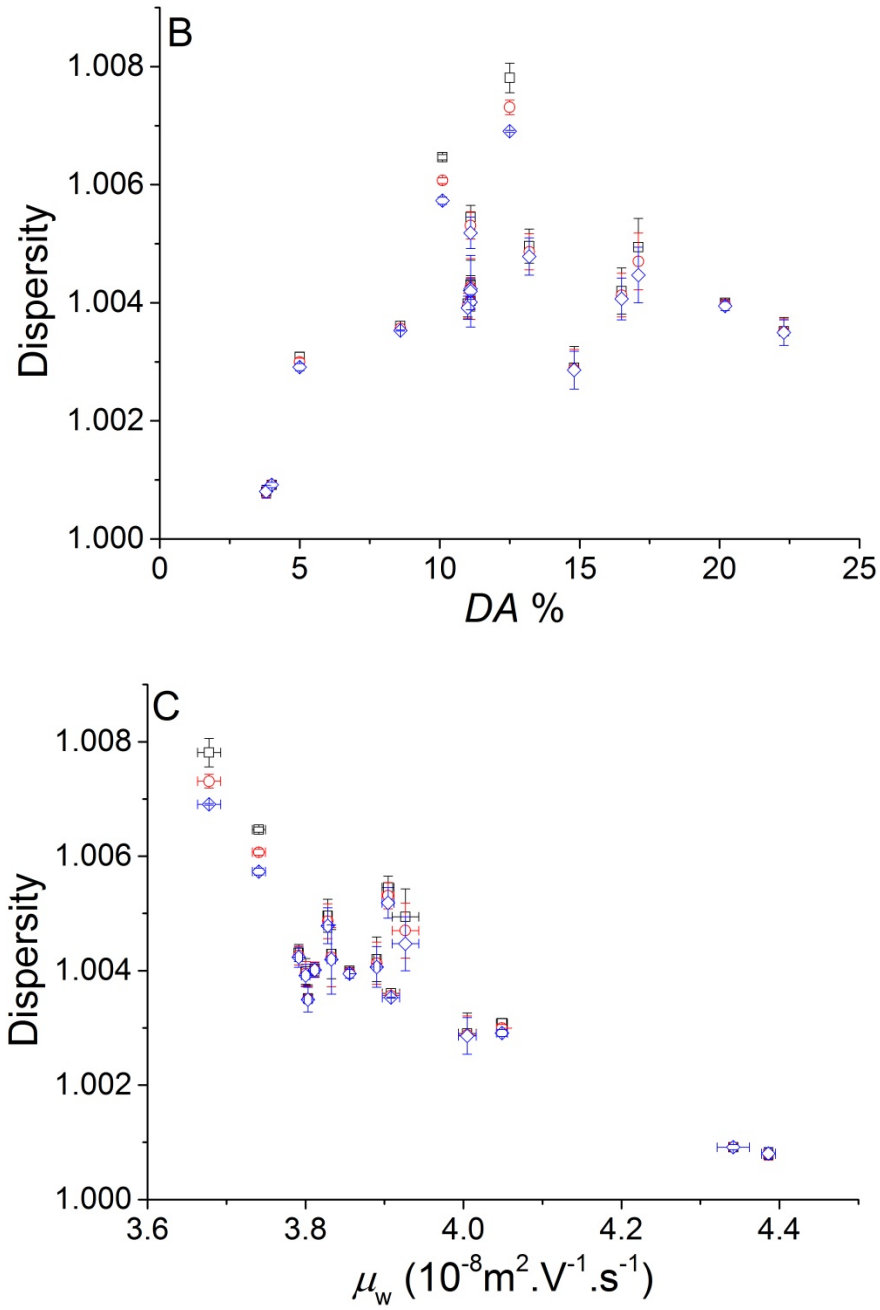

Figure 4-5. A. Distributions of electrophoretic mobilities, $W(\mu)$, of chitosan separated with PACE using LiPB100 with samples with an average *DA* below 5 % (green lines), between 5 % and 10 % (blue line), between 10 % and 15 % (red lines), between 15 % and 20 % (black lines) and above 20 % (purple line). Dispersity values for chitosan samples as $D(W(\mu),1,0)$ (black squares), $D(W(\mu),2,0)$ (red circles) and $D(W(\mu),3,0)$ (blue diamonds) against their (B) number-average degree of acetylation or (C) weight-average electrophoretic

mobility. See supporting information equation S4-1 to S4-3 for dispersity calculations [24].

Determining the dispersity of the electrophoretic mobility distributions is useful especially in the case of complex polyelectrolytes for which obtaining a correlation between the parameter of interest and mobility is challenging. Comparison of the dispersity values obtained from electrophoretic mobility distributions allows a direct qualitative comparison of the heterogeneity of the samples with respect to each other.

3.4. COMPOSITION DISTRIBUTIONS

3.4.1. CORRELATION BETWEEN MOBILITY AND COMPOSITION

To obtain composition distributions from electrophoretic mobility distributions a correlation is required between mobility and composition. Initial calibration curves which included all the chitosan samples used the average *DA* measured with solid-state NMR spectroscopy plotted against the weight-average electrophoretic mobility (Figure S4-3). The *DA* values were measured using solid-state NMR spectroscopy as it was proven that analyzing the *DA* by solution-state NMR spectroscopy was inaccurate due to both poor dissolution or to deacetylation in the most commonly used solvents [19]. The initial calibration curves seemed to show 2 separate populations with a very low correlation. However, calibration curves, especially in the case of molar mass distributions, are generally made with narrow standards and the chitosan samples analyzed do not fit this criterion due to their heterogeneities of composition. Therefore to obtain a calibration curve samples were removed

based on their dispersity value (below 1.0036 for LiPB100 ($r^2 > 0.75$) and 1.0040 for NaPB100 ($r^2 > 0.55$) until a correlation was obtained with a reasonable number of samples. This was undertaken for samples separated both in NaPB100 and Li-PB100. Using the least disperse samples for the calibration curve various fits including linear, polynomial, inverse and log functions were tested for the chitosan samples separated in NaPB100 (Figure S4-7). All of the trends suffered from low correlation and the linear, inverse and log functions resulted in distributions containing populations with negative *DA* values. As the *DA* cannot physically fall below 0, the fit should rather be performed with a mathematical function which is defined only between 0 and 1 (as is the *DA*). The Bradley function (double logarithmic reciprocal function) was thus tested and deemed the most appropriate fit (Equation 2 and Figure 4-6).

$$\mu = a \times \ln(-b \times \ln(DA)) \qquad \textbf{4-2}$$

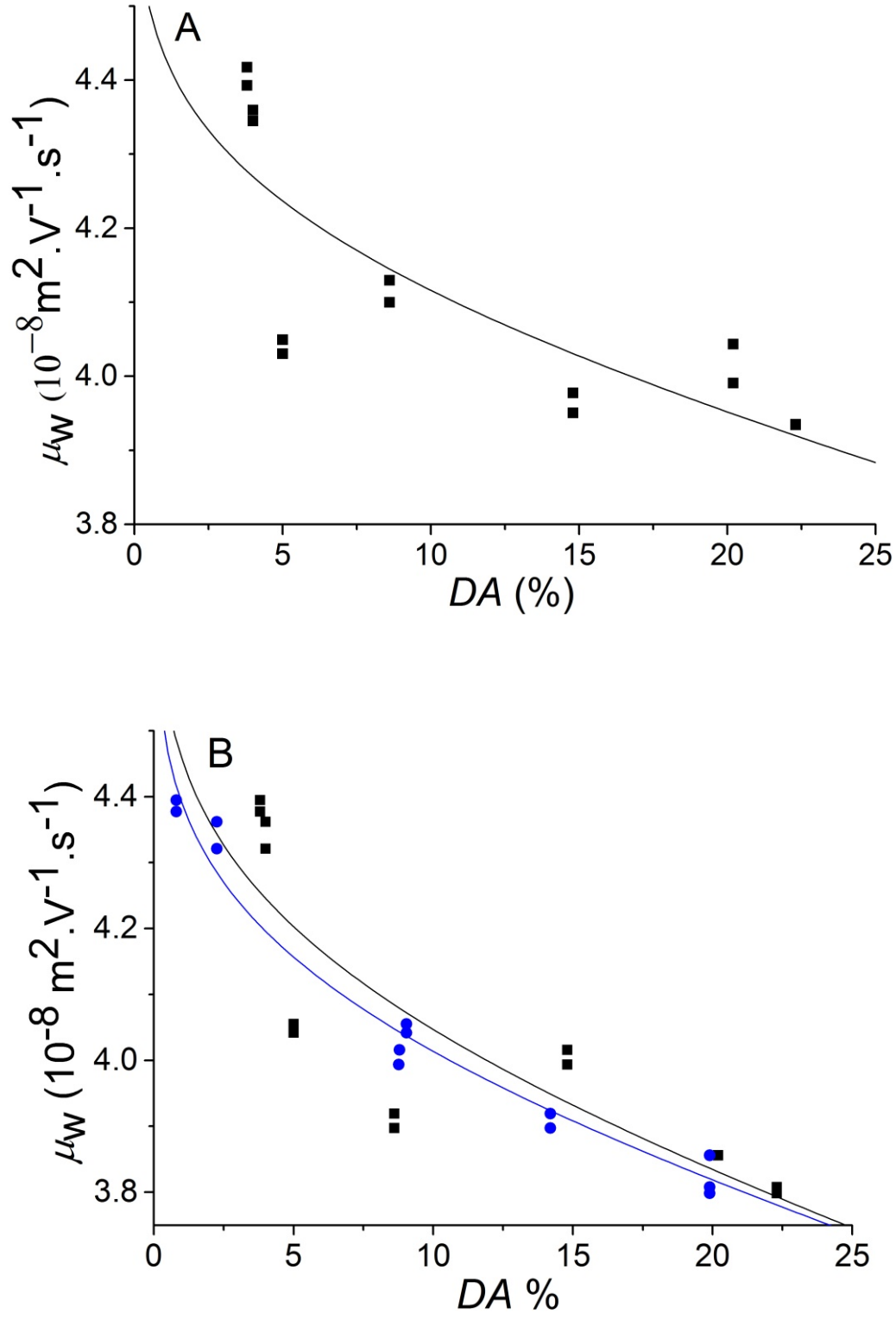

Figure 4-6: Calibration curve of the weight-average electrophoretic mobility in A. NaPB100 ($a = 4.58 \times 10^{-9}$, $b = 3447.2$, $r^2 = 0.62$) B. LiPB100 as a function of

DA for chitosan with a Bradley function fit first (black line) ($a = 5.44 \times 10^{-9}$, b = 693.77, $r^2 = 0.70$) and second iteration (blue line) ($a = 5.93 \times 10^{-9}$, b = 399.21, $r^2 = 0.97$), The electrophoretic mobilities were measured in duplicates; both duplicates are shown on the graph and included in the fit (see section 3.4.2)

Low correlations could be explained by a number of reasons. First the use of the Bradley fit is empirical (like that of the polynomial fit used for molar mass determination by SEC) but not based on a theory predicting the relation between μ and *DA*. Second, heterogeneity of the composition of chitosan is not just due to differences in average *DA* but may also be in the form of blocks of deacetylated groups. This would influence the separation as for the chitosan sample to be in the critical conditions for capillary electrophoresis the charges should be evenly distributed along the polymer chain. If there are blocks of charged species the chitosan chains may behave as a block copolymer [41] rather than a statistical copolymer. In this case the separation (electrophoretic mobility) is influenced by both the mobility of the charged species and the hydrodynamic friction of the uncharged species. Without an appropriate correction factor the occurrence of this bias cannot be accounted for. One reason for block deacetylation is the semi-crystalline structure of the precursor of chitosan, chitin [42]. To check if the occurrence of 2 populations was due to block deacetylation XRD measurements were undertaken. Crystallinity from the precursor chitin would likely play a role in the block deacetylation. However no significant difference was noted between the samples which exhibited diffractograms typical of amorphous chitosan samples [43] (Figure S4-8). This suggests that no long range order is in the chitosan samples; however, the occurrence of short chain blocks is still possible and would influence the mobility. Further reasons of a low correlation may include the dissolution and

the treatment of chitin to chitosan. The dissolution of the sample plays an important role in the meaningful characterization of the sample as a whole and bias in dissolution would prevent an accurate correlation between the accurate *DA* measured in solid-state NMR spectroscopy and the distributions of mobility. Although the problem of dissolution was not overcome and requires further investigation, composition distributions were obtained with the best current dissolution.

3.4.2. CALCULATION OF COMPOSITION DISTRIBUTIONS

Using the calibration curve the electrophoretic mobility distributions were transformed to composition distributions using the following equations:

$$DA = e^{\left(-\frac{\frac{\mu}{e}-a}{b}\right)} \quad \textbf{4-3}$$

$$W(DA) = W(\mu) \times \frac{-a}{DA \times \ln(DA)} \quad \textbf{4-4}$$

The composition distributions of the chitosan samples used in calibration curves were obtained (Figure 4-7). This is the first time composition distributions of chitosan are presented in the literature. The composition distributions reveal information on the amount of chains with a specific composition in the sample. The dispersities of the composition distributions were observed to be larger than those seen for electrophoretic mobility distributions (Figure 4-8). There is no expectation of the dispersities values for these two different types of distributions to be similar. However, larger variations in dispersity values of the composition distributions were seen between replicates. The dispersity values of the composition distributions are less repeatable than the ones of the electrophoretic mobility distributions; however, the variations were still small

(e.g. in comparison to the 2000 % variation for M_n and M_w determined in a round-robin test for poly(acrylic acid) using SEC [44]). The dispersity values were calculated for composition distributions for the first time. The dispersity values for $D(W(\mu),1,0)$ were determined to be larger than those for $D(W(\mu),2,0)$ and $D(W(\mu),3,0)$. A different trend of the dispersity values was seen compared to those calculated from the electrophoretic mobility distributions. This is likely due to the lower selectivity in terms of μ at low *DA* compared to intermediate *DA* (the calibration curve has a higher slope at low *DA* than intermediate *DA*). The conversion from $W(\mu)$ to $W(DA)$ thus corrects an artefact in a similar fashion as the conversion from SEC chromatograms to molar mass distributions corrects for an artefact when the SEC calibration is not linear in the region of interest [45]. Standard deviation values of $W(DA)$ showed a trend similar to that obtained with the dispersities of $W(\mu)$. The dispersity of $W(DA)$ and its standard deviation thus give different information on the composition and its heterogeneity. They may relate to different functional properties. The standard deviation values are corresponding to the visual comparison of the $W(DA)$: the distributions at the lowest *DA*s appear sharper. It is to note that the translation of the $W(DA)$ at higher *DA* (+0.05) led to a decrease of the dispersity values from around 2 (Figure 4-7) to 1.0001. The dispersity values are thus giving an interesting perspective on the $W(DA)$ that visual observation of the distributions in this work could not provide.

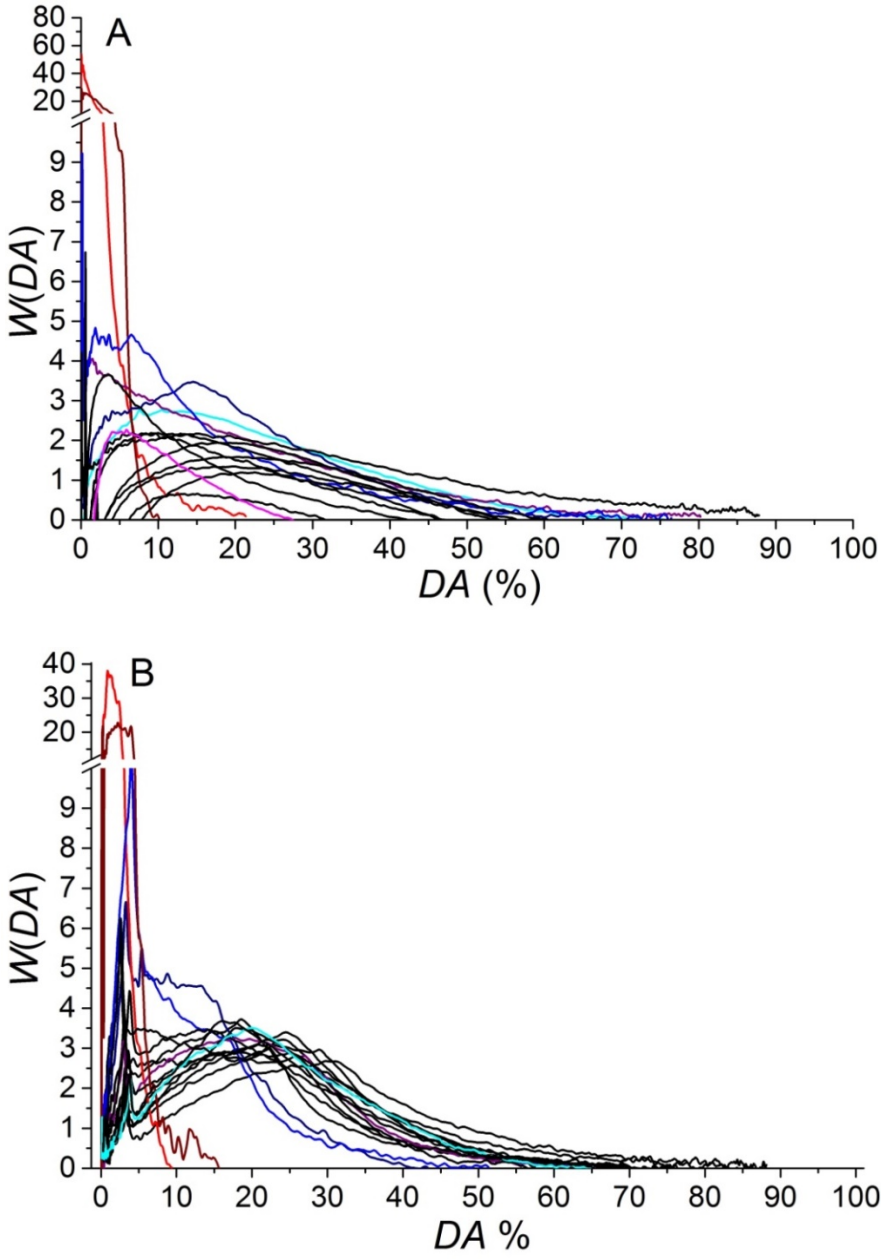

Figure 4-7: Composition distributions of chitosan samples separated in A. NaPB100 and B. LiPB100

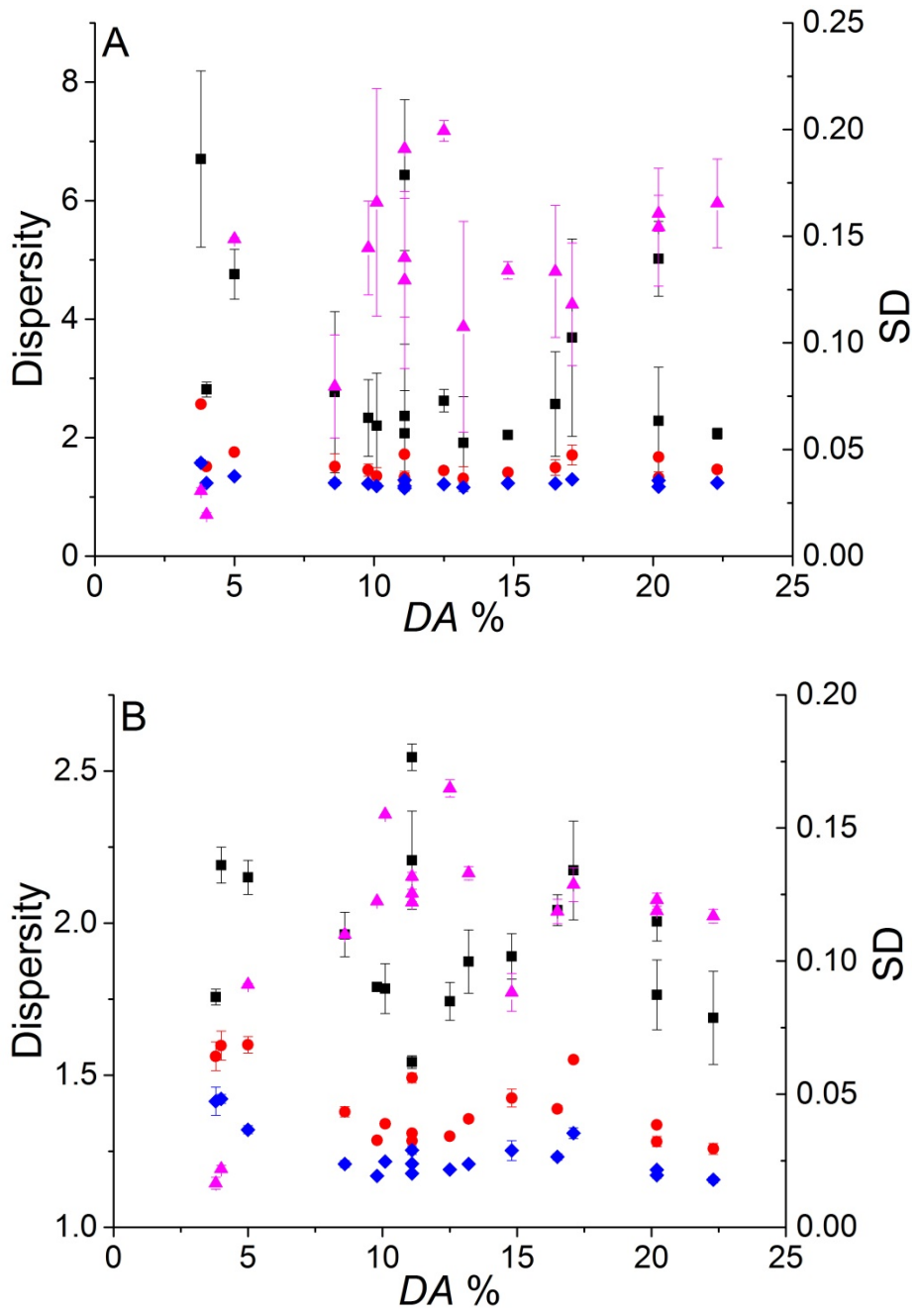

Figure 4-8. Dispersity of composition distributions as $D(W(DA),1,0)$ (black squares), $D(W(DA),2,0)$ (red circles), $D(W(DA),3,0)$ (blue diamonds) and standard deviation (pink triangles) for chitosan samples separated in A) NaPB100 and B) LiPB100. See supporting information equation S4-1 to S4-8 for dispersity calculations [24].

Using the composition distributions obtained (Figure 4-7B) a second iteration of the *DA* versus electrophoretic mobility calibration curve was determined for the chitosan samples separated in LiPB100. There is no reason for the average *DA* determined by NMR to correspond to μ_w. To obtain the second iteration the average *DA* values determined from the solid-state NMR measurements were thus replaced with those determined at the peak apex of the relevant composition distributions. This was re-plotted against the weight-average electrophoretic mobilities obtained by CE (Figure 4-6B). The correlation improved compared to the initial calibration curve. This was not the case for the chitosan samples separated in NaPB100 (Figure S4-9). Therefore, composition distributions were calculated for the chitosan samples using the 2nd iteration of the calibration curve only in LiPB100. Further the dispersity values of the composition distributions were plotted against the *DA* obtained by solid-state NMR spectroscopy (Figure 4-9B). The composition distributions exhibited minimal changes, although slightly more tailing may be noticed. The trend of the dispersity values is similar to that before the iteration. Once again the standard deviation supports the visual observation for the composition distributions; however, the corresponding values are higher in the re-treated composition distributions. The dispersity values are constant throughout the whole range of samples. Therefore a quantitative analysis of the composition distributions is possible using the standard deviation which discriminates the different chitosan in this work and potentially the dispersities for other samples.

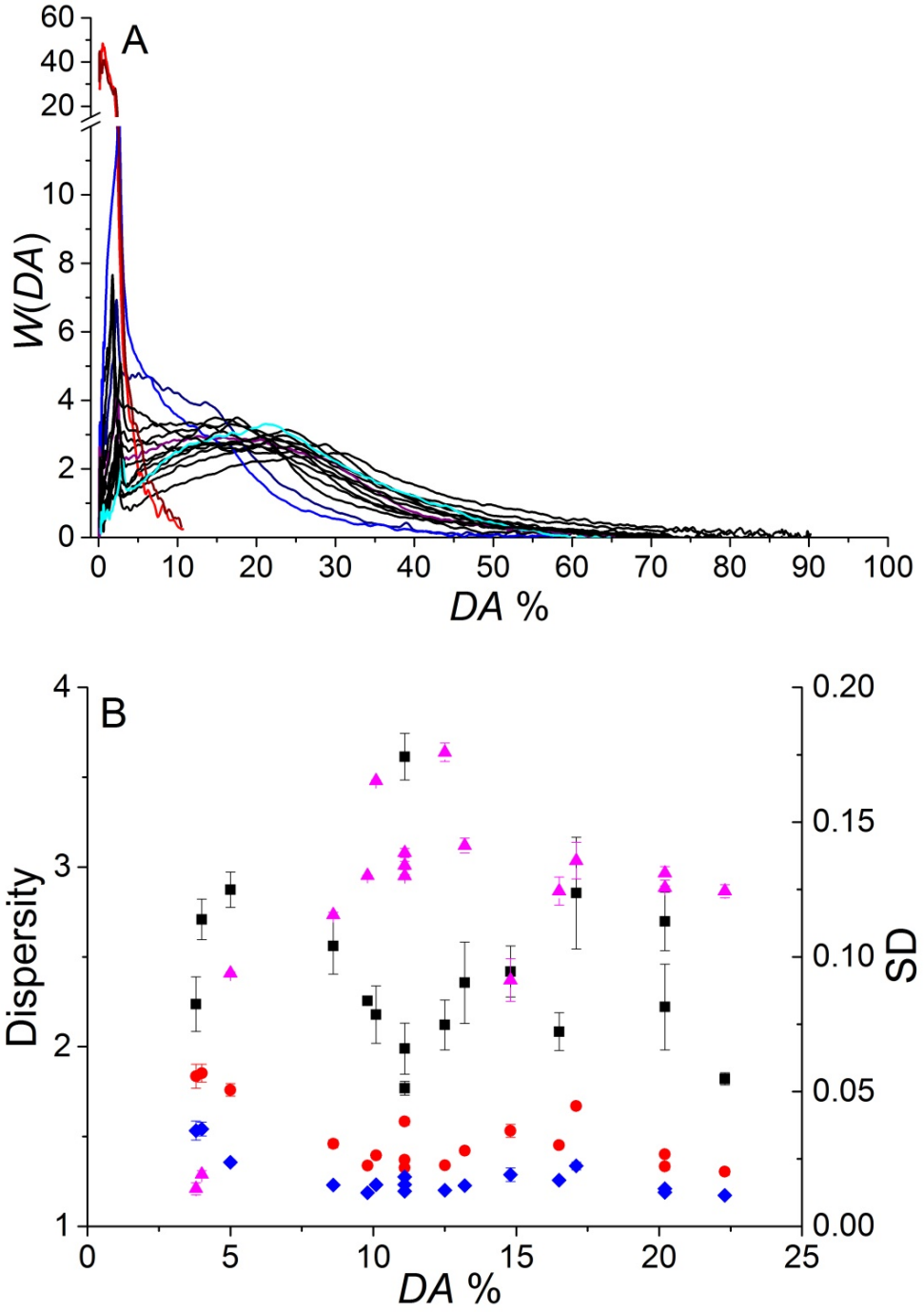

Figure 4-9. A. Composition distributions and B. Dispersity of composition distributions as *D*(*W*(*DA*),1,0) (black squares), *D*(*W*(*DA*),2,0) (red circles), *D*(*W*(*DA*),3,0) (blue diamonds) and standard deviation (pink triangles) for chitosan samples separated in LiPB100 and treated with the 2nd iteration. See supporting information equation S4-1 to S4-8 for dispersity calculations [24].

4. CONCLUSIONS

In this study distributions of electrophoretic mobilities and of compositions were obtained for a range of chitosan samples and their dispersity values were determined. Multilayer coatings were tested to prevent adsorption and a cationic polymer, polyamine sample poly(allylamine hydrochloride) was separated successfully. The selectivity of the chitosan separation was improved with the use of lithium as the counter-ion. The distribution of electrophoretic mobilities, $W(\mu)$, and its dispersity can be used for a quick and precise characterization of the heterogeneity of *DA* of chitosan (or the heterogeneity of composition of any statistical copolymer where at least one monomer unit is charged). The application of this methodology to the monitoring of the dissolution of chitosan confirmed that the *DA* can influence the dissolution of chitosan. Strategies to obtain the distribution of *DA*s, $W(DA)$, have been proposed and tested as well. The determination of $W(DA)$ requires establishing a correlation between the *DA* of several chitosan samples and their electrophoretic mobility. The usual mathematical functions (linear, polynomial) used to produce calibration curves (in SEC) did not provide any correlation. Bradley functions did provide some correlation between the weight-average electrophoretic mobility and the *DA* (composition) of chitosan samples which allowed composition distributions to be obtained for the first time. Standard with low dispersity of the distribution of *DA*s do not exist. The quality of the calibration can thus be rather improved by using an iteration process (in which the peak apex from the composition distributions is used as an improved *DA* value). For the specific example of chitosan, the standard deviation and dispersity were valuable in numerically representing the heterogeneity of the composition distributions and give different perspectives. This methodology

can be applied to any charged copolymer such as heparin, carboxymethylcelluloses and pectins and would truly be advantageous. Separations by composition with a high selectivity would allow a strong correlation between mobility and composition. Further work may also involve improving the selectivity specifically in the separation of chitosan. This would result in a greater precision in the resulting composition distributions. In conclusion, the calculation of composition distributions provides an improved characterization which influences the possible modification or functionalization of copolymers, quality control of the synthesis and a closer step towards understanding structure-property relationships of complex polymers, which has already been identified as crucial. For example the *DA* has been shown to influence significant properties such as bioadhesion [5], dissolution [19] and biodegradability [46,, 47]. The functional characterization of chitosan and its derivatives is nowadays one of the most productive research areas [3].

SUPPORTING INFORMATION

The supporting information contains the supplier information, kinetics of dissolution, separation of PAlAm, correlation of electrophoretic mobility and composition and X-ray diffraction of chitosan powders. This material is available free of charge via the Internet at http://pubs.acs.org.

ACKNOWLEDGMENTS

JJT thanks Leena Thevarajah for assistance with data treatment, Aidan Grosas for discussions, Alison Maniego and Melissa Meinel for assistance in the lab. JJT also thanks the Australian Government for an Endeavour Research fellowship to travel to the University of Montpellier, Montpellier, France. The authors thank Timothy Murphy and Richard Wuhrer from the Advanced Materials

Characterisation Facility (AMCF) at Western Sydney University for discussions and instrumentation training/assistance.

REFERENCES

1. M. Rinaudo, Chitin and chitosan: Properties and applications, Prog. Polym. Sci. 31 (2006) 603-632.
2. A. Domard, A perspective on 30 years research on chitin and chitosan, Carbohydr. Polym. 84 (2011) 696-703.
3. S.K. Shukla, A.K. Mishra, O.A. Arotiba, B.B. Mamba, Chitosan-based nanomaterials: A state-of-the-art review, Int. J. Biol. Macromol. 59 (2013) 46-58.
4. M.J. Barton, J.W. Morley, D.A. Mahns, D. Mawad, R. Wuhrer, D. Fania, S.J. Frost, C. Loebbe, A. Lauto, Tissue repair strength using chitosan adhesives with different physical-chemical characteristics, J. Biophotonics 7 (2014) 948-955.
5. B. Menchicchi, J.P. Fuenzalida, K.B. Bobbili, A. Hensel, M.J. Swamy, F.M. Goycoolea, Structure of Chitosan Determines Its Interactions with Mucin, Biomacromolecules 15 (2014) 3550-3558.
6. S. Nguyen, S. Hisiger, M. Jolicoeur, F.M. Winnik, M.D. Buschmann, Fractionation and characterization of chitosan by analytical SEC and H-1 NMR after semi-preparative SEC, Carbohydr. Polym. 75 (2009) 636-645.
7. M. Mnatsakanyan, J.J. Thevarajah, R.S. Roi, A. Lauto, M. Gaborieau, P. Castignolles, Separation of chitosan by degree of acetylation using simple free solution capillary electrophoresis, Anal. Bioanal. Chem. 405 (2013) 6873-6877.
8. I.A.H. Ahmad, A.M. Striegel, Determining the absolute, chemical-heterogeneity-corrected molar mass averages, distribution, and solution conformation of random copolymers, Anal. Bioanal. Chem. 396 (2010) 1589-1598.
9. H. Maier, F. Malz, W. Radke, Characterization of the Chemical Composition Distribution of Poly(n-butyl acrylate-stat-acrylic acid)s, Macromol. Chem. Phys. 216 (2015) 228-234.
10. M. Shakun, T. Heinze, W. Radke, Determination of the DS distribution of non-degraded sodium carboxymethyl cellulose by gradient chromatography, Carbohydr. Polym. 98 (2013) 943-950.

11. M. Shakun, T. Heinze, W. Radke, Characterization of sodium carboxymethyl cellulose by comprehensive two-dimensional liquid chromatography, Carbohydr. Polym. 130 (2015) 77-86.

12. M.K. Jang, B.G. Kong, Y.I. Jeong, C.H. Lee, J.W. Nah, Physicochemical characterization of alpha-chitin, beta-chitin, and gamma-chitin separated from natural resources, J. Polym. Sci. Pol. Chem. 42 (2004) 3423-3432.

13. T. Sannan, K. Kurita, Y. Iwakura, Studies on Chitin, 2. Effect of Deactylation on Solubility, Makromol. Chem. Macromol. Chem. Phys. 177 (1976) 3589-3600.

14. K. Kurita, S. Ishii, K. Tomita, S.I. Nishimura, K. Shimoda, Reactivity Characteristics of Squid Beta-Chitin as Compared with Those of Shrimp Chitin: High Potentials of Squid Chitin as a Starting Material for Facile Chemical Modifications, J. Polym. Sci. A Polym. Chem. 32 (1994) 1027-1032.

15. G. Lamarque, C. Viton, A. Domard, Comparative study of the first heterogeneous deacetylation of alpha- and beta-chitins in a multistep process, Biomacromolecules 5 (2004) 992-1001.

16. K. Kurita, T. Sannan, Y. Iwakura, Studies on Chitin, 4. Evidence for formation of block and random copolymers of N-Acetyl-D-glucosamine and D-glucosamine by Hetero- and Homogenous Hydrolyses, Macromol. Chem. Phys. 178 (1977) 3197-3202.

17. M.R. Kasaai, Various Methods for Determination of the Degree of N-Acetylation of Chitin and Chitosan: A Review, J. Agric. Food Chem. 57 (2009) 1667-1676.

18. A. Zajac, J. Hanuza, M. Wandas, L. Dyminska, Determination of N-acetylation degree in chitosan using Raman spectroscopy, Spectroc. Acta Pt. A-Molec. Biomolec. Spectr. 134 (2015) 114-120.

19. J.J. Thevarajah, J.C. Bulanadi, M. Wagner, M. Gaborieau, P. Castignolles, Towards a less biased dissolution of chitosan, Anal. Chim. Acta 935 (2016) 258-268.

20. M.H. Ottoy, K.M. Varum, O. Smidsrod, Compositional heterogeneity of heterogeneously deacetylated chitosans, Carbohydr. Polym. 29 (1996) 17-24.

21. L. Heux, J. Brugnerotto, J. Desbrieres, M.F. Versali, M. Rinaudo, Solid state NMR for determination of degree of acetylation of chitin and chitosan, Biomacromolecules 1 (2000) 746-751.

22. M. Gaborieau, P. Castignolles, Size-exclusion chromatography (SEC) of branched polymers and polysaccharides, Anal. Bioanal. Chem. 399 (2011) 1413-1423.

23. Z. Grubisic, P. Rempp, H. Benoit, A universal calibration for gel permeation chromatography (Reprinted from Polymer Letters, vol 5, pg 753-759, 1967), J. Polym. Sci. B Polym. Phys. 34 (1996) 1707-1713.

24. Y. Brun, P. Foster, Characterization of synthetic copolymers by interaction polymer chromatography: Separation by microstructure, J. Sep. Sci. 33 (2010) 3501-3510.

25. A. Favier, C. Petit, E. Beaudoin, D. Bertin, Liquid chromatography at the critical adsorption point (LC-CAP) of high molecular weight polystyrene: pushing back the limits of reduced sample recovery, E-Polymers 9 (2009) 15.

26. J.J. Thevarajah, M. Gaborieau, P. Castignolles, Separation and characterization of synthetic polyelectrolytes and polysaccharides with capillary electrophoresis, Adv. Chem. 2014 (2014) Article ID 798403.

27. J.J. Thevarajah, A.T. Sutton, A.R. Maniego, E.G. Whitty, S. Harrisson, H. Cottet, P. Castignolles, M. Gaborieau, Quantifying the Heterogeneity of Chemical Structures in Complex Charged Polymers through the Dispersity of Their Distributions of Electrophoretic Mobilities or of Compositions, Anal. Chem. 88 (2016) 1674-1681.

28. S.E. Guillotin, E.J. Bakx, P. Boulenguer, H.A. Schols, A.G.J. Voragen, Determination of the degree of substitution, degree of amidation and degree of blockiness of commercial pectins by using capillary electrophoresis, Food Hydrocoll. 21 (2007) 444-451.

29. K.A. Oudhoff, F.A. Ab Buijtenhuijs, P.H. Wijnen, P.J. Schoenmakers, W.T. Kok, Determination of the degree of substitution and its distribution of carboxymethylcelluloses by capillary zone electrophoresis, Carbohydr. Res. 339 (2004) 1917-1924.

30. T. Wielgos, K. Havel, N. Ivanova, R. Weinberger, Determination of impurities in heparin by capillary electrophoresis using high molarity phosphate buffers, J. Pharm. Biomed. Anal. 49 (2009) 319-326.

31. H.F. Wu, S.A. Allison, C. Perrin, H. Cottet, Modeling the electrophoresis of highly charged peptides: Application to oligolysines, J. Sep. Sci. 35 (2012) 556-562.

32. C.H. Wu, C.Y. Kao, S.Y. Tseng, K.C. Chen, S.F. Chen, Determination of the degree of deacetylation of chitosan by capillary zone electrophoresis, Carbohydr. Polym. 111 (2014) 236-244.

33. C. Lefay, Y. Guillaneuf, G. Moreira, J.J. Thevarajah, P. Castignolles, F. Ziarelli, E. Bloch, M. Major, L. Charles, M. Gaborieau, D. Bertin, D. Gigmes, Heterogeneous modification of chitosan via nitroxide-mediated polymerization, Polym. Chem. 4 (2013) 322-328.

34. J. Chamieh, M. Martin, H. Cottet, Quantitative Analysis in Capillary Electrophoresis: Transformation of Raw Electropherograms into Continuous Distributions, Anal. Chem. 87 (2015) 1050-1057.

35. M. Gaborieau, T. Causon, Y. Guillaneuf, E.F. Hilder, P. Castignolles, Molecular weight and tacticty of oligoacrylates by capillary electrophoresis - mass spectrometry, Aus. J. Chem. 63 (2010) 1219-1226.

36. H. Katayama, Y. Ishihama, N. Asakawa, Stable cationic capillary coating with successive multiple ionic polymer layers for capillary electrophoresis, Anal. Chem. 70 (1998) 5272-5277.

37. C.R. Morcombe, K.W. Zilm, Chemical shift referencing in MAS solid state NMR, J. Magn. Reson. 162 (2003) 479-486.

38. M.T. Bowser, E.D. Sternberg, D.D.Y. Chen, Development and application of a nonaqueous capillary electrophoresis system for the analysis of porphyrins and their oligomers, Anal. Biochem. 241 (1996) 143-150.

39. L. Chiappisi, M. Gradzielski, Co-assembly in chitosan-surfactant mixtures: thermodynamics, structures, interfacial properties and applications, Adv. Colloid Interface Sci. 220 (2015) 92-107.

40. J. Wu, K. Gerstandt, H. Zhang, J. Liu, B.J. Hinds, Electrophoretically induced aqueous flow through single-walled carbon nanotube membranes, Nat. Nano. 7 (2012) 133-139.

41. A.T. Sutton, E. Read, A.R. Maniego, J. Thevarajah, J.D. Marty, M. Destarac, M. Gaborieau, P. Castignolles, Purity of double hydrophilic block copolymers revealed by capillary electrophoresis in the critical conditions, J. Chromatogr. A 1372 (2014) 187-195.

42. C.K.S. Pillai, W. Paul, C.P. Sharma, Chitin and chitosan polymers: Chemistry, solubility and fiber formation, Prog. Polym. Sci. 34 (2009) 641-678.

43. C. Gartner, B.L. Lopez, L. Sierra, R. Graf, H.W. Spiess, M. Gaborieau, Interplay between Structure and Dynamics in Chitosan Films Investigated with Solid-State NMR, Dynamic Mechanical Analysis, and X-ray Diffraction, Biomacromolecules 12 (2011) 1380-1386.

44. D. Berek, Size exclusion chromatography - A blessing and a curse of science and technology of synthetic polymers, J. Sep. Sci. 33 (2010) 315-335.

45. M. Gaborieau, R.G. Gilbert, A. Gray-Weale, J.M. Hernandez, P. Castignolles, Theory of Size Exclusion Chromatography (SEC) of complex branched polymers, Macromol. Theory Simul. 16 (2007) 13-28.

46. Y. Shigemasa, K. Saito, H. Sashiwa, H. Saimoto, Enzymatic Degradation of Chitins and Partially Deacetylated Chitins, Int. J. Biol. Macromol. 16 (1994) 43-49.

47. S. Aiba, Studies on Chitosan 4. Lysozyme Hydrolysis of Partially N-Acetylated Chitosans, Int. J. Biol. Macromol. 14 (1992) 225-228.

4.2. Publication: Supporting information

Supporting Information

For

Determination of the Distribution of the Degrees of Acetylation of Chitosan

Joel J Thevarajah[1,2], Matthew P Van Leeuwen[1,3], Herve Cottet[4], Patrice Castignolles[2*], Marianne Gaborieau[1,2]

[1]Western Sydney University, Molecular Medicine Research Group (MMRG), Parramatta, 2150, Australia

[2]Western Sydney University, Australian Centre for Research on Separation Sciences (ACROSS), School of Science and Health, Parramatta, 2150, Australia

[3]Western Sydney University, School of Medicine, Parramatta, 2150, Australia

[4]Institut des Biomolécules Max Mousseron (IBMM, UMR 5247 CNRS-Université de Montpellier-Ecole Nationale Supérieure de Chimie de Montpellier), Place Eugène Bataillon CC 1706, 34095 Montpellier Cedex 5, France

CHITOSAN SAMPLES AND SUPPLIER INFORMATION

A number of chitosan samples were analyzed. The samples were commercially available from different suppliers.

Table S4-1: Information of chitosan samples studied in the manuscript provided by supplier and measured. *DA* is the degree of acetylation in % of monomer units (DA_{supp} was given by the supplier, DA_{SSNMR} was measured by solid-state NMR spectroscopy). The viscosity in cps was given by the supplier in the following conditions: [A] at 20°C; [B] at 1% in 1% AcOH; [C] at 1 % in 1 % AcOH, at 20 °C, according to DIN 45, 100S-1; [D] at 20°C, [B] at 1% in 1% AcOH.

Sample	*Supplier*	*Catalog number*	*Lot*	DA_{supp}	DA_{SSNMR}	*Viscosity*
HighMW1	Sigma-Aldrich	419419	MKBD7240V	22	11.1	1218 [B]
HighMW2	Sigma-Aldrich	419419	12913CJ	24	11.0	1540 [B]
MedMW2	Sigma-Aldrich	448877	03318AJ	20	20.2	590 [B]
MedMW3	Sigma-Aldrich	448877	MKBF1336V	20	13.2	503 [B]
MedMW1	Sigma-Aldrich	448877	MKBH1108V	24	22.3	563 [B]
MedMW4	Sigma-Aldrich	448877	09303PE	25	11.1	453 [B]
LowMW2	Sigma-Aldrich	448869	06714DJ	8.9	5	238 [B]
LowMW1	Sigma-Aldrich	448869	MKBG3334V	3.9	17.1	35 [B]
Sig	Sigma-Aldrich	C3646	120M0028V	12	9.8	

Fluk	Sigma-Aldrich (Fluka)	28191	440698/1	not indicated	8.6	337 [C]
AKbioV1	AK Biotech Ltd		090426V1	13.8	10.1	30 [A]
AKbioV2	AK Biotech Ltd		090423V2	14	16.5	320 [A]
AKbioV3	AK Biotech Ltd		090426V3	14	14.8	570 [A]
AKbioD1	AK Biotech Ltd		090422D1	13.9	12.5	35 [A]
AKbioD2	AK Biotech Ltd		090422D2	9.8	11.1	55 [A]
AKbioD3	AK Biotech Ltd		090422D3	4.4	3.8	55 [A]
chitAL	[1]			2.5	4.0	unknown

DISPERSITY OF THE ELECTROPHORETIC MOBILITY DISTRIBUTIONS AND OF THE COMPOSITION DISTRIBUTIONS (DISTRIBUTIONS OF *DA*S)

The expressions of dispersity for electrophoretic mobility distributions and composition distributions have recently been established [2]. The expressions are analogous to the calculation of dispersity of molar mass distributions by a ratio of moments. The discrete expressions used to calculate the dispersity are as below:

$$D(W(\mu),1,0) = \frac{[\sum_z W(\mu_z)\mu_z\,(\mu_{z+1}-\mu_z)][\sum_z W(\mu_z)\mu_z{}^{-1}(\mu_{z+1}-\mu_z)]}{[\sum_z W(\mu_z)\,(\mu_{z+1}-\mu_z)]^2} \quad \textbf{S4-1}$$

$$D(W(\mu),2,0) = \frac{[\sum_z W(\mu_z)\,\mu_z{}^2(\mu_{z+1}-\mu_z)][\sum_z W(\mu_z)\,(\mu_{z+1}-\mu_z)]}{[\sum_z W(\mu_z)\,\mu_z(\mu_{z+1}-\mu_z)]^2} \quad \textbf{S4-2}$$

$$D(W(\mu),3,0) = \frac{[\sum_z W(\mu_z)\,\mu_z{}^3(\mu_{z+1}-\mu_z)][\sum_z W(\mu_z)\,\mu_z(\mu_{z+1}-\mu_z)]}{[\sum_z W(\mu_z)\,\mu_z{}^2(\mu_{z+1}-\mu_z)]^2} \quad \textbf{S4-3}$$

$$D(W(DA)1,0) \quad = \frac{[\sum_z W(DA_z)\,DA_z\,(DA_{z+1}-DA_z)]\left[\sum_z W(DA_z)\,DA_z^{-1}\,(DA_{z+1}-DA_z)\right]}{[\sum_z W(DA_z)\,(DA_{z+1}-DA_z)]^2} \quad \textbf{S4-4}$$

$$D(W(DA),2,0) = \frac{[\sum_z W(DA_z)\,DA_z{}^2(DA_{z+1}-DA_z)][\sum_z W(DA_z)\,(DA_{z+1}-DA_z)]}{[\sum_z W(DA_z)\,DA_z(DA_{z+1}-DA_z)]^2} \quad \textbf{S4-5}$$

$$D(W(DA),3,0) = \frac{[\sum_z W(DA_z)\,DA_z{}^3(DA_{z+1}-DA_z)][\sum_z W(DA_z)DA_z\,(DA_{z+1}-DA_z)]}{\left[\sum_z W(DA_z)\,DA_z{}^2(DA_{z+1}-DA_z)\right]^2} \quad \textbf{S4-6}$$

$$D_\sigma = \left[\frac{[\sum_z W(\mu_z)\,(\mu_z-\mu_\mathrm{w})^2(\mu_{z+1}-\mu_z)}{[\sum_z W(\mu_z)\,(\mu_{z+1}-\mu_z)]}\right]^{0.5} \quad \textbf{S4-7}$$

$$D(W(DA),\sigma,DA_\mathrm{W}) = \left[\frac{[\sum_z W(DA_z)\,(DA_z-DA_\mathrm{w})^2(DA_{z+1}-DA_z)]}{[\sum_z W(DA_z)(DA_{z+1}-DA_z)]}\right]^{0.5} \quad \textbf{S4-8}$$

KINETICS OF CHITOSAN DISSOLUTION

Pressure assisted capillary electrophoresis (PACE) measurements of the dissolution of MewMW1 in either 50 mM HCl or 50 mM DCl in D_2O were undertaken with the carousel set to 60 °C.

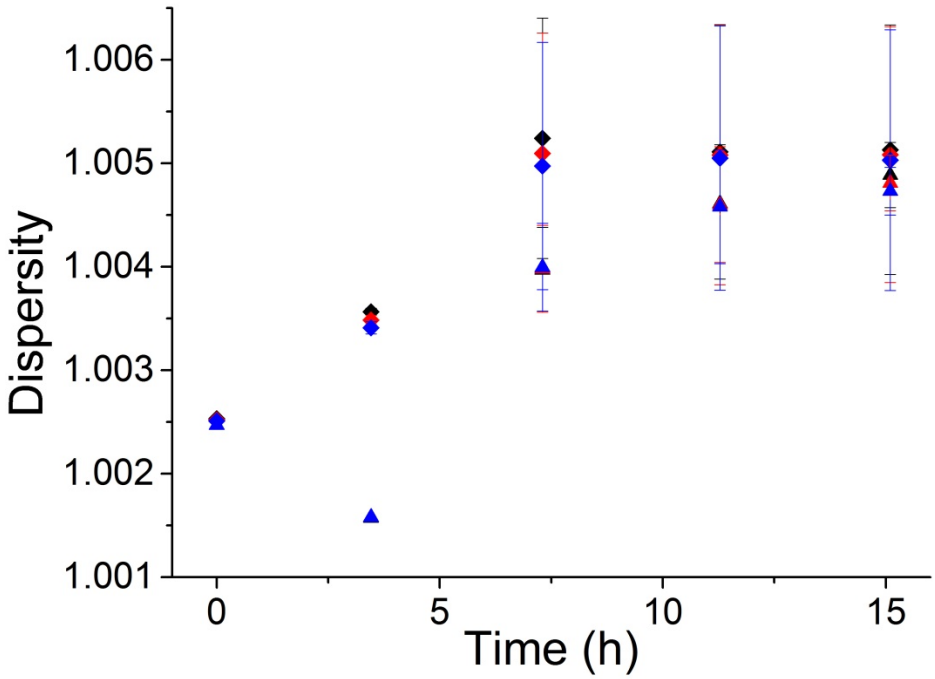

Figure S4-1: Dispersity of electrophoretic mobility distributions $D(W(\mu),1,0)$ (black), $D(W(\mu),2,0)$ (red), $D(W(\mu),3,0)$ (blue) of chitosan MedMW1 dissolved in 50 mM HCl in H_2O (diamonds) and 50 mM DCl in D_2O (triangles) during kinetic measurement using CE-CC with the carousel kept at 60 °C

SEPARATION OF PALAM

Separation of the cationic polymer poly(allylamine hydrochloride) was possible using a PDADMAC/alginate mulilayer coated capillary. The separation was undertaken using NaPB10 at pH 3. It was detected using both UV absorbance and conductivity.

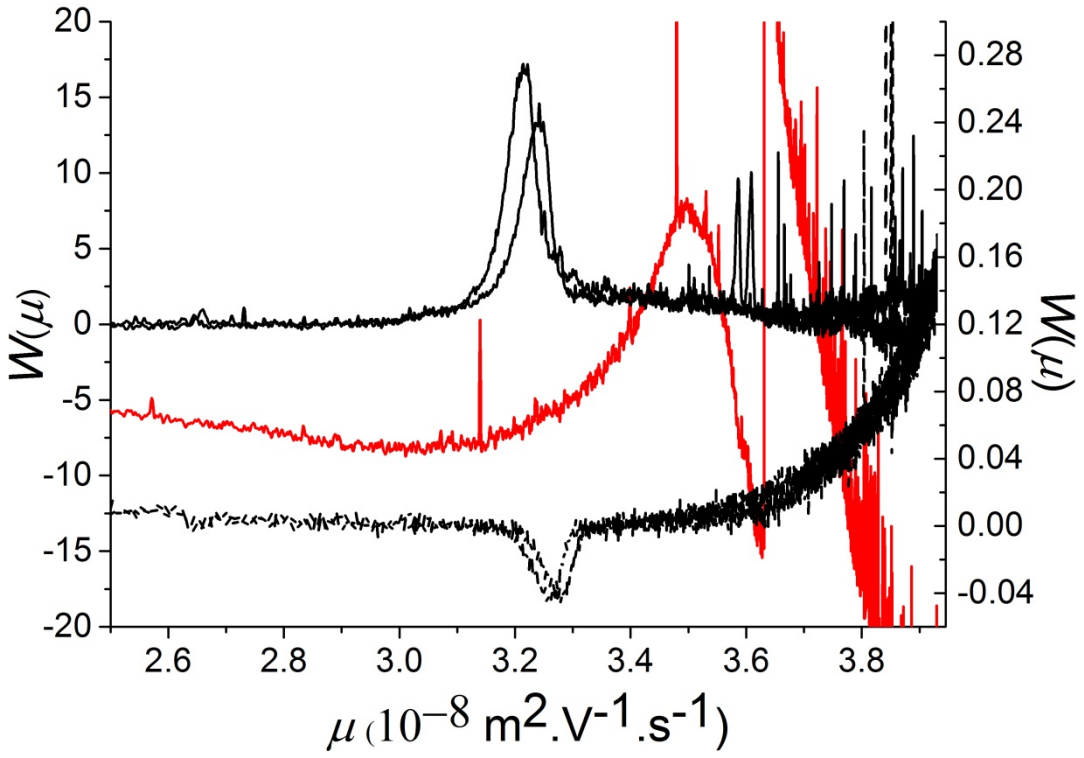

Figure S4-2: Electropherogram of PAlAm (black lines) and chitosan (red line) separated in a PDADMAC/alginate multilayer coated capillary in NaPB10, detected with UV (solid line – left y axis) or conductivity (dashed line – right y axis).

CORRELATION OF ELECTROPHORETIC MOBILITY AND COMPOSITION

The weight-average electrophoretic mobility of the complete range of chitosan samples separated in NaPB100 and LiPB100 were plotted against their average *DA* measured by solid-state NMR spectroscopy.

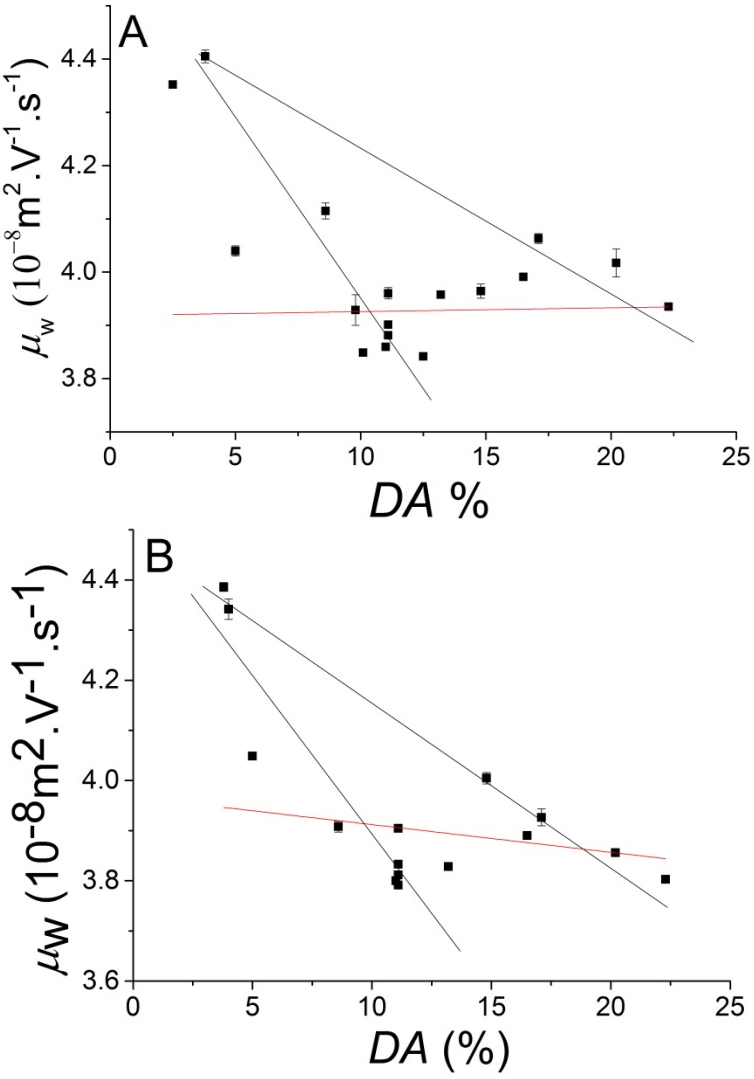

Figure S4-3 A. Calibration curve of the weight-average electrophoretic mobility (μ_w) of chitosan samples separated in A. NaPB100 and B. LiPB100. Red line represents linear fit and black lines represent possible population fits

Chitosan samples were removed in initial calibration curves based on their dispersity. This was to allow the calibration to curve mimic those made with "narrow" standards. Various fits were tested including linear, polynomial, inverse and log functions.

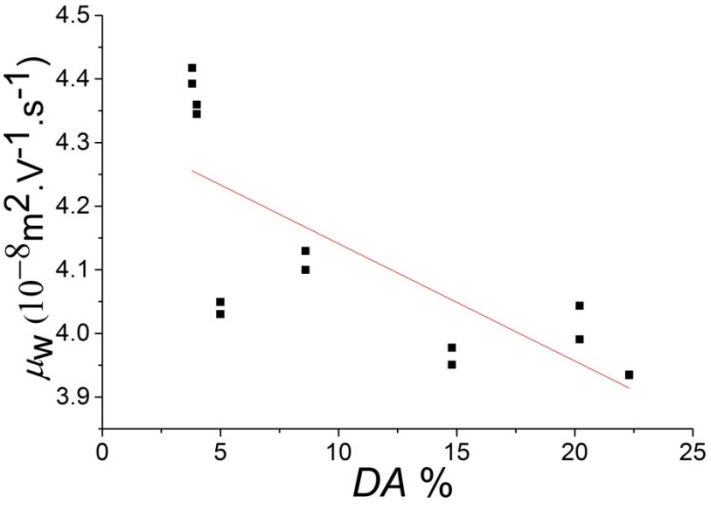

Figure S4-4: Calibration curve of weight-average electrophoretic mobility in NaPB100 as a function of DA for chitosan with a linear fit (red line) ($r^2 = 0.56$)

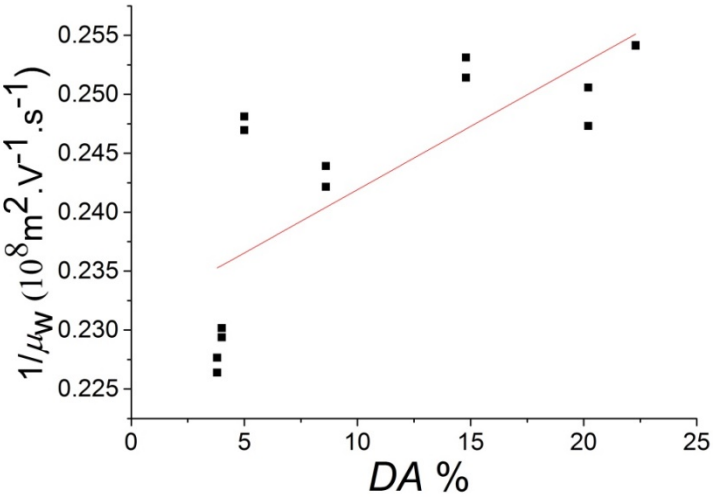

Figure S4-5: Calibration curve of the inverse function of weight-average electrophoretic mobility in NaPB100 as a function of DA for chitosan with a linear fit (red line) ($r^2 = 0.57$)

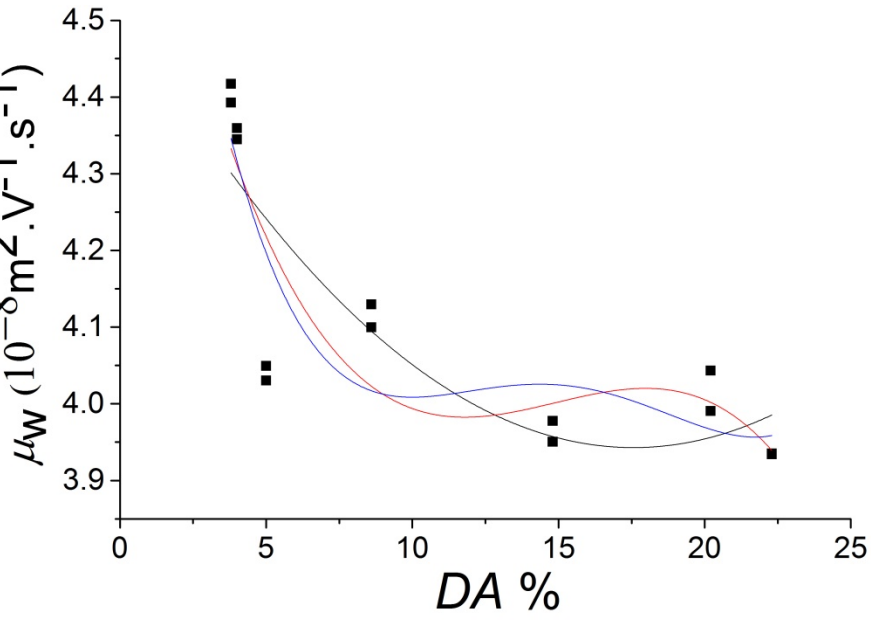

Figure S4-6: Calibration curve of weight-average electrophoretic mobility in NaPB100 as a function of DA for chitosan with order 2 (black line), 3 (red line) and 4 (blue line) polynomial fit.

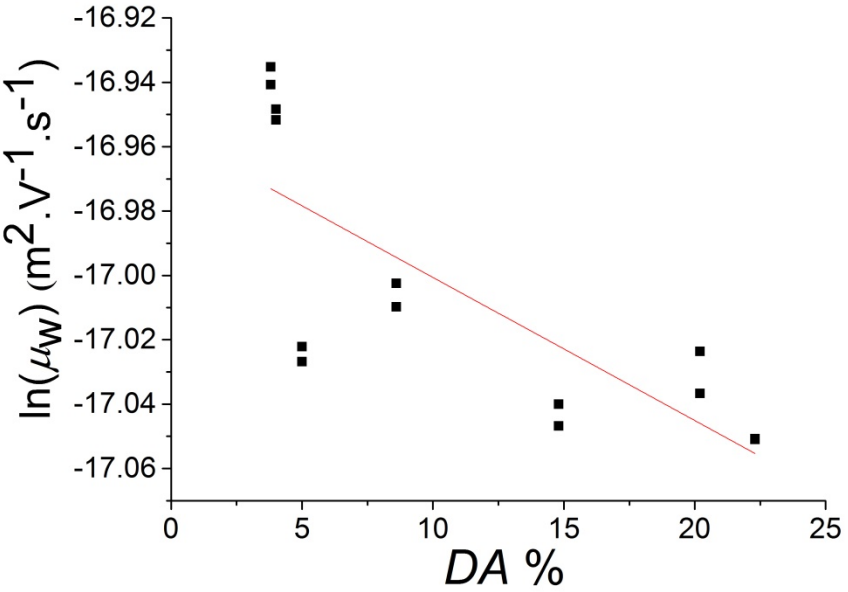

Figure S4-7: Calibration curve of the log function of weight-average electrophoretic mobility in NaPB100 as a function of DA for chitosan with a linear fit (red line) ($r^2 = 0.56$)

X-RAY DIFFRACTION OF CHITOSAN

Chitosan samples were measured with a Bruker D8 Advance Powder Diffractometer (XRD). Incident radiation was Cu Kα II with detection by a Bruker Lynx eye silicon drift detector. Samples were placed on a sample holder in powder form and levelled to a thin, flat layer.

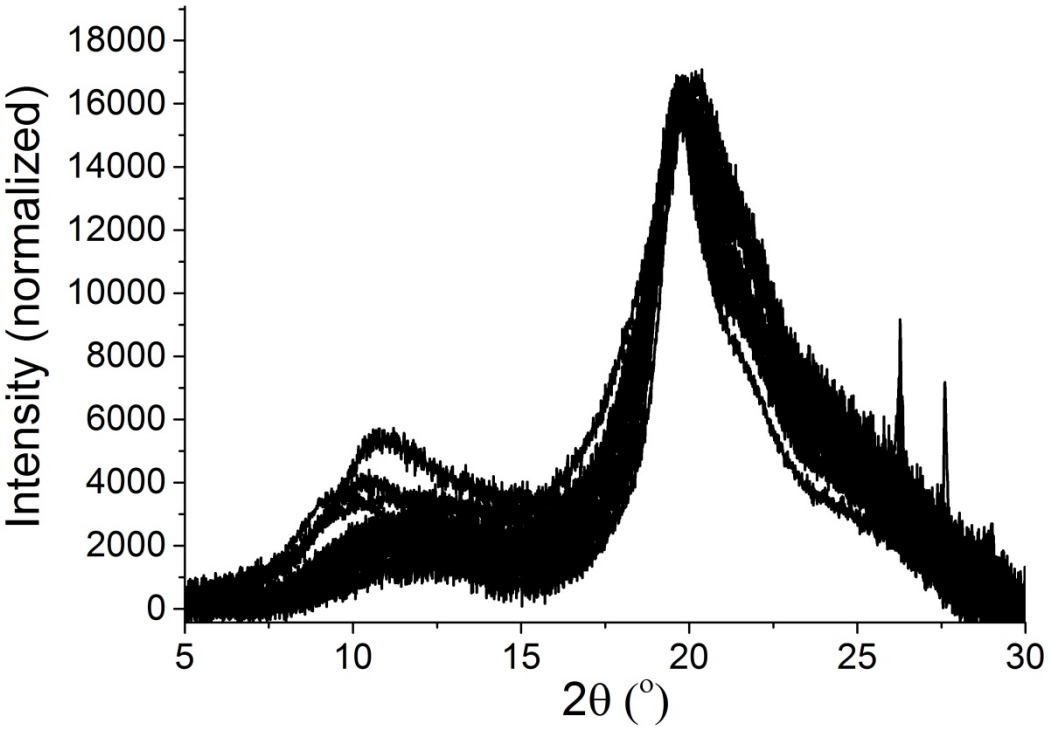

Figure S4-8: X-ray diffractograms of various chitosan samples normalized by the peak maximum between 18 and 22°.

COMPOSITION DISTRIBUTIONS

Using the initial composition distributions, the average *DA* at the peak apex could be determined. A second iteration of the calibration was calculated. For chitosan samples separated in NaPB100, the correlation between the *DA* from the peak apex and the weight-average electrophoretic mobility did not improve as seen below. Therefore composition distributions were not calculated.

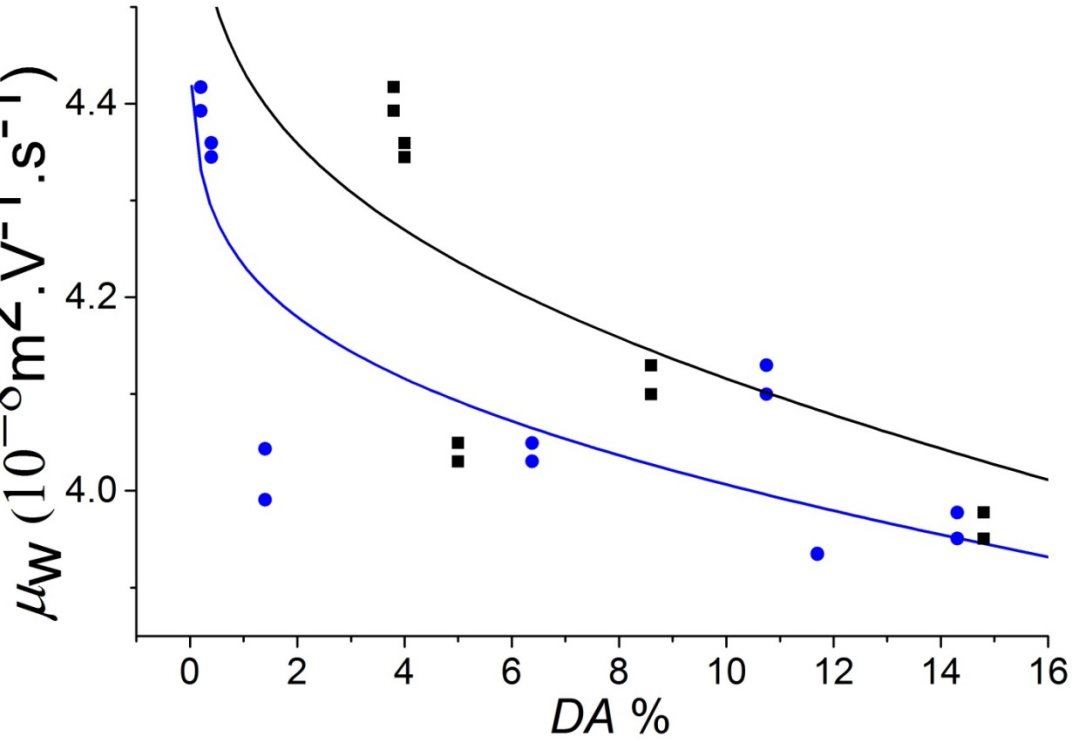

Figure S4-9: Calibration curve with a Bradley function fit of the weight-average electrophoretic mobility in NaPB100 as a function of *DA* from the solid-state NMR spectroscopy measurements (black) or the peak apex of the composition distributions (blue).

REFERENCES

1.Mnatsakanyan, M.; Thevarajah, J. J.; Roi, R. S.; Lauto, A.; Gaborieau, M.; Castignolles, P., Separation of chitosan by degree of acetylation using simple free solution capillary electrophoresis. *Analytical and Bioanalytical Chemistry* 2013, *405* , 6873-6877.

2.Thevarajah, J. J.; Sutton, A. T.; Maniego, A. R.; Whitty, E. G.; Harrisson, S.; Cottet, H.; Castignolles, P.; Gaborieau, M., Quantifying the Heterogeneity of Chemical Structures in Complex Charged Polymers through the Dispersity of Their Distributions of Electrophoretic Mobilities or of Compositions. *Analytical Chemistry* 2016, *88*, 1674-1681.

CHAPTER 5: Chitosan Films

A) Capillary electrophoresis to monitor peptide grafting onto chitosan films in real time

B) Fabrication and characterization of modified chitosan films- homogeneity of the surface and biocompatibility

5.1. A) Publication [128]

TITLE:

Capillary electrophoresis to monitor peptide grafting onto chitosan films in real time

AUTHORS:

Thevarajah, Joel J.

Western Sydney University

Molecular Medicine Research Group

Australian Centre for Research on Separation Science

School of Science and Health

Parramatta, Australia

Joel.Thevarajah@westernsydney.edu.au

O'Connor, Michael D.

Western Sydney University

Molecular Medicine Research Group

School of Medicine

Campbelltown, Australia

M.OConnor@westernsydney.edu.au

Castignolles, Patrice

Western Sydney University

Australian Centre for Research on Separation Science

School of Science and Health

Parramatta, Australia

P.Castignolles@westernsydney.edu.au

Gaborieau, Marianne

Western Sydney University

Molecular Medicine Research Group

Australian Centre for Research on Separation Science

School of Science and Health

Parramatta, Australia

M.Gaborieau@westersydney.edu.au

+61 2 9685 9905

CORRESPONDING AUTHOR:

Gaborieau, Marianne

KEYWORDS:

Capillary electrophoresis; reaction monitoring; real time; grafting; peptide; chitosan; films; epithelial cells; solid-state nuclear magnetic resonance (NMR) spectroscopy

SHORT ABSTRACT:

Free solution capillary electrophoresis is a fast, cheap and robust analytical method that enables the quantitative monitoring of chemical reactions in real time. Its utility for rapid, convenient and precise analysis is demonstrated here through analysis of covalent peptide grafting onto chitosan films for improved cell adhesion.

LONG ABSTRACT:

Free-solution capillary electrophoresis (CE) separates analytes, generally charged compounds in solution through the application of an electric field. Compared to other analytical separation techniques, such as chromatography, CE is cheap, robust and effectively requires no sample preparation (for a number of complex natural matrices or polymeric samples). CE is fast and can be used to follow the evolution of mixtures in real time (e.g., chemical reaction kinetics), as the signals observed for the separated compounds are directly proportional to their quantity in solution.

Here, the efficiency of CE is demonstrated for monitoring the covalent grafting of peptides onto chitosan films for subsequent biomedical applications. Chitosan's antimicrobial and biocompatible properties make it an attractive material for biomedical applications such as cell growth substrates. Covalently grafting the peptide RGDS (arginine – glycine – aspartic acid – serine) onto the surface of chitosan films aims at improving cell attachment. Historically, chromatography and amino acid analysis have been used to provide a direct measurement of the amount of grafted peptide. However, the fast separation and absence of sample preparation provided by CE enables equally accurate yet real-time monitoring of the peptide grafting process. CE is able to separate and quantify the different components of the reaction mixture: the (non-grafted) peptide and the chemical coupling agents. In this way the use of CE results in improved films for downstream applications.

The chitosan films were characterized through solid-state NMR (nuclear magnetic resonance) spectroscopy. This technique is more time-consuming and cannot be applied in real time, but yields a direct measurement of the peptide and thus validates the CE technique.

INTRODUCTION:

Free solution capillary electrophoresis (CE) is a technique that separates compounds in solutions based on their charge-to-friction ratio[1,2]. Charge-to-size ratio is often mentioned in the literature, but this simplification does not apply to polyelectrolytes, including polypeptides in this work, and was also shown not to be appropriate for small organic molecules[3]. CE differs from other

separation techniques in that it does not have a stationary phase, only a background electrolyte (usually a buffer). This allows the technique to be robust in its ability to analyze a large range of samples with complex matrices[4] such as plant fibers[5], fermentation brews[6] grafting onto synthetic polymers[7], food samples[8], and hardly soluble peptides[9] without tedious sample preparation and purification. This is especially significant for complex polyelectrolytes which have dissolution issues (such as chitosan[10] and gellan gum[11]) and therefore exist as aggregated or precipitated in solution and have been successfully analyzed without sample filtration. Further, the analysis of sugars in breakfast cereals involved injecting samples with particles of breakfast cereal samples precipitated in water[8]. This also extends to the analysis of branched polyelectrolytes or copolymers[12,13]. Extensive work has also been completed in the development of CE techniques specifically for the analysis of proteins for proteomics[14], chiral separation of natural or synthetic peptides[15] and microchip separations of proteins and peptides[16]. Since the separation and analysis take place in a capillary, only small volumes of sample and solvents are used which enables CE to have a lower running cost than other separation techniques including chromatography[5,6,17]. Since the separation by CE is fast, it allows the monitoring of reaction kinetics. This was demonstrated in the case of the grafting of peptides onto chitosan films for improved cell adhesion[18].

Chitosan is a polysaccharide derived from the *N*-deacetylation of chitin. Chitosan films can be used for various biomedical applications such as bioadhesives[19] and cell growth substrates[18,20], due to chitosan's biocompatibility[21]. Cell attachment to specific extracellular matrix proteins, such

as fibronectin, collagens and laminin, is directly linked to the survival of the cells[22]. Notably, different cell types often require attachment to different extracellular matrix proteins for survival and proper function. Cell attachment to chitosan films was shown to be enhanced through the grafting of fibronectin[23]; however, preparation, purification and grafting of such large proteins is not economically viable. Alternately a range of small peptides have been shown to be able to mimic the properties of large extracellular matrix proteins. For example, peptides such as the fibronectin mimetics RGD (arginine – glycine- aspartic acid) and RGDS (arginine – glycine- aspartic acid – serine) have been used to facilitate and increase cell attachment[24]. Covalent grafting of RGDS onto chitosan films resulted in improved cell attachment for cells known to attach to fibronectin in vivo[18]. Substituting larger proteins likes fibronectin with smaller peptides that have the same functionality provides a significant cost reduction.

Here, peptide grafting to chitosan was performed as previously published[18]. As previously demonstrated, this approach provides simple and efficient grafting by using the coupling agents EDC-HCl (1-ethyl-3-(3-dimethylaminopropyl)carbodiimide) and NHS (*N*-hydroxysuccinimide) to functionalize the carboxylic acid of the RGDS to be grafted onto the chitosan film. Two advantages of this grafting method are that it does not require any modification of the chitosan or of the peptide, and it is undertaken in aqueous medium to maximize compatibility with future cell culture applications[18,20]. As the coupling agents and the peptide can be charged, CE is a suitable method for the analysis of the reaction kinetics. Importantly, analysis of the reaction

kinetics via CE enables real-time monitoring of the grafting reaction, and thus enables both optimizing and quantifying the degree of grafting.

While it is not routinely necessary, the results of the CE analysis can be validated off-line by a direct measurement of the peptide grafting onto the chitosan films using solid-state NMR (nuclear magnetic resonance) spectroscopy[25,26] to demonstrate the covalent grafting of the peptide onto the film[18]. However, compared with solid-state NMR spectroscopy, the real-time analysis provided by CE enables the quantification of the peptide consumption in real time and thus the ability to assess the kinetics of the reaction.

The above mentioned method is simple and allows the real-time analysis of peptide grafting onto chitosan films with indirect quantification of the extent of the grafting. The demonstrated method can be extended to the real time quantitative assessment of different chemical reactions as long as the reactants or the products to be analyzed can be charged.

PROTOCOL:

1. Preparation of chitosan films

1.1) Weigh out 2 g of glacial acetic acid, complete to 100 mL with ultrapure water.

1.2) Weigh out 1.7 g of chitosan powder, add 100 mL of the 2 % m/m acetic acid aqueous solution. Stir for 5 days with stirring bar and magnetic stirring plate at room temperature either covered with aluminum foil or in the dark.

1.3) Centrifuge the chitosan dispersion at 1,076 x g at 23 °C for 1 hr. Collect the supernatant with a syringe and discard the precipitate.

1.4) For each film, aliquot 10 mL of the chitosan suspension into a 9 cm plastic Petri dish at room temperature. Leave the films covered to dry for at least 7 days.

1.5) Using scissors cut the dry films into 1x1 cm squares. Note: The experiment can be paused at this stage.

2. Preparation of phosphate-buffered saline (PBS)

2.1) Weigh out 8 g sodium chloride, 0.2 g potassium chloride, 1.44 g disodium hydrogen phosphate and 0.24 g potassium dihydrogen phosphate.

2.2) Dissolve these weighed out chemicals in 800 mL of ultrapure water and titrate the solution with concentrated hydrochloric acid to pH 7.4. Note: The experiment can be paused at this stage.

3. Preparation of 75 mM sodium borate buffer at pH 9.2

3.1) Weigh out 3.0915 g of boric acid. Dissolve it in 75 mL of ultrapure water.

3.2) Titrate the boric acid solution to a pH of 9.2 with a sodium hydroxide solution at a concentration of 10 M or higher.

Caution: Concentrated sodium hydroxide solutions are corrosive and should be handled with gloves.

3.3) Complete with ultrapure water to obtain 100 mL of solution. This yields a 500 mM sodium borate buffer at pH 9.2.

3.4) Dilute the 500 mM sodium borate buffer with ultrapure water to 75 mM sodium borate buffer. Note: The experiment can be paused at this stage.

4. Preparation of chitosan films for the grafting reaction

4.1) Rinse 10 square chitosan films (1x1 cm) in 5 mL of PBS for 2 hr in a Petri dish at room temperature.

4.2) During this time, prepare and validate the capillary electrophoresis instrument (step 5).

5. Preparation and validation of the capillary electrophoresis instrument

5.1) Prepare a 43.5 cm bare fused silica capillary with an internal diameter of 50 μm (43.5 cm is the total length, the effective length to the detection window is typically 35 cm) by weakening the polymer outer coating of the capillary at the set length with a blunt utensil then snapping the capillary.

5.1.1) Create a window for the capillary by using a lighter to burn the polymer coating at 8.5 cm from the inlet and after it cools wipe it clean with ethanol. Burn the coating of the capillary at each end for a few millimeters with a lighter, and after it cools wipe it clean with ethanol.

5.1.2) Place capillary inside detection window and install it in the capillary cassette by placing it at equal lengths in the inlet and outlet and winding it around the spindles of the cassette. Then install the cassette in the capillary electrophoresis instrument.

5.2) Set the parameters of the method for each separation. In the software menu select "method" then “edit the entire method”. Set the temperature, time, voltage, and vials used for the separation (for example 25 °C, 10 min, 30 kV).

5.2.1) In the pre-conditioning section, set the consecutive flushes: 10 min with 1 M sodium hydroxide (in water), 5 min with 0.1 M sodium hydroxide (in water), 5 min with ultrapure water and 5 min with 75 mM sodium borate buffer at pH 9.2 for the first method of a series of analyses.

5.2.2) For the subsequent methods, set the set the consecutive flushes in the pre-conditioning section: 1 min with 1 M sodium hydroxide (in water), 5 min with 75 mM sodium borate buffer at pH 9.2.

5.2.3) In the injection section, set parameters for a hydrodynamic injection with 30 mbar pressure for 10 sec for all methods. In the separation section, set the separation conditions to 30 kV at 25 °C for 9 min for all methods.
Note: Consult user manual of specific CE instrument as procedure for operating the CE instrument may vary between manufacturers. Prepare the 1 M sodium hydroxide solution on the day.
5.3) Inject and separate a neutral internal standard (10 µL of 10 %v/v dimethylsulfoxide (DMSO), in water diluted into 450 µL of 75 mM sodium borate buffer). Then inject and separate in the same way an oligoacrylate standard (dissolved in ultrapure water at 10 $g \cdot L^{-1}$; see Table of Materials) to check the validity of the capillary. Pause the sequence here until the grafting reaction is ready to start.
6. Grafting of RGDS onto chitosan film
6.1) Weigh out the peptide (1 mg RGDS) and the coupling agents (3 mg EDC-HCl and 2 mg NHS).
6.2) 2 hr after the start of the chitosan film soaking in PBS, dissolve the peptide and the coupling agents in 5 mL of PBS.
6.2.1) Take a 50 µL aliquot of this solution. Add 2 µL of 10 %v/v DMSO in water as an internal neutral standard to the aliquot. Analyze the aliquot with CE (see step 7).
6.3) Remove the 5 mL of PBS used to rinse the chitosan films from the Petri dish. Add the 5 mL solution of peptide and coupling agents to the Petri dish containing the chitosan films.
6.4) Cover the Petri dish with paraffin film and place it on an orbital shaker at room temperature. Take 50 µL aliquots of reaction media at set times.

Note: The total analysis time with CE is 15 min, thus an aliquot can be taken every 15 min (or every 30 min if two reactions are monitored in parallel, etc.).

6.4.1) Add 2 μL of 10 %v/v DMSO in water as an internal neutral standard to each aliquot.

Note: Aliquots should be analyzed with CE as soon as they are taken (see step 7).

6.5) After 4 hr of shaking and aliquot removal, remove the Petri dish from the shaker. Remove the reaction medium from the Petri dish. Add 5 mL of PBS to rinse the chitosan films.

6.6) Remove the PBS from the Petri dish, rinse the chitosan film with ultrapure water and allow them to dry overnight. Remove the ultrapure water and store the films at -20 °C in a plastic Petri dish.

7. Monitoring of grafting reaction using CE

7.1) Inject and separate aliquots of reaction media immediately after removal from the Petri dish using the analysis conditions as in section 5.2.

7.2) Upon completion of the separations rinse the capillary with ultrapure water for 10 min. Dry it through a flush with an empty vial (air) for 10 min.

Note: The experiment can be paused at this stage.

8. Data treatment for CE

8.1) Check the validity of each separation, by checking that both the current during the separation and the migration time of the electroosmotic mobility marker (DMSO in this case) are similar to the ones observed for the oligoacrylate standard separation.

Note: Up to 10-15% variation is acceptable from the expected current value of about 50 μA and migration time value of 1.3 min (electrophoretic mobility

values should be used instead of migration times if a higher repeatability is required).

8.2) For each successful separation, export the raw data from the capillary electrophoresis software by selecting a specific data set, right clicking on export and selecting an appropriate signal.

8.3) Convert the raw data recorded by the CE (presented as UV absorbance as a function of migration time). Convert the X-axis (migration time t_m) into an electrophoretic mobility μ following Equation 5-1:

$$\mu_{ep} = \frac{L_d \cdot L_t}{V} \cdot \left(\frac{1}{t_m} - \frac{1}{t_{eo}}\right) \quad \textbf{5.1-1}$$

where L_d is the length to the detector, L_t is the total length of the capillary, V is the voltage, and t_{eo} is the migration time of a neutral specie (the DMSO internal standard in this case)[27].

8.3.1) Convert the Y-axis of the raw data (absorbance in a.u.) to a distribution of electrophoretic mobilities $W(\mu)$ following Equation 2:[28].

$$W(\mu) = t_m * absorbance \quad \textbf{5.1-2}$$

9. Additional characterization of peptide-grafted films[18]

9.1) Insert peptide-grafted chitosan films, rolled around themselves, in a 4 mm solid-state NMR rotor. Fill the rotor with phosphate-buffered saline to swell the films, and close the rotor. Wait for a few hr.

9.2) Analyze the film with ^{13}C NMR spectroscopy[18].

REPRESENTATIVE RESULTS:

CE is well suited to monitoring the grafting of peptides (e.g., RGDS) onto chitosan films. Suitable coupling agents include EDC-HCl and NHS which activate the peptide to be grafted onto the chitosan (Figure 5.1-1). CE is able to separate the different molecules of interest from the reaction medium. To assign the peaks on the electropherogram, pure RGDS, EDC-HCl and NHS were dissolved, injected and separated separately. After the peak assignment, the reaction medium was injected and the various reactants were identified (Figure 5.1-2). EDC-HCl reacted into a side product EDH-HCl (3-(((ethylamino)(hydroxy)methylene)amino)-*N*,*N*-dimethylpropan-1-amine). Dimethyl sulfoxide (DMSO) is used as an internal standard for the CE separations. Chitosan is present in the grafting experiment in the form of insoluble films and is thus not injected or observed in CE. Note that for all raw data, the recorded migration time axis is converted into an electrophoretic mobility axis (Equation 5-1) and the UV absorbance axis into a distribution of electrophoretic mobilities $W(\mu)$ (Equation 5-2).

As the aliquots are taken from the reaction medium they are placed into the CE instrument and injected. The extent of the reaction is monitored through the decrease of the peak associated with RGDS (Figure 5.1-3). It can also be seen that the EDC-HCl peak decreases while the EDH-HCl peak increases over time. It is important to note that there is no signal that can be assigned to a product from a side reaction of the peptide, thus it is assumed that the RGDS being removed from the reaction medium is being grafted onto the chitosan film. Overlaid electropherograms (Figure 5.1-3A) allow the quantification of peptide

consumption from the start to the end of the reaction. It is to be noted that although the kinetics was initially measured for 18 hr (Figure 5.1-3B), 4 hr was deemed sufficient for the reaction to proceed to its maximal extent. To allow quantification an optimal injection volume is required to ensure the signal-to-noise ratio is high enough while preventing overloading (Figure 5.1-4A) and in the case of RGDS, injections were required to be completed in real time to prevent polycondensation (Figure 5.1-4B).

The CE-based technique described here to analyze peptide grafting to chitosan films is fast and simple; however, it does not quantify the grafting process directly. NMR spectroscopy is used to demonstrate the grafting; this measurement cannot be done in real time (it typically takes several hr) and needs to be completed post-reaction. The qualitative comparison of the chitosan films before and after grafting shows the successful grafting of the peptides through the appearance of a signal at 70 ppm in the grafted films corresponding to the amide bond between the chitosan and the peptide (Figure 5.1-5).

FIGURE LEGENDS:

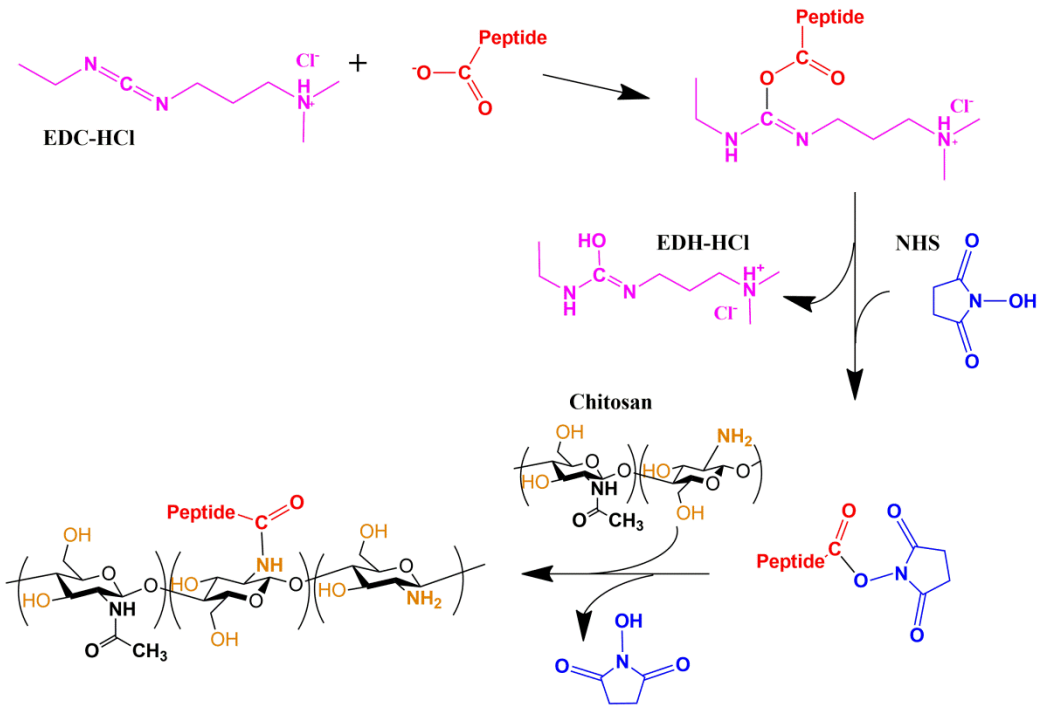

Figure 5.1-1: Scheme of the grafting reaction. Chemical reaction scheme showing the activation by EDC-HCl and NHS of the carboxylic acid functional group of RGDS followed by its grafting onto the chitosan's film surface.

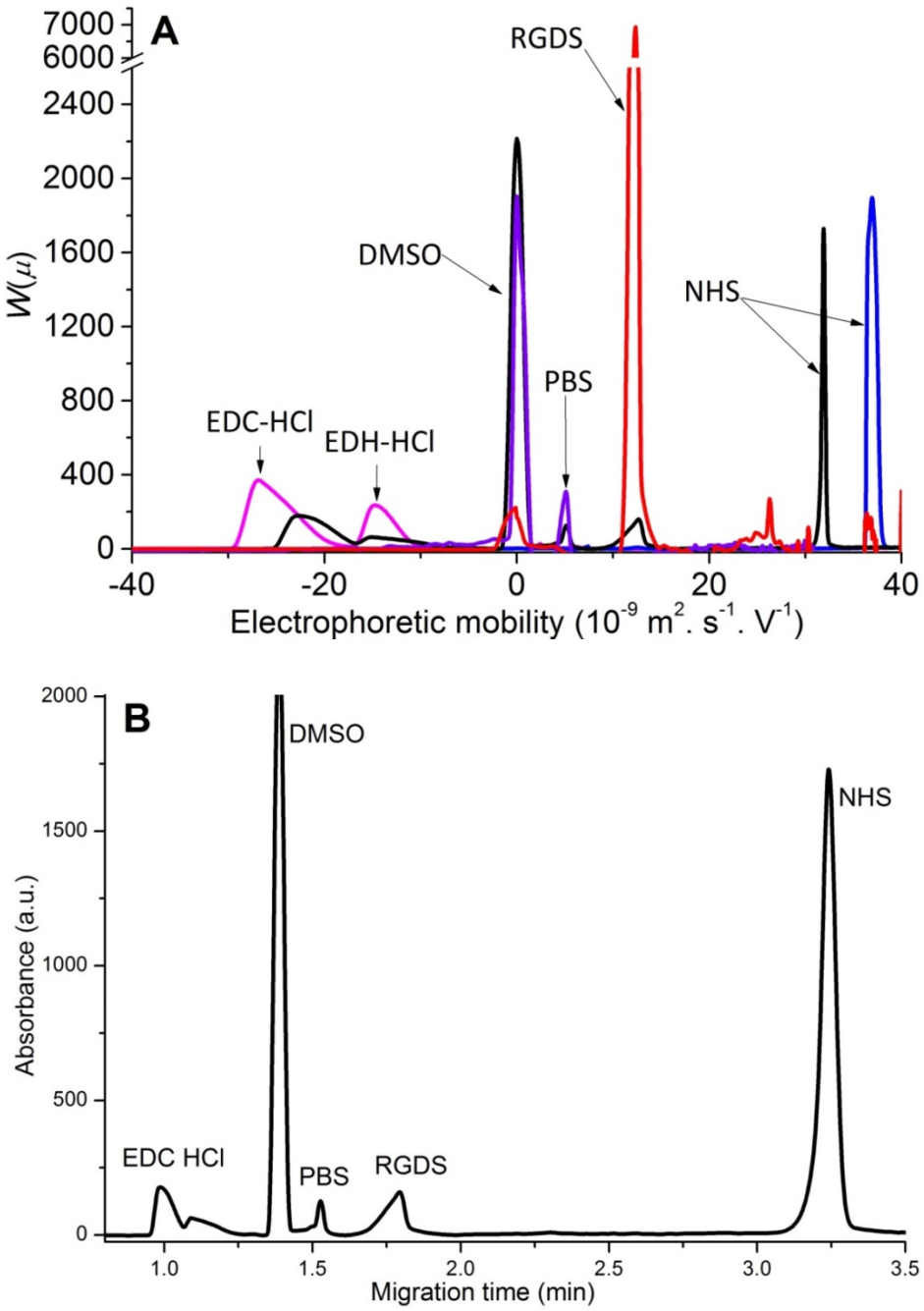

Figure 5.1-2: Peak assignment of the species present in the reaction medium. A. Separation and peak assignment for solutions of partially hydrolyzed EDC-HCl (pink), RGDS (red), NHS (blue), as well as for PBS (purple) and the reaction medium (black). B. Electropherograms of reaction media (black) presented as a function of migration time (electrophoretic mobility should be used to overcome poor repeatability in migration times).

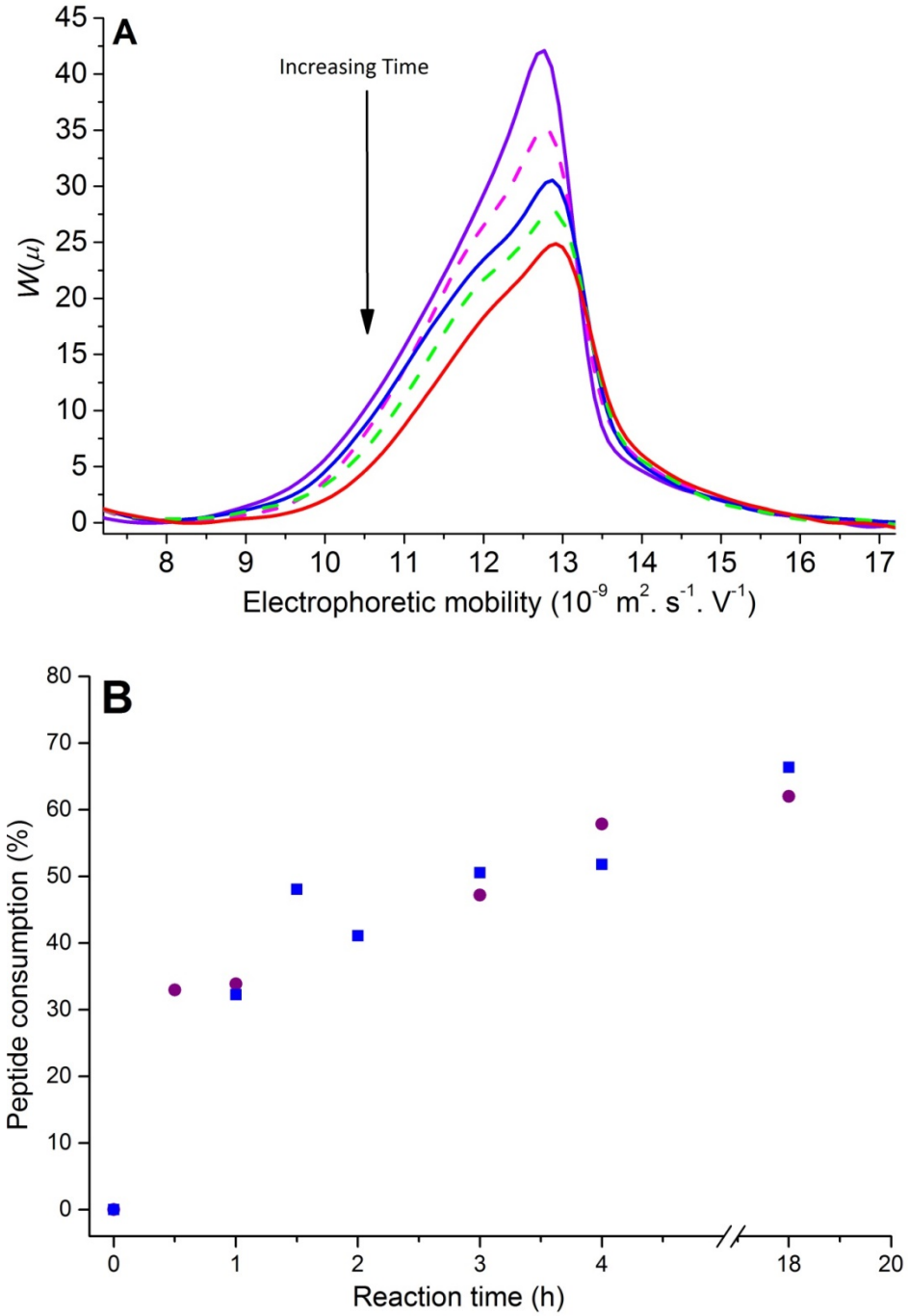

Figure 5.1-3: CE monitoring of RGDS consumption. (A) Overlaid peptide peaks at reaction time 30 min (purple solid line), 60 min (magenta dash line), 90 min (blue solid line), 120 min (green dash line), 150 min (red solid line) and (B) kinetics of grafting completed over 18 hr in replicates (square and circle).

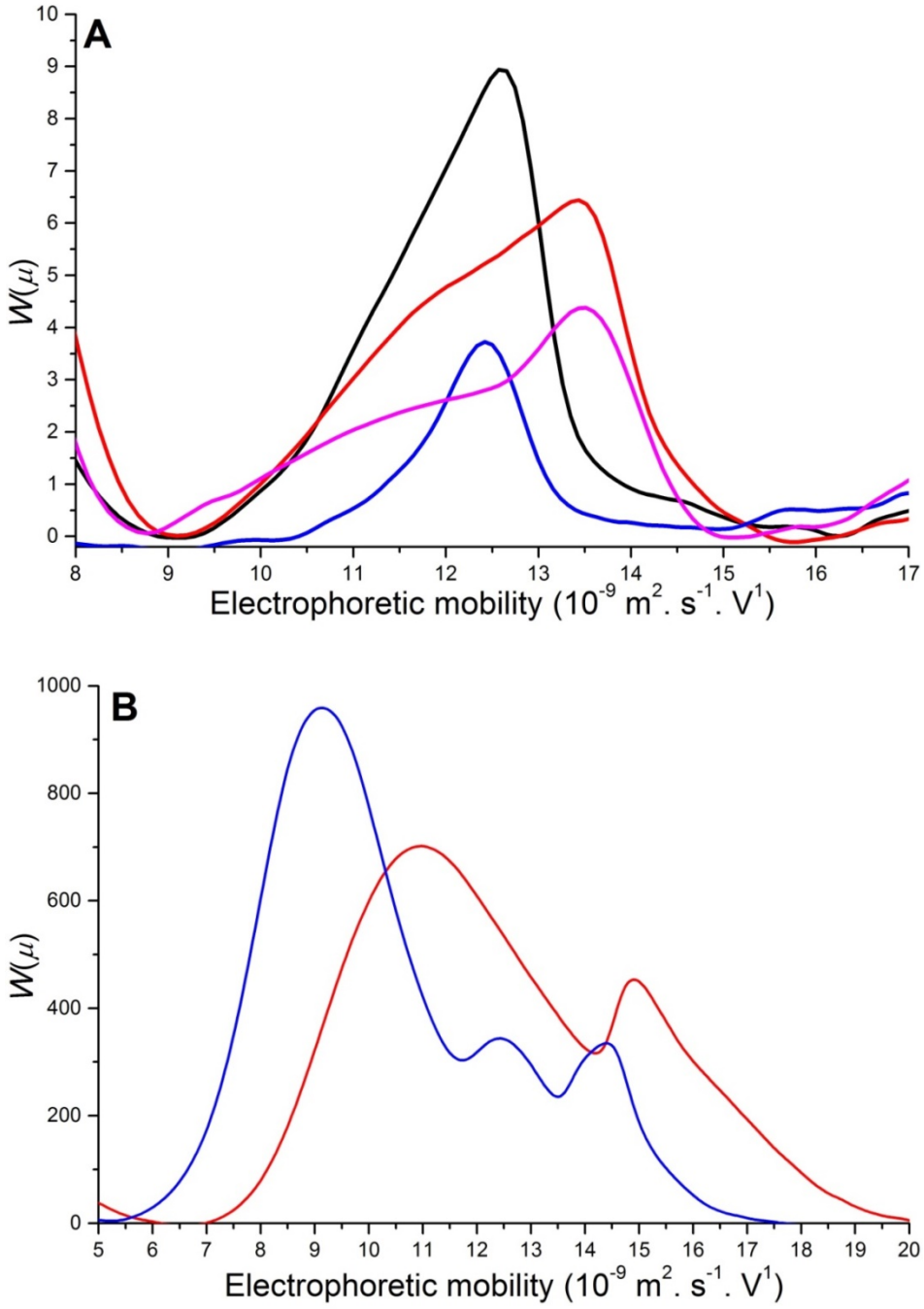

Figure 5.1-4: Overlaid peptide peaks in reaction media showing suboptimal results. (A) Varying (hydrodynamic) injection times: 5 sec (blue line), 10 sec (black line), 20 sec (red line) and 30 sec (magenta line). (B) Reaction media left in a CE vial for an extended period of time before injection: 30 min (red line) and 90 min (blue line).

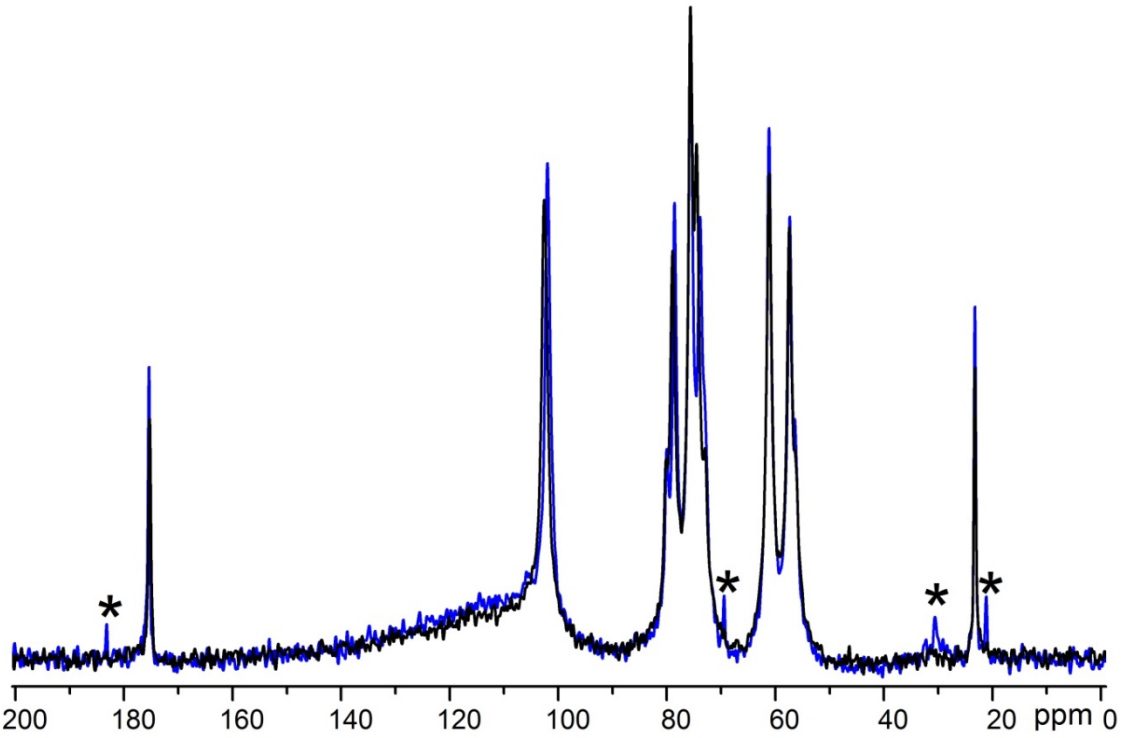

Figure 5.1-5: ^{13}C swollen-state NMR spectra of chitosan films. Comparison of the films before (black line) and after (blue line) peptide grafting. Signals present only in the spectrum recorded after grafting are indicated by asterisks.

DISCUSSION:

The simplicity of the protocol described here makes it ideally suited to widespread application. However, particular attention needs to be paid to of the following key steps.

PROPER CE INSTRUMENT PREPARATION

It is important to separate a known standard immediately prior to the separation of unknown samples (as well as at the end of a series of separations) to check the validity of the capillary and instrument on the day. This standard can be an oligoacrylate[27] or any sample known to give multiple peaks over a wide range of migration times. Monitoring the current during all separations and analyzing the migration of a neutral marker in each separation are key steps to identify issues. An unstable current or large variations (more than 10-15 %) in the plateau value of the current may be due to inconsistency in the buffer (pH or concentration). If it is followed by a delayed migration time of the neutral maker it may also be due to the capillary not being sufficiently clean. Routine checks of the pH of the buffer and an extra flush of the capillary for 10 min with 1 M sodium hydroxide (freshly prepared) can be used to prevent/amend this problem. During the experiment, extra cleaning steps can be employed to ensure an optimal separation, typically including or lengthening a flush with concentrated aqueous sodium hydroxide to regenerate the fuse silica capillary surface.

PROPER DATA TREATMENT

At the conclusion of the experiment, appropriate treatment of the raw data is essential when comparing results. This involves the conversion of the X and Y-axis obtained from the CE instrument (step 8.3). The migration times determined in CE have a relatively poor repeatability and we recommend using electrophoretic mobilities instead, leading to a much better repeatability. The significance of correctly treating data has been shown previously with the

separation and characterization of chitosan[10], poly(acrylic acid), [29] block copolymers[13] and the detection of sugars in breakfast cereals[8] through smaller standard deviations (RSD) observed between experiments for mobilities than for migration times. Further, CE has been shown to be more robust than HPLC in the separation of monosaccharides in complex matrices [5]. Other steps of optimization may include adjusting the injection volume (time of injection) to allow separation with good sensitivity without causing overloading which would prevent quantification. An injection time of 10 sec is deemed optimal at 30 mbar (Figure 5.1-4B): a shorter injection time leads to a reduced sensitivity while longer injection times lead to a peak shape distortion indicative of capillary overloading.

IMPORTANCE OF REAL-TIME MONITORING

A critical strength of this CE-based method is the ability to monitor reactions in real time. This requires optimal CE conditions for detection and separation of the relevant reactant(s) and/or product(s). Furthermore, for the analysis of chemical reactions an appropriate time zero must be taken as a benchmark of the reaction; this typically consists in the separation of the measured out reactants just prior to the reaction starting. This can be done for example before one particular reactant is introduced, before the temperature is increased, or before UV irradiation is started to trigger the reaction.

In the case of the grafting of the peptide RGDS (onto chitosan or onto another substrate), the peptide is able to react with itself to produce linear oligomers or branched structures through polycondensation[18]. This is because RGDS contains

both amine and carboxylic acid functional groups. These peptide oligomers do not have the same electrophoretic mobility as the initial peptide RGDS and therefore may cause an inaccurate quantification, through for example co-migration with other species. It is therefore important to ensure that aliquots of the reaction medium are injected and separated within a few minutes of being taken from the reaction medium (Figure 5.1-4B).

PROPER PREPARATION OF THE CHITOSAN FILMS

When specifically dealing with chitosan films there are a number of steps to adhere to. During the production of the chitosan films, the films need to be left to dry for at least 7 days (preferably more). If this is not completed, when the films are placed in PBS buffer to rinse they will dissolve rather than form a swollen film which then prevents the next steps. Additionally, it is important to neutralize the film prior to the grafting reaction to remove any remaining acetic acid which may leach out of the film and compete with the peptide for the grafting reaction[18]. This can be done through soaking in dilute aqueous sodium hydroxide or in PBS. The pH of the buffer used as solvent for the grafting reaction is also critical: if it is too acidic the films will partially or completely dissolve. During the grafting reaction it is important that the film is able to have maximum contact with the reaction solution. Therefore, the Petri dish containing the films and the reaction mixture are placed on a shaker. It is also imperative to prevent the evaporation of the reaction mixture to prevent uncontrolled concentration variations resulting in inaccurate quantifications; the use of paraffin film to cover the Petri dish was effective to prevent it.

The main limitation of the CE technique is that individually it is not able to confirm the grafting process. In the context of the chemical grafting process mentioned above, the quantification of the peptide grafting is indirect. This can be overcome with the use of a complementary technique such as solid-state NMR spectroscopy as previously mentioned. Other limitations of the CE technique include that it requires the compound of interest to be charged. Therefore neutral species will migrate at the same time. In certain cases this can be overcome if the compound of interest complexes with borate. Finally if the compound of interest does not contain chromophores detection other than UV such as conductivity may need to be used. This requires the additional purchase of a conductivity detector which requires optimization.

ADVANTAGES OF ANALYZING PEPTIDE GRAFTING VIA CE VS OTHER ANALYTICAL METHODS

The CE method has several advantages over alternative indirect methods including high performance liquid chromatography (HPLC), amino acid analysis (AAA) and the direct method of NMR spectroscopy. Compared to AAA it is a high-throughput, robust method which allows it to analyze complex samples efficiently without tedious sample preparation. This is advantageous especially in the analysis of chemical reactions in real time. HPLC has been used previously for peptide grafting analysis[30], however it was deemed only semi-quantitative. CE has a lower running cost than HPLC and does not require sample filtration prior to analysis, minimizing the risk of sample loss[5]. Although ^{13}C NMR spectroscopy is able to directly measure the product of interest, it is a costly technique and is unable to measure it in real time.

The protocol descripted here provides a rapid, efficient, inexpensive and reliable method for optimizing peptide grafting to chitosan film. This new approach thus provides significant advantages for tailoring the cell attachment properties of chitosan films compared to traditionally used methods such as chromatography and AAA. This CE method can be used to monitor a number of other chemical reactions in real time, typically reactions occurring on the timeframe of several hr, for which the reactants/products of interest can be charged. In this case, it is however important to note that the CE method should be optimized prior to the analysis of a different chemical reaction to allow a successful analysis. This includes the analysis of the pure reactants and products prior to the reaction to allow them to be identified and ensure that they can be detected and separated, as well as to ensure that no contaminants may prevent quantification. The separation may be improved and the total analysis time changed by varying the capillary length, buffer composition and voltage, and potentially using a capillary with coated walls. The detection may be improved by modifying the conditions in which the sample is injected to favor the charged reactants or by injecting a larger amount of the sample into the capillary. Further, other detectors apart from UV detection can be employed including fluorescence, contactless conductivity detectors or the CE can be coupled to a mass spectrometer. The ability to monitor reactions in real time enables the grafting reaction to be performed directly in a CE vial if the substrate is in solution and is able to be analyzed by CE. This can take place directly inside the CE instrument, as we recently performed it for grafting of aminoantipyrine on poly(acrylic acid)[7] Additionally, the approach is not limited to grafting reactions but can be extended to monitor various other chemical reactions. Further, the monitoring of the reactions allows optimization of the

reaction and may also be used to validate the product of the reaction. As long as the compound of interest can be dissolved and charged, the CE method allows fast, cheap and robust separation, detection and quantification.

ACKNOWLEDGMENTS: MG, MO'C and PC thank the Molecular Medicine Research Group at WSU for Research Seed Funding, as well as Michele Mason (WSU), Richard Wuhrer (Advanced Materials Characterisation Facility, AMCF, WSU) and Hervé Cottet (Montpellier) for discussions.

DISCLOSURES: The authors declare that they have no competing financial interests.

REFERENCES:

1 Muthukumar, M. Theory of electrophoretic mobility of a polyelectrolyte in semidilute solutions of neutral polymers. *Electrophoresis* **17**, 1167-1172, doi:10.1002/elps.1150170629 (1996).

2 Barrat, J. L. & Joanny, J. F. in *Advances in Chemical Physics, Vol Xciv* Vol. 94 *Advances in Chemical Physics* 1-66 (John Wiley & Sons Inc, 1996).

3 Fu, S. L. & Lucy, C. A. Prediction of electrophoretic mobilities. 1. Monoamines. *Anal. Chem.* **70**, 173-181, doi:10.1021/ac9706638 (1998).

4 Harvey, D. *Modern Analytical Chemistry*. (McGraw Hill, 2000).

5 Oliver, J. D., Gaborieau, M., Hilder, E. F. & Castignolles, P. Simple and robust determination of monosaccharides in plant fibers in complex mixtures by capillary electrophoresis and high performance liquid chromatography. *J. Chromatogr. A* **1291**, 179-186, doi:10.1016/j.chroma.2013.03.041 (2013).

6 Oliver, J. D., Sutton, A. T., Karu, N., Phillips, M., Markham, J., Peiris, P., Hilder, E. F. & Castignolles, P. Simple and robust monitoring of ethanol

fermentations by capillary electrophoresis. *Biotechnology and Applied Biochemistry* **62**, 329-342, doi:10.1002/bab.1269 (2015).

7 Thevarajah, J. J., Sutton, A. T., Maniego, A. R., Whitty, E. G., Harrisson, S., Cottet, H., Castignolles, P. & Gaborieau, M. Quantifying the Heterogeneity of Chemical Structures in Complex Charged Polymers through the Dispersity of Their Distributions of Electrophoretic Mobilities or of Compositions. *Anal. Chem.* **88**, 1674-1681, doi:10.1021/acs.analchem.5b03672 (2016).

8 Toutounji, M. R., Van Leeuwen, M. P., Oliver, J. D., Shrestha, A. K., Castignolles, P. & Gaborieau, M. Quantification of sugars in breakfast cereals using capillary electrophoresis. *Carbohydr. Res.* **408**, 134-141, doi:10.1016/j.carres.2015.03.008 (2015).

9 Miramon, H., Cavelier, F., Martinez, J. & Cottet, H. Highly Resolutive Separations of Hardly Soluble Synthetic Polypeptides by Capillary Electrophoresis. *Anal. Chem.* **82**, 394-399, doi:10.1021/ac902211f (2010).

10 Mnatsakanyan, M., Thevarajah, J. J., Roi, R. S., Lauto, A., Gaborieau, M. & Castignolles, P. Separation of chitosan by degree of acetylation using simple free solution capillary electrophoresis. *Anal. Bioanal. Chem.* **405**, 6873-6877, doi:10.1007/s00216-013-7126-4 (2013).

11 Taylor, D. L., Ferris, C. J., Maniego, A. R., Castignolles, P., in het Panhuis, M. & Gaborieau, M. Characterization of Gellan Gum by Capillary Electrophoresis. *Australian Journal of Chemistry* **65**, 1156-1164, doi:10.1071/CH12211 (2012).

12 Thevarajah, J. J., Gaborieau, M. & Castignolles, P. Separation and characterization of synthetic polyelectrolytes and polysaccharides with capillary electrophoresis. *Adv. Chem.* **2014**, Article ID 798503, doi:10.1155/2014/798503 (2014).

13 Sutton, A. T., Read, E., Maniego, A. R., Thevarajah, J., Marty, J.-D., Destarac, M., Gaborieau, M. & Castignolles, P. Purity of double hydrophilic block copolymers revealed by capillary electrophoresis in the critical conditions. *J. Chromatogr. A* **1372**, 187-195, doi:10.1016/j.chroma.2014.10.105 (2014).

14 Righetti, P. G., Sebastiano, R. & Citterio, A. Capillary electrophoresis and isoelectric focusing in peptide and protein analysis. *Proteomics* **13**, 325-340, doi:10.1002/pmic.201200378 (2013).

15 Ali, I., Al-Othman, Z. A., Al-Warthan, A., Asnin, L. & Chudinov, A. Advances in chiral separations of small peptides by capillary electrophoresis and chromatography. *J. Sep. Sci.* **37**, 2447-2466, doi:10.1002/jssc.201400587 (2014).

16 Kasicka, V. Recent developments in capillary and microchip electroseparations of peptides (2011-2013). *Electrophoresis* **35**, 69-95, doi:10.1002/elps.201300331 (2014).

17 JoVE Science Education Database. *Essentials of Analytical Chemistry*, Capillary Electrophoresis (CE), JoVE Cambridge, MA, doi:10.3791/10226 (2016)

18 Taylor, D. L., Thevarajah, J. J., Narayan, D. K., Murphy, P., Mangala, M. M., Lim, S., Wuhrer, R., Lefay, C., O'Connor, M. D., Gaborieau, M. & Castignolles, P. Real-time monitoring of peptide grafting onto chitosan films using capillary electrophoresis. *Anal. Bioanal. Chem.* **407**, 2543-2555, doi:10.1007/s00216-015-8483-y (2015).

19 Rinaudo, M. Chitin and chitosan: Properties and applications. *Prog. Polym. Sci.* **31**, 603-632, doi:10.1016/j.progpolymsci.2006.06.001 (2006).

20 Li, Z., Leung, M., Hopper, R., Ellenbogen, R. & Zhang, M. Feeder-free self-renewal of human embryonic stem cells in 3D porous natural polymer scaffolds. *Biomaterials* **31**, 404-412, doi:10.1016/j.biomaterials.2009.09.070 (2010).

21 Domard, A. A perspective on 30 years research on chitin and chitosan. *Carbohydr. Polym.* **84**, 696-703, doi:10.1016/j.carbpol.2010.04.083 (2011).

22 Shekaran, A. & Garcia, A. J. Nanoscale engineering of extracellular matrix-mimetic bioadhesive surfaces and implants for tissue engineering. *Biochim. Biophys. Acta Gen. Subj.* **1810**, 350-360, doi:10.1016/j.bbagen.2010.04.006 (2011).

23 Custodio, C. A., Alves, C. M., Reis, R. L. & Mano, J. F. Immobilization of fibronectin in chitosan substrates improves cell adhesion and proliferation. *J. Tissue Eng. Regen. Med.* **4**, 316-323, doi:10.1002/term.248 (2010).

24 Boateng, S. Y., Lateef, S. S., Mosley, W., Hartman, T. J., Hanley, L. & Russell, B. RGD and YIGSR synthetic peptides facilitate cellular adhesion identical to that of laminin and fibronectin but alter the physiology of neonatal cardiac myocytes. *Am. J. Physiol. Cell Physiol.* **288**, C30-38, doi:10.1152/ajpcell.00199.2004 (2005).

25 Lefay, C., Guillaneuf, Y., Moreira, G., Thevarajah, J. J., Castignolles, P., Ziarelli, F., Bloch, E., Major, M., Charles, L., Gaborieau, M., Bertin, D. & Gigmes, D. Heterogeneous modification of chitosan via nitroxide-mediated polymerization. *Polym. Chem.* **4**, 322-328, doi:10.1039/c2py20544k (2013).

26 Gartner, C., Lopez, B. L., Sierra, L., Graf, R., Spiess, H. W. & Gaborieau, M. Interplay between Structure and Dynamics in Chitosan Films Investigated with Solid-State NMR, Dynamic Mechanical Analysis, and X-ray Diffraction. *Biomacromolecules* **12**, 1380-1386, doi:10.1021/bm200193u (2011).

27 Castignolles, P., Gaborieau, M., Hilder, E. F., Sprong, E., Ferguson, C. J. & Gilbert, R. G. High resolution separation of oligo(acrylic acid) by capillary zone electrophoresis. *Macromol. Rapid Commun.* **27**, 42-46, doi:10.1002/marc.200500641 (2006).

28 Chamieh, J., Martin, M. & Cottet, H. Quantitative Analysis in Capillary Electrophoresis: Transformation of Raw Electropherograms into Continuous Distributions. *Anal. Chem.* **87**, 1050-1057, doi:10.1021/ac503789s (2015).

29 Maniego, A. R., Ang, D., Guillaneuf, Y., Lefay, C., Gigmes, D., Aldrich-Wright, J. R., Gaborieau, M. & Castignolles, P. Separation of poly(acrylic acid) salts according to topology using capillary electrophoresis in the critical conditions. *Anal. Bioanal. Chem.* **405**, 9009-9020, doi:10.1007/s00216-013-7059-y (2013).

30 Chung, T. W., Lu, Y. F., Wang, S. S., Lin, Y. S. & Chu, S. H. Growth of human endothelial cells on photochemically grafted Gly-Arg-Gly-Asp (GRGD) chitosans. *Biomaterials* **23**, 4803-4809, doi:10.1016/s0142-9612(02)00231-4 (2002).

5.2. B) Publication (in preparation)[129]

Fabrication and characterization of modified chitosan films – homogeneity of the surface and biocompatibility

Joel J. Thevarajah[1,2], Michele E. Mason[1,2,3], Daniel Bairamian[1,2], Timothy Murphy[4], Richard Wuhrer[4], Robert Graf[5] Michael D. O'Connor[3], Patrice Castignolles[2], Marianne Gaborieau[1,2]

[1] Western Sydney University, Molecular Medicine Research Group (MMRG), School of Science and Health, Parramatta, 2150, Australia

[2] Western Sydney University, Australian Centre for Research on Separation Sciences (ACROSS), School of Science and Health, Parramatta, 2150, Australia

[3] Western Sydney University, Molecular Medicine Research Group (MMRG), School of Medicine, Campbelltown, 2560, Australia

[4]Western Sydney University, Advanced Materials Characterisation Facility, Parramatta,. 2150, Australia

[5]Max Planck-Institut fur Polymerforschung, Ackermannweg 10, 55128 Mainz, Germany

KEYWORDS: Chitosan, Poly(ethylene glycol), Capillary electrophoresis, Thermogravimetric analysis, Solid-state NMR spectroscopy

ABSTRACT: Chitosan has promising properties for biomedical applications. However, this does not include low immunogenicity or proven permeability to nutrients required for cell growth. Poly(ethylene glycol) was grafted to the surface of chitosan films to improve immunogenicity. The grafting of this neutral polymer was monitored by capillary electrophoresis and 79-80% grafting efficiency was quantified. Thermogravimetric analysis (TGA) confirmed the grafting. Understanding the heterogeneity in chitosan is significant especially when considering chemical modifications. The heterogeneity of the chemical modification suggests an inherent heterogeneity of the chitosan films. Swollen-state NMR spectroscopy measurements identified the non-swollen and swollen fraction of chitosan films and powders to be similar; however observations on the orientation of the acetyl group and its interaction with the backbone were obtained.

INTRODUCTION

Chitosan is a polysaccharide derived from the *N*-deacetylation of chitin. It has many promising applications including as a bioadhesive [1] and cell growth substrate [2] due to its many promising properties including biocompatibility and biodegradability [3]. Further, it can be developed into various forms including nanoparticles [4], hydrogels, scaffolds [5] and films [6]. However, being a natural polymer, chitosan is plagued by batch to batch variations and a lack of a complete characterization prevents its extensive use.

Chitosan is a copolymer composed of *N*-acetyl-D-glucosamine and D-glucosamine units randomly distributed along its polymer chain. It is often characterized by the average degree of acetylation [7], which is the fraction of the

N-acetyl-D-glucosamine units in the bulk sample. Previously, it was discovered that distributions of degrees of acetylation exists in chitosan samples [8]. The distributions of *DA* were obtained using the separation of chitosan with capillary electrophoresis in the critical conditions (CE-CC) and their dispersity allowed the quantification of the heterogeniety of the composition distributions [9, 10].

Chitosan films for transplantation require improved properties and therefore require modification of the regular films. In the case of lens cell implantation, mechanical properties to allow easy manipulation, low immunogenicity and biodegradability are required to ensure successful transplantation of cells. It is essential that the films mimic the natural microenvironment and allow the transport of biomolecules throughout the film. Therefore a certain permeability of the film is also required. Previous studies have looked into the permeability of cross-linked chitosan films to aqueous ethanol solutions[11] however; currently no study has focused on the permeability of bare chitosan films.

In our study we aimed to further improve the biocompatibility of the chitosan films with the grafting of the non-charged poly(ethylene glycol), PEG, onto the chitosan surface and monitor the reaction using CE. Although PEG has been used extensively to improve the immunogenicity of proteins [12], drug delivery agents/nanoparticles [13] and chitosan [14], the grafting of PEG is not often monitored. Producing chitosan films with low immunogenicity is essential in expanding and improving the application of the films especially for use in transplantation. Previously the grafting of the charged peptide RGDS onto chitosan film was monitored using CE in real-time. Film characterization and cell culture of these chitosan films revealed information regarding an inherent

heterogeneity [15]. Therefore the heterogeneity was probed further in this study. The permeability of both native and thin films were also tested with both a mimic sugar solution and fibroblast growth factor (FGF). The focus of this study was to investigate and characterize the regular and modified chitosan films to progress in the understanding of the inherent heterogeneity using a range of techniques.

EXPERIMENTAL SECTION

MATERIALS

Chitosan powder (medium molecular weight, catalogue number 448877, lot number MKBH1108V), *N*-hydroxysuccinmide (NHS 98 %), 1-ethyl- 3-(3-dimethylaminopropyl)carbodiimide, (EDC-HCl 99 %), dimethylsulfoxide (DMSO 99.5 %), sodium hydroxide pellets, poly(ethylene glycol) 2-mercaptoethyl ether acetic acid (PEG-SH, Mn 5000) were purchased from Sigma-Aldrich. Acetic acid (AcOH, glacial, 99 %) and hydrochloric acid (32 %) were purchased from Unilab. Sodium hydrogen orthophosphate, potassium chloride, sodium chloride and potassium dihyrdogen phosphate were purchased from Univar. Boric acid was purchased from BDH AnalR, Merck Pty Ltd. Cascade beverages raspberry red cordial was purchased from a local supermarket. All water used in this study was of MilliQ quality.

METHODS

PREPARATION OF BUFFERS

Phosphate-buffered saline solution (PBS) at pH 7.4 was prepared by dissolving 8 g sodium chloride, 0.2 g potassium chloride, 1.44 g disodium hydrogen phosphate and 0.24 g potassium dihydrogen phosphate in 0.8 L Milli-Q water and titrating the solution with hydrochloric acid to pH 7.4. Sodium borate buffer (75 mM) was prepared from 0.5 M boric acid in Milli-Q water, titrated to pH 9.20 with 10 M sodium hydroxide and diluted with Milli-Q water. Sodium borate was filtered with a Millex GP syringe filter (0.22 μm).

PREPARATION OF CHITOSAN FILMS

Chitosan films were cast from an adapted protocol [15, 16]. A 1.7 wt% chitosan suspension in a 2 wt% acetic acid dispersion was produced by stirring for 5 days at room temperature (covered from UV light). The solution was then diluted (twice for thinner films with 2 wt% AcOH) or kept at the same concentration and centrifuged at 1,076xg and 23 °C for 1 h and the precipitate removed and discarded before 10 mL aliquots were cast in 9 cm diameter plastic Petri dishes at room temperature (covered from UV light). Chitosan films were then grafted with PEG using a protocol adapted from previous peptide grafting experiments [15, 16]. EDC-HCl (3 mg, 3.13 mM), NHS (2 mg, 3.48 mM), and PEG-SH (11.5 mg, 0.46 mM) were stirred in 5 mL PBS then immediately poured into a 5 cm diameter Petri dish containing 10 x 1 cm^2 chitosan films (total 10 cm^2) for 4 h at room temperature. Aliquots of 50 μL were taken at 30 min intervals for 4 h.

CHARACTERIZATION OF CHITOSAN SOLUTION AND FILMS

Capillary electrophoresis. Measurements were carried out using an Agilent 7100 CE (Agilent Technologies, Waldbronn, Germany) instrument equipped with a diode array detector. Polyimide-coated fused silica high sensitivity capillaries (50 μm internal diameter) were purchased from Agilent. The capillary (112.5 cm total length, 104 cm effective length) was initially pretreated by flushing for 10 min 1 M NaOH then 5 min with 0.1 M NaOH, MilliQ water and sodium borate, respectively, at the start of the series of experiments. An oligoacrylate with a known separation [17] and a broad range of mobilities was injected to validate the capillary and the instrument before each session. Separation was obtained in sodium borate buffer (75 mM, pH 9.3) applying 30 kV at 25 °C. Detection was set at 195 nm.

Thermogravimetric analysis (TGA) and differential scanning calorimetry (DSC). TGA and DSC measurements were conducted on a Netzsch STA449C Jupiter. Samples were placed in an aluminum crucible and the experiment was run with a 10 °C min^{-1} ramp from room temperature up to 600 °C in air.

Scanning electron microscopy. Electron micrographs were recorded on JEOL JSM-6510LV and 7001F-FEG scanning electron microscopes using both secondary (SEI) and backscatter (BSE) detectors for imaging.

Solid-State NMR spectroscopy. NOESY MAS NMR experiments were performed on a Bruker Avance console operating at 500 MHz ^{1}H Larmor frequency with a commercial double resonance probe supporting zirconia MAS rotors with 2.5 mm outer diameter at a MAS spinning frequency of 25 kHz. ^{1}H double quantum correlation and REDOR-based heteronuclear (^{1}H-^{13}C) correlation spectra were recorded at 5 and 25 kHz MAS and 700 MHz ^{1}H Larmor frequency on a Bruker Avance spectrometer using a Bruker 1.3 mm double resonance MAS probe with

140 kHz rf nutation frequency (1.8 μs 90° pulse length). Double quantum excitation was achieved using the Back-to-Back recoupling pulse sequence with 40 μs recoupling time, whereas the REPT-HSQC sequence has been applied for ^{1}H -^{13}C heteronuclear correlation experiments with 80 μs recoupling time. (see figure captions for individual experiments).

PERMEABILITY TEST OF CHITOSAN FILMS

The films were placed on top of a 2 mL glass vial filled with water which created a concave section in the chitosan film (Figure S5.2-12) and 30 μL of red cordial solution was pipetted on top. The samples were left for 1.5 and 3 h. The permeability of the film was then quantified by UV spectrophotometry (Agilent Technologies Cary 100 UV-Vis Spectrophotometer) by analysis of the solution in the vial. A control solution of red cordial was first analyzed by UV-Vis spectrophotometry (Figure S5.2-14) for which and a wavelength of 525 nm was chosen as an optimal absorbance (Figure S5.2-13).

RESULTS AND DISCUSSION

Permeability of chitosan films. As a requirement for transplantation and effective cell proliferation, chitosan films are required to be permeable to certain molecules such as nutrients and growth factors. The permeability of chitosan films to water vapor has been shown to vary depending on numerous factors including pH, solvent and degree of acetylation [18]. Newly modified films were produced to have a structure which allowed physical manipulation as well permeability to biomolecules with improved biocompatibility. The thickness of

native films were measured with a digimatic micrometer, initial native films were measured to be between 24.3 ± 2.6 μm in thickness. Thinner films were produced by diluting chitosan dispersion used to make films with 2 wt% acetic acid by a factor of 2, 3, 4 and 5. Films produced with dilutions between 3 and 5 were seen to be inappropriate as they tore with minimal stress. Small variations in the thickness of the twice diluted films were noticed however the average film thickness was measured to be 14.8 ± 2.8 μm (Table S1). The permeability of the chitosan films was initially tested with red cordial as a mimic for the nutrients. Both the native and thin films showed similar permeability to the red cordial (Figure 5.2-1). As expected the chitosan film with MilliQ had an insignificant increase in UV absorbance. The results from the cordial test suggest that the native chitosan is permeable to small molecules. Further testing with twice and three times thinner films showed that they were inappropriate for further study as they were deemed too fragile especially when in contact with water for prolonged periods of time.

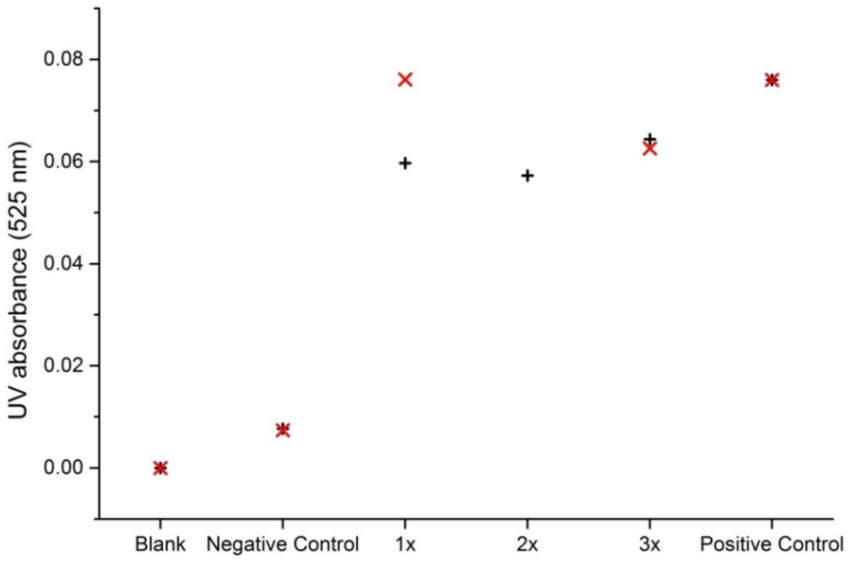

Figure 5.2-1. Permeability of regular and thin blank chitosan films, experiment completed in duplicate (red and black crosses). Negative control

was chitosan films without cordial and the positive control was the experiment without chitosan film.

Monitoring of RGDS and PEG-SH grafting through distribution of electrophoretic mobility W(μ). A recently developed method allows further characterization of polyelectrolytes from CE data. Their dispersity [10] of the chosen polyelectrolyte can be analyzed by a transformation of the raw CE data [19]. In a previous study, the peptide RGDS was grafted onto the surface of chitosan films. Due to the detection of oligo- and polyRGDS it was assumed that the branched structures of RGDS were grafted to the surface rather than singular peptides [15]. Branched/oligo RGDS was detected by a notable shift in the peak maximum of the RGDS. A similar experiment was conducted with PEG-SH, although PEG-SH was not expected to react or polycondense in the presence of the coupling agents without chitosan. Rather than using the peak maximum as applied previously, the weight-average electrophoretic mobility was analyzed as it gives a more accurate representation especially of non-Gaussian peaks (Figure 5.2-2A). It was seen that the PEG-SH remained at a seemingly constant electrophoretic mobility, as expected. In contrast, the RGDS peak had a sharp decrease in the weight-average electrophoretic mobility, indicating polycondensation and then remained at a seemingly constant mobility.

Using the data obtained previously from the grafting of RGDS onto chitosan film [15] the dispersity of both the PEG-SH and RGDS were calculated (Figure 5.2-2B). Similarly to its weight-average mobility, the dispersity of PEG-SH remained constant throughout the monitoring time. The RGDS had a very small dispersity value (close to 1) at the start of the reaction and then it increased significantly

when the branched/oligo RGDS was formed. Although there are slight variations between replicates, the general trend of the dispersity of the RGDS seems to increase and then begin to decrease. This is consistent with the notion that RGDS before the reaction is most homogenous and as branching occurs polyRGDS becomes increasingly heterogeneous. Once most of the polyRGDS units are branched, the dispersity will decrease as the polyRGDS starts to become more homogenous in its branching as seen with poly(sodium acrylate) [10].

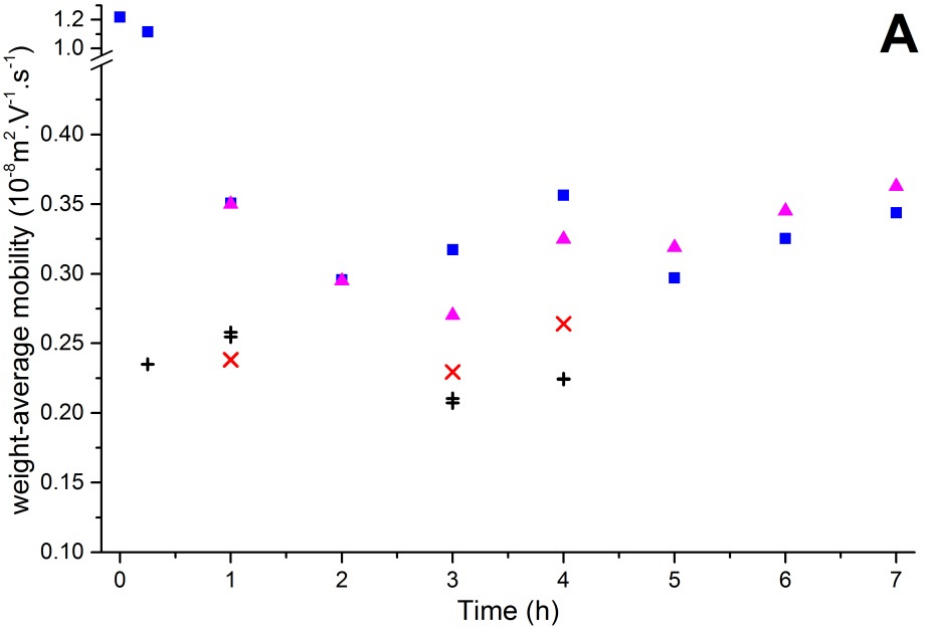

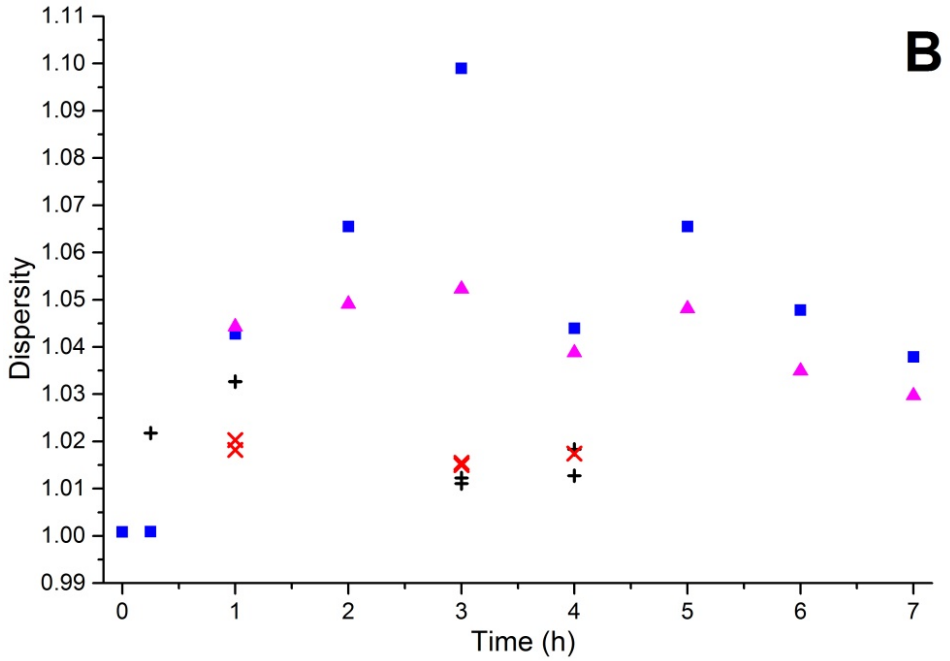

Figure 5.2-2.A) Weight-average mobility of RGDS (blue and pink triangles) and PEG-SH (black and red crosses) against the reaction time B) Dispersity of RGDS (blue and pink triangles) and PEG-SH (black and red crosses) against the reaction time.

Grafting and characterization of PEG grafted chitosan films. PEG-SH was grafted onto the chitosan surface using the reactants EDC-HCl and NHS (Figure S5.2-1). A supplier M_n of 5000 was chosen to prevent potential uptake of PEG with genotoxic effects [20]. The PEG-SH grafted has a carboxylic acid and thiol functional (SH) group per chain. The singular carboxylic acid allows it to be grafted onto the surface of the chitosan films without polycondensing as in the case of the unprotected peptide RGDS [15].Therefore a more even distribution of PEG grafted over the surface is expected.

The SH functional group allows the potential of further functionality following grafting onto chitosan films, such as a chemical grafting of proteins. The reactants were able to be separated by CE with good resolution and no sample

preparation (Figure 5.2-3). The Joule heating was calculated according to the literature [130] to be 0.3 K, which is negligible. Although PEG-SH is not charged, it is able to complex with borate. This and the carboxylic acid functional group enable it to be charged and separated from the neutral species such as the electroosmotic flow marker (DMSO). The LOD and LOQ of PEG in CE were calculated to be 0.0323 $g.L^{-1}$ and 0.108 $g.L^{-1}$ correspondingly (Figure S5.2-2).

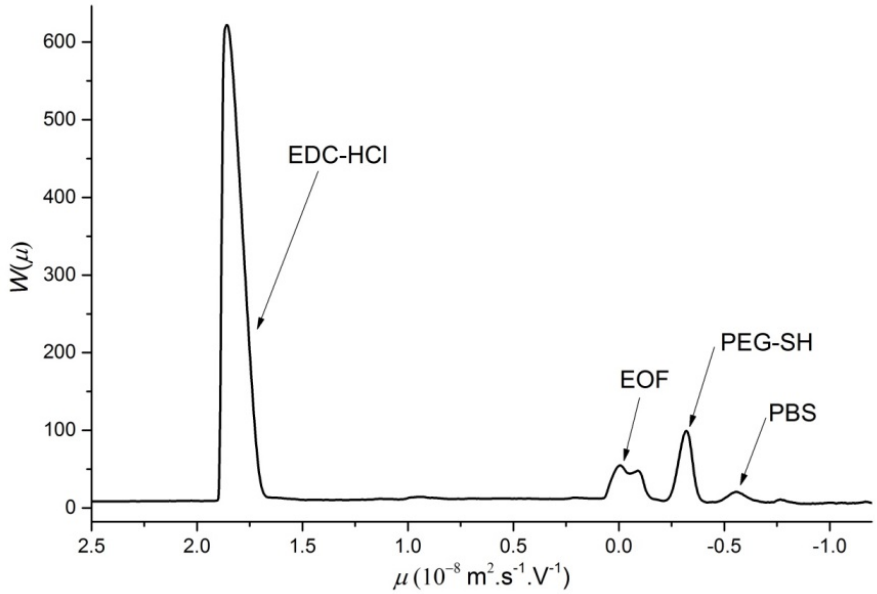

Figure 5.2-3. Electropherogram of reactants of grafting reaction EDC-HC and PEG-SH, of the EOF marker, and PBS shown as the weight distribution W(μ) of electrophoretic mobilities (μ).

The kinetics of the grafting was monitored over 4 hours and a decrease of the PEG-SH peak area was seen (Figure 5.2-4). Using a calibration curve (Figure S5.2-3), the amount of PEG ($g.L^{-1}$) grafted onto the surface of chitosan was able to be quantified. The regression coefficient r^2 was greater than 0.97 as seen in previous work [22]. To ensure accuracy in the quantification of the PEG-SH in the grafting solution, the aliquots were injected in duplicate and an average area of

the PEG-SH was taken. Slight variations between the reactions are seen as previously observed in the case of peptide grafting [15]. This is likely due to the inherent heterogeneity that exists in the chitosan film surface which may limit the chemical reaction. Following the grafting reaction the films were rinsed to remove any adsorbed PEG-SH and this was plotted as the 5 hour point. It is important to note that the consumption of the PEG-SH remains fairly constant after the 3-4 hour mark and there is not a large amount of PEG-SH in the rinse which supports the notion that only a small amount of PEG-SH was adsorbed onto the films surface.

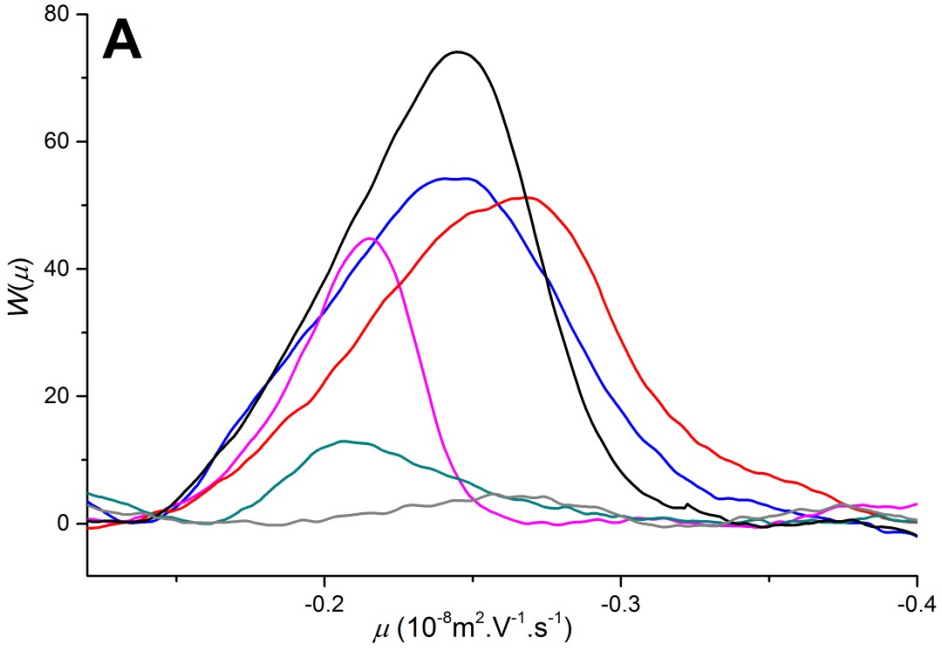

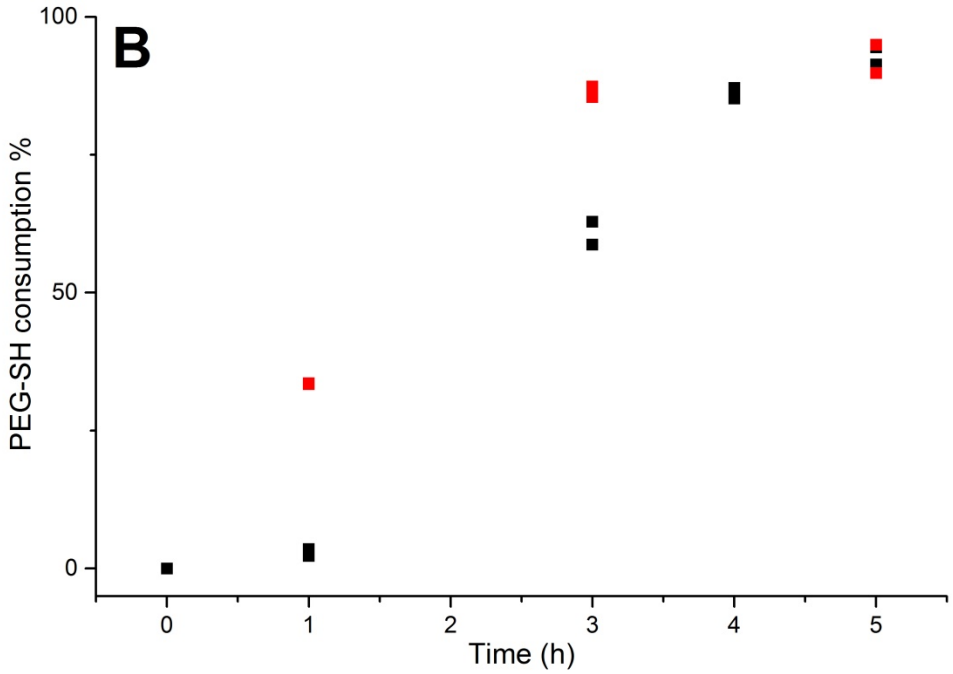

Figure 5.2-4. A) Distribution of electrophoretic mobility of PEG-SH signal of grafting reaction solution over 0 min (black), 60 min (red), 120 min (blue), 180 min (magenta), 240 min (green) and after rinsing the chitosan film following the end of the grafting (grey). B) Quantification of PEG-SH consumption over 4 hours in replicates (black and red squares). The point at 5 hours represents rinsing of the chitosan film at the completion of the grafting.

Taking into account the amount of PEG-SH that was adsorbed onto the chitosan film (6-7%) by the analysis of the PBS rinse used after grafting (Figure 5.2-4A), the grafting efficiency of PEG-SH onto the surface of the chitosan film was calculated to be between 79-80 % for the repeat experiments. Using the same calculation to obtain the surface coverage of the peptide previously[15], it was calculated that 549-557 chains of PEG-SH was grafted per nm^2 of the nominal surface. The large calculated coverage of PEG-SH on the surface also needs to take into account that the surface of chitosan is not flat on the microscopic level, as revealed by atomic force microscopy (Figure S5.2-10). The number of PEG-SH chains bound to the surface of the chitosan film is less than that which was

calculated for the RGDS (5,600)[15]. This may be due to steric hindrance (the PEG being larger than RGDS). However, the previous calculation of RGDS did not take into account the polycondensation confirmed in this study.

Characterization of grafted chitosan films. Although indirect detection of the PEG-SH grafting and further characterization was possible through CE, direct detection of the PEG-SH on the surface of the chitosan was challenging due to the similar organic nature of both the PEG and chitosan. Direct detection of the sulfur group of the PEG-SH would directly confirm grafting specifically on the surface of the chitosan however, this was unable to be completed with X-ray detection during SEM imaging of the surface (Figure S5.2-5). This is likely due to the relatively low concentration of sulfur in the PEG and PEG's scarcity over the surface of the film. FTIR spectroscopy of both the PEG-SH powder of the PEG films was also unable to resolve the SH band between 2500 and 2600 cm^{-1} and further there was no distinguishable difference between regular and grafted films (Figure S5.2-6). Raman spectroscopy of the films could also not resolve the SH band (Figure S5.2-7). The SEM analysis of the films surface also showed no difference between PEG-SH and regular chitosan films (Figure S5.2-8 and S5.2-9). The SEM images allow an analysis of the surface roughness of the films on the scale that is important for its use as a cell culture substrate. It showed that both the grafted and non-grafted films were smooth. AFM images allowed the analysis of the surface roughness of the film at a much smaller scale. This is important as surface roughness at a 2 μm scale would affect chemical grafting processes of small molecules such as peptides and would therefore affect the homogeneity of peptides readily available to allow cell attachment (Figure S5.2-

10). As previously conducted for RGDS [15], swollen-state NMR spectroscopy was also used to try and detect the grafted species onto the surface of the chitosan film (Figure S5.2-11). Non-grafted and grafted chitosan were swollen with D_2O and PBS at pH 7.4, however, no difference was noted. The swollen-state NMR measurements however did allow confirmation that the PEGylation of the film did not cause any compositional differences in the film.

To detect the PEG-SH in the bulk of the film, TGA and DSC experiments were undertaken on blank chitosan films, chitosan grafted with PEG-SH films and PEG-SH powder. TGA of the blank chitosan films showed a large mass loss before 300 °C as seen previously [21] (Figure 5.2-5A). TGA of the PEG-SH powder showed a later and more extensive mass loss close to 400 °C with a second step at 500 °C. The chitosan grafted with PEG-SH onto the surface had a very similar degradation as the blank chitosan film with the exception of the second step at 500 °C similarly to the PEG-SH powder (Figure 5.2-5A). The DSC results (Figure 5.2-5B) showed a very similar result to the TGA results with the chitosan film grafted with the PEG-SH having a distinct endothermic process near 500 °C which was seen in the PEG-SH but not in the blank chitosan film. These results confirm the presence of PEG-SH in the bulk of the sample, which can be assumed to be on the surface even after extensive rinsing. The derivatives of the TGA and DSC curves were also analyzed (Figure S5.2-4).

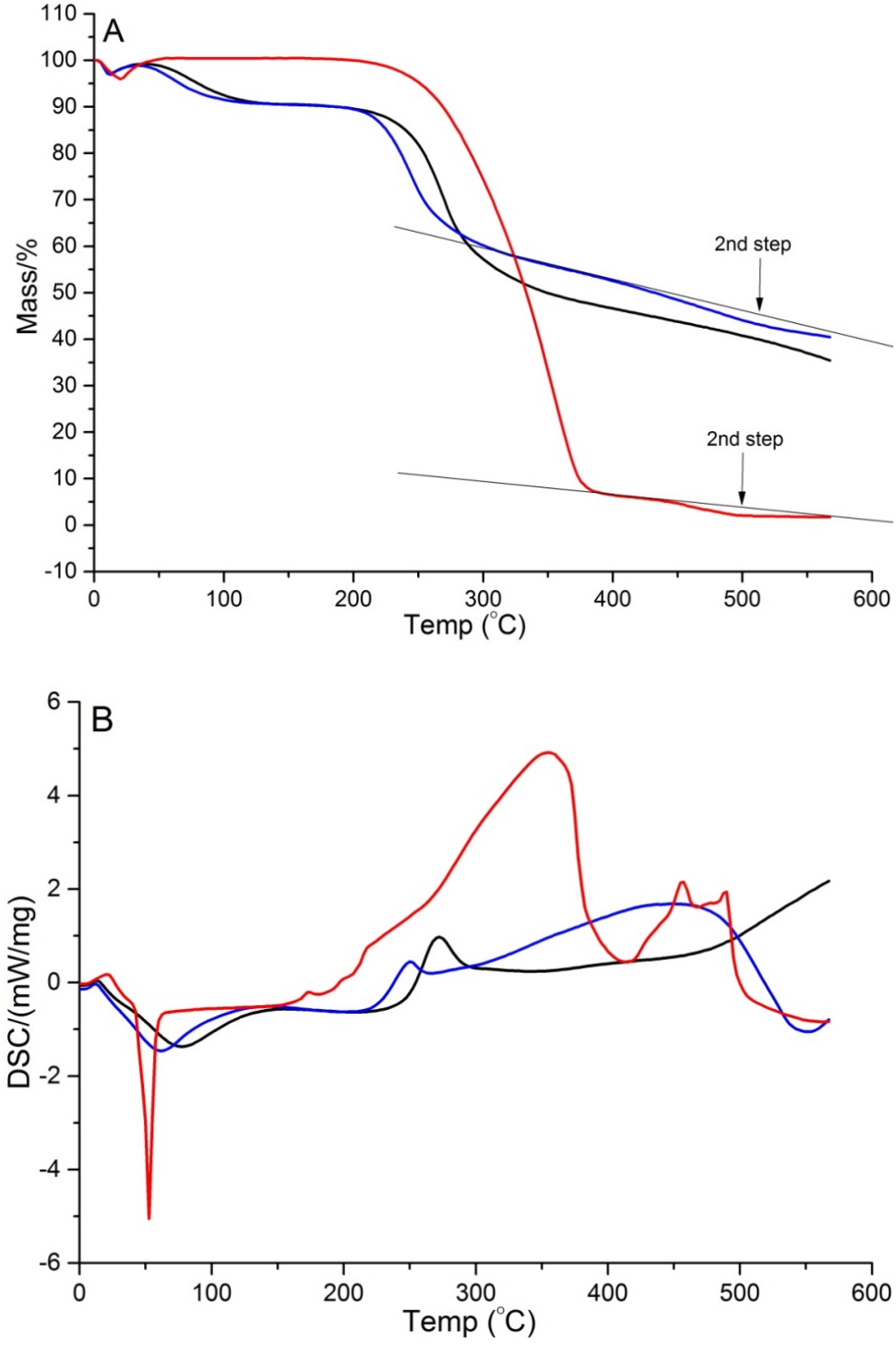

Figure 5.2-5. A. TGA and B. DSC of blank chitosan film (black line), chitosan film with PEG-SH grafted onto the surface (blue line) and PEG-SH powder (red line). Derivatives of TGA and DSC curves are shown in the supporting information Figure S5.2-4.

Heterogeneity of native chitosan film and powder. In a previous study the growth of cells was seen to occur in specific regions [15]. This indicated the possible heterogeneity in the grafting of the peptide RGDS onto the surface. This was attributed to an inherent heterogeneity of the chitosan film surface. The heterogeneity of chitosan in both powder and films is significant especially when trying to chemically modify homogenously. The mobile and rigid fractions of the sample were analyzed through solid-state NMR spectroscopy. Nuclear Overhauser enhancement spectroscopy (NOESY) measurements are used in solution-state NMR spectroscopy to identify dipolar coupling and motions [22]. NOESY measurements were undertaken on chitosan films and powder in the swollen state to identify heterogeneity in through-space coupling of the mobile fraction of the sample. It was seen that there was weak dipolar coupling between the methyl (1 to 2 ppm) and backbone of chitosan film (2 to 5 ppm) which increased with longer mixing times as expected (Figure S5.2-15). Both chitosan powders (Figure 5.2-6 to 5.2-8) had a weaker NOE signal compared to chitosan films and generally less signal intensity, which is likely due to less swelling occurring in the powder form.

a)

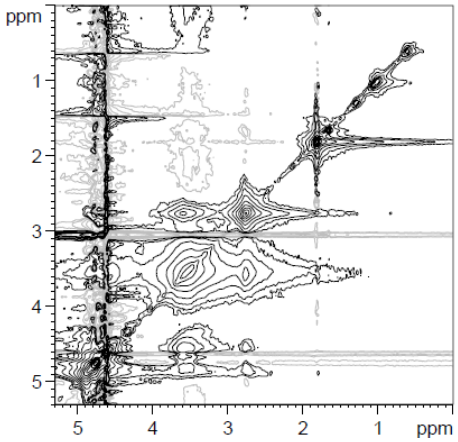

b)

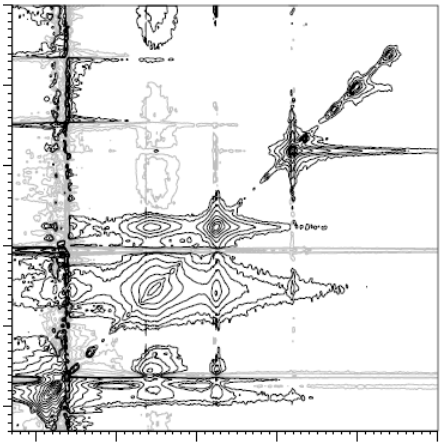

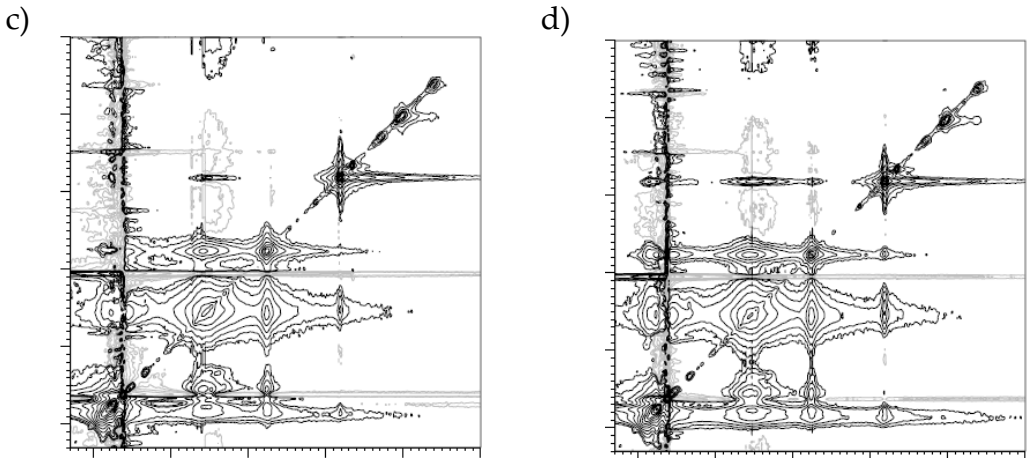

Figure 5.2-6: NOESY measurements of chitosan films swollen in PBS at pH 7 with varying mixing times a) 5 ms b) 10 ms c) 20 ms d) 50 ms

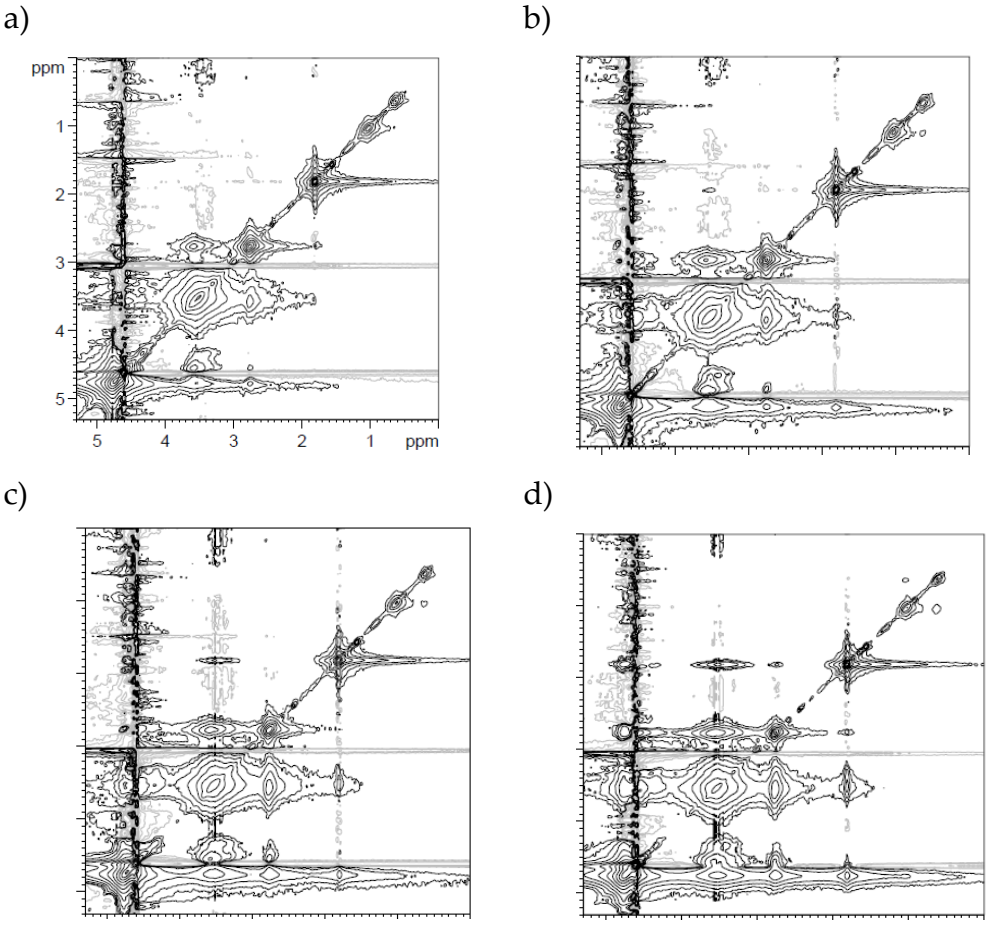

Figure 5.2-7: NOESY measurements of chitosan powder ChitPar1 swollen in PBS at pH 7 with varying mixing times a) 5 ms b) 10 ms c) 20 ms d) 50 ms

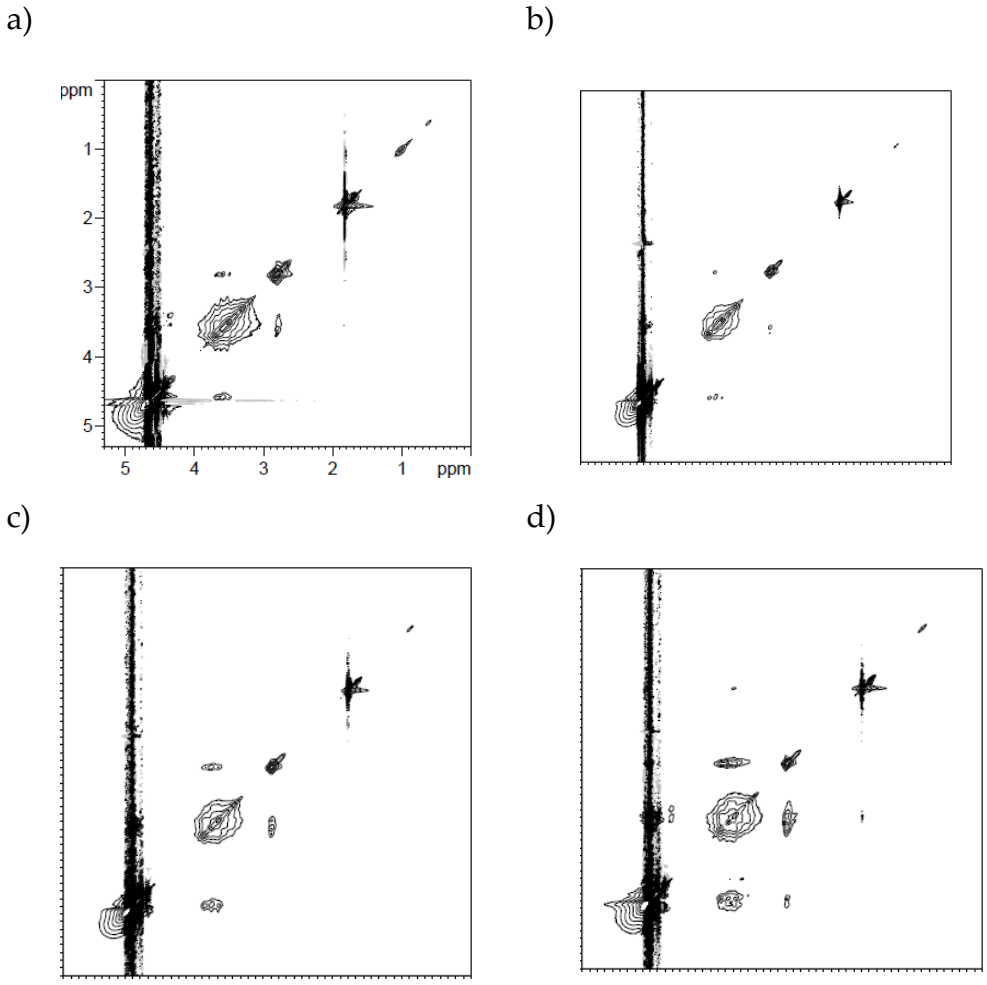

Figure5.2-8: NOESY measurements of chitosan powder ParraMedMW swollen in PBS at pH 7 with varying mixing times a) 5 ms b) 10 ms c) 20 ms d) 50 ms

To analyze the rigid parts of the sample, back-to-back (BaBa) homonuclear double-quantum (DQ) MAS recoupling experiments which have been previously used for rigid and soft solids were undertaken [23] (Figure 5.2-9 to 5.2-11). The coupling in BaBa-DQ experiments allows the coupling between ^{1}H to be quantified even in inhomogenous samples. It was noted for the films that once again there was a weak cross peak between the methyl and backbone signals. This was in agreement with the NOESY measurements and suggests

similarities between mobile and non-mobile fractions of the chitosan film. Further this also suggests that the geometry of the chitosan backbone is that the acetyl groups are likely protruding away from the backbone and have little to no interaction with the backbone. The measurements were repeated at higher spinning speeds and it was noted that the methyl and backbone interaction increased; however, significant broadening was noted with the methyl peak suggesting heterogeneity of the methyl orientation.

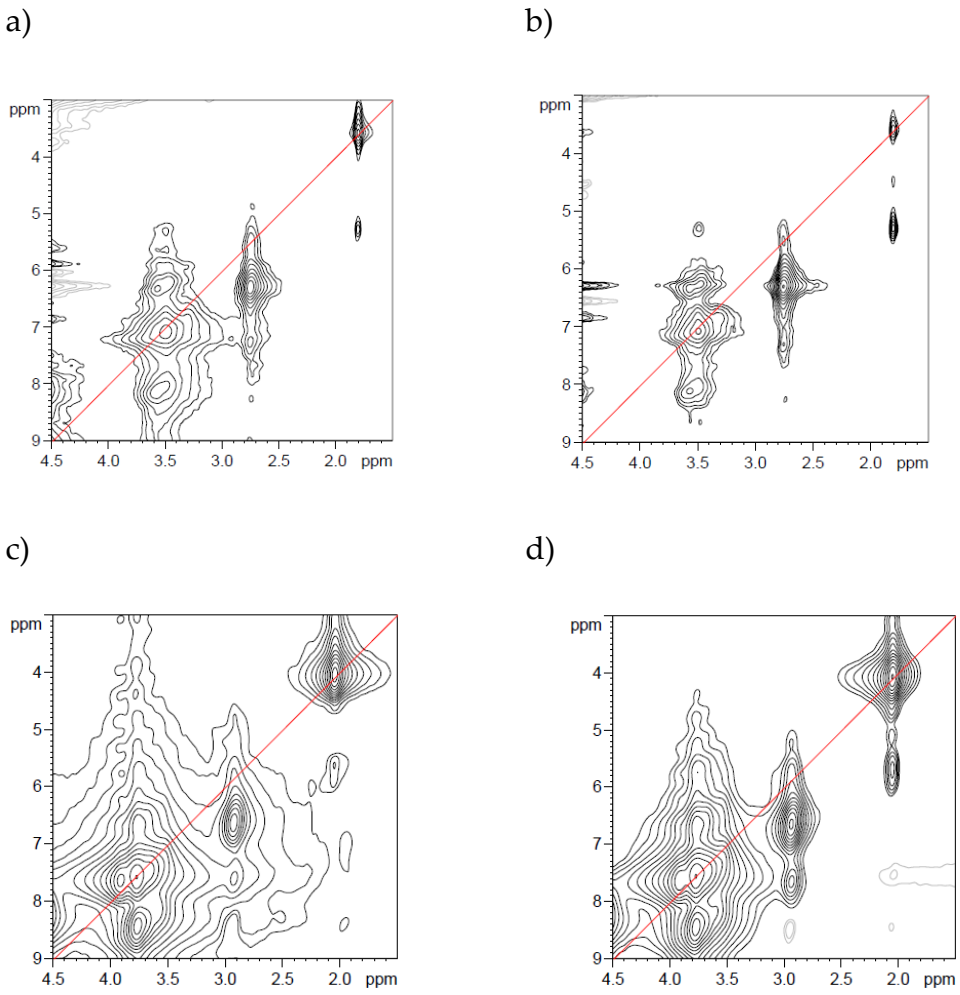

Figure 5.2-9: ^{1}H-^{1}H double quantum correlation of chitosan film swollen in PBS at pH 7 with varying spinning rates and recoupling times a) 2 tr 5 kHz b) 4 tr 5 kHZ c) 2 tr 25 kHz d) 4 tr 25 kHz

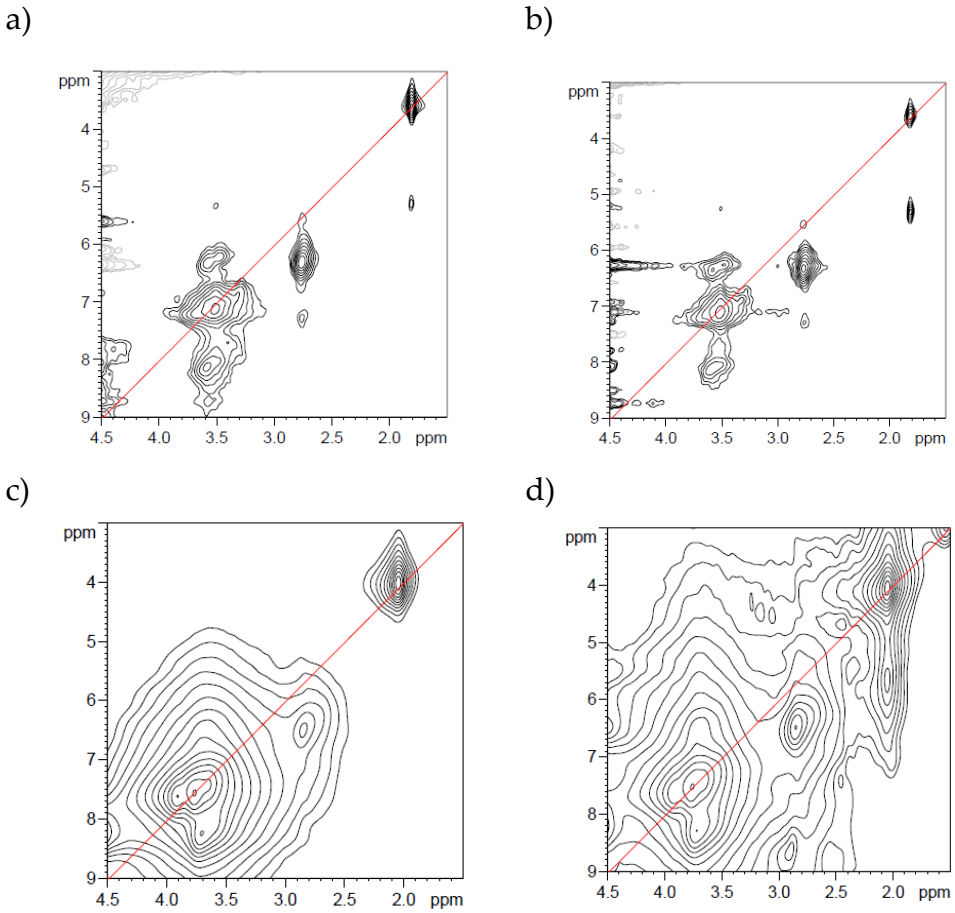

Figure 5.2-10: ^{1}H-^{1}H double quantum correlation of chitosan powder Chitpar1 swollen in PBS at pH 7 with varying spinning rates and recoupling times a) 2 tr 5 kHz b) 4 tr 5 kHZ c) 2 tr 25 kHz d) 4 tr 25 kHz

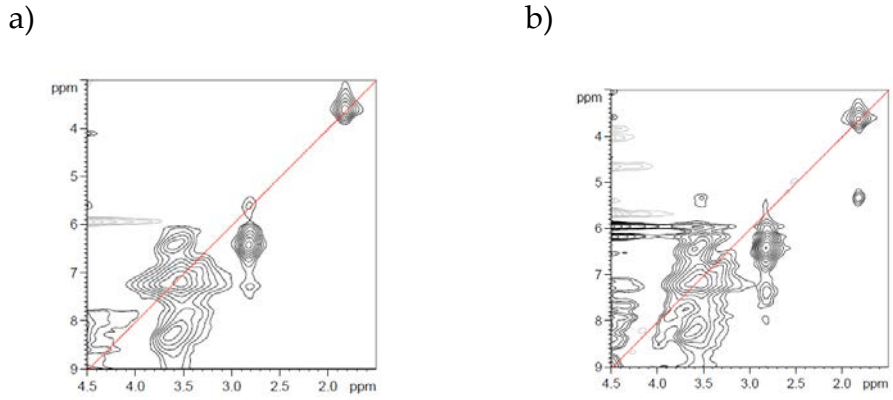

c)

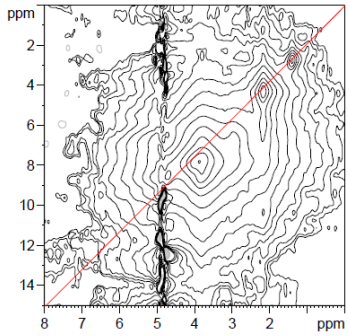

d)

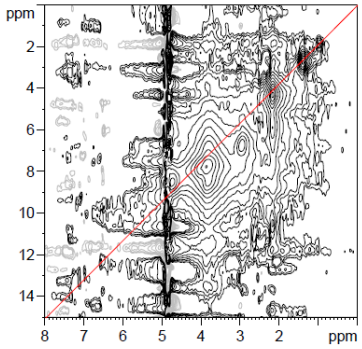

Figure 5.2-11: ^{1}H-^{1}H double quantum correlation of chitosan powder ParraMedMW swollen in PBS at pH 7 with varying spinning rates and recoupling times a) 2 tr 5 kHz b) 4 tr 5 kHZ c) 2 tr 25 kHz d) 4 tr 25 kHz

DQ and NOESY showed that the chitosan powders were much more rigid when compared to the film. The methyl peak of the ParraMedMW powder was seen to be considerably broader than that of the ChitPar1. This is in agreement with previous capillary electrophoresis measurements which have shown a larger compositional heterogeneity in the ParraMedMW powder[9]. Further, measurements were taken using D_2O to swell the chitosan and it was seen to be much more rigid in comparison with samples swollen with PBS (see supporting information). ^{13}C (^{1}H) correlation experiments showed that even though the rigid and mobile fractions were different in different solvents, correlation between ^{13}C and ^{1}H was not affected (see supporting information). This suggests that the ^{13}C and ^{1}H interaction of both the chitosan powders and films remains similar even in different swelling conditions.

CONCLUSION

The grafting of PEG onto the surface of chitosan films to improve biocompatibility was indirectly quantified using capillary electrophoresis. The grafting was then validated with TGA and DSC. Analysis of the weight-average mobility of RGDS [15] and PEG allowed the detection of different structures of RGDS, i.e oligomers or highly branched. This data also confirmed that PEG-SH remained as singular chains during the grafting into the chitosan films. The permeability of the films to small molecules was also tested and chitosan films were seen to be permeable to red cordial. The complexity in probing the inherent heterogeneity of chitosan was further illustrated in this manuscript. Initial NOESY and DQ-BaBa NMR measurements results comparing the mobile and rigid fractions of the chitosan powders and films showed similarities between the two. However, it was seen that the acetyl region may have an orientation that places it away from the backbone.

Future work may involve using deuterated chitosan to possibly allow quantification of the heterogeneity of the surface or the grafting of deuterated molecules and detection by IR microscopy. Also the permeability could be tested with a specific biomolecule such as fibroblast growth factor. With the successful grafting of PEG-SH onto the surface of the chitosan films completed in this study, peptides such as RGDS could be grafted to the SH functional group of PEG. This would allow bi-functionality of the chitosan films. Further testing of the biocompatibility of the film could also be an area of study and this may involve implantation of chitosan films.

REFERENCES

1.Lauto, A., Integration of Extracellular Matrix With Chitosan Adhesive Film for Sutureless Tissue Fixation. *Lasers in Surgery and Medicine* **2009,** 41, 366-371.

2.Li, Z.; Leung, M.; Hopper, R.; Ellenbogen, R.; Zhang, M., Feeder-free self-renewal of human embryonic stem cells in 3D porous natural polymer scaffolds. *Biomaterials* **2010,** 31, 404-412.

3.Boryniec, S.; Strobin, G.; Struszczyk, H.; Niekraszewicz, A.; Kucharska, M., GPC studies of chitosan degradation. *International Journal of Polymer Analysis and Characterization* **1997,** 3, 359-368.

4.Bodnar, M.; Hartmann, J. F.; Borbely, J., Preparation and characterization of chitosan-based nanoparticles. *Biomacromolecules* **2005,** 6, 2521-7.

5.Gartner, C.; Lopez, B. L., Influence of the critical concentration parameters on the morphology of chitosan scaffolds for chondrocyte culture. *Polymer Engineering and Science* **2012,** 52, 2269-2276.

6.Gartner, C.; Lopez, B. L.; Sierra, L.; Graf, R.; Spiess, H. W.; Gaborieau, M., Interplay between Structure and Dynamics in Chitosan Films Investigated with Solid-State NMR, Dynamic Mechanical Analysis, and X-ray Diffraction. *Biomacromolecules* **2011,** 12, 1380-1386.

7.Mnatsakanyan, M.; Thevarajah, J. J.; Roi, R. S.; Lauto, A.; Gaborieau, M.; Castignolles, P., Separation of chitosan by degree of acetylation using simple free solution capillary electrophoresis. *Analytical and Bioanalytical Chemistry* **2013,** 405, 6873-6877.

8.Nguyen, S.; Hisiger, S.; Jolicoeur, M.; Winnik, F. M.; Buschmann, M. D., Fractionation and characterization of chitosan by analytical SEC and H-1 NMR after semi-preparative SEC. *Carbohydrate Polymers* **2009,** 75, 636-645.

9.Thevarajah, J. J.; Van Leeuwen, M. P.; Cottet, H.; Castignolles, P.; Gaborieau, M., Determination of the Distributions of the Degrees of Acetylation of Chitosan. *Biomacromolecules* **2016,** Submitted, Manuscript ID: bm-2016-01205s.

10.Thevarajah, J. J.; Sutton, A. T.; Maniego, A. R.; Whitty, E. G.; Harrisson, S.; Cottet, H.; Castignolles, P.; Gaborieau, M., Quantifying the Heterogeneity of Chemical Structures in Complex Charged Polymers through the Dispersity of Their Distributions of Electrophoretic Mobilities or of Compositions. *Analytical Chemistry* **2016,** 88, 1674-1681.

11. Uragami, T.; Kinoshita, H.; Okuno, H., Characteristics of Permeation and Separation of Aqueous Alcoholic Solutions with Chitosan Derivative Membranes. *Angewandte Makromolekulare Chemie* **1993,** 209, 41-53.

12. Abuchowski, A.; Vanes, T.; Palczuk, N. C.; Davis, F. F., Alteration of Immunological Properties of Bovine Serum-Albumin by Covalent Attachment of Polyethylene-Glycol. *Journal of Biological Chemistry* **1977,** 252, 3578-3581.

13. Du, X.-J.; Wang, J.-L.; Liu, W.-W.; Yang, J.-X.; Sun, C.-Y.; Sun, R.; Li, H.-J.; Shen, S.; Luo, Y.-L.; Ye, X.-D.; Zhu, Y.-H.; Yang, X.-Z.; Wang, J., Regulating the surface poly(ethylene glycol) density of polymeric nanoparticles and evaluating its role in drug delivery invivo. *Biomaterials* **2015,** 69, 1-11.

14. Casettari, L.; Vllasaliu, D.; Castagnino, E.; Stolnik, S.; Howdle, S.; Illum, L., PEGylated chitosan derivatives: Synthesis, characterizations and pharmaceutical applications. *Progress in Polymer Science* **2012,** 37, 659-685.

15. Taylor, D. L.; Thevarajah, J. J.; Narayan, D. K.; Murphy, P.; Mangala, M. M.; Lim, S.; Wuhrer, R.; Lefay, C.; O'Connor, M. D.; Gaborieau, M.; Castignolles, P., Real-time monitoring of peptide grafting onto chitosan films using capillary electrophoresis. *Analytical and Bioanalytical Chemistry* **2015,** 407, 2543-2555.

16. Thevarajah, J. J.; O'Connor, M. D.; Castignolles, P.; Gaborieau, M., Capillary electrophoresis to monitor peptide grafting onto chitosan films in real time. *Journal of Visualized Experiments* **2016,** In Press, DOI: 10.3791/54549.

17. Gaborieau, M.; Causon, T. J.; Guillaneuf, Y.; Hilder, E. F.; Castignolles, P., Molecular weight and tacticty of oligoacrylates by capillary electrophoresis - mass spectrometry. *Australian Journal of Chemistry* **2010,** 63, 1219-1226.

18. Kim, K. M.; Son, J. H.; Kim, S.-K.; Weller, C. L.; Hanna, M. A., Properties of Chitosan Films as a Function of pH and Solvent Type. *Journal of Food Science* **2006,** 71, E119-E124.

19. Chamieh, J.; Martin, M.; Cottet, H., Quantitative Analysis in Capillary Electrophoresis: Transformation of Raw Electropherograms into Continuous Distributions. *Analytical Chemistry* **2015,** 87, 1050-1057.

20. Biondi, O.; Motta, S.; Mosesso, P., Low molecular weight polyethylene glycol induces chromosome aberrations in Chinese hamster cells cultured in vitro. *Mutagenesis* **2002,** 17, 261-264.

21. Lefay, C.; Guillaneuf, Y.; Moreira, G.; Thevarajah, J. J.; Castignolles, P.; Ziarelli, F.; Bloch, E.; Major, M.; Charles, L.; Gaborieau, M.; Bertin, D.; Gigmes, D., Heterogeneous modification of chitosan via nitroxide-mediated polymerization. *Polymer Chemistry* **2013,** 4, 322-328.

22. Novoa-Carballal, R.; Fernandez-Megia, E.; Riguera, R., Dynamics of Chitosan by H-1 NMR Relaxation. *Biomacromolecules* **2010,** 11, 2079-2086.

23. Saalwachter, K.; Lange, F.; Matyjaszewski, K.; Huang, C. F.; Graf, R., BaBa-xy16: Robust and broadband homonuclear DQ recoupling for applications in rigid and soft solids up to the highest MAS frequencies. *Journal of Magnetic Resonance* **2011,** 212, 204-215.

5.3. B) Supporting Information

Supporting information

for

Fabrication and characterization of modified chitosan films – homogeneity of the surface and improved biocompatibility

Joel J. Thevarajah[1,2], Michele E. Mason[1,2,3], Daniel Bairamian[1,2], Timothy Murphy[4], Richard Wuhrer[4], Robert Graf[5] Michael D. O'Connor[3], Patrice Castignolles[2], Marianne Gaborieau[1,2]

[1] Western Sydney University, Molecular Medicine Research Group (MMRG), School of Science and Health, Parramatta, 2150, Australia

[2] Western Sydney University, Australian Centre for Research on Separation Sciences (ACROSS), School of Science and Health, Parramatta, 2150, Australia

[3] Western Sydney University, Molecular Medicine Research Group (MMRG), School of Medicine, Campbelltown, 2560, Australia

[4]Western Sydney University, Advanced Materials Characterisation Facility, Parramatta,. 2150, Australia

[5]Max Planck-Institut fur Polymerforschung, Ackermannweg 10, 55128 Mainz, Germany

GRAFTING INTO CHITOSAN FILM

The reaction scheme is shown in Fig. S1. The calibration curve of the signal-to-noise ratio and peak area of PEG-SH are shown in Fig S2 and S3.

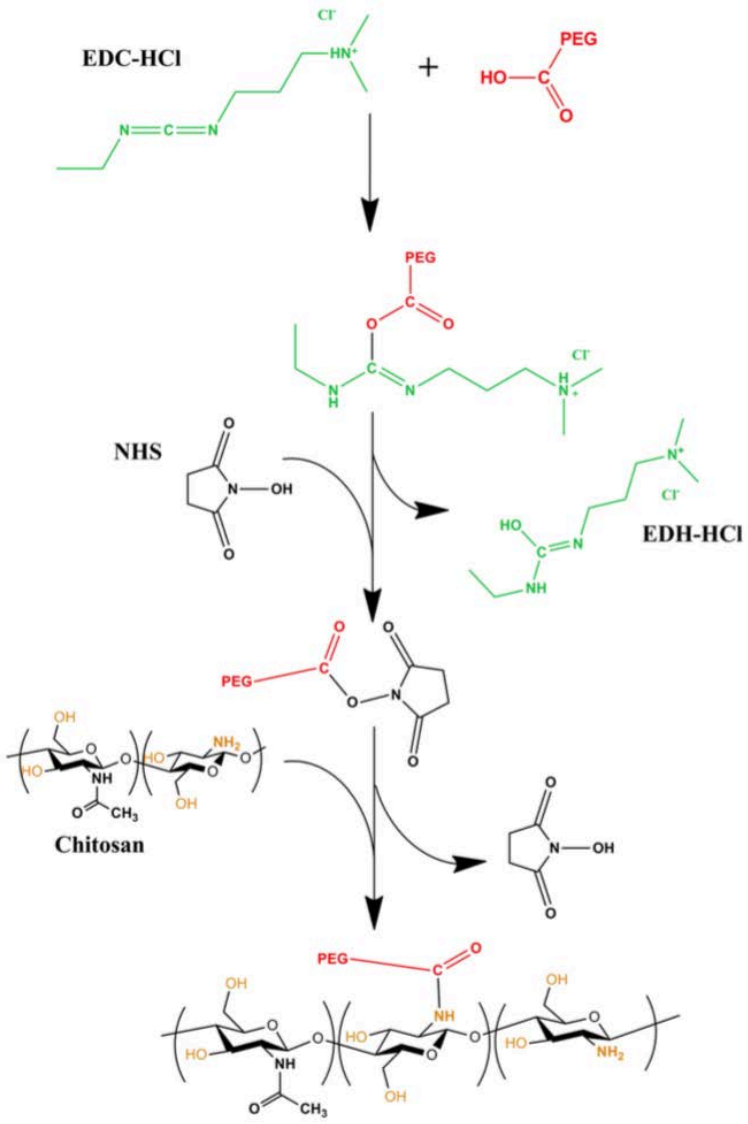

Figure S5.2-1. Reaction scheme for PEG-SH grafting to chitosan films, adapted from previous research.[1]

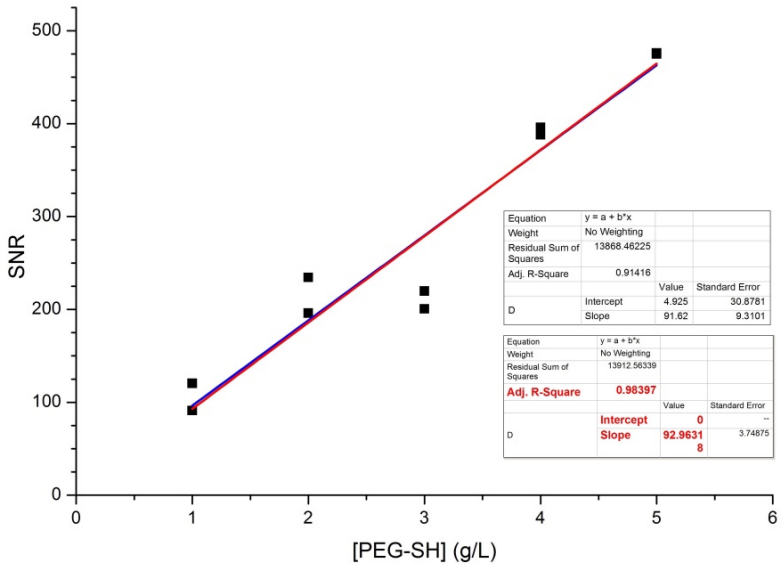

Figure S5.2-2. Calibration curve of signal-to-noise ratio (SNR) as a function of PEG-SH concentration with a line of best fit with (blue) or without (red) intercept set to 0.

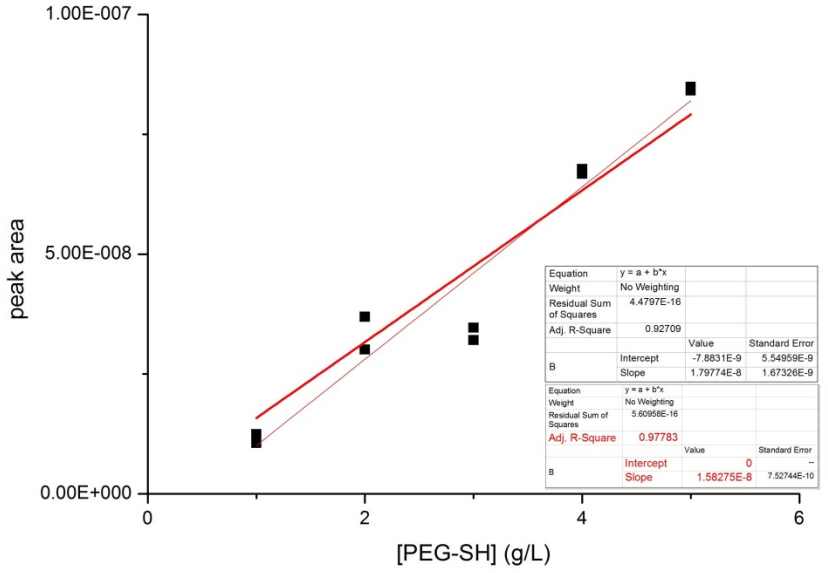

Figure S5.2-3. Calibration curve of peak area of PEG-SH as a function of concentration with a line of best fit with (thick red) or without (thin red) the intercept set to 0.

THERMOGRAVIMETRIC ANALYSIS (TGA) AND DIFFERENTIAL SCANNING CALORIMETRY (DSC) OF CHITOSAN FILM

TGA and DSC were undertaken on blank chitosan film, chitosan films grafted with PEG-SH on the surface and PEG-SH powder. A second mass loss was seen around 500 °C for the chitosan-PEG-SH film and the PEG-SH powder which was not seen in the blank chitosan film. The DSC results showed an endothermic energy peak in the same area which was again only visisble in the PEG-SH powder and the CS-PEG-SH film. The derivatives are shown in Fig S4.

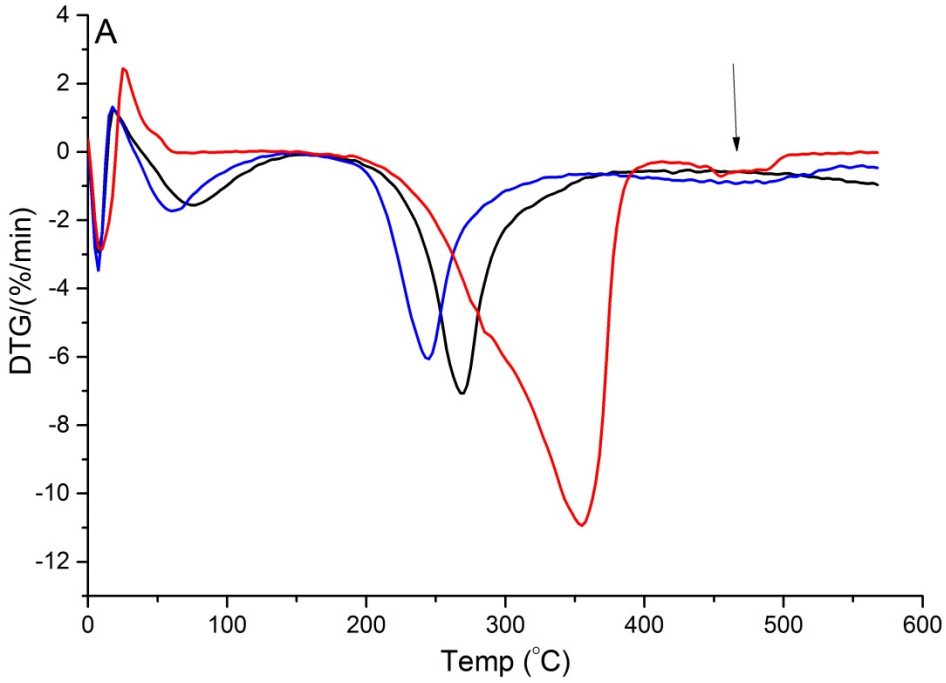

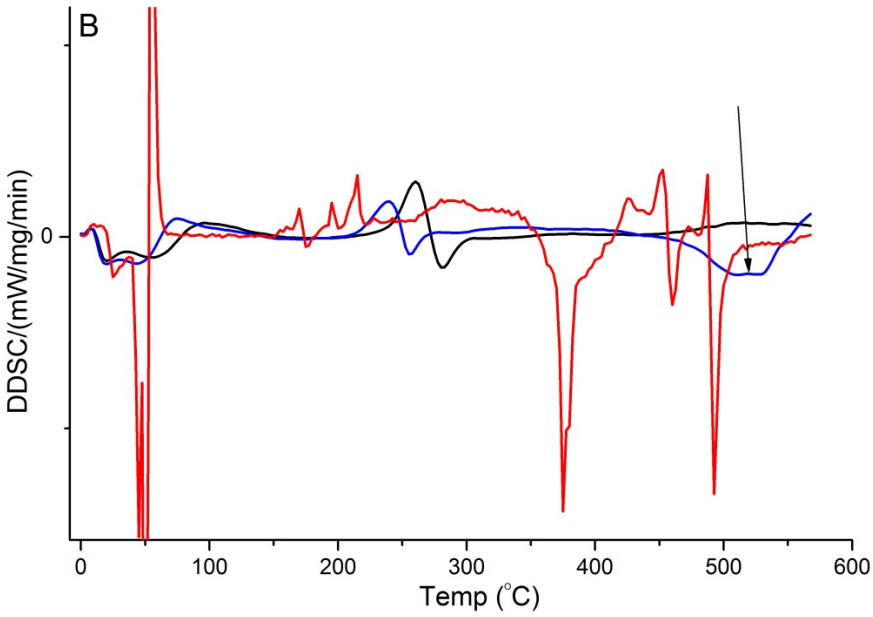

Figure S5.2-4: A. Derivative thermogravimetric (DTG) curve B. Derivative differential scanning calorimetry (DDSC) curve of blank chitosan film (black line), chitosan film grafted with PEG-SH (blue line) and PEG-SH powder (red line).

X-RAY SPECTROMETRY OF FILMS

X-ray spectrometry of the films was undertaken during the SEM (JEOL 6510 Low Vacuum with EDS microanalysis) analysis of the chitosan films. Detection of the sulfur in the SH group of the PEG chains was not possible likely due to a low concentration over a large surface area. The result is shown in Fig S5.2-5.

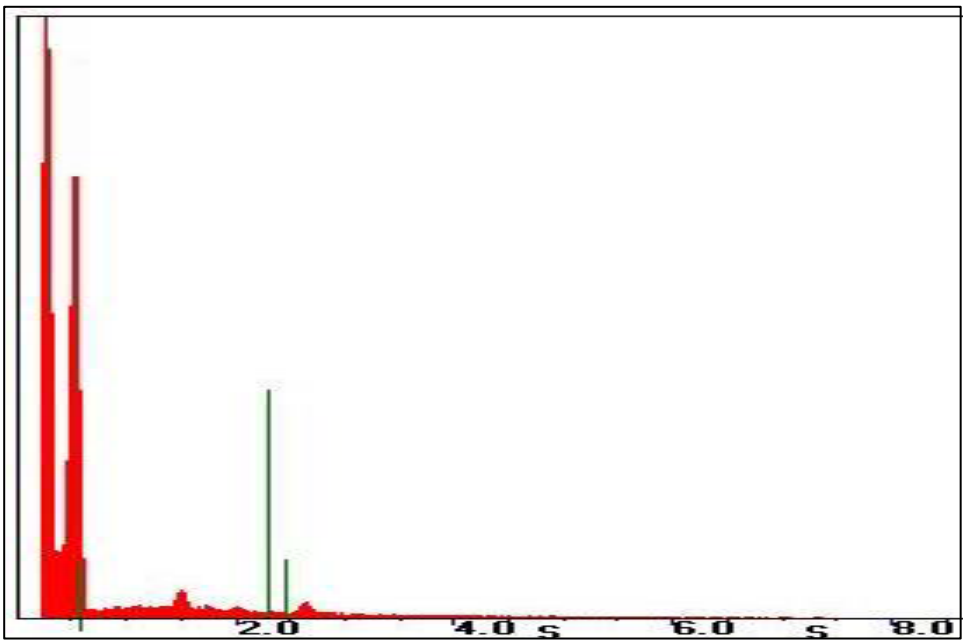

Figure S5.2-5. X-ray spectrometry of chitosan grafted with PEG-SH (red), no significant counts of sulfur (green).

FTIR SPECTROSCOPY OF CHITOSAN FILMS

Attenuation Total Reflectance (ATR) Fourier-Transform (FT) Infrared (IR) Spectroscopy was performed on a Bruker Vertex 70 spectrometer. Spectra were acquired on all the film samples with 32 scans and a recording speed of 1 cm^{-1}/s. No significant difference was seen between the samples and additionally no detection of the SH group of the PEG-SH.

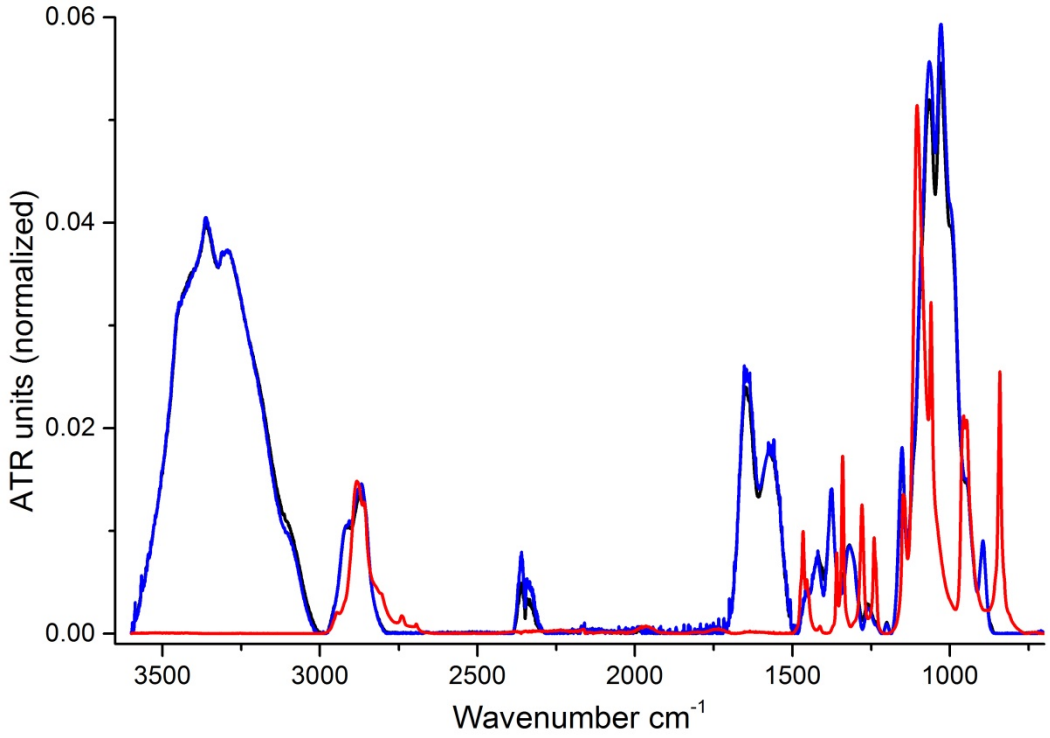

Figure S5.2-6: ATR FTIR spectroscopy of chitosan film (black), chitosan film grafted with PEG-SH (blue) and PEG-SH powder (red).

RAMAN SPECTROSCOPY OF CHITOSAN FILMS

Raman spectroscopy (Bruker Ramanscope III Senterra) was conducted on blank chitosan films and chitosan films with PEG-SH grafted onto the surface. A 633 nm laser at 10 mW with 40 s integration time and 10 co-additions was used. Polystyrene was used as a standard to ensure the instrument was running optimally. No significant difference was seen between each of the samples and additionally no detection of the SH group of the PEG-SH.

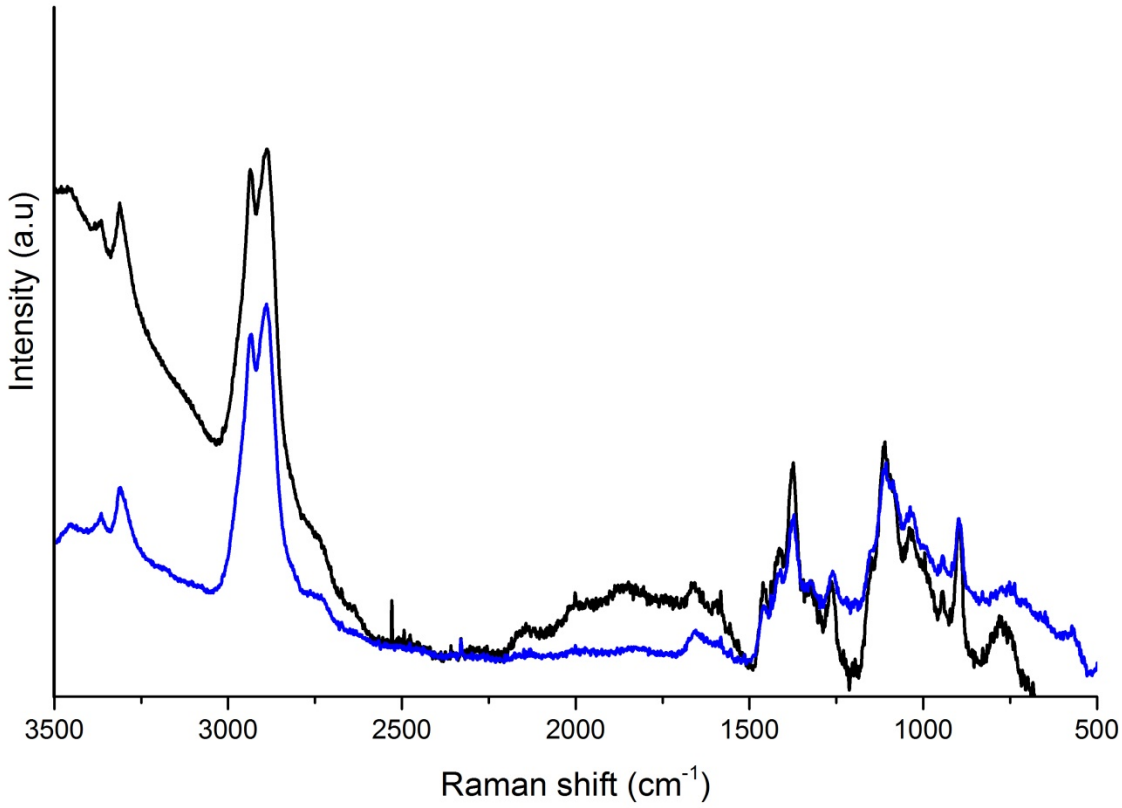

Figure S5.2-7: Raman spectroscopy of chitosan film (black) and chitosan film grafted with PEG-SH (blue).

SCANNING ELECTRON MICROSCOPY (SEM)

SEM (JEOL 6510 Low Vacuum with EDS microanalysis) images were taken on the blank chitosan film and the PEG-grafted chitosan film. The images show that the PEGylation of the film did not cause any adverse effects or compromise the surface of the film. Further, the surface roughness of the film can be analyzed on a scale that is important for cell culture.

a) b)

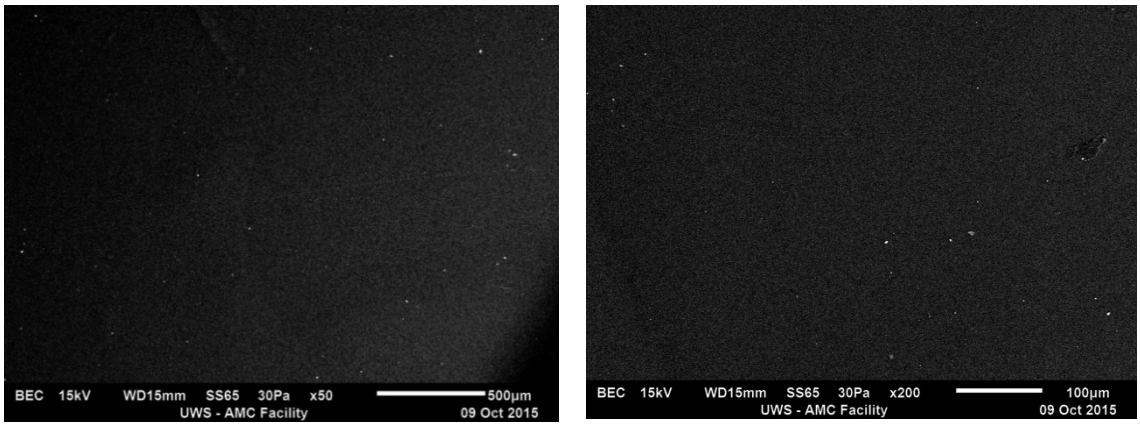

c) d)

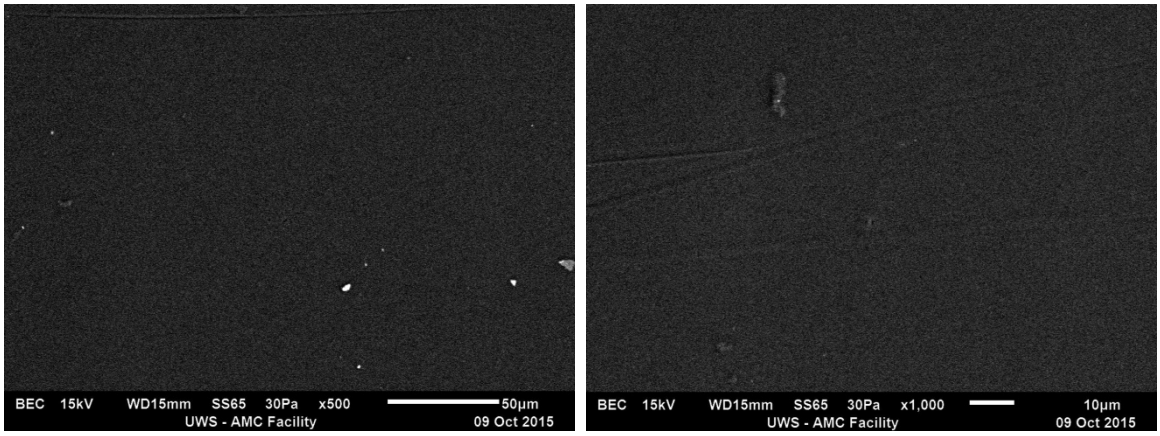

Figure S5.2-8: SEM image of chitosan films grafted with PEG-SH on the surface at a a) 500 μm b) 100 μm c) 50 μm and d) 10 μm (see scale bar of images)

a) b)

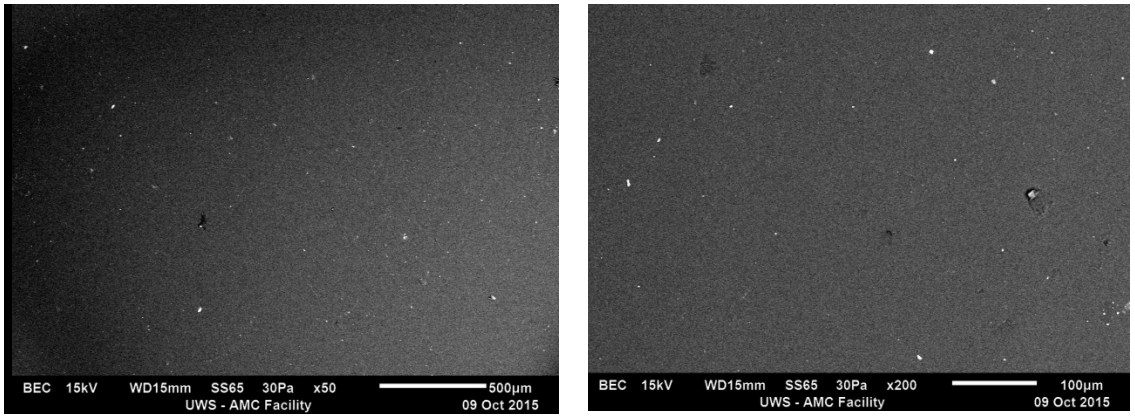

c) d)

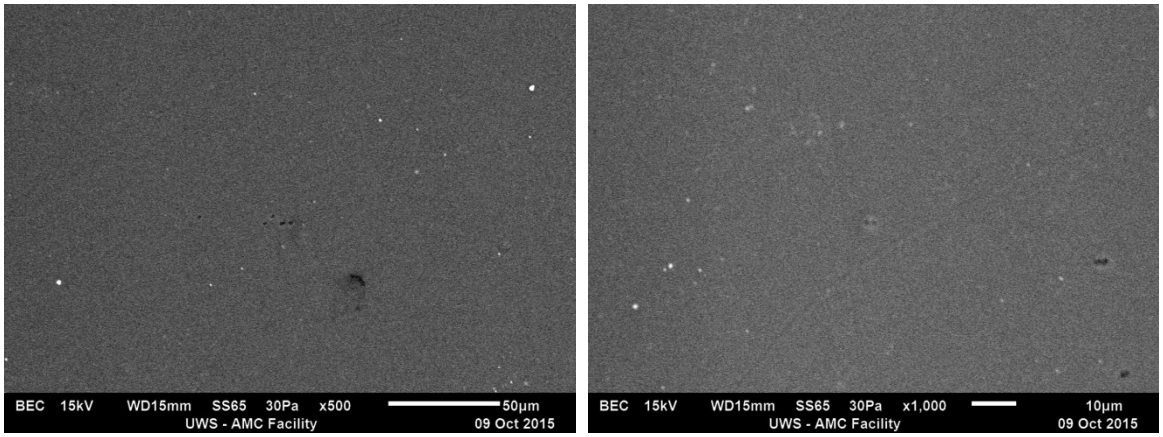

Figure S5.2-9: SEM image of native chitosan films at a) 500 μm b) 100 μm c) 50 μm and d) 10 μm (see scale bar of images)

ATOMIC FORCE MICROSCOPY (AFM)

AFM (Digital Nanoscope III) measurements allowed the analysis of the surface roughness of the film on a smaller scale which is significant for the grafting reaction. The film was shown to be quite rough on a 2 μm scale.

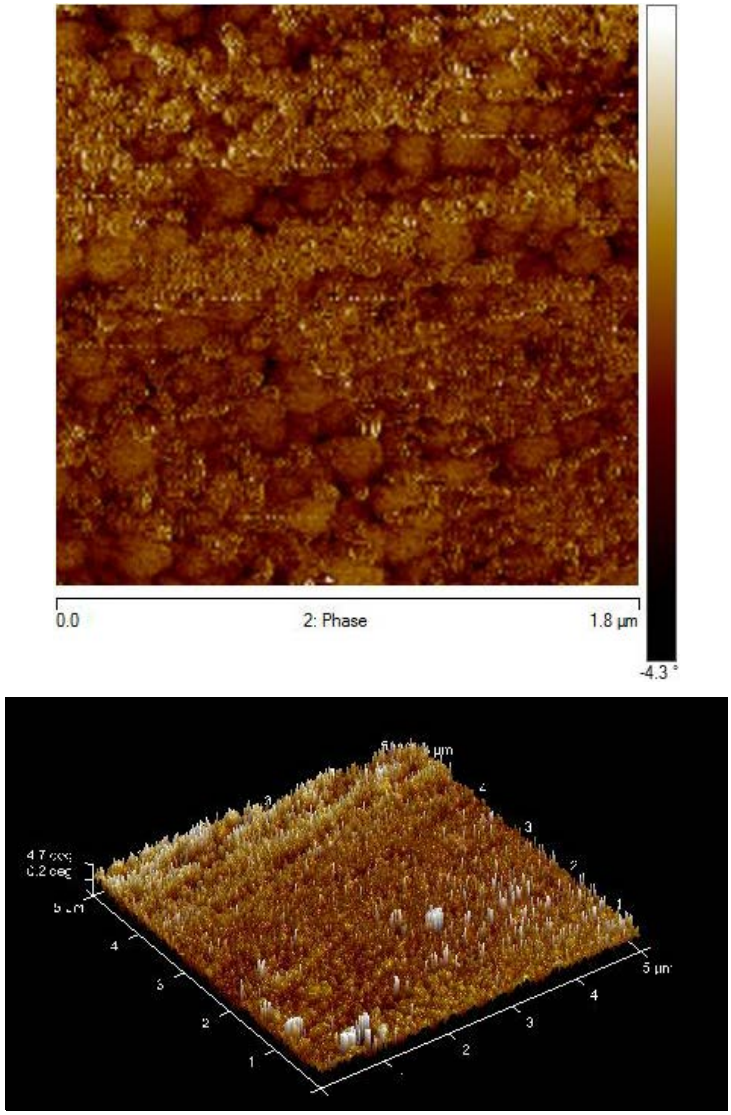

Figure S5.2-10. Surface roughness of native chitosan film with AFM a) 2d image and b) 3d image

NMR SPECTROSCOPY

^{13}C swollen-state NMR spectroscopy was conducted on chitosan grafted with PEG-SH on the surface. The films were swollen with either PBS at pH 7.4 or D_2O. No significant difference was seen between chitosan film and PEG-SH was not detected.

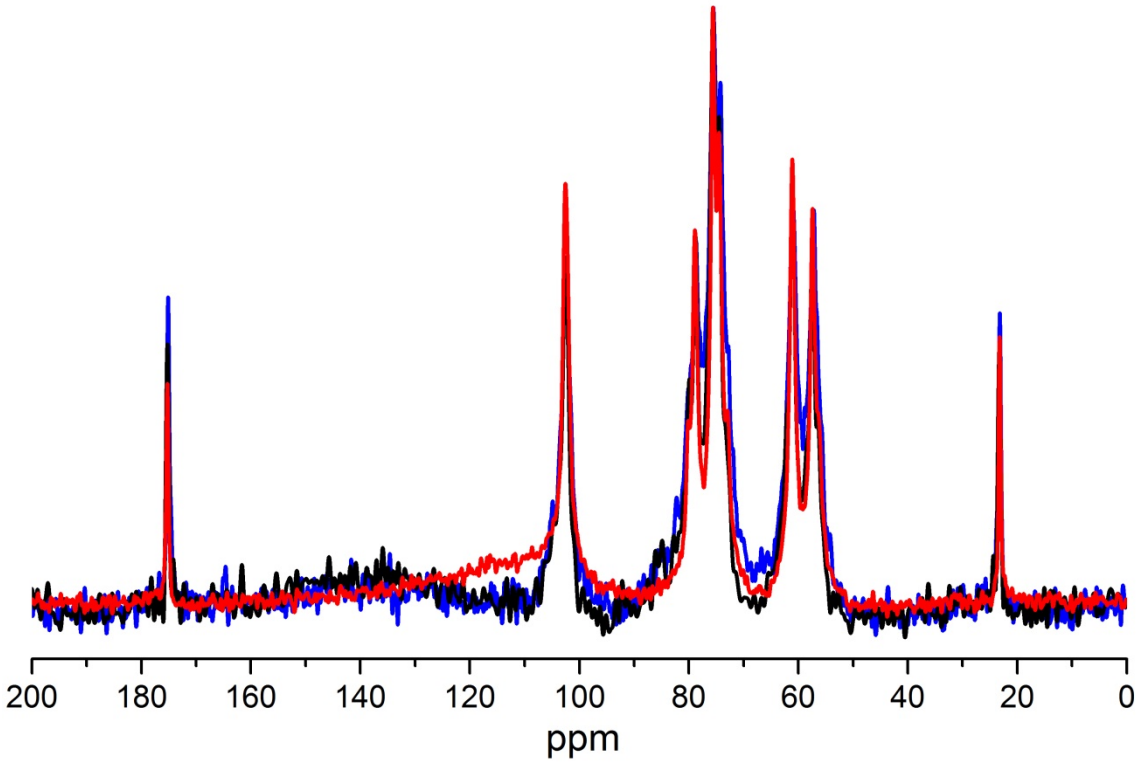

Figure S5.2-11: ^{13}C spectra of chitosan film (red), grafted with PEG-SH swollen in PBS (black) and D_2O (blue).

CHITOSAN PERMEABILITY

Thinner films were made by diluting the concentration of chitosan with acetic acid by twice or three times. The resulting films were thinner and the thickness measured is shown in Table S5.2-1. To allow optimal detection, UV-Vis spectrophotometry was undertaken on the cordial solution Figure S5.2-13. A calibration of the cordial was also undertaken shown in Figure S5.2-14.

Table S5.2-1: Chitosan films were measured using a Digimatic micrometer at 4 random points around the film. Average thickness results shown are mean ± SD.

Dilution	Film Thickness (μm)				Average thickness (μm)
1X	24	22	28	23	24.3 ± 2.6
2X	16	13	18	12	14.8 ± 2.8
3X	10	12	8	10	10.0 ± 1.6

Figure S5.2-12: Permeability test setup for 1X, 2X and 3X chitosan film samples for both 1.5 h and 3 h wait times with 30μL red cordial pipetted above.

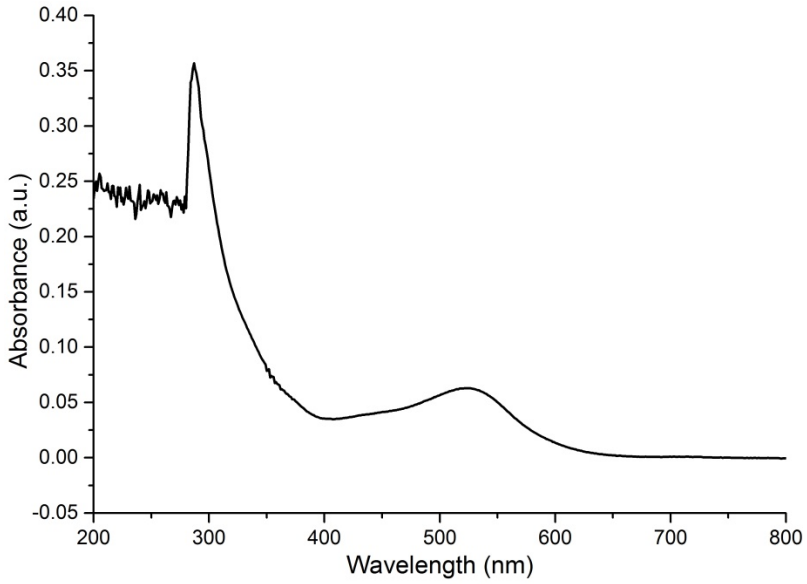

Figure S5.2-13: UV-Vis absorption across 200-800 nm for a 0.15% (v/v) red cordial solution.

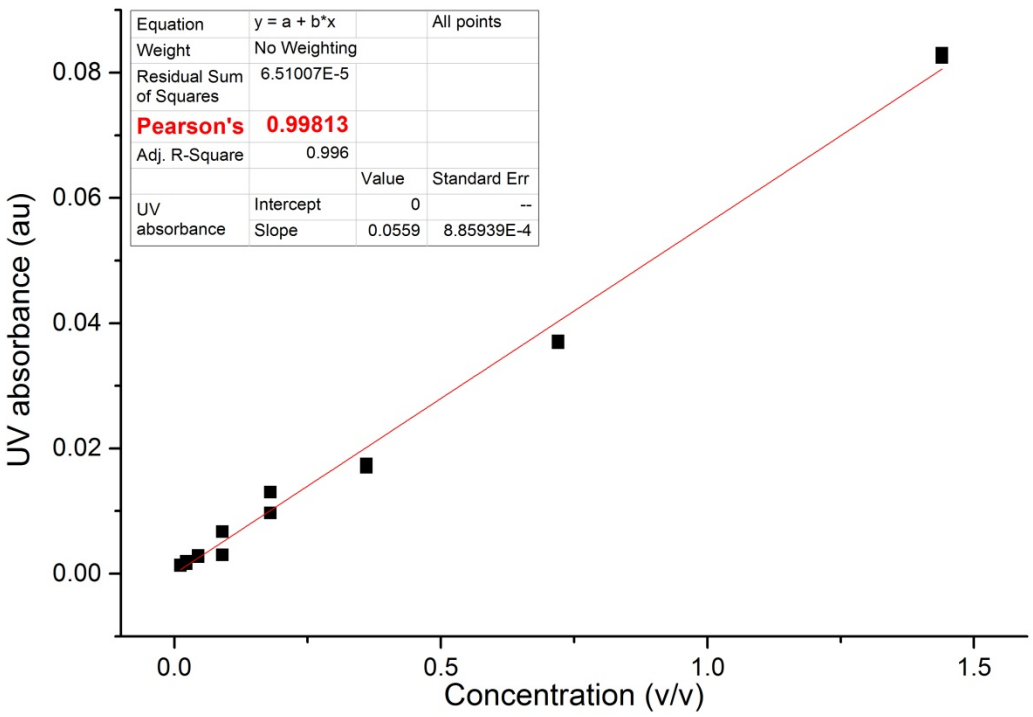

Figure S5.2-14: Calibration of UV absorbance of red cordial solutions with linear fit (red).

^{1}H-^{1}H Double wuantum correlation spectra of chitosan films swollen in D_2O.

a) b)

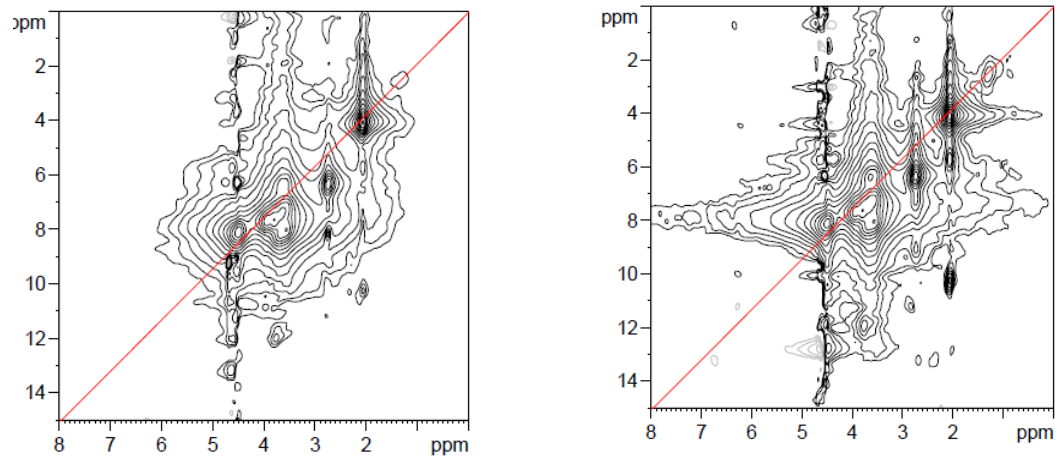

Figure S5.2-15: ^{1}H-^{1}H double quantum correlation of chitosan films swollen in D_2O with varying spinning rates and recoupling times a) 2 tr 25 kHz b) 4 tr 25 kHz

a) b)

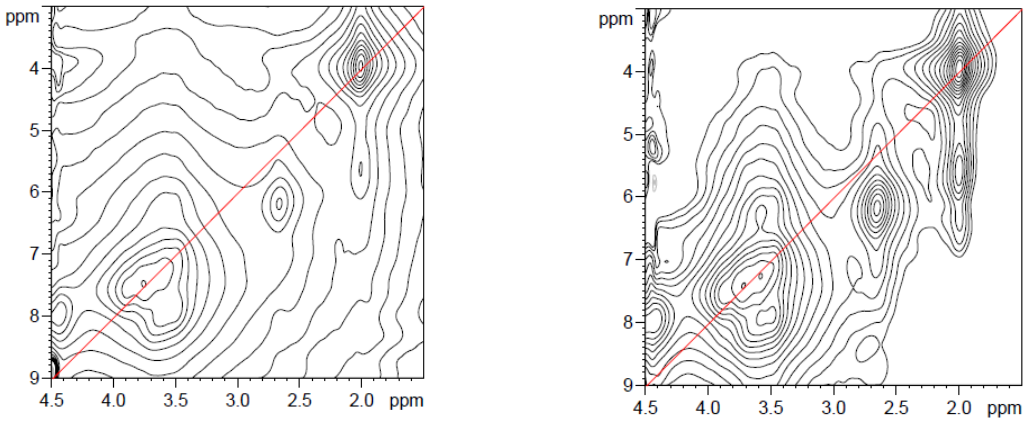

Figure S5.2-16: ^{1}H-^{1}H double quantum correlation of ChitPar1 swollen in D_2O with varying spinning rates and recoupling times a) 2 tr 25 kHz b) 4 tr 25 kHz

a) b)

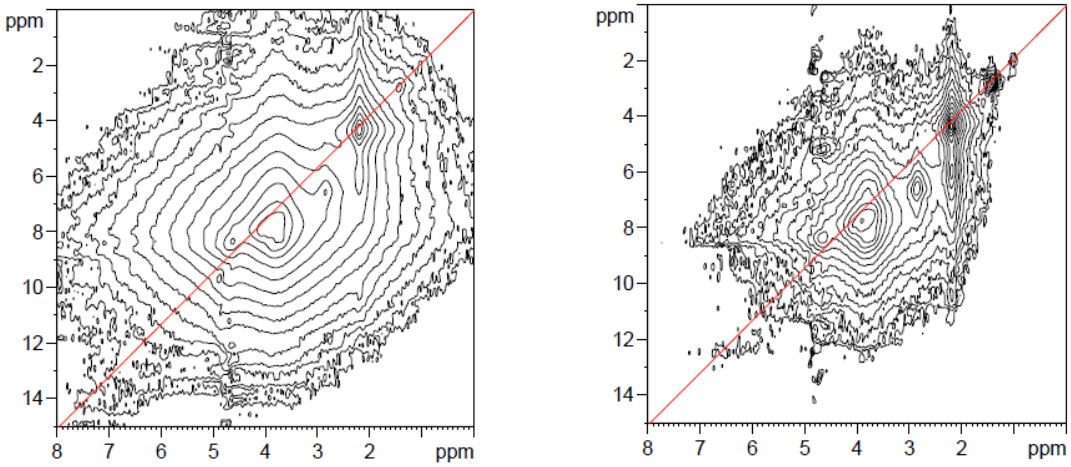

Figure S5.2-17: ^{1}H-^{1}H double quantum correlation of ParraMedMW swollen in $D_2O$with varying spinning rates and recoupling times a) 2 tr 25 kHz b) 4 tr 25 kHz

^{13}C (^{1}H) CORRELATION:

a) b)

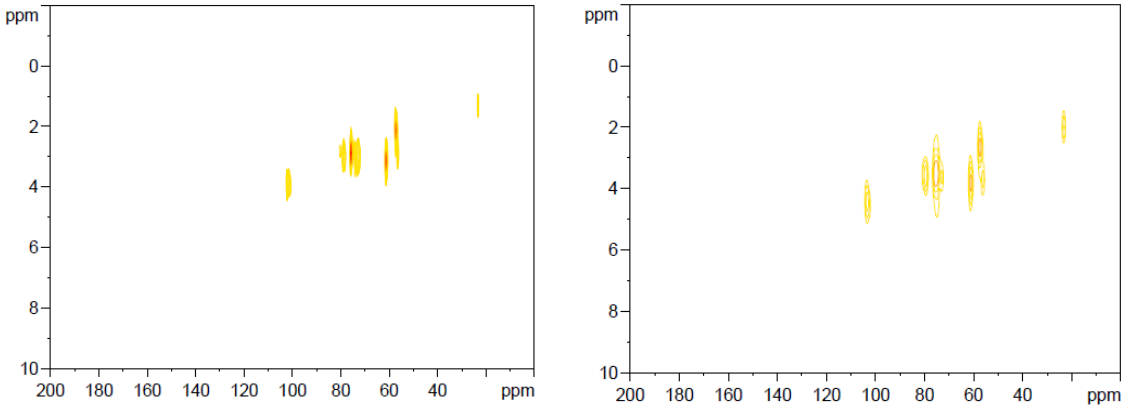

Figure S5.2-18: ^{13}C (^{1}H) correlation measurement of chitosan film swollen in a) PBS at pH 7 and b) D_2O

a) b)

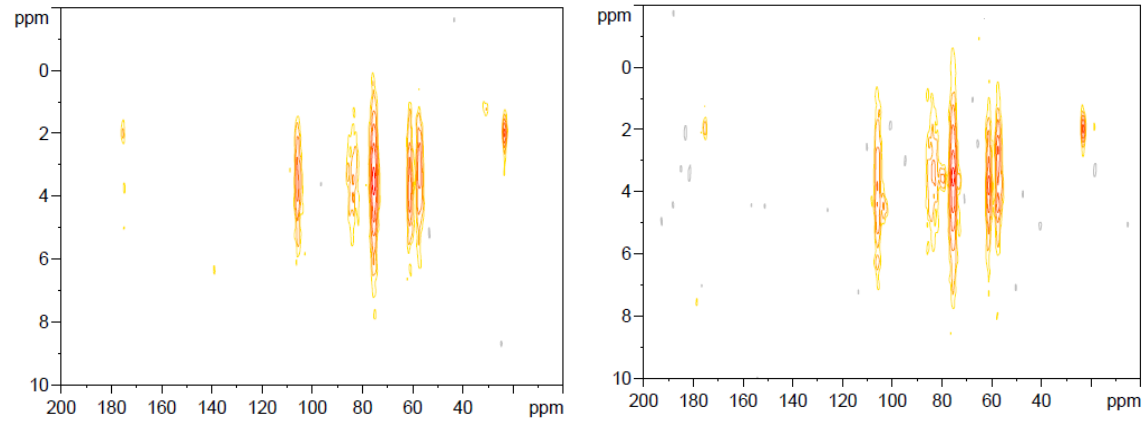

Figure S5.2-19: ^{13}C (^{1}H) correlation measurement of ChitPar1 swollen in a) PBS at pH 7 and b) D_2O

a) b)

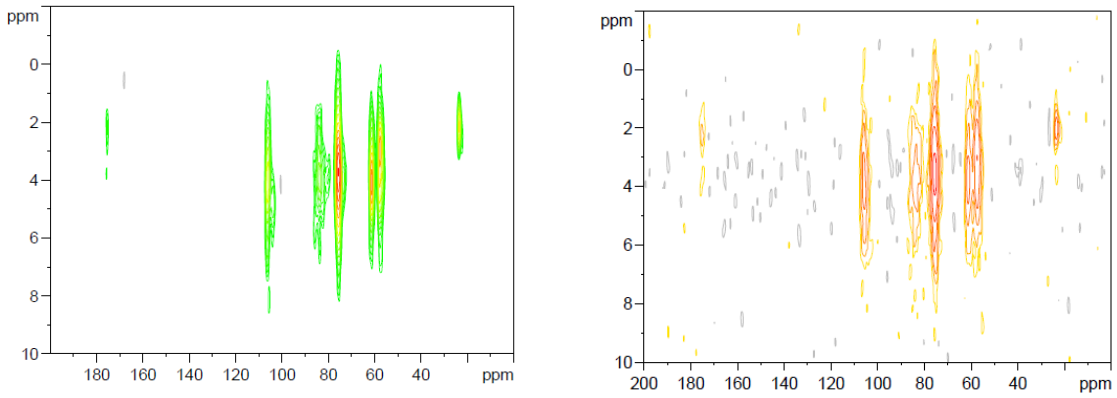

Figure S5.2-20: ^{13}C (^{1}H) correlation measurement of ParraMedMW swollen in a) PBS at pH 7 and b) D_2O

Reference

[1] D.L. Taylor, J.J. Thevarajah, D.K. Narayan, P. Murphy, M.M. Mangala, S. Lim, R. Wuhrer, C. Lefay, M.D. O'Connor, M. Gaborieau, P. Castignolles, Real-time monitoring of peptide grafting onto chitosan films using capillary electrophoresis, Analytical and Bioanalytical Chemistry, 407 (2015) 2543-2555.

CHAPTER 6: Conclusion and Future work

6.1. Fulfilled aims

The overall aim of this work was to develop new methods for the characterization of chitosan to allow its further use for biomedical applications. Chitosan being a natural polymer is known for being complicated to analyze and current methods are insufficient for a complete characterization.

Methods such as CE-CC and NMR spectroscopy were successfully used to explore the area of dissolution in the analysis of chitosan. The robustness of CE allowed the analysis of partially dissolved samples and the monitoring of the kinetics of dissolution of chitosan with no sample preparation. The results showed that the current widely used solvent (aqueous AcOH) was inefficient in dissolution, while DCl in D_2O caused deacetylation at high temperature. For a more complete dissolution of chitosan, aqueous 50 mM HCl at 60 °C for ~2 h should be used. Further work in obtaining a true solution would have flow on effects in the characterization of chitosan in solution. More accurate composition distributions compared to those obtained in this thesis would be possible. Further work could also be completed to improve the selectivity of the separation. Finally, solid-state measurements should be used to determine the average *DA* of chitosan samples.

Using CE-CC, a methodology was developed to calculate the dispersity of distributions of electrophoretic mobilities or of composition distributions thus enabling the quantification of the heterogeneity of composition or of branching. This was successfully applied to a range of complex polyelectrolytes. This included the heterogeneity of the composition of chitosan, poly(sodium acrylate-*co*-*N*-antipyrine acrylamide), poly(acrylic acid-*b*-acrylamide) and the heterogeneity of branching of poly(sodium acrylate).. Further development in the selectivity of chitosan separation also allowed composition distributions of chitosan to be obtained for the first time.

The robustness of CE was further outlined in its ability to monitor chemical reactions such as the grafting of peptides and PEG onto the surface of chitosan films. Chitosan films were improved in functionality and possible reduction in immunogenecity through the grafting of poly(ethylene glycol) on their surface which was successfully validated through TGA.Swollen-state NMR spectroscopy allowed confirmation of grafting of RGDS onto the surface of chitosan and also allowed probing into the behavior of chitosan powder and films in different swelling conditions. The results from this thesis also identified some key areas for further areas of study including further work on assessing the heterogeneity of chitosan and its films.

6.2. Further method development

As a consequence of trying to improve the analysis of chitosan, a method was developed to analyze distributions of parameters other than size for polymers.

This method has significant positive implications in the field of polymer science as it can be used extensively for polyelectrolyte characterization. It is already being used in the analysis of poly(acrylic acid) (possible anticancer drug delivery agent), starch (significant effect on glycemic index and global diet), DNA (possible identification of methylation in DNA found in cancer cells), double hydrophilic block copolymers (various industrial applications including coatings) and proteins (significant for example in the study of Alzheimer's disease). Further knowledge and development of this method would allow its use in an even wider range of areas of study.

Another method which is of interest is TDA. TDA has the possibility to be an extremely effective tool in size analysis of polymers. If coupled to CE-CC both size and composition/branching/end group information could be obtained with one instrument. Another possibility to allow a more complete characterization includes coupling SEC to CE to allow size and composition information to be obtained. Unfortunately, this would require optimal conditions for the SEC, which would also require better dissolution conditions of chitosan and an appropriate SEC eluent. Additionally the sensitivity the CE analysis would need to be tested and optimized. Together these methods would allow a much more complete characterization of polyelectrolytes.

In further analysis of chitosan films, the use of labeled peptides and PEG would allow easier detection with NMR spectroscopy. The use of deuterated chitosan or peptides would allow detection by IR microscopy. Both of which could give further information regarding the heterogeneity of the surface of chitosan films.

6.3. Design of materials based on chitosan

This thesis has shown that the use of chitosan for biomedical applications is a possibility. However it also outlined the various limitations that exist currently. The first of these is in the dissolution of chitosan. Not having a true solution prevents accurate characterization in solution. To obtain a more complete dissolution, solvents such as ionic liquids or the use of salts to disrupt hydrogen bonds as in the case of starch should be tested.

The growth of cells in specific regions of chitosan films gave evidence of heterogeneity of the surface. The quantification of the heterogeneity of composition that influenced the surface of the films was challenging to prove. Possible techniques to quantify the heterogeneity of chitosan and chitosan films may include IR microscopy on deuterated chitosan. Using deuterated chitosan would allow the detection of the acetyl rich and poor regions as the resolution of the IR band would be higher than that measured with current non-deuterated films. Deuterated chitosan films could also be used to map the grafting of peptides or polymers such as PEG onto the surface for the same reason and allow more information on the heterogeneity of the films surface as well as the grafting itself.

For chitosan films grafted with PEG, implantation studies would need to take place to test whether the biocompatibility had improved compared to that of bare films. The grafting of peptides such as RGDS onto the SH functionality of

PEG would also allow the chitosan films to be bi-functional. The improved biocompatibility of the chitosan films due to the presence of PEG and the cell attachment from the peptides would allow the films to be an interesting product to be tested for various biomedical applications. Another parameter of interest which would need to be studied is the degradation of the chitosan films. To prevent an immune response is required; however, proper removal of the material after it has been implanted on an appropriate time scale is also necessary. Films produced from low molar mass chitosan for easier degradation may need to be considered.

The methods developed in this thesis will enable chitosan to reach its potential for various applications ranging from tissue regeneration, through bioplastics to drug delivery.

CHAPTER 7: References

1.Thevarajah, J. J.; Gaborieau, M.; Castignolles, P., Separation and characterization of synthetic polyelectrolytes and polysaccharides with capillary electrophoresis. *Advances in Chemistry* **2014,** 2014, Article ID 798403.

2.Sutton, A. T.; Read, E.; Maniego, A. R.; Thevarajah, J.; Marty, J. D.; Destarac, M.; Gaborieau, M.; Castignolles, P., Purity of double hydrophilic block copolymers revealed by capillary electrophoresis in the critical conditions. *Journal of Chromatography A* **2014,** 1372, 187-195.

3.Taylor, D. L.; Thevarajah, J. J.; Narayan, D. K.; Murphy, P.; Mangala, M. M.; Lim, S.; Wuhrer, R.; Lefay, C.; O'Connor, M. D.; Gaborieau, M.; Castignolles, P., Real-time monitoring of peptide grafting onto chitosan films using capillary electrophoresis. *Analytical and Bioanalytical Chemistry* **2015,** 407, 2543-2555.

4.Trombotto, S.; Ladaviere, C.; Delolme, F.; Domard, A., Chemical preparation and structural characterization of a homogeneous series of chitin/chitosan oligomers. *Biomacromolecules* **2008,** 9, 1731-1738.

5.Domard, A., A perspective on 30 years research on chitin and chitosan. *Carbohydrate Polymers* **2011,** 84, 696-703.

6.Rinaudo, M., Chitin and chitosan: Properties and applications. *Progress in Polymer Science* **2006,** 31, 603-632.

7.Lauto, A., Integration of Extracellular Matrix With Chitosan Adhesive Film for Sutureless Tissue Fixation. *Lasers in Surgery and Medicine* **2009,** 41, 366-371.

8.Li, Z.; Leung, M.; Hopper, R.; Ellenbogen, R.; Zhang, M., Feeder-free self-renewal of human embryonic stem cells in 3D porous natural polymer scaffolds. *Biomaterials* **2010,** 31, 404-412.

9.Wen, Y. H.; Grondahl, L.; Gallego, M. R.; Jorgensen, L.; Moller, E. H.; Nielsen, H. M., Delivery of Dermatan Sulfate from Polyelectrolyte Complex-Containing Alginate Composite Microspheres for Tissue Regeneration. *Biomacromolecules* **2012,** 13, 905-917.

10.Patel, M. P.; Patel, R. R.; Patel, J. K., Chitosan Mediated Targeted Drug Delivery System: A Review. *Journal of Pharmacy and Pharmaceutical Sciences* **2010,** 13, 536-557.

11.Song, J.; Chen, Q.; Zhang, Y.; Diba, M.; Kolwijck, E.; Shao, J.; Jansen, J. A.; Yang, F.; Boccaccini, A. R.; Leeuwenburgh, S. C. G., Electrophoretic Deposition of Chitosan Coatings Modified with Gelatin Nanospheres To Tune the Release of Antibiotics. *ACS Applied Materials & Interfaces* **2016,** 8, 13785-13792.

12.Morrow, B. H.; Payne, G. F.; Shen, J., pH-Responsive Self-Assembly of Polysaccharide through a Rugged Energy Landscape. *Journal of the American Chemical Society* **2015,** 137, 13024-13030.

13.Boryniec, S.; Strobin, G.; Struszczyk, H.; Niekraszewicz, A.; Kucharska, M., GPC studies of chitosan degradation. *International Journal of Polymer Analysis and Characterization* **1997,** 3, 359-368.

14.Gopalakannan, A.; Arul, V., Immunomodulatory effects of dietary intake of chitin, chitosan and levamisole on the immune system of Cyprinus carpio and control of Aeromonas hydrophila infection in ponds. *Aquaculture* **2006,** 255, 179-187.

15.Martínez-Camacho, A. P.; Cortez-Rocha, M. O.; Ezquerra-Brauer, J. M.; Graciano-Verdugo, A. Z.; Rodriguez-Félix, F.; Castillo-Ortega, M. M.; Yépiz-Gómez, M. S.; Plascencia-Jatomea, M., Chitosan composite films: Thermal, structural, mechanical and antifungal properties. *Carbohydrate Polymers* **2010,** 82, 305-315.

16.Pillai, C. K. S.; Paul, W.; Sharma, C. P., Chitin and chitosan polymers: Chemistry, solubility and fiber formation. *Progress in Polymer Science* **2009,** 34, 641-678.

17.Kusek, K., Promising solution to plastic pollution. *Harvard Gazette* 2014, pp http://news.harvard.edu/gazette/story/2014/05/promising-solution-to-plastic-pollution/.

18.Nguyen, S.; Hisiger, S.; Jolicoeur, M.; Winnik, F. M.; Buschmann, M. D., Fractionation and characterization of chitosan by analytical SEC and H-1 NMR after semi-preparative SEC. *Carbohydrate Polymers* **2009,** 75, 636-645.

19.Peniche, C.; Argüelles-Monal, W.; Goycoolea, F. M., Chapter 25 - Chitin and Chitosan: Major Sources, Properties and Applications. In *Monomers, Polymers and Composites from Renewable Resources*, Mohamed Naceur, B.; Alessandro, G., Eds. Elsevier: Amsterdam, 2008; pp 517-542.

20.Gartner, C.; Lopez, B. L.; Sierra, L.; Graf, R.; Spiess, H. W.; Gaborieau, M., Interplay between Structure and Dynamics in Chitosan Films Investigated

with Solid-State NMR, Dynamic Mechanical Analysis, and X-ray Diffraction. *Biomacromolecules* **2011,** 12, 1380-1386.

21. Yanagisawa, M.; Kato, Y.; Yoshida, Y.; Isogai, A., SEC-MALS study on aggregates of chitosan molecules in aqueous solvents: Influence of residual N-acetyl groups. *Carbohydrate Polymers* **2006,** 66, 192-198.

22. Striegel, A. M.; Kirkland, J. J.; Yau, W. W.; Bly, D. D., *Modern Size Exclusion Chromatography*. 2nd ed.; Wiley: Hoboken, 2009; p 494.

23. Bruessau, R. J., Experiences with interlaboratory GPC experiments. *Macromolecular Symposia* **1996,** 110, 15-32.

24. Lacík, I.; Stach, M.; Kasák, P.; Semak, V.; Uhelská, L.; Chovancová, A.; Reinhold, G.; Kilz, P.; Delaittre, G.; Charleux, B.; Chaduc, I.; D'Agosto, F.; Lansalot, M.; Gaborieau, M.; Castignolles, P.; Gilbert, R. G.; Szablan, Z.; Barner-Kowollik, C.; Hesse, P.; Buback, M., SEC Analysis of Poly(Acrylic Acid) and Poly(Methacrylic Acid). *Macromolecular Chemistry and Physics* **2015,** 216, 23-37.

25. Berek, D., Size exclusion chromatography - A blessing and a curse of science and technology of synthetic polymers. *Journal of Separation Science* **2010,** 33, 315-335.

26. Barth, H. G.; Carlin, F. J., A review of polymer shear degradation in size-exclusion chromatography. *Journal of Liquid Chromatography* **1984,** 7, 1717-1738.

27. Uliyanchenko, E.; van der Wal, S.; Schoenmakers, P. J., Deformation and degradation of polymers in ultra-high-pressure liquid chromatography. *Journal of Chromatography A* **2011,** 1218, 6930-6942.

28. Kostanski, L. K.; Keller, D. M.; Hamielec, A. E., Size-exclusion chromatography - a review of calibration methodologies. *Journal of Biochemical and Biophysical Methods* **2004,** 58, 159-186.

29. Netopilik, M.; Kratochvil, P., Polystyrene-equivalent molecular weight versus true molecular weight in size-exclusion chromatography. *Polymer* **2003,** 44, 3431-3436.

30. Guillaneuf, Y.; Castignolles, P., Using apparent Molecular Weight from SEC in controlled/living polymerization and kinetics of polymerization. *Journal of Polymer Science, Part A: Polymer Chemistry* **2008,** 46, 897-911.

31.Hamielec, A. E.; Ouano, A. C., Generalized Universal Molecular-Weight Calibration Parameter in GPC. *Journal of Liquid Chromatography* **1978,** 1, 111-120.

32.Gaborieau, M.; Gilbert, R. G.; Gray-Weale, A.; Hernandez, J. M.; Castignolles, P., Theory of Size Exclusion Chromatography (SEC) of complex branched polymers. *Macromolecular Theory and Simulations* **2007,** 16, 13-28.

33.Gaborieau, M.; Nicolas, J.; Save, M.; Charleux, B.; Vairon, J.-P.; Gilbert, R. G.; Castignolles, P., Multiple-detection size-exclusion chromatography of complex branched polyacrylates. *Journal of Chromatography A* **2008,** 1190, 215-233.

34.Couvreur, L.; Piteau, G.; Castignolles, P.; Tonge, M.; Coutin, B.; Charleux, B.; Vairon, J. P., Pulsed-laser radical polymerization and propagation kinetic parameters of some alkyl acrylates. *Macromolecular Symposia* **2001,** 174, 197-207.

35.Castignolles, P.; Graf, R.; Parkinson, M.; Wilhelm, M.; Gaborieau, M., Detection and quantification of branching in polyacrylates by size-exclusion chromatography (SEC) and melt-state 13C NMR spectroscopy. *Polymer* **2009,** 50, 2373-2383.

36.Castignolles, P., Transfer to Polymer and Long-Chain Branching in PLP-SEC of Acrylates. *Macromolecular Rapid Communications* **2009,** 30, 1995 - 2001.

37.Junkers, T.; Schneider-Baumann, M.; Koo, S. S. P.; Castignolles, P.; Barner-Kowollik, C., Determination of Propagation Rate Coefficients for Methyl and 2-Ethylhexyl Acrylate via High Frequency PLP–SEC under Consideration of the Impact of Chain Branching. *Macromolecules* **2010,** 43, 10427-10434.

38.Gaborieau, M.; Castignolles, P., Size-exclusion chromatography (SEC) of branched polymers and polysaccharides. *Analytical and Bioanalytical Chemistry* **2011,** 399, 1413-1423.

39.Uliyanchenko, E.; van der Wal, S.; Schoenmakers, P. J., Challenges in polymer analysis by liquid chromatography. *Polymer Chemistry* **2012,** 3, 2313-2335.

40.Rollet, M.; Gle, D.; Phan, T. N. T.; Guillaneuf, Y.; Bertin, D.; Gigmes, D., Characterization of Functional Poly(ethylene oxide)s and Their Corresponding Polystyrene Block Copolymers by Liquid Chromatography

under Critical Conditions in Organic Solvents. *Macromolecules* **2012,** 45, 7171-7178.

41. Al Samman, M.; Radke, W.; Khalyavina, A.; Lederer, A., Retention Behavior of Linear, Branched, and Hyperbranched Polyesters in Interaction Liquid Chromatography. *Macromolecules* **2010,** 43, 3215-3220.

42. Lee, W.; Cho, D. Y.; Chang, T. Y.; Hanley, K. J.; Lodge, T. P., Characterization of polystyrene-b-polyisoprene diblock copolymers by liquid chromatography at the chromatographic critical condition. *Macromolecules* **2001,** 34, 2353-2358.

43. Favier, A.; Petit, C.; Beaudoin, E.; Bertin, D., Liquid chromatography at the critical adsorption point (LC-CAP) of high molecular weight polystyrene: pushing back the limits of reduced sample recovery. *E-Polymers* **2009**, 15.

44. Beaudoin, E.; Favier, A.; Galindo, C.; Lapp, A.; Petit, C.; Gigmes, D.; Marque, S.; Bertin, D., Reduced sample recovery in liquid chromatography at critical adsorption point of high molar mass polystyrene. *European Polymer Journal* **2008,** 44, 514-522.

45. Weinberger, R., *Practical capillary electrophoresis*. Academic Press: San Diego, CA 2000.

46. Cottet, H.; Gareil, P., Separation of synthetic (Co)polymers by capillary electrophoresis techniques. In *Capillary Electrophoresis*, Schmitt-Kopplin, P., Ed. Humana Press Inc.: Totowa, NJ, United States, 2008; Vol. 384, pp 541-567.

47. Tran, N. T.; Taverna, M.; Miccoli, L.; Angulo, J. F., Poly(ethylene oxide) facilitates the characterization of an affinity between strongly basic proteins with DNA by affinity capillary electrophoresis. *Electrophoresis* **2005,** 26, 3105-3112.

48. Miramon, H.; Cavelier, F.; Martinez, J.; Cottet, H., Highly Resolutive Separations of Hardly Soluble Synthetic Polypeptides by Capillary Electrophoresis. *Analytical Chemistry* **2010,** 82, 394-399.

49. Vayaboury, W.; Giani, O.; Cottet, H.; Bonaric, S.; Schue, F., Mechanistic study of alpha-amino acid N-carboxyanhydride (NCA) polymerization by capillary electrophoresis. *Macromolecular Chemistry and Physics* **2008,** 209, 1628-1637.

50. Aguilar, M. R.; Gallardo, A.; Roman, J. S.; Cifuentes, A., Micellar electrokinetic chromatography: A powerful analytical tool to study

copolymerization reactions involving ionic species. *Macromolecules* **2002,** 35, 8315-8322.

51.Spiridon, I.; Popa, V. I., Chapter 13 - Hemicelluloses: Major Sources, Properties and Applications. In *Monomers, Polymers and Composites from Renewable Resources*, Belgacem, M. N.; Gandini, A., Eds. Elsevier: Amsterdam, 2008; pp 289-304.

52.Brudin, S.; Schoenmakers, P., Analytical methodology for sulfonated lignins. *Journal of Separation Science* **2010,** 33, 439-452.

53.Oliver, J. D.; Gaborieau, M.; Hilder, E. F.; Castignolles, P., Simple and robust determination of monosaccharides in plant fibers in complex mixtures by capillary electrophoresis and high performance liquid chromatography. *Journal of Chromatography A* **2013,** 1291, 179-186.

54.Verzele, M.; Simoens, G.; Vandamme, F., A Critical-Review of Some Liquid-Chromatography Systems for the Separation of Sugars. *Chromatographia* **1987,** 23, 292-300.

55.Rovio, S.; Yli-Kauhaluoma, J.; Siren, H., Determination of neutral carbohydrates by CZE with direct UV detection. *Electrophoresis* **2007,** 28, 3129-3135.

56.Rovio, S.; Simolin, H.; Koljonen, K.; Siren, H., Determination of monosaccharide composition in plant fiber materials by capillary zone electrophoresis. *Journal of Chromatography A* **2008,** 1185, 139-144.

57.Oliver, J. D.; Sutton, A. T.; Karu, N.; Phillips, M.; Markham, J.; Peiris, P.; Hilder, E. F.; Castignolles, P., Simple and robust monitoring of ethanol fermentations by capillary electrophoresis. *Biotechnology and Applied Biochemistry* **2015,** 62, 329-342.

58.Oliver, J. D.; Gaborieau, M.; Castignolles, P., Ethanol determination using pressure mobilization and free solution capillary electrophoresis by photo-oxidation assisted UV detection. *Journal of Chromatography A* **2014,** 1348, 150-157.

59.Sarazin, C.; Delaunay, N.; Costanza, C.; Eudes, V.; Mallet, J. M.; Gareil, P., New Avenue for Mid-UV-Range Detection of Underivatized Carbohydrates and Amino Acids in Capillary Electrophoresis. *Analytical Chemistry* **2011,** 83, 7381-7387.

60.Oliver, J. D.; Rosser, A. A.; Fellows, C. M.; Guillaneuf, Y.; Clement, J. L.; Gaborieau, M.; Castignolles, P., Understanding and improving direct UV

detection of monosaccharides and disaccharides in free solution capillary electrophoresis. *Analytica Chimica Acta* **2014,** 809, 183-193.

61.Schmid, T.; Himmelsbach, M.; Oliver, J. D.; Gaborieau, M.; Castignolles, P.; Buchberger, W., Investigation of photochemical reactions of saccharides during direct ultraviolet absorbance detection in capillary electrophoresis. *Journal of Chromatography A* **2015,** 1388, 259-266.

62.Cottet, H.; Gareil, P., From small charged molecules to oligomers: A semiempirical approach to the modeling of actual mobility in free solution. *Electrophoresis* **2000,** 21, 1493-1504.

63.Siauw, M.; Hawkett, B. S.; Perrier, S., Short Chain Amphiphilic Diblock Co-Oligomers via RAFT Polymerization. *Journal of Polymer Science Part a-Polymer Chemistry* **2012,** 50, 187-198.

64.Castignolles, P.; Gaborieau, M.; Hilder, E. F.; Sprong, E.; Ferguson, C. J.; Gilbert, R. G., High resolution separation of oligo(acrylic acid) by capillary zone electrophoresis. *Macromolecular Rapid Communications* **2006,** 27, 42-46.

65.Ferguson, C. J.; Hughes, R. J.; Nguyen, D.; Pham, B. T. T.; Gilbert, R. G.; Serelis, A. K.; Such, C. H.; Hawkett, B. S., Ab initio emulsion polymerization by RAFT-controlled self-assembly. *Macromolecules* **2005,** 38, 2191-2204.

66.Lacik, I.; Beuermann, S.; Buback, M., PLP-SEC study into free-radical propagation rate of nonionized acrylic acid in aqueous solution. *Macromolecules* **2003,** 36, 9355-9363.

67.Gaborieau, M.; Causon, T. J.; Guillaneuf, Y.; Hilder, E. F.; Castignolles, P., Molecular weight and tacticty of oligoacrylates by capillary electrophoresis - mass spectrometry. *Australian Journal of Chemistry* **2010,** 63, 1219-1226.

68.Guttman, C. M.; Flynn, K. M.; Wallace, W. E.; Kearsley, A. J., Quantitative Mass Spectrometry and Polydisperse Materials: Creation of an Absolute Molecular Mass Distribution Polymer Standard. *Macromolecules* **2009,** 42, 1695-1702.

69.Chojnacka, A.; Kempe, K.; van de Ven, H. C.; Englert, C.; Hoogenboom, R.; Schubert, U. S.; Janssen, H. G.; Schoenmakers, P., Molar mass, chemical-composition, and functionality-type distributions of poly(2-oxazoline)s revealed by a variety of separation techniques. *Journal of Chromatography A* **2012,** 1265, 123-132.

70.Fitzgerald, E. B.; Fuoss, R. M., Polyelectrolytes .11. Electrophoresis in Solutions of Poly-4-Vinyl-N-N-Butylpyridinium Bromide. *Journal of Polymer Science* **1954,** 14, 329-339.

71.Rollet, M.; Pelletier, B.; Altounian, A.; Berek, D.; Maria, S.; Beaudoin, E.; Gigmes, D., Separation of Parent Homopolymers from Polystyrene-b-poly(ethylene oxide)-b-polystyrene Triblock Copolymers by Means of Liquid Chromatography: 1. Comparison of Different Methods. *Analytical Chemistry* **2014,** 86, 2694-2702.

72.Flory, P. J., Configurational and frictional properties of the polymer molecule in dilute solution. In *Principles of Polymer Chemistry*, 1st ed.; Cornell University Press: Ithaca, New York, 1953; Vol. XIV, pp 595-639.

73.Muthukumar, M., Theory of electrophoretic mobility of a polyelectrolyte in semidilute solutions of neutral polymers. *Electrophoresis* **1996,** 17, 1167-1172.

74.Barrat, J. L.; Joanny, J. F., Theory of polyelectrolyte solutions. In *Advances in Chemical Physics*, John Wiley & Sons Inc: New York, 1996; Vol. 94, pp 1-66.

75.Stellwagen, N. C.; Gelfi, C.; Righetti, P. G., The free solution mobility of DNA. *Biopolymers* **1997,** 42, 687-703.

76.Cottet, H.; Gareil, P.; Theodoly, O.; Williams, C. E., A semi-empirical approach to the modeling of the electrophoretic mobility in free solution: Application to polystyrenesulfonates of various sulfonation rates. *Electrophoresis* **2000,** 21, 3529-3540.

77.Zhong, H. J.; Williams, M. A. K.; Keenan, R. D.; Goodall, D. M.; Rolin, C., Separation and quantification of pectins using capillary electrophoresis: a preliminary study. *Carbohydrate Polymers* **1997,** 32, 27-32.

78.Oudhoff, K. A.; Ab Buijtenhuijs, F. A.; Wijnen, P. H.; Schoenmakers, P. J.; Kok, W. T., Determination of the degree of substitution and its distribution of carboxymethylcelluloses by capillary zone electrophoresis. *Carbohydrate Research* **2004,** 339, 1917-1924.

79.Jiang, C. M.; Wu, M. C.; Chang, W. H.; Chang, H. M., Determination of random- and blockwise-type de-esterified pectins by capillary zone electrophoresis. *Journal of Agricultural and Food Chemistry* **2001,** 49, 5584-5588.

80.Williams, M. A. K.; Foster, T. J.; Schols, H. A., Elucidation of pectin methylester distributions by capillary electrophoresis. *Journal of Agricultural and Food Chemistry* **2003,** 51, 1777-1781.

81.Jiang, C. M.; Liu, S. C.; Wu, M. C.; Chang, W. H.; Chang, H. M., Determination of the degree of esterification of alkaline de-esterified pectins by capillary zone electrophoresis. *Food Chemistry* **2005,** 91, 551-555.

82.Guillotin, S. E.; Bakx, E. J.; Boulenguer, P.; Schols, H. A.; Voragen, A. G. J., Determination of the degree of substitution, degree of amidation and degree of blockiness of commercial pectins by using capillary electrophoresis. *Food Hydrocolloids* **2007,** 21, 444-451.

83.Ferris, C. J.; Gilmore, K. J.; Wallace, G. G.; in het Panhuis, M., Modified gellan gum hydrogels for tissue engineering applications. *Soft Matter* **2013,** 9, 3705-3711.

84.Taylor, D. L.; Ferris, C. J.; Maniego, A. R.; Castignolles, P.; in het Panhuis, M.; Gaborieau, M., Characterization of Gellan Gum by Capillary Electrophoresis. *Australian Journal of Chemistry* **2012,** 65, 1156-1164.

85.Ferris, C. J.; in het Panhuis, M., Conducting bio-materials based on gellan gum hydrogels. *Soft Matter* **2009,** 5, 3430-3437.

86.Cottet, H.; Biron, J. P.; Martin, M., Taylor Dispersion Analysis of mixtures. *Analytical Chemistry* **2007,** 79, 9066-9073.

87.Cherney, L. T.; Petrov, A. P.; Krylov, S. N., One-Dimensional Approach to Study Kinetics of Reversible Binding of Protein on Capillary Walls. *Analytical Chemistry* **2015,** 87, 1219-1225.

88.Mnatsakanyan, M.; Thevarajah, J. J.; Roi, R. S.; Lauto, A.; Gaborieau, M.; Castignolles, P., Separation of chitosan by degree of acetylation using simple free solution capillary electrophoresis. *Analytical and Bioanalytical Chemistry* **2013,** 405, 6873-6877.

89.Lefay, C.; Guillaneuf, Y.; Moreira, G.; Thevarajah, J. J.; Castignolles, P.; Ziarelli, F.; Bloch, E.; Major, M.; Charles, L.; Gaborieau, M.; Bertin, D.; Gigmes, D., Heterogeneous modification of chitosan via nitroxide-mediated polymerization. *Polymer Chemistry* **2013,** 4, 322-328.

90.Nicolas, J.; Guillaneuf, Y.; Lefay, C.; Bertin, D.; Gigmes, D.; Charleux, B., Nitroxide-mediated polymerization. *Progress in Polymer Science* **2012,** 38, 63-235.

91.Maniego, A. R.; Ang, D.; Guillaneuf, Y.; Lefay, C.; Gigmes, D.; Aldrich-Wright, J. R.; Gaborieau, M.; Castignolles, P., Separation of poly(acrylic acid) salts according to topology using capillary electrophoresis in the critical conditions. *Analytical and Bioanalytical Chemistry* **2013,** 405, 9009-9020.

92.Gigmes, D.; Bertin, D.; Lefay, C.; Guillaneuf, Y., Kinetic Modeling of Nitroxide-Mediated Polymerization: Conditions for Living and Controlled Polymerization. *Macromolecular Theory and Simulations* **2009,** 18, 402-419.

93.Ouano, A. C., Diffusion in Liquid Systems.1. Simple and Fast Method of Measuring Diffusion Constants. *Industrial & Engineering Chemistry Fundamentals* **1972,** 11, 268-271.

94.Pratt, K. C.; Wakeham, W. A., Mutual Diffusion-Coefficient of Ethanol-Water Mixtures - Determination by a Rapid, New Method. *Proceedings of the Royal Society of London Series a-Mathematical Physical and Engineering Sciences* **1974,** 336, 393-406.

95.Callendar, R.; Leaist, D. G., Diffusion coefficients for binary, ternary, and polydisperse solutions from peak-width analysis of taylor dispersion profiles. *Journal of Solution Chemistry* **2006,** 35, 353-379.

96.Cottet, H., New analytical strategies in capillary electrophoresis: application to the characterization of polymers and polypeptides. *Actualite Chimique* **2007**, 4-10.

97.Cottet, H.; Martin, M.; Papillaud, A.; Souaid, E.; Collet, H.; Commeyras, A., Determination of dendrigraft poly-L-lysine diffusion coefficients by Taylor dispersion analysis. *Biomacromolecules* **2007,** 8, 3235-3243.

98.Le Saux, T.; Cottet, H., Size-based characterization by the coupling of capillary electrophoresis to Taylor dispersion analysis. *Analytical Chemistry* **2008,** 80, 1829-1832.

99.Ibrahim, A.; Meyrueix, R.; Pouliquen, G.; Chan, Y. P.; Cottet, H., Size and charge characterization of polymeric drug delivery systems by Taylor dispersion analysis and capillary electrophoresis. *Analytical and Bioanalytical Chemistry* **2013,** 405, 5369-5379.

100.Lakowicz, J. R., *Principles of Fluorescence Spectroscopy*. Springer US: New York, 2007.

101.Claridge, T. D. W., *High-Resolution NMR Techniques in Organic Chemistry*. 2nd ed.; Elsevier: Amsterdam, 2009.

102.Spiess, H. W., Interplay of Structure and Dynamics in Macromolecular and Supramolecular Systems. *Macromolecules* **2010,** 43, 5479-5491.

103.Gaborieau, M. Solid-state NMR investigation of spatial and dynamic heterogeneity in acrylic pressure sensitive adhesives (PSAs) compared to

model poly(n-alkyl acrylates) and poly(n-alkyl methacrylates). PhD thesis, University Louis Pasteur, http://scd-theses.u-strasbg.fr/956/, Strasbourg, France, 2005.

104. Andrew, E. R., Magic Angle Spinning. In *Encyclopedia of Magnetic Resonance*, John Wiley & Sons, Ltd: 2007.

105. Bruker Very High Speed MAS. https://www.bruker.com/products/mr/nmr/probes/probes/solids/very-fast-mas/07-mm/overview.html (03/08/2016),

106. Heux, L.; Brugnerotto, J.; Desbrieres, J.; Versali, M. F.; Rinaudo, M., Solid state NMR for determination of degree of acetylation of chitin and chitosan. *Biomacromolecules* **2000,** 1, 746-751.

107. Kasaai, M. R., Determination of the degree of N-acetylation for chitin and chitosan by various NMR spectroscopy techniques: A review. *Carbohydrate Polymers* **2010,** 79, 801-810.

108. Kumirska, J.; Czerwicka, M.; Kaczyński, Z.; Bychowska, A.; Brzozowski, K.; Thöming, J.; Stepnowski, P., Application of Spectroscopic Methods for Structural Analysis of Chitin and Chitosan. *Marine Drugs* **2010,** 8, 1567-1636.

109. Prashanth, K. V. H.; Kittur, F. S.; Tharanathan, R. N., Solid state structure of chitosan prepared under different N-deacetylating conditions. *Carbohydrate Polymers* **2002,** 50, 27-33.

110. Nah, J. W.; Jang, M. K., Spectroscopic characterization and preparation of low molecular, water-soluble chitosan with free-amine group by novel method. *Journal of Polymer Science Part a-Polymer Chemistry* **2002,** 40, 3796-3803.

111. Walls, J. M., Smith, R, *Surface Science Techniques*. Elsevier Loughborough University of Technology, Leicestershire, UK, 2013.

112. Lawrie, G.; Keen, I.; Drew, B.; Chandler-Temple, A.; Rintoul, L.; Fredericks, P.; Grondahl, L., Interactions between alginate and chitosan biopolymers characterized using FTIR and XPS. *Biomacromolecules* **2007,** 8, 2533-2541.

113. Pauloehrl, T.; Welle, A.; Bruns, M.; Linkert, K.; Börner, H. G.; Bastmeyer, M.; Delaittre, G.; Barner-Kowollik, C., Spatially Controlled Surface Immobilization of Nonmodified Peptides. *Angewandte Chemie International Edition* **2013,** 52, 9714-9718.

114. Park, S. I.; Daeschel, M. A.; Zhao, Y., Functional Properties of Antimicrobial Lysozyme-Chitosan Composite Films. *Journal of Food Science* **2004,** 69, M215-M221.

115. Rhim, J. W.; Hong, S. I.; Park, H. M.; Ng, P. K. W., Preparation and characterization of chitosan-based nanocomposite films with antimicrobial activity. *Journal of Agricultural and Food Chemistry* **2006,** 54, 5814-5822.

116. Pinotti, A.; Garcia, M. A.; Martino, M. N.; Zaritzky, N. E., Study on microstructure and physical properties of composite films based on chitosan and methylcellulose. *Food Hydrocolloids* **2007,** 21, 66-72.

117. Casariego, A.; Souza, B. W. S.; Cerqueira, M. A.; Teixeira, J. A.; Cruz, L.; Diaz, R.; Vicente, A. A., Chitosan/clay films' properties as affected by biopolymer and clay micro/nanoparticles' concentrations. *Food Hydrocolloids* **2009,** 23, 1895-1902.

118. Tchemtchoua, V. T.; Atanasova, G.; Aqil, A.; Filee, P.; Garbacki, N.; Vanhooteghem, O.; Deroanne, C.; Noel, A.; Jerome, C.; Nusgens, B.; Poumay, Y.; Colige, A., Development of a Chitosan Nanofibrillar Scaffold for Skin Repair and Regeneration. *Biomacromolecules* **2011,** 12, 3194-3204.

119. Bhuvaneshwari, S.; Sruthi, D.; Sivasubramanian, V.; Kalyani, N.; Sugunabai, J., Development and characterization of chitosan films. *International Journal of Engineering Research and Applications* **2010,** 1, 292-299.

120. Praxedes, A. P. P.; da Silva, A. J. C.; da Silva, R. C.; Lima, R. P. A.; Tonholo, J.; Ribeiro, A. S.; de Oliveira, I. N., Effects of UV irradiation on the wettability of chitosan films containing dansyl derivatives. *Journal of Colloid and Interface Science* **2012,** 376, 255-261.

121. Inthanon, K.; Saranwong, N.; Wongkham, W.; Wanichapichart, P.; Prakrajang, K.; Suwannakachorn, D.; Yu, L. D., PIII-induced enhancement and inhibition of human cell attachment on chitosan membranes. *Surface & Coatings Technology* **2013,** 229, 112-119.

122. Du, X.-J.; Wang, J.-L.; Liu, W.-W.; Yang, J.-X.; Sun, C.-Y.; Sun, R.; Li, H.-J.; Shen, S.; Luo, Y.-L.; Ye, X.-D.; Zhu, Y.-H.; Yang, X.-Z.; Wang, J., Regulating the surface poly(ethylene glycol) density of polymeric nanoparticles and evaluating its role in drug delivery invivo. *Biomaterials* **2015,** 69, 1-11.

123. Casettari, L.; Vllasaliu, D.; Castagnino, E.; Stolnik, S.; Howdle, S.; Illum, L., PEGylated chitosan derivatives: Synthesis, characterizations and pharmaceutical applications. *Progress in Polymer Science* **2012,** 37, 659-685.

124. Boateng, S. Y.; Lateef, S. S.; Mosley, W.; Hartman, T. J.; Hanley, L.; Russell, B., RGD and YIGSR synthetic peptides facilitate cellular adhesion identical to that of laminin and fibronectin but alter the physiology of neonatal cardiac myocytes. *American Journal of Physiology - Cell Physiology* **2005,** 288, C30-8.

125. Thevarajah, J. J.; Bulanadi, J. C.; Wagner, M.; Gaborieau, M.; Castignolles, P., Towards a less biased dissolution of chitosan. *Analytica Chimica Acta* **2016,** 935, 258-268.

126. Thevarajah, J. J.; Sutton, A. T.; Maniego, A. R.; Whitty, E. G.; Harrisson, S.; Cottet, H.; Castignolles, P.; Gaborieau, M., Quantifying the Heterogeneity of Chemical Structures in Complex Charged Polymers through the Dispersity of Their Distributions of Electrophoretic Mobilities or of Compositions. *Analytical Chemistry* **2016,** 88, 1674-1681.

127. Thevarajah, J. J.; Van Leeuwen, M. P.; Cottet, H.; Castignolles, P.; Gaborieau, M., Determination of the Distributions of the Degrees of Acetylation of Chitosan. *International Journal of Biological Macromolecules* **2016,** 95, 40-48.

128. Thevarajah, J. J.; O'Connor, M. D.; Castignolles, P.; Gaborieau, M., Capillary electrophoresis to monitor peptide grafting onto chitosan films in real time. *Journal of Visualized Experiments* **2016,** In Press, DOI: 10.3791/54549.

129. Thevarajah, J. J.; Mason, M. E.; Bairamian, D.; Murphy, T.; Wuhrer, R.; Graf, R.; O'Connor, M. D.; Castignolles, P.; Gaborieau, M., Fabrication and Characterization of Modified Chitosan Films - Homogeniety of the surface and Biocompatability. In Preparation.

130. Evenhuis, C. J.; Guijt, R. M.; Macka, M.; Marriott, P. J.; Haddad, P. R., Temperature profiles and heat dissipation in capillary electrophoresis. *Analytical Chemistry* **2006,** 78, 2684-2693.

CHAPTER 8: Appendix

This appendix contains the published version of each publication represented in this thesis.

Hindawi Publishing Corporation
Advances in Chemistry
Volume 2014, Article ID 798503, 11 pages
http://dx.doi.org/10.1155/2014/798503

Review Article

Separation and Characterization of Synthetic Polyelectrolytes and Polysaccharides with Capillary Electrophoresis

Joel J. Thevarajah,[1,2] Marianne Gaborieau,[1,2] and Patrice Castignolles[1]

[1] *University of Western Sydney (UWS), School of Science and Health, Australian Centre for Research on Separation Sciences (ACROSS), Parramatta, NSW 2751, Australia*
[2] *University of Western Sydney (UWS), School of Science and Health, Molecular Medicine Research Group (MMRG), Parramatta, NSW 2751, Australia*

Correspondence should be addressed to Patrice Castignolles; p.castignolles@uws.edu.au

Received 30 April 2014; Revised 31 July 2014; Accepted 31 July 2014; Published 14 September 2014

Academic Editor: Alejandro Sosnik

The development of macromolecular engineering and the need for renewable and sustainable polymer sources make polymeric materials progressively more sophisticated but also increasingly complex to characterize. Size-exclusion chromatography (SEC or GPC) has a monopoly in the separation and characterization of polymers, but it faces a number of proven, though regularly ignored, limitations for the characterization of a number of complex samples such as polyelectrolytes and polysaccharides. Free solution capillary electrophoresis (CE), or capillary zone electrophoresis, allows usually more robust separations than SEC due to the absence of a stationary phase. It is, for example, not necessary to filter the samples for analysis with CE. CE is mostly limited to polymers that are charged or can be charged, but in the case of polyelectrolytes it has similarities with liquid chromatography in the critical conditions: it does not separate a charged homopolymer by molar mass. It can thus characterize the topology of a branched polymer, such as poly(acrylic acid), or the purity or composition of copolymers, either natural ones such as pectin, chitosan, and gellan gum or synthetic ones.

1. Introduction to CE and Limitations of Size-Exclusion Chromatography (SEC/GPC)

Free solution capillary electrophoresis (CE), or capillary zone electrophoresis, is a robust polymer separation method. CE differs from the commonly known slab electrophoresis or capillary gel electrophoresis as the capillary does not contain any stationary phase: it is just filled with a buffer (also named background electrolyte). CE does not require tedious sample preparation, not even filtration (e.g., see later in Section 3.2.2). It has several advantages over traditional separation techniques for the characterization of polyelectrolytes which will be outlined in this review. The most commonly used method for the separation and characterization of polymers is size-exclusion chromatography (SEC, also known as GPC). SEC is relatively quick and affordable in obtaining data regarding the size or molar mass of a polymer with good repeatability [1]. Among SEC's main limitations is its poor reproducibility in terms of molar mass analysis: round-robin tests often show poor accuracy of the values of the determined molar mass [2]. This is detailed in Berek's recent critical review [3]. The review linked the common accuracy issue to the difficulties in obtaining a pure size-exclusion separation: secondary retention mechanisms, side processes, parasitic processes, osmotic effects, secondary exclusion, concentration effects, preferential interactions, and SEC band broadening. For the ultrahigh molar masses, the sample is generally thought to be degraded by shear [4], although a change of conformation of the polymer chains may also take place, leading to a new separation mechanism [5]. In addition, even in ideal conditions (pure size-exclusion mechanism, no degradation), SEC separates by hydrodynamic volume not by molar mass [6]. Apparent molar masses determined by SEC (e.g., polystyrene-equivalent molar masses) thus have a variable and sometimes limited accuracy [7, 8]. Different topologies

(branching) or compositions of the polymer sample influence the hydrodynamic volume and the separation is then incomplete in terms of molar mass when a range of branching structures or of compositions is present in a sample [9–11]. This can render the simple determination of molar mass using Mark-Houwink-Sakurada parameters inaccurate, like in the case of most poly(alkyl acrylates) [12, 13]. Up to 100% error in the determination of the molar mass of branched polymers has been measured using multiple detection SEC (light scattering and viscometry) [14, 15].

We recently discussed the SEC of branched polymers and polysaccharides in a review [16]. Composition of copolymers, branching, and purity are often overlooked in polymer characterization, since SEC has a quasi-monopoly and is not suited for these types of characterization. However, alternative methods are being developed, especially alternative liquid chromatography methods [17]. Liquid chromatography in critical conditions (or at the critical conditions) [18] is one of the most prominent alternative chromatography technique: the critical conditions for one homopolymer correspond to the absence of separation by molar mass for this homopolymer, allowing for separation solely by its topology if branched [19] or solely by its composition if copolymerized [20]. These critical conditions are, however, tedious to establish and low recoveries have been observed [21, 22]. CE offers an alternative and the objective of this review is to present and discuss the potential of CE for synthetic polymers and polysaccharides.

CE (defined here as free solution capillary electrophoresis) involves separation in a capillary filled with only buffer (no stationary phase) under high voltage [23]. The use of only a buffer and no stationary phase prevents the common problem of adsorption onto the stationary phase (and of degradation or deformation of the ultrahigh molar mass chains) commonly faced in SEC. The velocity of different analytes is proportional to the electric field: the proportional constant is named the electrophoretic mobility, μ_{ep}. The selectivity of CE separation relates to the difference in electrophoretic mobility of the analytes (see Figure 1 for the experimental determination of μ_{ep}). The electroosmotic flow (EOF) is created by the movement of the ions of the background electrolyte through the capillary under electric field. The EOF is contributing to the migration of all molecules, even neutral ones. At a high pH the silanol groups of the glass layer of the capillary are completely ionized. This generates a strong zeta potential and an electrical double layer of silanolate groups and positive ions from the background electrolyte. The higher the pH, the higher the density of the electrical double layer which increases the EOF [23].

Successful applications of CE to polymer characterization have been the object of a number of publications, especially by Cottet's group, and the earliest works have been reviewed [24]. Building on these advances, using CE, our group was able to reliably characterize several natural and synthetic polymers, especially polysaccharides and poly(acrylic acid) as discussed in this review.

2. Free Solution Capillary Electrophoresis (CE)

Characterization of polymers by CE can be divided into at least four categories: separation of monomer units after depolymerization (see Section 2.1), separation of oligoelectrolytes (see Section 2.2), and separation of longer polyelectrolytes (see Section 3). The fourth category is the separation of polymers bearing a single charge or no charge. For the latter category, the reader is referred to the pioneering work of the groups of Cottet [25, 26] and Cifuentes [24, 27].

2.1. Average Composition of Polysaccharides

2.1.1. Robust Separation of a Mixture of Monosaccharides. A number of polysaccharides, such as hemicellulose [28, 29], have highly complex chemical structures: they are composed of several different monomer units, mainly monosaccharides. The analysis of these polysaccharides is extremely difficult. The average composition can be determined after depolymerization (hydrolysis) and quantification of the different resulting monosaccharides. Currently high performance liquid chromatography (HPLC) is used to separate carbohydrates using different modes; however, this technique and the different modes used have limitations in regard to coelution [30], tedious sample preparation, and short column life [31]. The detection of monosaccharides is another difficulty. CE is most easily and classically applied to analytes that are charged and possess chromophores. The pKa of most mono- and disaccharides is around 12 [32, 33] and separation in CE was obtained at high pH [34] but initially indirect UV detection, conductivity detection, or derivatization was required for detection. Rovio et al. showed that different hemicelluloses can be characterized not only with CE but also with direct UV detection [32, 33]. This method was applied to plant fiber samples without any derivatization: CE achieved a high-resolution separation of the depolymerized fiber samples (Figure 1) and was compared to the various common HPLC methods and IC (HPAEC) [30, 32]. The CE separation can be optimized at minimal cost by changing the capillary length, buffer counter-ion, and/or the buffer concentration [35]. The main advantage of CE is the robustness of the technique, especially the minimum sample preparation that is required. The precision of the peak identification and the quantification were greatly improved with the use of an electroosmotic flow (EOF) marker and an internal standard [30]. Figure 1 shows electropherograms when raw data (migration time) are compared to corrected data (electrophoretic mobility). Figure 1 also gives the equation used to perform this transformation. In the equation, μ_{ep} is electrophoretic mobility, V is voltage, L_d is the length to the detector, L_t is the total length of the capillary, t_m is the time of migration, and t_{eo} is the migration of a neutral species. Using electrophoretic mobility (thus correcting for EOF variations) allows easy visual comparison of results, for example, to allow identification of trace sugars in ethanol fermentation [36].

CE was able to resolve and quantify mannose, galactose, and xylose. The CE quantification of these sugars results in larger amounts when compared to the HPLC results. This might indicate incomplete recovery in HPLC possibly due

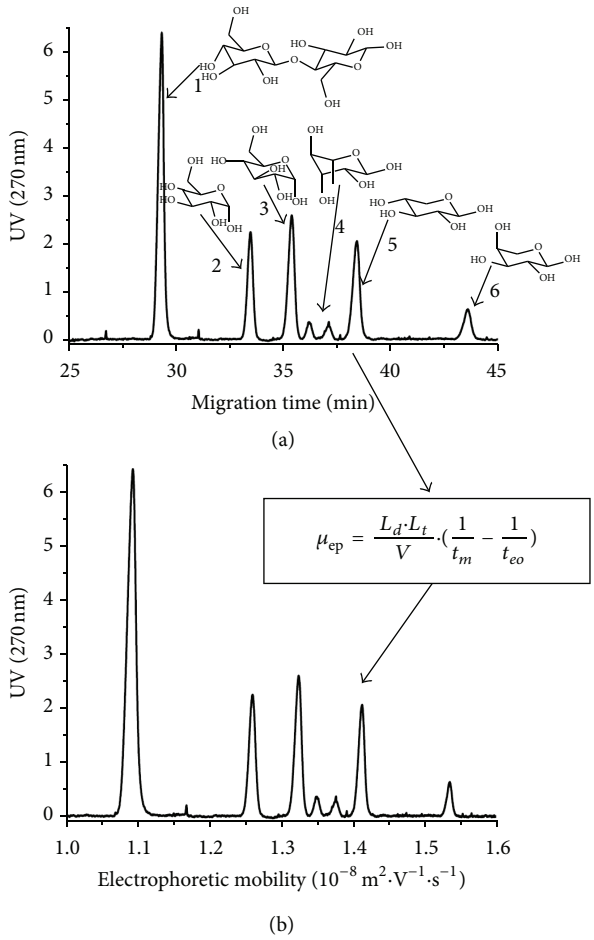

Figure 1: Separation by CE at high pH (12.6) and with direct UV detection of a depolymerized plant fiber sample plotted as a function of electrophoretic mobility (a) and of migration time (b). The sample contains (1) cellobiose, (2) galactose, (3) glucose, (4) rhamnose, (5) arabinose, and (6) xylose (the molecular structures are given for the sole purpose of identification, and they are in equilibrium with a number of linear and charged forms) [30].

to adsorption onto the stationary phase, which is a common problem associated with the HPLC of samples in complex matrices. There were weaknesses in the direct UV detection in CE which have been addressed recently (see Section 2.1.2).

2.1.2. Direct Detection due to the Photooxidation of Sugars. Rovio et al. [33] showed that the detection of monosaccharides was possible at 270 nm at pH 12.6. Sarazin et al. [43] suggested the method of detection was due to a photooxidation reaction occurring at the detection window. We confirmed that the detection is by photooxidation using a combination of simulation, multidimensional CE migration, and NMR spectroscopy analysis [30, 37]. The detection occurs without the electric field (i.e., in pressure mobilization instead of CE) but the electric field enhances the sensitivity of the detection. The photooxidation is initiated either by hydroxyl radicals formed by minimal but sufficient water decomposition or by direct decomposition of the carbohydrates under UV irradiation [35]. The diode-array detector (DAD) emits UV light down to 190 nm. These wavelengths are not leading to any known sample degradation, except for the photooxidation of carbohydrates at high pH. The photooxidation is a type of *in situ* derivatization. If one wishes to avoid the photooxidation reaction taking place, then the lowest wavelengths need to be filtered out: on commercial equipment this simply means using UV detection and not a DAD. Even by using a DAD, most of the sugar molecules are not photooxidized (in the timeframe of the detection). The UV-absorbing species are intermediates in the photooxidation process [37]. These intermediates are present at low concentration but have a high UV absorption coefficient. The final products do not absorb UV and are likely obtained after reacting with oxygen. NMR spectroscopy used as offline detection after CE migration allowed for the identification of a number of carboxylated compounds in the final products. This CE method is ideally suited for the separation of mono- and disaccharides in complex matrices. Direct detection has the advantage of simplicity and of using the most common detector in CE (diode-array detection). The detection of the CE was found to have a limit of detection 10–100x better than HPLC and a better selectivity of detection. Direct detection in CE is not as sensitive as more convoluted methods based on derivatization or pulsed-amperometric detection in ion-chromatography [36]. The method will thus need further improvement to be used for trace detection. Preliminary results showed that using a radical photoinitiator can increase the sensitivity of the direct UV detection [37].

The CE method (Figure 2) is useful not only to determine the average composition of complex polysaccharides, but also to monitor carbohydrates, for example, in a fermentation process. The latest developments showed that fermentation products such as ethanol can also be determined [35]. Ethanol is inhibiting the photooxidation process and this leads to indirect detection of ethanol in the presence of a sugar, such as sucrose. This indirect detection was successfully applied to monitoring lignocellulosic fiber fermentation in terms of both ethanol and sugars alcohols [36].

2.2. Oligoelectrolytes. Cottet and Gareil have shown that oligo(styrene sulfonate)s can be separated by their molar mass up to a degree of polymerization of 9 [44]. Oligo(sodium acrylates)—oligoAAs—are used in the paint and coating industries to stabilize emulsions [45]. Controlled polymerization methods such as reversible addition-fragmentation chain transfer (RAFT) allow the controlled synthesis of oligoAA. CE can separate oligoAAs (Figure 3) at a higher resolution than that ever obtained with SEC (for oligomers) [38] even using optimal SEC conditions [46, 47].

CE was able to separate and quantify the residual RAFT agent used to obtain the oligoAAs as well as the species of degrees of polymerization (DP) of one, two, and three. The identification of these peaks was obtained by the online coupling of CE with ESI-MS-TOF (electrospray ionization-mass spectrometry-time of flight) [48]. MS analysis showed that the oligomers are separated not only according to their

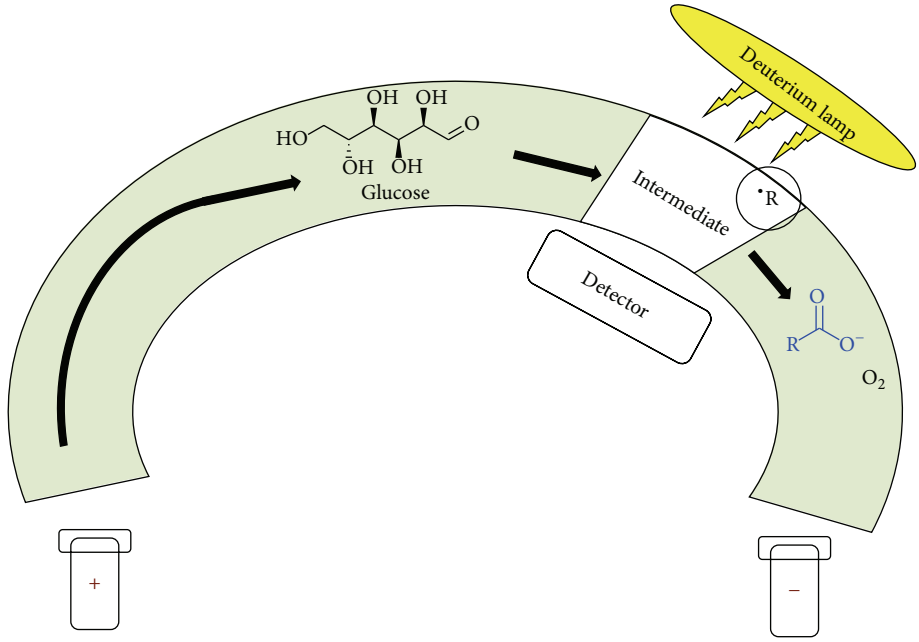

Figure 2: Mechanism of direct UV detection in CE of carbohydrates owing to a photooxidation reaction [37].

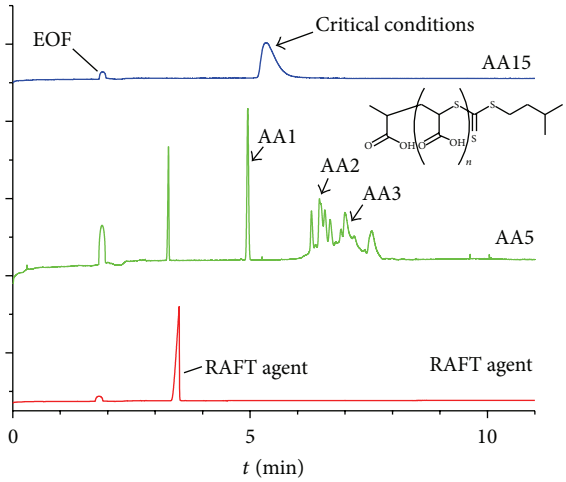

Figure 3: Electropherograms in lithium borate for two different oligoAAs, AA5 and AA15, produced by RAFT polymerization, where 5 and 15 correspond to the degree of polymerization obtained at the maximum of the mass spectrum from ESI-MS-TOF (electrospray ionization-mass spectrometry-time of flight) direct infusion (adapted from [38]). AA15 is not separated by molar mass; it is thus in the critical conditions. The bottom electropherogram is of the RAFT agent, that is, the control agent for the polymerization.

degree of polymerization and end-group, but also according to their tacticity. The shortest oligoAAs were shown to contain 50% of unreacted RAFT agent, while the direct infusion in ESI-MS estimated that the sample contained only 2% of unreacted RAFT agent. This large discrepancy is due to the known issue of the bias of the ionization towards low degrees of polymerization and hydrophilic species in MS analysis [49]. CE was shown to be a relevant and fast method in the study of kinetics of polymerization of RAFT. It has also been used to shed light on the kinetics and mechanism of ring opening polymerization of either 2-oxazoline [50] or *N*-carboxyanhydrides [26].

Most importantly, the high-resolution separation of CE by molar mass is limited to oligoelectrolytes, with degrees of polymerization below about 10. For large polyelectrolytes, no separation by molar mass is obtained, which corresponds to the "critical conditions" described below.

3. CE in the Critical Conditions

3.1. Explanation of "Critical Conditions". The first example of analysis of synthetic polyelectrolytes by electrophoresis dealt with poly(4-vinyl-*N*-*n*-butylpyridinium bromide) more than half a century ago [51]. The authors concluded that "the electrophoretic behavior of polyvinylbutylpyridinium is not very sensitive to molecular weight." CE in the "critical conditions" differs from the CE undertaken in the separation and characterization of oligoelectrolytes such as oligoAA. Critical conditions refer to the conditions sought in liquid chromatography (LC) in which a homopolymer is not separated by molar mass (see Section 1). While these critical conditions are of no use to characterize simple (homo)polymers, most, if not all, polymers are not simple in the sense that they possess a distribution of molar masses as well as different end-groups, distribution(s) of compositions for copolymers, distribution of branch molar masses and of positions of branching points for branched polymers, and so forth. Polymeric samples are multidimensional: the critical conditions allow separation by one (or only a few) dimension at one time (since the distribution of molar masses does not influence the separation any more). The critical conditions thus enable the characterization of complex polymers through the

simplification of a multidimensional problem. While a lot of research has been devoted to LC and critical conditions, the method remains tedious and plagued with low accuracy and recovery [21]. Applications to hydrophilic and/or charged polymers are very limited. CE is an alternative to LC in this specific, but important, case of complex polyelectrolytes. The molecular reasons behind critical conditions in LC and CE are completely different and are not widely accepted in any case. The electrophoretic mobility always depends on the charge to friction ratio. It does not depend on the ratio of the charge to the size in the case of polyelectrolytes, since the friction is not only hydrodynamic in this case. The critical conditions do not correspond to the free draining model as proposed by Flory, in which the solvent penetrates the polymer chains freely [52]. Electrostatic friction, however, screens the hydrodynamic friction [53, 54] and leads to the electrophoretic mobility having a very weak dependence on molar mass for a degree of polymerization generally above 15–20 [44, 55, 56]. Thus, CE leads to migration independent from molar mass for polyelectrolytes and this corresponds to the critical conditions sought in LC-CC. CE has been used in the critical conditions outside of our group in the separation of pectins [57] and carboxymethylcellulose [58] according to their composition. In our group using CE in the critical conditions (CE-CC) has allowed the investigation of the composition of natural polymers as well as of synthetic polymers. Further, we have also been able to look at the degree of branching of synthetic polymers.

3.2. Separation by Composition

3.2.1. Pectin and Carboxymethylcellulose (CMC). CE-CC effectively separates the polysaccharide pectin by composition. Several studies reported the separation of pectin by its degree of substitution (DS, which may include either esterification or methyl-esterification) [57, 59–62]. Within one sample, pectins macromolecules with different degrees of esterification (DE) could be separated. It was later hypothesized that the shape of the peaks could additionally be used to indicate a distribution of methyl esters of pectin within samples [60]. Guillotin et al. [62] established a protocol in which pectin's degree of amidification, degree of methyl-esterification, and subsequently the degree of substitution could be determined.

Other research involved the use of capillary electrophoresis to determine the DS of carboxymethylcellulose [58]. The study showed the possibility of not only determining the average DS but also determining the heterogeneity/distribution of the compositions of CMC.

3.2.2. Gellan Gum. Gellan gum is a natural polymer which is widely distributed in the environment. Due to its rheological properties it is viewed as a possible stabilizing agent in various industries [63]. Gellan gum's monomer unit structure contains D-glucuronic acid, D-glucose either with or without acyl substituents, and L-rhamnose. The proportion of acyl chains attached to the glucose and the distribution of these

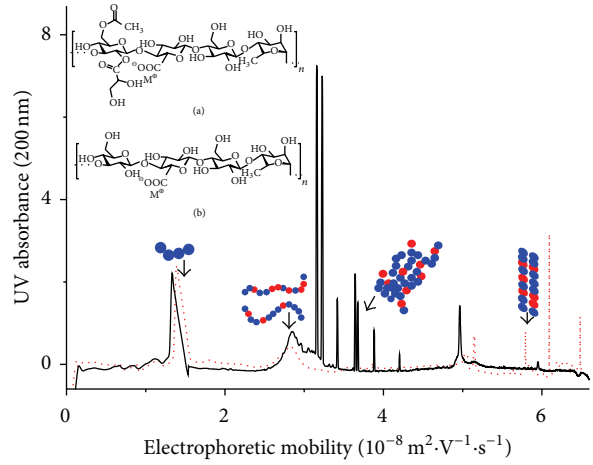

FIGURE 4: Electropherograms of a low acyl gellan gum (dotted red line) and a high-acyl gellan gum (solid black line) (in potassium borate, pH 9.2), after a few hours of dissolution [39].

acyl chains along the polysaccharide vary from sample to sample. Gellan gum is often characterized by its degree of acylation, which affects its desired properties. CE allowed some separation of gellan gum oligomers according to their degree of polymerization and separation of polymers by their degree of acylation (composition) [39]. CE gave a unique separation of gellan gums that could not be attained with any other existing separation methods. CE could characterize not only a low acyl gellan gum but also a high acyl gellan gum (Figure 4). The latter sample was a turbid dispersion: while obtaining a true solution was not possible, the characterization of this dispersion is relevant for its applications such as the stabilization of carbon nanotubes [64]. Characterization of the high acyl gellan gum showed the presence of aggregates forming during the dissolution of the gellan gum samples and appearing as very narrow peaks due to their very low diffusion coefficients. This illustrates the robustness of the method as it did not require sample filtration (while the background electrolyte still requires filtration). Filtration would have changed the nature of this colloidal sample and should thus not be performed for a meaningful characterization. Complementing the CE separation with a simple pressure mobilization analysis (a qualitative version of Taylor dispersion analysis [65]; see 3.4), the presence of oligomers of gellan gum was confirmed while they had never been identified previously in these gellan gums. Through the CE separation, the oligomers could be separated and quantified. Separation and characterization of this dispersion could only be obtained by CE or field flow fractionation (FFF). In the most common form of FFF, flow FFF, the oligomers would have been lost through the membrane. The low acyl samples contained more oligomers than the high acyl samples suggesting the occurrence of some degradation during the deacylation process. The electrophoretic mobility is also sensitive to the conformation of gellan gum and complementary to light scattering characterization. A high mobility peak, present in the high acyl sample and becoming more intense in the presence of potassium borate ions, suggests the possibility

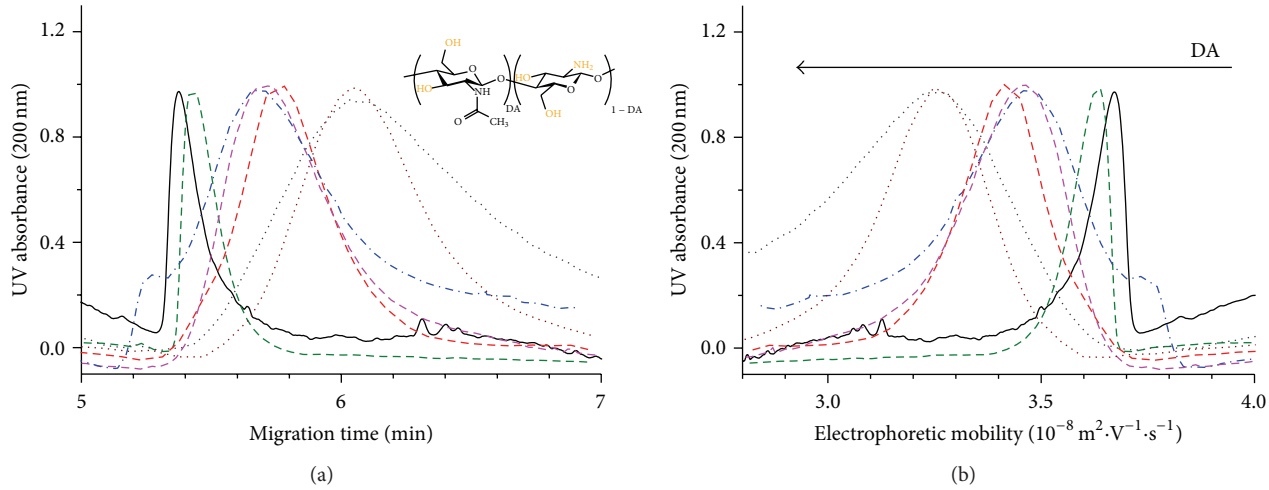

Figure 5: Separation of chitosan samples by their DA with CE (sodium phosphate, pH 3): electropherogram shown as a function of (a) migration time and (b) apparent electrophoretic mobility. Samples with different degrees of acetylation (weight-average DA determined by NMR spectroscopy) are shown: black solid line (4%), green dashed line (4.3%), blue dashed-dotted line (16.5%), red dashed line (18.7%), pink dashed line (19.8%), brown dotted line (22.4%), and black dotted line (23.6%) [40].

of a double-helix conformation. This peak differs in mobility and, thus, also suggests that the rest of the macromolecules are in a random coil conformation.

In order of increasing mobility, the electropherograms show the presence of gellan gum oligomers, then gellan gum polymer chains containing different degrees of acylation (random coil conformation), then aggregates of gellan gum chains, and finally gellan gum polymer chains in a helix conformation. The gellan gums studied in this work are copolymers containing both repeating units (not necessarily forming blocks). The top molecular structure represents fully acetylated gellan gum and the bottom one represents fully deacylated gellan gum. The monomer unit is constituted from left to right of one D-glucose with two acyl substituents (one acetyl and one glycerate bearing a diol or glycol), one D-glucuronic acid, one D-glucose without substituents, and one L-rhamnose.

The study undertaken on gellan gum is an example of the robustness of the CE technique. Whilst allowing the successful separation of complex samples by composition, it also provides information on the conformation of the polymer chains and the presence of aggregates.

3.2.3. Chitosan. Chitosan is a polysaccharide produced from the *N*-deacetylation of chitin. Chitin is the main component of the shells of crabs and shrimps and can also be found in the cell wall of fungi. It is a renewable resource that it is a large waste product. Chitosan's structure contains *N*-acetyl-D-glucosamine as well as D-glucosamine units. The composition of this copolymer is quantified by the degree of acetylation (DA), which is the fraction of *N*-acetyl-D-glucosamine. Chitosan is receiving extensive research interest due to its inherent properties. It is biocompatible, antimicrobial, antifungal, biodegradable, and pH-responsive [66, 67]. However, one limitation of chitosan is in the incomplete characterization by current methods; while being a natural product, there is a large variation among samples. Chitosan is often characterized by its average degree of acetylation (DA) [40]. Chitosan samples are, however, not composed of polymer chains with all the same DA, but they contain a distribution of DAs. The complexity and importance of the distribution of DAs have been revealed recently through a coupling of SEC with ^{1}H NMR spectroscopy [68]; however, it still has not been measured. ^{1}H NMR spectroscopy can determine number-average as well as weight-average DAs [40]. The measurements are accurate, but precise results are time-consuming and alternative methods are often considered. Chitosan is often characterized by only one of its average DAs, which is implicitly and incorrectly assuming the sample is homogeneous in terms of DA, that is, does not have a distribution of DAs.

CE-CC separates chitosan by its degree of acetylation (Figure 5) [40]. Chitosan macromolecules with a lower DA have a higher mobility (at low pH below the glucosamine monomer unit pKa) since they have a higher number of free amino groups which increase their charge and therefore their electrophoretic mobility. Another important attribute revealed in the CE separation is the broadness and shape of the peaks of the chitosan samples. The broadness corresponds to the distribution of DAs and some samples have broader distributions than others (Figure 5). These differences in distributions will likely affect functional properties such as adhesion, biodegradability, and bacteriostaticity [68]. With proper calibration, the CE separation will allow the determination of the distribution of DAs. The distribution can be calculated from the UV signal taking into account the nonlinear relation between electrophoretic mobility and migration, as it is done to calculate molar mass distributions in SEC [10].

We have also used CE to assist in the grafting of synthetic polymers, poly(sodium styrene sulfonate) and poly(methyl methacrylate-*co*-acrylonitrile), onto a chitosan backbone [41]

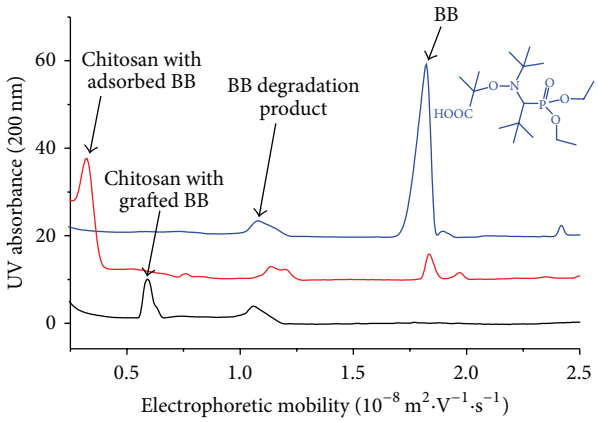

FIGURE 6: CE of pure BlocBuilder (BB, blue line), chitosan with adsorbed BB (red line), and chitosan with grafted BB (red line) in sodium borate buffer (pH 9.2) [41].

to address the variability of the mechanical properties of chitosan films [69]. CE could analyze samples produced along the synthetic pathway. This allowed the validation of the grafting process. Chitosan was first functionalized with the introduction of an acrylamide and/or acrylate function. This was followed by a radical addition of BlocBuilder (BB) alkoxyamine to allow a controlled (nitroxide-mediated) polymerization [70] of the grafted monomers. The limited solubility of chitosan, added to the hydrophobicity of the grafted compound, made the complete solubilization of the samples impossible. Despite incomplete dissolution, the robustness of CE allowed us to analyze these samples: chitosan functionalized with BlocBuilder was separated from pure BlocBuilder (Figure 6). This experiment was undertaken in a high pH buffer and therefore the negative charge expressed by BB results in a nonzero mobility in the CE electropherogram whilst the neutral chitosan has no mobility. Pure BB, chitosan covalently functionalized with BB, and chitosan physically mixed with BB (control) were then injected at the same pH. The chitosan grafted with BB encounters more hydrodynamic friction than BB alone which reduces the electrophoretic mobility of the chitosan grafted with BB in comparison to the pure BB. The method even allowed the discrimination of covalently grafted BB from BB adsorbed to chitosan since the latter has a lower electrophoretic mobility in comparison to the grafted sample. This type of separation, neutral polymer chain from slightly modified polymer chain, was also used by the group of Schoenmakers with nonaqueous CE to prove the presence of charged end-groups in part of their poly(2-oxazoline) samples [50].

Using both CE and CE-CC a more thorough analysis can be completed on both pure and modified chitosan samples. There is also a possibility of extending the research on chitosan with CE in terms of the determination of the distribution of the degrees of acetylation which has not been previously examined [40].

3.3. Separation by Topology (Branching). There is a large interest in the characterization of water-soluble polyacrylates as their use has increased to include a range of applications from industrial protective coatings to food packaging. The poly(sodium acrylate)s, PNaA, studied by our group were produced by nitroxide-mediated polymerisation (NMP) [70]. The aim of the study was to characterize the branching in PAA using CE-CC. Different topologies of the PAA samples, linear, hyperbranched, and three-arm star, were separated within 15 min [42]. Figure 7 presents the CE results both as raw data, as a function of migration time and as EOF corrected data, as a function of electrophoretic mobility. This highlights the importance of converting the results to electrophoretic mobility plots as a trend is not seen in the migration time results due to the variation in EOF between injections. When the EOF correction is made, it can be seen that the hyperbranched polymer exhibits the lowest electrophoretic mobility followed by three-arm star and finally the linear ones. The differences in electrophoretic mobility can be explained by a decrease in the effective charge of the branched samples when compared to the linear samples. The results obtained were highly repeatable and reproducible with relative standard deviations (RSD) values below 1.6%. The separations were also successfully reproduced in a different buffer and whilst they produced different electrophoretic mobility values (as expected, due to the different counterions), the electrophoretic mobility remained lower for the more branched structures. This study highlights also the accuracy (related to the reproducibility of the separation) of the technique.

The CE results obtained also provided information regarding the homogeneity of the branching topology. These samples are expected to have a controlled molar mass owing to the reversible termination with the nitroxide but the broadness of the peaks obtained suggests some heterogeneity in the branching structure. The broad range of electrophoretic mobilities is attributed to a broad range of branching topologies produced in the polymerization.

The CE-CC separation was also shown to be influenced by end-groups. In Figure 8 the red solid line represents PAA with a SG1 [N-tert-butyl-N-(1-diethylphosphono-2,2-dimethylpropyl) nitroxide] moiety as the end-group. There is a marked difference between this sample and the sample with the PAA that has been heated in the presence of thiophenol to replace the SG1 end-groups with hydrogen. The electrophoretic mobility increases with the removal of the SG1 end-group, as expected, since the bulky SG1 molecule would contribute to the hydrodynamic friction of the PAA chains more than hydrogen (and neither contributes to its charge). The result also suggests heterogeneity of the sample in terms of branching. The thiophenol treatment was also applied to a PAA sample obtained from the hydrolysis of poly(*t*-butyl acrylate) and CE-CC showed that the hydrolysis of poly(*t*-butyl acrylate) did not just cleave the targeted *t*-butyl groups, but also likely lead to some degradation of the SG1 end-group. This led to a greater heterogeneity of the sample and is expressed in the broadness of the peak.

Through CE-CC, we were able to separate polymers by their topology (branching) as well as by their end-groups. The ability of CE-CC to separate based on the presence of SG1 (control agent used for nitroxide-mediated polymerization)

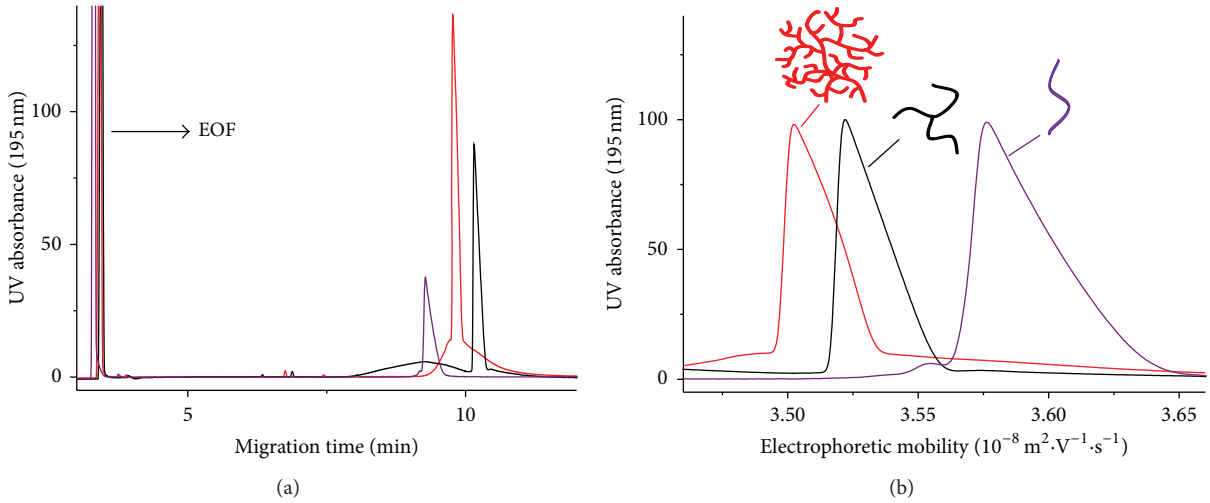

FIGURE 7: Separation of linear (purple line), three-arm star (black line), and hyperbranched (red line) poly(sodium acrylate) by capillary electrophoresis in sodium borate buffer (pH 9.2) shown as a function of (a) migration time and (b) electrophoretic mobility, which is a more reproducible quantity than the former [42].

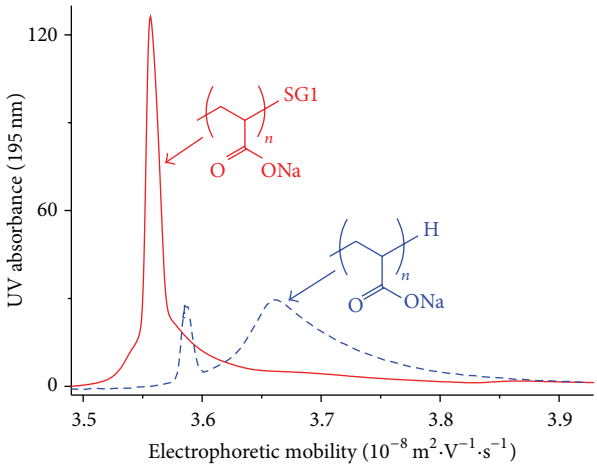

FIGURE 8: Electrophoretic mobility distributions of a PNaA obtained by nitroxide-mediated polymerization of acrylic acid initiated by the monofunctional initiator Monams (red solid line) followed by cleavage of the SG1 end-group by treatment with thiophenol (blue dashed line) in sodium borate (pH 9.2) [42].

reveals information regarding the "livingness" of the obtained sample (allowing continuing reacting through NMP) [42, 71]. This allows the optimization of the method used to produce the sample and provides information regarding further functionalization of the PAA.

3.4. Size Determination with TDA. One limitation of CE for polymer characterization, compared to multiple detection SEC [16], is the limited number of detectors, especially the lack of molar mass sensitive detectors. The group of Cottet is, however, bridging this gap rapidly by demonstrating that the CE separation can be coupled to Taylor dispersion analysis (TDA). TDA is a method that does not involve separation but allows the determination of the diffusion coefficient/hydrodynamic radius of a sample. TDA has been looked at previously to obtain diffusion coefficients in liquid systems [72, 73]. Further it has proven to be practical in the size characterization of macromolecules and particles of virtually any molar mass [65, 74]. TDA has several advantages including that it is an absolute method, meaning that no calibration is required. The group of Cottet has shown that a CE instrument is particularly well suited to carry out TDA [65, 75]. Le Saux and Cottet [76] coupled CE and TDA. A copolymer mixture of 2-acrylamido-2-methylpropanesulfonate/acrylamide and DNA was injected into a fused silica capillary. The mixture was separated in CE conditions (with an electric field) and then pressure was used to push the samples to the detection window where the analysis took place. The experiment proved that the coupling of CE and TDA allowed not only a complete separation of the copolymer from the DNA in the mixture, but also the successful determination of the diffusion coefficient of both the copolymer and the DNA. A successful coupling of CE with TDA allowed a combination of a high performance and throughput method with an absolute method for the calculation of diffusion coefficients [77]. The diffusion coefficient can then be related to the hydrodynamic volume of the macromolecule as it is classically done in light scattering by the following equation:

$$D = kT6\pi\eta r, \quad (1)$$

where k is the Boltzmann constant, T is the temperature, η is the viscosity of the solvent, and r is the hydrodynamic radius of the macromolecule [78].

The relation of the hydrodynamic radius to the molar mass is complex and is influenced by branching and copolymer composition as discussed in Section 1 for SEC [16].

4. Conclusions and Future Directions

Characterization by capillary electrophoresis involves both separation and characterization of complex polymers. This review outlined the broad range of samples that can be analyzed with CE. The characterization of complex polymers is significant for various industries including food, biomedical, energy/fuel, and materials (such as paint and bioplastics) industries. The robustness of the method, especially the minimal sample preparation, is one of the main strengths of the method (shared with field flow fractionation). The continual development of the methods in CE and their coupling with other techniques such as TDA widens the scope and depth of the possible characterization and meets the ever-growing needs of progressively increasing complex macromolecular structures for increasingly advanced applications. CE in the critical conditions (CE-CC) has the most potential and can be applied to a wide variety of charged polymers to characterize their topology, composition, or end-groups. The method is complementary to SEC.

Future directions will look into further characterizing complex polyelectrolytes, for example, in terms of determination of the molar mass distribution of one block in block copolymers, or in terms of sugars quantification in food samples. The different distributions related to branching will also be studied. CE coupled with TDA is a very useful and simple technique that will definitely be examined further as it is able to provide extremely valuable information regarding the size and shape of sample molecules by the calculation of their diffusion coefficient. Its simplicity and being an absolute method mean that it can be applied to a variety of samples investigated by our research group and other polymer research groups.

Conflict of Interests

The authors declare that there is no conflict of interests regarding the publication of this paper.

Acknowledgments

Patrice Castignolles and Marianne Gaborieau would like to thank Professor Herve Cottet (University of Montpellier II) and Professor Emily Hilder (ACROSS, University of Tasmania) for discussions over the last 10 years. The authors thank Alison Maniego, Adam Sutton, James Oliver, Danielle Taylor, and their entire macromolecular characterization team.

References

[1] A. M. Striegel, J. J. Kirkland, W. W. Yau, and D. D. Bly, *Modern Size Exclusion Chromatography*, John Wiley & Sons, Hoboken, NJ, USA, 2009.

[2] R. J. Bruessau, "Experiences with interlaboratory GPC experiments," *Macromolecular Symposia*, vol. 110, pp. 15–32, 1996.

[3] D. Berek, "Size exclusion chromatography—a blessing and a curse of science and technology of synthetic polymers," *Journal of Separation Science*, vol. 33, no. 3, pp. 315–335, 2010.

[4] H. G. Barth and F. J. Carlin Jr., "A review of polymer shear degradation in size-exclusion chromatography," *Journal of Liquid Chromatography*, vol. 7, no. 9, pp. 1717–1738, 1984.

[5] E. Uliyanchenko, S. van der Wal, and P. J. Schoenmakers, "Deformation and degradation of polymers in ultra-high-pressure liquid chromatography," *Journal of Chromatography A*, vol. 1218, no. 39, pp. 6930–6942, 2011.

[6] L. K. Kostanski, D. M. Keller, and A. E. Hamielec, "Size-exclusion chromatography—A review of calibration methodologies," *Journal of Biochemical and Biophysical Methods*, vol. 58, no. 2, pp. 159–186, 2004.

[7] M. Netopilík and P. Kratochvíl, "Polystyrene-equivalent molecular weight versus true molecular weight in size-exclusion chromatography," *Polymer*, vol. 44, no. 12, pp. 3431–3436, 2003.

[8] Y. Guillaneuf and P. Castignolles, "Using apparent molecular weight from SEC in controlled/living polymerization and kinetics of polymerization," *Journal of Polymer Science A: Polymer Chemistry*, vol. 46, no. 3, pp. 897–911, 2008.

[9] A. E. Hamielec and A. C. Ouano, "Generalized universal molecular-weight calibration parameter in GPC," *Journal of Liquid Chromatography*, vol. 1, pp. 111–120, 1978.

[10] M. Gaborieau, R. G. Gilbert, A. Gray-Weale, J. M. Hernandez, and P. Castignolles, "Theory of multiple-detection size-exclusion chromatography of complex branched polymers," *Macromolecular Theory and Simulations*, vol. 16, no. 1, pp. 13–28, 2007.

[11] M. Gaborieau, J. Nicolas, M. Save et al., "Separation of complex branched polymers by size-exclusion chromatography probed with multiple detection," *Journal of Chromatography A*, vol. 1190, no. 1-2, pp. 215–223, 2008.

[12] L. Couvreur, G. Piteau, P. Castignolles et al., "Pulsed-laser radical polymerization and propagation kinetic parameters of some alkyl acrylates," *Macromolecular Symposia*, vol. 174, pp. 197–207, 2001.

[13] P. Castignolles, R. Graf, M. Parkinson, M. Wilhelm, and M. Gaborieau, "Detection and quantification of branching in polyacrylates by size-exclusion chromatography (SEC) and melt-state 13C NMR spectroscopy," *Polymer*, vol. 50, no. 11, pp. 2373–2383, 2009.

[14] T. Junkers, M. Schneider-Baumann, S. S. P. Koo, P. Castignolles, and C. Barner-Kowollik, "Determination of propagation rate coefficients for methyl and 2-ethylhexyl acrylate via high frequency PLP-SEC under consideration of the impact of chain branching," *Macromolecules*, vol. 43, no. 24, pp. 10427–10434, 2010.

[15] P. Castignolles, "Transfer to polymer and long-chain branching in PLP-SEC of acrylates," *Macromolecular Rapid Communications*, vol. 30, no. 23, pp. 1995–2001, 2009.

[16] M. Gaborieau and P. Castignolles, "Size-exclusion chromatography (SEC) of branched polymers and polysaccharides," *Analytical and Bioanalytical Chemistry*, vol. 399, no. 4, pp. 1413–1423, 2011.

[17] E. Uliyanchenko, P. J. C. H. Cools, S. van der Wal, and P. J. Schoenmakers, "Comprehensive two-dimensional ultrahigh-pressure liquid chromatography for separations of polymers," *Analytical Chemistry*, vol. 84, no. 18, pp. 7802–7809, 2012.

[18] M. Rollet, D. Glé, T. N. T. Phan, Y. Guillaneuf, D. Bertin, and D. Gigmes, "Characterization of functional poly(ethylene oxide)s and their corresponding polystyrene block copolymers by liquid chromatography under critical conditions in organic solvents," *Macromolecules*, vol. 45, no. 17, pp. 7171–7178, 2012.

[19] M. Al Samman, W. Radke, A. Khalyavina, and A. Lederer, "Retention behavior of linear, branched, and hyperbranched

polyesters in interaction liquid chromatography," *Macromolecules*, vol. 43, no. 7, pp. 3215–3220, 2010.

[20] W. Lee, D. Cho, T. Chang, K. J. Hanley, and T. P. Lodge, "Characterization of polystyrene-b-polyisoprene diblock copolymers by liquid chromatography at the chromatographic critical condition," *Macromolecules*, vol. 34, no. 7, pp. 2353–2358, 2001.

[21] A. Favier, C. Petit, E. Beaudoin, and D. Bertin, "Liquid chromatography at the critical adsorption point (LC-CAP) of high molecular weight polystyrene: pushing back the limits of reduced sample recovery," *E-Polymers*, pp. 1–15, 2009.

[22] E. Beaudoin, A. Favier, C. Galindo et al., "Reduced sample recovery in liquid chromatography at critical adsorption point of high molar mass polystyrene," *European Polymer Journal*, vol. 44, no. 2, pp. 514–522, 2008.

[23] R. Weinberger, *Practical Capillary Electrophoresis*, CA Academic Press, San Diego, Calif, USA, 2000.

[24] H. Cottet and P. Gareil, "Separation of synthetic (co)polymers by capillary electrophoresis techniques.," *Methods in Molecular Biology*, vol. 384, pp. 541–567, 2008.

[25] H. Miramon, F. Cavelier, J. Martinez, and H. Cottett, "Highly resolutive separations of hardly soluble synthetic polypeptides by capillary electrophoresis," *Analytical Chemistry*, vol. 82, no. 1, pp. 394–399, 2010.

[26] W. Vayaboury, O. Giani, H. Cottet, S. Bonaric, and F. Schué, "Mechanistic Study Of α-amino acid N-carboxyanhydride (NCA) polymerization by capillary electrophoresis," *Macromolecular Chemistry and Physics*, vol. 209, no. 15, pp. 1628–1637, 2008.

[27] M. R. Aguilar, A. Gallardo, J. San Román, and A. Cifuentes, "Micellar electrokinetic chromatography: a powerful analytical tool to study copolymerization reactions involving ionic species," *Macromolecules*, vol. 35, no. 22, pp. 8315–8322, 2002.

[28] I. Spiridon and V. I. Popa, "Hemicelluloses: major sources, properties and applications," in *Monomers, Polymers and Composites from Renewable Resources*, M. N. Belgacem and A. Gandini, Eds., chapter 13, Elsevier, Amsterdam, The Netherlands, 2008.

[29] S. Brudin and P. Schoenmakers, "Analytical methodology for sulfonated lignins," *Journal of Separation Science*, vol. 33, no. 3, pp. 439–452, 2010.

[30] J. D. Oliver, M. Gaborieau, E. F. Hilder, and P. Castignolles, "Simple and robust determination of monosaccharides in plant fibers in complex mixtures by capillary electrophoresis and high performance liquid chromatography," *Journal of Chromatography A*, vol. 1291, pp. 179–186, 2013.

[31] M. Verzele, G. Simoens, and F. van Damme, "A critical review of some liquid chromatography systems for the separation of sugars," *Chromatographia*, vol. 23, no. 4, pp. 292–300, 1987.

[32] S. Rovio, H. Simolin, K. Koljonen, and H. Sirén, "Determination of monosaccharide composition in plant fiber materials by capillary zone electrophoresis," *Journal of Chromatography A*, vol. 1185, no. 1, pp. 139–144, 2008.

[33] S. Rovio, J. Yli-Kauhaluoma, and H. Sirén, "Determination of neutral carbohydrates by CZE with direct UV detection," *Electrophoresis*, vol. 28, no. 17, pp. 3129–3135, 2007.

[34] A. E. Vorndran, P. J. Oefner, H. Scherz, and G. K. Bonn, "Indirect UV detection of carbohydrates in capillary zone electrophoresis," *Chromatographia*, vol. 33, no. 3-4, pp. 163–168, 1992.

[35] J. D. Oliver, M. Gaborieau, and P. Castignolles, "Ethanol determination using pressure mobilization and free solution capillary electrophoresis by photo-oxidation assisted UV detection," *Journal of Chromatography A*, vol. 1348, pp. 150–157, 2014.

[36] J. D. Oliver, A. T. Sutton, N. Karu et al., "Simple and robust monitoring of ethanol fermentations by capillary electrophoresis," *Biotechnology and Applied Biochemistry*, 2014.

[37] J. D. Oliver, A. A. Rosser, C. M. Fellows et al., "Understanding and improving direct UV detection of monosaccharides and disaccharides in free solution capillary electrophoresis," *Analytica Chimica Acta*, vol. 809, pp. 183–193, 2014.

[38] P. Castignolles, M. Gaborieau, E. F. Hilder, E. Sprang, C. J. Ferguson, and R. G. Gilbert, "High-resolution separation of oligo(acrylic acid) by capillary zone electrophoresis," *Macromolecular Rapid Communications*, vol. 27, no. 1, pp. 42–46, 2006.

[39] D. L. Taylor, C. J. Ferris, A. R. Maniego, P. Castignolles, M. In Het Panhuis, and M. Gaborieau, "Characterization of gellan gum by capillary electrophoresis," *Australian Journal of Chemistry*, vol. 65, no. 8, pp. 1156–1164, 2012.

[40] M. Mnatsakanyan, J. J. Thevarajah, R. S. Roi, A. Lauto, M. Gaborieau, and P. Castignolles, "Separation of chitosan by degree of acetylation using simple free solution capillary electrophoresis," *Analytical and Bioanalytical Chemistry*, vol. 405, no. 21, pp. 6873–6877, 2013.

[41] C. Lefay, Y. Guillaneuf, G. Moreira et al., "Heterogeneous modification of chitosan via nitroxide-mediated polymerization," *Polymer Chemistry*, vol. 4, no. 2, pp. 322–328, 2013.

[42] A. R. Maniego, D. Ang, Y. Guillaneuf et al., "Separation of poly(acrylic acid) salts according to topology using capillary electrophoresis in the critical conditions," *Analytical and Bioanalytical Chemistry*, vol. 405, no. 28, pp. 9009–9020, 2013.

[43] C. Sarazin, N. Delaunay, C. Costanza, V. Eudes, J. Mallet, and P. Gareil, "New avenue for mid-UV-range detection of underivatized carbohydrates and amino acids in capillary electrophoresis," *Analytical Chemistry*, vol. 83, no. 19, pp. 7381–7387, 2011.

[44] H. Cottet and P. Gareil, "From small charged molecules to oligomers: a semiempirical approach to the modeling of actual mobility in free solution," *Electrophoresis*, vol. 21, pp. 1493–1504, 2000.

[45] M. Siauw, B. S. Hawkett, and S. Perrier, "Short chain amphiphilic diblock co-oligomers via RAFT polymerization," *Journal of Polymer Science A: Polymer Chemistry*, vol. 50, no. 1, pp. 187–198, 2012.

[46] C. J. Ferguson, R. J. Hughes, D. Nguyen et al., "Ab initio emulsion polymerization by RAFT-controlled self-assembly," *Macromolecules*, vol. 38, no. 6, pp. 2191–2204, 2005.

[47] I. Lacík, M. Stach, P. Kasak et al., "SEC analysis of poly(acrylic acid) and poly(methacrylic acid)," *Macromolecular Chemistry and Physics*, 2014.

[48] M. Gaborieau, T. J. Causon, Y. Guillaneuf, E. F. Hilder, and P. Castignolles, "Molecular weight and tacticity of oligoacrylates by capillary electrophoresis-mass spectrometry," *Australian Journal of Chemistry*, vol. 63, no. 8, pp. 1219–1226, 2010.

[49] C. M. Guttman, K. M. Flynn, W. E. Wallace, and A. J. Kearsley, "Quantitative mass spectrometry and polydisperse materials: creation of an absolute molecular mass distribution polymer standard," *Macromolecules*, vol. 42, no. 5, pp. 1695–1702, 2009.

[50] A. Chojnacka, K. Kempe, H. C. van de Ven et al., "Molar mass, chemical-composition, and functionality-type distributions of poly(2-oxazoline)s revealed by a variety of separation techniques," *Journal of Chromatography A*, vol. 1265, pp. 123–132, 2012.

[51] E. B. Fitzgerald and R. M. Fuoss, "Polyelectrolytes .11. electrophoresis in solutions of poly-4-vinyl-N-N-butylpyridinium bromide," *Journal of Polymer Science*, vol. 14, pp. 329–339, 1954.

[52] P. J. Flory, "Configurational and frictional properties of the polymer molecule in dilute solution," in *Principles of Polymer Chemistry*, Cornell University Press, Ithaca, NY, USA, 1st edition, 1953.

[53] M. Muthukumar, "Theory of electrophoretic mobility of a polyelectrolyte in semidilute solutions of neutral polymers," *Electrophoresis*, vol. 17, no. 6, pp. 1167–1172, 1996.

[54] J. L. Barrat and J. F. Joanny, "Theory of polyelectrolyte solutions," in *Advances in Chemical Physics, Vol Xciv*, John Wiley & Sons, New York, NY, USA, 1996.

[55] N. C. Stellwagen, C. Gelfi, and P. G. Righetti, "The Free Solution Mobility of DMA," *Biopolymers*, vol. 42, no. 6, pp. 687–703, 1997.

[56] H. Cottet, P. Gareil, O. Theodoly, and C. E. Williams, "A semi-empirical approach to the modeling of the electrophoretic mobility in free solution: application to polystyrenesulfonates of various sulfonation rates," *Electrophoresis*, vol. 21, no. 17, pp. 3529–3540, 2000.

[57] H. J. Zhong, M. A. K. Williams, R. D. Keenan, D. M. Goodall, and C. Rolin, "Separation and quantification of pectins using capillary electrophoresis: a preliminary study," *Carbohydrate Polymers*, vol. 32, no. 1, pp. 27–32, 1997.

[58] K. A. Oudhoff, F. A. Buijtenhuijs, P. H. Wijnen, P. J. Schoenmakers, and W. T. Kok, "Determination of the degree of substitution and its distribution of carboxymethylcelluloses by capillary zone electrophoresis," *Carbohydrate Research*, vol. 339, no. 11, pp. 1917–1924, 2004.

[59] C.-M. Jiang, M.-C. Wu, W.-H. Chan, and H.-M. Chang, "Determination of random- and blockwise-type de-esterified pectins by capillary zone electrophoresis," *Journal of Agricultural and Food Chemistry*, vol. 49, no. 11, pp. 5584–5588, 2001.

[60] M. A. K. Williams, T. J. Foster, and H. A. Schols, "Elucidation of pectin methylester distributions by capillary electrophoresis," *Journal of Agricultural and Food Chemistry*, vol. 51, no. 7, pp. 1777–1781, 2003.

[61] C.-M. Jiang, S.-C. Liu, M.-C. Wu, W.-H. Chang, and H.-M. Chang, "Determination of the degree of esterification of alkaline de-esterified pectins by capillary zone electrophoresis," *Food Chemistry*, vol. 91, no. 3, pp. 551–555, 2005.

[62] S. E. Guillotin, E. J. Bakx, P. Boulenguer, H. A. Schols, and A. G. J. Voragen, "Determination of the degree of substitution, degree of amidation and degree of blockiness of commercial pectins by using capillary electrophoresis," *Food Hydrocolloids*, vol. 21, no. 3, pp. 444–451, 2007.

[63] C. J. Ferris, K. J. Gilmore, G. G. Wallace, and M. in het Panhuis, "Modified gellan gum hydrogels for tissue engineering applications," *Soft Matter*, vol. 9, no. 14, pp. 3705–3711, 2013.

[64] C. John Ferrisa and M. in het Panhuism, "Conducting biomaterials based on gellan gum hydrogels," *Soft Matter*, vol. 5, no. 18, pp. 3430–3437, 2009.

[65] H. Cottet, J. Biron, and M. Martin, "Taylor dispersion analysis of mixtures," *Analytical Chemistry*, vol. 79, no. 23, pp. 9066–9073, 2007.

[66] A. Domard, "A perspective on 30 years research on chitin and chitosan," *Carbohydrate Polymers*, vol. 84, no. 2, pp. 696–703, 2011.

[67] I. Aranaz, M. Mengíbar, R. Harris et al., "Functional characterization of chitin and chitosan," *Current Chemical Biology*, vol. 3, no. 2, pp. 203–230, 2009.

[68] S. Nguyen, S. Hisiger, M. Jolicoeur, F. M. Winnik, and M. D. Buschmann, "Fractionation and characterization of chitosan by analytical SEC and 1H NMR after semi-preparative SEC," *Carbohydrate Polymers*, vol. 75, no. 4, pp. 636–645, 2009.

[69] C. Gartner, B. L. López, L. Sierra, R. Graf, H. W. Spiess, and M. Gaborieau, "Interplay between structure and dynamics in chitosan films investigated with solid-state NMR, dynamic mechanical analysis, and X-ray diffraction," *Biomacromolecules*, vol. 12, no. 4, pp. 1380–1386, 2011.

[70] J. Nicolas, Y. Guillaneuf, C. Lefay, D. Bertin, D. Gigmes, and B. Charleux, "Nitroxide-mediated polymerization," *Progress in Polymer Science*, vol. 38, no. 1, pp. 63–235, 2013.

[71] D. Gigmes, D. Bertin, C. Lefay, and Y. Guillaneuf, "Kinetic modeling of nitroxide-mediated polymerization: conditions for living and controlled polymerization," *Macromolecular Theory and Simulations*, vol. 18, no. 7-8, pp. 402–419, 2009.

[72] A. C. Ouano, "Diffusion in liquid systems. I. A simple and fast method of measuring diffusion constants," *Industrial and Engineering Chemistry Fundamentals*, vol. 11, no. 2, pp. 268–271, 1972.

[73] K. C. Pratt and W. A. Wakeham, "Mutual diffusion-coefficient of ethanol-water mixtures—determination by a rapid, new method," *Proceedings of the Royal Society of London A-Mathematical Physical and Engineering Sciences*, vol. 336, pp. 393–406, 1974.

[74] R. Callendar and D. G. Leaist, "Diffusion coefficients for binary, ternary, and polydisperse solutions from peak-width analysis of Taylor dispersion profiles," *Journal of Solution Chemistry*, vol. 35, no. 3, pp. 353–379, 2006.

[75] H. Cottet, M. Martin, A. Papillaud, E. Souaïd, H. Collet, and A. Commeyras, "Determination of dendrigraft poly-L-lysine diffusion coefficients by Taylor dispersion analysis," *Biomacromolecules*, vol. 8, no. 10, pp. 3235–3243, 2007.

[76] T. le Saux and H. Cottet, "Size-based characterization by the coupling of capillary electrophoresis to taylor dispersion analysis," *Analytical Chemistry*, vol. 80, no. 5, pp. 1829–1832, 2008.

[77] A. Ibrahim, R. Meyrueix, G. Pouliquen, Y. P. Chan, and H. Cottet, "Size and charge characterization of polymeric drug delivery systems by Taylor dispersion analysis and capillary electrophoresis," *Analytical and Bioanalytical Chemistry*, vol. 405, no. 16, pp. 5369–5379, 2013.

[78] J. R. Lakowicz, *Principles of Fluorescence Spectroscopy*, Springer, New York, NY, USA, 2007.

Journal of Chromatography A, 1372 (2014) 187–195

Contents lists available at ScienceDirect

Journal of Chromatography A

journal homepage: www.elsevier.com/locate/chroma

Purity of double hydrophilic block copolymers revealed by capillary electrophoresis in the critical conditions☆

Adam T. Sutton[a,b], Emmanuelle Read[c], Alison R. Maniego[a,b], Joel J. Thevarajah[a,b], Jean-Daniel Marty[c], Mathias Destarac[c], Marianne Gaborieau[a,b], Patrice Castignolles[a,*]

[a] University of Western Sydney (UWS), Australian Centre for Research on Separation Science (ACROSS), School of Science and Health, Locked Bag 1797, Penrith 2751, NSW, Australia
[b] University of Western Sydney (UWS), Molecular Medicine Research Group, School of Science and Health, Locked Bag 1797, Penrith 2751, NSW, Australia
[c] University Paul Sabatier, IMRCP, CNRS UMR 5623, 118 route de Narbonne, 31062 Toulouse, France

ARTICLE INFO

Article history:
Received 10 August 2014
Received in revised form 28 October 2014
Accepted 29 October 2014
Available online 6 November 2014

Keywords:
Capillary electrophoresis
Critical conditions
Block copolymers
Residual homopolymer quantification
Purity
Pressure assisted CE–CC

ABSTRACT

Block copolymers enable combining properties of different polymers; double hydrophilic block copolymers are innovative examples. Size-exclusion chromatography (SEC or GPC) has a quasi-monopoly in separation-based characterization methods for polymers, including block copolymers. However, in terms of purity determination (unintended homopolymers present in the copolymers), SEC resolution proves insufficient except for the extreme compositions for which the second block is much larger than the first one. The free solution capillary electrophoresis (capillary zone electrophoresis) technique does not separate charged homopolymers by their molar mass and we thus named the corresponding method capillary electrophoresis in the critical condition (CE–CC). CE–CC provides a means to assess the purity of poly(acrylic acid-*b*-acrylamide) – P(AA-*b*-AM) – copolymers, as well as of the more challenging cationic poly(acrylamido-*N*-propyltrimethylammonium chloride-*b*-*N*-isopropylacrylamide)—P(APTAC-*b*-NIPAM). In addition it can identify that a block copolymer has been produced. It is to be noted that P(APTAC-*b*-NIPAM) block copolymers cannot be eluted in SEC due to their exceptional ability to adsorb onto surfaces, while some information is obtained from CE–CC. Both possible parent homopolymers can be detected and their quantity estimated in a single injection by CE–CC. In both cases, one of the parent homopolymers is neutral and comes with the electro-osmotic flow. If the electro-osmotic flow is weak (conditions used for the cationic copolymer) then pressure assisted CE–CC is used to detect this homopolymer.

1. Introduction

Block copolymers provide a means of incorporating the properties of multiple polymers into the one material. Stimulus-responsive or 'smart' polymers can be included to provide, for example, the pH-responsiveness in one block and adhesion in another. For this reason they have a wide variety of potential applications including improving medical imaging [1], drug delivery [2], capacitors [3] and removable coatings [4]. Double hydrophilic block copolymers (DHBCs) are especially innovative [5], for example in the field of controlled mineralization [6,7] or quantum dots [8]. With further development, these applications may become a reality.

To continue the advance of these block copolymers more accurate means of characterizing them are required. There is no established method for the control of the purity of DHBCs. The most common tool for separating and characterizing polymers is size exclusion chromatography (SEC), also known as gel permeation chromatography (GPC) [9,10]. SEC separates according to hydrodynamic volume and not according to molar mass [10,11]. When the hydrodynamic volume is altered not only by molar mass, but also by copolymer composition or branching, there is an incomplete separation according to molar mass leading to errors of up to 100% in the determined molar mass [12,13]. Moreover, if any unintended homopolymers are present in the block copolymer sample it is unlikely to be detected by routine NMR spectroscopy and SEC experiments, leading to further errors in the determined molar mass. The difference in hydrodynamic volumes of a copolymer

☆ Selected papers presented at 21st Annual RACI Research and Development Conference 11th to 13th December 2013 for the ML VSI.

* Corresponding author. Tel.: +61 2 9685 9970; fax: +61 2 9685 9915.
E-mail addresses: destarac@chimie.ups-tlse.fr (M. Destarac), m.gaborieau@uws.edu.au (M. Gaborieau), p.castignolles@uws.edu.au (P. Castignolles).

http://dx.doi.org/10.1016/j.chroma.2014.10.105
0021-9673/

and of the corresponding homopolymers is usually not sufficient to allow their baseline separation to occur using SEC. Furthermore, SEC of smart polymers such as polyelectrolytes can be plagued with aggregation [14] and 'ion exclusion' [15–17]. This can then lead to low accuracy of the determined molar mass values [10,18]. More particularly, interactions of the polycations with the SEC stationary phase is a challenge, which limits reproducibility and separation efficiency. These interactions can generally be suppressed with high salt eluents and co-solvents [19,20] however in some cases there is a risk of precipitation and poor recovery. Columns for aqueous SEC of cationic polymers at low salt conditions are being developed as shown in application notes [21–23]. In the case of DHBCs, these SEC conditions for polycations are however incompatible with the SEC conditions for some second (neutral) block. For example, poly(*N*-isopropylacrylamide)—PNIPAM is a very challenging polymer to properly characterize using aqueous SEC due to its thermoresponsiveness in water [24]. PNIPAM requires polar organic mobile phases such as dimethylformamide (DMF) containing LiBr [25]. Therefore, the analysis of block copolymers such as poly(acrylamido-*N*-propyltrimethylammonium chloride-*b*-NIPAM) – P(APTAC-*b*-NIPAM) – or P(APTAC-*b*-*N*-vinyl pyrrolidone) by SEC is usually unsuccessful [26–29]. Both PAPTAC and PNIPAM homopolymers can be analysed by SEC with some success but no common conditions for the related DHBCs characterisation could be found. Therefore, the development of applications of cationic DHBCs such as P(APTAC-*b*-NIPAM) has been hindered by their lack of characterization.

Liquid chromatography under critical conditions (LC–CC) is a separation technique which separates polymers independently from molar mass [30]. By having one block in critical conditions the other block can be separated according to its molar mass providing the molar mass distribution of this other block. LC–CC leads to complete separation of the block copolymer from one of the corresponding homopolymers. However, determining the critical conditions is tedious, LC–CC suffers from poor recovery [31,32] and the mobile phase is usually required to be a mixture of solvents leading to preferential solvations and adsorption on the stationary phase [33]. Therefore, easier alternatives to LC–CC are highly desired. One example is Liquid Chromatography under Limiting Conditions of Desorption (LC–LCD), which is capable of separating block copolymers from their corresponding homopolymers [34–36]. LC–LCD has been used to show that a number of commercial poly(methyl methacrylate-*b*-styrene) block copolymers contained small amounts of both poly(methyl methacrylate) and polystyrene [35,37]. Furthermore, LC–LCD has been applied to poly(methyl methacrylate-*b*-styrene) copolymers synthesized by nitroxide mediated polymerization (NMP) and a significant amount of residual homopolymer was detected [38]. However, LC–LCD has not been applied to highly polar and charged polymers for which finding the correct solvent conditions would be particularly challenging.

An alternative method for quantifying the unintended homopolymers of polar and charged polymers is free solution capillary electrophoresis (CE), or capillary zone electrophoresis. Free solution CE can be used to separate a wide variety of compounds from sugars [39] to proteins [40]. Free solution CE separates compounds according to their charge to friction ratio. Free solution CE can separate poly(acrylic acid-*co*-diallyldimethylammonium chloride) from residual poly(diallyldimethyl ammonium chloride), PDADMAC, homopolymer and from its monomers [41]. The amount of unreacted poly(acrylic acid), PAA, in an amphiphilic block copolymer has also been previously determined by free solution CE [42,43]. DNA has similarly been separated from some of its block copolymers by free solution CE, the method being called end labeled free solution electrophoresis (ELFSE), which involved attaching a large uncharged protein or synthetic polymer (second block) to the end of DNA (first block) causing a change in the overall charge to friction ratio [44]. The additional friction resulted in separation of the free DNA (residual homopolymer) from the labeled DNA (copolymer) [45].This is because in the case of polyelectrolytes, when the chain reaches a certain size, the electrophoretic mobility is independent of molar mass, as shown for poly(styrene sulfonate) [46], single and double stranded DNA [47,48] and PAA [49]. The absence of separation according to molar mass is due the electrostatic friction outweighing the hydrodynamic friction [50,51]. This situation of electrophoretic mobility being independent of molar mass is analogous to the 'critical conditions' observed in LC–CC. Free solution CE can separate with different modes, in the case of free solution CE of large polyelectrolytes, we refer to it as CE in the critical conditions (CE–CC). The nomenclature is extensively discussed and defined in a recent review [52]. In this mode, separation of polymers can occur according to structure or to end groups. Previous work has already used CE–CC to separate polyacrylates according to branching [53], statistical copolymers such as chitosan and gellan gum by their composition (degree of acetylation) and conformation [54,55] as recently reviewed [52].

Herein we present a method for the quantification of parent homopolymers and thus an assessment of the purity of complex charged block copolymers exhibiting either a weak anionic block (PAA) or a cationic block (PAPTAC). The capabilities of SEC and CE–CC were compared and assessed to quantify homopolymers in block copolymer samples. Poly(acrylic acid-*b*-acrylamide) – P(AA-*b*-AM) – samples spiked with PAA were used to develop this method since P(AA-*b*-AM) samples with minimal residual homopolymer could be synthesized. This method was then applied to cationic P(APTAC-*b*-NIPAM) to quantify the amount of parent PAPTAC and PNIPAM homopolymers.

2. Material and methods

2.1. Materials

Acrylic acid (AA, 98%), (3-acrylamidopropyl)trimethylammonium chloride solution (APTAC, 75 wt% in water) and *N*-isopropylacrylamide (NIPAM, 97%) were purchased from Sigma Aldrich. Acrylamide (AM, 50 wt% in water stabilized with 100 ppm MEHQ, *p*-methoxyphenol) was obtained from SNF. *O*-ethyl-*S*-(1-methoxycarbonyl)ethyldithiocarbonate agent (Rhodixan A1) was obtained from Solvay. 4,4′azobis(4-cyanopentanoic)acid (ACVA, >98%) was obtained from Fluka. 2,2′-Azobis(2-methylpropionamidine)dihydrochloride (V-50, 98%), ammonium persulfate (APS, 98+%), sodium formaldehyde sulfoxylate dihydrate (NAFS, 98%) and L(+)-ascorbic acid (AsAc, 99%) were obtained from Acros Organics. Ethanol and deionized water were used as solvent for polymer syntheses. Diethyl ether was used to purify the diblock copolymers.

Water of Milli *Q* quality (Millipore, Bedford, MA, USA) was used in SECs and Free solution CE. Agilent fused-silica capillaries with an extended light path detection window (50 μm i.d., 360 μm o.d.) and poly(ethylene oxide) coated (named "WAX") and fluorocarbon coated (named "FC") fused-silica capillaries (50 μm i.d., 360 μm o.d.) were purchased from Pacific Laboratory Products (Australia). Sodium hydroxide (98%) pellets were obtained from Univar (Ingleburn, NSW, Australia). Boric acid (≥98%) and sodium azide (99%) were purchased from BDH AnalaR, Merck Pty Limited. Phosphoric acid (≥99.0%) was purchased from Fusions (Homebush, Australia). Hexaamminecobalt(III) chloride (≥99.5%), absolute ethanol, dimethyl sulfoxide (DMSO, >99%), disodium hydrogen phosphate (99%), ammonium nitrate (≥99.0%), acetonitrile (HPLC grade, ≥99.99%), and poly(diallyldimethyl ammonium

Table 1
Homopolymers and block copolymers investigated in this study.

Sample Code	Polymer	Theoretical molar mass (g mol^{-1})
PAA2k	PAA	2000
PAA2kPAM10k	P(AA-*b*-AM)	2000-*b*-10,000
PAA10k	PAA	10,000
PAA10kPAM10k	P(AA-*b*-AM)	10,000-*b*-10,000
PAPTAC5k	PAPTAC	5000
PNIPAM5k	PNIPAM	5000
PAPTAC5kPNIPAM5k	P(APTAC-*b*-NIPAM)	5000-*b*-5000
PAPTAC2k	PAPTAC	2000
PAPTAC2kPNIPAM8k	P(APTAC-*b*-NIPAM)	2000-*b*-8000
PAPTAC2kPNIPAM3k	P(APTAC-*b*-NIPAM)	2000-*b*-3000
PAPTAC1k	PAPTAC	1000
PAPTAC1kPNIPAM9k	P(APTAC-*b*-NIPAM)	1000-*b*-9000
PAPTAC1kPNIPAM3k	P(APTAC-*b*-NIPAM)	1000-*b*-3000
PAPTAC3k	PAPTAC	3000
PAPTAC3kPNIPAM3k	P(APTAC-*b*-NIPAM)	3000-*b*-3000
PAPTAC6k	PAPTAC	6000
PAPTAC6kPNIPAM3k	P(APTAC-*b*-NIPAM)	6000-*b*-3000

chloride) (PDADMAC, 'average M_w' 200,000–350,000, 20 wt% in H_2O) were supplied by Sigma Chemical company. Pullulan standards were purchased from PSS (Mainz, Germany).

2.2. Polymer samples

All polymers (Table 1) were synthesized by Reversible-Addition Fragmentation chain Transfer/Macromolecular Design via Interchange of Xanthates (RAFT/MADIX). PAA homopolymers were synthesized as in [5]. The synthesis of the P(AA-b-AM) block copolymers is shown in supporting information. PNIPAM homopolymer was synthesized as in [25], with the procedure detailed in supporting information.

PAPTAC homopolymers and P(APTAC-*b*-NIPAM) block copolymers were typically synthesized as follows: APTAC solution (10.7 g) corresponding to 7.98 g of pure APTAC (38.6 mmol), Rhodixan A1 (0.24 g, 1.15 mmol), V-50 (0.06 g, 0.19 mmol), ethanol (1.81 g) and deionized water (7.39 g) were placed in a 50 mL two neck round bottom flask. The solution was degassed by argon bubbling for 30 min before heating at 60 °C for 3 h. Conversion was monitored using ^{1}H NMR, on a Bruker Avance 300 taking aliquots until it reached 100%. The mixture was evaporated under reduced pressure to remove ethanol and then the solid content in the solution was determined by gravimetry (50.7%) in order to use this PAPTAC solution as macroMADIX agent for the synthesis of the diblock copolymer. PAPTAC solution (11.8 g, 0.80 mmol), NIPAM (9.77 g, 86.0 mmol), APS (0.20 g, 0.90 mmol) and deionized water (15.8 g) were placed in a 100 mL round bottom flask. The solution was degassed for 30 min by argon bubbling. AsAc (0.15 g, 0.86 mmol) was separately dissolved in 2.00 g of water and degassed for 30 min the same way. Then AsAc was added to the mixture to initiate the reaction that was left for 24 h until completion. The solution was evaporated under reduced pressure and the residue was dissolved in ethanol before precipitating in diethyl ether to yield a white powder.

2.3. SECs

Two different SEC set ups were used. SEC of PAA homopolymers and block copolymers was conducted with a Malvern Triple Detector Array (TDA) SEC Model 305 with an online degasser, pump and a manual injector. They were eluted through one SEC SUPREMA pre-column (particle size of 5 μm) then through three SEC SUPREMA columns (two 1000 Å, particle size of 5 μm and one 30 Å, particle size of 5 μm) from Polymer Standards Service (PSS, Mainz) with an aqueous eluent containing 0.1 mol L^{-1} Na_2HPO_4 and 200 ppm NaN_3 at 50 °C and 1 mL min^{-1} flow rate. The TDA includes the following detectors: right-angle laser light scattering (RALLS) and 7° low angle laser light scattering (LALLS) at 670 nm, refractometer and viscometer. Data was treated using OmniSEC version 4.7.0 and was plotted using OriginPro 8.5. Injections of PAA homopolymers and block copolymers used ethylene glycol as a flow rate marker. All samples were filtered through 0.45 μm PES or PVDF membrane filter before injection. The system was calibrated using 10 pullulan standards ranging from 342 to 708,000 g mol^{-1} (molar mass at the peak) with dispersity inferior to 1.27. The obtained calibration curve was fitted with a 4th order polynomial: $\log M = 142.9 - 20.76x + 1.184x^2 - 0.0301x^3 + 0.0002824x^4$ ($R^2 = 0.9994$), calibration curve shown in Fig. S-1.

SEC of PAPTAC homopolymers and block copolymers was conducted on an Agilent 1100 HPLC system with model 2424 refractive index and a DAWN HELEOS (Wyatt) light scattering detector. A guard column Shodex SB806-MT and two 8 mm × 300 mm Shodex columns (SB 806 M HQ, 13 μm, and 802.5 HQ, 13 μm) were used with as eluent 1 M NH_4NO_3 solution of water/acetonitrile (80/20, w/w) containing 100 ppm of PDADMAC (flowrate 1 mL min^{-1}). All samples were filtered through 0.45 μm filter before injection. The data were recorded using Astra and plotted using OriginPro 8.5.

2.4. Capillary electrophoresis

Separations were performed on an Agilent 7100 (Agilent Technologies Waldbronn, Germany) with a Diode Array Detector (DAD) monitoring at 200 and 285 nm with 10 and 20 nm bandwidths, respectively. Buffers were sonicated for 5 min and filtered before use. All samples were injected hydrodynamically by applying 30 mbar of pressure for 5 s followed by the running buffer injected in the same manner. All separations were performed at 30 kV and 25 °C unless specified. Data was acquired using Chemstation A.10.01 and plotted, integrated and migration time was converted to electrophoretic mobility using OriginPro 8.5. Electrophoretic mobility was calculated as shown in supporting information. The peak areas were corrected by dividing them by the migration time at the relevant apex.

2.4.1. PAA based samples

PAA based samples were dissolved at 5 g L^{-1} in 10 mM NaOH aqueous solution. 1 μL of DMSO was added to each 500 μL sample to mark the electro-osmotic flow (EOF). 110 mM sodium borate buffer (NB110, pH 9.2) was prepared as stated in reference [53]. All separations were carried out in NB110 buffer, with an extended light path fused-silica capillary with a total length of 60.6 cm (effective length 52.1 cm). The capillary was pre-treated prior to use by flushing for 10 min with 1 M NaOH, for 5 min with 0.1 M NaOH, for 5 min with water and for 5 min with NB110. Preconditioning between injections involved a 2 min flush with 1 M NaOH followed by a 5 min flush with NB110. After the last injection, the capillary was flushed for 1 min with 1 M NaOH, for 4 min with 0.1 M NaOH, for 10 min with water and for 10 min with air.

2.4.2. PAPTAC-based samples

PAPTAC-based samples were dissolved at 5 g L^{-1} in 1 mM $[Co(NH_3)_6]Cl_3$ aqueous solution unless stated otherwise. 10 mM NaH_2PO_4 (PB10) was prepared by taking 1 M H_3PO_4 and diluting it to 0.5 M; the resulting solution was titrated to pH 2 with 1 M NaOH, and then diluted to 10 mM. Preconditioning involved a 20 min flush with 10 mM H_3PO_4 followed by a 5 min flush with ethanol and then 5 min PB10. All separations were carried out in PB10 buffer, in a 'WAX' capillary with a total length of 34.5 cm (effective length 28.0 cm) unless stated otherwise. After the last injection, the

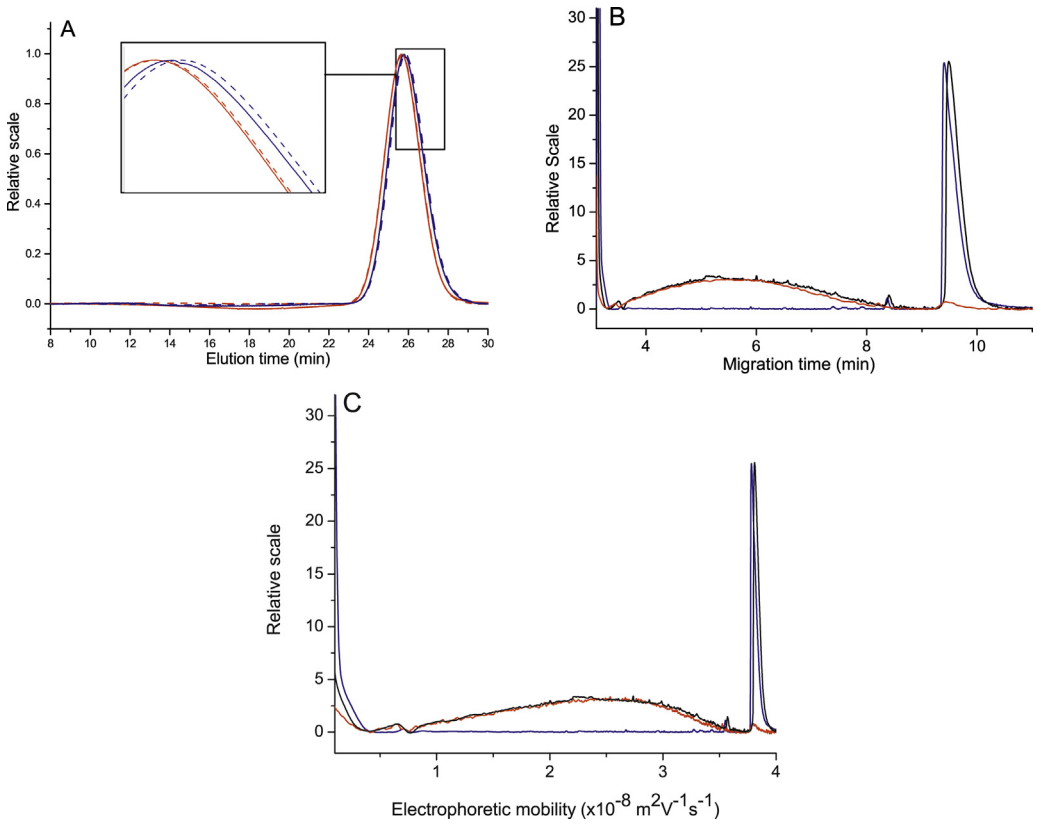

Fig. 1. Separation of PAA10k homopolymer (blue) from PAA10kPAM10k copolymer (red) using (A) SEC and (B and C) CE–CC. Dashed lines in A show repeat chromatograms. The black line in B and C is the electropherogram of PAA10kPAM10k spiked with PAA10k. CE–CC electropherograms are shown as a function of migration time (B) and of electrophoretic mobility (C). The injection concentrations were 2 g L^{-1} each for SEC and 5 g L^{-1} for CE–CC (except for the mixture of PAA10k and PAA10kPAM10k, for which 5 g L^{-1} of each component was injected). (For interpretation of the references to color in this figure legend, the reader is referred to the web version of this article.)

capillary was flushed for 20 min with 10 mM H_3PO_4, for 5 min with ethanol, for 20 min with water and for 10 min with air.

2.5. Pressure mobilization and pressure assisted free solution CE

All conditions were the same as those stated for PAPTAC based samples, except for the following. For pressure mobilization, samples were dissolved in PB10 and 50 mbar of pressure was applied instead of an electric field during the migration. For pressure assisted free solution CE, 50 mbar of internal pressure was applied in addition to the electric field during the separation.

3. Results and discussion

3.1. Comparison of the separation of homopolymers and block copolymers by SEC and CE–CC

The separation of a PAA homopolymer from a P(AA-*b*-AM) block copolymer is easily achieved by CE–CC, using standard conditions in under 14 min (see Fig. 1B for PAA10kPAM10k) with a relative standard deviation (RSD) of the electrophoretic mobility at the peak maximum of PAA10k being 0.5% ($n = 8$). In contrast, when the same samples were analyzed by SEC, minimal separation of the homopolymer from the block copolymer was observed (Fig. 1A). Only a 0.6% shift in elution time (calculated from the average at the peak maximum of the repeat injections) was detected for the block copolymer in SEC using established conditions for SEC of PAA and PAM [56–58]. In contrast CE–CC led to a narrow PAA peak at a higher electrophoretic mobility and a broad P(AA-*b*-AM) at a lower electrophoretic mobility, which were resolved (Fig. 1B and C). The narrow PAA peak in CE–CC is due to the critical conditions, so the absence of separation by molar mass for PAA. The SEC chromatograms of the corresponding PAAs are broader than the pullulan standards one indicating the PAA has a molar mass distribution with a dispersity above 1.1 (Fig. S-2A). The complete separation of the block copolymer from the corresponding homopolymer in CE–CC was confirmed through spiking P(AA-*b*-AM) samples with the corresponding PAA homopolymer (Fig. 1). The narrow peak of PAA confirms that it is under critical conditions. PAA oligomers were also present in the PAA samples with small peaks around 3.5×10^{-8} m^2 V^{-1} s^{-1} (Fig. 1C and Fig. S-2C) [49]. The lower electrophoretic mobility of P(AA-*b*-AM) compared to PAA indicates that the attached PAM neutral block is changing the overall charge to friction ratio by providing additional hydrodynamic friction but no charge [59]. In a controlled polymerization, this change in electrophoretic mobility can be used to confirm whether a homopolymer, used as a macroinitiator or macro-chain transfer agent, has been reinitiated and a block copolymer formed. The broadness of the block copolymer peak shows that there is a distribution of electrophoretic mobilities in the block copolymer sample, relating to the ratio of both block lengths in the sample. The block copolymer separation is the same as that which occurs in ELFSE where the electrophoretic mobility was linked to the ratio of the block lengths [59,60].

The success of a block copolymer synthesis is often probed through a shift in SEC elution time towards the higher molar masses [61–65]. The molar masses of block copolymers determined with SEC can be inaccurate due to the change of solvation properties between monomer units leading to local dispersity above 1 [10,66]. In the case of the symmetric block copolymer PAA10kPAM10k, SEC analysis fails to indicate if a block copolymer has been formed. Even if an additional method such as diffusion NMR (also named

DOSY) indicated the presence of block copolymer [28], SEC does not allow the detection or quantification of any homopolymer contaminant (Fig. 1A). Therefore, it is possible to have a situation where a large amount of homopolymer is present that would be assumed to be block copolymer resulting in an impure sample with an incorrect molar mass determined. However, from CE–CC, a clear shift in migration time (Fig. 1B) and in electrophoretic mobility (Fig. 1C) is observed, providing evidence that a block copolymer was produced and whether any homopolymers are present (discussed below). Therefore, CE–CC can be used to qualitatively identify when a block copolymer is produced, as well as if any homopolymers are present, which cannot always be said for SEC, especially in the case of adsorbing cationic block copolymers. In addition, CE–CC has a lower running cost and higher throughput than chromatography based techniques [39] and does not require sample filtration [52].

3.2. Cationic copolymers: Minimizing adsorption onto the capillary surface in CE–CC

SEC and CE–CC separations are now compared on more challenging cationic DHBCs. PAPTAC homopolymers did not initially elute from the column [67]. However, using the conditions developed for PDADMAC, the SEC of PAPTAC led to repeatable separations [19]. This procedure involves the addition of PDADMAC to the mobile phase, creating a positively charged coating on the stationary phase. These SEC conditions provide some indication of the size and dispersity of the PAPTAC homopolymer (Figs. S-3 and S-4). At the lowest elution volumes a signal is detected on the light scattering signal only, indicating the presence of aggregates (in minute amounts). Ion exclusion and finding appropriate standards for conventional calibration are also still a concern. In the same conditions P(APTAC-*b*-NIPAM) block copolymer yielded similar chromatograms to that of the corresponding homopolymer but with a lower signal intensity at identical sample injection concentrations (Figs. S-3 and S-4). It may seem that no block copolymer was formed; however, it is more likely that the PAPTAC homopolymer present in the block copolymer sample is eluting while the block copolymer is strongly adsorbing in the column and not eluting out of the column or only as a tail. Therefore CE–CC was used to investigate these block copolymer samples.

Cationic polymers have a tendency to adsorb onto surfaces with a negative zeta potential. PAPTAC injected in a fused-silica capillary led to a very weak signal even at pH 2 likely because of strong adsorption on the glass surface (Fig. S-5). To prevent the adsorption, capillaries with a fluorocarbon (FC) coating or a poly(ethylene oxide) (PEO) coating were used. Both coatings limited the adsorption of PAPTAC as indicated by the signal intensity being orders of magnitude higher than with uncoated fused-silica capillaries (Fig. S-5 and S-6). Joule heating was also found to not be a concern for these (thermoresponsive) polymers (supporting information). When using a FC coating the results were not repeatable likely due the adsorption attributed to hydrophobic interactions between the PNIPAM block and the hydrophobic (fluorinated) coating (Fig. S-6). The PEO coating yielded both sensitivity and repeatability with the RSD of the electrophoretic mobility of the homopolymer at the peak maximum being 0.6% ($n = 7$) – similar to PAA – for PAPTAC2k and 2.4% ($n = 3$) for PAPTAC5kPNIPAM5k.

Pressure mobilization was used to identify if the analyte interacted with the capillary surface. If no interaction is present then a Gaussian peak (or superimposed Gaussian peaks) is (are) observed with the cause of peak broadening being the diffusion of the analyte [68]. It was observed that a small fraction of PAPTAC was interacting with the capillary surface (Fig. 2). It is suspected to be due to an uneven distribution of the PEO coating, some areas of the capillary wall may have little or no coating allowing for the PAPTAC to adsorb. However, at least 75% of the homopolymer was

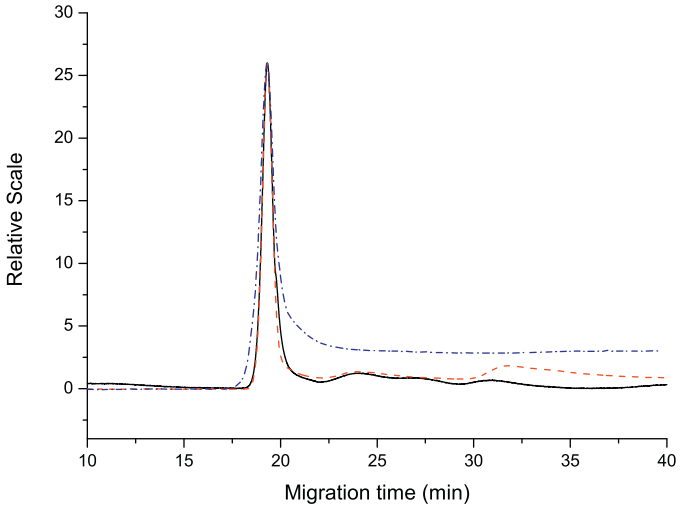

Fig. 2. Pressure mobilization of PAPTAC5k (black solid line), PNIPAM5k (red dashed line) and PAPTAC5kPNIPAM5k (blue dashed-dotted line) through a 74.8 cm PEO coated capillary. Injection concentration of each polymer was 5 g L^{-1}. (For interpretation of the references to color in this figure legend, the reader is referred to the web version of this article.)

unaffected and the remaining homopolymer was present in peaks which returned to the baseline shortly after the main peak and thus no permanent adsorption was observed. Similar results were also observed for the PNIPAM with 46% of it being unaffected but tailing peaks were broader and migrated further than that shown for PAPTAC (Fig. 2). The block copolymer P(APTAC-*b*-NIPAM) showed permanent adsorption with the peak tailing giving a consistent elevated baseline (Fig. 2). The adsorption appears to be mainly due to the hydrophobic interactions of the PNIPAM with the capillary surface. The improved repeatability using a PEO coating instead of a FC coating could be attributed to PEO being a more polar coating. Since the block copolymer shows the strongest adsorption both the ionic interactions of PAPTAC and the hydrophobic interactions of PNIPAM with the coating were contributing to the adsorption. The adsorption of the homopolymers would likely result in some peak tailing. To remove the adsorbed polymer the capillary was flushed with 10 mM H_3PO_4 for 20 min and ethanol for 5 min during the preconditioning of each injection. This prevented the adsorption from impacting subsequent injections.

The PAPTAC homopolymers in CE–CC showed well defined peaks with little effects of adsorption. (Short) oligomers were detected in the majority of the PAPTAC samples as indicated by the small peaks at lower electrophoretic mobilities (Fig. 3) [46,49]. For the lower molar mass samples such as PAPTAC1k and PAPTAC2k the oligomers made approximately 13% (w/w) of the sample, while for all other samples it represented no more than 1% (w/w) of the sample. This indicates that the majority of the PAPTAC samples contained mainly chain lengths longer than a few monomer units.

Although P(APTAC-*b*-NIPAM) is adsorbing, as clearly shown by the elevated baseline in Fig. 3, a prominent PAPTAC signal was noticeable in all samples. This enabled the quantification of residual PAPTAC in the P(APTAC-*b*-NIPAM) samples. Furthermore, in the case of PAPTAC1kPNIPAM9k the oligomers in the PAPTAC homopolymer were detected in the block copolymer in minute amounts (Fig. 3). These oligomers could be removed by dialysis if necessary using CE–CC to assess the success of the purification.

To further combat the adsorption of the block copolymer, pressure assisted CE–CC was used. This technique uses the same conditions as regular CE but with the addition of internal pressure during the separation so that the species migrate due to both the electric field and pressure (the separation still being due only to the electric field). Pressure assisted CE has previously been used

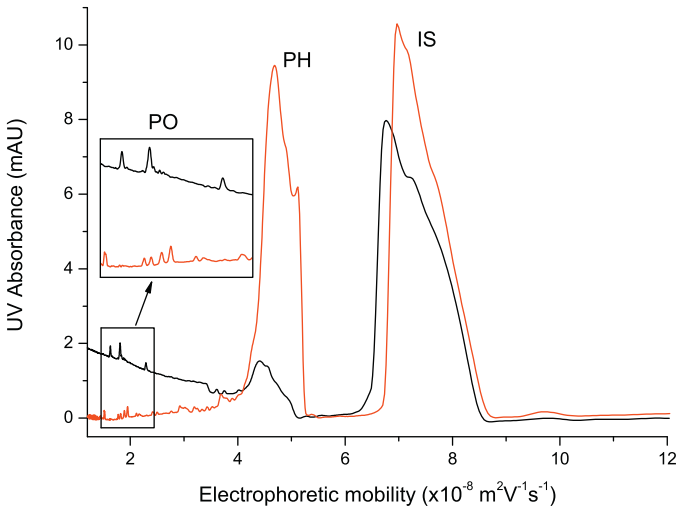

Fig. 3. CE–CC electropherograms of PAPTAC1k homopolymer (red) and PAPTAC1kPNIPAM9k block copolymer (black). The homopolymer and the internal standard (labeled as PH and IS, respectively) have mobilities between 4 and 5×10^{-8} m^2 V^{-1} s^{-1}, and between 6 and 9×10^{-8} m^2 V^{-1} s^{-1}, respectively. Oligomer peaks (labeled as PO) occur around 2×10^{-8} m^2 V^{-1} s^{-1} as shown in the insert. The injection concentrations were 0.625 g L^{-1} each for PAPTAC1k and 5 g L^{-1} for PAPTAC1kPNIPAM9k. (For interpretation of the references to color in this figure legend, the reader is referred to the web version of this article.)

to aid in the separation of polyelectrolytes [69]. Pressure assisted CE–CC helps migrate the adsorbed block copolymer along the capillary enabling its detection. Furthermore with a PEO coating at pH 2 there is no measureable EOF, meaning the detection of neutral species is very difficult using free solution CE, but with the aid of pressure the presence of neutral species in the sample can be more easily detected. The pressure assisted CE–CC of a mixture of PAPTAC and PNIPAM homopolymers produced well separated and relatively narrow peaks (Fig. 4 and Fig. S-7). The pressure assisted CE–CC of the P(APTAC-*b*-NIPAM) samples detected some species migrating at the same speed as the PAPTAC homopolymer,

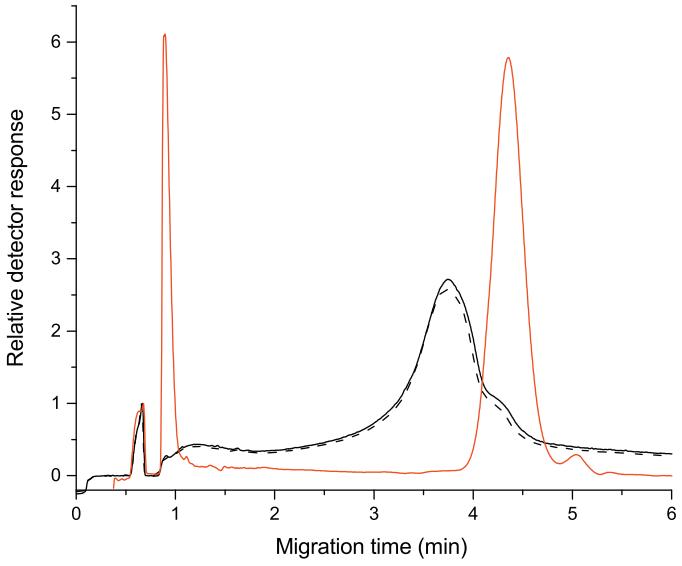

Fig. 4. Pressure assisted CE–CC of a mixture of PAPTAC5k and PNIPAM5k homopolymers (red) and of PAPTAC2kPNIPAM8k block copolymer (black, with repeat shown as dashed line). The mixture of homopolymers (red) indicate the migration time of the individual homopolymers in the critical conditions. The separation of another copolymer PATAC5kPNIPAM5k is presented on Fig. S-7. Injection concentration of each individual polymer was 5 g L^{-1}. Internal standard occurs at 0.6 min. (For interpretation of the references to color in this figure legend, the reader is referred to the web version of this article.)

demonstrating the presence of residual PAPTAC in the samples. This was then followed by a broad peak which mainly migrated slower than the PAPTAC homopolymer but mainly faster than the neutral species showing that a block copolymer was produced and makes up the majority of the sample (Fig. 4). In the P(APTAC-*b*-NIPAM) samples, a shoulder was observed which migrates at the same time as the PNIPAM homopolymer showing that some PNIPAM homopolymer is also present in the sample. Therefore in a single run, both parent homopolymers and the block copolymer can be detected. The identification of both homopolymers has been shown for block copolymers produced by anionic polymerization [35] and RAFT/MADIX [43]. In the case of RAFT/MADIX block copolymers this is likely due to the need of an external source of radicals for initiating the polymerization. Therefore, the formation of a secondary homopolymer would be less likely with living anionic polymerization or NMP which do not require an external initiator for the second block [38]. The presence of one or two parent homopolymers in the sample would influence the properties of the final product [37,42,70].

3.3. Homopolymer quantification by CE–CC

Assessing how accurately a separation method can quantify a polymer is rarely demonstrated in the literature. The group of Cottet however proved CE a reliable method to determine the cationic PDADMAC homopolymer within PAA-PDADMAC statistical copolymers [41]. To accurately quantify the amount of the PAA homopolymer in this work, a calibration curve between the homopolymer peak area and the concentration was established (Table 2). The alternative would be to compare the correct area of homopolymer and the block copolymer signals, however this is less accurate due to the different absorptivity of the different monomer units. UV detection in CE–CC showed sufficient linearity with all samples having a regression coefficient (R^2) greater than 0.979. The end group was shown to affect the calibration curve since the same homopolymers with different molar masses produced different calibration curves. Therefore the precursor homopolymers were used to quantify homopolymer in the corresponding copolymers to prevent bias from the end group.

CE–CC has the advantage of using a DAD unlike LC–CC and LC–LCD which usually require an evaporative light scattering detector (ELSD) due to the use of organic solvent and gradients. Although the linearity of the UV detector response for the PAA homopolymers is not as high as wanted, establishing linearity with an ELSD detector can be equally as difficult and in some cases there is no linear response between the detector signal and concentration of the polymer [71,72], as the molar mass of the polymer also influences the ELSD response. The imperfect linearity of the detector response for the PAA homopolymers is likely due to variations in injection volumes between injections since the samples were injected hydrodynamically and the pressure may vary from injection to injection. At higher concentrations the PAA homopolymers also change the solution viscosity which can influence the injection volume. To account for these differences between injections the internal standard, hexaaminecobalt(III) chloride, was used for the PAPTAC based polymers, which resulted in higher linearity than for the PAA homopolymers. The internal standard migrated before the PAPTAC homopolymer, had strong molar absorptivity and showed no sign of interaction with capillary coating or polymers as shown previously with chitosan [73]. In the case of polymer lacking chromophore, indirect UV detection and conductivity detection both were proved successful at quantifying PDADMAC with even lower LOD than the direct UV detection used in this work [41].

The recovery of LC based techniques has been shown to be a problem [36,72,74]. The recovery of CE–CC is quantitative in the case of PAA (Table 2). Recoveries of 113% and 95% are considered

Table 2
Linearity of homopolymer quantification, recovery and LOD CE–CC for PAA and PAPTAC homopolymers.

Sample	Concentration range (g L^{-1})	Equation	R^2	Number of points	Recovery* (%)	LOD# (g L^{-1})
PAA2k	2.50–20.0	$y = 0.431x - 0.402$	0.979	10	113	0.121
PAA10k	1.25–20.0	$y = 0.475x - 0.487$	0.984	12	95	0.095
PAPTAC2k	0.63–5.0	$y = 0.835x - 0.096$	0.998	10	ND	0.005
PAPTAC5k	0.63–5.0	$y = 0.769x - 0.005$	0.999	10	ND	0.008

* Recovery was measured for the homopolymer when mixed with its corresponding block copolymer; when the homopolymer was already present in the block copolymer the recovery was measured through the change in homopolymer peak upon spiking with homopolymer.
# The Limit Of Detection (LOD) was defined as the concentration at which the signal-noise ratio is equal to 3. ND stands for 'not determined'.

Table 3
Quantification of residual PAA/PAPTAC homopolymer in block copolymer samples for determination of sample purity.

Sample	C_H (g L^{-1})	RSD (%) $n = 3$	Amount of residual homopolymer^		Estimated amount of block copolymer#	
			(w/w) %	(mol/mol) %*	(w/w) %	(mol/mol) %*
PAA2kPAM10k	BLOD	CD	CD	CD	100	100
PAA10kPAM10k	0.11	ND	2.14	4.19	98	96
PAPTAC5kPNIPAM5k	1.27	0.88	18.87	31.75	80	67
PAPTAC2kPNIPAM8k	0.12	4.04	1.79	8.36	96	89

ND stands for 'not determined'.
* Calculated from the theoretical molar masses shown in Table 1.
# Assuming no significant amount of PAM in P(AA-*b*-AM) block copolymers.
^ PAA and PAPTAC homopolymer in corresponding block copolymer. BLOD stands for 'below the LOD'. C_H stands for concentration of homopolymer. CD stands for 'could not be determined'.

quantitative within experimental error. The LOD of the PAPTAC homopolymers was found to be significantly lower than that of the PAA homopolymers likely due to the higher UV absorption coefficient of the amide in the APTAC unit compared to the carboxylate in the AA unit. Minute amounts of PAPTAC homopolymer can be detected in block copolymer samples.

3.4. Quantification of parent homopolymers in block copolymer samples

Even when trying to prevent the presence of homopolymers in a block copolymer sample, there is inevitably the formation of 'dead chains' which form residual homopolymer in the block copolymer sample [38,75]. Using the equation determined above (Table 2), 2% (w/w) of PAA homopolymer was found in PAA10kPAM10k while none was detected in PAA2kPAM10k (Table 3). Assuming ideal polymerization kinetics and that all the initiator and MADIX agent reacted, the ratio of initiator to MADIX agent reflects the maximum possible fraction of 'dead' PAA homopolymer chains, 7.5 (mol/mol)% in this work for PAA10kPAM10k. Using the value of the theoretical molar mass, the fraction of dead PAA chains was estimated by CE–CC of PAA10kPAM10k to be 4 (mol/mol)%, thus 96% of the macro-chain transfer agent was converted to a block copolymer. The discrepancy may be due to the difference between values of the actual and theoretical molar masses (the non-ideal kinetics of polymerization of acrylic acid [76] leads to branching [77]) or to incomplete decomposition of the initiator. In the case of PAA2kPAM10k, given the theoretical maximal number of 'dead chains' the w/w% of PAA homopolymer would be below the LOD at the given injection concentration. Detection of PAM homopolymer is also possible with CE–CC as long as no EOF marker is used since as a neutral species it would migrate with the EOF.

Although there was incomplete separation of the PAPTAC homopolymer from the P(APTAC-*b*-NIPAM) block copolymer, it can be quantified with a RSD below 5% (Table 3). A significant amount of PAPTAC homopolymer was found in all P(APTAC-*b*-NIPAM) samples although the amount was found to vary greatly between samples (Table 3). For PAPTAC5kPNIPAM5k it was found that around 30% of the homopolymer chains did not reinitiate. Such information about the amount of homopolymer chains present in the crude block copolymer sample and can help to indicate the reactivity of the end group and whether the synthetic conditions used favor the formation of a block copolymer. The end group shows absorbance at 285 nm independent of the monomer units. However, the sensitivity of the detection of the xanthate end group was insufficient to determine whether the residual homopolymer had the end group present (i.e., "livingness" could not be assessed in this work).

The amount of PNIPAM present in the P(APTAC-*b*-NIPAM) samples was estimated by adjusting the maximum of the PNIPAM peak to the height of the shoulder. It was then estimated that the P(APTAC-*b*-NIPAM) samples likely contained between 1 and 3% (w/w) of PNIPAM homopolymer (Fig. 4). Therefore, the P(APTAC-*b*-NIPAM) samples contain a majority of block copolymer but also significant amounts of both homopolymers.

4. Conclusions

Determining the purity of block copolymers is important for having a complete characterization of the sample. CE–CC provides a fast and cost effective means of determining the amount of homopolymers present in a block copolymer in a single injection as well as qualitatively identifying the formation of a block copolymer. The purity of the block copolymer (and of the materials they are incorporated in) as well as blocking efficiency can be assessed by CE–CC, which is not possible with SEC and NMR. In the case of a P(AA-*b*-AM) block copolymer, CE–CC was shown to easily identify the formation of a block copolymer and measure the amount of residual PAA. SEC may be able to assess the distribution of molar masses in the initial homopolymer, however, SEC was unable to identify the presence of any homopolymers in the block copolymer and in this case it was difficult to show that a block copolymer had formed.

CE–CC uses a background electrolyte with a single component (no mixed-solvent) contrary to what is usually used in LC–CC (temperature can also be varied in LC to reach the CC) and adsorption events are limited in CE–CC since it is based on free solution CE (no stationary phase). This makes CE–CC an excellent method to characterize highly adsorbing polymers such as P(APTAC-*b*-NIPAM) and other cationic DHBCs. CE–CC was found to have linearity and recovery equal if not greater than that of LC–CC for homopolymers. SEC of P(APTAC-*b*-NIPAM) block copolymers was found not to be

possible, while CE–CC and pressure assisted CE–CC were able to show that the majority of the sample was a block copolymer but significant amounts of both parent homopolymers were present in the sample. With a means to quantify homopolymers in a block copolymer a relationship between the purity and the properties can be established. Furthermore, kinetic and 'livingness' studies of the polymerization are possible since the quantity of both the block copolymer and homopolymers can be determined. The effectiveness of purification techniques such as dialysis and precipitation can also be assessed by the use of CE–CC.

Acknowledgements

PC and MG thank the College of Health and Science of the University of Western Sydney for a College Equipment Grant for the purchase of the Capillary Electrophoresis instrument. We thank Malvern Instruments and ATA Scientific, especially Bryn McDonagh, for the loan of a Triple Detector Array (TDA) SEC. We thank Maryanne Selim and Erin Lans for technical assistance with sample preparation and early CE tests.

Appendix A. Supplementary data

Supplementary data associated with this article can be found, in the online version, at http://dx.doi.org/10.1016/j.chroma.2014.10.105.

References

[1] B. Dubertret, P. Skourides, D.J. Norris, V. Noireaux, A.H. Brivanlou, A. Libchaber, In vivo imaging of quantum dots encapsulated in phospholipid micelles, Science 298 (2002) 1759–1762.
[2] B. Jeong, Y.H. Bae, D.S. Lee, S.W. Kim, Biodegradable block copolymers as injectable drug-delivery systems, Nature 388 (1997) 860–862.
[3] T. Brezesinski, J. Wang, J. Polleux, B. Dunn, S.H. Tolbert, Templated nanocrystal-based porous TiO_2 films for next-generation electrochemical capacitors, J. Am. Chem. Soc. 131 (2009) 1802–1809.
[4] H. Fu, X. Hong, A. Wan, J.D. Batteas, D.E. Bergbreiter, Parallel effects of cations on PNIPAM graft wettability and PNIPAM solubility, ACS Appl. Mater. Interf. 2 (2010) 452–458.
[5] D. Taton, A.-Z. Wilczewska, M. Destarac, Direct synthesis of double hydrophilic statistical di- and triblock copolymers comprised of acrylamide and acrylic acid units via the MADIX process, Macromol. Rapid Commun. 22 (2001) 1497–1503.
[6] S.H. Yu, H. Colfen, Bio-inspired crystal morphogenesis by hydrophilic polymers, J. Mater. Chem. 14 (2004) 2124–2147.
[7] N. Sanson, F. Bouyer, M. Destarac, M. In, C. Gérardin, Hybrid polyion complex micelles formed from double hydrophilic block copolymers and multivalent metal ions: size control and nanostructure, Langmuir 28 (2012) 3773–3782.
[8] K. Tarasov, D. Houssein, M. Destarac, N. Marcotte, C. Gerardin, D. Tichit, Stable aqueous colloids of ZnS quantum dots prepared using double hydrophilic block copolymers, New J. Chem. 37 (2013) 508–514.
[9] A.M. Striegel, W.W. Yau, J.J. Kirkland, D.D. Bly, Modern Size-Exclusion Liquid Chromatography: Practice of Gel Permeation and Gel Filtration Chromatography, second ed., John Wiley & Sons Inc., Hoboken, NJ, 2009.
[10] M. Gaborieau, P. Castignolles, Size-exclusion chromatography (SEC) of branched polymers and polysaccharides, Anal. Bioanal. Chem. 399 (2011) 1413–1423.
[11] Z. Grubisic, P. Rempp, H. Benoit, A universal calibration for gel permeation chromatography, J. Polym. Sci. B: Polym. Lett. 5 (1967) 753–759.
[12] P. Castignolles, R. Graf, M. Parkinson, M. Wilhelm, M. Gaborieau, Detection and quantification of branching in polyacrylates by size-exclusion chromatography (SEC) and melt-state 13C NMR spectroscopy, Polymer 50 (2009) 2373–2383.
[13] T. Junkers, M. Schneider-Baumann, S.S.P. Koo, P. Castignolles, C. Barner-Kowollik, Determination of propagation rate coefficients for methyl and 2-ethylhexyl acrylate via high frequency PLP–SEC under consideration of the impact of chain branching, Macromolecules 43 (2010) 10427–10434.
[14] G. Delaittre, M. Save, M. Gaborieau, P. Castignolles, J. Rieger, B. Charleux, Synthesis by nitroxide-mediated aqueous dispersion polymerization, characterization, and physical core-crosslinking of pH- and thermoresponsive dynamic diblock copolymer micelles, Polym. Chem. 3 (2012) 1526–1538.
[15] I.V. Perminova, F.H. Frimmel, D.V. Kovalevskii, G. Abbt-Braun, A.V. Kudryavtsev, S. Hesse, Development of a predictive model for calculation of molecular weight of humic substances, Water Res. 32 (1998) 872–881.
[16] B. Porsch, L.O. Sundelöf, Size-exclusion chromatography and dynamic light scattering of dextrans in water: explanation of ion-exclusion behaviour, J. Chromatogr. A 669 (1994) 21–30.
[17] S. Mori, Secondary effects in aqueous size exclusion chromatography of sodium poly(styrenesulfonate) compounds, Anal. Chem. 61 (1989) 530–534.
[18] D. Berek, Size exclusion chromatography—a blessing and a curse of science and technology of synthetic polymers, J. Sep. Sci. 33 (2010) 315–335.
[19] M. Destarac, A. Guinaudeau, R. Geagea, S. Mazieres, E. Van Gramberen, C. Boutin, S. Chadel, J. Wilson, Aqueous MADIX/RAFT polymerization of diallyldimethylammonium chloride: extension to the synthesis of poly(DADMAC)-based double hydrophilic block copolymers, J. Polym. Sci., A: Polym. Chem. 48 (2010) 5163–5171.
[20] M. Destarac, I. Blidi, O. Coutelier, A. Guinaudeau, S. Mazieres, E. Van Gramberen, J. Wilson, Aqueous RAFT/MADIX polymerization: same monomers, new polymers? ACS Symp. Ser. 1100 (2012) 259–275.
[21] TOSOH Bioscience LLC, Aqueous SEC Columns for Analysis of Cationic Polymers TSKgel PWXL-CP Series, TOSOH Bioscience LLC, 2013.
[22] Polymer Standards Service, Characterization of Poly(DADMAC), Polymer Standards Service, 2014.
[23] R. Roemling, K. Tokunaga, H. Moriyama, Analysis of Cationic Polymers by Size Exclusion Chromatography with TSK-GEL® PWXL-CP, LC GC Application Notebooks, Tosoh Bioscience GmbH, 2008.
[24] F. Ganachaud, M.J. Monteiro, R.G. Gilbert, M.-A. Dourges, S.H. Thang, E. Rizzardo, Molecular weight characterization of poly(*N*-isopropylacrylamide) prepared by living free-radical polymerization, Macromolecules 33 (2000) 6738–6745.
[25] E. Read, A. Guinaudeau, D. James Wilson, A. Cadix, F. Violleau, M. Destarac, Low temperature RAFT/MADIX gel polymerisation: access to controlled ultra-high molar mass polyacrylamides, Polym. Chem. 5 (2014) 2202–2207.
[26] M.L. Patrizi, M. Diociaiuti, D. Capitani, G. Masci, Synthesis and association properties of thermoresponsive and permanently cationic charged block copolymers, Polymer 50 (2009) 467–474.
[27] S. Utsel, E.E. Malmstrom, A. Carlmark, L. Wagberg, Thermoresponsive nanocomposites from multilayers of nanofibrillated cellulose and specially designed *N*-isopropylacrylamide based polymers, Soft Matter 6 (2010) 342–352.
[28] A. Guinaudeau, O. Coutelier, A. Sandeau, S. Mazières, H.D. Nguyen Thi, V. Le Drogo, D.J. Wilson, M. Destarac, Facile access to poly(*N*-vinylpyrrolidone)-based double hydrophilic block copolymers by aqueous ambient RAFT/MADIX polymerization, Macromolecules 47 (2014) 41–50.
[29] E. Read, W. Moussa, J.-D. Marty, M. Destarac, Room temperature, aqueous RAFT/MADIX synthesis of thermoresponsive cationic diblock copolymers and their temperature-induced aggregation properties, Polymer Preprints (Am. Chem. Soc., Div. Polym. Chem.) 52 (2011) 655–656.
[30] M. Rollet, D. Glé, T.N.T. Phan, Y. Guillaneuf, D. Bertin, D. Gigmes, Characterization of functional poly(ethylene oxide)s and their corresponding polystyrene block copolymers by liquid chromatography under critical conditions in organic solvents, Macromolecules 45 (2012) 7171–7178.
[31] E. Beaudoin, A. Favier, C. Galindo, A. Lapp, C. Petit, D. Gigmes, S. Marque, D. Bertin, Reduced sample recovery in liquid chromatography at critical adsorption point of high molar mass polystyrene, Eur. Polym. J. 44 (2008) 514–522.
[32] A. Favier, C. Petit, E. Beaudoin, D. Bertin, Liquid chromatography at the critical adsorption point (LC–CAP) of high molecular weight polystyrene: pushing back the limits of reduced sample recovery, E-Polymers (2009) 15.
[33] W. Lee, S. Park, T. Chang, Liquid chromatography at the critical condition for polyisoprene using a single solvent, Anal. Chem. 73 (2001) 3884–3889.
[34] D. Berek, Coupled liquid chromatographic techniques for the separation of complex polymers, Prog. Polym. Sci. 25 (2000) 873–908.
[35] D. Berek, Separation of parent homopolymers from diblock copolymers by liquid chromatography under limiting conditions desorption, 1—Principle of the method, Macromol. Chem. Phys. 209 (2008) 695–706.
[36] D. Berek, Separation of parent homopolymers from diblock copolymers by liquid chromatography under limiting conditions of desorption 3. Role of column packing, Polymer 51 (2010) 587–596.
[37] D. Berek, Separation of minor macromolecular constituents from multicomponent polymer systems by means of liquid chromatography under limiting conditions of enthalpic interactions, Eur. Polym. J. 45 (2009) 1798–1810.
[38] P. Astolfi, L. Greci, P. Stipa, C. Rizzoli, C. Ysacco, M. Rollet, L. Autissier, A. Tardy, Y. Guillaneuf, D. Gigmes, Indolinic nitroxides: evaluation of their potential as universal control agents for nitroxide mediated polymerization, Polym. Chem. 4 (2013) 3694–3704.
[39] J.D. Oliver, M. Gaborieau, E.F. Hilder, P. Castignolles, Simple and robust determination of monosaccharides in plant fibers in complex mixtures by capillary electrophoresis and high performance liquid chromatography, J. Chromatogr. A 1291 (2013) 179–186.
[40] P.D. Grossman, J.C. Colburn, H.H. Lauer, R.G. Nielsen, R.M. Riggin, G.S. Sittampalam, E.C. Rickard, Application of free-solution capillary electrophoresis to the analytical scale separation of proteins and peptides, Anal. Chem. 61 (1989) 1186–1194.
[41] N. Anik, M. Airiau, M.-P. Labeau, C.-T. Vuong, H. Cottet, Characterization of cationic copolymers by capillary electrophoresis using indirect UV detection and contactless conductivity detection, J. Chromatogr. A 1219 (2012) 188–194.
[42] M. Jacquin, P. Muller, G. Lizarraga, C. Bauer, H. Cottet, O. Théodoly, Characterization of amphiphilic diblock copolymers synthesized by MADIX polymerization process, Macromolecules 40 (2007) 2672–2682.
[43] M. Jacquin, P. Muller, R. Talingting-Pabalan, H. Cottet, J.F. Berret, T. Futterer, O. Théodoly, Chemical analysis and aqueous solution properties of charged amphiphilic block copolymers PBA-*b*-PAA synthesized by MADIX®, J. Colloid Interface Sci. 316 (2007) 897–911.

[44] P. Mayer, G.W. Slater, G. Drouin, Theory of DNA sequencing using free-solution electrophoresis of protein–DNA complexes, Anal. Chem. 66 (1994) 1777–1780.
[45] H. Ren, A.E. Karger, F. Oaks, S. Menchen, G.W. Slater, G. Drouin, Separating DNA sequencing fragments without a sieving matrix, Electrophoresis 20 (1999) 2501–2509.
[46] H. Cottet, P. Gareil, O. Theodoly, C.E. Williams, A semi-empirical approach to the modeling of the electrophoretic mobility in free solution: Application to polystyrenesulfonates of various sulfonation rates, Electrophoresis 21 (2000) 3529–3540.
[47] C. Heller, G.W. Slater, P. Mayer, N. Dovichi, D. Pinto, J.-L. Viovy, G. Drouin, Free-solution electrophoresis of DNA, J. Chromatogr. A 806 (1998) 113–121.
[48] E. Stellwagen, N.C. Lu, Unified description of electrophoresis and diffusion for DNA and other polyions, Biochemistry 42 (2003) 11745–11750.
[49] M. Gaborieau, T.J. Causon, Y. Guillaneuf, E.F. Hilder, P. Castignolles, Molecular weight and tacticity of oligoacrylates by capillary electrophoresis–mass spectrometry, Aust. J. Chem. 63 (2010) 1219–1226.
[50] M. Muthukumar, Theory of electrophoretic mobility of a polyelectrolyte in semidilute solutions of neutral polymers, Electrophoresis 17 (1996) 1167–1172.
[51] J.L. Barrat, J.F. Joanny, Advances in Chemical Physics, vol. XCIV, John Wiley & Sons Inc., New York, NY, 1996, pp. 1–66.
[52] J.J. Thevarajah, M. Gaborieau, P. Castignolles, Separation and characterization of synthetic polyelectrolytes and polysaccharides with capillary electrophoresis, Adv. Chem. 2014 (2014), Article ID: 798503.
[53] A.R. Maniego, D. Ang, Y. Guillaneuf, C. Lefay, D. Gigmes, J.R. Aldrich-Wright, M. Gaborieau, P. Castignolles, Separation of poly(acrylic acid) salts according to topology using capillary electrophoresis in the critical conditions, Anal. Bioanal. Chem. 405 (2013) 9009–9020.
[54] D.L. Taylor, C.J. Ferris, A.R. Maniego, P. Castignolles, M. in het Panhuis, M. Gaborieau, Characterization of gellan gum by capillary electrophoresis, Aust. J. Chem. 65 (2012) 1156–1164.
[55] M. Mnatsakanyan, J.J. Thevarajah, R.S. Roi, A. Lauto, M. Gaborieau, P. Castignolles, Separation of chitosan by degree of acetylation using simple free solution capillary electrophoresis, Anal. Bioanal. Chem. 405 (2013) 6873–6877.
[56] I. Lacik, S. Beuermann, M. Buback, Aqueous phase size-exclusion-chromatography used for PLP–SEC studies into free-radical propagation rate of acrylic acid in aqueous solution, Macromolecules 34 (2001) 6224–6228.
[57] S.A. Seabrook, M.P. Tonge, R.G. Gilbert, Pulsed laser polymerization study of the propagation kinetics of acrylamide in water, J. Polym. Sci., A: Polym. Chem. 43 (2005) 1357–1368.
[58] I. Lacík, S. Beuermann, M. Buback, PLP–SEC study into free-radical propagation rate of nonionized acrylic acid in aqueous solution, Macromolecules 36 (2003) 9355–9363.
[59] W.N. Vreeland, C. Desruisseaux, A.E. Karger, G. Drouin, G.W. Slater, A.E. Barron, Molar mass profiling of synthetic polymers by free-solution capillary electrophoresis of DNA–polymer conjugates, Anal. Chem. 73 (2001) 1795–1803.
[60] L.C. McCormick, G.W. Slater, A.E. Karger, W.N. Vreeland, A.E. Barron, C. Desruisseaux, G. Drouin, Capillary electrophoretic separation of uncharged polymers using polyelectrolyte engines: theoretical model, J. Chromatogr. A 924 (2001) 43–52.
[61] A.H. Soeriyadi, C. Boyer, F. Nyström, P.B. Zetterlund, M.R. Whittaker, High-order multiblock copolymers via iterative Cu(0)-mediated radical polymerizations (SET–LRP): toward biological precision, J. Am. Chem. Soc. 133 (2011) 11128–11131.
[62] G.H. Li, P.P. Yang, Z.S. Gao, Y.Q. Zhu, Synthesis and micellar behavior of poly(acrylic acid-*b*-styrene) block copolymers, Colloid. Polym. Sci. 290 (2012) 1825–1831.
[63] I. Javakhishvili, K. Jankova, S. Hvilsted, Neutral, anionic, cationic, and zwitterionic diblock copolymers featuring poly(2-methoxyethyl acrylate) hydrophobic segments, Polym. Chem. 4 (2013) 662–668.
[64] V. Delplace, A. Tardy, S. Harrisson, S. Mura, D. Gigmes, Y. Guillaneuf, J. Nicolas, Degradable and comb-like PEG-Based copolymers by nitroxide-mediated radical ring-opening polymerization, Biomacromolecules 14 (2013) 3769–3779.
[65] V. Delplace, S. Harrisson, A. Tardy, D. Gigmes, Y. Guillaneuf, J. Nicolas, Nitroxide-mediated radical ring-opening copolymerization: chain-end investigation and block copolymer synthesis, Macromol. Rapid Commun. 35 (2014) 484–491.
[66] E. Hosseini Nejad, P. Castignolles, R.G. Gilbert, Y. Guillaneuf, Synthesis of methacrylate derivatives oligomers by dithiobenzoate-RAFT-mediated polymerization, J. Polym. Sci., A: Polym. Chem. 46 (2008) 2277–2289.
[67] M. Beija, E. Palleau, S. Sistach, X. Zhao, L. Ressier, C. Mingotaud, M. Destarac, J.-D. Marty, Control of the catalytic properties and directed assembly on surfaces of MADIX/RAFT polymer-coated gold nanoparticles by tuning polymeric shell charge, J. Mater. Chem. 20 (2010) 9433–9442.
[68] J. Chamieh, H. Cottet, Comparison of single and double detection points Taylor dispersion analysis for monodisperse and polydisperse samples, J. Chromatogr. A 1241 (2012) 123–127.
[69] L. Leclercq, H. Cottet, Fast characterization of polyelectrolyte complexes by inline coupling of capillary electrophoresis to Taylor dispersion analysis, Anal. Chem. 84 (2012) 1740–1743.
[70] M.W. Matsen, Phase-behavior of block-copolymer homopolymer blends, Macromolecules 28 (1995) 5765–5773.
[71] M.I. Malik, G.W. Harding, M.E. Grabowsky, H. Pasch, Two-dimensional liquid chromatography of polystyrene–polyethylene oxide block copolymers, J. Chromatogr. A 1244 (2012) 77–87.
[72] A. Šišková, E. MacOvá, D. Corradini, D. Berek, Liquid chromatography of synthetic polymers under critical conditions of enthalpic interactions 4: Sample recovery, J. Sep. Sci. 36 (2013) 2979–2985.
[73] C. Wu, C.Y. Kao, S.Y. Tseng, K.C. Chen, S.F. Chen, Determination of the degree of deacetylation of chitosan by capillary zone electrophoresis, Carbohydr. Polym. 111 (2014) 236–244.
[74] M.I. Malik, H. Pasch, Novel developments in the multidimensional characterization of segmented copolymers, Prog. Polym. Sci. 39 (2014) 87–123.
[75] D.J. Keddie, A guide to the synthesis of block copolymers using reversible-addition fragmentation chain transfer (RAFT) polymerization, Chem. Soc. Rev. 43 (2014) 496–505.
[76] M. Buback, P. Hesse, I. Lacik, Propagation rate coefficient and fraction of mid-chain radicals for acrylic acid polymerization in aqueous solution, Macromol. Rapid Commun. 28 (2007) 2049–2054.
[77] P. Castignolles, Transfer to polymer and long-chain branching in PLP–SEC of acrylates, Macromol. Rapid Commun. 30 (2009) 1995–2001.

Purity of double hydrophilic block copolymers revealed by capillary electrophoresis in the critical conditions

SUPPORTING INFORMATION

Adam T. Sutton,[1,2] Emmanuelle Read,[3] Alison R. Maniego,[1,2] Joel J. Thevarajah,[1,2] Jean-Daniel Marty,[3] Mathias Destarac,[3] Marianne Gaborieau,[1,2] Patrice Castignolles[1]*

[1]University of Western Sydney (UWS), Australian Centre for Research on Separation Science (ACROSS), School of Science and Health, Locked Bag 1797, Penrith NSW 2751, Australia, p.castignolles@uws.edu.au

[2]University of Western Sydney (UWS), Molecular Medicine Research Group, School of Science and Health, Locked Bag 1797, Penrith NSW 2751, Australia, m.gaborieau@uws.edu.au

[3]University Paul Sabatier, IMRCP, CMRS UMR 5623, 118 route de Narbonne 31062 Toulouse, France, destarac@chimie.ups-tlse.fr

Polymer synthesis

Synthesis of PAA, procedure for PAA2k:

In a Schlenk flask, a solution of AA (7.00 g, 97.0 mmol), Rhodixan A1 (0.81 g, 3.90 mmol), ACVA (45.5 mg, 0.16 mmol), ethanol (1.92 g), and distilled water (8.00 g) was degassed by bubbling argon for 30 min before heating at 60 °C for 4.5 h. Conversion was monitored by ^{1}H NMR spectroscopy of aliquots until the completion (>99 %) of the reaction. Ethanol was evaporated under reduced pressure. Finally the aqueous solution of PAA was freeze dried to yield a white powder.

Synthesis of the P(AA-b-AM) diblock copolymer, procedure for PAA2kPAM10k:

In a Schlenk flask, a solution of PAA2k (0.81 g, 0.40 mmol), AM (8.00 g, 56.0 mmol) and water (6.50 g) was degassed by bubbling argon for 30 min. Then 2 mL of each solution (0.06 % w/w) of APS and NAFS were added simultaneously to the mixture at 10 °C. After 24 h, the reaction was complete and the solution was freeze dried to yield a white polymer powder.

Synthesis of PNIPAM, procedure for PNIPAM5k:

NIPAM (2.19 g, 19.3 mmol), APS (39.6 mg, 0.17 mmol), distilled water (3.97 g) and PDMA-XA1 (0.55 g, 0.49 mmol) macroinitiator whose synthesis is described in [E. Read, A. Guinaudeau, D. James Wilson, A. Cadix, F. Violleau, M. Destarac, Polymer Chemistry, 5 (2014) 2202-2207], were placed in a two-neck round-bottom flask and thermostated at 25°C. The solution was degassed for 30 min by argon bubbling. AsAc (35.6 mg, 0.17 mmol) was separately dissolved in 2.00 g of water and degassed for 30 min in the same manner. Then AsAc was added to the mixture under a stream of argon to initiate the reaction that was left for 24 h.

SEC

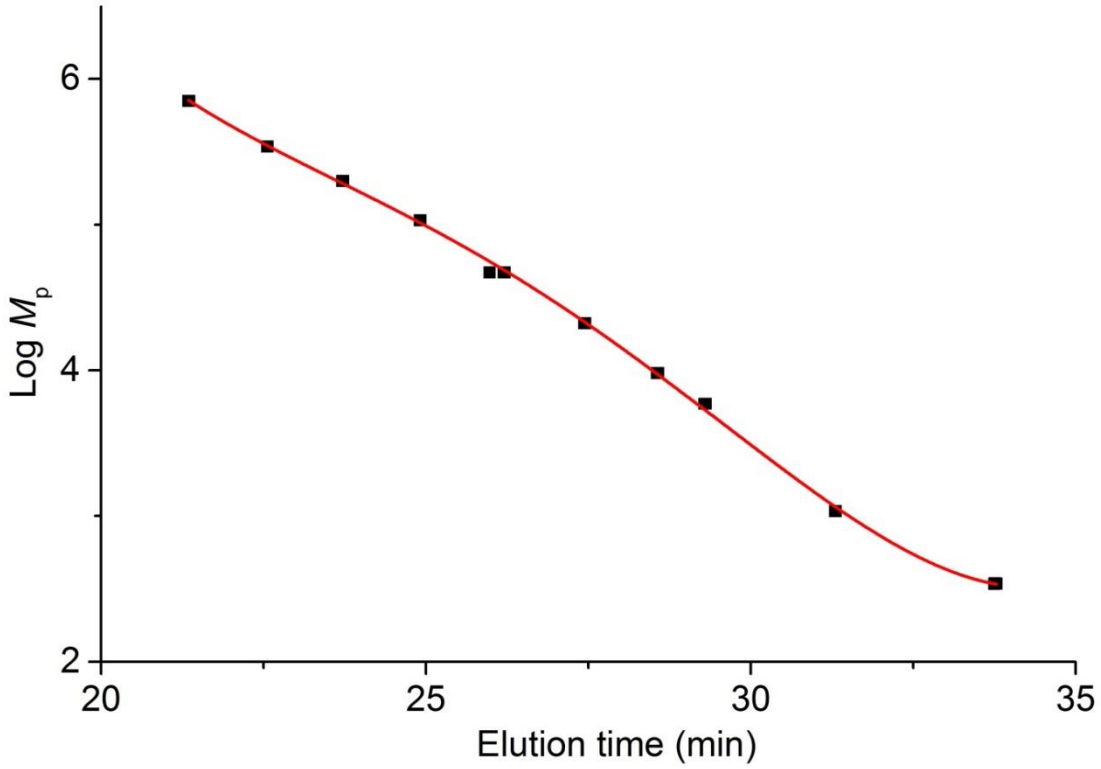

Fig. S-1. Calibration curve of the pullulan standards ranging from 342 to 708000 g·mol^{-1} (molar mass at the peak) fitted with a 4th order polynomial: log M = 142.9 - 20.76x + 1.184x^2 - 0.0301x^3 + 0.0002824x^4 (R^2=0.9994).

Capillary electrophoresis

The electrophoretic mobility (μ) was determined using Equation S-1:

$$\mu = \frac{l_d l_t}{V}\left(\frac{1}{t_m} - \frac{1}{t_{EOF}}\right) \quad \text{(S-1)}$$

where l_d is the length to the detection window (effective length), l_t is the total length of the capillary, V is the applied voltage, t_m is the migration time of the analyte and t_{EOF} is the migration time of the electro-osmotic flow (EOF) marker [P. Castignolles, M. Gaborieau, E.F. Hilder, E. Sprong, C.J. Ferguson, R.G. Gilbert, Macromolecular Rapid Communications, 27 (2006) 42-46].

In the case of the cationic polymers which were separated at pH 2, in a PEO coated capillary there is no measurable EOF within 60 min so the t_{EOF} term is negligible in the determination of electrophoretic mobility. The internal standard hexaaminecobalt(III) chloride was used to correct for injection to injection variations to give a relative electrophoretic mobility. Therefore Equation S-2 was used to calculate the μ of the cationic polymers:

$$\mu = \frac{l_d l_t}{V}\left(\frac{1}{t_m} . \frac{t_{ref}}{t_{is}}\right) \quad \text{(S-2)}$$

Where t_{ref} is the average migration time of the peak maximum of the internal standard and t_{is} is the migration time at the peak maximum of the internal standard in the electropherogram. When no internal standard was used t_{ref}/t_{is} was equal to 1.

The increase in temperature due to Joule heating inside the PEO coated capillaries was found to be 0.2 °C using the equations in [C.J. Evenhuis, R.M. Guijt, M. Macka, P.J. Marriott, P.R. Haddad, Analytical Chemistry, 78 (2006) 2684-2693]. Therefore there is little to no effect of Joule heating in the separation.

Results

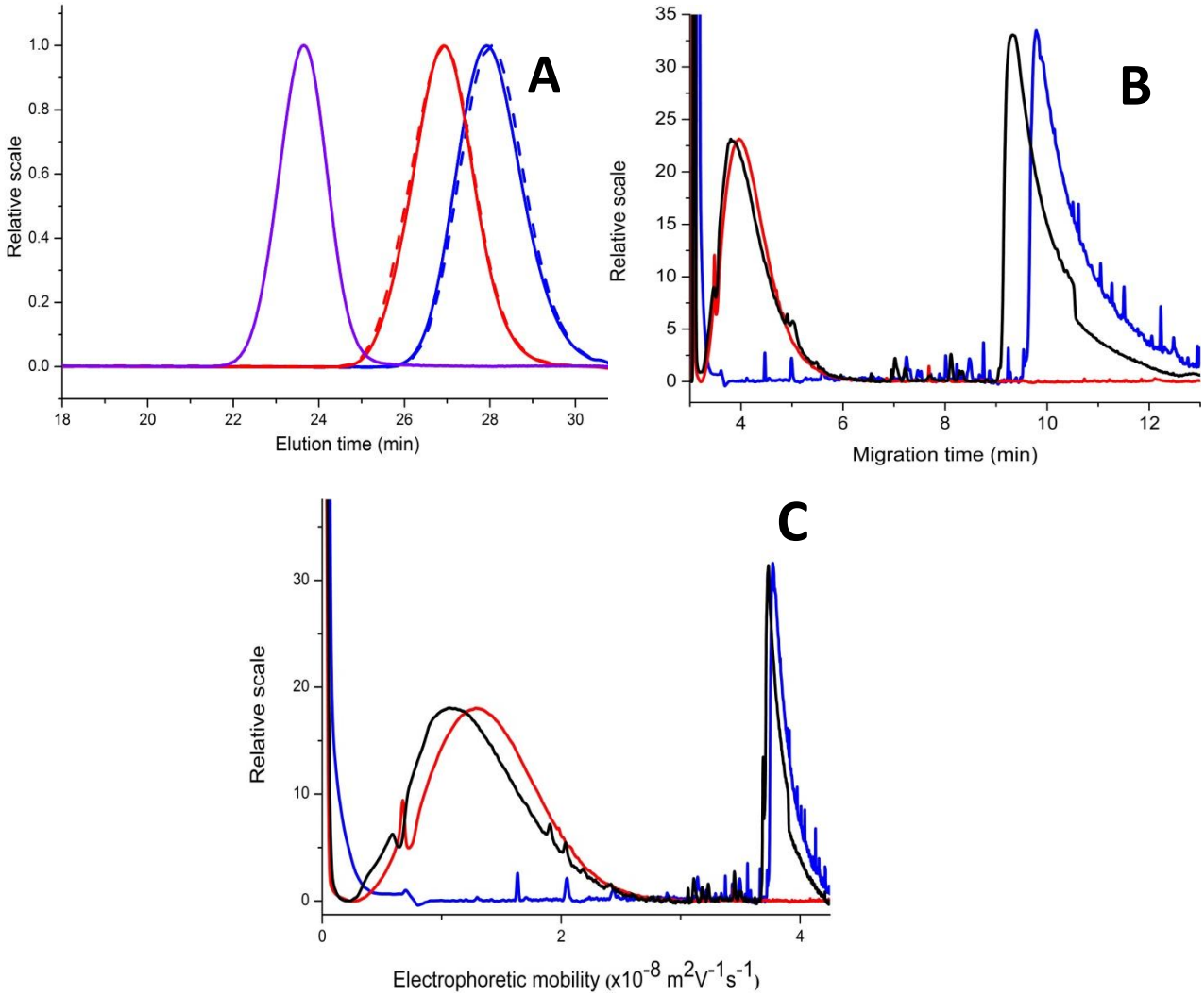

Fig. S-2. Separation of PAA2k homopolymer(blue) from PAA2kPAM10k copolymer (red) using (A) SEC and (B, C) CE-CC. Dashed lines in A show repeat chromatograms and the purple line shows the chromatogram of a pullulan standard with 200 000 g mol^{-1} molar mass. The black line in B and C is the electropherogram of PAA2kPAM10k spiked with PAA2k. CE-CC electropherograms are shown as a function of migration time (**B**) and of electrophoretic mobility (**C**). The injection concentrations were 8 and 5 g L^{-1}respectively for SEC and 5 g L^{-1} for CE (except for the mixture of PAA2k and PAA2kPAM10k, for which 5 g L^{-1} of each component was injected).

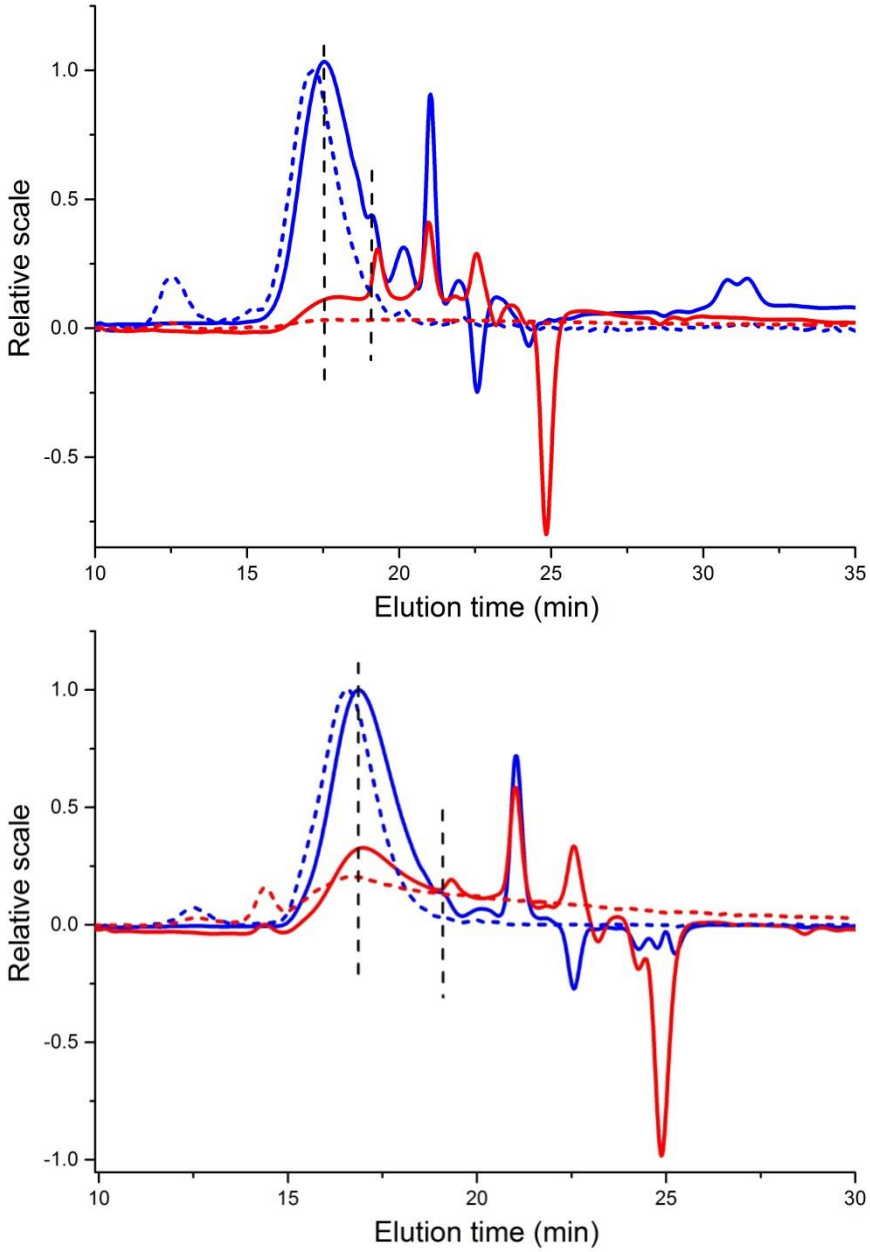

Fig. S-3. SEC chromatograms of PAPTAC homopolymers (blue) and P(APTAC-*b*-NIPAM) block copolymers (red). Figure S-3a (top) shows PAPTAC1k and PAPTAC1kPNIPAM3k while Figure S-3b (bottom) shows PAPTAC2k and PAPTAC2kPNIPAM3k. Solid and dashed lines represent signals obtained by refractive index and light scattering detectors respectively.

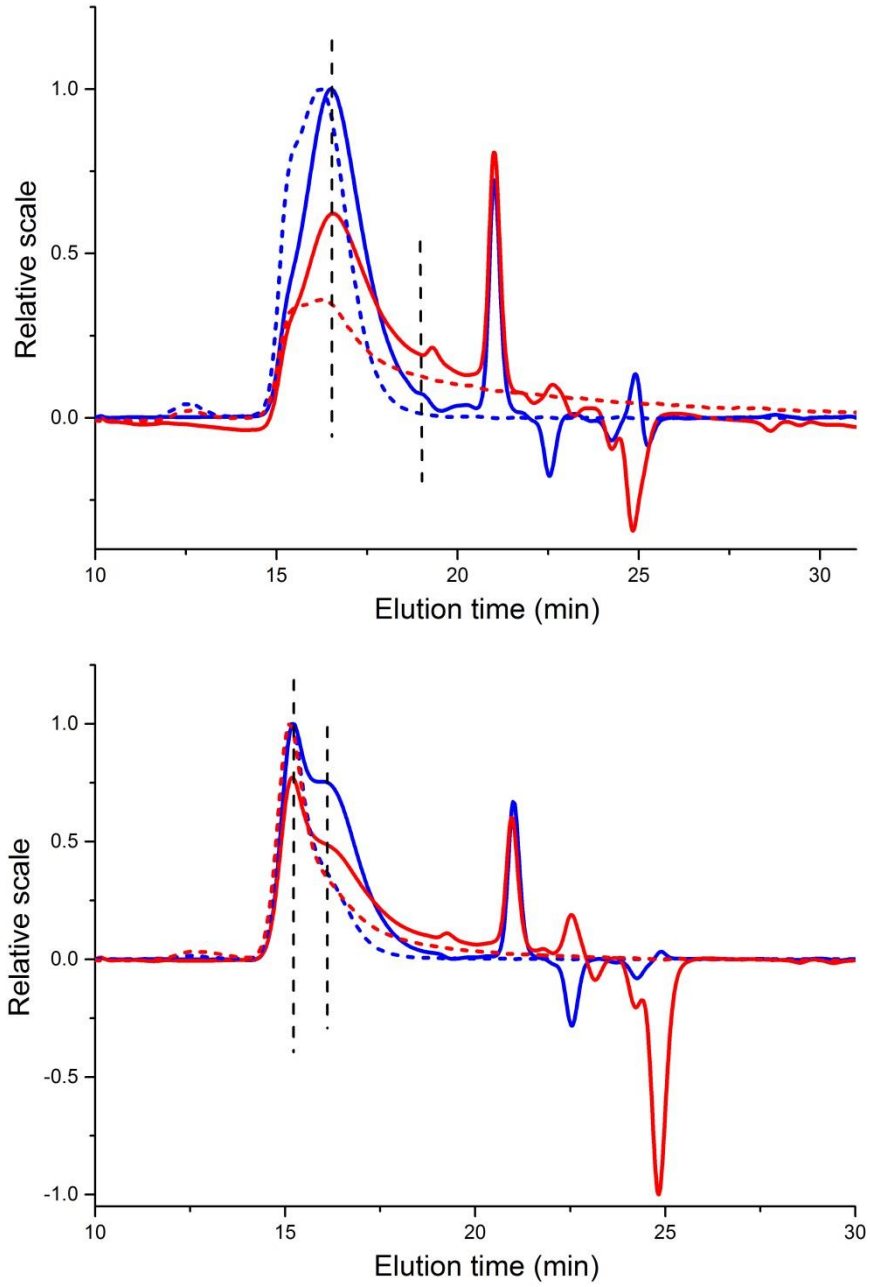

Fig. S-4 .SEC chromatograms of PAPTAC homopolymers (blue) and P(APTAC-*b*-NIPAM) block copolymers (red). Figure S-4a (top) shows PAPTAC3k and PAPTAC3kPNIPAM3k while Figure S-4b (bottom) shows PAPTAC6k and PAPTAC6kPNIPAM3k. Solid and dashed lines represent signals obtained by refractive index and light scattering detectors respectively.

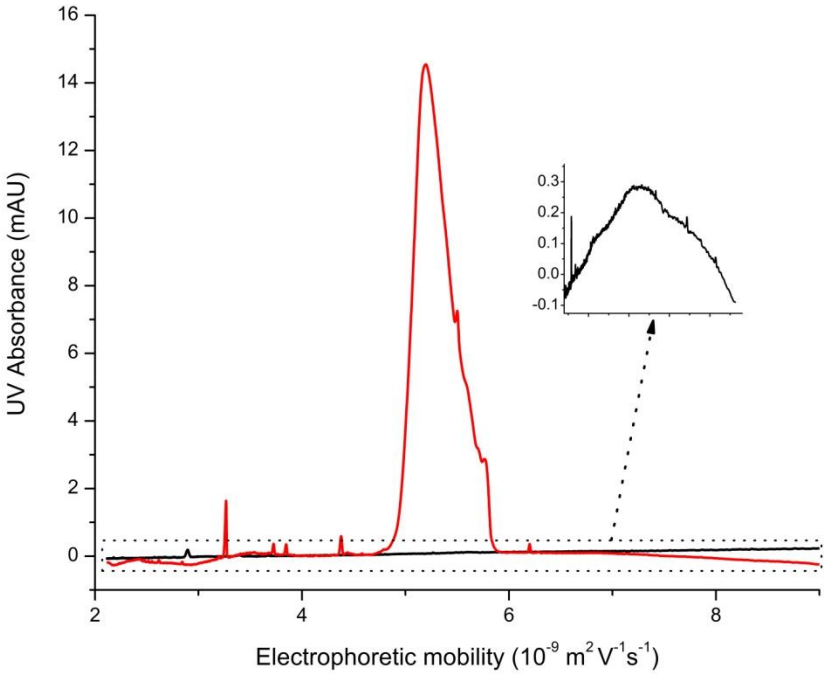

Fig. S-5. Separation of PAPTAC6k in an uncoated fused silica capillary (black) with 58.6 cm total length and a 83.8 cm PEO coated capillary (red). Both separations occurred at 13 °C with the samples dissolved in water to 8 mg mL^{-1}.

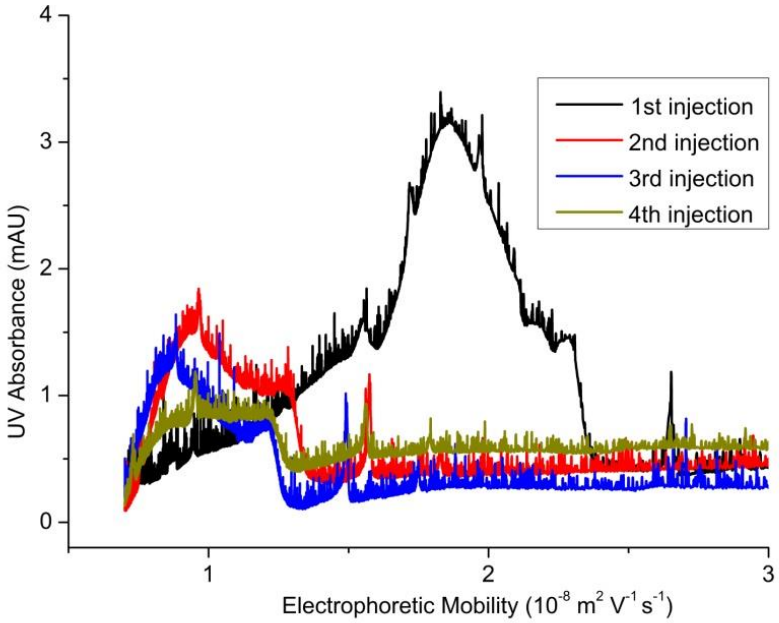

Fig. S-6. Repeatability of PAPTAC3kPNIPAM3k injected using an 83.8 cm FC coated capillary at 13°C with the samples dissolved in water to 7 mg mL^{-1}.

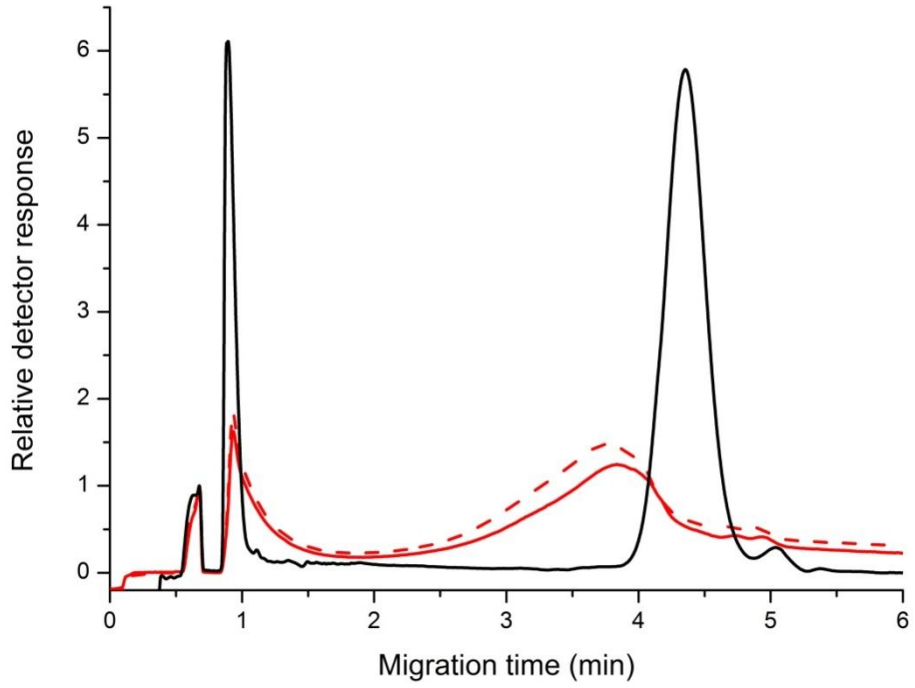

Fig. S-7. Pressure assisted CE-CC of a mixture of PAPTAC5k and PNIPAM5k homopolymers (black) and PAPTAC5kPNIPAM5k block copolymer (red). Dashed line is a repeat electropherogram. Injection concentration of each individual polymer was 5 g L^{-1}.

Anal Bioanal Chem (2015) 407:2543–2555
DOI 10.1007/s00216-015-8483-y

RESEARCH PAPER

Real-time monitoring of peptide grafting onto chitosan films using capillary electrophoresis

Danielle L. Taylor · Joel J. Thevarajah · Diksha K. Narayan · Patricia Murphy · Melissa M. Mangala · Seakcheng Lim · Richard Wuhrer · Catherine Lefay · Michael D. O'Connor · Marianne Gaborieau · Patrice Castignolles

Received: 16 October 2014 / Revised: 22 December 2014 / Accepted: 12 January 2015 / Published online: 14 February 2015

Abstract Chitosan, being antimicrobial and biocompatible, is attractive as a cell growth substrate. To improve cell attachment, arginine–glycine–aspartic acid–serine (RGDS) peptides were covalently grafted to chitosan films, through the widely used coupling agents 1-ethyl-3-(3-dimethylaminopropyl)carbodiimide (EDC-HCl) and *N*-hydroxysuccinimide (NHS), via the carboxylic acid function of the RGDS molecule. The grafting reaction was monitored, for the first time, in real time using free-solution capillary electrophoresis (CE). This enabled fast separation and determination of the peptide and all other reactants in one separation with no sample preparation. Covalent RGDS peptide grafting onto the chitosan film surface was demonstrated using solid-state NMR of swollen films. CE indicated that oligomers of RGDS, not simply RGDS, were grafted on the film, with a likely hyperbranched structure. To assess the functional properties of the grafted films, cell growth was compared on control and peptide-grafted chitosan films. Light microscopy and polymerase chain reaction (PCR) analysis demonstrated greatly improved cell attachment to RGDS-grafted chitosan films.

Keywords Chitosan · Peptide · Capillary electrophoresis · Solid-state NMR spectroscopy · Retinal pigment epithelial cells

Danielle L. Taylor and Joel J. Thevarajah contributed equally to this work.

Electronic supplementary material The online version of this article (doi:10.1007/s00216-015-8483-y) contains supplementary material, which is available to authorized users.

D. L. Taylor · J. J. Thevarajah · D. K. Narayan · P. Murphy · M. M. Mangala · S. Lim · M. D. O'Connor · M. Gaborieau
University of Western Sydney (UWS), Molecular Medicine Research Group (MMRG), Parramatta 2150, Australia

D. L. Taylor · J. J. Thevarajah · D. K. Narayan · M. Gaborieau (✉) · P. Castignolles
University of Western Sydney, Australian Centre for Research on Separation Sciences (ACROSS), School of Science and Health, Parramatta 2150, Australia
e-mail: m.gaborieau@uws.edu.au

D. K. Narayan · P. Murphy · M. M. Mangala · S. Lim · M. D. O'Connor (✉)
University of Western Sydney, School of Medicine, Campbelltown 2560, Australia
e-mail: m.oconnor@uws.edu.au

R. Wuhrer
University of Western Sydney, Advanced Materials Characterisation Facility (AMCF), Parramatta 2150, Australia

C. Lefay
Aix-Marseille Université, CNRS, ICR UMR 7273, 13397 Marseille, France

Introduction

Chitin is the second most abundant polysaccharide in the world (by volume after cellulose) and is the main component extracted from discarded shells and gladii of crustaceans and molluscs; it is thus readily available, inexpensive, and abundant [1, 2]. Chitosan is derived from the *N*-deacetylation of chitin. It can be dispersed in acidic media and easily cast into fibers, gels, beads, scaffolds, nanoparticles, and films [3]. Chitosan exists as a linear copolymer of β-[1,4]-linked 2-acetamido-2-deoxy-D-glucopyranose and 2-amino-2-deoxy-D-glucopyranose (monomer units bearing different functional

groups, see Electronic Supplementary Material (ESM) Fig. S1) [4]. Its antifungal [5], antibacterial [6], and low immunological [7] properties make it promising for various biomedical applications including as a substrate for culture of stem cells [8–11] and other cell types [12].

Cell survival and appropriate functioning are intimately linked with cell attachment to cell type-specific extracellular matrix proteins [13]. For example, biomaterials used in prostheses, vascular grafting, and artificial skin require substantial anchorage and adhesion to cells [14]. The peptides arginine–glycine–aspartic acid (RGD) and arginine–glycine–aspartic acid–serine (RGDS) are fibronectin mimetics that have been extensively used in cell attachment studies due to their ability to increase and mediate cell adhesion on biomedical components. When grafted to a silicone surface, RGD was shown to trigger similar cell attachment as the whole fibronectin protein [15]. Short peptides containing the tri-amino sequence RGD are thus cheaper substitutes for fibronectin when attempting to produce cell attachment to artificial surfaces. The RGD sequence acts as a ligand for cell surface integrin receptors as shown through their grafting on the thermoresponsive poly(*N*-isopropylacrylamide-*co*-*N*-acryloxysuccinimide) [16]. Covalent grafting of RGD peptides can occur through amidification of the amine at the N-terminus of the peptide with the succinimide group of the corresponding co-monomer. In the case of chitosan films, grafting with the fibronectin protein (containing the RGDS sequence) has been achieved by amidification (or esterification) of the protein's carboxylic acid groups onto the amine (or alcohol) moieties on the chitosan surface via the coupling agents 1-ethyl-3-(3-dimethylaminopropyl)carbodiimide (EDC-HCl) and *N*-hydroxysuccinimide (NHS) [17]. The resulting covalently grafted fibronectin-chitosan surface promoted the adhesion and proliferation of SaOs-2 human osteoblast-like cells compared to bare chitosan films. This grafting method has been applied to RGD or RGDS, but usually to graft the peptide through its amine (not carboxylic acid) functional group onto carboxylic acid functional groups of the substrate, requiring a chemical modification of chitosan [11]. The use of EDC-HCl/NHS appears more straightforward, and thus preferable, in comparison to grafting through the photochemical activation of RGDS [18–20] or the thiolation reaction using *N*-succinimidyl-3-(2-pyridyldithio)propionate [21]. Grafting with EDC-HCl and NHS is often assumed to lead to quantitative grafting of RGD(S).

Knowledge of the grafting reaction enables adjustments to be made to the reaction time. Similarly, determination of the actual final peptide consumption enables adjustment of its initial concentration to avoid wastage. To analyze peptide grafting processes, appropriate determination of the reactants and products is necessary. For chitosan films, the grafting process has previously been monitored by direct characterization of the grafted films. For example, amino acid analysis (AAA) has been used on a chitosan scaffold with peptide grafted from the chitosan amine [22] and also a carboxymethylated chitosan with peptide grafted from the carboxylic acid functional group introduced on the chitosan surface [23]. In the first of these studies, the yield of grafted peptide was not reported, with only the final peptide density on the surface reported. In the second study, the yield of the grafted peptide was reported as 10 to 12 %.

Critically, the AAA method used in these two studies is tedious and incompatible with simple and/or high-throughput assessment of the grafting process. It should also be noted that RGDS grafting onto chitosan does not yield an imide bond [22] but rather an amide bond. As an alternative to the AAA method, grafting of RGD onto chitosan via EDC-HCl and NHS has been assessed through the fluorescence of a model system containing RGD labeled with fluorescein isothiocyanate (FITC) [24]. Unfortunately, no comparison of the grafted RGD quantity to the RGD originally introduced was made in this study, so the kinetics and the extent of the reaction cannot be accurately assessed. Moreover, the presence of the bulky FITC groups could alter the grafting process mediated by EDC-HCl and NHS. This is particularly relevant for processes involving RGD(S) polycondensation described in this work.

Solid-state characterization can also be used to characterize the grafting process, but as with AAA, it has specific limitations such as the inability to be performed in real time. As an alternative, the grafting process can be characterized indirectly by monitoring the disappearance of the peptide from the reactant solution. Indirect monitoring may not differentiate between covalent grafting and adsorption; however, adsorption experiments can be carried out in parallel to assess the extent of adsorption. Reverse-phase HPLC has been used to quantify glycine-arginine-glycine-aspartic acid (GRGD) grafting on chitosan, but the method was deemed as only semi-quantitative [20]. In contrast, capillary electrophoresis (CE) has never been applied to monitor peptide grafting. However, in other systems, CE has been used extensively to characterize both cationic and anionic peptides and proteins with relatively high recovery [25, 26]. It can also be used as an indirect method to monitor reactions in real time [27]. Additionally, free-solution CE has a lower running cost and is more robust than common HPLC methods [28] and allows characterization in complex matrices, for example of polysaccharides without sample preparation, not even filtration [29] including for chitosan [30]. Therefore, free-solution CE (also known as capillary zone electrophoresis) was assessed here to test whether the real-time monitoring advantages of CE are suitable for monitoring peptide consumption during peptide grafting onto chitosan films.

The physical characteristics of chitosan films may affect the grafting process and the application properties of biomedical products. Solid-state NMR spectroscopy under magic-angle spinning (MAS) enabled the characterization of various properties of chitosan films (e.g., composition, mechanical

strength, elasticity) [3, 31, 32]. Additionally, ^{13}C and ^{15}N NMR spectroscopy was used to determine the average composition of the chitosan in terms of degree of acetylation [31]. ^{1}H, ^{13}C, and ^{15}N NMR spectroscopy, combined with X-ray scattering, was used to reveal the molecular origin of several properties of chitosan films (e.g., mechanical strength, elasticity) depending on the film preparation (e.g., casting from weak or strong acid solution, neutralization or not) [3].

A range of cell types are relevant to regenerative medicine applications, including ocular retinal pigment epithelium (RPE) that plays a key role in the development of macular degeneration. In vivo, the RPE requires attachment to Bruch's membrane to provide key regulatory signals for RPE survival and function [33]. Transplantation of RPE from various sources, in conjunction with synthetic Bruch's membrane, is widely viewed as a promising and viable method to restore vision in patients with diseased RPE [33]. Importantly, the RPE is known to attach to extracellular matrix proteins such as fibronectin within Bruch's membrane [34], thus allowing transmission of bioactive signals to enhance cell adhesion and survival [35].

In this context, we report a simple method to graft biologically relevant peptides onto chitosan films, to monitor the grafting reaction with CE, and to characterize the films by solid-state NMR spectroscopy. In doing so, we demonstrate a simple, inexpensive, and widely applicable method to successfully generate cell type-specific substrates that promote cell attachment and proliferation for downstream cell culture and other biomedical applications (e.g., transplantation).

Materials and methods

Materials

Chitosan powder (medium molecular weight, lot number MKBH1108V, average degree of acetylation, DA, of 24 % of monomer units and viscosity of 563 cP in 1 % acetic acid), NHS (98 %), EDC-HCl (99 %), trifluoroacetic acid (TFA, 99 %), dimethylsulfoxide (DMSO), sodium hydroxide pellets, and adamantane (99 %) were purchased from Sigma-Aldrich. Glucosamine (GLcN, 1,000-mg capsules, batch number 23249) was purchased from Health Care, Australia. Boric acid (98 %) and orthophosphoric acid (85 %) were purchased from BDH AnalR, Merck Pty Ltd. Acetic acid (AcOH, glacial, 99 %) and hydrochloric acid (32 %) were purchased from Unilab. Singly labeled ^{13}C-labeled alanines (1-^{13}C, 2-^{13}C, 3-^{13}C; 99 %) were purchased from Cambridge Isotope laboratories, Inc. The peptide RGDS (97 %) was obtained from Auspep Pty Ltd, Australia. Phosphate-buffered saline solution (PBS) at pH 7.4 was prepared by dissolving 8 g sodium chloride, 0.2 g potassium chloride, 1.44 g disodium hydrogen phosphate, and 0.24 g potassium dihydrogen phosphate in 0.8 L Milli-Q water and titrating the solution with hydrochloric acid to pH 7.4. Sodium borate buffer (75 mM) was prepared from 0.5 M boric acid in Milli-Q water, titrated to pH 9.20 with 10 M sodium hydroxide, and diluted with Milli-Q water. Sodium borate buffers were filtered with a Whatman (0.2 μm) or Millex GP syringe filter (0.22 μm). A 1.33 wt/vol% glucosamine solution in Milli-Q water was prepared for a control experiment.

Preparation of chitosan films

Chitosan films were cast from acetic acid dispersion according to a protocol adapted from Gartner et al. [3]. A 1.7 wt% chitosan suspension in a 2 wt% acetic acid aqueous dispersion was produced by stirring for 5 days at room temperature in the dark. The dispersion was centrifuged at 1,076×*g* and 23 °C for 1 h, and the precipitate discarded before 10-mL aliquots of the suspension were cast in 9 cm diameter plastic Petri dishes at room temperature. The resulting chitosan films were clear, colorless, and 20 to 40 μm thick (ESM Fig. S2).

Peptide grafting onto chitosan films

The grafting protocol was adapted from Cheng and Cao (ESM Fig. S3) [19]. Briefly, EDC-HCl (3 mg, 3.13 mM), NHS (2 mg, 3.48 mM), and peptide (RGDS, 1 mg, 0.46 mM) were stirred in 5 or 10 mL PBS for 15 min at room temperature (except for the films Grafted-18h and Grafted-18h-d, for which the reaction medium was stirred for 5 min). The mixture was then poured into a glass Petri dish (9 or 5 cm diameter for 10- or 5-mL reaction medium, respectively) containing 10×1 cm^2 chitosan films (total 10 cm^2) (Table 1) covered with Parafilm and placed on a shaker for up to 18 h at room temperature (shaking exposes both surfaces of the film to the reaction medium). Aliquots of 50 μL were removed from the reaction medium at the commencement of the reaction and at variable intervals and analyzed via CE within 15 min after removal. Chitosan films were subsequently rinsed with PBS and Milli-Q water then left to dry and stored in a −20 °C freezer. In one control experiment (Control-NoFilm), no chitosan film was used and RGDS was grafted instead on glucosamine (0.74 M) with EDC-HCl and NHS, as described above for all parameters other than chitosan and glucosamine (Table 1).

Monitoring peptide grafting via CE

Free-solution CE experiments were carried out using an Agilent 7100 CE (Agilent Technologies, Waldbronn, Germany) instrument equipped with a diode array detector. Polyimide-coated fused silica high sensitivity capillaries (50 μm internal diameter) were purchased from Agilent. The electrolyte was sodium borate (75 mM, pH 9.2). The capillary

Table 1 Chitosan samples (films were 10 cm^2 films unless otherwise stated)

Sample	Description
Powder	Chitosan powder—used as received
Non-treated	Films, untreated
Control-soaked	Films gently shaken for 2 h in 10 mL PBS
Neutralized	Films immersed in 1 vol% NaOH aqueous solution, then washed thoroughly with Milli-Q water
Ethanol-washed	Films gently shaken for 2 h in 10 mL PBS, then washed with 0.1 M ethanol in Milli-Q water, fresh PBS, and Milli-Q water
Grafted-2h, Grafted-2h-d (duplicates)	Films gently shaken for 2 h in 10 mL PBS, then immersed in 10 mL reaction medium containing RGDS, NHS, and EDC-HCl for up to 2 h, then washed with fresh PBS and Milli-Q water
Grafted-3h, Grafted-3h-d (duplicates)	Films gently shaken for 2 h in 10 mL PBS, then immersed in 5 mL reaction medium containing RGDS, NHS, and EDC-HCl for 3 h covered with Parafilm, then washed with fresh PBS and Milli-Q water (9 and 8 cm^2 films, respectively)
Grafted-18h, Grafted-18h-d (duplicates), Grafted-18h-r1, and Grafted-18h-r2 (replicates)	Films gently shaken for 2 h in 10 mL PBS, then immersed in 5 mL reaction medium containing RGDS, NHS, and EDC-HCl for up to 18 h covered with Parafilm, then washed with fresh PBS and Milli-Q water
Control-GLcN	10 mL of GLcN solution mixed with 2.5 mL reaction medium containing RGDS, NHS, and EDC-HCl. Solution then gently shaken for 2 h covered with Parafilm
Control-NoCoupling	Films soaked in PBS for 2 h, then immersed in 5 mL PBS containing RGDS only (no EDC-HCl or NHS) for 4 h covered with Parafilm
Control-NoFilm	5 mL reaction medium containing RGDS, NHS, and EDC-HCl for 4 h but no chitosan film

(43.5 cm total length, 35 cm effective length) was pretreated by a 10 min flush with NaOH (1 M) and then 5 min successive flushes with NaOH (0.1 M), Milli-Q water, and sodium borate (75 mM, pH 9.2). The capillary surface was regenerated between separations through a 1 min flush with NaOH (1 M) then a 5 min flush with sodium borate (75 mM, pH 9.2). All injections were hydrodynamic, i.e., pressure (30 mbar) was applied for 10 s. Detection was set at 195 nm. Separation was obtained applying 30 kV at 25 °C. Each injected solution contained 0.22 vol% DMSO as an electroosmotic flow marker. An oligoacrylate with a known separation [36] and a broad range of mobilities was injected to validate the capillary and the instrument before each session.

The peptide consumption was calculated by determining the area under the curve of the identified RGDS peak divided by the migration time at each time interval and then normalizing it to the area determined for the aliquot just before the peptide mixture was introduced to the chitosan films.

Solid-state NMR spectroscopy

Chitosan powder was packed as received from the manufacturer into a 4 mm outer diameter rotor (with 3 mm internal diameter), and 10×1 cm^2 films were stacked and rolled to be packed into a 4 mm outer diameter rotor (with 2.5 mm internal diameter). This method of rotor packing was used for Non-treated, Control-soaked, Neutralized, Ethanol-washed, Grafted-2h, and Grafted-2h-d films. Grafted-18h-r1 films were cut into small circles using a hole punch and then stacked in a 4 mm outer diameter rotor (with 2.5 mm internal diameter). The 10×1 cm^2 fresh (wet) Grafted-18h films and control-soaked films were swollen with fresh PBS buffer by soaking for 1 h, stacking, and then rolling to be packed in a 4 mm outer diameter rotor (with 3 mm internal diameter). Additional PBS was added to the rotors, and films were left to soak for a half hour.

The ^{13}C cross-polarization (CP) and ^{1}H and ^{13}C single-pulse excitation (SPE) NMR spectra were recorded under MAS on a Bruker DPX200 spectrometer operating at 200 and 50 MHz Larmor frequencies for ^{1}H and ^{13}C, respectively. A commercial double resonance probe supporting high-speed zirconia MAS rotors with a 4 mm outer diameter was used at a spinning frequency of 10 kHz. The ^{1}H MAS NMR spectra were recorded with a 3 s relaxation delay and 64 scans. For ^{13}C NMR experiments, ^{1}H decoupling was used during the acquisition. The ^{13}C CP-MAS NMR spectra [3] were recorded with a 2 ms contact time and a 5 s relaxation delay, 10,240 scans for the

powder and 20,480 scans for the films (Non-treated, Control-soaked, Neutralized, Ethanol-washed, Grafted-2h, Grafted-3h, Grafted-18h-r1). The ^{13}C SPE-MAS NMR spectra were recorded with a 5 s relaxation delay and 61,945 scans for the powder and the same films (102,400 scans for Grafted-18h-r1). The ^{13}C CP-MAS NMR spectra of swollen films were recorded with a 0.2 ms contact time and a 3 s relaxation delay, 56,896 scans for control-soaked and 81,920 scans for Grafted-18h. The ^{13}C SPE-MAS NMR spectra of swollen films were recorded with a 3 s relaxation delay and 112,640 scans for control-soaked and Grafted-18h. The ^{1}H and ^{13}C pulses were calibrated with adamantane and a mixture of 3 singly ^{13}C labeled alanines. The ^{1}H and ^{13}C chemical shift scales were externally referenced to tetramethylsilane (TMS) at 0.0 ppm using adamantane by setting the CH resonance to 1.64 and 38.5 ppm, respectively [37].

Cell culture

The ARPE-19 (retinal pigment epithelial) and FHL124 (lens epithelial) cell lines used here were obtained from the American Type Culture Collection, and all cell culture [38, 39] was performed in a Class II Biological Safety Cabinet (Gelaire, Sydney, Australia). Cultured cells were maintained in DMEM containing 10 % fetal bovine serum and 1× penicillin/streptomycin (Life Technologies, Australia) using a Heracell 150 CO_2 incubator set at 37 °C with an atmosphere of 5 % CO_2 (ThermoFisher Scientific, Melbourne, Australia). Cells were passaged every 7 days as single cells using TrypLE (Life Technologies) and plated onto tissue culture plastic. For experiments, cells were plated at a density of 7×10^5 in 24-well plates either onto tissue culture plastic, 1 cm^2 non-grafted chitosan film, or 1 cm^2 RGDS peptide-grafted chitosan film. Imaging was performed using an Olympus CKX41 inverted microscope, digital camera (Olympus, Melbourne, Australia), and QCapture Pro™ 6 software (QImaging, Sydney, Australia).

RNA purification and PCR

RNA was harvested from cells using an ISOLATE RNA Purification Kit (Bioline, Australia) and complementary DNA (cDNA) produced via reverse transcription (Bioline). Polymerase chain reaction (PCR) [38, 39] was performed for key transcription factors known to be expressed by ARPE-19 cells; PAX6 and MITF use the following primers: PAX6 Fwd CCCCACATATGCAGACACAC, PAX6 Rev TCAC TTCCGGGAACTTGAAC; MITF Fwd CGAAAGTTGC AACGAGAACA, MITF Rev GAGCCTGCATTTCAAGTT CC. PCR amplification was performed using an Eppendorf AG thermocycler (Hamburg, Germany) and involved 45 cycles of 95 °C, 30 s; 55 °C, 30 s; and 72 °C, 45 s. PCR products were separated on a 2 wt/vol% agarose/TAE gel and imaged via a GelDock transilluminator (BioRad, Australia).

Results and discussion

Monitoring the grafting by free-solution CE

The peptide RGDS was grafted onto chitosan films with the aim to provide improved cell adhesion and proliferative properties compared to non-grafted chitosan films. Amidification of the carboxylic acid groups of the peptide onto the amine moieties on the chitosan surface was obtained using EDC-HCl to activate the carboxylic acid functions, with NHS used to create a more stable intermediate [19]. As the NHS reacts with the peptide activated by EDC-HCl, a side product of 3-(((ethyl amino)(hydroxy)methylene)amino)-*N*,*N*-dimethylpropan-1-amine (EDH-HCl) is produced (ESM Fig. S3).

Separation of reactants and products

The reactants and soluble products of RGDS peptide grafting were monitored using free-solution CE in sodium borate buffer, leading to a strong electroosmotic flow (EOF, 1.99 to 3.68×10^{-6} m^2 V^{-1} s^{-1}). The pure reactants EDC-HCl, NHS, and RGDS were first injected individually (Fig. 1a). Each of the components was fully separated within 4 min, and no sample preparation was required (neither for purification nor for derivatization): this fast separation (10 min in total including

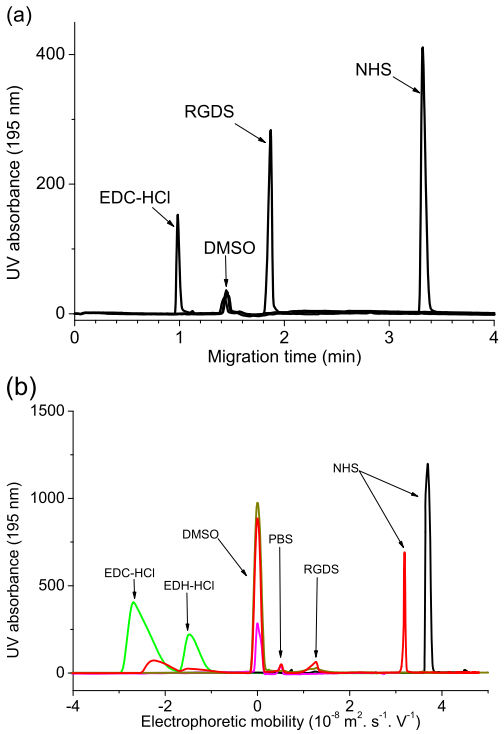

Fig. 1 Monitoring of the grafting by free-solution CE: **a** separation of reactants, injected individually, as a function of migration time and **b** electrophoretic mobility distribution of the reaction medium after 15 min reaction (*red*) and of the individual reactants (*other colors*)

Table 2 Repeatability and reproducibility of the electrophoretic mobilities of reactants and products

Compound	Repeatability RSD (%)	Reproducibility RSD (%)
EDC-HCl	6.97/3.10	5.03
EDH-HCl	5.61/3.91	4.76
PBS	12.6/3.89	8.25
RGDS	9.85/2.92	6.39
NHS	15.5/1.90	8.70

Repeatabilities for different operators are separated by a slash (n=8 for operator 1, n=15 for operator 2)

flushes) allowed real-time monitoring of the grafting reaction (Fig. 1b and ESM Fig. S5) throughout the 18 h reaction period. The positively charged ammonium group of EDC-HCl resulted in electrophoretic mobility in the same direction as the EOF, thus allowing it to migrate towards the detector the fastest. Conversely, anionic compounds under these conditions, such as NHS and the peptide RGDS, had an electrophoretic mobility in the opposite direction to the EOF (due to their hydroxyl and carboxylic acid groups, respectively) leading to a counter-EOF separation and a slower migration (ESM Fig. S4). The repeatability and reproducibility of the separation were determined (Table 2) and showed that the precision and accuracy of the electrophoretic mobility were sufficient to prevent any error in peak identification. The UV absorbance of the peptide solution increased linearly with concentration with a correlation coefficient of 0.992 (ESM Fig. S7a) thus allowing its accurate quantification. The limit of detection (LOD) was 6.0 μM, and the limit of quantification (LOQ) was 20.3 μM (ESM Fig. S7b), well below the peptide concentration in the grafting mixture that was typically around 500 μM.

Control experiments

The importance of removing acetic acid adsorbed in the chitosan films was demonstrated by failed preliminary grafting experiments (see ESM, page 4, as well as characterization by CE, see ESM Fig. S11, and by ^{1}H and ^{13}C SPE-MAS NMR spectroscopy, see ESM Fig. S14). It is also important to consider leaching of acetic acid from the chitosan films for other applications where chitosan films cast from acetic acid are used such as bioadhesives or for drug delivery. A low (3 %) yield of consumed peptide (and therefore low yield of grafting onto the chitosan films) was attributed to a competing reaction where the acetic acid was grafted onto the films instead of the RGDS. The grafting was thus repeated after rinsing the initial films in PBS. The consumption of peptide was monitored and reached 52–58 % after 4 h and 60–66 % after 18 h (Fig. 2). This compares well with the 53 and 83 % grafting determined by HPLC for photochemically grafted GRGD peptide on chitosan [20]. Rinsing the films removed excess acetic acid and

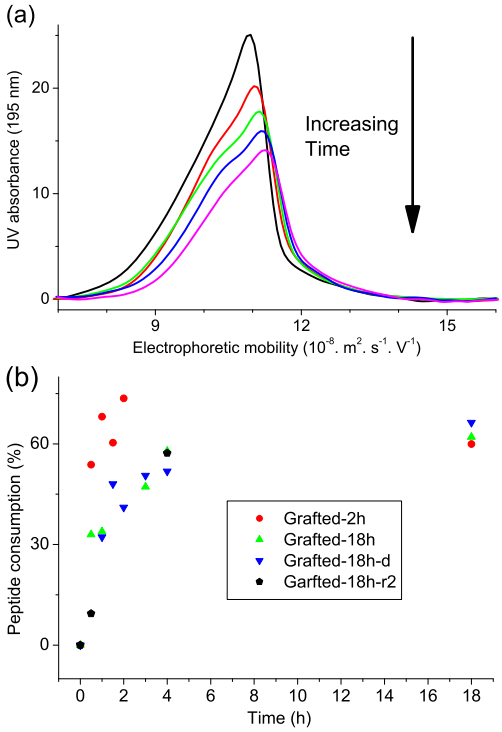

Fig. 2 **a** Electropherograms of RGDS signal showing its consumption over the reaction time in real time (*curves* are shown for 30, 60, 90, 120, 150 min reaction times, full electropherograms are in ESM Fig. S5). **b** Real-time monitoring of RGDS peptide consumption during the grafting onto chitosan films with CE (*different symbols* refer to different grafting reactions, see Table 1)

thereby prevented the competing reaction. However, as a result of soaking in PBS, the chitosan films swelled. The adsorption (and potentially absorption) of RGDS onto (into) the film could lead to peptide consumption as monitored by CE, a clearly undesirable event as covalent binding of the peptide to the film is required for optimal reproducible cell attachment. To test for adsorption/absorption, control experiments were undertaken without possible grafting or without possible adsorption/absorption by performing sham grafting experiments without the coupling agents (EDC-HCl and NHS) and without the chitosan film, respectively. The control experiment Control-NoCoupling showed peptide adsorbing onto the film (Fig. 3) but in relatively limited amounts, with less than 20 % of peptide consumption compared to 60–66 % in the presence of the coupling agents (see Fig. 2 and corresponding text below). These data demonstrate that at least two thirds of the consumed peptide was covalently grafted onto the chitosan film and not adsorbed. Moreover, when the reaction medium (not the film) was replaced with fresh PBS after 120 min, the fresh PBS monitored 42 min after replacement showed that only about 2 % of the initial peptide was released from the film (Fig. 3). This data indicated that the peptide adsorbed on the film would only be removed by a strong washing procedure.

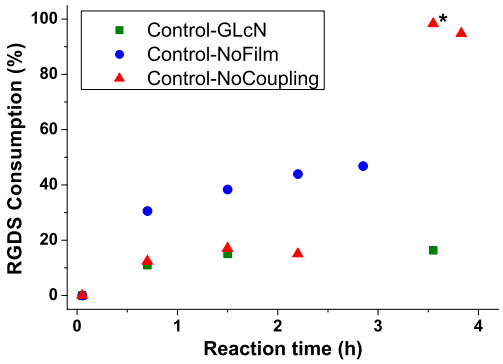

Fig. 3 RGDS consumption monitored in real time by free-solution CE in control experiments: GLcN solution (*Control-GLcN*, see electropherograms in ESM Fig. S6), RGDS with coupling agent (*Control-NoFilm*) and RGDS without coupling agent showing peptide adsorption (*Control-NoCoupling*) (Table 1). *Asterisk* indicates that the reaction medium (not the film) was replaced with fresh PBS: the high peptide consumption then was not an indication of grafting or adsorption on the film but simply an indication that all peptide was removed by taking away the reaction medium, and little peptide was released from the film into the fresh PBS

Another control was performed by replacing the chitosan film with a GLcN solution (Figs. 2 and 3). The reaction medium with GLcN showed signals with the same electrophoretic mobility as in the case of grafting to the film when monitored by CE, with additional detection of the GLcN coupled to the RGDS peptide at a lower mobility (ESM Fig. S6). In the GLcN solution, the RGDS consumption was about 16 %, whereas the peptide consumption in the presence of the film was much greater (even taking into account the adsorption onto the film, which may be up to the amount observed in the absence of the coupling agent). This indicated a higher amount of free $–NH_2$ functional groups on the film compared to the GLcN solution and also that the amount of available amine (or potentially alcohol group) may be the limiting factor in this grafting experiment. Consequently, the reactant quantities used in this study were adequate for the films and enabled the maximal possible amount of peptide to be covalently grafted onto the films. By scaling the evolution of the peak area of the peptide in the presence of GLcN to the evolution of this peak area in the presence of the film, the ratio of free amine groups between the GlcN and the chitosan film could be determined (ESM Fig. S10). This showed that the maximum amount of peptide that could be covalently bound to the chitosan surface of the film was 5,600 RGDS units per nominal nm^2 (the nominal surface largely underestimates the effective surface as discussed below). This, however, does not consider that the peptides could also be coupled to one another.

Polycondensation

The last control experiment investigated whether the RGDS polymerized through a polycondensation reaction in the (dilute and typical) conditions used. The RGDS peptide possesses one amine functional group and two different carboxylic acids per molecule; thus, it could undergo an ABB' polycondensation. Other possibilities of side reactions include degradation or precipitation. However, the disappearance or lower UV absorbance of the peptide from the reaction medium for Control-NoFilm (Fig. 3) related more to the peptide polycondensation (the peptide bonding leading to polypeptide formation). The polycondensation yielded an oligoelectrolyte or polyelectrolyte, with a nominal charge (at pH 9.2) that increased linearly with the degree of polymerization. The electrophoretic mobility of the oligoelectrolytes very likely increases with the degree of polymerization as observed for DNA (for which the degree of polymerization is often named number of base pairs) [40], oligo(styrene sulfonate) [41], and oligoacrylate [36]. If the polycondensation occurred through only one of the two carboxylic acid moieties in the RGDS, then it would form linear oligomers of RGDS (oligoRGDS). However, if both the –COOH groups were bound to $–NH_2$ of other peptides, then hyperbranched oligoRGDS would be formed. The polycondensation of RGDS was therefore analyzed (Fig. 4). The pure RGDS peptide (two carboxylic acid moieties) had an electrophoretic mobility of 2.5×10^{-8} m^2 V^{-1} s^{-1}. After 15 min of reaction, the electrophoretic mobility of the peptide peak decreased by 9 % which could be explained by an RGDS functionalized by NHS. Linear oligomers of RGDS at different degrees of polymerization likely corresponded to the small peaks at 2.8, 3.4, and 3.6×10^{-8} m^2 V^{-1} s^{-1} and would be consistent with the literature and oligoRGDS, respectively, bearing three charges (dimer), four charges (trimer), and five charges (tetramer). These peaks represented only a small percentage of the sample. After 15 min, the electrophoretic mobility of the main peptide-related peak decreased to less than half of the original value. The electrophoretic mobility of the main peak (0.3 to 1×10^{-8} m^2 V^{-1} s^{-1} after 15 min) was too low to correspond to linear oligoRGDS or polyRGDS chains of higher degrees of

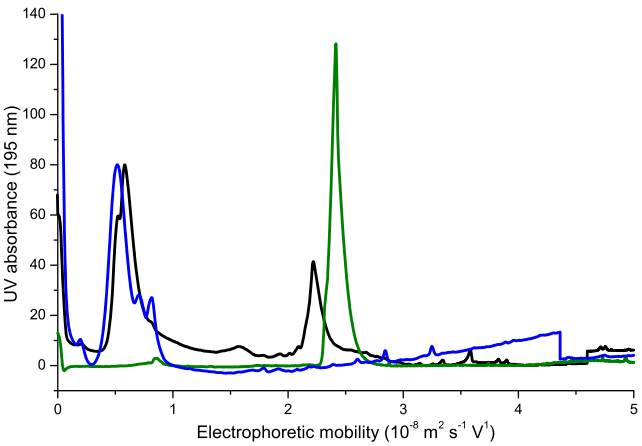

Fig. 4 Electropherograms of pure RGDS (*green*) and of the reaction medium initially containing RGDS, EDC-HCl, and NHS, also containing oligo/polyRGDS after 15 min (*black*) and 75 min (*blue*) reaction

polymerization. A decrease in electrophoretic mobility can also be caused by branching in the macromolecular structure, as observed for dendrimers [42] and hyperbranched polymers [43]. In addition, the low RGDS concentration did not favor the obtainment of high molecular weights (polymers). The RGDS polycondensation thus likely led to branched oligoRGDS. The electrophoretic mobility of the oligoRGDS peak during the grafting process (1.1×10^{-9} m^2 V^{-1} s^{-1}, Fig. 2a) was observed to be significantly lower than that of RGDS (2.4×10^{-9} m^2 V^{-1} s^{-1}, Fig. 4). This polypeptide formation results in some heterogeneity on the surface of the grafted chitosan film since the grafted oligoRGDS have a distribution of molecular weights as well as likely a distribution of branching topologies. Importantly, the formation of the oligoRGDS could increase the accessibility of RGDS to cells should the peptides be grafted in nanometric crevices of the chitosan film.

Peptide quantification

The quantification of the peptide by CE exhibited a good repeatability (Table 2). The grafting as monitored by CE first appeared to be poorly reproducible (see data recorded for Grafted-2h and Grafted-2h-d in ESM Fig. S8). This was attributed to the polycondensation, evidenced above, continuing during the storage of aliquots of the reaction medium before their analysis by CE. The grafting was therefore monitored in real time with the aliquots injected into the capillary less than 15 min after sampling. The grafting was then observed to be reproducible from film to film, although some small variations were still observed (Fig. 2b). Online monitoring of the grafting, as developed for fermentation processes [44], would lead to an even more accurate monitoring. This is however beyond the scope of this work, for which our offline monitoring was of sufficient accuracy to optimize the grafting process.

The consumption of both EDC-HCl and NHS was also calculated and compared to the peptide consumption (ESM Fig. S9) with the EDC-HCl consumption showing a somewhat greater variability compared to the peptide consumption. EDC-HCl consumption also reached a point (at 18 h) where it was not detected anymore. This was potentially due to adsorption of EDC-HCl onto the capillary (due to the positive charge of the capillary and the negative zeta potential of the EDC-HCl) as well as the slow hydrolysis of EDC-HCl in the aqueous medium. By comparison, the concentration of NHS within the reaction mixture was determined with greater precision than that of EDC-HCl. This was expected since the NHS charge is the same as that of the capillary wall, minimizing adsorptive interactions. However, NHS consumption cannot be used to indicate peptide grafting, as NHS is regenerated to its original structure after reaction with RGDS. Together, these data indicate that the RGDS signal was the most appropriate to use for a robust, real-time monitoring of peptide consumption via CE during the grafting experiments.

Reaction monitoring

The amount of peptide used in comparison to the amount of chitosan film used was taken from values obtained from literature [19]. The reaction was continued for at least 18 h, with no significant increase in the amount of grafted peptide observed compared to 4 h of reaction (Fig. 2b). The maximal possible extent of grafting was thus achieved in 4 h in these conditions. Several factors might have influenced the grafting efficiency on different films (Fig. 2b). Assuming that the amount of grafted RGDS equals the amount of RGDS consumed during the CE monitoring, then the 60–66 % yield corresponded to 417–460 RGDS peptide units per nominal nm^2. Taking into account the control data showing RGDS adsorption in the absence of the coupling reagents, the percentage of RGDS calculated as grafted to the surface was reduced to 43–49 % of the initial RGDS. This corresponded to 280–320 RGDS molecules per nominal nm^2 or about 5.10^{-8} mol cm^{-2}. This is more than one order of magnitude higher than the grafting of 10^{-9} mol cm^{-2} determined by AAA for the grafting of GRGDS through its amine function on modified (carboxylated) chitosan [45]. The discrepancy between the two grafting assessments is likely explained by the different grafting procedures or by an underestimate of the grafting with AAA. The data shown here indicate that the effective surface of the film (including surface roughness) has to be at least two orders of magnitude larger than the nominal one (i.e., the surface of a perfectly smooth film of equivalent dimensions). Note that oligoRGDS chains of a few RGDS units are grafted rather than individual RGDS peptides which only reduces the number of grafted molecules by a small factor, not an order of magnitude. Since the chitosan films were not cast in a controlled environment (e.g., humidity, temperature), they might have exhibited variations in their surface roughness that could have resulted in the films having different actual surface areas for the same nominal surface area (and thus different grafting efficiencies). To examine this, the film surface before grafting was observed via scanning electron microscopy (SEM) (ESM Fig. S12). From this data, the film surfaces appeared relatively flat and homogeneous on the micrometer scale (the micrometric indentations and ripples observed in ESM Fig. S12b are not present throughout the entire films and are an indication of the film drying process). Higher resolution SEM to better resolve the surface of the films was not possible due to film melting caused by the electron beam (ESM Fig. S12c). The homogeneous, even, and non-porous topography of the films on the micrometer scale is beneficial as it provides an even surface area for substantial cell adhesion. However, the structure of the films surface may be different at the nanometer scale, which is relevant

for the peptide grafting (RGDS only has four amino acids; thus, RGDS or its oligomers cannot be resolved at the micrometer scale). Spectroscopy-based techniques were thus used to assess the presence of the peptides on the grafted films.

Characterization of the films by FT-IR and solid-state NMR

To complement the indirect measurement of peptide grafting onto the film with a direct measurement, solid-state characterization methods were used. Attenuation total reflectance infrared (ATR IR) analysis was first chosen as it provides a fast and simple spectroscopy method compared to other methods such as solid-state NMR (i.e., ATR IR requires no tedious sample packing and only takes several minutes). The free amine groups and their disappearance through grafting have previously been detected by other groups using IR [22], while the amide on GRGD peptide has previously also been selectively detected [20]. The ATR IR spectra of chitosan powder and films (ESM Fig. S13) were in agreement with those shown in the literature, confirming the molecular structure of the chitosan used [46]. The RGDS grafted onto the chitosan films (expected at 1,566 and 1,414 cm^{-1} [18]) could not be detected here using ATR IR spectroscopy because of insufficient resolution (overlap of chitosan and peptide signals) or of insufficient sensitivity (due to the limited peptide quantity relative to the chitosan which constitutes the bulk of the films). The free amine group on the chitosan films could not be detected, as shown by comparison with the IR spectrum of glucosamine, and may indicate their involvement in extensive hydrogen bonding.

Due to the limited data obtained through ATR IR, solid-state NMR was performed. ^{13}C NMR spectra of chitosan Control-soaked film (ESM Fig. S14) corresponded to those found in the literature and confirmed the chitosan molecular structure [3, 31]. The ^{13}C SPE-MAS NMR spectra of the samples Control-soaked and Grafted-3h (ESM Fig. S15) showed no significant difference and therefore no indication of RGDS grafted onto the chitosan film. This may have been due to the low concentration of peptide within the samples. Attempts to increase the films' packing into the rotor by stacking discs of films instead of rolling the films, by altering the contact time and relaxation delays, and by significantly increasing the number of scans were unsuccessful at detecting the peptide's signals. However, swelling the chitosan films with PBS yielded spectra with increased resolution via increased molecular dynamics. Note that sample swelling also introduces a likely heterogeneity of chain dynamics and relaxation behaviors in the samples, rendering any quantification hazardous even with long relaxation delays; for that reason, shorter relaxation delays were chosen to increase sensitivity of the ^{13}C NMR experiments. The ^{1}H MAS NMR spectrum of Grafted-18h films swollen with PBS revealed two additional peaks, at 1.3 and 4.72 ppm, compared to that of the Control-soaked films swollen with PBS (Fig. 5). The peak at 4.72 ppm was assigned to the α-H of aspartic acid of RGDS (in agreement with the reported value of 4.75 ppm [47]). Although the reported signal assignment of RGDS was sparse and incomplete, a ChemNMR estimation yielded a ^{1}H NMR signal for β-H of arginine at 1.55 ppm which is in agreement with the peak observed at 1.3 ppm. ChemNMR estimations yielded a signal at 4.86 ppm corresponding to the α-H of aspartic acid. The slight difference in chemical shift could be accounted for by molecular packing effects experienced in solid-state NMR spectroscopy [48]. The discussion above assumes that the grafting occurred on the amine groups of the chitosan. Estimations by ChemNMR for grafting occurring at the alcohol groups of the chitosan yielded signals at 1.55, 4.86, and 4.62 ppm (ESM Fig. S17), where the signal at 4.62 ppm was assigned to the α-H of serine and could also account for the signal observed at 4.72 ppm. However, the signal observed at 4.62 ppm was broad, and the assignment could belong to either signal yielded from the ChemNMR estimations, with no significant difference to determine which grafting site was favored. Furthermore, ^{1}H NMR signals are reported at 0.9 ppm and between 2 and 4 ppm for the coupling agent

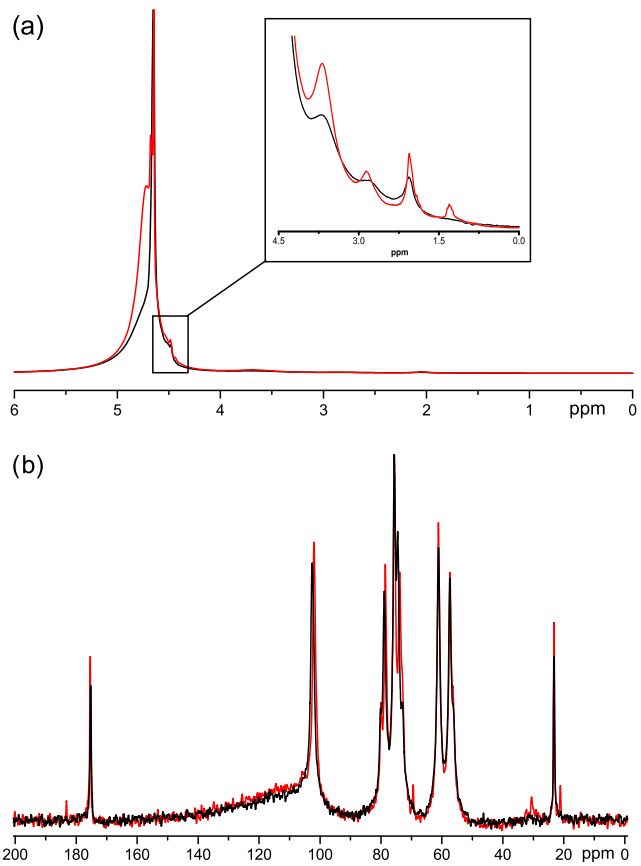

Fig. 5 NMR spectra of Grafted-18h (*red line*) and Control-soaked (*black line*) films swollen with PBS: **a** ^{1}H MAS NMR spectra, with *inset* showing a magnification of spectra between 0 and 4.5 ppm, and **b** ^{13}C-SPE-MAS NMR spectra

EDC-HCl [49], at 2.79 and 4.84 ppm for NHS [50]. These signals were either absent or overlapping with the large chitosan signal in the ^{1}H MAS NMR spectrum of Grafted-18h (Fig. 5a). These data confirm that the coupling reagents were removed from the swollen films during the soakings in PBS and water after grafting.

The ^{13}C SPE-MAS NMR spectra for the Grafted-18h films swollen with PBS revealed five additional peaks, at 21.2, 30.6, 32.2, 69.4, and 183.2 ppm, compared to control-soaked films swollen with PBS (Fig. 5b). No ^{13}C NMR spectra of RGDS-grafted chitosan have been reported in the literature. However, the ^{13}C NMR signals observed after grafting in this study are in agreement with signals reported for RGDS at 24.27, 28.69, and 37.65 ppm (γ-C of arginine, β-C of arginine, and β-C of aspartic acid, respectively) [47]. The expected RGDS signals reported between 50 and 60 ppm were masked by the chitosan signals. The peak observed at 69.4 ppm was absent from both the published ^{13}C NMR spectra and the ChemNMR estimations for non-grafted RGDS. However, it was present in the ChemNMR estimation of the grafted RGDS–chitosan polymer as the RGDS α-C of serine. This confirms that RGDS peptides were covalently bound to the chitosan through the terminal carboxylic acid function as expected. Grafting at the amine functional group of the chitosan yielded a signal at 61.4 ppm, in agreement with the experimental value of 69.4 ppm. When assuming the grafting of RGDS occurred on the alcohol groups of chitosan, the signal shifted upfield slightly to 62.5 ppm which was in better agreement with the experimental value. Chitosan is expected to yield signals at similar values which were absent from both Grafted-18h and control-soaked films spectra; this can be explained by the increased dynamics of the α-C compared to the dynamics of the bulk chitosan film. The ChemNMR estimation produced peaks from 173.2 to 170.3 ppm, corresponding to the various carbonyl α-C when grafted at the amine and the alcohols. A grafting site bias between the amine and the alcohol groups cannot be conclusively determined.

A ChemNMR estimation for NHS and EDC-HCl yielded ^{13}C NMR signals at 25.7 and 169 ppm and 25.2 and 35.4 ppm, respectively, that may correspond to some of the peaks identified as RGDS. However, they do not account for the additional signals obtained in the NMR analysis of Grafted-18h films compared to the control-soaked film spectra. The ^{13}C SPE-MAS NMR spectra (Fig. 5b) cannot reveal if the EDC-HCl and NHS coupling agents were removed from the films, but this can be concluded from the ^{1}H MAS NMR (Fig. 5a). Overall, both the ^{13}C and ^{1}H NMR spectra confirmed that RGDS was successfully covalently grafted onto the chitosan films.

Cell culture

To assess whether covalent grafting of the RGDS peptide increased cell attachment to the chitosan film, ARPE-19 and FHL124 cell lines were plated onto non-grafted and grafted films. Both cell lines preferentially attached to the RGDS-grafted chitosan film compared to the non-grafted film (Fig. 6a, b). For the ARPE-19 cell line, these cells maintained their morphology and subsequently proliferated to confluence on the RGDS-grafted chitosan films similar to ARPE-19 cells cultured on tissue culture plastic (Fig. 6a, c). In contrast, the FHL124 cells attached briefly (overnight) to the grafted films but not to the non-grafted films; however, they did not proliferate to confluence and eventually detached from the film. These findings are consistent with the RGDS-grafted chitosan film mimicking fibronectin and thus being better suited to supporting the retinal ARPE-19 cell line (as fibronectin is a component of Bruch's membrane) [51] but not the lens epithelial FHL124 cell line (as laminin and collagen are the major components of the lens capsule) [52]. It should be noted that some variability in cell attachment was seen between different RGDS-grafted films. This was likely due to the expected heterogeneity in the chitosan film structure (since the films were cast from a dispersion and not a true solution) which would have then affected the uniform distribution of grafted peptides. It could also be due in part to the attachment of some RGDS peptides to the chitosan through the side chain of aspartate, which contains a carboxylic acid group, rather than through their C-terminal. The formation of longer peptide chains as a result of polycondensation would decrease the number of RGDS-containing molecules grafted onto the film, which in turn could result in incomplete coverage over the film surface.

To determine whether the ARPE-19 cells retained key molecular features after culture on the RGDS-grafted chitosan, messenger RNA (mRNA) expression of the transcription factors *PAX6* and *MITF* was assessed via RT-PCR. These data clearly show that both of these key genes remain expressed after at least 6 days of culture on the RGDS-grafted chitosan (Fig. 6d).

Conclusion

The production of chitosan films grafted with RGDS is not possible by a simple adsorption process. Alternatively, peptides such as RGDS can be covalently grafted onto free-standing chitosan films using the coupling agents EDC-HCl and NHS in one step without prior chitosan modification. The grafting takes place through the carboxylic acid functional group(s) of the peptide and the amine (or alcohol) functional groups on the chitosan surface. This grafting should be monitored in real time, and this can be achieved using free-solution CE. CE can separate all reactants and products in only 10 min, and it requires no sample preparation: it is thus an ideal indirect technique for real-time monitoring of the grafting process. The data presented here revealed that adsorption of RGDS

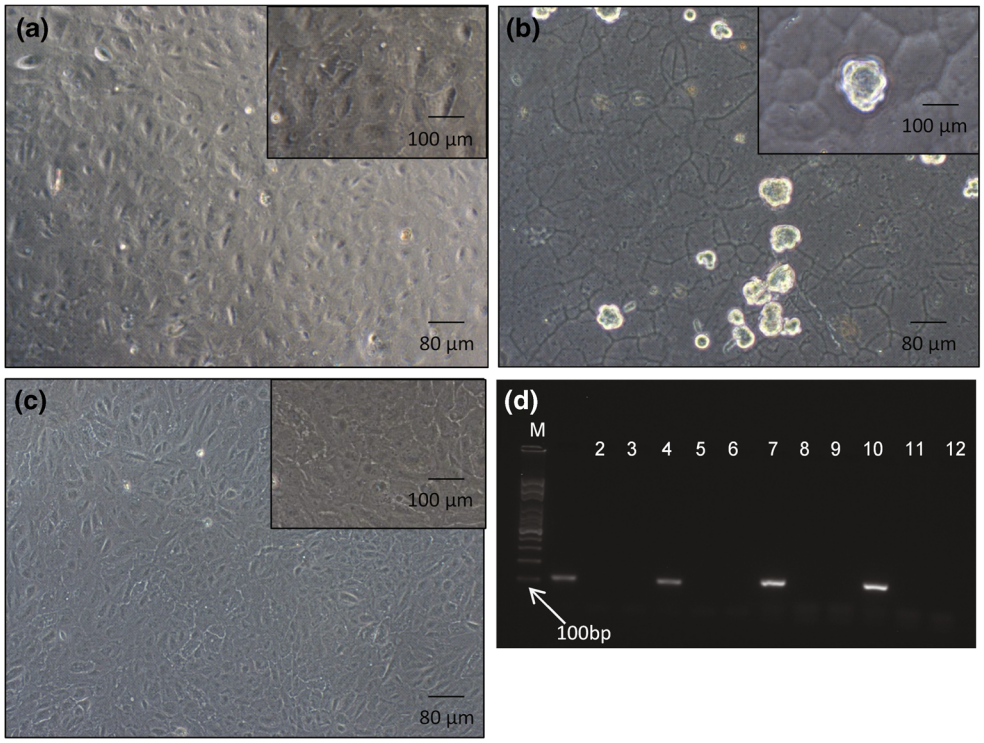

Fig. 6 Phenotypic characterization of chitosan-cultured cells. **a** ARPE-19 cells attached and proliferated to confluence on RGDS-grafted chitosan films. **b** ARPE-19 did not attach to the non-grafted chitosan. **c** Control ARPE-19 cells plated onto tissue culture plastic (**a** to **c**: images shown were taken 7 days after cell seeding, and the *insets* show a higher magnification). **d** Separated PCR products via agarose gel electrophoresis showing expression of control ARPE-19 cells cultured on plastic for 6 days for *PAX6* (*lane 1*) and *MITF* (*lane 7*) and cultured for 6 days on RGDS-grafted films for *PAX6* and *MITF* (*lanes 4 and 10*, respectively). All amplicons were of the expected size as shown by comparison with the nucleotide marker (*M*). The control PCR reactions (shown in *lanes 2*, *3*, *5*, *6*, *8*, *9*, *11*, and *12*) indicate that the detected *PAX6* and *MITF* amplicons did not arise from contaminating genomic DNA or DNA-contaminated reagents

peptide on the chitosan film takes place but is not the main method of RGDS attachment to the chitosan. While covalent grafting had been considered as a "more involved process" than adsorption [11], it was shown in the present work that grafting directly on the amine of the chitosan allows for a simple covalent grafting method. Side reactions of the RGDS peptide, such as polycondensation, are significant in the absence of chitosan film, and it is thus important to monitor the grafting in real time to obtain accurate results. The ^{1}H and ^{13}C NMR spectroscopy of the swollen films directly demonstrated the covalent grafting of RGDS onto the film. All available free amine (alcohol) functional groups on the chitosan film surface had reacted, leading to a high density of RGDS on the surface. The RGDS was present in the form of (likely branched) oligomers of RGDS. The SEM data indicated the RGDS-grafted films had a flat surface on the micrometer (cell) scale, but nanometric-scale crevices likely exist [53]. Given the approximate 5–10 µm diameter of the ARPE-19 and FHL124 cells used here, these nanometer-scale crevices would be inaccessible for cell attachment. Considering the order of magnitude difference between the size of a cell and the size of the RGDS, the formation of oligoRGDS might help bring a higher number of RGDS moieties in contact with the cells, rather than being inaccessible in nanometric crevices. However, the surface of the films may also present some chemical heterogeneity with zones richer in acetyl groups, thus poorer in free amine groups on which RGDS grafting occurs. This could account for some of the inter-film cell attachment variability seen.

Further development of chitosan films could be undertaken by casting them from solutions or other dispersions, in order to circumvent potential differences in surface roughness and surface chemical heterogeneity between films and thereby produce films with a more homogeneous/accessible peptide grafting surface for cell attachment. Film preparation prior to grafting could also be completed to deacetylate the surface of the films; this could increase the number of active sites available for peptide attachment in order to further decrease variability in cell attachment. The use of isotopically labeled peptides would increase the sensitivity for the detection and quantification of peptide grafting through NMR spectroscopy. Further studies of the chitosan film itself could be carried out by ^{13}C and ^{15}N MAS NMR spectroscopy [3]. While both ARPE-19 and FHL124 are ocular cell lines, they are derived from different tissues that require different extracellular matrix interactions. This was supported by the ability of the ARPE-19

cells, but not the FHL124 cells, to attach and proliferate on the RGDS-grafted chitosan. Thus, the above CE-based method will enable future chitosan films to be optimized for attachment by particular cell types, through the ability to monitor in real time the attachment of different extracellular matrix peptide mimetics. Importantly, these peptide mimetics can be chosen based on the in vivo extracellular matrix requirements for the particular cell type(s) of interest.

Acknowledgments CL, MO'C, and MG thank the University of Western Sydney for an International Research Initiatives Scheme (IRIS) grant. Mariam Mnatsakanyan (UWS) is thanked for the production of some of the chitosan films. We would like to acknowledge the Advanced Materials Characterisation Facility (AMCF) of UWS for assistance and access to the instrumentation.

Conflict of interest The authors declare that they have no conflict of interest.

References

1. Dash M, Chiellini F, Ottenbrite RM, Chiellini E (2011) Chitosan-A versatile semi-synthetic polymer in biomedical applications. Prog Polym Sci 36:981–1014
2. Domard A (2011) A perspective on 30 years research on chitin and chitosan. Carbohydr Polym 84:696–703
3. Gartner C, Lopez BL, Sierra L, Graf R, Spiess HW, Gaborieau M (2011) Interplay between structure and dynamics in chitosan films investigated with solid-state NMR, dynamic mechanical analysis, and X-ray diffraction. Biomacromolecules 12:1380–1386
4. Rinaudo M (2006) Chitin and chitosan: properties and applications. Prog Polym Sci 31:603–632
5. Martínez-Camacho AP, Cortez-Rocha MO, Ezquerra-Brauer JM, Graciano-Verdugo AZ, Rodriguez-Félix F, Castillo-Ortega MM, Yépiz-Gómez MS, Plascencia-Jatomea M (2010) Chitosan composite films: thermal, structural, mechanical and antifungal properties. Carbohydr Polym 82:305–315
6. Shi CM, Zhu Y, Ran XZ, Wang M, Su YP, Cheng TM (2006) Therapeutic potential of chitosan and its derivatives in regenerative medicine. J Surg Res 133:185–192
7. Bodnar M, Hartmann JF, Borbely J (2005) Preparation and characterization of chitosan-based nanoparticles. Biomacromolecules 6: 2521–2527
8. Wise JK, Alford A, Goldstein S, Stegemann JP (2014) Comparison of uncultured marrow mononuclear cells and culture-expanded mesenchymal stem cells in 3D collagen-chitosan microbeads for orthopaedic tissue engineering. Tissue Eng A 20:210–224
9. de la Mata A, Nieto-Miguel T, López-Paniagua M, Galindo S, Aguilar MR, García-Fernández L, Gonzalo S, Vázquez B, Román JS, Corrales RM, Calonge M (2013) Chitosan-gelatin biopolymers as carrier substrata for limbal epithelial stem cells. J Mater Sci Mater Med 24:2819–2829
10. Chien Y, Liao YW, Liu DM, Lin HL, Chen SJ, Chen HL, Peng CH, Liang CM, Mou CY, Chiou SH (2012) Corneal repair by human corneal keratocyte-reprogrammed iPSCs and amphiphatic carboxymethyl-hexanoyl chitosan hydrogel. Biomaterials 33:8003–8016
11. Jiang T, Kumbar SG, Nair LS, Laurencin CT (2008) Biologically active chitosan systems for tissue engineering and regenerative medicine. Curr Top Med Chem 8:354–364
12. Li Z, Leung M, Hopper R, Ellenbogen R, Zhang M (2010) Feeder-free self-renewal of human embryonic stem cells in 3D porous natural polymer scaffolds. Biomaterials 31:404–412
13. Shekaran A, Garcia AJ (2011) Nanoscale engineering of extracellular matrix-mimetic bioadhesive surfaces and implants for tissue engineering. Biochim Biophys Acta Gen Subj 1810:350–360
14. Gristina A (1987) Biomaterial-centered infection: microbial adhesion versus tissue integration. Science 237:1588–1595
15. Boateng SY, Lateef SS, Mosley W, Hartman TJ, Hanley L, Russell B (2005) RGD and YIGSR synthetic peptides facilitate cellular adhesion identical to that of laminin and fibronectin but alter the physiology of neonatal cardiac myocytes. Am J Physiol Cell Physiol 288:C30–38
16. Smith E, Yang J, McGann L, Sebald W, Uludag H (2005) RGD-grafted thermoreversible polymers to facilitate attachment of BMP-2 responsive C2C12 cells. Biomaterials 26:7329–7338
17. Custodio CA, Alves CM, Reis RL, Mano JF (2010) Immobilization of fibronectin in chitosan substrates improves cell adhesion and proliferation. J Tissue Eng Regen Med 4:316–323
18. Karakecili AG, Gumusderelioglu M (2008) Physico-chemical and thermodynamic aspects of fibroblastic attachment on RGDS-modified chitosan membranes. Colloids Surf B: Biointerfaces 61: 216–223
19. Cheng N, Cao XD (2011) Photosensitive chitosan to control cell attachment. J Colloid Interface Sci 361:71–78
20. Chung TW, Lu YF, Wang SS, Lin YS, Chu SH (2002) Growth of human endothelial cells on photochemically grafted Gly-Arg-Gly-Asp (GRGD) chitosans. Biomaterials 23:4803–4809
21. Han HD, Mangala LS, Lee JW, Shahzad MMK, Kim HS, Shen D, Nam EJ, Mora EM, Stone RL, Lu C, Lee SJ, Roh JW, Nick AM, Lopez-Berestein G, Sood AK (2010) Targeted gene silencing using RGD-labeled chitosan nanoparticles. Clin Cancer Res 16:3910–3922
22. Ho MH, Wang DM, Hsieh HJ, Liu HC, Hsien TY, Lai JY, Hou LT (2005) Preparation and characterization of RGD-immobilized chitosan scaffolds. Biomaterials 26:3197–3206
23. Hansson A, Hashom N, Falson F, Rousselle P, Jordan O, Borchard G (2012) In vitro evaluation of an RGD-functionalized chitosan derivative for enhanced cell adhesion. Carbohydr Polym 90:1494–1500
24. Shi ZL, Neoh KG, Kang ET, Poh C, Wang W (2008) Bacterial adhesion and osteoblast function on titanium with surface-grafted chitosan and immobilized RGD peptide. J Biomed Mater Res A 86A: 865–872
25. Kašička V (2012) Recent developments in CE and CEC of peptides (2009–2011). Electrophoresis 33:48–73
26. Bao JJ (2000) Separation of proteins by capillary electrophoresis using an epoxy based hydrophilic coating. J Liq Chromatogr Relat Technol 23:61–78
27. Geiger M, Hogerton AL, Bowser MT (2011) Capillary electrophoresis. Anal Chem 84:577–596
28. Oliver JD, Gaborieau M, Hilder EF, Castignolles P (2013) Simple and robust determination of monosaccharides in plant fibers in complex mixtures by capillary electrophoresis and high performance liquid chromatography. J Chromatogr A 1291:179–186
29. Thevarajah JJ, Gaborieau M, Castignolles P (2014) Separation and characterization of synthetic polyelectrolytes and polysaccharides with capillary electrophoresis. Adv. Chem. 2014:Article ID 798503
30. Mnatsakanyan M, Thevarajah JJ, Roi RS, Lauto A, Gaborieau M, Castignolles P (2013) Separation of chitosan by degree of acetylation using simple free solution capillary electrophoresis. Anal Bioanal Chem 405:6873–6877
31. Heux L, Brugnerotto J, Desbrieres J, Versali MF, Rinaudo M (2000) Solid state NMR for determination of degree of acetylation of chitin and chitosan. Biomacromolecules 1:746–751
32. Lefay C, Guillaneuf Y, Moreira G, Thevarajah JJ, Castignolles P, Ziarelli F, Bloch E, Major M, Charles L, Gaborieau M, Bertin D, Gigmes D (2013) Heterogeneous modification of chitosan via nitroxide-mediated polymerization. Polym Chem 4:322–328

33. Lee E, MacLaren RE (2011) Sources of retinal pigment epithelium (RPE) for replacement therapy. Br J Ophthalmol 95:445–449
34. Priglinger SG, Alge CS, Neubauer AS, Kristin N, Hirneiss C, Eibl K, Kampik A, Welge-Lussen U (2004) TGF-beta 2-induced cell surface tissue transglutaminase increases adhesion and migration of RPE cells on fibronectin through the gelatin-binding domain. Invest Ophthalmol Vis Sci 45:955–963
35. Olivero DK, Furcht LT (1993) Type-IV collagen, laminin, and fibronectin promote the adhesion and migration of rabbit lens epithelial-cells in-vitro. Invest Ophthalmol Vis Sci 34:2825–2834
36. Gaborieau M, Causon TJ, Guillaneuf Y, Hilder EF, Castignolles P (2010) Molecular weight and tacticty of oligoacrylates by capillary electrophoresis-mass spectrometry. Aust J Chem 63:1219–1226
37. Morcombe CR, Zilm KW (2003) Chemical shift referencing in MAS solid state NMR. J Magn Reson 162:479–486
38. Ungrin M, O'Connor M, Eaves C, Zandstra PW (2007) Phenotypic analysis of human embryonic stem cells. Curr Protoc Stem Cell Biol 1B(3):1–25
39. O'Connor MD, Wederell E, Robertson G, Delaney A, Morozova O, Poon SSS, Yap D, Fee J, Zhao YJ, McDonald H, Zeng T, Hirst M, Marra MA, Aparicio S, Eaves CJ (2011) Retinoblastoma-binding proteins 4 and 9 are important for human pluripotent stem cell maintenance. Exp Hematol 39:866–879
40. Stellwagen NC, Gelfi C, Righetti PG (1997) The free solution mobility of DNA. Biopolymers 42:687–703
41. Cottet H, Gareil P, Theodoly O, Williams CE (2000) A semi-empirical approach to the modeling of the electrophoretic mobility in free solution: application to polystyrenesulfonates of various sulfonation rates. Electrophoresis 21:3529–3540
42. Ibrahim A, Koval D, Kasicka V, Faye C, Cottet H (2013) Effective charge determination of dendrigraft poly-L-lysine by capillary isotachophoresis. Macromolecules 46:533–540
43. Maniego AR, Ang D, Guillaneuf Y, Lefay C, Gigmes D, Aldrich-Wright JR, Gaborieau M, Castignolles P (2013) Separation of poly(-acrylic acid) salts according to topology using capillary electrophoresis in the critical conditions. Anal Bioanal Chem 405:9009–9020
44. Turkia H, Holmström S, Paasikallio T, Sirén H, Penttilä M, Pitkänen J-P (2013) Online capillary electrophoresis for monitoring carboxylic acid production by yeast during bioreactor cultivations. Anal Chem 85:9705–9712
45. Li J, Yun H, Gong YD, Zhao NM, Zhang XF (2006) Investigation of MC3T3-E1 cell behavior on the surface of GRGDS-coupled chitosan. Biomacromolecules 7:1112–1123
46. Silva SML, Braga CRC, Fook MVL, Raposo CMO, Carvalho LH, Canedo EL (2012) Application of infrared spectroscopy to analysis of chitosan/clay nanocomposites. In: Theophile T (ed) Materials science. Engineering and Technology, InTech, Rijeka
47. Mickos H, Bahr J, Lüning B (1990) The three-dimensional structure of the RGD (Arg-Gly-Asp) adhesion sequence of fibronectin; NMR studies of the peptides RGDS and GRGDSP. Acta Chem Scand 44: 161–164
48. Schmidt-Rohr K, Spiess HW (1994) Multidimensional solid-state NMR and polymers. Academic Press Ltd, San Diego, USA
49. Castillo JJ, Torres MH, Molina DR, Castillo-León J, Svendsen WE, Escobar P, Martínez OF (2012) Monitoring the functionalization of single-walled carbon nanotubes with chitosan and folic acid by two-dimensional diffusion-ordered NMR spectroscopy. Carbon 50:2691–2697
50. Spectral database for organic compounds SDBS (2014) National Institute of Advanced Industrial Science and Technology, AIST, Japan. http://sdbs.db.aist.go.jp/sdbs/cgi-bin/cre_index.cgi
51. Das A, Frank RN, Zhang NL, Turczyn TJ (1990) Ultrastructural-localization of extracellular-matrix components in human retinal-vessels and Bruch's membrane. Arch Ophthalmol 108:421–429
52. Wederell ED, de Iongh RU (2006) Extracellular matrix and integrin signaling in lens development and cataract. Semin Cell Dev Biol 17: 759–776
53. Inthanon K, Saranwong N, Wongkham W, Wanichapichart P, Prakrajang K, Suwannakachorn D, Yu LD (2013) PIII-induced enhancement and inhibition of human cell attachment on chitosan membranes. Surf Coat Technol 229:112–119

Analytical and Bioanalytical Chemistry

Electronic Supplementary Material

Real-time monitoring of peptide grafting onto chitosan films using capillary electrophoresis

Danielle L. Taylor, Joel J. Thevarajah, Diksha K. Narayan, Patricia Murphy, Melissa M. Mangala, Seakcheng Lim, Richard Wuhrer, Catherine Lefay, Michael D. O'Connor, Marianne Gaborieau, Patrice Castignolles

Chitosan structure and grafting onto chitosan films

The structure of the polysaccharide chitosan includes varying proportions of D-glucosamine and *N*-acetyl-D-glucosamine (Fig. S1). A photograph of a chitosan film cast form acetic acid solution is shown on Fig. S2. The reaction scheme is shown on Fig. S3.

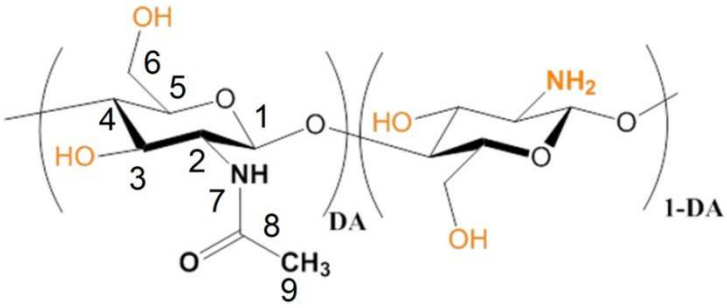

Fig. S1 Chemical structure of chitosan with a degree of acetylation DA. Chitin corresponds to DA=1

Fig. S2 Photograph of chitosan film cast from aqueous acetic acid

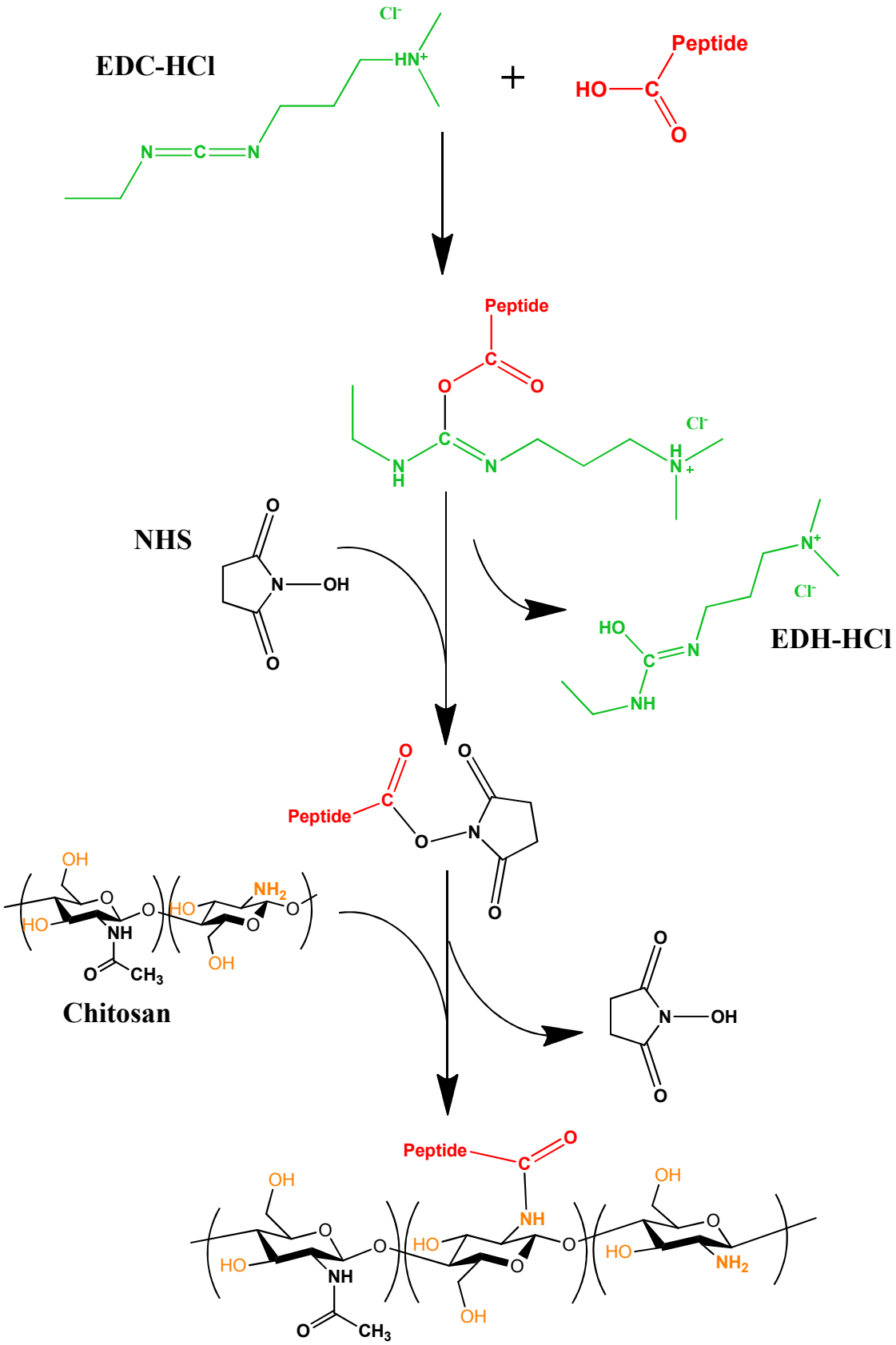

Fig. S3 Reaction scheme for peptide grafting onto chitosan film. Note: activated peptide may react with either an amine or an alcohol group of chitosan

Preliminary grafting experiments indicated that only 3 % of peptide was consumed after 2 h. These films were observed to kill cells in less than 24 h (data not shown) if not thoroughly rinsed with PBS indicating either the residual presence of reactant (EDC-HCl is cytotoxic) [1] or the release of acetic acid (as the chitosan films had been cast from suspensions in aqueous acetic acid). Acetic acid was proved to be the cause of the low grafting yield and of the cells death through its identification with capillary electrophoresis (see Fig. S11) as well as ^{1}H and ^{13}C SPE-MAS NMR spectroscopy (Fig. S14) as follows. A non-neutralized chitosan film was placed in MilliQ water: a decrease in pH from 6.00 to 5.36 was observed consistent with the release of acetic acid. This solution in which the film had been immersed was further analyzed via CE, which confirmed that the released molecule had the same electrophoretic mobility as acetic acid (see Fig. S11). Finally, ^{1}H and ^{13}C SPE-MAS NMR spectroscopy showed that the film contained acetic acid that was eliminated upon rinsing with PBS for 2 h (Fig. S14).

Capillary electrophoresis

The principle of free solution capillary electrophoresis at high pH in fused silica capillaries is given in Fig. S4, followed by a calibration curve for the RGDS quantification (Fig. S7). Fig. S8 show the results of monitoring the grafting not in real time (defined here as injecting the reaction medium more than 15 min after the aliquot was withdrawn). The consumption of peptide is compared to the one of the coupling agents on Fig. S9. Fig. S11 shows the electropherogram of solutions used to rinse the chitosan films, and the comparison with acetic acid solution.

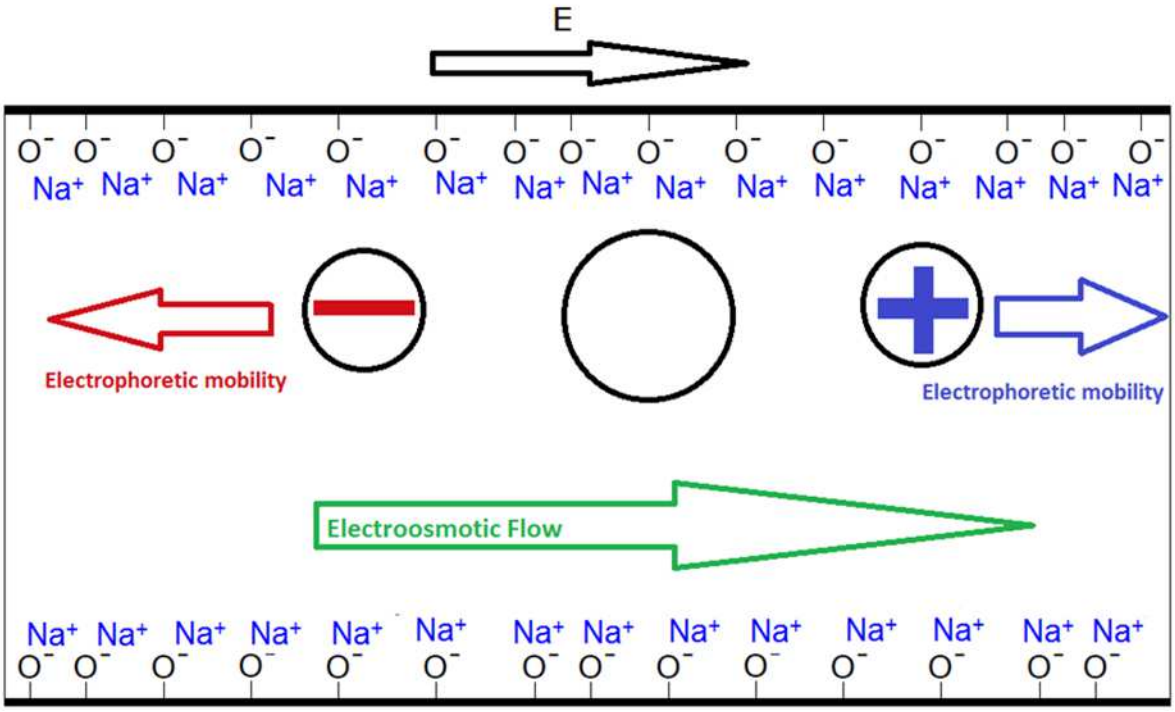

Fig. S4 Principle of the separation of compounds by their charge-to-friction ratio under basic conditions (sodium borate, pH 9.2) and a positive voltage (30 kV)

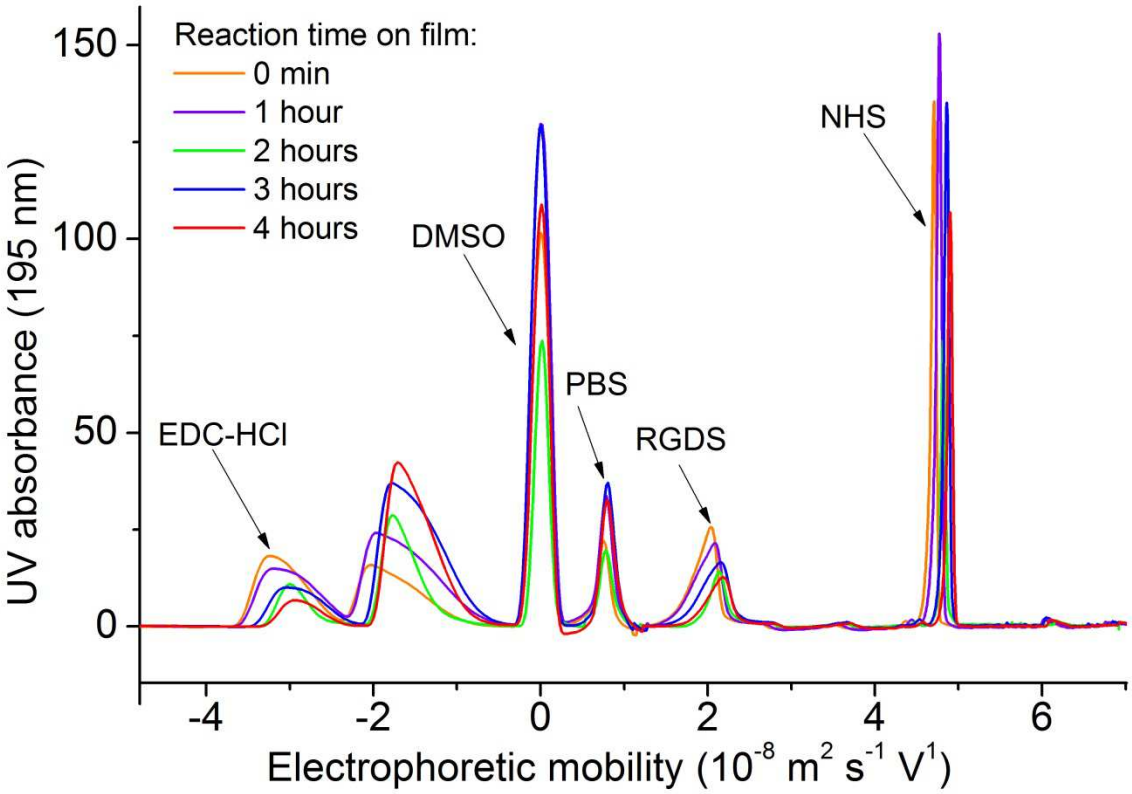

Fig. S5 Electropherograms of peptide in the reaction medium in real-time

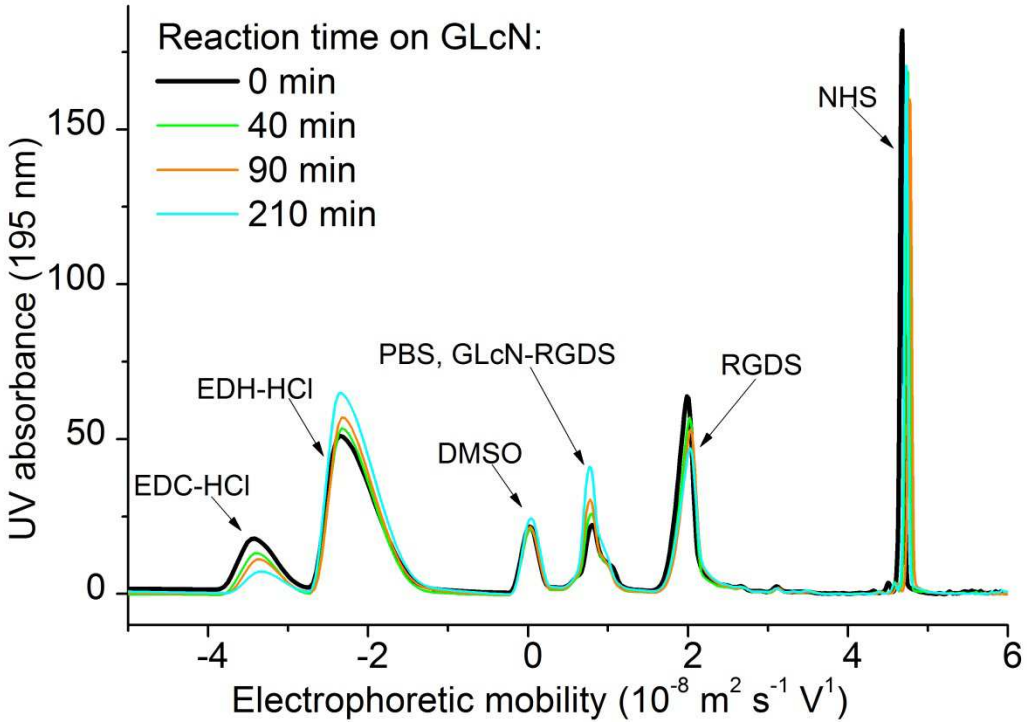

Fig. S6 Electropherograms of GLcN solution in the reaction medium in real-time. The shoulder on the right side of the PBS signal at 2.10-8 m2s-1V-1 is the signal of the GLcN grafted with RGDS

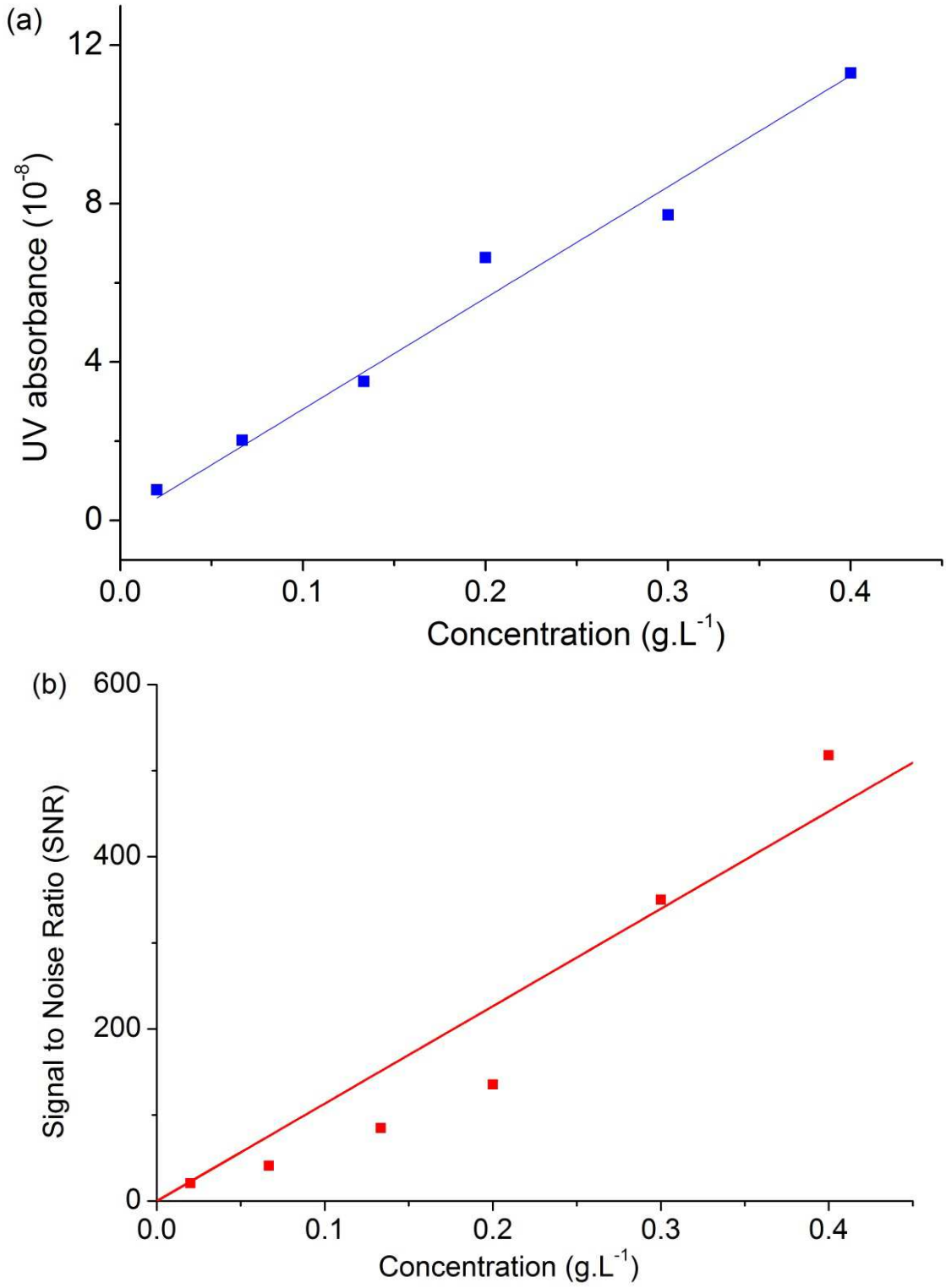

Fig S7 Calibration curves for (a) UV absorbance (abs) vs RGDS concentration: abs=2.81×10-7*concentration (R2=0.992) and (b) Signal to Noise Ratio (SNR) vs RGDS concentration: SNR=1132*concentration (R2=0.948)

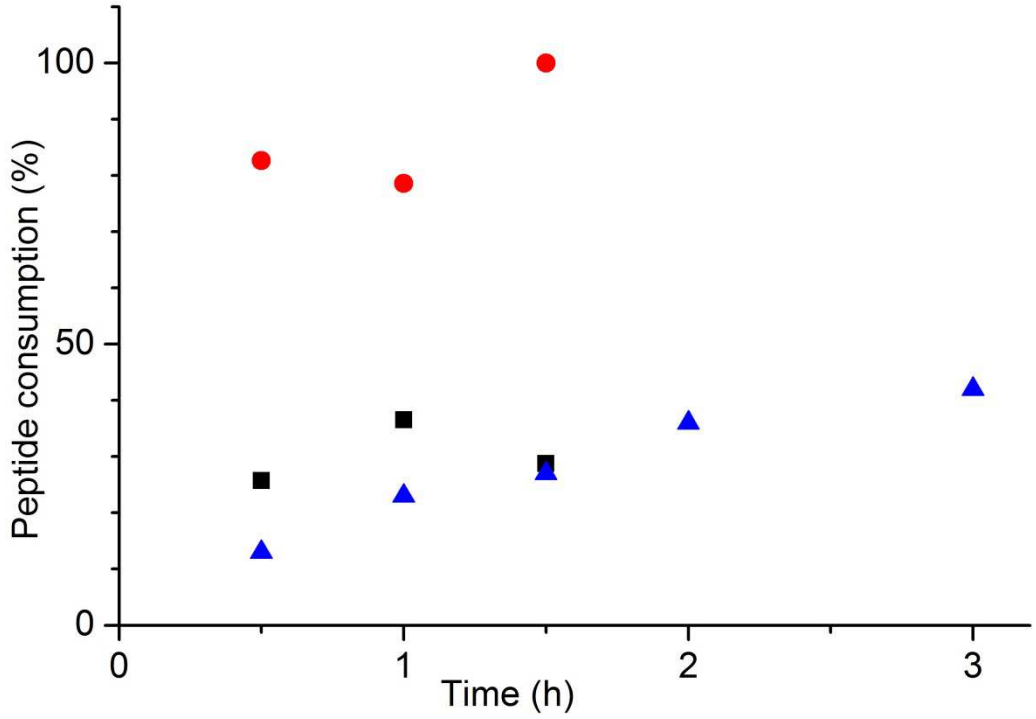

Fig. S8 Monitoring grafting not in real time: data for Grafted-2h (black squares), Grafted-2h-d (red circle) and Grafted-3h-d (blue triangles)

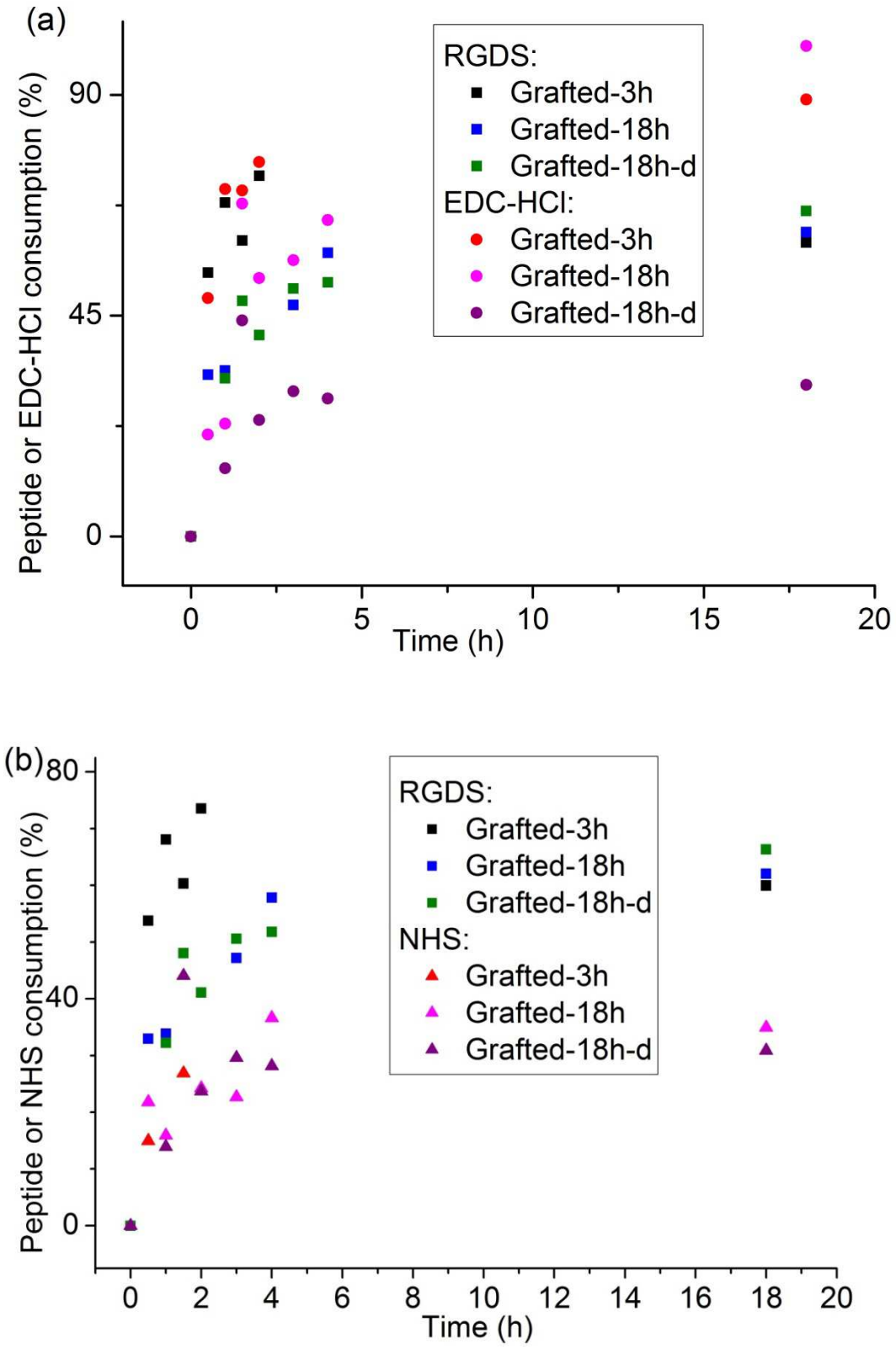

Fig. S9 Peptide consumption (squares) compared to a) EDC-HCl (circles) and b) NHS (triangles) consumption

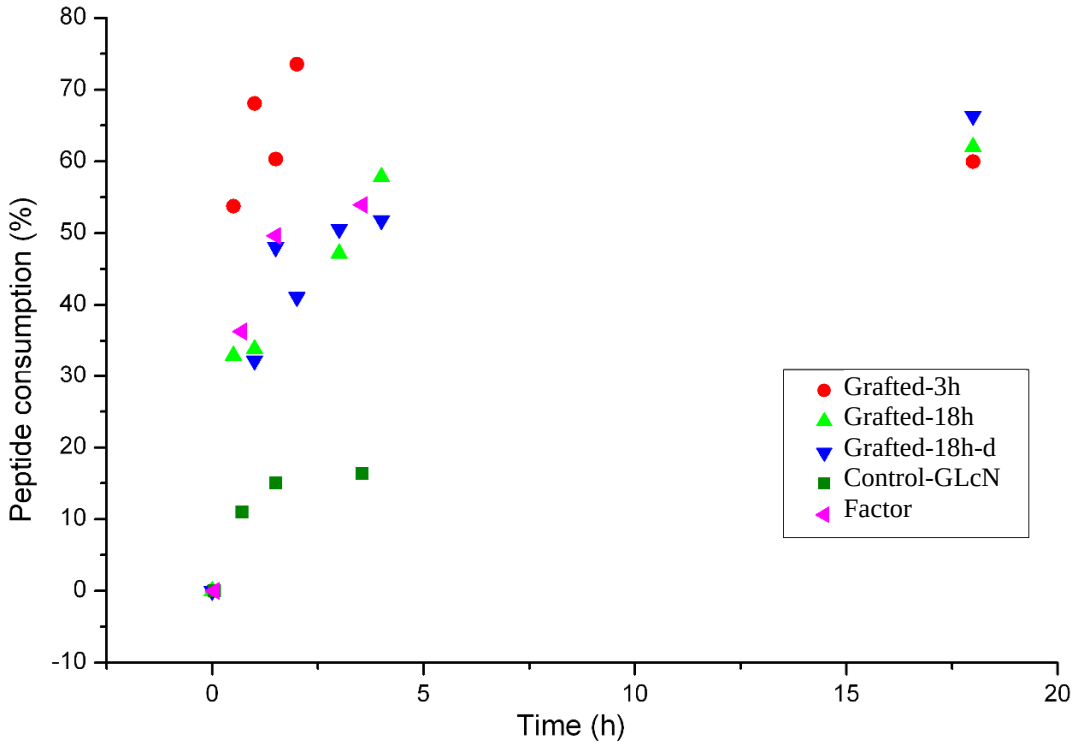

Fig. S10 Real-time monitoring of RGDS peptide consumption during the grafting onto chitosan films and GLcN solution with capillary electrophoresis. Factor shows the Control-GLcN data scale up by a factor 2.7 to illustrate the amount of free NH2 on the chitosan films in the other grafting experiments

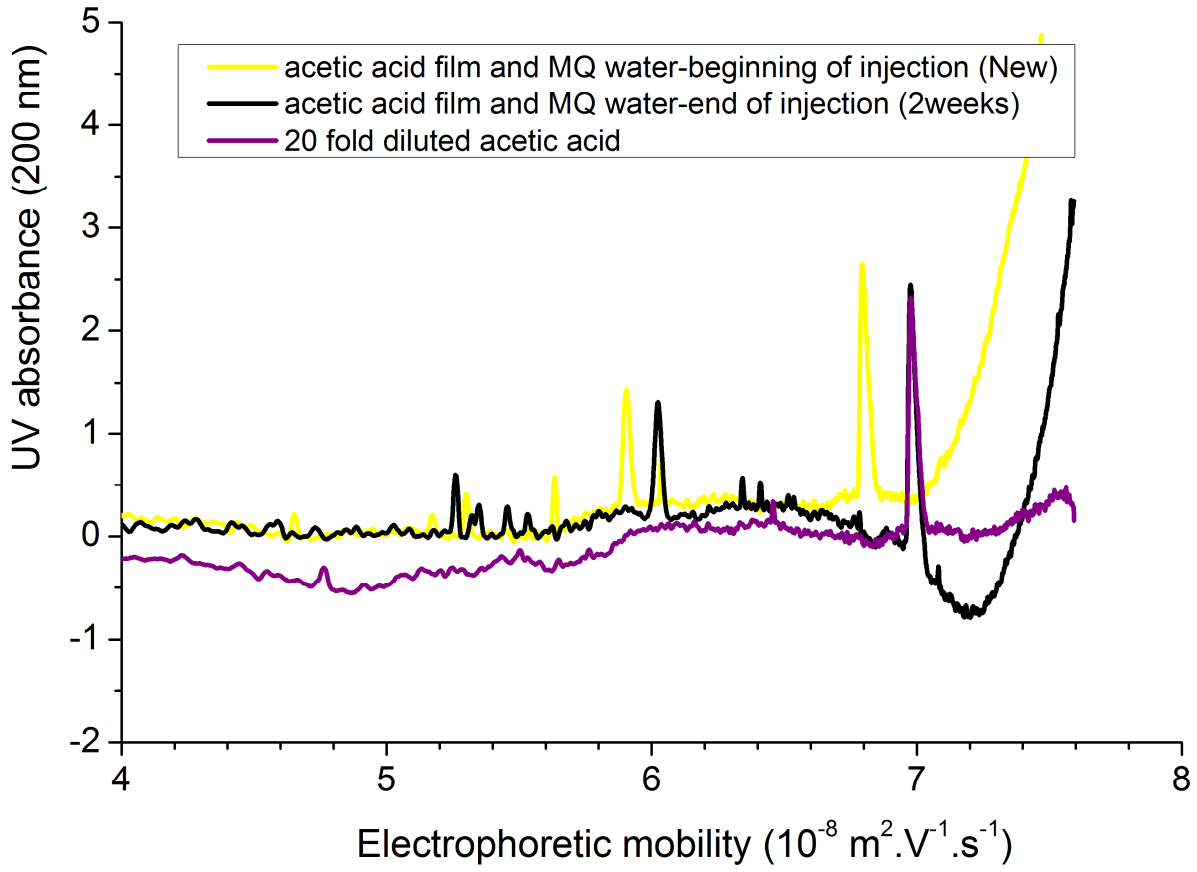

Fig. S11 Electropherograms of Milli-Q water exposed to a Non-treated chitosan film for a few hours and a few weeks, and of acetic acid in MilliQ water, showing the rapid leaching of acetic acid from the film placed in Milli-Q water

Scanning Electron Microscopy (SEM)

A JEOL JSM-6510LV scanning electron microscope was used to analyze the topography of the chitosan films before RGDS grafting. Analysis was performed using a low, 5 kV accelerating voltage to avoid charging.[2, 3] Both secondary (SEI) and backscatter (BSE) detectors were used for imaging.

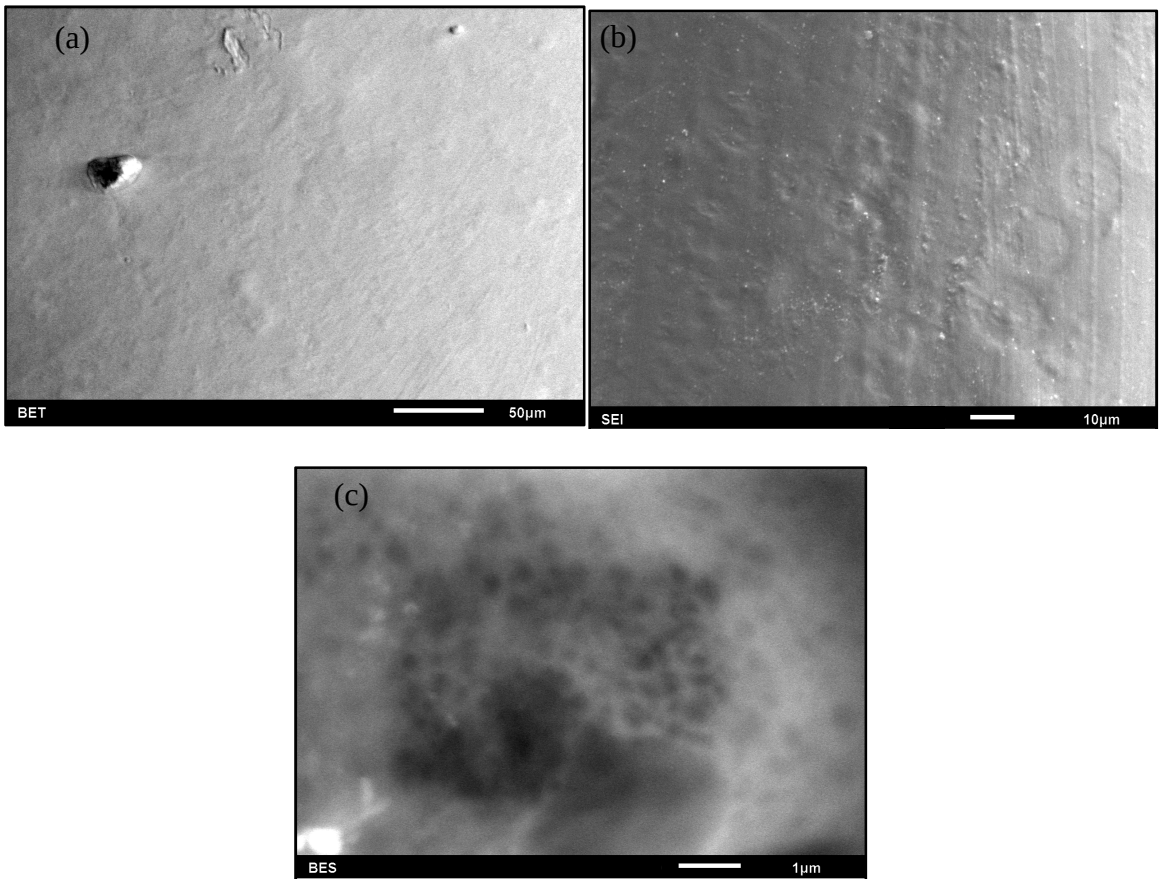

Fig. S12 SEM images for unmodified chitosan films. (a, b) Surface at different magnifications, and (c) beam damage to the film

FT-IR spectroscopy

Attenuation Total Reflectance (ATR) Fourier-Transform (FT) Infrared (IR) Spectroscopy was performed on a Perkin-Elmer Spectrum 100 FT-IR spectrometer equipped with a universal ATR sampling accessory. Spectra were acquired on the powder and films with 16 scans and a recording speed of 1 cm^{-1}/s.

IR spectroscopy analysis was completed on the chitosan powder and all films as shown in Fig. S13. The spectra are in agreement with those obtained in the literature and confirm the molecular structure of chitosan.[4] There are no significant differences identified between any of the samples analyzed. RGDS grafted onto the chitosan films was not detected. The RGDS is usually detected by peaks at 1566 and 1414 cm^{-1}.[5] These peaks correspond to the amide II region and the carboxyl functional groups, respectively. These peaks are not apparent and are masked by the signals corresponding to the chitosan film.

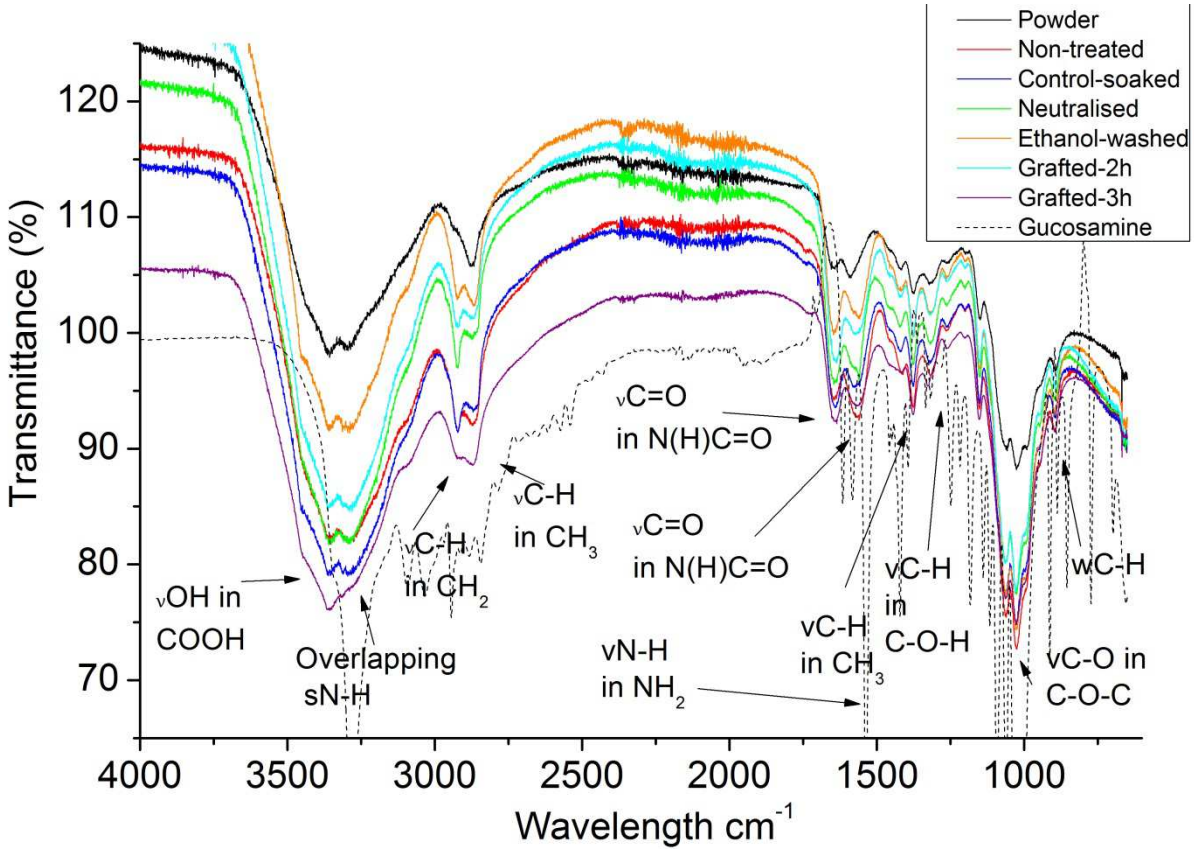

Fig S13 ATR –FTIR spectra of chitosan powder and film samples

Solid-State NMR of Chitosan Films

^{1}H MAS NMR spectra of all samples exhibited the expected broad signal of chitosan centered at 4.7 ppm [6]. Sample Non-treated presents a small signal superimposed on the main signal and shifted to the right, centered at 1.35 ppm (Fig. S14). This peak was tentatively identified as acetic acid from the preparation of the chitosan film and displays a slight shift from those reported in the literature.[7] The slight shift can be accounted for by the difference in molecular packing experienced in solid-state and solution state NMR spectroscopy. Due to the low resolution of ^{1}H NMR spectroscopy, ^{13}C NMR spectroscopy was undertaken and was able to confirm results obtained. An extra peak not characterized as chitosan [6] was observed at a high chemical shift of 181 ppm. Similarly to the results obtained in ^{1}H NMR spectroscopy analysis, a slight shift is observed in the acetic acid peak compared to the literature.[7] The ^{1}H and ^{13}C NMR spectroscopy demonstrated that the acetic acid peak disappears after simply soaking the film in PBS. The importance of rinsing the chitosan film after its production was demonstrated.

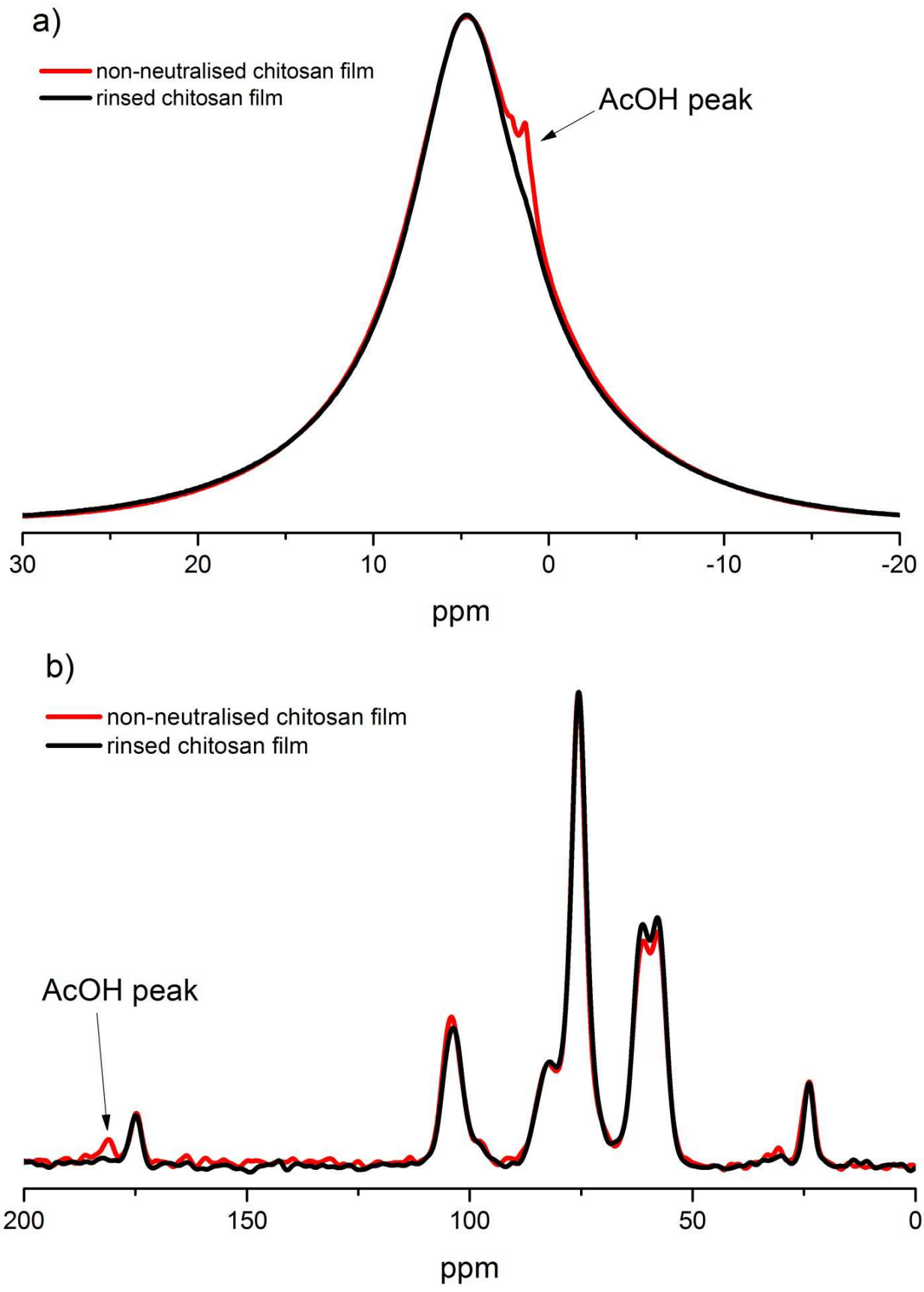

Fig. S14 Solid-state NMR spectra of chitosan film (Non-treated) and chitosan film rinsed with PBS (Control-soaked): 1H MAS (a) and 13C SPE-MAS (b)

Solid-state NMR spectroscopy analysis of the grafted films showed no indication of grafted RGDS peptide. This is illustrated in the 13C SPE-MAS NMR spectra of Control-soaked and Graft-2a samples in Fig. S15a and the 1H spectra of these samples in Fig. S15b. There is no significant difference between the spectra of the control samples and of the grafted samples. These grafting experiments were done on films not soaked in PBS and thus with films that retained acetic acid.

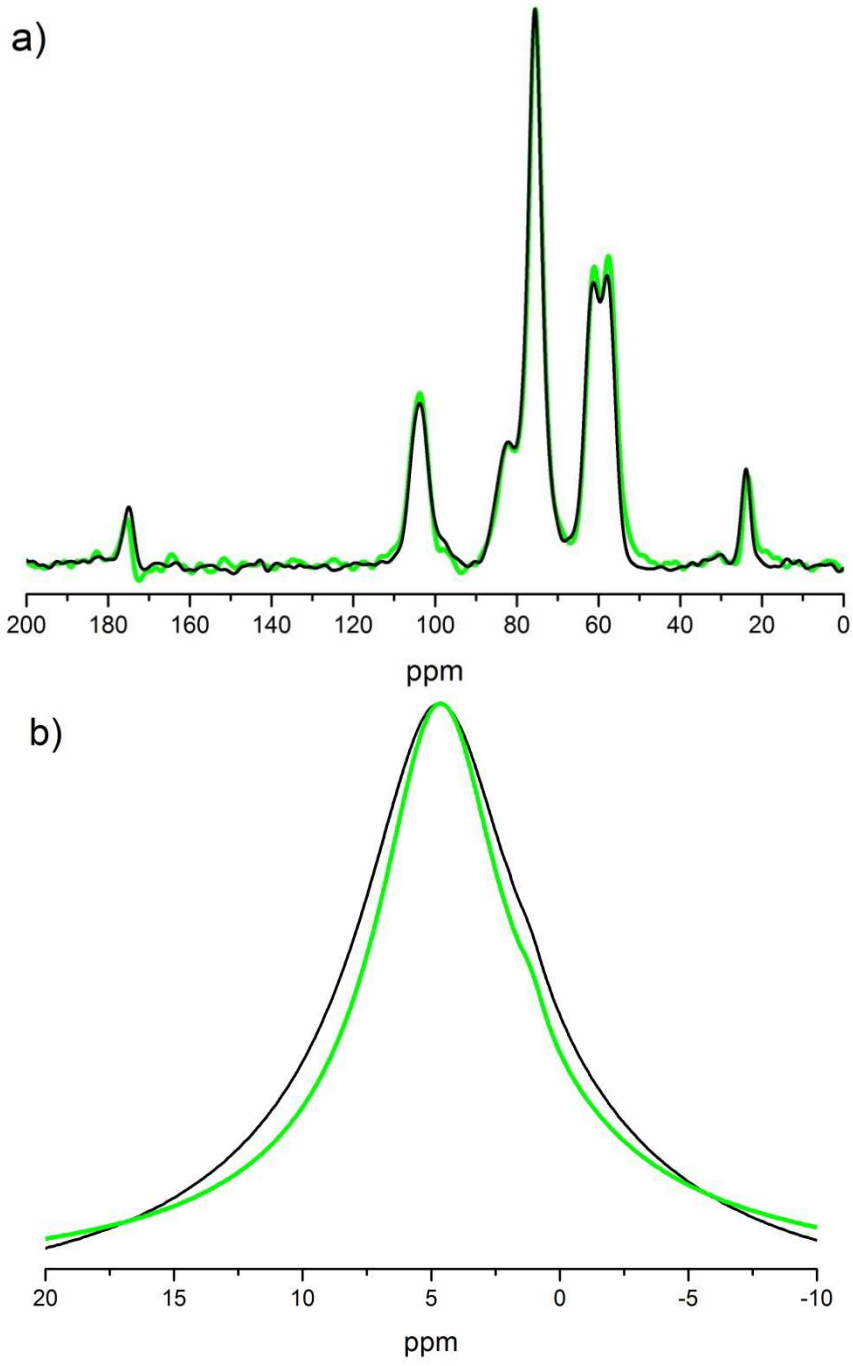

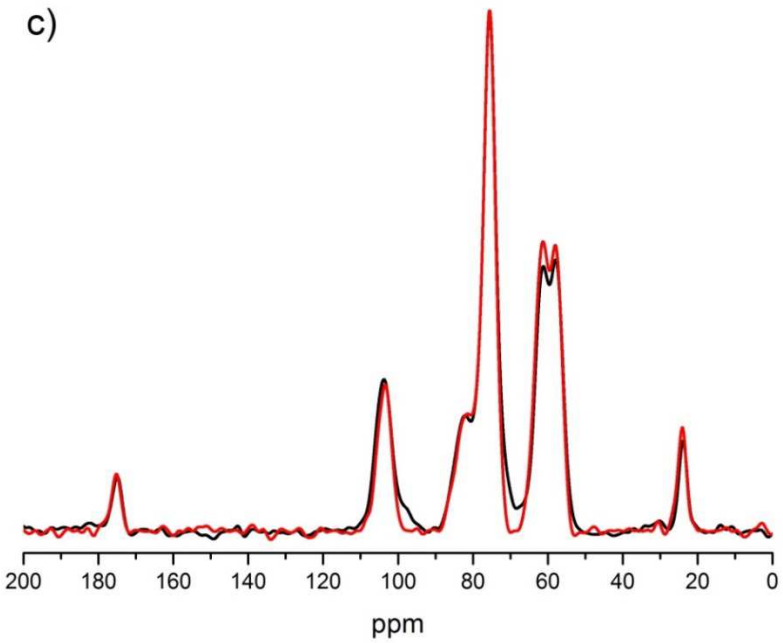

Fig. S15 Comparison of a) 13C SPE-MAS NMR spectra and b) 1H NMR spectra of Control-soaked (black line), Graft-1a (green line) and, ; c) comparison of 13C SPE-MAS NMR spectra of Control-soaked (black line) and Graft-2a (red line)

The comparison of ^{13}C CP-MAS and ^{13}C SPE-MAS spectra reveals additional molecular dynamic information. The higher relative intensity in SPE-MAS compared to CP-MAS of C6, C8 and C9 carbons indicates a higher molecular mobility of the pending CH_2OH group and of the pending acetyl group as compared to the glucose ring (Fig. S16).

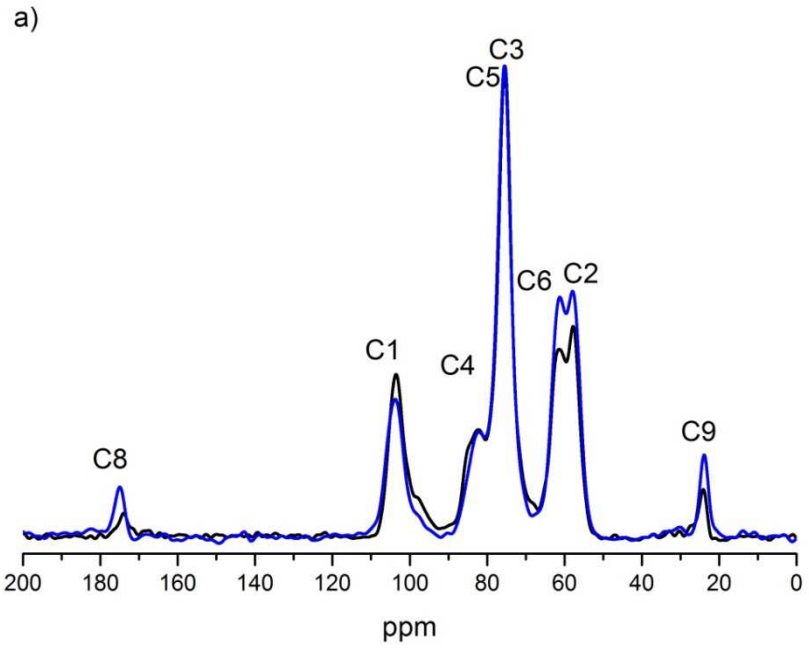

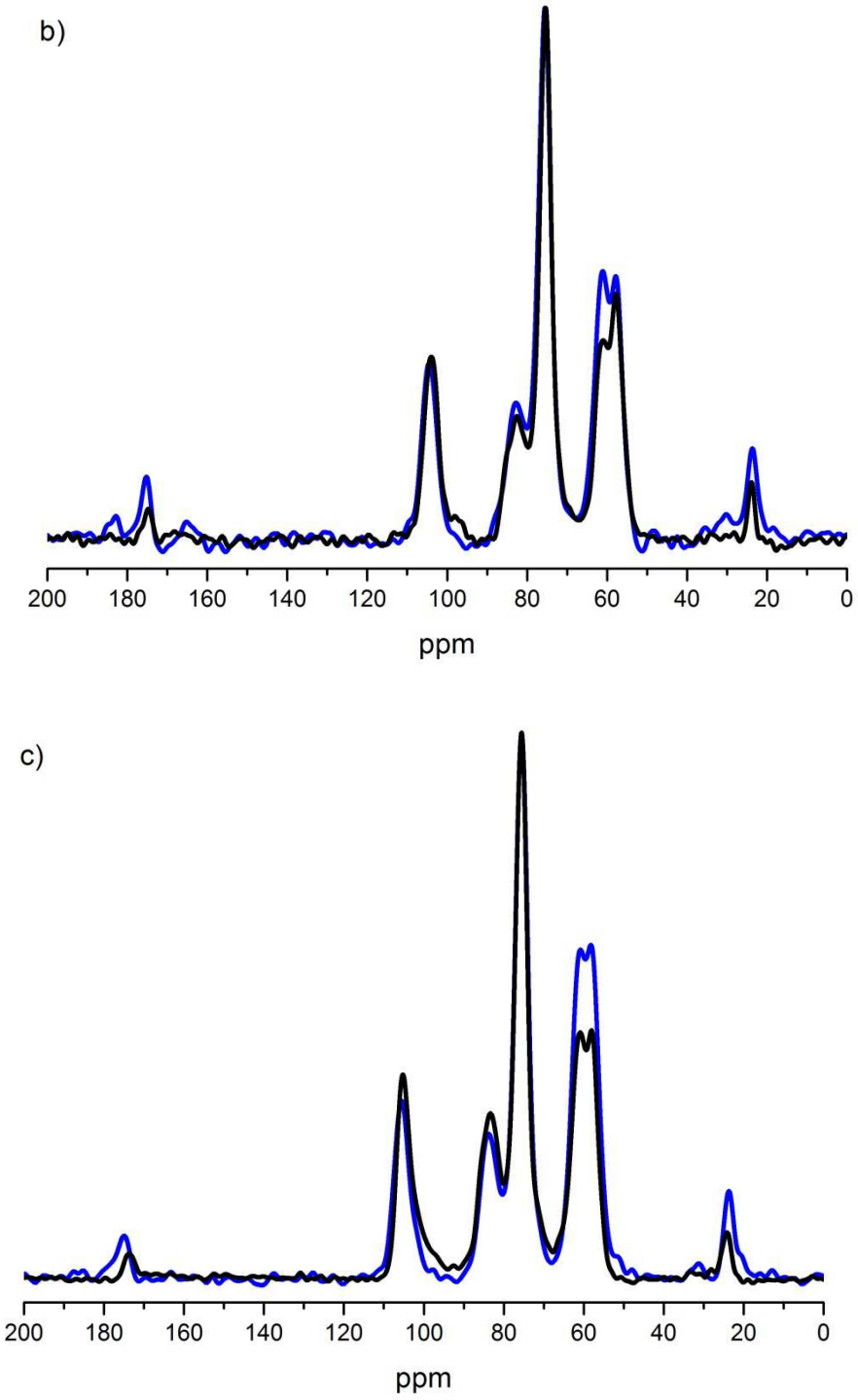

Fig. S16 Comparison of 13C CP-MAS (black lines) and 13C SPE-MAS (blue lines) NMR spectra of the a) Control-soaked film, b) Neutralized and c) Powder. The peak assignment of chitosan corresponds to the numbers shown in Fig. S1

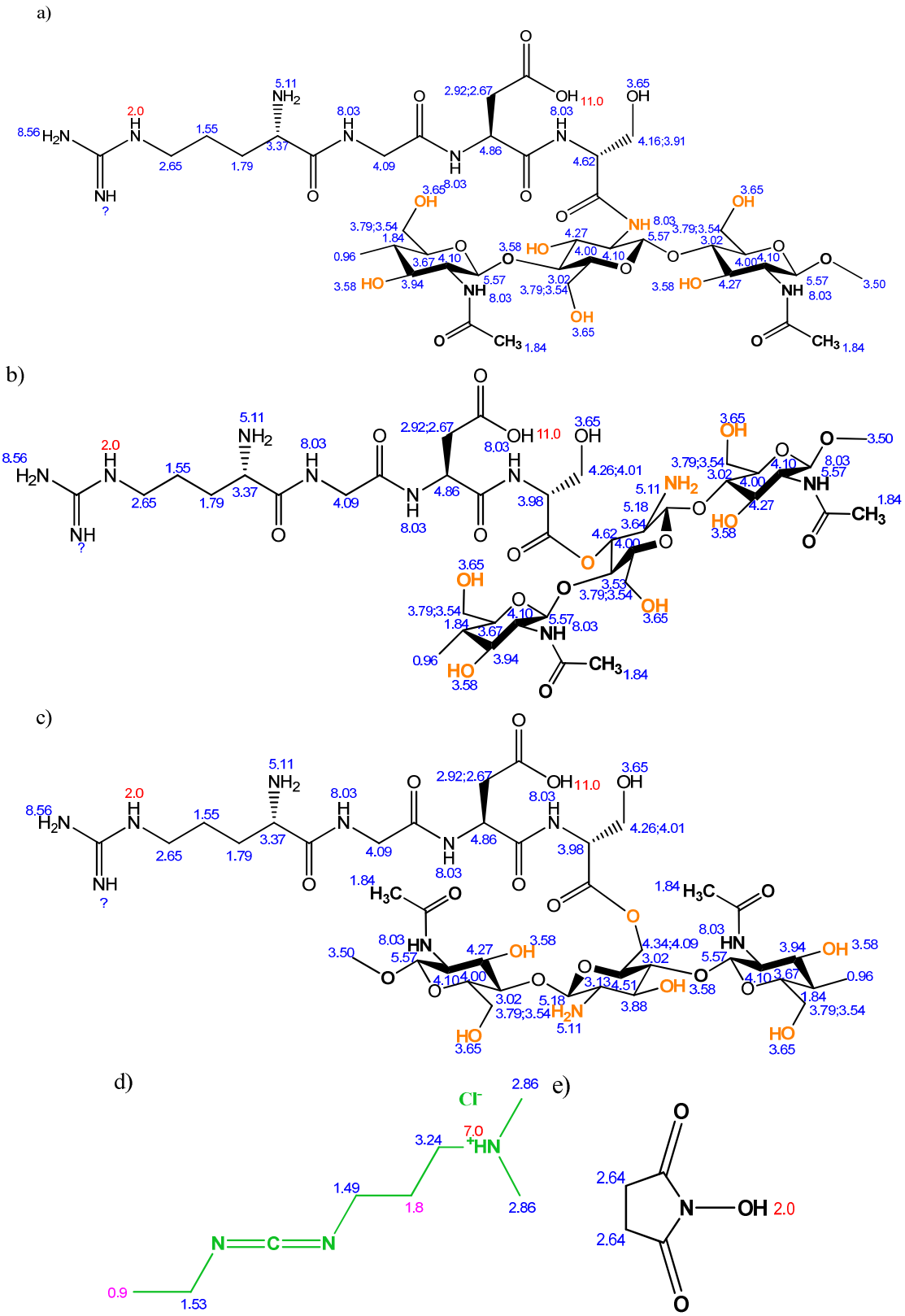

Fig. S17 ChemNMR estimations of 1H NMR chemical shifts of RGDS grafted to a) at an amine group of chitosan, b) at a secondary alcohol group of chitosan and c) at a primary alcohol group of the chitosan, and of d) EDC-HCl and e) NHS

a)

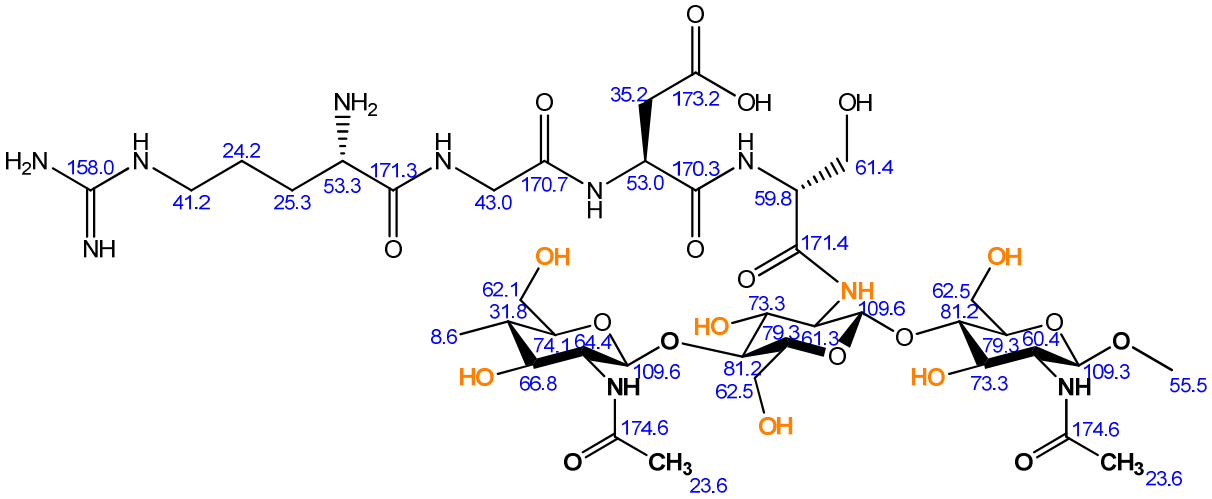

b)

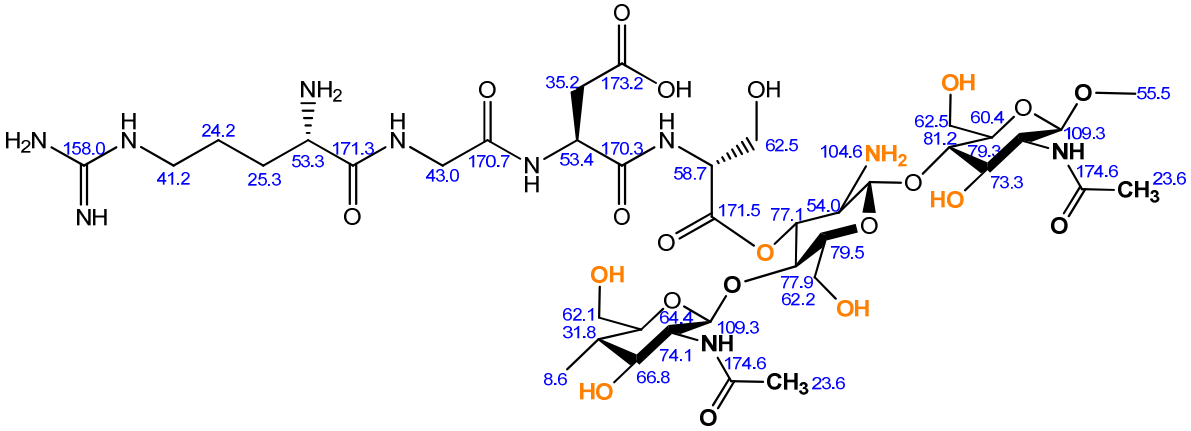

c)

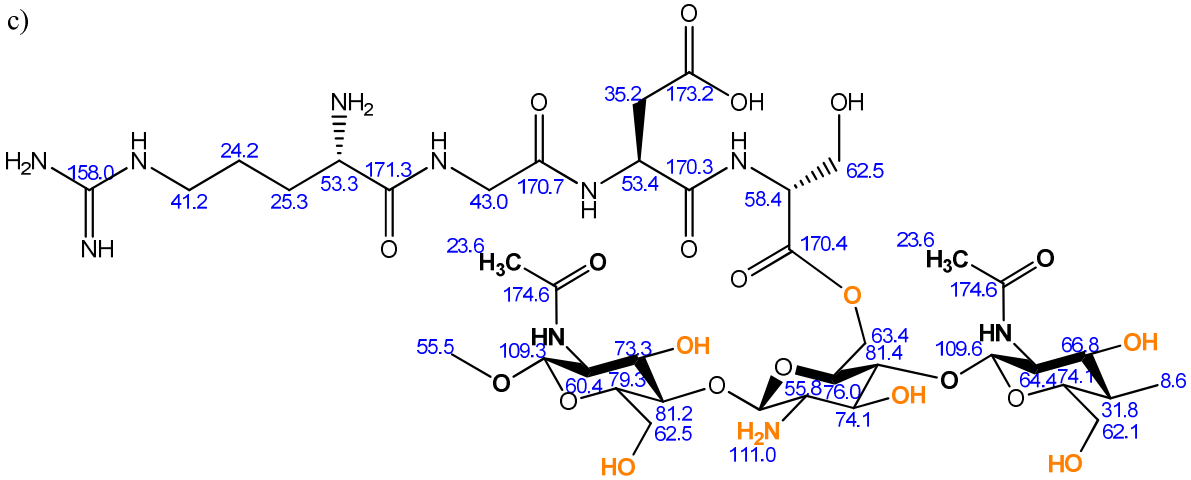

d)

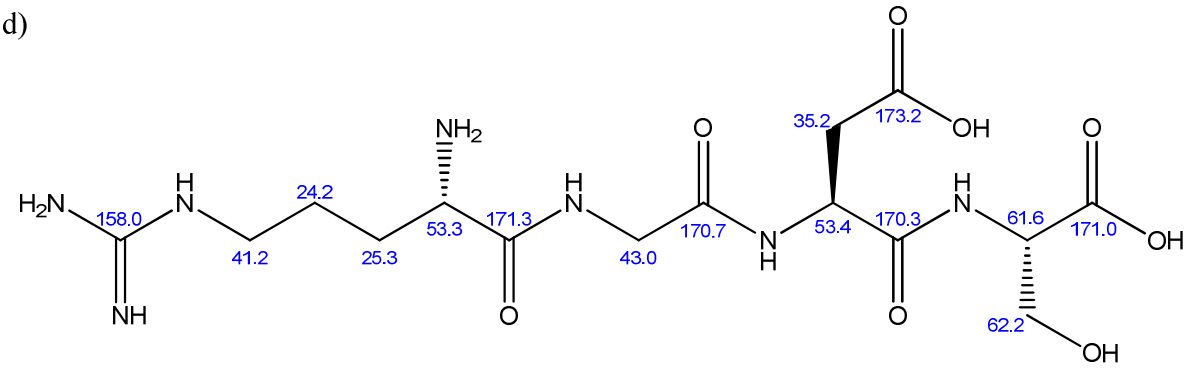

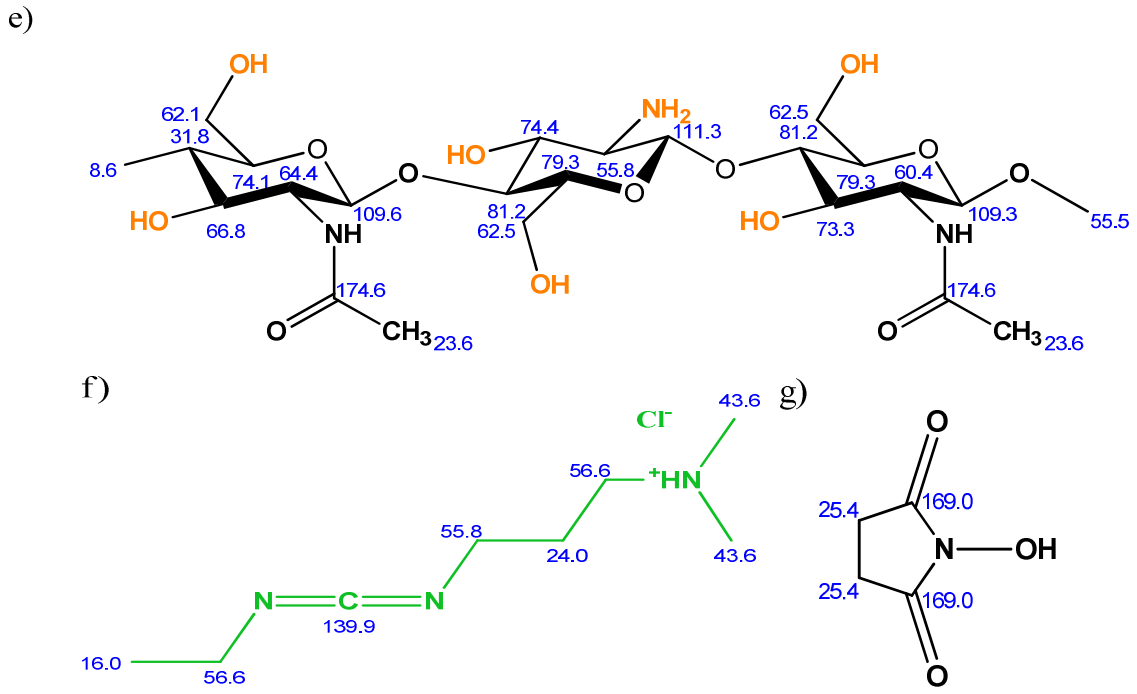

Fig. S18 ChemNMR estimations of 13C NMR chemical shifts of RGDS grafted to a) at an amine group of chitosan, b) at a secondary alcohol group of chitosan, c) at a primary alcohol group of chitosan, d) non-grafted RGDS, and e) chitosan, f) EDC-HCl and g) NHS

References

1. Moshnikova AB, Afanasyev VN, Proussakova OV, Chernyshov S, Gogvadze V, Beletsky IP (2006) Cytotoxic activity of 1-ethyl-3-(3-dimethylaminopropyl)-carbodiimide is underlain by DNA interchain cross-linking. Cell. Mol. Life Sci. 63:229-234
2. Park SI, Daeschel MA, Zhao Y (2004) Functional Properties of Antimicrobial Lysozyme-Chitosan Composite Films. J. Food Sci. 69:M215-M221
3. Pinotti A, García MA, Martino MN, Zaritzky NE (2007) Study on microstructure and physical properties of composite films based on chitosan and methylcellulose. Food Hydrocoll. 21:66-72
4. Silva SML, Braga CRC, Fook MVL, Raposo CMO, Carvalho LH, Canedo EL (2012) Application of Infrared Spectroscopy to Analysis of Chitosan/Clay Nanocomposites. In: T. Theophile, (Ed.), Materials Science, Engineering and Technology, InTech, Rijeka.
5. Karakecili AG, Gumusderelioglu M (2008) Physico-chemical and thermodynamic aspects of fibroblastic attachment on RGDS-modified chitosan membranes. Coll. Surf. B Biointerf. 61:216-223
6. Gartner C, Lopez BL, Sierra L, Graf R, Spiess HW, Gaborieau M (2011) Interplay between Structure and Dynamics in Chitosan Films Investigated with Solid-State NMR, Dynamic Mechanical Analysis, and X-ray Diffraction. Biomacromolecules 12:1380-1386
7. Gottlieb HE, Kotlyar V, Nudelman A (1997) NMR chemical shifts of common laboratory solvents as trace impurities. J. Org. Chem. 62:7512-7515

Analytica Chimica Acta 935 (2016) 258–268

Contents lists available at ScienceDirect

Analytica Chimica Acta

journal homepage: www.elsevier.com/locate/aca

Towards a less biased dissolution of chitosan

Joel J. Thevarajah [a, b, c], Jerikho C. Bulanadi [a], Manfred Wagner [c], Marianne Gaborieau [a, b, *], Patrice Castignolles [a]

[a] Western Sydney University, School of Science and Health, Australian Centre for Research on Separation Sciences (ACROSS), Parramatta, 2150, Australia
[b] Western Sydney University, Molecular Medicine Research Group (MMRG), School of Science and Health, Parramatta, 2150, Australia
[c] Max Planck Institute for Polymer Research, Ackermannweg 10, 55128 Mainz, Germany

HIGHLIGHTS

- Clear solutions of chitosan do not ensure complete solubility.
- Aggregation of chitosan is observed in size-exclusion chromatography conditions.
- HCl and DCl cause deacetylation of chitosan during dissolution in water.
- The extent of chitosan dissolution is more limited in aqueous acetic acid than in aqueous HCl.
- The dissolution of chitosan in aqueous HCl is relatively quick; however, it may not be complete.

GRAPHICAL ABSTRACT

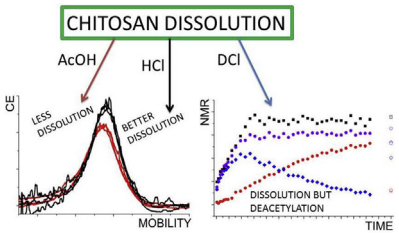

ARTICLE INFO

Article history:
Received 14 March 2016
Received in revised form
17 June 2016
Accepted 19 June 2016
Available online 21 June 2016

Keywords:
Chitosan
Dissolution
Solid-state NMR spectroscopy
Solution-state NMR spectroscopy
Capillary electrophoresis
Size-exclusion chromatography (SEC)

ABSTRACT

The dissolution of polysaccharides is notoriously challenging, especially when one needs a “true” solution. Factors influencing chitosan's solubility include composition, also known as degree of acetylation (*DA*). The dissolution of chitosan was investigated by visual observation, size-exclusion chromatography (SEC), pressure mobilization (PM), free-solution capillary electrophoresis (CE) and real-time solution-state NMR spectroscopy. Aqueous HCl dissolves around 15% more chitosan than the commonly used aqueous acetic acid (AcOH), however aggregates were detected in SEC suggesting incomplete dissolution. Significant deacetylation of chitosan over the period needed for dissolution at high temperature was observed by NMR spectroscopy in DCl by about 20% of the initial *DA* value. Accurate *DA* determination by NMR spectroscopy may thus be possible only in the solid state (with a precision within 1% on the *DA* % scale above a *DA* of 10%). Overall a compromise between maximum solubilization and minimum degradation is required in attempting to obtain a “true” solution of chitosan. The completeness of the dissolution may be more influenced by the average *DA* than by molar mass.

1. Introduction

Chitosan is a polysaccharide derived from the *N*-deacetylation of chitin. Chitin is the second most abundant polysaccharide in the world (by volume after cellulose) and is synthesized by many organisms [1]. Its natural occurrence includes the exoskeletons of arthropods such as shrimps, crabs and the cell walls of yeasts [2]. It is a major waste product of the seafood industry. Its most promising derivative, chitosan, was shown to be biocompatible, biodegradable and antimicrobial, which make it an appropriate material for

* Corresponding author. Western Sydney University, Molecular Medicine Research Group (MMRG), School of Science and Health, Parramatta, 2150, Australia.
E-mail address: m.gaborieau@westernsydney.edu.au (M. Gaborieau).

http://dx.doi.org/10.1016/j.aca.2016.06.021
0003-2670/

biomedical applications such as stem cell growth substrate [3,4]. Chitosan's structure contains varying proportions of D-glucosamine and *N*-acetyl-D-glucosamine units. The degree of acetylation (*DA*) of chitosan refers to the proportion of the *N*-acetyl-D-glucosamine monomer units. It is often characterized only by its average *DA* which does not take into account the complex arrangement of monomer units along the polymer chain [5]. The *DA* and the distribution of the acetyl groups along chitosan chains affect the dissolution or hydrolysis of chitosan [6,7].

A significant factor that hinders a meaningful characterization of chitosan is the difficulty to fully dissolve it without degrading it. To allow for the proper separation and characterization of a polysaccharide (by chromatography, light scattering, etc.), true solutions are required as in the case of starch [8]. A true (dilute) solution is defined in this work as a solution where all macromolecules (chitosan chains) are surrounded by solvent molecules [9]. True solutions are also necessary to allow the homogenous chemical modification of chitosan [10]. The dissolution of polysaccharides is generally complex, and various techniques have been used to assess it in different ways. A dissolved sample will visually appear as a clear and transparent liquid; however, obtaining a clear and transparent liquid does not always mean that the sample is completely dissolved. In the case of starch, quantitative ^{1}H NMR spectroscopy of a transparent liquid proved it to contain undissolved starch (up to 15% of the initial starch) for some starches, possibly due to the presence of aggregates which were invisible to the naked eye [8]. Unlike chitin, which is largely insoluble in aqueous and organic solvents, chitosan is partially soluble owing to the amine group of its D-glucosamine monomer. However, the actual extent of dissolution of chitosan is often overlooked and is dependent on structural characteristics including the distributions of the degrees of acetylation and environmental conditions such as pH, ionic strength, temperature, time and the dielectric constant of the solvent [3,11]. UV spectrophotometry at 600 nm has been used to analyze the dissolution by analysis of the turbidity, however this overlooks the presence of aggregates or non-dissolved parts of the chitosan small enough to produce minimal scattering of visible light [12]. A range of methods has been used to monitor the dissolution of macromolecules [9], but a number of these methods do not discriminate between true solution and dispersion (aggregation) such as viscometry [13], FT-IR spectroscopy [14], or pyrolysis gas chromatography [15,16].

Light scattering (static and dynamic) was used to analyze the dissolution of chitosan, unfortunately, there were several limitations. Chitosan dissolution is often complicated by the presence of (concentration dependent) aggregation. Common methods to remove aggregates are ultracentrifugation and filtration. However, in the case of chitosan, these methods were shown to remove high molar mass chains and caused the light scattering results to be strongly influenced by the filtration procedure undertaken [17]. Size-exclusion chromatography (SEC) coupled to multi-angle light scattering (MALS) identified aggregation in chitosan samples and heterogeneity of the solution [18]. It was further identified that the aggregates are stable in solution and thus light scattering cannot accurately characterize chitosan [17,18]. The extent of the aggregation did not correlate with the average *DA* in this work.

SEC is a commonly used method in the characterization of polysaccharides [19]. It has been used in an attempt to obtain molar mass distributions of chitosan [2]. Unfortunately, as identified previously, chitosan's poor solubility and aggregation causes difficulty in choosing an appropriate solvent. Solvents such as 0.1 M acetic acid/0.2 M sodium chloride were shown to cause an overestimation of molar mass due to the promotion of aggregation. It was also noted that light scattering was sensitive to the aggregation of highly acetylated chitosan samples [20].

Beyond light scattering, Taylor dispersion analysis (TDA) can be used to determine the diffusion coefficient of macromolecules, but has never been applied to chitosan. The diffusion coefficient is related to the size of the macromolecules and thus TDA can provide information regarding the presence of aggregates or dissolved molecules. The detection of narrow and broad peaks allows a clear distinction between the dissolved sample and aggregate formation [21]. Free-solution capillary electrophoresis (CE) or capillary zone electrophoresis has been applied in a limited but successful fashion to the characterization of polysaccharides, including the separation of chitosan samples by their *DA* [5,22]. CE proved to separate the samples by their *DA* with no sample preparation required, not even sample filtration. The area of the peaks on the CE electropherograms could thus be used to analyze the dissolution of chitosan, with no bias due to sample preparation. It is important to note that aggregates, as long as their diffusion coefficient is much lower than that of the macromolecules of interest, lead to very sharp peaks in CE. These sharp peaks are easily distinguished from the polymer peak as in the case of gellan gum [23].

In this paper the dissolution of chitosan samples is investigated with various techniques: capillary electrophoresis and pressure mobilization, multiple-detection SEC, as well as solution-state and solid-state NMR spectroscopy. Aggregation, extent of dissolution and possible chemical degradation are assessed.

2. Experimental

2.1. Materials

Chitosan powders were purchased from Aldrich, Castle Hill, Australia and from AK Biotech, Jinan, China (Table 1). Samples were prepared at 1 g L^{-1}. Orthophosphoric acid (85%) was purchased from BDH AnalR, Merck Pty Ltd. Acetic acid (AcOH, glacial, 99%) and hydrochloric acid (32%) were purchased from Unilab. Sodium hydroxide pellets, sodium chloride, trifluoroacetic acid (TFA, 99%), hexaamminecobalt(III) chloride (≥99.5%), dimethyl sulfoxide (DMSO, 99%) and adamantane (99%) were purchased from Sigma-Aldrich. Deuterium chloride (35%) was purchased from Cambridge Isotope Laboratories. All water used in this study was of Milli-Q quality. The SEC eluent was prepared from TFA at 0.3% (w/v) with 0.1 M NaCl. The eluent was filtered with 0.22 μm nylon 6,6 filter. Nine pullulan standards (with weight-average molar masses between 342 and 805,000 g mol^{-1} and dispersity values between 1.00 and 1.27) were purchased from Polymer Standard Service, Mainz, Germany. Sodium borate buffer (75 mM) was prepared from 0.5 M boric acid in Milli-Q water, titrated to pH 9.20 with 10 M sodium hydroxide, and diluted with Milli-Q water. Sodium phosphate buffer (100 mM) was prepared from 0.5 M sodium dihydrogen phosphate, titrated with phosphoric acid, and diluted with Milli-Q water. Sodium borate and phosphate buffers were sonicated for 5 min and filtered with a Whatman (0.2 μm) or Millex GP PES syringe filter (0.22 μm) before use.

2.2. Capillary electrophoresis and pressure mobilization

Free-solution capillary electrophoresis (CE) and pressure mobilization (PM) experiments were carried out using an Agilent 7100 CE (Agilent Technologies, Waldbronn, Germany) instrument equipped with a diode array detector and external circulating bath with MX temperature controller (Polyscience, USA). Polyimide-coated fused silica high sensitivity capillaries (50 μm internal diameter) were purchased from Agilent. The capillary (104 cm total length, 95.5 cm effective length) was initially pretreated by flushing with 1 M NaOH for 10 min, then with 0.1 M NaOH, Milli-Q water and sodium borate buffer for 5 min each at the start of the series of

Table 1
Visual evaluation of the dissolution of chitosan samples with varied *DA*s in aqueous solvents: 50 mM HCl, 0.3% (w/v) trifluoroacetic acid (TFA), as well as 0.3% (w/v) TFA with 0.1 M NaCl (Eluent).

Sample	Supplier	Batch (Catalogue)	DA_n^{SS-NMR} (%)[a]	DA_n^{NMR} (%)[b]	HCl	TFA	Eluent
LowMW1	Sigma	MKBG3334V (448869)	17.1 ± 0.3		2h[c]	2h	2h
MedMW1	Sigma	MKBH1108V (448877)	22.3 ± 0.3		2h	2h	1n[d]
MedMW2	Sigma	03318AJ (448877)	20.2 ± 0.3	15.5 ± 1.6	1n	1n	
HighMW	Sigma	MKBD7240V (419419)	11.8 ± 0.3		1n	1n	
Sig	Sigma	120M0028V (C3646)	10.1 ± 0.3		1n	1n	
AKbioV1	AK Biotech	090426V1	10.1 ± 0.3		1n	1n	
AKbioV2	AK Biotech	090423V2	16.5 ± 0.3	18.7 ± 1.9	1n	1n	
AKbioV3	AK Biotech	090426V3	14.8 ± 0.3	16.5 ± 1.7	1n	1n	
AKbioD1	AK Biotech	090422D1	12.5 ± 0.3	19.8 ± 2.0	1n	1n	
AKbioD2	AK Biotech	090422D2	11.1 ± 0.3	13.6 ± 1.4	1n	1n	
AKbioD3	AK Biotech	090422D3	3.8 ± 0.3	3.5 ± 0.4	1n	1n	
AKbioC	AK Biotech	090430C			2w[e]	2w	
ChitAl	[5]		4.0 ± 0.3	2.5 ± 0.3	2h		

[a] Number-average *DA* obtained by solid-state NMR spectroscopy in this work for which the *SD* was determined as the error caused by phasing (see Section 3.5.).
[b] Number-average *DA* obtained by solution-state NMR spectroscopy [5].
[c] Sample was visually dissolved after 2 h at 60 °C.
[d] Sample was visually dissolved after 2 h at 60 °C and an overnight shaking at room temperature.
[e] Sample was visually dissolved after 2 h at 60 °C followed by overnight shaking at room temperature followed by 2 weeks without shaking at room temperature.

experiments. An oligo(sodium acrylate) was separated [24] in sodium borate (75 mM, pH 9.3) to validate the capillary and the instrument before each session. The electrolyte for chitosan analysis was sodium phosphate (100 mM, pH 2 or 3). Before each experiment the capillary was rinsed with HCl (50 mM) and sodium phosphate (100 mM, pH 2 or 3) for 5 min, respectively. Hydrodynamic injections for PM were carried out with 75 mbar for 10 s and for capillary electrophoresis with 40 mbar for 20 s (both corresponding to injection volumes of 0.14% of the total capillary volume, see Eq. S1 in supporting information). CE was undertaken by applying 30 kV at 25 or 55 °C. PM was undertaken at a pressure of 72 or 63 mbar (without electric field). For PM the sample was mixed with the background electrolyte with the electric field. This involved ramping the voltage up to 30 kV and then down to −30 kV and back up to 0 kV over the first 4 min of separation (Fig S-3). The mixing of the chitosan with the carrier liquid is due to the electroneutrality of the solution needing to be maintained at all times, even during the ramping process. This is possible due to the reservoirs of buffer which represent an infinite source of the liquid carrier's ions compared to the capillary volume. As the anions and cations of the buffer migrate with the electric field, the counter-ions migrate as well to maintain electroneutrality which results in mixing. When the electric field is off, the sample is allowed to migrate through the capillary within the carrier liquid. Pressure-assisted capillary electrophoresis (PACE) was undertaken with both an electric field (30 kV) and pressure (50 mbar) at 55 °C. For kinetic measurements undertaken using PACE, the CE carousel was kept at 60 °C using an external circulating bath. Detection was set at 195 nm. All CE and PM data were treated with the software Origin 9 and the x and y axes were normalized based on previous studies [25,26], converting the y axis into a time-corrected y axis $h(t)$, or a weight distribution of electrophoretic mobilities $W(\mu)$ (see supporting information).

2.3. Multiple-detection size-exclusion chromatography

The analysis of chitosan was undertaken with a Malvern Viscotek triple-detector size-exclusion chromatography instrument triple detector array consisting of an online degasser, pump, automatic sample injector, one precolumn and three NOVEMA columns (one low molar mass column: 30 Å and two medium molar mass columns: 1000 Å, both with particle sizes of 10 μm) from Polymer Standards Service, Mainz, Germany. The triple detector array included in series RALS (right-angle light scattering, 670 nm), refractometer (660 nm) and viscometer thermostated at 50 °C, controlled by the software OmniSEC. The flow rate was 0.85 mL min^{-1}. Ethylene glycol was used as a flow rate marker and the injection volume was set at 100 μL. The eluent was regularly injected to check for the absence of system peaks on all the detectors' signals and the absence of bleeding from the columns.

2.4. Solid-state NMR spectroscopy

Solid-state ^1H and ^{13}C NMR spectra were recorded on a Bruker Avance DPX200 spectrometer operating at Larmor frequencies of 200 MHz and 50 MHz, respectively. A commercial double resonance probe supporting zirconia MAS rotors with a 4 mm outer diameter and a 3 mm inner diameter was used, and samples were spun at 10 kHz at the magic angle. ^1H experiments were recorded using a 90° pulse, a 3 s repetition delay with at least 64 scans accumulated. ^{13}C CP-MAS NMR experiments were adapted from quantitative measurements found in the literature [27,28]. They were recorded with a 1 ms contact time and a 4 s repetition delay, and 21,586 to 104,924 scans. For ^1H experiments the 90° pulse was optimized using adamantane and power levels for the ^{13}C CP-MAS experiments were optimized using a mixture of three ^{13}C singly labeled alanines. The ^1H and ^{13}C chemical shifts scales were externally referenced using adamantane by setting the CH resonance to 1.64 and 38.48 ppm, respectively [29]. The degree of acetylation was measured through Eq. (1) [27]:

$$DA_n^{SSNMR}(\%) = \frac{I_{CH_3}}{(I_1 + I_2 + I_3 + I_4 + I_5 + I_6)/6} \quad (1)$$

Where I_{CH3} is the integral of the methyl group of the acetyl group and I_1 to I_6 are the integrals of the signals assigned to the chitosan backbone.

To measure the deacetylation by solid-state NMR spectroscopy 250 mg chitosan (MedMW1) was dissolved at 1 gL^{-1} in 50 mM HCl in Milli-Q water or in 50 mM DCl in D_2O. Each sample was then kept in an oven at 60 °C for 55 h. After removing the sample from the oven the dispersion was neutralized with excess 1 M NaOH. The dispersion was then filtered and rinsed with 500 mL of Milli-Q water, freeze-dried and measured by solid-state NMR spectroscopy.

2.5. Solution-state NMR spectroscopy

The kinetic measurements were recorded on a Bruker 500 MHz

Avance III system operating at a Larmor frequency of 500 MHz, equipped with a 5 mm z-gradient BBFO 1H/X probe with z-gradient using TopSpin 3.2 (Bruker). The ^{1}H NMR spectra were measured in deuterium oxide at 333 K. The accuracy of the temperature was controlled with a methanol sample. The sample was prepared at 1 g L^{-1} in approximately 0.8 M DCl in D_2O. A standard kinetic ^{1}H NMR experiment was started immediately after the chitosan was mixed with solvent, and recorded with 32 transients per spectrum with a 10.6 μs 90° pulse, a spectral width of 11,000 Hz and a repetition delay of 8.6 s (3.6 s acquisition time and 5 s relaxation delay). A total of 800 successive spectra were recorded over 61 h. The relaxation rate (T_1) of the protons was measured before and after the kinetic run with the inversion recovery method and the T_1 values for the acetyl peak and the peak associated to the backbone were determined to be 1.2 s and 943 ms, respectively. Therefore the kinetic experiment conducted was quantitative. Repeat monitoring experiments were conducted on a Bruker DRX300 spectrometer operating at a Larmor frequency of 300.13 MHz equipped with a 5-mm dual ^{1}H/^{13}C probe at 333 K. The temperature was calibrated with 80% glycol in DMSO. The measurements were undertaken with 64 transients per spectrum with a 1.7 μs 30° pulse and a repetition delay of 18.3 s (4.3 s acquisition time and 14 s relaxation delay).

The solution-state NMR measurements for quantifying *DA* conditions were as previously [5].

3. Results and discussion

3.1. Visual observation of dissolution

Pillai [11] suggested that the dissolution of chitosan does not occur in inorganic solvents and therefore the first qualitative measurement of the dissolution of chitosan was through visual observation in aqueous solvents (also more suitable for biomedical applications). Chitosan can be soluble only at a pH below 6 [11]. Aqueous solvents (Table S1) were used at different acid concentrations, limiting them to low concentrations to prevent chitosan degradation. No dissolution took place at 5 mM or 10 mM hydrochloric, acetic, trifluoroacetic, phosphoric, and boric acid. 50 mM concentration of hydrochloric, trifluoroacetic or acetic acid produced clear transparent suspensions after 15 min at room temperature. Trifluoracetic acid has been suggested to be more effective at dissolving chitosan but also samples with a higher *DA* [30]. Phosphoric and boric acid even at higher concentrations were unable to produce a visually clear sample. The acids that were unable to produce a clear solution at room temperature were tested at higher temperatures (Table S2 and Table 1). It was observed that only phosphoric acid was able to produce a clear solution if it was left at 60 °C for 1 h. Using the conditions previously established other chitosan samples with a range of different average *DA*s were also evaluated visually for dissolution in HCl 50 mM, TFA 0.3% and SEC eluent at 60 °C for 2 h. Samples that were not visually dissolved were left overnight on a shaker at room temperature (Table 1). It was concluded from the visual observations that different samples varied in the time needed to produce a clear suspension. This confirmed that the dissolution process was complex and further analysis was required.

3.2. Size-exclusion chromatography and aggregation

SEC is the gold standard for the characterization of polymers especially for the determination of molar mass distributions. This, as well as the degradation and oligomers of chitosan, was characterized using a SEC instrument equipped with PSS NOVEMA columns [31–33]. Aqueous HCl was not chosen to prevent the corrosion of the SEC instrument. A TFA-based eluent was indicated as an appropriate running buffer for the PSS NOVEMA columns for chitosan by PSS in an application note [34]. In this study SEC was used to analyze chitosan samples with different *DA*s. Pullulans were used as standards to generate a conventional calibration curve (Figure S-1). Pullulan-equivalent molar masses of the chitosan samples (Table S3) were repeatable, but not reproducible, as commonly observed in SEC [35]. The reproducibility was investigated only by varying the injection concentration, but this already led to significant variations as observed for other polysaccharides [36]. Importantly, the determined apparent molar masses were 7 orders of magnitude larger than that of the largest pullulan standard. The values obtained are physically impossible, well beyond the experimental error associated to pullulan-equivalent (or any apparent) molar masses [37]. This is likely explained by aggregation in these conditions as observed also with other SEC conditions [18]. Analysis of the refractive index and right angle light scattering detector traces (Fig. 1) revealed that all chitosan samples were bimodal. The different samples exhibited 2 different populations and bimodal peaks: a peak at a lower elution time and a peak at a higher elution time. The peak at a low elution time infers a large molar mass and is assigned to the aggregates and the peak at a higher elution time is inferred to be the dissolved chitosan. The large molar mass values obtained and the intensity of the LS signal which is sensitive to large molar masses [38] were in good

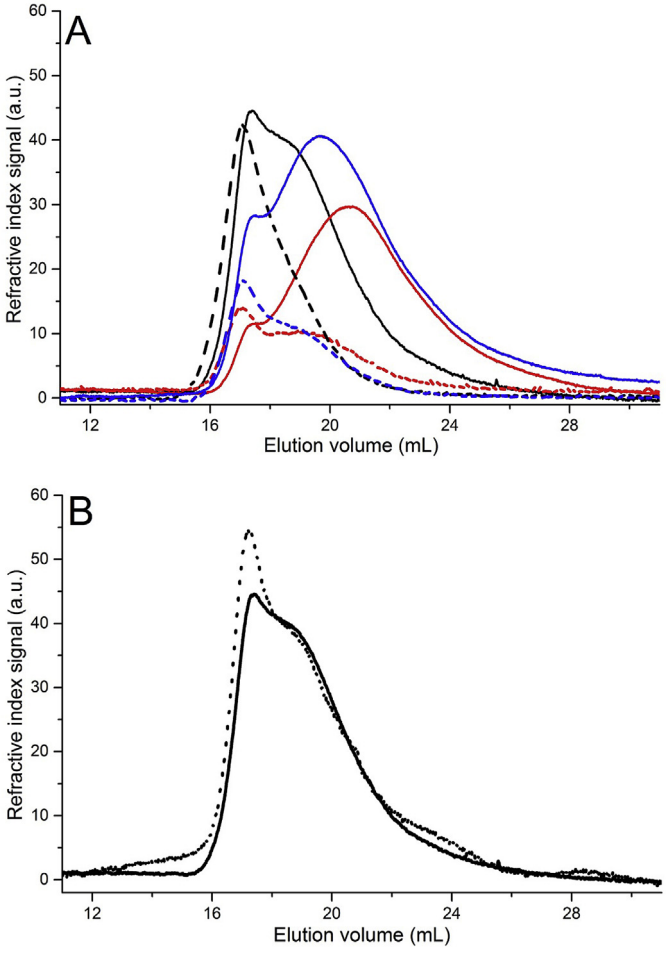

Fig. 1. A) RI (solid lines) and RALS (dashed lines) traces of chitosan MedMW1 (black), LowMW1 (red) and AKbioD3 (blue). B) RI trace of MedMW1 in 50 mM HCl at 1 g L^{-1} (solid line) and diluted to 0.25 g L^{-1} (normalized by concentration, dotted line).

agreement of the existence of aggregation.

Samples that exhibited a separation of aggregates and dissolved polymer (analysis of elution profile) were then diluted (up to 1/100) to assist in breaking apart the aggregates. However, the aggregation remained in the diluted sample suggesting a high stability (Fig. 1B) as suggested in the case of starch [39].

3.3. Evaluation of dissolution by pressure mobilization

Chitosan MedMW1 dissolved in aqueous HCl and AcOH was chosen to be analyzed by pressure mobilization (PM) based on initial visual observations. The sample was heated for 2 h at 60 °C to ensure a clear liquid was obtained. PM was used for the first time to analyze the dissolution of chitosan. It was initially performed with phosphate buffer at pH 3 at 25 °C as the carrier liquid without mixing of the chitosan suspension with the phosphate buffer. A large peak with considerable tailing was observed for chitosan dissolved in aqueous HCl and a small peak with tailing for the chitosan dissolved in aqueous AcOH (Fig. S2). The large UV absorbance of the sample dissolved in HCl is uncharacteristic of chitosan; however, the presence of tailing suggests adsorption onto the capillary surface [40]. Repeatable results were obtained with the sample dissolved in HCl; however, samples dissolved in AcOH exhibited adsorption and poor repeatability. Therefore conditions were adapted and PM experiments were carried out with a slightly different carrier liquid of pH 2 phosphate buffer (100 mM) with mixing (Fig. 2) at 55 °C. The mixing involved the adjustment of the electric field between 30 kV and −30 kV (Fig. S3) immediately after the injection and the addition of pressure (which was reduced from 72 mbar to 63 mbar). Chitosan dissolved in HCl produced 2 signals slightly separated from each other and the blank (no chitosan) produced a large signal from HCl 50 mM (Fig. 2A). The large signal was assigned to the Cl^- from HCl [41]. To analyze the chitosan signal the intensity of the Cl^- signal was normalized based on the viscosity difference between the solutions (Eq. S2). The peak of Cl^- has a similar migration to blanks with injection of the carrier liquid spiked with DMSO. The injection of 50 mM HCl was then superimposed and subtracted from the chitosan dissolved in 50 mM HCl (Fig. 2B). The remaining peak is identified as chitosan. The unexpected separation of chitosan and Cl^- may be due to the occurrence of ion exclusion of the Cl^- and the adsorption of the chitosan. Tailing toward high elution times, indicative of slight adsorption [40] could still be seen; however, this was less pronounced than for chitosan dissolved in 50 mM AcOH.

Chitosan dissolved in aqueous AcOH exhibited a sharp peak (also present in the blank) coeluting with a broad peak. The sharp peak is thus assigned to acetate. The area of the chitosan dissolved in AcOH was calculated by integrating the chitosan with the acetate peak superimposed and subtracting the peak area of the acetate peak (Fig. S4). The peak area of chitosan dissolved in aqueous HCl was determined to be 17% greater than that dissolved in aqueous AcOH ($n = 2$). This is consistent with the CE results (see section 3.4.). PM experiments were also conducted with the solvent as the background electrolyte as is used for TDA (Fig. S5). Chitosan in aqueous HCl had the Cl^- peak superimposed on top of the chitosan peak in these conditions, while it was not the case of the chitosan in aqueous AcOH with the AcO^- migrating earlier. From the PM results it was concluded that aqueous HCl was able to dissolve chitosan to a greater extent than aqueous AcOH.

3.4. Evaluation of dissolution by capillary electrophoresis and pressure-assisted capillary electrophoresis

CE is growing in use for the characterization of macromolecules such as chitosan [22]. CE in the critical conditions has previously been studied to separate polylysine with a degree of polymerization below 10 [42] and chitosan samples by their *DA* [5]. CE in the critical conditions was used in this work to analyze the dissolution of chitosan in different solvents (Fig. 3). All separations were repeatable, but chitosan dissolved in aqueous HCl systematically led to higher recovery in CE. The dissolution of chitosan in aqueous HCl is seen to be more effective than in aqueous AcOH, both at room temperature and at 60 °C. The integration of the chitosan peak showed that the chitosan dissolved in aqueous HCl had at least a 13% greater peak area compared to that dissolved in aqueous AcOH ($n = 3$). The dissolution in aqueous TFA is as effective as in aqueous HCl at room temperature but at 60 °C it is not (being then comparable to dissolution in aqueous AcOH). These results are consistent with the initial results obtained from the pressure mobilization and it shows that aqueous AcOH is less efficient as a solvent for chitosan than aqueous HCl even though clear suspensions are produced in both cases. To increase the precision of the determination of the mobility, PACE was undertaken. PACE is CE with an added pressure during the separation. This is beneficial as the separation of chitosan takes place in a shorter time and the electroosmotic flow (EOF) is detected. The detection of the EOF allows a more precise determination of the electrophoretic mobilities of chitosan through a double correction with the use of an EOF marker and an electrophoretic mobility marker (Fig. 4). Further, it allows the correction of the area of the chitosan by the hexaamminecobalt(III) chloride internal standard area (to compensate

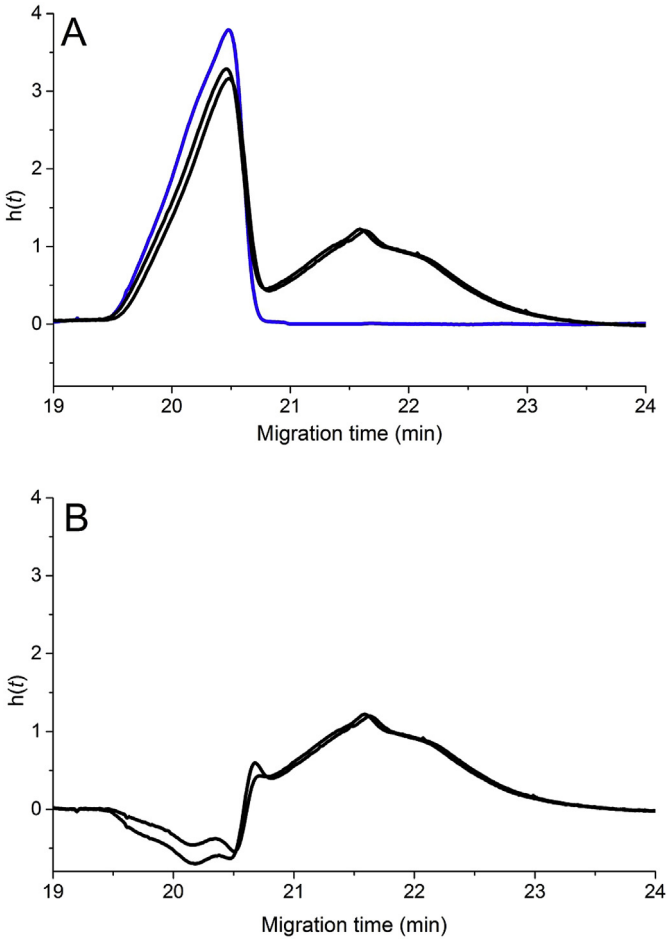

Fig. 2. PM (with viscosity normalization for Cl^-) of 50 mM HCl (blue) and of chitosan (MedMW1) dissolved in 50 mM HCl (black, 2 repeat experiments shown) A) before and B) after Cl^- subtraction.

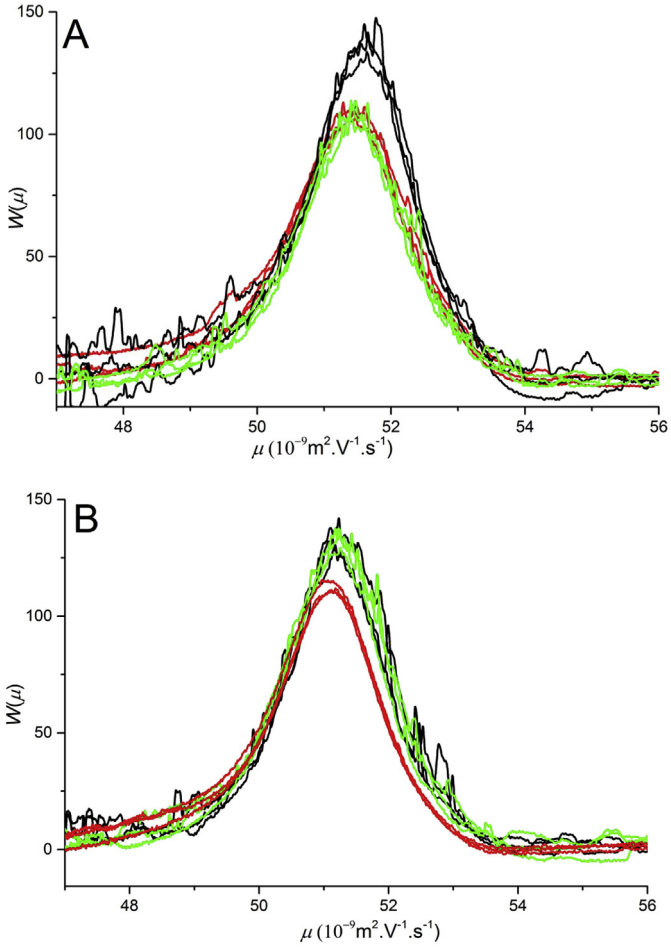

Fig. 3. Electropherogram of chitosan (MedMW1) dissolved in 50 mM HCl (black line), AcOH (red line) and TFA (green line) prepared at A) 60 °C for 2 h B) 25 °C for 2 h.

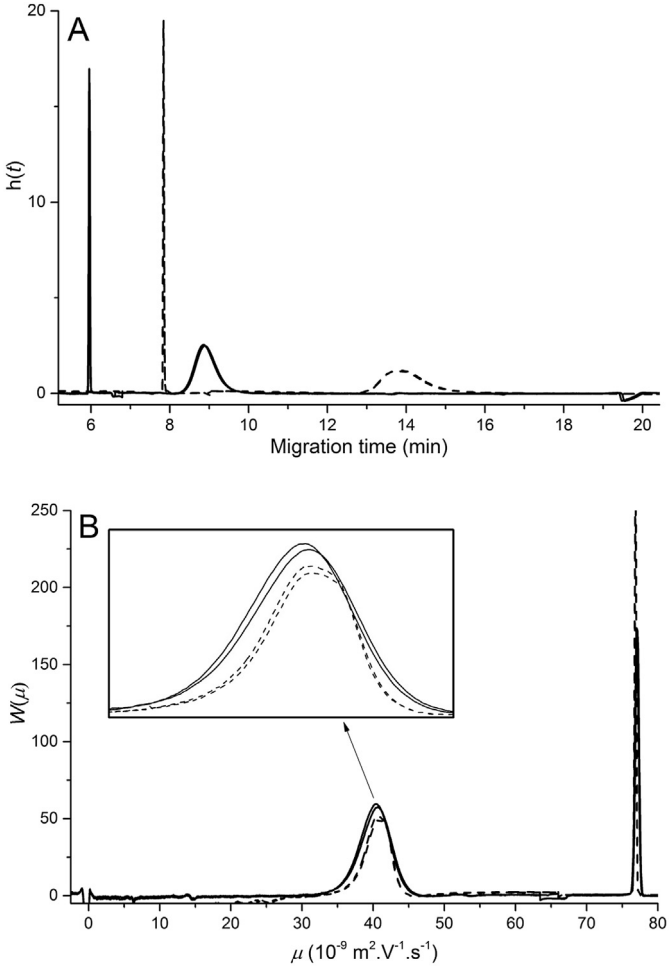

Fig. 4. Electropherogram of chitosan (MedMW1) dissolved in 50 mM HCl separated using CE (dashed line) and PACE (solid line) in a) migration time and b) electrophoretic mobility. The electrophoretic mobility marker is seen at a mobility of 76.9×10^{-9} m^2 V^{-1} s^{-1} and a migration time between 6 and 8 min. The EOF is seen at a mobility of 0.

for variations in injection volumes) and the detection of any neutral impurities that could not be seen in CE of chitosan without very long measuring times. The increase in precision is extremely important as any shifts in mobility caused by possible deacetylation (loss of charge) would be noticed during PACE measurements and be more accurately measured. Therefore, experiments monitoring the kinetics of dissolution (see sections 3.6. and 3.7.) with CE were undertaken using PACE.

3.5. Bias in dissolution evaluated with NMR spectroscopy

The measurement of the average degree of acetylation of chitosan is routine in its characterization. Solid-state NMR spectroscopy measurements allow the analysis of the whole sample and an accurate degree of acetylation to be attained. This is further significant taking into account the aforementioned difficulties in obtaining a true solution. A comparison of results from solid-state and solution-state NMR spectroscopy further identifies this bias. The error bars for the solution-state NMR spectroscopy results are based on the relative standard deviation *RSD* estimated from the signal-to-noise ratio *SNR* (Eq. (2) [43]).

$$RSD(\%) = \frac{238}{SNR^{1.28}} \quad (2)$$

The error bars for the solid-state NMR spectroscopy results are based on error caused by phasing and *SNR*. Limited *SNR* may not only result in a limited precision but it can also affect the way the user will phase the spectrum. This is especially true in the case of solid-state NMR spectroscopy in which the signals are generally quite broad. Therefore the error caused by phasing was tested (Table S5). It was measured by having 4 different users phase 8 different experimental data sets. The *DA* was measured and a *RSD* value was obtained for each data set. The *RSD* from phasing was observed to correlate with the *RSD* from *SNR* (Fig. 5A). Therefore, when the *SNR* was less than 50 the *RSD* of *DA* was estimated as a sum of the error from phasing and the error from *SNR* (Eq. (3)). The *RSD* was estimated from the *SNR* (Eq. (2)) for measurements with a *SNR* greater than 50, for which it was deemed that the error from phasing would be negligible.

$$RSD(\%) = 11 \times \frac{238}{SNR^{1.28}} - 16 \quad (3)$$

The MedMW2 sample (Table 1 and Fig. 5B) has a significantly higher *DA* value when measured with solid-state NMR spectroscopy compared to solution-state NMR spectroscopy which is not the case for the rest of the samples. The error on the average *DA* obtained by solution-state NMR may thus not be systematic. Solution-state NMR measurements can therefore not be calibrated, for example with chitosan samples standardized by solid-state

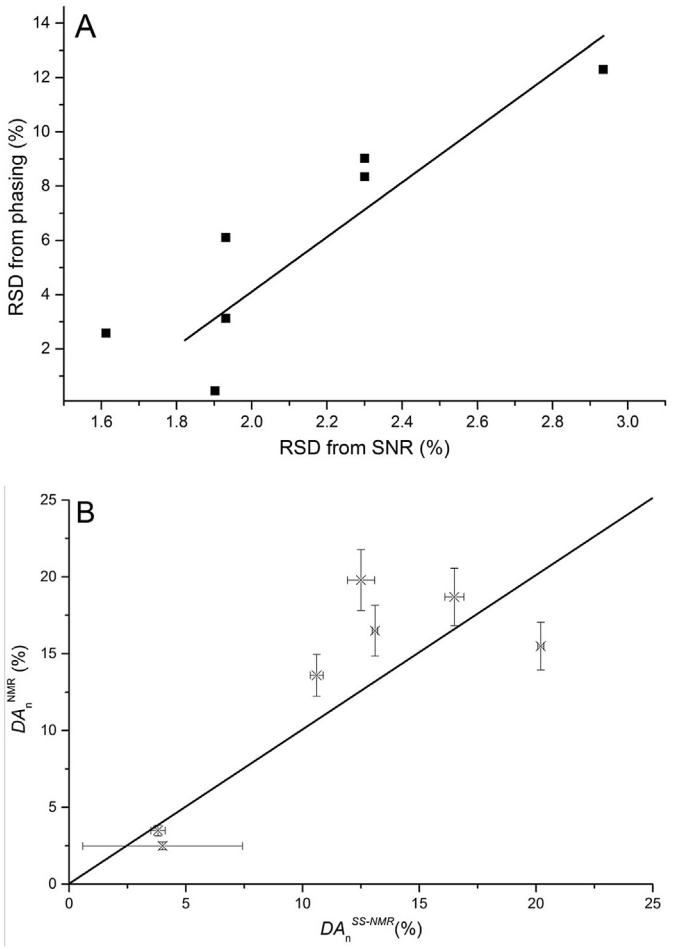

Fig. 5. A. Error of solid-state NMR spectroscopy measurements estimated as *RSD* from *SNR* and as *RSD* from phasing. The straight line represents a linear fit (y = 10x-16, $R^2 = 0.79$). B. *DA* values obtained by solution- and solid-state NMR spectroscopy for the same chitosan samples. The straight line is the diagonal.

NMR spectroscopy.

The analysis undertaken in solution state shows only the *DA* of the dissolved fraction of the partially dissolved sample which introduces a bias in the determination of the *DA* of the whole sample. The solid-state NMR spectroscopy measurements considered more accurate due to the fact that they measure the whole sample and not just its soluble fraction. For the solution-state NMR spectroscopy the difficulty in dissolving chains with many acetyl groups was previously noted [2] and therefore it is likely chitosan chains with a large *DA* may remain undissolved and influence the determination of *DA*. The influence may also cause variance in the total amount of D-glucosamine units in solution as a chain with a block of *N*-acetyl-D-glucosamine units that remain out of solution may cause the rest of the chain to remain out of solution. Such an occurrence would be explained by chitosan's precursor chitin, as chitin has a semi-crystalline structure with extended hydrogen bonding [11]. The deacetylation of chitin may cause some chains to have a tendency towards blocks of *N*-acetyl-D-glucosamine [3]. These blocks depending on their size may cause these chitosan chains to remain out of solution and cause an incomplete dissolution. This would explain the overestimation (AK Bio D2, D3) of the *DA* values by solution-state NMR spectroscopy. The solution-state measurements may also be influenced by the use of deuterated HCl (DCl) as explored below (see section 3.6).

3.6. Kinetics of dissolution monitored by solution-state NMR spectroscopy and PACE

The kinetics of the dissolution was monitored using solution-state NMR spectroscopy, as previously achieved in the case of starch [44]. Before the kinetics measurement, T_1 relaxation time of the chitosan was measured to allow a quantitative measurement. The T_1 relaxation time of the acetyl peak was 1.2 s which was very similar to that of the backbone signal. Chitosan was suspended in 0.8 M DCl in D_2O. Measurements were taken over a 61 h period with a total of 800 measurements and the probe's temperature was controlled at 60 °C during the experiment. From the second measurement the signals assigned to the backbone between 3 and 5 ppm start to be seen (Fig. S6). A signal in the region of the acetyl signal (1.8–2 ppm) is also seen. However, as the measurements progress a second signal is seen in the same region slightly shifted downfield (Fig. S6).

As the kinetics measurement continues this new signal becomes more intense. An integration of this peak shows a steady increase even after the plateau of the chitosan backbone signal intensity is reached (Fig. 6); this signal is therefore assigned to a product of the deacetylation of chitosan [45]. The sharp signal is indicative of a small/mobile group which supports the hypothesis of deacetylation. The intensity of the signal at 2.2 ppm reduces over time (after 15 h); this signal is thus assigned to the acetyl group of the chitosan. To check the assignment of the signals, chitosan and chitosan spiked with 50 mM AcOH dissolved in 50 mM DCl in D_2O were measured at 60 °C. The signal of the deacetylation product of chitosan was assigned to free AcOH confirming the occurrence of deacetylation (Fig. S7).

The intensity of the chitosan backbone signal is stable after 10 h (Fig. 6A) however, the signal associated with the acetyl peak and the peak associated to the deacetylation increase and decrease over time, respectively. The detection and quantification of the free AcOH allowed the monitoring of the kinetics of the deacetylation (which is not possible using the acetyl group on the chitosan backbone since it is affected by both dissolution and deacetylation simultaneously). The deacetylation was assumed to follow a 2nd order kinetics [46]: S_N2 reaction with a first order in *N*-acetyl-D-glucosamine units (see Equation S-10). This hypothesis was tested using the acetyl peak of the free AcOH (see Fig. 6B and C). A linear correlation is observed when the concentration of the *N*-acetyl-D-glucosamine units is determined as the sum of the integrals of the free AcOH and *N*-acetyl-D-glucosamine signals (NG) on the plateau (Fig. 6B). This NG concentration at the plateau $[NG]_\infty$ corresponds to the total concentration of *N*-acetyl-D-glucosamine units that can be dissolved, regardless of whether they are deacetylated or not in solution. When the total concentration of *N*-acetyl-D-glucosamine units is taken as the dissolved fraction of the initial *N*-acetyl-D-glucosamine units (real time value of [NG] on Fig. 6A), a non-linear relationship is seen (Fig. 6C). This result suggests that deacetylation is able to take place as soon as the chitosan is in contact with the solvent. The use of DCl for the dissolution over HCl may cause the dissolution to be slower since the hydrogen bonding that would normally occur in aqueous HCl is stronger than deuterium bonding. Studies have looked into the deacetylation and hydrolysis of chitin and chitosan in concentrated hydrochloric acid [47,48] with temperatures of 25 and 30 °C. It was seen that the concentration of the HCl or DCl used and the composition influenced the rate of hydrolysis and deacetylation [7]. In these conditions, the concentration of HCl (high concentrations) was shown to play a significant role over temperature (only tested 25 and 35 °C). However, deacetylation was 4 times faster at 35 °C compared to 25 °C and 6 M HCl was shown to be the most efficient in hydrolysis [47]. It was further suggested that the formation of a glucofuranosyl

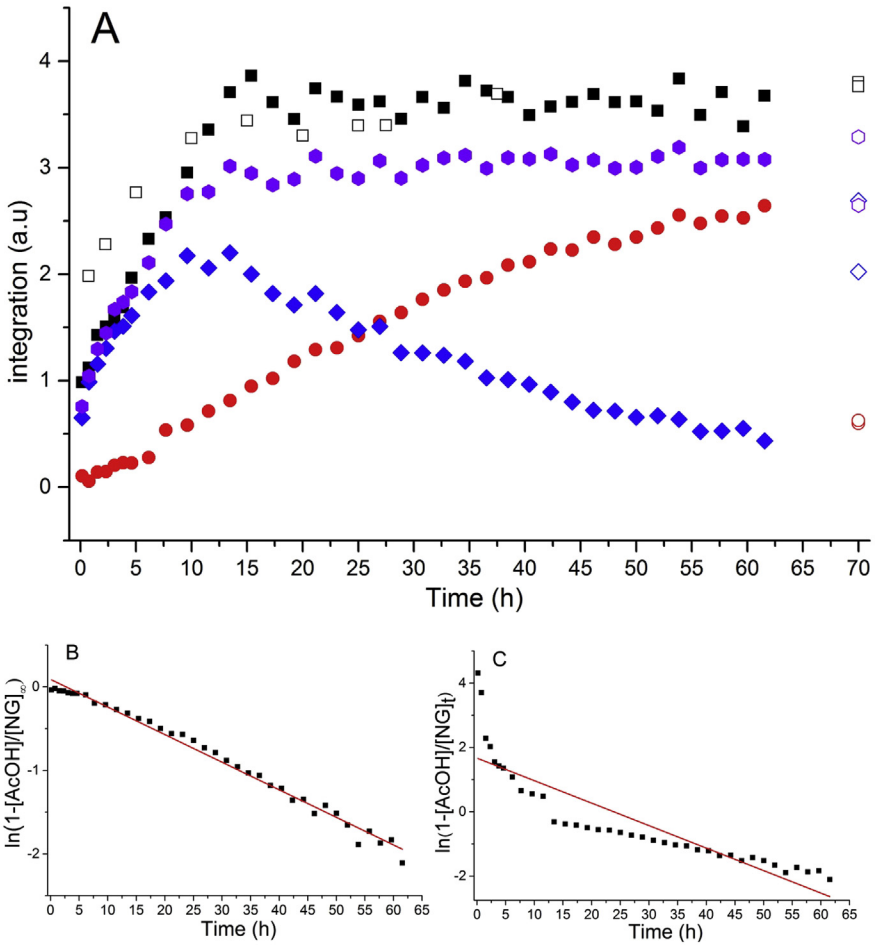

Fig. 6. A. Integration of solution-state NMR signals measured over 61 h at 60 °C: chitosan backbone (black squares), chitosan acetyl group (blue diamonds), free AcOH (red circles) and the sum of the acetyl group and free AcOH (NG, purple hexagons). The full symbols correspond to measurements in 0.8 M DCl in D_2O, the empty symbols to measurements in 50 mM DCl in D_2O. Evolution on a logarithmic scale of the consumption of the acetyl groups on *N*-acetyl-D-glucosamine units, with the *N*-acetyl-D-glucosamine concentration taken as (B) the total available initial *N*-acetyl-D-glucosamine units $[NG]_\infty$ (plateau of NG purple curve in A) or (C) as the dissolved fraction of the initial *N*-acetyl glucosamine units $[NG]_t$ (real time value of NG purple curve in A). Red lines represent linear fits with a r^2 of 0.99 (B) and 0.77 (C). (For interpretation of the references to colour in this figure legend, the reader is referred to the web version of this article.)

oxazolinium ion occurs in concentrated DCl, however this was not noted in our spectra as there was an absence of the corresponding 3 ^{1}H NMR signals at 7 and between 5 and 4.7 ppm. A lower concentration of acid (0.8 M) was used in this work than in previous research and the glucofuranosyl oxazolinium, if present, is below its limit of detection. Further, the low concentration of DCl used in this work would not support hydrolysis over deacetylation as seen previously.

The monitoring was then repeated with 16 times lower concentration of DCl in D_2O (50 mM) to see if the deacetylation still occurred. The rate of dissolution was surprisingly comparable. Deacetylation was once again detected and confirmed, but more limited. Deacetylation was seen to be between 18 and 24% of the initial *DA* value (±3.5 on the *DA* scale). A dissolution experiment was also undertaken with chitosan dissolved for 55 h in 50 mM HCl and DCl in D_2O. The 2 chitosan samples were precipitated and measured with solid-state NMR spectroscopy. Between 14 and 16% of the initial *DA* value (±1.5 on the *DA* scale) deacetylation was determined after dissolution. The results suggest that the deacetylation and dissolution of chitosan is complex however occurs even at low concentrations of DCl.

This NMR method is not a high-throughput method to monitor dissolution. Measurements of chitosan in 50 mM DCl and HCl were also undertaken on a Magritek Spinsolve benchtop NMR spectrometer to try and detect the deacetylation of chitosan in aqueous HCl. However, the signals of chitosan were unable to be distinctly resolved at the low concentration (1 g L^{-1}) chosen for minimal aggregation (Fig. S8).

To compare the effects of HCl and DCl on the deacetylation of chitosan, PACE was used to run a kinetic measurement at 60 °C. CE has an advantage over ^{1}H NMR spectroscopy in its ability to test both DCl and HCl and a shift in the mobility would be an indication of the deacetylation of chitosan. Samples were kept in the sample tray (set at 60 °C) during the course of the kinetic experiment. The PACE results show an insignificant difference in the extent of chitosan dissolution between 50 mM HCl in water and 50 mM DCl in D_2O (Figs. 7 and S9). Further, the peak area of both samples does not significantly change over the course of the kinetics after reaching a plateau at 7 h (within experimental error). This is quicker than the 10 h needed for the plateau to be observed in NMR spectroscopy. This might be due to strong intramolecular interactions persisting in the chitosan macromolecules between 7 and 10 h dissolution (this might be related to the tendency towards blocks of *N*-acetyl-D-glucosamine units).

The deacetylation of chitosan at 60 °C in 50 mM DCl in D_2O was detected in solution-state NMR spectroscopy and it was observed to

occur almost immediately. This should correspond in PACE to a shift to higher electrophoretic mobility because of the higher charge [5] as well as a decrease in peak area since the main chromophore of the chitosan should be the acetamide functional group. However, the evidence of deacetylation was not detected in the PACE results: the electrophoretic mobility remains constant throughout the dissolution apart from the first 5 h in which aggregation affects the dissolution and the peak area of the chitosan dissolved in both aqueous solvents remained constant after reaching a plateau after 7 h (Fig. 7). In both cases, the dissolution as well as the deacetylation contribute: some low *DA* chitosan chains may dissolve a lot quicker than the high *DA* ones (before the first measurement). The dissolution may thus lead to a shift to lower mobility during the dissolution and this may counterbalance the shift to higher mobility due to deacetylation. A similar effect would be observed on peak area. The absence of mixing of the sample in PACE compared to the rotation of the NMR tube might lead to a lower difference in rate of deacetylation in both systems, but this was not observed in the case of the dissolution. It can be hypothesized through the comparison of the NMR and CE results that higher *DA* chitosan chains dissolve quicker and that, at least in DCl, deacetylation of chitosan takes place at a similar rate as the dissolution.

This finding is extremely significant as solution-state NMR spectroscopy is used routinely for the molecular characterization of chitosan especially for *DA* measurements (Table S4). These measurements often use DCl as the methyl from any residual CHD_2COOD in CD_3COOD is likely to overlap with that of the chitosan. DCl causes degradation and therefore inaccurate measurements are obtained. Conditions used for the solution-state NMR results obtained previously [5] are unlikely to have caused a strong deacetylation due to the short period at higher temperatures; however, the sample would not have been completely dissolved during the measurement and therefore a bias on the measurement of *DA* is clear. Further research is required on obtaining of a "true solution", however it can be concluded that solution-state NMR spectroscopy using 50 mM DCl in D_2O as a solvent yields inaccurate *DA* values.

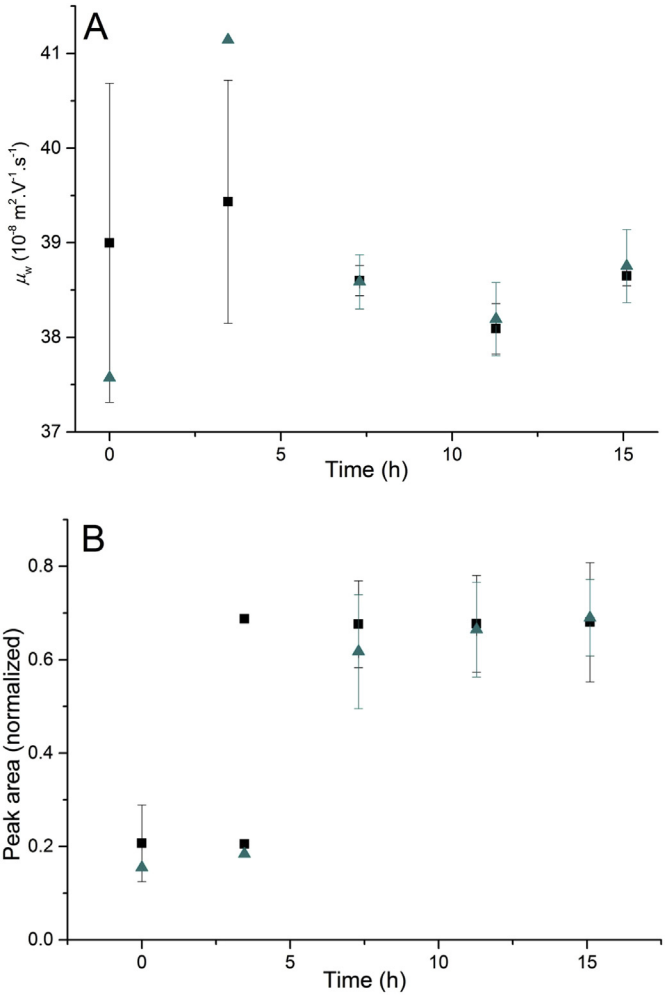

Fig. 7. A. Weight-average mobility μ_w and B. Integral of chitosan peak in kinetics of dissolution monitored with PACE in 50 mM HCl in water (black squares) and DCl in D_2O (green triangles). (For interpretation of the references to colour in this figure legend, the reader is referred to the web version of this article.)

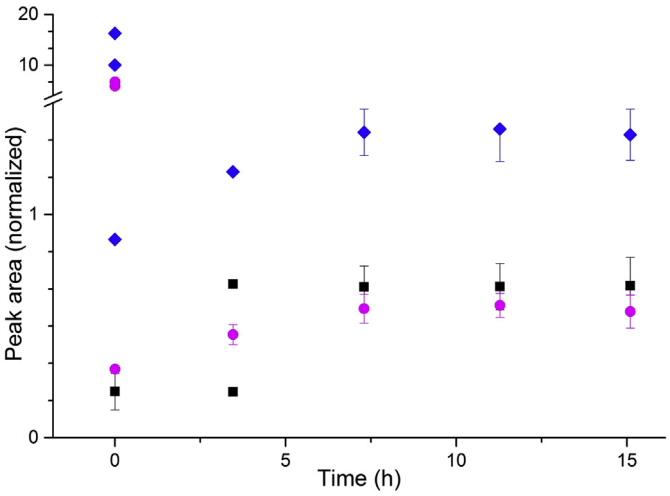

Fig. 8. Integration of the peak area in a kinetics of dissolution of MedMW1 (black squares), LowMW1 (magenta circles) and HighMW (blue diamonds) chitosan undertaken with PACE in 50 mM HCl (n = 2). (For interpretation of the references to colour in this figure legend, the reader is referred to the web version of this article.)

The effect of acid on the hydrodynamic volume of chitosan was also investigated and compared in the literature [49]. It was concluded that AcOH caused acid hydrolysis when compared to malic acid through a measurement of intrinsic viscosity. This may, however, also be due to a more complete dissolution taking place when compared to malic acid as results undertaken in this study express that chitosan is complicated to dissolve even in aqueous solvents.

3.7. Comparison of the kinetics of dissolution of different chitosan samples

The dissolution of 3 different chitosan samples (MedMW1, LowMW1, HighMW) in 50 mM HCl was analyzed with PACE to compare the effect of molar mass and of *DA* on dissolution. The samples were prepared after the preconditioning of the capillary to obtain an accurate data point at the beginning of the kinetics (t_0). It was seen that the area of the peak for LowMW1, MedMW1 and HighMW reached a plateau (within experimental error) after 7.5 h (from the 3rd measurement, Fig. 8, S9-11). The peak area was corrected by the average *DA* obtained from the solid-state NMR spectroscopy measurements. The t_0 measurement of HighMW and LowMW1 had a very large signal at the same electrophoretic mobility as chitosan (Fig. S12). This was due to non-repeatable aggregates causing light scattering which would explain the immense absorbance. The dissolution of all 3 samples followed a similar kinetics reaching a plateau after 5 h. The samples

dissolution seems to behave similarly with the exception of the t_0 of the HighMW and the LowMW1 which undergoes aggregation. The LowMW1 and MedMW1 are notably less soluble in aqueous HCl than the HighMW with approximately 35% difference in the peak area (n = 2). Low or medium molar masses are expected to lead to faster and potentially more complete dissolution than higher molar masses. It should be noted that the molar masses are of limited accuracy notably due to aggregation (as see with SEC in this work) and incomplete dissolution or deacetylation. Therefore the molar mass supplied may not be representative of the sample. More importantly, HighMW has the lowest average *DA*. A lower *DA* is known to lead to faster and more complete dissolution. Assuming the relative difference of molar mass of the three chitosan samples is true, the results signify *DA* has a greater role in dissolution than molar mass.

4. Conclusions

Through this study we have showed that the dissolution of chitosan is quite challenging and often overlooked. The presence of aggregates even at low concentrations of chitosan complicates the dissolution and prevents from obtaining a true solution. However, this study was able to show that aqueous AcOH was less efficient at dissolving chitosan when compared to aqueous HCl and the dissolution in aqueous TFA is as efficient only at room temperature. This information is significant due to the prominent use of AcOH in the dissolution of chitosan for various applications, as well as characterization methods such as SEC for molar mass calculations or CE for the separation of chitosan by its *DA*. Several studies characterize the average *DA* or the molar mass of chitosan on the assumption that all the chains of chitosan are dissolved and the result obtained is representative of the whole sample [11]. A study undertaken to analyze the *DA* of chitosan and its distribution by SEC concluded that the characterization in solution may have been impeded by artifacts [50]. These artifacts could, however, have been the presence of aggregates due to the use of AcOH as a solvent as identified in a later study [18]. Due to the presence of aggregates and the inability to remove them from the solution, it was concluded that characterization was only possible for a small number of samples. The SEC results obtained in our study further supports the presence of aggregation through the extremely large molar mass values determined. The kinetics measurements gave further information regarding the behavior of chitosan in solution and showed the increase in deacetylation caused by long periods at high temperature as well as partial deacetylation in shorter time periods. Samples with different *DA*s measured by NMR spectroscopy were successfully studied and the effects of *DA* on the dissolution were compared by PACE. The average *DA* may play a more important role in the completeness of dissolution than the molar mass. Further, time-resolved NMR spectroscopy and PACE showed that 50 mM DCl is an inappropriate solvent for chitosan due to deacetylation. Following these results, previous measurements of the average *DA* of chitosan in 50 mM DCl using solution-state NMR spectroscopy (Table S4), including from our team [5] should be considered very carefully and rather replaced with values obtained by solid-state NMR spectroscopy as published by others [27,28] and as obtained in this work. Future work should focus on improving the solubility while minimizing the degradation and this may involve the use of salts as a hydrogen bond disruptor as in the cases of cellulose [51] and starch [8] or the use of ionic liquids [52]. The stability of chitosan in simulated gastric fluid (SGF) and simulated intestinal fluid (SIF) could also be analyzed to help assess the use of chitosan as a drug delivery agent.

Acknowledgements

JJT thanks Matthew Van Leeuwen (WSU) for assistance in the lab, Alison Maniego (WSU), Michelle Toutounji (WSU) and Lucie Seiler (University Paul Sabatier, Toulouse, France) for assistance with NMR spectroscopy data treatment, and the Australian Government for the Endeavour Research Fellowship to travel to the Max Planck Institute for Polymer Research, Mainz, Germany. MG and PC thank the Molecular Medicine Research Group at WSU for Research Seed Funding. We thank Robert Graf (MPIP), Michael O'Connor (WSU) and Richard Wuhrer (AMCF, WSU) for insightful discussions, Malvern Instruments and ATA Scientific, especially Bryn McDonagh, for the loan of a Triple Detector Array SEC, as well as and Magritek, especially Mitchell Goshert, Peter Hulmston and Andrew Coy, for the loan of a benchtop NMR spectrometer.

Appendix A. Supplementary data

Supplementary data related to this article can be found at http://dx.doi.org/10.1016/j.aca.2016.06.021.

References

[1] S. Trombotto, C. Ladaviere, F. Delolme, A. Domard, Chemical preparation and structural characterization of a homogeneous series of chitin/chitosan oligomers, Biomacromolecules 9 (2008) 1731–1738.
[2] M. Rinaudo, Chitin and chitosan: properties and applications, Prog. Polym. Sci. 31 (2006) 603–632.
[3] A. Domard, A perspective on 30 years research on chitin and chitosan, Carbohydr. Polym. 84 (2011) 696–703.
[4] Z. Li, M. Leung, R. Hopper, R. Ellenbogen, M. Zhang, Feeder-free self-renewal of human embryonic stem cells in 3D porous natural polymer scaffolds, Biomaterials 31 (2010) 404–412.
[5] M. Mnatsakanyan, J.J. Thevarajah, R.S. Roi, A. Lauto, M. Gaborieau, P. Castignolles, Separation of chitosan by degree of acetylation using simple free solution capillary electrophoresis, Anal. Bioanal. Chem. 405 (2013) 6873–6877.
[6] G. Lamarque, C. Viton, A. Domard, Comparative study of the first heterogeneous deacetylation of alpha- and beta-chitins in a multistep process, Biomacromolecules 5 (2004) 992–1001.
[7] A. Einbu, K.M. Varum, Characterization of chitin and its hydrolysis to GlcNAc and GlcN, Biomacromolecules 9 (2008) 1870–1875.
[8] S. Schmitz, A.C. Dona, P. Castignolles, R.G. Gilbert, M. Gaborieau, Assessment of the extent of starch dissolution in dimethyl sulfoxide by 1H NMR spectroscopy, Macromol. Biosci. 9 (2009) 506–514.
[9] B.A. Miller-Chou, J.L. Koenig, A review of polymer dissolution, Prog. Polym. Sci. 28 (2003) 1223–1270.
[10] C. Lefay, Y. Guillaneuf, G. Moreira, J.J. Thevarajah, P. Castignolles, F. Ziarelli, E. Bloch, M. Major, L. Charles, M. Gaborieau, D. Bertin, D. Gigmes, Heterogeneous modification of chitosan via nitroxide-mediated, polymerization 4 (2013) 322–328.
[11] C.K.S. Pillai, W. Paul, C.P. Sharma, Chitin and chitosan polymers: chemistry, solubility and fiber formation, Prog. Polym. Sci. 34 (2009) 641–678.
[12] Y.I. Jeong, D.G. Kim, M.K. Jang, J.W. Nah, Preparation and spectroscopic characterization of methoxy poly(ethylene glycol)-grafted water-soluble chitosan, Carbohydr. Res. 343 (2008) 282–289.
[13] T.P. Kravtchenko, J. Renoir, A. Parker, G. Brigand, A novel method for determining the dissolution kinetics of hydrocolloid powders, Food Hydrocolloids 13 (1999) 219–225.
[14] Y. Zhang, S.K. Mallapragada, B. Narasimhan, A novel high throughput method to investigate polymer dissolution, Macromol. Rapid Commun. 31 (2010) 385–390.
[15] A. Chojnacka, H.G. Janssen, P. Schoenmakers, Detailed study of polystyrene solubility using pyrolysis-gas chromatography-mass spectrometry and combination with size-exclusion chromatography, Anal. Bioanal. Chem. 406 (2014) 459–465.
[16] A. Chojnacka, A. Ghaffar, A. Feilden, K. Treacher, H.G. Janssen, P. Schoenmakers, Pyrolysis-gas chromatography-mass spectrometry for studying N-vinyl-2-pyrrolidone-co-vinyl acetate copolymers and their dissolution behaviour, Anal. Chim. Acta 706 (2011) 305–311.
[17] M.W. Anthonsen, K.M. Varum, A.M. Hermansson, O. Smidsrod, D.A. Brant, Aggregates in acidic solutions of chitosans detected by static laser-light scattering, Carbohydr. Polym. 25 (1994) 13–23.
[18] M. Yanagisawa, Y. Kato, Y. Yoshida, A. Isogai, SEC-MALS study on aggregates of chitosan molecules in aqueous solvents: influence of residual N-acetyl groups, Carbohydr. Polym. 66 (2006) 192–198.
[19] M. Gaborieau, P. Castignolles, Size-exclusion chromatography (SEC) of branched polymers and polysaccharides, Anal. Bioanal. Chem. 399 (2011)

1413–1423.
[20] M.H. Ottoy, K.M. Varum, B.E. Christensen, M.W. Anthonsen, O. Smidsrod, Preparative and analytical size-exclusion chromatography of chitosans, Carbohydr. Polym. 31 (1996) 253–261.
[21] T. Le Saux, H. Cottet, Size-based characterization by the coupling of capillary electrophoresis to Taylor dispersion analysis, Anal. Chem. 80 (2008) 1829–1832.
[22] J.J. Thevarajah, M. Gaborieau, P. Castignolles, Separation and characterization of synthetic polyelectrolytes and polysaccharides with capillary electrophoresis, Adv. Chem. 2014 (2014). Article ID 798403.
[23] D.L. Taylor, C.J. Ferris, A.R. Maniego, P. Castignolles, M. in het Panhuis, M. Gaborieau, Characterization of Gellan Gum by capillary electrophoresis, Aus. J. Chem. 65 (2012) 1156–1164.
[24] M. Gaborieau, T. Causon, Y. Guillaneuf, E.F. Hilder, P. Castignolles, Molecular weight and tacticty of oligoacrylates by capillary electrophoresis - mass spectrometry, Aus. J. Chem. 63 (2010) 1219–1226.
[25] J.J. Thevarajah, A.T. Sutton, A.R. Maniego, E.G. Whitty, S. Harrisson, H. Cottet, P. Castignolles, M. Gaborieau, Quantifying the heterogeneity of chemical structures in complex charged polymers through the dispersity of their distributions of electrophoretic mobilities or of compositions, Anal. Chem. 88 (2016) 1674–1681.
[26] J. Chamieh, M. Martin, H. Cottet, Quantitative analysis in capillary electrophoresis: transformation of raw electropherograms into continuous distributions, Anal. Chem. 87 (2015) 1050–1057.
[27] M.H. Ottoy, K.M. Varum, O. Smidsrod, Compositional heterogeneity of heterogeneously deacetylated chitosans, Carbohydr. Polym. 29 (1996) 17–24.
[28] L. Heux, J. Brugnerotto, J. Desbrieres, M.F. Versali, M. Rinaudo, Solid state NMR for determination of degree of acetylation of chitin and chitosan, Biomacromolecules 1 (2000) 746–751.
[29] C.R. Morcombe, K.W. Zilm, Chemical shift referencing in MAS solid state NMR, J. Magn. Reson. 162 (2003) 479–486.
[30] R. Novoa-Carballal, E. Fernandez-Megia, R. Riguera, Dynamics of chitosan by H-1 NMR relaxation, Biomacromolecules 11 (2010) 2079–2086.
[31] C. Prego, D. Torres, E. Fernandez-Megia, R. Novoa-Carballal, E. Quinoa, M.J. Alonso, Chitosan-PEG nanocapsules as new carriers for oral peptide delivery - effect of chitosan pegylation degree, J. Control. Release 111 (2006) 299–308.
[32] E. Fernandez-Megia, R. Novoa-Carballal, E. Quiñoá, R. Riguera, Optimal routine conditions for the determination of the degree of acetylation of chitosan by 1H-NMR, Carbohydr. Polym. 61 (2005) 155–161.
[33] M. de la Fuente, B. Seijo, M.J. Alonso, Bioadhesive hyaluronan-chitosan nanoparticles can transport genes across the ocular mucosa and transfect ocular tissue, Gene Ther. 15 (2008) 668–676.
[34] Polymer Standards Service, Characterization of Chitin/Chitosan, GPC/SEC application note 10280.
[35] D. Berek, Size exclusion chromatography - a blessing and a curse of science and technology of synthetic polymers, J. Sep. Sci. 33 (2010) 315–335.
[36] D. Muller, M. Ndoumenze, J. Jozefonvicz, High-pressure size-exclusion chromatography of anticoagulant materials, J. Chromatogr. 297 (1984) 351–358.
[37] Y. Guillaneuf, P. Castignolles, Using apparent Molecular Weight from SEC in controlled/living polymerization and kinetics of polymerization, J. Polym. Sci. A Polym. Chem. 46 (2008) 897–911.
[38] M. Gaborieau, J. Nicolas, M. Save, B. Charleux, J.-P. Vairon, R.G. Gilbert, P. Castignolles, Multiple-detection size-exclusion chromatography of complex branched polyacrylates, J. Chromatogr. A 1190 (2008) 215–233.
[39] W. Praznik, A. Huber, De facto molecular weight distributions of glucans by size-exclusion chromatography combined with mass/molar-detection of fluorescence labeled terminal hemiacetals, J. Chromatogr. B 824 (2005) 295–307.
[40] L.T. Cherney, A.P. Petrov, S.N. Krylov, One-dimensional approach to study kinetics of reversible binding of protein on capillary walls, Anal. Chem. 87 (2015) 1219–1225.
[41] N. Higashi, Y. Ozaki, Potential of far-ultraviolet absorption spectroscopy as a highly sensitive quantitative and qualitative analysis method for aqueous solutions, Part I: determination of hydrogen chloride in aqueous solutions, Appl. Spectrosc. 58 (2004) 910–916.
[42] H.F. Wu, S.A. Allison, C. Perrin, H. Cottet, Modeling the electrophoresis of highly charged peptides: application to oligolysines, J. Sep. Sci. 35 (2012) 556–562.
[43] P. Castignolles, R. Graf, M. Parkinson, M. Wilhelm, M. Gaborieau, Detection and quantification of branching in polyacrylates by size-exclusion chromatography (SEC) and melt-state 13C NMR spectroscopy, Polymer 50 (2009) 2373–2383.
[44] A. Dona, C.-W.W. Yuen, J. Peate, R.G. Gilbert, P. Castignolles, M. Gaborieau, A new NMR method for directly monitoring and quantifying the dissolution kinetics of starch in DMSO, Carbohydr. Res. 342 (2007) 2604–2610.
[45] M. Lavertu, Z. Xia, A.N. Serreqi, M. Berrada, A. Rodrigues, D. Wang, M.D. Buschmann, A. Gupta, A validated 1H NMR method for the determination of the degree of deacetylation of chitosan, J. Pharma. Biomed. Anal. 32 (2003) 1149–1158.
[46] K.M. Varum, M.H. Ottoy, O. Smidsrod, Acid hydrolysis of chitosans, Carbohydr. Polym. 46 (2001) 89–98.
[47] A. Einbu, K.M. Varum, Depolymerization and de-N-acetylation of chitin oligomers in hydrochloric acid, Biomacromolecules 8 (2007) 309–314.
[48] A. Einbu, H. Grasdalen, K.M. Varum, Kinetics of hydrolysis of chitin/chitosan oligomers in concentrated hydrochloric acid, Carbohydr. Res. 342 (2007) 1055–1062.
[49] R.H. Chen, W.Y. Chen, S.T. Wang, C.H. Hsu, M.L. Tsai, Changes in the Mark-Houwink hydrodynamic volume of chitosan molecules in solutions of different organic acids, at different temperatures and ionic strengths, Carbohydr. Polym. 78 (2009) 902–907.
[50] G. Berth, H. Dautzenberg, The degree of acetylation of chitosans and its effect on the chain conformation in aqueous solution, Carbohydr. Polym. 47 (2002) 39–51.
[51] M. Kostag, T. Liebert, T. Heinze, Acetone-based cellulose solvent, Macromol. Rapid Commun. 35 (2014) 1419–1422.
[52] M. Gericke, P. Fardim, T. Heinze, Ionic liquids - promising but challenging solvents for homogeneous derivatization of cellulose, Molecules 17 (2012) 7458–7502.

Supporting information
For
Towards a less biased dissolution of chitosan

Joel J. Thevarajah [a,b,c], Jerikho C. Bulanadi [a], Manfred Wagner [c], Marianne Gaborieau [a,b]*, Patrice Castignolles [a]

[a] Western Sydney University, School of Science and Health, Australian Centre for Research on Separation Sciences (ACROSS), Parramatta, 2150, Australia

[b] Western Sydney University, Molecular Medicine Research Group (MMRG), School of Science and Health, Parramatta, 2150, Australia [c] Max Planck Institute for Polymer Research, 55128 Mainz, Ackermannweg 10, Germany

*Corresponding author : Marianne Gaborieau, m.gaborieau@westernsydney.edu.au

Visual observation of dissolution

A range of aqueous acids were chosen at different concentrations to assess the dissolution of chitosan at room temperature, 40 °C and 60 °C (see Tables S1 and S2).

Table S1: Visual evaluation of MedMW2 chitosan dissolution in various aqueous acids and sodium borate buffer at room temperature. "Yes" indicates transparency within 15 minutes.

	Concentration				
Acid	5 mM	10 mM	50 mM	1 % [a)]	5 % [a)]
Hydrochloric	No	No	Yes	Yes	-
Acetic	No	No	Yes	Yes	-
Trifluoroacetic	No	No	Yes	Yes	-
Phosphoric	-	-	No	No	No
Boric	-	-	No	No	No
Borate Buffer	-	-	No	-	-
Trifluoroacetic acid (0.3%) [a)]	-	-	No	-	-

- indicates that the experiment was not conducted

[a)] Unit was % w/v for boric acid and % v/v for the others

Table S2: Visual evaluation of MedMW2 chitosan dissolution at higher temperatures in various aqueous acids and sodium borate buffer. “Yes” indicates transparency after 1 hour.

Temperature	40 °C		60 °C	
Concentration	50 mM	1 %	50 mM	1 %
Phosphoric acid	Partial	Partial	Yes	Yes
Boric acid	No	No	No	No
Borate Buffer	No	-	No	-
Trifluoroacetic acid eluent	No	-	No	-

SEC of chitosan

Aqueous SEC of different chitosan samples dissolved with 3 different solvents was conducted. The pullulan-equivalent number-average and weight-average molar masses M_w and M_n were calculated.

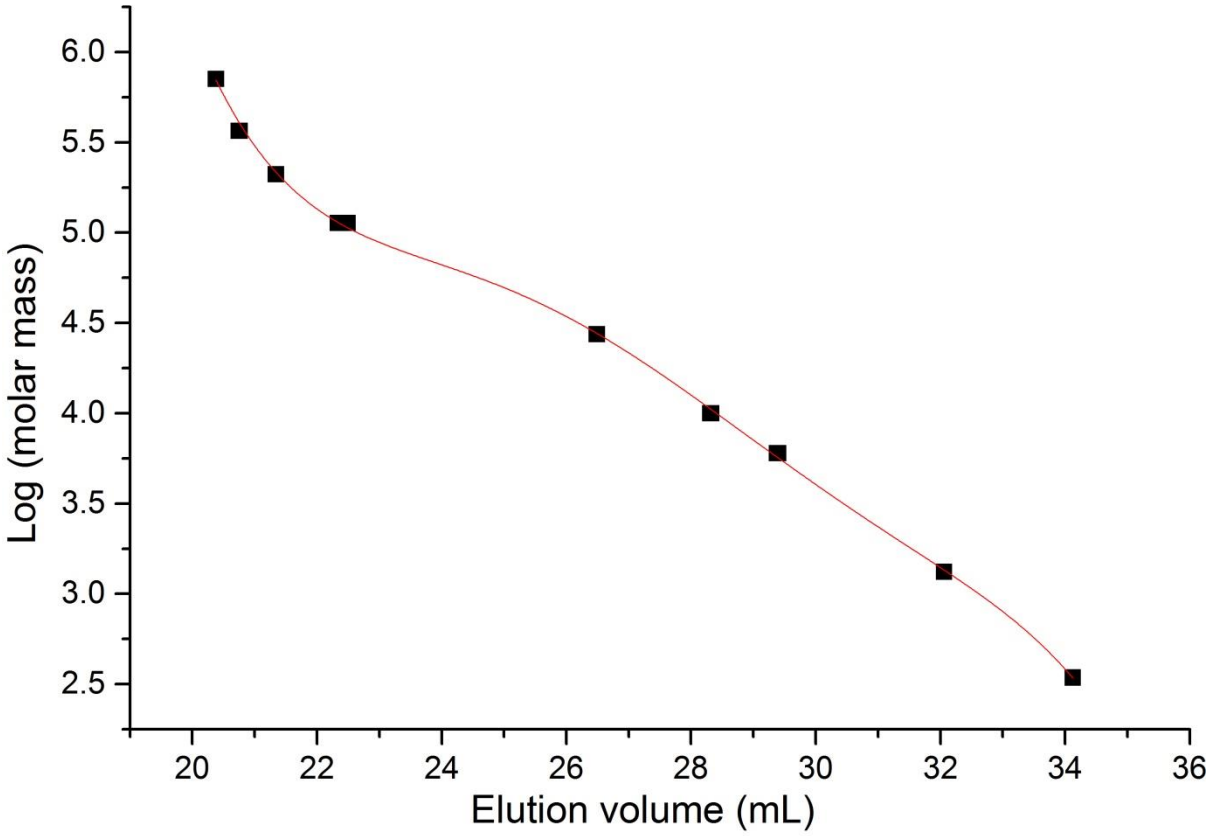

Figure S1: Conventional calibration curve of pullulan standards

Table S3: Pullulan-equivalent M_n and M_w of different chitosan samples injected at different concentrations and dissolved in different aqueous solvents (eluent is composed of 0.3 % (w/v) TFA and 0.1 M NaCl)

Sample	Solvent	Injection concentration ($g \cdot L^{-1}$)	M_n ($g \cdot mol^{-1}$)	M_w ($g \cdot mol^{-1}$)
LowMW1	50 mM HCl	1	830,000	$16{,}000 \times 10^{10}$
		1	1,100,000	$98{,}000 \times 10^{10}$
		1	960,000	$39{,}000 \times 10^{11}$
		1	950,000	$42{,}000 \times 10^{10}$

		0.5	700,000	$77{,}000 \times 10^{12}$
		0.25	950,000	$59{,}000 \times 10^{10}$
	0.3% (w/v) TFA	1	840,000	$55{,}000 \times 10^{10}$
		1	1,100,000	$76{,}000 \times 10^{10}$
		0.5	860,000	$70{,}000 \times 10^{10}$
		0.25	910,000	$17{,}000 \times 10^{10}$
	eluent	1	1,000,000	$91{,}000 \times 10^{10}$
		1	990,000	$76{,}000 \times 10^{10}$
		0.5	1,300,000	$36{,}000 \times 10^{11}$
		0.25	820,000	$17{,}000 \times 10^{11}$
LowMW2	50mM HCl	1	1,400,000	$15{,}000 \times 10^{12}$
		1	1,600,000	$32{,}000 \times 10^{11}$
		0.5	1,600,000	$91{,}000 \times 10^{14}$
		0.25	1,700,000	$90{,}000 \times 10^{10}$
MedMW1	50mM HCl	1	2,100,000	$73{,}000 \times 10^{12}$
		1	3,300,000	$65{,}000 \times 10^{11}$
		0.5	1,600,000	$57{,}000 \times 10^{12}$
		0.25	5,300,000	$62{,}000 \times 10^{13}$
	0.3% (w/v) TFA	1	1,400,000	$41{,}000 \times 10^{12}$
		1	1,600,000	$10{,}000 \times 10^{13}$
		0.5	2,100,000	$90{,}000 \times 10^{11}$
		0.25	4,200,000	$57{,}000 \times 10^{11}$
	eluent	1	1,900,000	$12{,}000 \times 10^{12}$
		1	1,400,000	$85{,}000 \times 10^{12}$
		0.5	1,500,000	$84{,}000 \times 10^{11}$
		0.25	2,300,000	$19{,}000 \times 10^{12}$
MedMW4	50mM HCl	1	1,900,000	$23{,}000 \times 10^{10}$
		1	2,100,000	$51{,}000 \times 10^{12}$
		0.5	1,400,000	$35{,}000 \times 10^{12}$
		0.25	2,000,000	$37{,}000 \times 10^{13}$
MedMW2	50mM HCl	1	1,300,000	$90{,}000 \times 10^{10}$
		0.5	1,900,000	$13{,}000 \times 10^{12}$
		0.25	950,000	$41{,}000 \times 10^{12}$
MedMW3	50mM HCl	1	3,900,000	$38{,}000 \times 10^{14}$
		0.5	1,300,000	$47{,}000 \times 10^{15}$
		0.25	5,400,000	$80{,}000 \times 10^{13}$
Fluk	50mM HCl	1	4,400,000	$65{,}000 \times 10^{13}$
		0.5	5,500,000	$21{,}000 \times 10^{12}$
		0.25	1,300,000	$66{,}000 \times 10^{12}$

Sig	50mM HCl	1	2,900,000	$99{,}000 \times 10^{11}$
		0.5	1,500,000	$48{,}000 \times 10^{12}$
		0.25	3,800,000	$12{,}000 \times 10^{12}$
HighMW	50mM HCl	1	3,600,000	$74{,}000 \times 10^{13}$
		0.5	3,500,000	$31{,}000 \times 10^{12}$
		0.25	1,600,000	$35{,}000 \times 10^{13}$
AKbioD1	50mM HCl	1	930,000	$25{,}000 \times 10^{11}$
		1	920,000	$75{,}000 \times 10^{12}$
		1	940,000	$51{,}000 \times 10^{11}$
		1	910,000	$52{,}000 \times 10^{11}$
		0.5	910,000	$78{,}000 \times 10^{10}$
		0.25	750000	$13{,}000 \times 10^{11}$
AKbioD2	50mM HCl	1	1,500,000	$14{,}000 \times 10^{11}$
		0.5	980,000	$14{,}000 \times 10^{11}$
		0.25	860,000	$50{,}000 \times 10^{11}$
AKbioD3	50mM HCl	1	1,400,000	$70{,}000 \times 10^{10}$
		0.5	1,000,000	$13{,}000 \times 10^{11}$
		0.25	2,300,000	$34{,}000 \times 10^{11}$
AKbioV1	50mM HCl	1	910,000	$54{,}000 \times 10^{10}$
		1	870,000	$40{,}000 \times 10^{10}$
		1	510,000	$97{,}000 \times 10^{10}$
		0.5	730,000	$40{,}000 \times 10^{9}$
		0.25	720,000	$18{,}000 \times 10^{11}$
AKbioV2	50mM HCl	1	2,400,000	$45{,}000 \times 10^{11}$
		0.5	1,900,000	$88{,}000 \times 10^{18}$
		0.25	2,900,000	$11{,}000 \times 10^{13}$
AKbioV3	50mM HCl	1	1,600,000	$12{,}000 \times 10^{13}$
		0.5	2,600,000	$29{,}000 \times 10^{12}$
		0.25	910,000	$57{,}000 \times 10^{12}$

Table S4: Chitosan samples not mentioned in Table 1

Sample	Supplier	Batch number	Catalogue number
HighMW2	Sigma	12913CJ	419419
MedMW3	Sigma	MKBF1336V	448877
MedMW4	Sigma	09303PE	448877
LowMW2	Sigma	06714DJ	448869
Fluk	Sigma (Fluka)	440698/1	28191

Optimization of pressure mobilization of chitosan

Pressure mobilisation was used to assess the dissolution between samples dissolved in 50 mM HCl and AcOH. A number of optimisation steps, mainly of the background electrolyte, were required to analyse the samples.

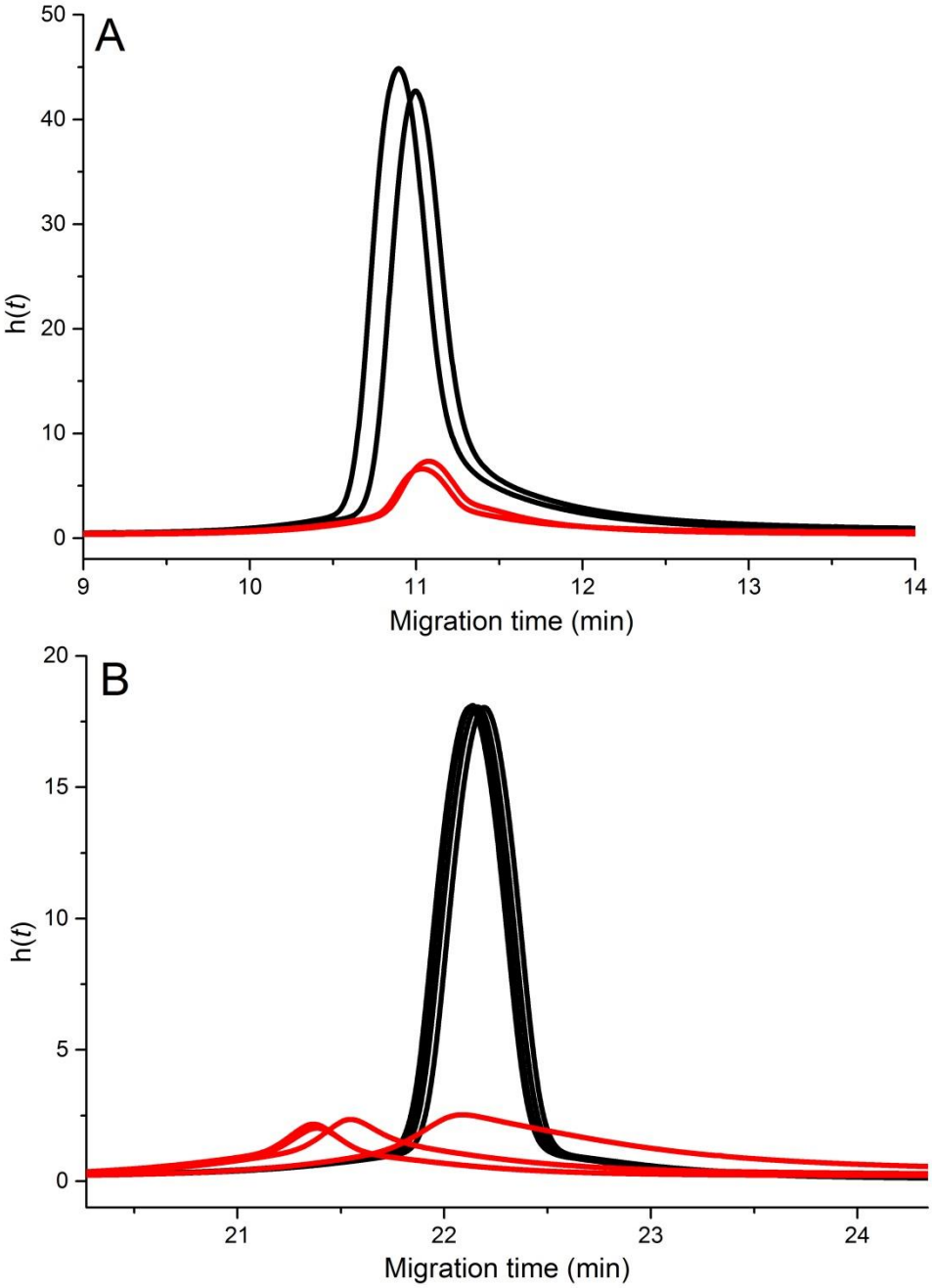

Figure S2: Pressure mobilisation of MedMW1 (no mixing) dissolved in 50 mM HCl (black) and AcOH (red) while the rest of the capillary contains A. phosphate buffer 100 mM pH 3 and at 25 ºC B. phosphate buffer 100 mM pH 2 and at 55 ºC

Mixing using voltage

Pressure mobilization experiments used an inversion of voltage at the start of the experiment to mix the sample with the background electrolyte.

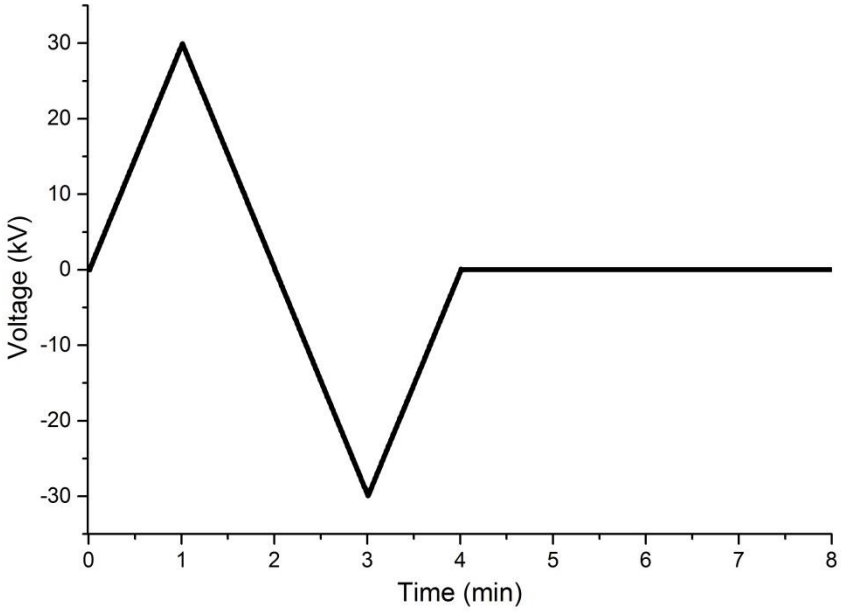

Figure S3: Mixing with inversion of voltage at the beginning of pressure mobilization experiments

Pressure mobilization of chitosan dissolved in aqueous AcOH

A comparison of chitosan dissolved in AcOH using the same conditions as for chitosan dissolved in 50 mM HCl (Fig. 2) produced a narrow peak superimposed on a broader peak. Using the premixing with the electric field as described above did not separate the peak of the chitosan from that of the AcOH solution. Subtracting the peak of AcOH would introduce a large error. It was interesting to note the behavioral differences and interaction of the chitosan with the capillary in different solvents, however, the lack of separation of the narrow peak superimposed onto the chitosan peak prevents an accurate analysis of the dissolution of chitosan in AcOH. (Fig. S4).

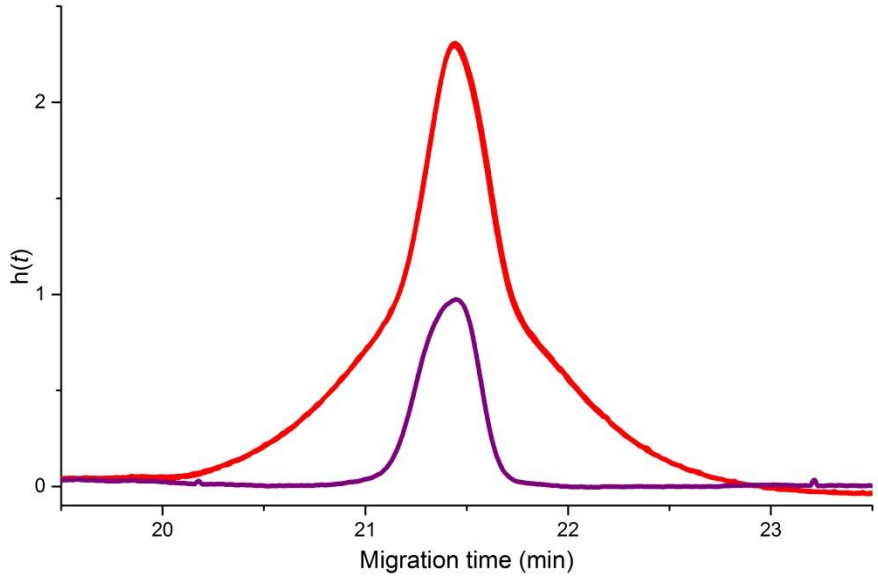

Figure S4: Pressure mobilisation (with mixing) of 50 mM AcOH (purple) and of MedMW1 in 50 mM AcOH (red)

Normalization based on viscosity

To subtract the peak assigned to Cl^-, area normalization was required. The viscosity difference between the chitosan solution and the aqueous HCl (50 mM) was taken into account. The difference between the migration of the apex of the Cl^- peak in the aqueous HCl and the Cl^- peak in the CS solution was measured and used to normalize the y-axis intensity of the Cl^- elugram based on the viscosity difference. The Cl^- peak was then subtracted from the CS elugram.

$$Normalized\ absorbance\ of\ Cl^- = \text{Absorbance of } Cl^- \times \frac{t_2}{t_1} \quad \text{(S1)}$$

Where t_1 is the time at the peak apex of chitosan and t_2 is the time at the peak apex of Cl^-.

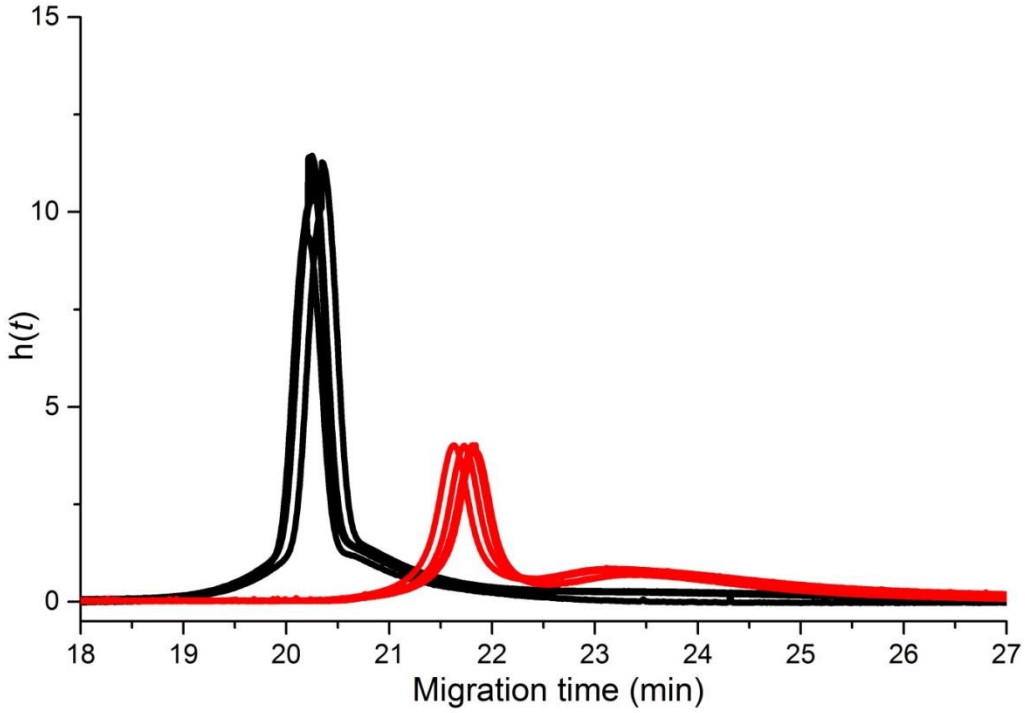

Figure S5: Pressure mobilization of chitosan dissolved in 50 mM HCl (4 black lines) and AcOH (4 red lines) at 55 °C and running in 50 mM HCl and 50 mM AcOH respectively.

Calculation of injection volume for CE and PM experiments

The injection volume *V* is calculated using a rearranged Poiseuille equation as follows:[1, 2]

$$V_t = \frac{\Delta P D^4 \pi}{128 \eta L} \quad \text{(S2)}$$

Where η is the viscosity (1.00 x 10^{-3} kg·m^{-1}·s^{-1}), *L* is the length of the capillary (104 cm total and effective length respectively) , *D* is the diameter of the capillary (50 µm), Δ*P* is the pressure (72 mbar) and *t* is the injection time (10 s).

Correction of raw data

For PM experiments, the y axes of the raw data needs to be time corrected with the following equation:

$$h(t) = \frac{absorbance}{time} \quad \text{(S3)}$$

where absorbance is the raw UV signal obtained from the CE instrument and the time is the x axes obtained from the raw data

For CE experiments both the x and y axes need to be converted to electrophoretic mobility and a weight distribution of electrophoretic mobilities respectively with the following equations:

$$\mu = \frac{l_t l_d}{V}\left(\frac{1}{t_m} - \frac{1}{t_{eof}}\right) \quad \text{(S4)}$$

$$W(\mu) = time \times absorbance \quad \text{(S5)}$$

where l_t and l_d are the length of the capillary and the length to the detector, respectively, *V* is the voltage, t_m is the migration time and t_{eof} is the migration time of a neutral species (electroosmotic flow).

Solution-state NMR spectroscopy

Solution-state NMR spectroscopy measurements were conducted over 61 hours to analyze the behavior of chitosan kept at 60 °C for an extended period of time.

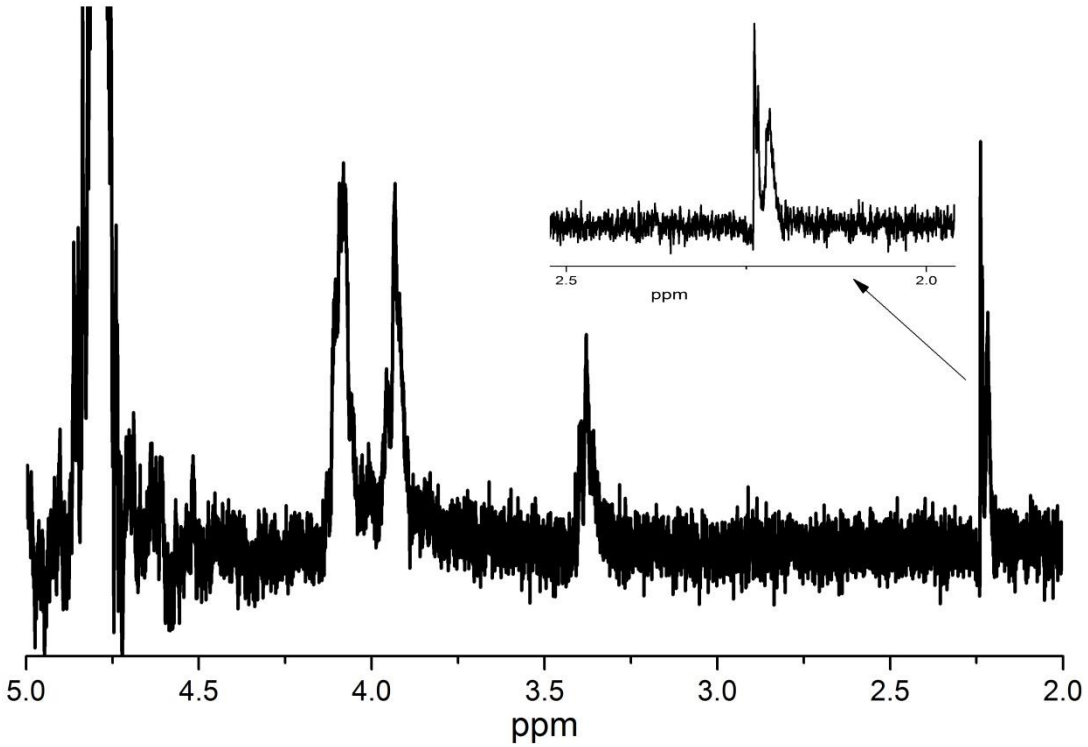

Figure S6. ^{1}H NMR spectrum of chitosan (MedMW1) in D_2O/DCl (50 mM) at 60 °C after several hours

Kinetics of deacetylation

If it obeyed a first order kinetics, the deacetylation of the *N*-acetyl-D-glucosamine unit would follow Eq. S6:

$$\frac{-d[NG]}{dt} = k[NG] \tag{S6}$$

where NG is the *N*-acetyl-D-glucosamine and *t* is the time.

Eq. S6 can be rearranged into

$$\frac{-d[NG]}{[NG]} = k \cdot dt \tag{S7}$$

which integrates into a typical first order kinetics:

$$\ln[NG] - \ln([NG]_\infty) = -kt \tag{S8}$$

Since free AcOH is only created by the deacetylation of NG:

$$[AcOH] = [NG]_\infty - [NG] \tag{S9}$$

Combining Eq. S8 and S9 leads to Eq. S10

$$\ln\left(\frac{[NG]}{[NG]_\infty}\right) = \ln(1 - \frac{[AcOH]}{[NG]_\infty}) = -\mathrm{kt} \tag{S10}$$

Previous solution-state NMR spectroscopy experiments of chitosan

There are several examples of the analysis of chitosan using solution-state NMR spectroscopy. Tabulated below are the various conditions including temperature, solvent and dissolution time.

Table S4: Published examples of conditions for solution-state NMR spectroscopy of chitosan

Year Published, First Author	Solvent	Dissolution Time	Temperature	Reference
1996 Ottoy	1 % v/v AcOH	Overnight	Not specified	[3]
2000 Heux	DCl in D_2O (pH 4)	Not specified	Not specified	[4]
2003 Lavertu	D_2O 1.96 mL + DCl 0.04 mL	30 min	Room temperature	[5]
2014 Dahmane	2 % DCl in D_2O	1 hour	70 ºC	[6]
2014 Lago	1 % CD_3COOD in D_2O	Not specified	not specified	[7]

Signal assignment for ^{1}H NMR spectra of chitosan

To assign the signals of the ^{1}H NMR spectroscopy kinetics, chitosan was dissolved in 50 mM DCl in D_2O for 65 h at 60 °C. The sample was measured and then spiked with 50 mM AcOH and re-measured (Fig. S7). The chemical shift scales were calibrated with the signal of water at 4.717 ppm at 60 °C [8].

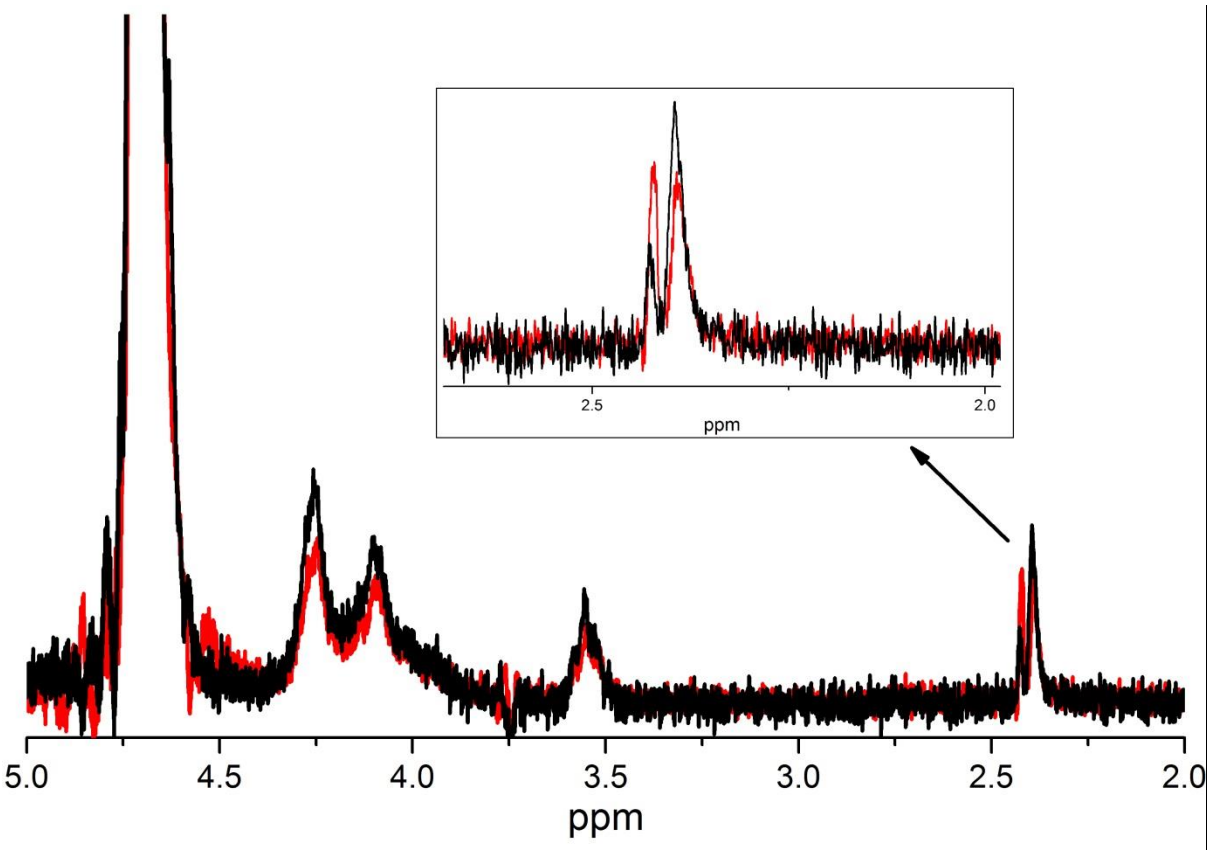

Figure S7. ^{1}H NMR spectrum of chitosan (black line) and chitosan spiked with 50 mM AcOH (red line) dissolved in 50 mM DCl in D_2O.

Magritek Spinsolve benchtop NMR

Solution-state NMR spectra were recorded of chitosan (1 $g \cdot L^{-1}$) prepared in 50 mM DCl in D_2O and 50 mM HCl.

a)

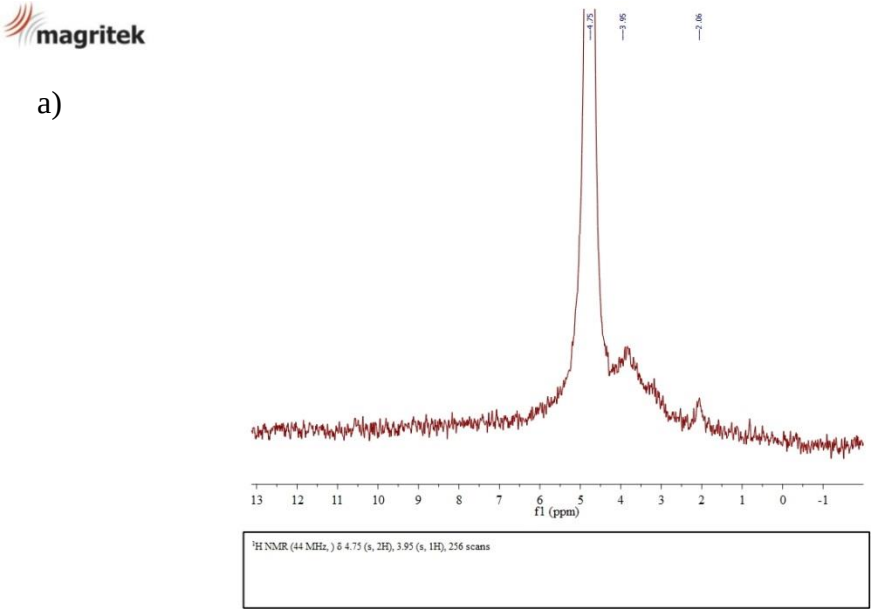

b)

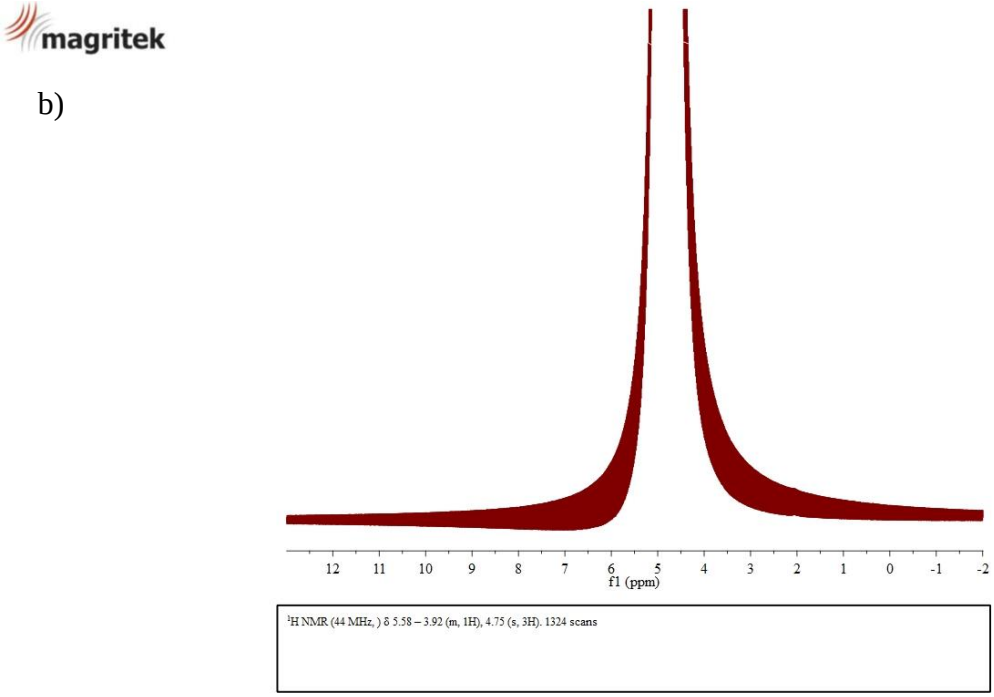

Figure S8. ^{1}H NMR spectrum of chitosan (MedMW1) dissolved in a) 50 mM DCl in D_2O b) 50 mM HCl

Calculation of phasing error on solid-state NMR measurements

The error from phasing was measured by having 4 different users phase 8 different experimental data sets. The results are presented in Table S5.

Table S5. Calculation of error caused by phasing of 8 different solid-state NMR spectroscopy data sets. The *DA* was measured after phasing by 4 different users.

	User - Calculated *DA* (%)						
	1	2	3	4	Average *DA*	*SD*	*RSD* (%)
1	9.53	10.44	8.29	8.30	9.14	1.04	11.41
2	12.09	13.21	11.34	10.56	11.80	1.13	9.56
3	6.85	6.04	6.43	6.44	6.44	0.33	5.14
4	10.27	11.65	10.37	11.07	10.84	0.65	5.97
5	3.48	2.51	2.85	3.43	3.07	0.47	15.23
6	16.34	16.47	16.43	16.51	16.44	0.07	0.45
7	14.24	14.12	14.25	14.87	14.37	0.34	2.35
8	10.73	10.50	10.56	12.36	11.04	0.89	8.05

Kinetics of chitosan dissolution using PACE

The dissolution of chitosan (MedMW1) over time in either 50 mM HCl or 50 mM DCl in D_2O at 60 °C was compared using PACE. The dissolution of different chitosan samples prepared in 50 mM HCl was also compared. The electrophoretic mobility was corrected with both the electroosmotic flow and an additional internal standard. The area was corrected through the integral of the internal standard.

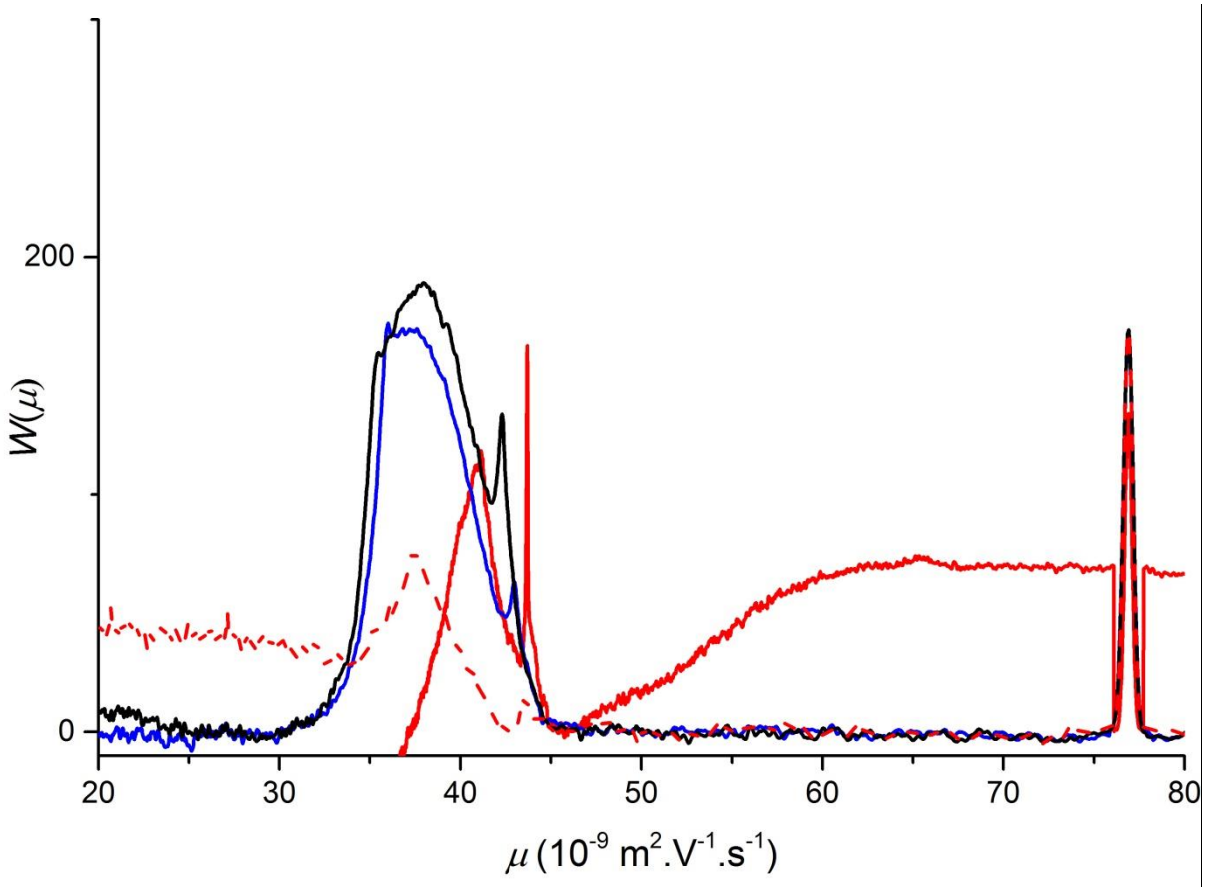

Figure S9. Typical electropherograms of chitosan dissolved in 50 mM DCl in D_2O over 20 hours with a dissolution time of less than 2 h (red lines), 2-10 h (blue line) and 10-20 h (black line).

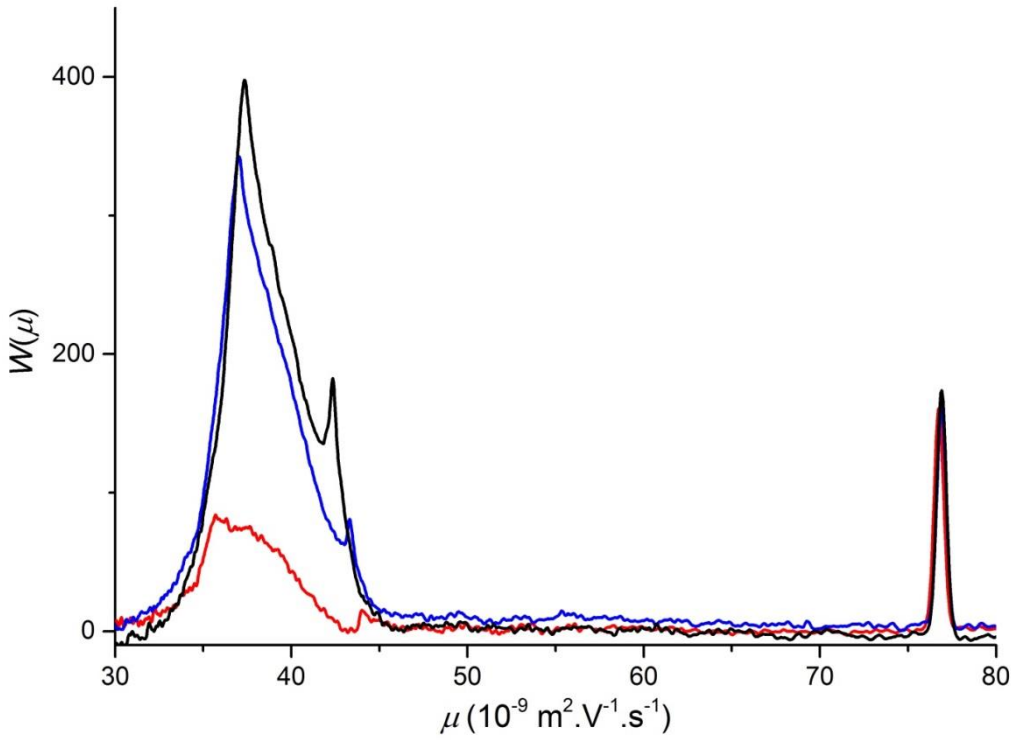

Figure S10. Typical electropherograms of MedMW1 chitosan dissolved in 50 mM HCl over 20 hours with a dissolution time of less than 2 h (red line), 2-10 h (blue line) and 10-20 h (black line).

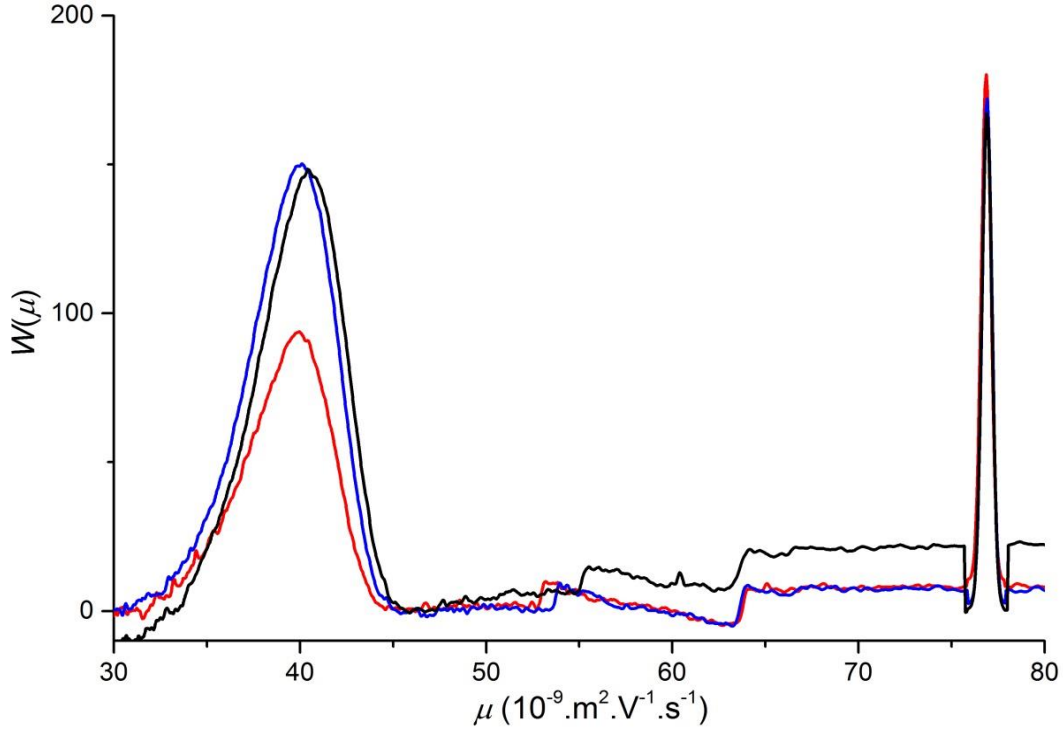

Figure S11. Typical electropherograms of LowMW1 chitosan dissolved in 50 mM HCl over 20 hours with a dissolution time of less than 2 h (red line), 2-10 h (blue line) and 10-20 h (black line).

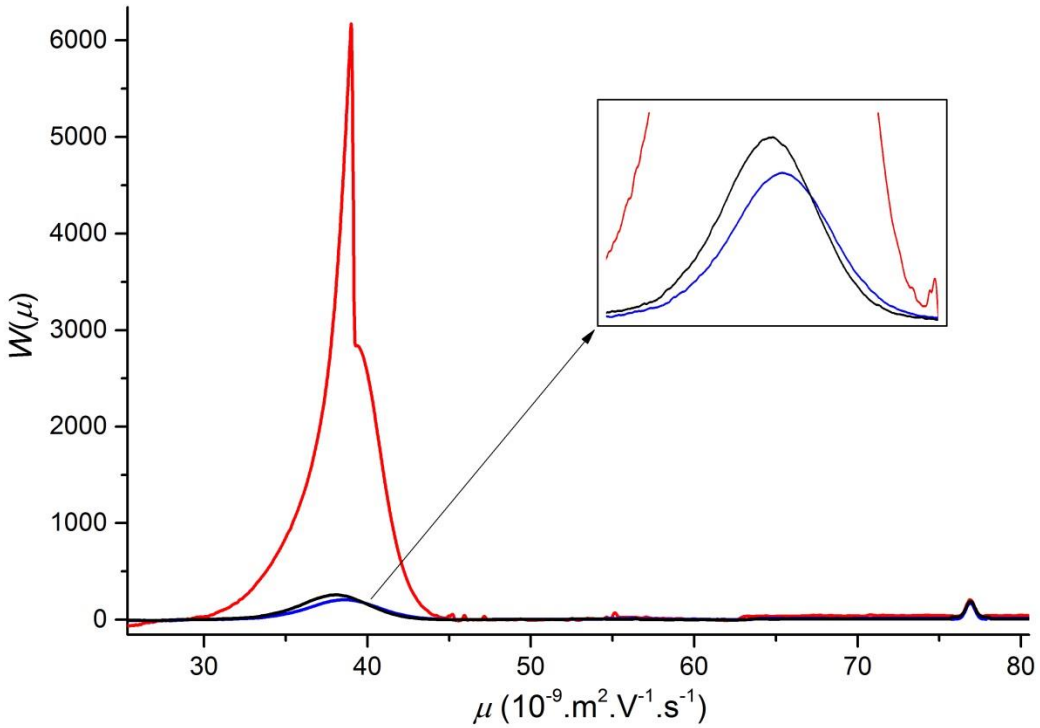

Figure S12. Typical electropherograms of HighMW Par1 chitosan dissolved in 50 mM HCl over 20 hours with a dissolution time of less than 2 h (red line), 2-10 h (blue line) and 10-20 h (black line).

References

[1] G. Taylor, Dispersion of Soluble Matter in Solvent Flowing Slowly through a Tube, Proc. Royal Soc. London A Math. Phys. Sci., 219 (1953) 186-203.

[2] R. Aris, On the Dispersion of a Solute in a Fluid flowing through a Tube, Proceedings of the Royal Society of London Series a-Mathematical and Physical Sciences, 235 (1956) 67-77.

[3] M.H. Ottoy, K.M. Varum, O. Smidsrod, Compositional heterogeneity of heterogeneously deacetylated chitosans, Carbohydr. Polym., 29 (1996) 17-24.

[4] L. Heux, J. Brugnerotto, J. Desbrieres, M.F. Versali, M. Rinaudo, Solid state NMR for determination of degree of acetylation of chitin and chitosan, Biomacromolecules, 1 (2000) 746-751.

[5] M. Lavertu, Z. Xia, A.N. Serreqi, M. Berrada, A. Rodrigues, D. Wang, M.D. Buschmann, A. Gupta, A validated 1H NMR method for the determination of the degree of deacetylation of chitosan, J. Pharma. Biomed. Anal., 32 (2003) 1149-1158.

[6] E.M. Dahmane, M. Taourirte, N. Eladlani, M. Rhazi, Extraction and Characterization of Chitin and Chitosan from Parapenaeus longirostris from Moroccan Local Sources, Int. J. Polym. Anal. Charact., 19 (2014) 342-351.

[7] M.A. Lago, R. Sendon, A.R.B. de Quiros, A. Sanches-Silva, H.S. Costa, D.I. Sanchez-Machado, H.S. Valdez, I. Angulo, G.P. Aurrekoetxea, E. Torrieri, J. Lopez-Cervantes, P. Paseiro, Preparation and Characterization of Antimicrobial Films Based on Chitosan for Active Food Packaging Applications, Food and Bioprocess Technology, 7 (2014) 2932-2941.

[8] R.E. Hoffman, Standardization of chemical shifts of TMS and solvent signals in NMR solvents, Magn. Reson. Chem., 44 (2006) 606-616.

analytical chemistry

Article

pubs.acs.org/ac

Quantifying the Heterogeneity of Chemical Structures in Complex Charged Polymers through the Dispersity of Their Distributions of Electrophoretic Mobilities or of Compositions

Joel J. Thevarajah,[†,‡] Adam T. Sutton,[†,‡] Alison R. Maniego,[†,‡] Elizabeth G. Whitty,[†,‡] Simon Harrisson,[§] Hervé Cottet,[∥] Patrice Castignolles,[*,†] and Marianne Gaborieau[†,‡]

Western Sydney University, [†]School of Science and Health, Australian Centre for Research of Separation Science (ACROSS), and [‡]Molecular Medicine Research Group, School of Science and Health, Parramatta NSW 2150, Australia

[§]IMRCP, UMR 5623, Université de Toulouse, 118 route de Narbonne, F-31062 Toulouse Cedex 9, France

[∥]Institut des Biomolécules Max Mousseron (IBMM, UMR 5247 CNRS, Université de Montpellier, Ecole Nationale Supérieure de Chimie de Montpellier), Place Eugène Bataillon CC 1706, 34095 Montpellier Cedex 5, France

Supporting Information

ABSTRACT: The complexity of synthetic and natural polymers used in industrial and medical applications is expanding; thus, it becomes increasingly important to improve and develop methods for their molecular characterization. Free-solution capillary electrophoresis is a robust technique for the separation and characterization of both natural and synthetic complex charged polymers. In the case of polyelectrolytes, free-solution capillary electrophoresis is in the "critical conditions" (CE-CC): it allows their separation by factors other than molar mass for molar masses typically higher than 20000 g/mol. This method is thus complementary to size-exclusion chromatography (SEC). SEC is widely used to determine molar mass distributions and their dispersities. Utilizing CE-CC, an analogous calculation of dispersity based on the distributions of electrophoretic mobilities was derived and the heterogeneity of composition or branching in different polysaccharides or synthetic polymers was obtained in a number of experimental cases. Calculations are based on a ratio of moments and could therefore be compared to simulations of polymerization processes, in analogy to the work performed on molar mass distributions. Among four possible types of dispersity, the most precise values were obtained with the calculation analogous with the dispersity of molar mass distribution M_w/M_n. In addition, the dispersity value allows conclusions based on a single value: the closer the dispersity is to 1, the more homogeneous the polymer is in terms of composition or branching. This approach allows the analysis of dispersity of important molecular attributes of polymers other than molar mass and aims at improving the overall molecular characterization of both synthetic and natural polymers. The dispersity can also be monitored online while performing a chemical reaction within the CE instrument.

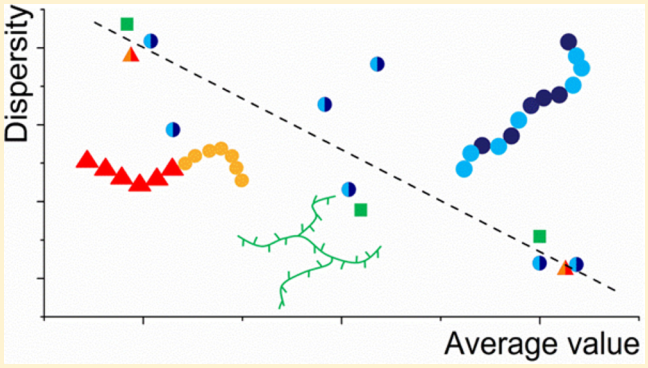

The accurate molecular characterization of polymers is a necessity as their production and development expands in both industry and research. This requires rigorous method development for the characterization of more complex polymers. Complex polymers can vary in a range of molecular attributes including molar mass, composition, type of copolymer, branching, charge, and chain-ends. Each of these attributes exists as distribution(s) in a given sample. These distributions can vary further and be for example broad, narrow, and uni- or bimodal.[1] Therefore, the distributions of particular molecular attributes should be characterized.

Currently, the commonly assessed molecular attribute of polymers is molar mass. The heterogeneity of molar mass in a polymer sample can be assessed through the determination of its dispersity typically by size-exclusion chromatography (SEC, also known as GPC).[2] The dispersity is calculated as the weight-average molar mass divided by the number-average molar mass and most, if not all, commercial software operating SEC instruments routinely performs this calculation for its users. The average molar masses and the dispersity are also predicted using simulations of polymerization processes by the method of the moments.[3]

Heterogeneity is not often quantified for the other molecular attributes of polymers such as composition (of copolymers) or branching. A number of methods for separating by composition or branching exist.[4] Following the SEC separation of copolymers of methyl methacrylate and styrene a quadruple detection was implemented, which included heavy reliance on

Received: September 29, 2015
Accepted: December 16, 2015

DOI: 10.1021/acs.analchem.5b03672
Anal. Chem. XXXX, XXX, XXX−XXX

the differential UV absorbance of each monomer unit.[5] It was further shown that a relation between sequence length heterogeneity and the molar mass distribution could be achieved; however, a number of conditions were required, including the intrachain interaction of the different monomers to be different to the monomers of the same type, appropriate solvation conditions for the chemical functionalities, and the architecture of the copolymer should remain the same as a function of the molar mass.[6] SEC gradient was shown to be able to determine the chemical composition distribution of statistical copolymers.[7] The coupling of SEC and gradient elution liquid chromatography[8,9] was shown to be required for the analysis of both synthetic and artificial copolymers since both dimensions suffered from coelution when performed individually. The dispersity of the distribution of compositions is not determined in the literature. This may result from the absence of a straightforward separation and characterization method for the composition or branching of polymers, especially for hydrophilic ones, as well as from the absence of a recognized method to calculate their dispersity. SEC separates by hydrodynamic volume, which depends on molar mass as well as on composition or branching. A local dispersity at a given hydrodynamic volume can be determined using multiple-detection SEC, which assesses the accuracy of the determined molar mass or the local heterogeneity at a given hydrodynamic volume; however, it does not directly assess the heterogeneity of the branching or composition distributions.[1,10] Various forms of liquid chromatography[11] as well as thermal field flow fractionation[12] have been shown to separate polymers according to composition or branching.

Capillary electrophoresis (CE) has been proven to be an appropriate technique for the separation of polyelectrolytes[13] and specifically the analysis of copolymers (natural[14,15] and synthetic[16,17]) and branched polymers.[18,19] Free-solution capillary zone electrophoresis of evenly charged polyelectrolytes (with regularly distributed charges along the polymer backbone) leads to analogous separations to liquid chromatography in the critical conditions (with different separation mechanisms) in which separation is not dependent on molar mass.[20] The technique free-solution capillary electrophoresis (CE) is thus defined here as the method CE in the critical conditions (CE-CC). This method allows the separation and analysis of polymers according to composition or branching as will be discussed. It further allows the distributions of these attributes to be obtained. Importantly, the determination of mass-relative distributions of electrophoretic mobilities, or of any other characteristic parameter, such as chemical composition, has been recently addressed by Chamieh et al.[21] The theoretical background required to convert the electropherogram into a distribution of electrophoretic mobilities was described with an emphasis on the fact that both x and y axes should be converted. Estimation of sample dispersity was performed via the determination of the standard deviation (or RSD) of the sample's chemical composition distribution.

We propose different expressions of the dispersity based on different moments of the distributions. In this work, they were used to estimate the dispersity of distributions obtained through CE-CC (distributions of electrophoretic mobilities and of compositions). The different types of dispersity were then compared by applying them to various natural and synthetic (co)polymers.

THEORY

Dispersities of Molar Mass Distributions. The expressions of dispersity obtained in this paper are analogous to expressions of dispersity of molar mass distributions. Shortt[22] demonstrated that the number-, weight-, and z-average molar mass, M_n, M_w, and M_z, can be obtained from the ratio of moments of molar mass distributions from SEC. To calculate the dispersity of molar mass distributions, the ratio M_w/M_n is quasi-exclusively used nowadays, but the ratio M_z/M_w has also been used for example to establish relations between the radius of gyration and M_w. The dispersity calculated as M_w/M_n (eq S1) is related to the standard deviation σ through a simple expression:[23]

$$Đ - 1 = \frac{M_w}{M_n} - 1 = \frac{\sigma^2}{M_n^2} \tag{1}$$

Dispersities of Electrophoretic Mobility Distributions. In this work, weight distributions of electrophoretic mobilities (and of compositions) are considered. $W(\mu)$, the weight fraction of polyelectrolyte chains with electrophoretic mobility μ, can be obtained from a mass-sensitive detection such as UV detection of the monomer units. The number distribution is usually not straightforward to obtain except in the case of end-labeled polymers (derivatization may be required).[24] The number-average electrophoretic mobility is thus generally not accessible by CE and it is not possible to access it by single detection contrary to the case of molar mass averages in SEC, where M_n and M_w are both determined with single-detection. In this work, ratios of moments were used to express the dispersity of electrophoretic mobility distributions (see Table S1 for the expression of the individual moments).

Let $D(W(A),b,c)$ be the dispersity of the weight distribution of the variable A (which can be either mobility or composition), as a function of the $(b\text{-}2)^{th}$, $(b\text{-}1)^{th}$, and b^{th} order moments, with respect to the reference c. The general expression of the moment, $\overline{A_c^b}$, (eq 2) and dispersity, $D(W(A),b,c)$ (eq 3), is given by

$$\overline{A_c^b} = \frac{\int_0^\infty W(A)(A-c)^b \mathrm{d}A}{\int_0^\infty W(A)\mathrm{d}A} \tag{2}$$

$$D(W(A), b, c) = \frac{\overline{A_c^b} \times \overline{A_c^{b-2}}}{[\overline{A_c^{b-1}}]^2} \tag{3}$$

It is noted that the number-average mobility could be mathematically defined as the ratio of the zeroth and the −1st order moments in analogy to molar mass distribution dispersity,[22] but this does not correspond to the definition of the number-average electrophoretic mobility based on the number distribution (see Supporting Information, eqs S28 and S29). Two reference values were used for the calculation of the moments of the distributions: either $c = 0$ as in the Shortt equations,[22] or the weight-average mobility, $c = \mu_w$, as for the standard deviation (SD). μ_w is determined as the ratio of the first and the zeroth order moments of the mobility distributions:

$$\mu_w = \frac{\overline{\mu_0^1}}{\overline{\mu_0^0}} = \frac{\int W(\mu)\mu \mathrm{d}\mu}{\int W(\mu)\mathrm{d}\mu} \tag{4}$$

DOI: 10.1021/acs.analchem.5b03672
Anal. Chem. XXXX, XXX, XXX−XXX

In the first approach, an analogy with M_w/M_n is used, and the dispersity is calculated as the ratio of first and zeroth order moments divided by the ratio of zeroth and −1st order moments. Eq 5 shows this dispersity with the reference (c) taken as 0:

$$D(W(\mu), 1, 0) = \frac{\overline{\mu_0^1} \times \overline{\mu_0^{-1}}}{[\overline{\mu_0^0}]^2} \tag{5}$$

In the second approach, an analogy with M_z/M_w is used, and the dispersity is calculated as the ratio of second and first order moments (or z-average) divided by the ratio of first and zeroth order moments (eq 6):

$$D(W(\mu), 2, 0) = \frac{\overline{\mu_0^2} \times \overline{\mu_0^0}}{[\overline{\mu_0^1}]^2} \tag{6}$$

In the third approach, dispersity is calculated as the ratio of third and second order moments divided by the ratio of second and first order moments (eq 7).

$$D(W(\mu), 3, 0) = \frac{\overline{\mu_0^3} \times \overline{\mu_0^1}}{[\overline{\mu_0^2}]^2} \tag{7}$$

The SD of the weight distribution of electrophoretic mobilities, taking μ_w as reference, is represented by eq 8:

$$D_\sigma = \left[\frac{\overline{\mu_{\mu_w}^2}}{\overline{\mu_{\mu_w}^0}}\right]^{0.5} \tag{8}$$

The integral expression of eqs 3−8 are given as eqs S6−S13. μ_w can be used as a reference instead of 0 similarly to the calculation for SD. However, eqs S3−S5 never give a finite value different from 0 (see Supporting Information).

Dispersities of Composition Distributions for Copolymers. The determination of distributions of compositions from electrophoretic mobility distributions first requires establishing a correlation between the electrophoretic mobility and the composition. This can be completed using the weight-average mobility of standard samples and a complementary method to measure their average composition such as NMR spectroscopy;[14] for synthetic polymers the composition may also be estimated from the monomer concentrations used in the synthesis. The challenge faced with establishing a correlation is the requirement of having appropriate samples to cover the whole range of compositions (as for any calibration curve). Samples with particularly broad distributions such as the natural samples studied in this paper could not be studied through composition distributions without acknowledgment of the possibility of significant error caused by the calibration curve.

The (weight-average) composition C is defined as the weight of one type of monomer unit over the weight of all monomer units. Assuming a linear correlation between the electrophoretic mobility and composition,[14,25,26] the weight fraction $W(C)$ of the polyelectrolyte chains with the composition C is calculated as

$$W(C) = \frac{W(\mu)}{\mathrm{d}C/\mathrm{d}\mu} = \frac{W(\mu)}{m} \tag{9}$$

where m is the slope of the calibration curve of the composition versus mobility. Linear correlation between mobility and composition is generally observed for evenly charged polyelectrolytes when charge densities are either below or above the Manning condensation threshold with a breaking slope at the condensation threshold.[27,28] The weight-average composition C_w is calculated as

$$C_w = \frac{\overline{C_0^1}}{\overline{C_0^0}} = \frac{\int W(C) C \mathrm{d}C}{\int W(C) \mathrm{d}C} \tag{10}$$

In analogy with the dispersities of the mobility distributions, the dispersities of the composition distributions are calculated as ratios of moments using 0 as a reference (eqs S20−S23).

Note that in the calculation of dispersity values for experimental cases for both mobility and composition distributions, the discrete forms were used in the software Origin for the moments (eq S14−S17 and S24−S27).

Estimating the Uncertainty on the Dispersity Values. In order to compare the calculated dispersity values on different samples it is necessary to estimate the precision of their determination. The error on the dispersity values caused by the uncertainty on the electrophoretic mobility values was calculated for each type of dispersity in eqs 5−7 (eq S30−S32 for the derivation) using experimental data. This resulted in eqs 11−13 for electrophoretic mobility dispersities.

$$\frac{\mathrm{d}D(W(\mu), 1, 0)}{D(W(\mu), 1, 0)} = \frac{\mathrm{d}\mu}{\mu}\sqrt{\left(\frac{W(\mu)\mu^2}{\int W(\mu)\mu \mathrm{d}\mu}\right)^2 + \left(\frac{W(\mu)}{\int W(\mu)\mu^{-1}\mathrm{d}\mu}\right)^2 + 2\left(\frac{W(\mu)\mu}{\int W(\mu)\mathrm{d}\mu}\right)^2} \tag{11}$$

$$\frac{\mathrm{d}D(W(\mu), 2, 0)}{D(W(\mu), 2, 0)} = \frac{\mathrm{d}\mu}{\mu}\sqrt{\left(\frac{W(\mu)\mu}{\int W(\mu)\mathrm{d}\mu}\right)^2 + \left(\frac{W(\mu)\mu^3}{\int W(\mu)\mu^2\mathrm{d}\mu}\right)^2 + 2\left(\frac{W(\mu)\mu^2}{\int W(\mu)\mu\mathrm{d}\mu}\right)^2} \tag{12}$$

$$\frac{\mathrm{d}D(W(\mu), 3, 0)}{D(W(\mu), 3, 0)} = \frac{\mathrm{d}\mu}{\mu}\sqrt{\left(\frac{W(\mu)\mu^2}{W(\mu)\mu\mathrm{d}\mu}\right)^2 + \left(\frac{W(\mu)\mu^4}{W(\mu)\mu^3\mathrm{d}\mu}\right)^2 + 2\left(\frac{W(\mu)\mu^3}{\int W(\mu)\mu^2\mathrm{d}\mu}\right)^2} \tag{13}$$

For the uncertainty of the dispersity of the distribution of compositions, the same expressions apply and only require the substitution of μ with C. In addition, the error due to the calibration may play an important additional role.

The derivation of the uncertainty of the electrophoretic dispersity expressed as a SD (eq 8) is shown in Supporting Information (eqs S36−S38) and yields eq 14:

$$\frac{\mathrm{d}D_\sigma}{D_\sigma} = \frac{\mathrm{d}\mu}{\mu}\sqrt{0.5\left(\frac{W(\mu)(\mu-\mu_w)^2\mu}{\int W(\mu)(\mu-\mu_w)^2}\mathrm{d}\mu\right)^2 + 0.5\left(\frac{W(\mu)\mu}{\int W(\mu)}\mathrm{d}\mu\right)^2} \tag{14}$$

The relative uncertainty of the electrophoretic mobility $\mathrm{d}\mu/\mu$ was taken as 1% corresponding to the order of magnitude of the relative SD of the electrophoretic mobility for free-solution CE of polyelectrolytes[18] and sugars[29,30] (Table S2). The calculated relative uncertainties were shown to be lower than 4×10^{-6} (sometimes by orders of magnitude), which shows that the error caused by the mobility is negligible for the dispersity values calculated (Table S3). Although there does not seem to be a correlation between the samples and the uncertainty, it is noted that D(W(μ),1,0) seems to have the lowest uncertainty.

DOI: 10.1021/acs.analchem.5b03672
Anal. Chem. XXXX, XXX, XXX−XXX

The major contributor of the uncertainty on the dispersity value is thus not the error on the determination of μ but likely other factors such as the error in setting the baselines and the start/end limits of the integration. Therefore, six significant digits (corresponding to five decimal places) were considered for the dispersity values. In the case of composition distributions, a higher order of magnitude (10^{-1}–10^{-6}) for the relative uncertainty of the dispersity and of SD (10^{-6}) were calculated (Table S4). As mentioned previously, a significant error can be introduced through the imperfect correlation between mobility and composition for the dispersity of composition.

EXPERIMENTAL SECTION

Separation conditions were as previously described for chitosan,[14] poly(sodium acrylate)/poly(sodium acrylate-*co*-*N*-antipyrine acylamide),[18] and poly(acrylic acid-*b*-acrylamide).[16]

RESULTS AND DISCUSSION

Dispersity of Electrophoretic Mobility Distributions. The treatment of CE-CC data allows the calculation of dispersity values based on electrophoretic mobility distributions. As mentioned previously, CE-CC separates evenly charged polymers based on molecular attributes other than molar mass, provided the polyelectrolyte degree of polymerization is typically higher than 10.[20,31] Three experimental cases are presented, two based on the heterogeneity of composition and one on the heterogeneity of branching.

Chitosan. Chitosan is a polysaccharide derived from the deacetylation of chitin. It is a copolymer of *N*-acetyl-D-glucosamine and D-glucosamine in varying proportions (Figure S1A). Its composition is generally referred to as degree of acetylation, DA (the fraction of *N*-acetyl-D-glucosamine units). Being a natural product, chitosan varies in a range of molecular attributes including molar mass and composition (including the distribution of units along the chain being rather in blocks or statistical). Using CE-CC, different chitosan samples had been separated based on their DA and through appropriate data treatment[21] the weight distributions of the mobilities have been obtained (Figure 1).[14] The heterogeneity of DA, which is the distribution of the compositions of different chains within a chitosan sample, is represented by the distribution of electrophoretic mobilities.

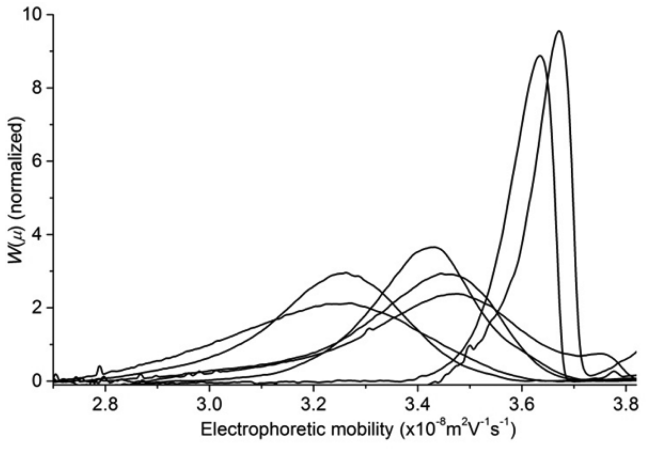

Figure 1. Mobility weight distributions obtained by CE-CC for chitosan samples with varying degrees of acetylation.

Using eqs 5–8, dispersity values were obtained for the different chitosan samples (Table S5). Dispersity values calculated as $D(W(\mu),1,0)$, $D(W(\mu),2,0)$, $D(W(\mu),3,0)$, and SD were in good agreement in terms of the trend observed (Figure 2). They showed an overall decreasing trend in which

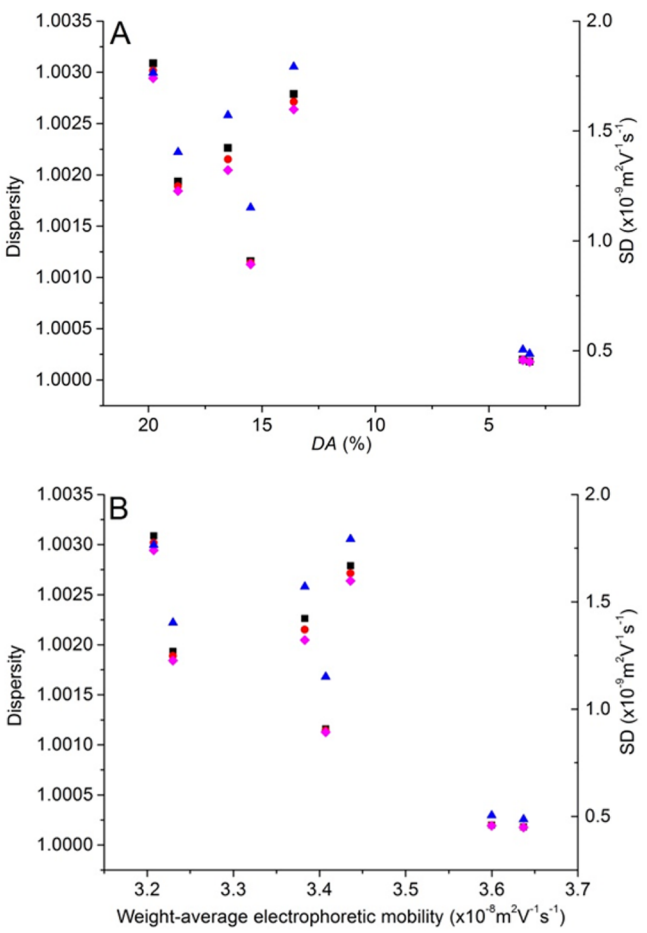

Figure 2. (A) Dispersity values shown for chitosan samples as $D(W(\mu),1,0)$ (red circles, eq 5), $D(W(\mu),2,0)$ (black squares, eq 6), $D(W(\mu),3,0)$ (magenta diamonds, eq 7), and SD (blue triangles, eq 8) against (A) their number-average degree of acetylation or (B) against their weight-average electrophoretic mobility.

the chitosan samples with higher average electrophoretic mobilities (lower average DAs) have more narrow distributions of compositions (lower D values). Thus, the calculation of the dispersity values provided a valid numerical demonstration of the data which was represented graphically. The lower selectivity above the counterion condensation, at the lowest DA, may contribute to this trend. The trend of the dispersity with DA might also be due to the rate of deacetylation varying for different parts of the chitosan sample which can lead to heterogeneity and may also explain the variation in dispersity of samples between the weight-average electrophoretic mobility of 3.3 and 3.4 × 10^{-8} $m^2 \cdot V^{-1} \cdot s^{-1}$. This effect would be weaker at low DA, since the DA cannot (physically) go below 0. It shows the importance of the chemical treatment to which many polysaccharides are subjected in their preparation. This overall trend may not extend to other families of polymers, as seen below.

Despite the relatively low selectivity of the separation, dispersity values calculated on the mobility distributions still

DOI: 10.1021/acs.analchem.5b03672
Anal. Chem. XXXX, XXX, XXX–XXX

allows information regarding the sample heterogeneity to be obtained.

Poly(sodium acrylate-*co*-*N*-antipyrine acrylamide), P(NaA-*co*-APA). This copolymer is synthesized using a known coupling reaction[32] between the amine of the 4-amino-antipyrine, AAP, and the carboxylate of the PNaA (Figure S1B). The grafting reaction was performed within a CE vial and monitored in real time using capillary electrophoresis in previously established conditions[33,34] (Figure 3). The increase

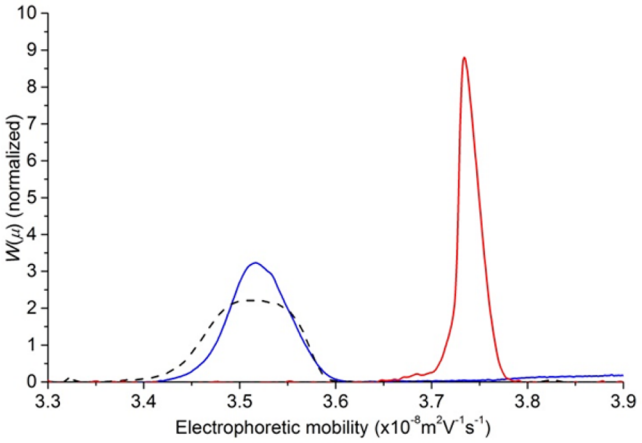

Figure 3. Electrophoretic mobility distributions of P(NaA-*co*-APA) samples at time 0 (red), 5 min (blue) and 4 h (black dash).

of the copolymer peak area with reaction time is consistent with the much larger UV absorption (Beer−Lambert coefficient) for AAP than PNaA which was calculated to be greater by a factor of almost 20 (see Supporting Information). The decrease of the electrophoretic mobility with grafting is consistent with both the reduced charge (loss of carboxylate units) and the increased hydrodynamic friction (increased size). As the reaction time increases the P(NaA-*co*-APA) peak becomes broader, indicating a larger heterogeneity of composition.

The dispersity of electrophoretic mobility of the copolymer was obtained from eqs 5−8 (Table S6). The linear PNaA homopolymer was used as a reference and its dispersity subtracted from the P(NaA-*co*-APA) dispersity values. This enabled us to monitor the grafting reaction and assess the heterogeneity of composition of the P(NaA-*co*-APA). The values of $D(W(\mu),1,0)$, $D(W(\mu),2,0)$, $D(W(\mu),3,0)$, and SD are in good agreement in terms of the trend observed (Figure 4). They increase reaching a maximum at approximately 4 h. The dispersity allows a numerical representation of the change in composition. The heterogeneity of the copolymer increases during the first 4 h, as most of the grafting proceeds. The reaction then slows down and it might lead to a more homogeneous copolymer.

Branched Poly(sodium acrylate), PNaA. This synthetic polymer (Figure S1C) is industrially produced using conventional polymerization; in this study it was synthesized using a controlled radical polymerization: nitroxide-mediated polymerization (NMP).[35] The occurrence of branching in PNaA has been noted[36] and it is an important factor which can be overlooked in PNaA characterization. The branching of PNaA can be used to tailor polymers for specific applications through the choice of an appropriate polymerization technique. CE-CC was shown to separate different PNaA samples based on their branching (Figure 5).[18]

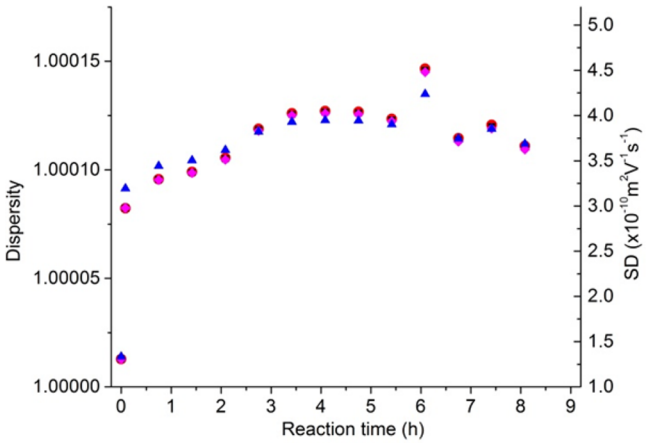

Figure 4. Dispersity values shown for P(NaA-*co*-APA) samples as $D(W(\mu),1,0)$ (black square, eq 5), $D(W(\mu),2,0)$ (red circle, eq 6), $D(W(\mu),3,0)$ (magenta diamonds, eq 7), and SD (blue triangle, eq 8) against reaction time.

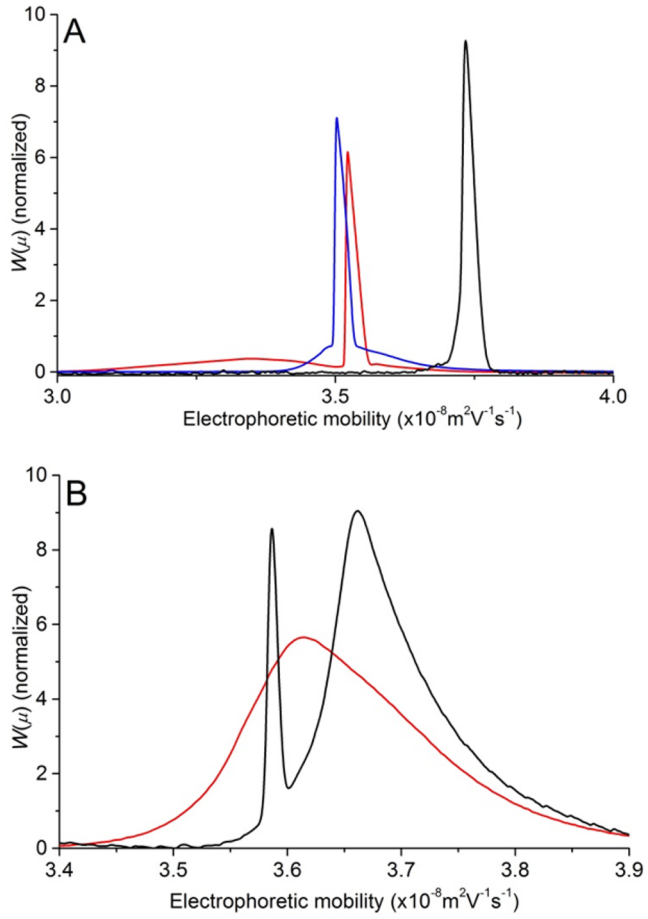

Figure 5. Electrophoretic mobility distributions of PNaA samples. (A) PNaAs with different topologies: linear injected at a lower concentration than previously[18] (black), 3-arm star (red) and hyperbranched (blue). (B) PNaAs synthesized by NMP of acrylic acid (black) and *tert*-butyl acrylate (red).

Dispersity values were obtained for the three samples (Figure 6 and Table S7). It is to be noted that the linear sample does not have any branching since it has been obtained by anionic polymerization[18] and thus the broadness of the peak results from intrinsic experimental factors. Considering the dispersity

DOI: 10.1021/acs.analchem.5b03672
Anal. Chem. XXXX, XXX, XXX−XXX

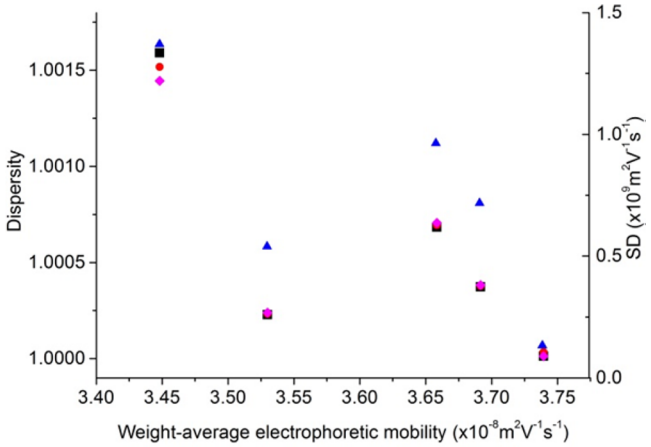

Figure 6. Dispersity values shown for PNaA samples as $D(W(\mu),1,0)$ (black square, eq 5), $D(W(\mu),2,0)$ (red circle, eq 6), $D(W(\mu),3,0)$ (magenta diamonds, eq 7), and SD (blue triangle, eq 8) against their weight-average electrophoretic mobility. The samples in increasing order of average electrophoretic mobility are 3-arm star (3.45×10^{-8} $m^2 \cdot V^{-1} \cdot s^{-1}$), hyperbranched ($3.53 \times 10^{-8}$ $m^2 \cdot V^{-1} \cdot s^{-1}$), NMP of *t*-BA ($3.66 \times 10^{-8}$ $m^2 \cdot V^{-1} \cdot s^{-1}$), NMP of AA ($3.69 \times 10^{-8}$ $m^2 \cdot V^{-1} \cdot s^{-1}$), and linear ($3.74 \times 10^{-8}$ $m^2 \cdot V^{-1} \cdot s^{-1}$).

values are representative of the heterogeneity of branching, the linear (which had the lowest dispersity value and the highest mobility), and the hyperbranched (at a weight-average mobility of 3.53×10^{-8} $m^2 \cdot V^{-1} \cdot s^{-1}$) samples have dispersity values, which are quite close (and low). As expected due to its branching architecture, 3-arm star had the highest dispersity and the lowest mobility. This is because although the hyperbranched sample is more branched than 3-arm star it was designed to have homogeneous branching through the use of an inimer for its synthesis.

Similar samples synthesized from different monomers were analyzed with the same method (Figure 5b). PNaA samples synthesized by the NMP of acrylic acid and of *tert*-butyl acrylate (*t*BA) had different distributions and dispersities. It is to be noted that different end groups[18] can also contribute to the heterogeneity of the electrophoretic mobility distribution.

Dispersity of Composition Distributions. Poly(acrylic acid-*b*-acrylamide), P(AA-*b*-AM), block copolymers were synthesized by Reversible-Addition-Fragmentation Chain Transfer/Macromolecular Design via Interchange of Xantates (RAFT/MADIX) polymerization. Using CE-CC the block copolymers could be separated (Figure 7).[16] The P(AA-*b*-AM) was synthesized with different ratios of the monomers (2K and 10K in the sample name refer to 2000 and 10000 g·mol^{-1} theoretical molar mass of the corresponding block). The electrophoretic mobility distributions were simple to obtain as shown previously, extra treatment was required to obtain composition distributions.

The separation of P(NaA-*b*-AM) using CE-CC is dependent on both the charge of the PNaA monomer units and the hydrodynamic friction of the charged PNaA and uncharged PAM blocks. Therefore, to obtain meaningful composition distributions, both the charged and uncharged blocks of the block copolymer need to be taken into account (eqs S38 and S39). However, the necessary rescaling factor α is challenging to obtain (see Supporting Information). The weight-average composition of both samples was determined from the theoretical values of the uncharged and charged block lengths.

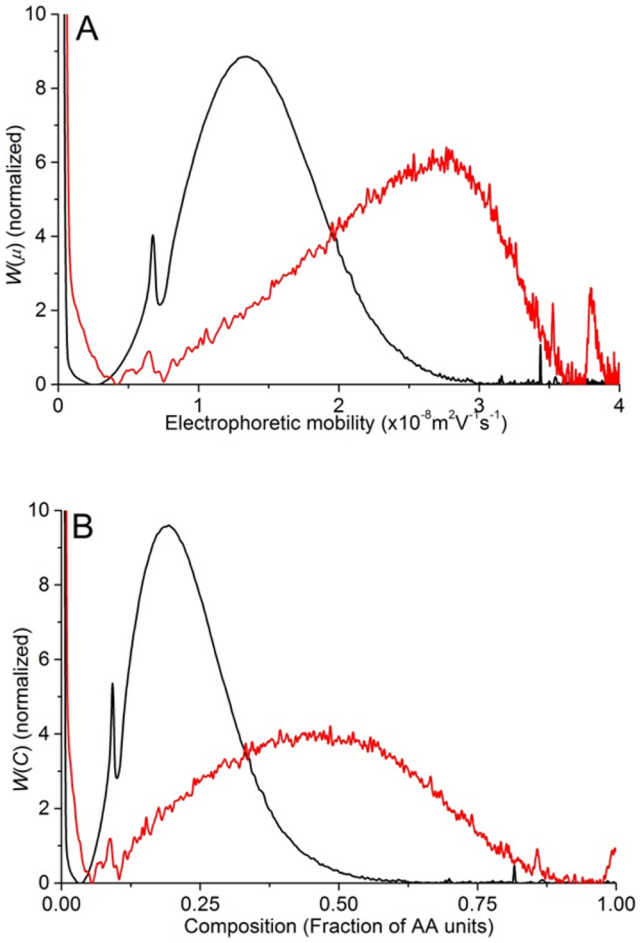

Figure 7. (A) Electrophoretic mobility distribution and (B) composition distribution of P(NaA-*b*-AM) samples: PAA2kPAM10k (black) and PAA10kPAM10k (red). The theoretical M_n values were listed for each sample previously.[16]

Dispersity values were obtained for the distributions of both mobilities and compositions (Table S8).

The accuracy of the composition distributions of P(AA-*b*-AM) and of their dispersity depends on the accuracy of α[16] (eq S39) and of the correlation between electrophoretic mobility and composition. In the case of statistical copolymers α would not need to be calculated and therefore the accuracy of the composition distribution would depend only on the correlation between mobility and composition. The larger uncertainty obtained for dispersities of composition distributions (Table S4) compared to that of electrophoretic mobility distributions (Table S3) is likely due to a weak correlation between mobility and composition (despite the high selectivity in this case). In some cases, a complementary method such as NMR spectroscopy could be used to obtain the average composition of specific samples, thus, allowing a more accurate α to be obtained.

CONCLUSIONS

In this study both synthetic and natural polymers were characterized. The distributions of compositions and the heterogeneity of branching were analyzed using the dispersity of the distributions. Using the correct treatment of CE-CC data, the dispersity was quantified, including the monitoring of grafting on polymers. Further, using the dispersity values, a

DOI: 10.1021/acs.analchem.5b03672
Anal. Chem. XXXX, XXX, XXX−XXX

numerical representation of the mobility and composition distributions were calculated and allowed comparisons between samples. Dispersity values using 0 as a reference were in good agreement with SD calculations in terms of trends observed. With further research dispersity values obtained through CE-CC can be used as commonly as molar mass dispersity values. Dispersity values calculated using D_σ and $D(W(\mu),1,0)$ were in good agreement. The dispersity values obtained in this work are closer to unity than typical values obtained on molar mass dispersity by SEC. It is, however, to be noted that SEC overestimates $Đ$ and this is largely due to band broadening.[37,38] Temperature gradient interaction chromatography[39] and molecular radius analysis with multiangle light scattering combined with SEC[40] were shown to reduce this effect. In analogy to SEC characterization of molar mass distributions of polymers, we recommend $D(W(\mu),1,0)$ to quantify the heterogeneity due to either composition (copolymers) or branching. However, the four different types of quantification of the dispersity should be further compared, especially in the cases of nonsymmetric distributions (with a tail) or bimodal distributions. It would also be very interesting to compare the CE method established in obtaining composition distributions with other methods, typically based on liquid chromatography;[41] however, this has been noted as tedious[42] or was not attempted yet for hydrophilic polymers. Field-flow fractionation, especially thermal,[12] may provide very interesting comparisons. In addition, simulation of polymerization processes should allow the prediction of $D(W(\mu),1,0)$ and the results can be compared with the values determined by CE-CC.

■ ASSOCIATED CONTENT

Supporting Information

The Supporting Information is available free of charge on the ACS Publications website at DOI: 10.1021/acs.analchem.5b03672.

Derivation and expressions of moments, dispersity, and uncertainty; dispersity values for experimental data; molar absorptivity and rescaling factor determination (PDF).

■ AUTHOR INFORMATION

Corresponding Author

*E-mail: p.castignolles@westernsydney.edu.au. Fax: +61 2 9685 9915.

Notes

The authors declare no competing financial interest.

■ ACKNOWLEDGMENTS

The authors would like to thank Matthew Van Leeuwen, Michelle Toutounji (Western Sydney University), and Aidan Grosas (Australian National University) for insightful discussions. J.J.T. thanks the Australian Government for the Endeavour Research Fellowship to visit the University of Montpellier.

■ REFERENCES

(1) Berek, D. *J. Sep. Sci.* **2010**, *33*, 315−335.
(2) Gilbert, R. G.; Hess, M.; Jenkins, A. D.; Jones, R. G.; Kratochvil, R.; Stepto, R. F. T. *Pure Appl. Chem.* **2009**, *81*, 779−779.
(3) Zabisky, R. C. M.; Chan, W. M.; Gloor, P. E.; Hamielec, A. E. *Polymer* **1992**, *33*, 2243−2262.
(4) Philipsen, H. J. A. *J. Chromatogr. A* **2004**, *1037*, 329−350.
(5) Haidar Ahmad, I. A.; Striegel, A. M. *Anal. Bioanal. Chem.* **2010**, *396*, 1589−1598.
(6) Haidar Ahmad, I. A.; Striegel, D. A.; Striegel, A. M. *Polymer* **2011**, *52*, 1268−1277.
(7) Maier, H.; Malz, F.; Radke, W. *Macromol. Chem. Phys.* **2015**, *216*, 228−234.
(8) Reingruber, E. M.; Chojnacka, A.; Jellema, E.; de Bruin, B.; Buchberger, W.; Schoenmakers, P. J. *J. Chromatogr. A* **2012**, *1255*, 259−266.
(9) Shakun, M.; Heinze, T.; Radke, W. *Carbohydr. Polym.* **2015**, *130*, 77−86.
(10) Gaborieau, M.; Castignolles, P. *Anal. Bioanal. Chem.* **2011**, *399*, 1413−1423.
(11) Radke, W. *J. Chromatogr. A* **2014**, *1335*, 62−79.
(12) Ponyik, C. A.; Wu, D. T.; Williams, S. K. R. *Anal. Bioanal. Chem.* **2013**, *405*, 9033−9040.
(13) Cottet, H.; Gareil, P. In *Capillary Electrophoresis*; Schmitt-Kopplin, P., Ed.; Humana Press Inc.: Totowa, NJ, U.S.A., 2008; pp 541−567.
(14) Mnatsakanyan, M.; Thevarajah, J. J.; Roi, R. S.; Lauto, A.; Gaborieau, M.; Castignolles, P. *Anal. Bioanal. Chem.* **2013**, *405*, 6873−6877.
(15) Taylor, D. L.; Ferris, C. J.; Maniego, A. R.; Castignolles, P.; in het Panhuis, M.; Gaborieau, M. *Aust. J. Chem.* **2012**, *65*, 1156−1164.
(16) Sutton, A. T.; Read, E.; Maniego, A. R.; Thevarajah, J. J.; Marty, J. D.; Destarac, M.; Gaborieau, M.; Castignolles, P. *J. Chromatogr. A* **2014**, *1372*, 187−195.
(17) Oukacine, F.; Bernard, S.; Bobe, I.; Cottet, H. *J. Controlled Release* **2014**, *196*, 139−145.
(18) Maniego, A. R.; Ang, D.; Guillaneuf, Y.; Lefay, C.; Gigmes, D.; Aldrich-Wright, J. R.; Gaborieau, M.; Castignolles, P. *Anal. Bioanal. Chem.* **2013**, *405*, 9009−9020.
(19) Sisavath, N.; Le Saux, T.; Leclercq, L.; Cottet, H. *Langmuir* **2014**, *30*, 4450−4457.
(20) Thevarajah, J. J.; Gaborieau, M.; Castignolles, P. *Adv. Chem.* **2014**, *9*, No. 798503.
(21) Chamieh, J.; Martin, M.; Cottet, H. *Anal. Chem.* **2015**, *87*, 1050−1057.
(22) Shortt, D. W. *J. Liq. Chromatogr.* **1993**, *16*, 3371−3391.
(23) Burchard, W. *Adv. Polym. Sci.* **1999**, *143*, 113−194.
(24) Yao, Y.; Guiltinan, M. J.; Thompson, D. B. *Carbohydr. Res.* **2005**, *340*, 701−710.
(25) Zhong, H. J.; Williams, M. A. K.; Keenan, R. D.; Goodall, D. M.; Rolin, C. *Carbohydr. Polym.* **1997**, *32*, 27−32.
(26) Guillotin, S. E.; Bakx, E. J.; Boulenguer, P.; Schols, H. A.; Voragen, A. G. J. *Food Hydrocolloids* **2007**, *21*, 444−451.
(27) Hoagland, D. A.; Smisek, D. L.; Chen, D. Y. *Electrophoresis* **1996**, *17*, 1151−1160.
(28) Cottet, H.; Biron, J. P. *Macromol. Chem. Phys.* **2005**, *206*, 628−634.
(29) Oliver, J. D.; Gaborieau, M.; Hilder, E. F.; Castignolles, P. *J. Chromatogr. A* **2013**, *1291*, 179−186.
(30) Oliver, J. D.; Sutton, A. T.; Karu, N.; Phillips, M.; Markham, J.; Peiris, P.; Hilder, E. F.; Castignolles, P. *Biotechnol. Appl. Biochem.* **2015**, *62*, 329−342.
(31) Cottet, H.; Gareil, P.; Theodoly, O.; Williams, C. E. *Electrophoresis* **2000**, *21*, 3529−3540.
(32) Taylor, D. L.; Thevarajah, J. J.; Narayan, D. K.; Murphy, P.; Mangala, M. M.; Lim, S.; Wuhrer, R.; Lefay, C.; O'Connor, M. D.; Gaborieau, M.; Castignolles, P. *Anal. Bioanal. Chem.* **2015**, *407*, 2543−2555.
(33) Castignolles, P.; Gaborieau, M.; Hilder, E. F.; Sprong, E.; Ferguson, C. J.; Gilbert, R. G. *Macromol. Rapid Commun.* **2006**, *27*, 42−46.
(34) Gaborieau, M.; Causon, T.; Guillaneuf, Y.; Hilder, E. F.; Castignolles, P. *Aust. J. Chem.* **2010**, *63*, 1219−1226.
(35) Couvreur, L.; Lefay, C.; Belleney, J.; Charleux, B.; Guerret, O.; Magnet, S. *Macromolecules* **2003**, *36*, 8260−8267.

DOI: 10.1021/acs.analchem.5b03672
Anal. Chem. XXXX, XXX, XXX−XXX

(36) Lacik, I.; Stach, M.; Kasak, P.; Semak, V.; Uhelska, L.; Chovancova, A.; Reinhold, G.; Kilz, P.; Delaittre, G.; Charleux, B.; Chaduc, I.; D'Agosto, F.; Lansalot, M.; Gaborieau, M.; Castignolles, P.; Gilbert, R. G.; Szablan, Z.; Barner-Kowollik, C.; Hesse, P.; Buback, M. *Macromol. Chem. Phys.* **2015**, *216*, 23−37.
(37) Vander Heyden, Y.; Popovici, S. T.; Staal, B. B. P.; Schoenmakers, P. J. *J. Chromatogr. A* **2003**, *986*, 1−15.
(38) Popovici, S. T.; Kok, W. T.; Schoenmakers, P. J. *J. Chromatogr. A* **2004**, *1060*, 237−252.
(39) Park, S.; Chang, T. *Macromolecules* **2006**, *39*, 3466−3468.
(40) Shortt, D. W. *J. Chromatogr. A* **1994**, *686*, 11−20.
(41) Rollet, M.; Pelletier, B.; Altounian, A.; Berek, D.; Maria, S.; Beaudoin, E.; Gigmes, D. *Anal. Chem.* **2014**, *86*, 2694−2702.
(42) Beaudoin, E.; Favier, A.; Galindo, C.; Lapp, A.; Petit, C.; Gigmes, D.; Marque, S.; Bertin, D. *Eur. Polym. J.* **2008**, *44*, 514−522.

DOI: 10.1021/acs.analchem.5b03672
Anal. Chem. XXXX, XXX, XXX−XXX

Supporting Information

for

Quantifying the heterogeneity of chemical structures in complex charged polymers through the dispersity of their distributions of electrophoretic mobilities or of compositions

Joel J. Thevarajah,[†,‡] Adam T. Sutton,[†,‡] Alison R. Maniego,[†,‡] Elizabeth G. Whitty,[†,‡] Simon Harrisson,[§] Hervé Cottet,[‖] Patrice Castignolles,[*,†] Marianne Gaborieau[†,‡]

Western Sydney University, [†]School of Science and Health, Australian Centre for Research of Separation Science (ACROSS), and [‡]Molecular Medicine Research Group, School of Science and Health, Parramatta NSW 2150, Australia

[§]IMRCP, UMR 5623, Université de Toulouse, 118 route de Narbonne, F-31062 Toulouse Cedex 9, France

[‖]Institut des Biomolécules Max Mousseron (IBMM, UMR 5247 CNRS, Université de Montpellier, Ecole Nationale Supérieure de Chimie de Montpellier), Place Eugène Bataillon CC 1706, 34095 Montpellier Cedex France

* Corresponding author : Patrice Castignolles, p.castignolles@westernsydney.edu.au, Fax: +61 2 9685 9915

Dispersity calculated through M_w and M_n

Integral expression of the dispersity using M_w and M_n

$$\frac{M_w}{M_n} = \frac{[\int W(M) M \mathrm{d}M][\int W(M) M^{-1} \mathrm{d}M]}{[\int W(M) \mathrm{d}M]^2} \quad \text{S1}$$

Moments and dispersity of electrophoretic mobility distributions

The moments are defined as in Table S1[1].

Table S1. Summary of the integrals and discrete expressions of the moments relevant to this work

Moment order	Integral form	Discrete form
-1	$\int W(\mu)\, \mu^{-1}\, d\mu$	$\sum_z W(\mu_z)\, \mu_z^{-1}\, (\mu_{z+1} - \mu_z)$
0	$\int W(\mu)\ d\mu$	$\sum_z W(\mu_z)\, (\mu_{z+1} - \mu_z)$
1	$\int W(\mu)\, \mu\, d\mu$	$\sum_z W(\mu_z)\, \mu_z\, (\mu_{z+1} - \mu_z)$
2	$\int W(\mu)\, \mu^2\, d\mu$	$\sum_z W(\mu_z)\, \mu_z^2\, (\mu_{z+1} - \mu_z)$
3	$\int W(\mu)\, \mu^3\, d\mu$	$\sum_z W(\mu_z)\, \mu_z\ \ (\mu_{z+1} - \mu_z)$

$$\mu_w = \frac{[\sum_z W(\mu_z)\mu_z\,(\mu_{z+1}-\mu_z)]}{[\sum_z W(\mu_z)\,(\mu_{z+1}-\mu_z)]} \quad \text{S2}$$

The general expressions for the equations taking μ_{w} as a reference are as follows:

$$D(W(\mu),1,\mu_{\mathrm{w}}) = \frac{\overline{\mu^1_{\mu_{\mathrm{w}}}} \times \overline{\mu^{-1}_{\mu_{\mathrm{w}}}}}{[\overline{\mu^0_{\mu_{\mathrm{w}}}}]^2} \quad \text{S3}$$

$$D(W(\mu),2,\mu_{\mathrm{w}}) = \frac{\overline{\mu^2_{\mu_{\mathrm{w}}}} \times \overline{\mu^0_{\mu_{\mathrm{w}}}}}{[\overline{\mu^1_{\mu_{\mathrm{w}}}}]^2} \quad \text{S4}$$

$$D(W(\mu),3,\mu_{\mathrm{w}}) = \frac{\overline{\mu^3_{\mu_{\mathrm{w}}}} \times \overline{\mu^1_{\mu_{\mathrm{w}}}}}{[\overline{\mu^2_{\mu_{\mathrm{w}}}}]^2} \quad \text{S5}$$

The integral forms of the general equations (eq 3, 5 to 8 and S3 to S4) are defined as:

$$D(W(A),b,c) = \frac{\left[\int W(A)(A-c)^b \mathrm{d}A\right]\left[\int W(A)(A-c)^{b-2}\mathrm{d}A\right]}{[\int W(A)(A-c)^{b-1}\mathrm{d}A]^2} \quad \text{S6}$$

$$D(W(\mu),1,0) = \frac{[\int W(\mu)\mu \mathrm{d}\mu][\int W(\mu)\mu^{-1}\mathrm{d}\mu]}{[\int W(\mu)\mathrm{d}\mu]^2} \quad \text{S7}$$

$$D(W(\mu),1,\mu_{\mathrm{w}}) = \frac{[\int W(\mu)(\mu-\mu_w)\mathrm{d}\mu]\left[\int W(\mu)(\mu-\mu_w)^{-1}\mathrm{d}\mu\right]}{[\int W(\mu)\mathrm{d}\mu]^2} \quad \text{S8}$$

$$D(W(\mu),2,0) = \frac{\left[\int W(\mu)\mu^2\mathrm{d}\mu\right][\int W(\mu)\mathrm{d}\mu)]}{[\int W(\mu)\mu\mathrm{d}\mu]^2} \quad \text{S9}$$

$$D(W(\mu),2,\mu_{\mathrm{w}}) = \frac{[\int W(\mu)(\mu-\mu_{\mathrm{w}})^2\,\mathrm{d}\mu][\int W(\mu)\mathrm{d}\mu]}{[\int W(\mu)(\mu-\mu_{\mathrm{w}})\mathrm{d}\mu]^2} \quad \text{S10}$$

$$D(W(\mu),3,0) = \frac{\left[\int W(\mu)\mu^3\mathrm{d}\mu\right][\int W(\mu)\mu\mathrm{d}\mu)]}{[\int W(\mu)\mu^2\mathrm{d}\mu]^2} \quad \text{S11}$$

$$D(W(\mu),3,\mu_{\mathrm{w}}) = \frac{[\int W(\mu)(\mu-\mu_{\mathrm{w}})^2\,\mathrm{d}\mu][\int W(\mu)(\mu-\mu_{\mathrm{w}})\mathrm{d}\mu]}{[\int W(\mu)(\mu-\mu_{\mathrm{w}})^2\mathrm{d}\mu]^2} \quad \text{S12}$$

$$D_\sigma = \left[\frac{[\int W(\mu)(\mu-\mu_{\mathrm{w}})^2\mathrm{d}\mu]}{[\int W(\mu)\mathrm{d}\mu]}\right]^{0.5} \quad \text{S13}$$

In the calculation of dispersity values for the experimental cases in the article, the discrete forms were used for the moments. Eq S5, S7 and S9 thus became:

$$D(W(\mu),1,0) = \frac{[\sum_z W(\mu_z)\mu_z\,(\mu_{z+1}-\mu_z)][\sum_z W(\mu_z){\mu_z}^{-1}(\mu_{z+1}-\mu_z)]}{[\sum_z W(\mu_z)\,(\mu_{z+1}-\mu_z)]^2} \quad \text{S14}$$

$$D(W(\mu),2,0) = \frac{[\sum_z W(\mu_z)\ {\mu_z}^2(\mu_{z+1}-\mu_z)][\sum_z W(\mu_z)\ (\mu_{z+1}-\mu_z)]}{[\sum_z W(\mu_z)\ \mu_z(\mu_{z+1}-\mu_z)]^2} \quad \text{S15}$$

$$D(W(\mu),3,0) = \frac{[\sum_z W(\mu_z)\ {\mu_z}^3(\mu_{z+1}-\mu_z)][\sum_z W(\mu_z)\ \mu_z(\mu_{z+1}-\mu_z)]}{[\sum_z W(\mu_z)\ {\mu_z}^2(\mu_{z+1}-\mu_z)]^2} \quad \text{S16}$$

$$D_\sigma = \left[\frac{[\sum_z W(\mu_z)\ (\mu_z-\mu_w)^2(\mu_{z+1}-\mu_z)]}{[\sum_z W(\mu_z)\ (\mu_{z+1}-\mu_z)]}\right]^{0.5} \quad \text{S17}$$

μ_w as a reference

In eq S7, S9 and S11 the term $W(\mu)(\mu-\mu_w)d\mu$, can be split. According to eq 4 the 2 resulting terms in eq S18 are equal and therefore the first order moment remains undefined. As this term is undefined it explains why the results using μ_w as a reference do not produce the same trend as $D(W(\mu),1,0)$, $D(W(\mu),2,0)$ and $D(W(\mu),3,0)$.

$$\int W(\mu)(\mu-\mu_w)d\mu = \int W(\mu)\mu d\mu - \mu_w \int W(\mu)d\mu = 0 \quad \text{S18}$$

Dispersity of composition distributions

The discrete form used in the calculation derived from eq 10 is defined as:

$$C_w = \frac{[\sum_z W(C_z)C_z\ (C_{z+1}-C_z)]}{[\sum_z W(C_z)\ (C_{z+1}-C_z)]} \quad \text{S19}$$

The integral forms of the general equations (eq 5 to 8) for composition are defined as:

$$D(W(C)1,0) \quad = \frac{[\int W(C)CdC][\int W(C)C^{-1}dC]}{[\int W(C)dC]^2} \quad \text{S20}$$

$$D(W(C),2,0) \quad = \frac{[\int W(C)C^2\mathrm{d}C][\int W(C)\mathrm{d}C]}{[\int W(C)C\mathrm{d}C]^2} \quad \text{S21}$$

$$D(W(C),3,0) \quad = \frac{[\int W(C)C^3\mathrm{d}C][\int W(C)C\mathrm{d}C]}{[\int W(C)C^2\mathrm{d}C]^2} \quad \text{S22}$$

$$D(W(C),\sigma,C_\mathrm{W}) = \left[\frac{[\int W(C)(C-C_w)^2\ \mathrm{d}C]}{[\int W(C)dC]}\right]^{0.5} \quad \text{S23}$$

In the calculation of dispersity values for the experimental cases in the article, the discrete forms were used for the moments. Eq S20 to S23 thus became:

$$D(W(C)1,0) \quad = \frac{[\sum_z W(C_z)\, C_z\, (C_{z+1}-C_z)]\left[\sum_z W(C_z)\, C_z^{-1}\, (C_{z+1}-C_z)\right]}{[\sum_z W(C_z)\, (C_{z+1}-C_z)]^2} \qquad \text{S24}$$

$$D(W(C),2,0) = \frac{\left[\sum_z W(C_z)\, {C_z}^2 (C_{z+1}-C_z)\right][\sum_z W(C_z)\, (C_{z+1}-C_z)]}{[\sum_z W(C_z)\, C_z (C_{z+1}-C_z)]^2} \qquad \text{S25}$$

$$D(W(C),3,0) = \frac{\left[\sum_z W(C_z)\, {C_z}^3 (C_{z+1}-C_z)\right][\sum_z W(C_z) C\, (C_{z+1}-C_z)]}{\left[\sum_z W(C_z)\, {C_z}^2 (C_{z+1}-C_z)\right]^2} \qquad \text{S26}$$

$$D(W(C),\sigma,C_{\mathrm{W}}) = \left[\frac{\left[\sum_z W(C_z)\, (C_z-C_{\mathrm{w}})^2 (C_{z+1}-C_z)\right]}{[\sum_z W(C_z)(C_{z+1}-C_z)]}\right]^{0.5} \qquad \text{S27}$$

Number average electrophoretic mobility

By definition the number-average electrophoretic mobility can be expressed as:

$$\mu_n = \frac{\int N(\mu)\mu d\mu}{\int N(\mu) d\mu} \qquad \text{S28}$$

Where $N(\mu)$ is the number distribution of electrophoretic mobility (which could be obtained by the detection of end-groups of the polymer after derivatization and use of a fluorescence detector). The ratio between the weight distribution and the number distribution of chains at a given electrophoretic mobility is the number-average molar mass of all polymer chains having the same electrophoretic mobility μ, $M_n(\mu)$. $M_n(\mu)$ has never been determined experimentally. Its determination by coupling the CE separation to a SEC second dimension is highly unlikely due to the injected volume in the CE being several orders of magnitude smaller than in SEC. The number distribution of electrophoretic mobility is thus not considered further in this work.

In this work, the dispersity of the electrophoretic mobility (or composition) distributions are calculated using the ratio of the zeroth to the -1st order moments of the relevant distribution. In the case of M_n, the ratio of the zeroth to the -1st order moments of the molar mass distribution leads to a different but corresponding expression to the definition of M_n[2,3]. In the case of μ_n the ratio of the zeroth to the -1st order moments of the electrophoretic mobility distribution does not correspond to the definition above:

$$\frac{\int W(\mu) d\mu}{\int \frac{W(\mu)}{\mu} d\mu} = \frac{\int \frac{N(\mu)}{M_n(\mu)} d\mu}{\int \frac{N(\mu)}{\mu M_n(\mu)} d\mu} \neq \mu_n \qquad \text{S29}$$

Estimation of the uncertainty on the electrophoretic mobility dispersity

To estimate the uncertainty of the dispersity due to the experimental error of the electrophoretic mobility, each of the dispersity equations was derived as follows. Each of the electrophoretic mobility dispersities expressed in eq 5 to 7 as a function of μ (except the standard deviation) can be expressed as a combination of other functions of μ: f, g and h (each of them being a moment). The fractional uncertainties add in quadrature.

$$D = \frac{f \cdot g}{h^2} \qquad \text{S30}$$

The differentiation of eq S30 results in:

$$\frac{dD}{D} = \sqrt{\left(\frac{df}{f}\right)^2 + \left(\frac{dg}{g}\right)^2 + 2\left(\frac{dh}{h}\right)^2} \qquad \text{S31}$$

Eq S31 can be rearranged in:

$$\frac{dD}{D} = \frac{d\mu}{\mu}\sqrt{\left(\frac{\mu \cdot f'}{f}\right)^2 + \left(\frac{\mu \cdot g'}{g}\right)^2 + 2\left(\frac{\mu \cdot h'}{h}\right)^2} \qquad \text{S32}$$

For example for eq 5 with $D(W(\mu)1,0)$, $f = \int W(\mu)\mu d\mu$; $g = \int W(\mu)\mu^{-1} d\mu$; and $h = \int W(\mu)\, d\mu$

Therefore $f' = W(\mu)\mu$; $g' = W(\mu)\mu^{-1}$; and $h' = W(\mu)\mu$

The expression of eq S32 in the case of the derivation of eq 5 to 7 are given in eq 11 to 13.

To calculate the relative uncertainty of the dispersity values based on eq 11 to 13, the discrete forms below were used (eq S33 to S35). Peak areas of the appropriate functions were used for sums, and peak heights for μ_z values outside of sums.

$$\frac{dD(W(\mu),1,0)}{D(W(\mu),1,0)} = \frac{d\mu}{\mu}\sqrt{\left(\frac{W(\mu)\mu^2}{\sum_z W(\mu)\mu_z(\mu_{z+1}-\mu_z)}\right)^2 + \left(\frac{W(\mu)}{\sum_z W(\mu){\mu_z}^{-1}(\mu_{z+1}-\mu_z)}\right)^2 + 2\left(\frac{W(\mu)\mu_z}{\sum_z W(\mu)(\mu_{z+1}-\mu_z)}\right)^2} \qquad \text{S33}$$

$$\frac{dD(W(\mu),2,0)}{D(W(\mu),2,0)} = \frac{d\mu}{\mu}\sqrt{\left(\frac{W(\mu)\mu^3}{\sum_z W(\mu){\mu_z}^2(\mu_{z+1}-\mu_z)}\right)^2 + \left(\frac{W(\mu)\mu}{\sum_z W(\mu)(\mu_{z+1}-\mu_z)}\right)^2 + 2\left(\frac{W(\mu)\mu^2}{\sum_z W(\mu)\mu_z(\mu_{z+1}-\mu_z)}\right)^2} \qquad \text{S34}$$

$$\frac{dD(W(\mu),3,0)}{D(W(\mu),3,0)} = \frac{d\mu}{\mu}\sqrt{\left(\frac{W(\mu)\mu^4}{\sum_z W(\mu){\mu_z}^3(\mu_{z+1}-\mu_z)}\right)^2 + \left(\frac{W(\mu)\mu^2}{\sum_z W(\mu)\mu(\mu_{z+1}-\mu_z)}\right)^2 + 2\left(\frac{W(\mu)\mu^3}{\sum_z W(\mu){\mu_z}^2(\mu_{z+1}-\mu_z)}\right)^2}$$

S35

The differentiation of the electrophoretic mobility dispersity expressed in eq 8 as a standard deviation follows a different path, as this dispersity can be expressed as a combination of functions f and g of μ (each of them being a moment):

$$D = \left(\frac{f}{g}\right)^{0.5}$$ S36

The differentiation of eq S36 results in:

$$\frac{dD}{D} = \sqrt{0.5\left(\frac{df'}{f}\right)^2 + 0.5\left(\frac{\mu g'}{g}\right)^2}$$ S37

Eq S37 can be rearranged in:

$$\frac{dD}{D} = \frac{d\mu}{\mu}\sqrt{0.5\left(\frac{\mu f'}{f}\right)^2 + 0.5\left(\frac{\mu g'}{g}\right)^2}$$ S38

In eq 8 with D_σ, $f = \int W(\mu)(\mu-\mu_w)^2 d\mu$ and $g = \int W(\mu)d\mu$,

Therefore $f' = W(\mu)(\mu-\mu_w)^2$ and $g' = W(\mu)$

Substituting f, g, f', g' in eq S38 yields eq 14. To calculate the uncertainty of the dispersity values based on eq 8, the discrete form below was used (eq S39).

Peak areas of the appropriate functions were used for sums, and peak heights for μ values outside of sums.

$$\frac{dD_\sigma}{D_\sigma} = \frac{d\mu}{\mu}\sqrt{\left(\frac{W(\mu)(\mu-\mu_w)^2\mu}{2\sum_z W(\mu)(\mu_z-\mu_w)^2(\mu_{z+1}-\mu_z)}\right)^2 + \left(\frac{W(\mu)\mu}{2\sum_z W(\mu)(\mu_{z+1}-\mu_z)}\right)^2}$$ S39

The value of the dispersity uncertainty was calculated for a sample of each of the experimental cases through eq S33 to S35 and S39, using 1 % for $\frac{d\mu}{\mu}$ as an estimate of the published RSDs of the electrophoretic mobilities (Table S2). Results are listed in Table S3.

Table S2. RSD of the electrophoretic mobilities of polyelectrolytes[4] and sugars[5,6] in the literature.

Sample	RSD (%)		
Linear PNaA	1.63		
3-arm star PNaA	1.34		
Hyperbranched PNaA	1.15		
Cellobiose	0.39		
Galactose	0.41	0.53	0.17
Glucose	0.45	0.63	0.06
Rhamnose	0.63	0.76	
Mannose	0.40	0.77	0.71
Arabinose	0.57	0.60	0.46
Xylose	0.40	0.54	0.29
Arabitol	0.74	1.33	

Table S3. Relative uncertainty values of the dispersity of the electrophoretic mobility distribution, calculated for a sample of each of the experimental cases using eq S33 to S35 and S39. The chitosan sample with a DA of 19.8, P(NaA-*co*-APA) at 5 minutes reaction time, PNaA 3 arm star and PAAkPAM10k were chosen. The uncertainty is given in $m^2V^{-1}s^{-1}$.

Sample	$\frac{dD(W(\mu),1,0)}{D(W(\mu),1,0)}$	$\frac{dD(W(\mu),2,0)}{D(W(\mu),2,0)}$	$\frac{dD(W(\mu),3,0)}{D(W(\mu),3,0)}$	$\frac{dD(W(\mu),\sigma,\mu_w)}{D(W(\mu),\sigma,\mu_w)}$
Chitosan	3.6×10^{-17}	1.3×10^{-12}	4.3×10^{-9}	1.3×10^{-12}
P(NaA-*co*-APA)	4.4×10^{-17}	1.1×10^{-12}	4.8×10^{-10}	1.3×10^{-12}
PNaA	9.3×10^{-18}	2.8×10^{-14}	1.4×10^{-13}	9.5×10^{-14}
PAA2kPAM10k	8.0×10^{-18}	5.5×10^{-14}	2.3×10^{-12}	2.0×10^{-13}

Estimation of the uncertainty on the composition dispersity

The differentiation of the composition dispersity follows the same approach as detailed above for the electrophoretic mobility dispersity. The resulting equations are similar to eq S33 to S35 and S39, except that *C* must be substituted for μ. The values of the dispersity uncertainty were calculated for block copolymer samples (Table S4).

Table S4. Relative uncertainty values of the dispersity of the composition distribution, for block copolymer samples (calculated from equations analogous to S33 to S35 and S39, with *C* substituted for μ)

Sample	$\frac{dD(W(C),1,0)}{D(W(C),1,0)}$	$\frac{dD(W(C),2,0)}{D(W(C),2,0)}$	$\frac{dD(W(C),3,0)}{D(W(C),3,0)}$	$\frac{dD(W(C),\sigma,C_w)}{D(W(C),\sigma,C_w)}$
PAA2kPAM10k	2.3×10^{-3}	5.4×10^{-7}	1.2×10^{-6}	3.1×10^{-6}
PAA10kPAM10k	5.6×10^{-3}	2.2×10^{-6}	2.7×10^{-6}	2.8×10^{-6}

Experimental samples

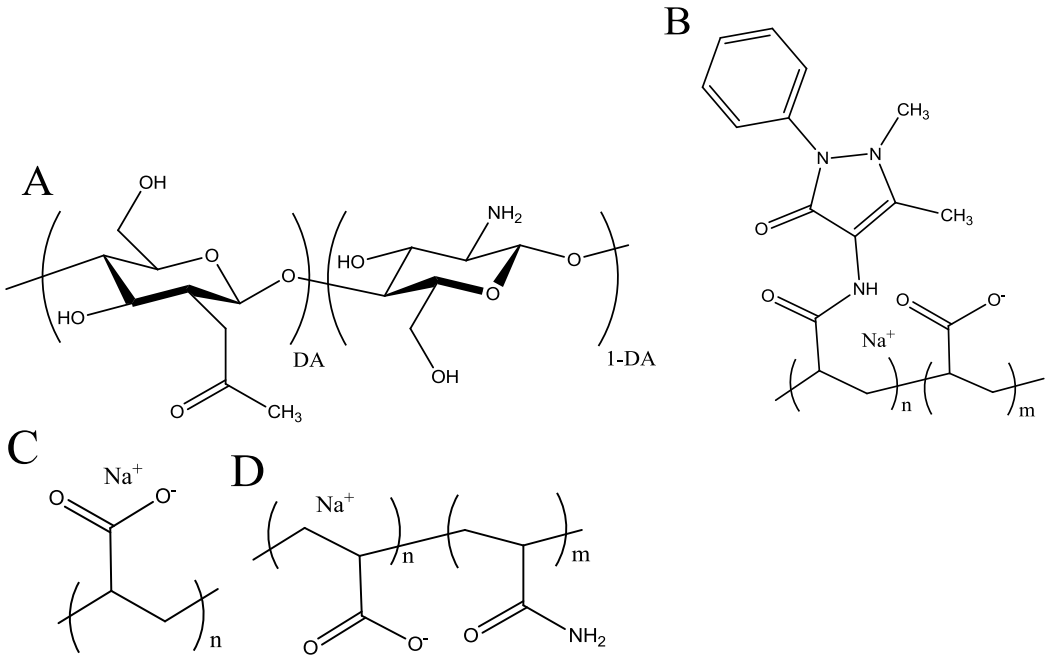

Figure S1. The molecular structure of (A) chitosan with *N*-acetyl-D-glucosamine and D-glucosamine units[7] (B) P(NaA-*co*-APA), (C) PNaA and (D) P(NaA-*b*-AM).

Table S5. Dispersity of chitosan samples

DA[a]	μ_w[b]	SD[c] (10^{-10})	D(*W*(*μ*),1,0)-1 (10^{-4})	*D*(*W(μ)*,2,0)-1 (10^{-4})	*D*(*W(μ)*,3,0)-1 (10^{-4})
19.8	3.21	17.6	30.9	30.2	29.4
13.6	3.44	17.9	27.9	27.1	26.4
3.5	3.60	5.05	2.00	1.97	1.94
18.7	3.23	14.0	19.4	18.9	18.4
16.5	3.38	15.7	22.6	21.5	20.5
3.2	3.64	4.86	1.81	17.9	1.77
15.5	3.41	11.5	11.6	11.4	11.3

[a] number-average *DA* measured using quantitative ^{1}H NMR spectroscopy at 90°C[8]

[b] the weight-average electrophoretic mobility is given in $10^{-8}.m^2V^{-1}s^{-1}$

[c] the standard deviation is given in $m^2V^{-1}s^{-1}$

Molar absorptivity P(NaA-*co*-APA)

The UV absorbance of PNaA and AAP were calculated using the absorbance obtained experimentally in the conditions of the separation (195 nm wavelength, sodium borate buffer 110 mM at 25 °C).

Linear PNaA: $1.7 \cdot 10^{-6}$ a.u.·V·s·m^{-2}

AAP: $3.4 \cdot 10^{-5}$ a.u.·V·s·m^{-2}

.

Table S6. Dispersity values of P(NaA-*co*-APA) samples. The values are first given as determined from eq 5 to 8; the value obtained for the linear PNaA (sample at time 0) was then subtracted from these values.

					After subtracting value for Linear PNaA			
Time (min)	$D(W(\mu),1,0)$ -1 (10^{-4})	$D(W(\mu),2,0)$ -1 (10^{-4})	$D(W(\mu),3,0)$ -1 (10^{-4})	SD[a] (10^{-10})	$D(W(\mu),1,0)$ -1 (10^{-4})	$D(W(\mu),2,0)$ -1 (10^{-4})	$D(W(\mu),3,0)$ -1 (10^{-4})	SD[a] (10^{-10})
0	0.13	0.13	0.13	1.33	0	0	0	0
5	0.82	0.82	0.825	3.20	0.696	0.696	0.697	1.86
45	0.96	0.96	0.954	3.44	0.830	0.828	0.826	2.11
85	0.99	0.99	0.986	3.51	0.863	0.861	0.859	2.17
125	1.05	1.05	1.05	3.62	0.927	0.923	0.92	2.28
165	1.19	1.18	1.18	3.82	1.06	1.06	1.05	2.49
205	1.26	1.26	1.25	3.93	1.13	1.13	1.12	2.60
245	1.27	1.27	1.26	3.95	1.14	1.14	1.13	2.61
285	1.27	1.26	1.26	3.94	1.14	1.13	1.13	2.61
325	1.24	1.23	1.22	3.90	1.11	1.10	1.1	2.57
365	1.47	1.46	1.45	4.24	1.34	1.33	1.32	2.90
405	1.15	1.14	1.13	3.75	1.02	1.01	1	2.41
445	1.21	1.2	1.19	3.85	1.08	1.07	1.06	2.52
485	1.11	1.1	1.09	3.69	0.983	0.97	0.967	2.35

[a] the standard deviation is given in $m^2V^1s^{-1}$

Branched PNaA

Table S7. Summary of PNaA dispersity values representing the heterogeneity of samples with different branching topologies and samples produced from different monomers

Sample	μ_w $10^{-8}.m^2V^1s^{-1}$	SD (10^{-10}) $m^2V^1s^{-1}$	$D(W(\mu),1,0)$-1 (10^{-4})	$D(W(\mu),2,0)$-1 (10^{-4})	$D(W(\mu),3,0)$-1 (10^{-4})
3-Arm star	3.45	13.7	15.9	15.2	14.4
Hyper-branched	3.53	5.4	2.28	2.34	2.39
Linear	3.74	1.33	0.10	0.10	0.13
PNaA-AA	3.69	7.18	3.73	3.78	3.83
PNaA-tBA	3.66	9.64	6.84	6.95	7.06

P(AA-*b*-AM) composition calculation

The composition *C* taken as the molar fraction of acrylic acid monomer units in the copolymer is linked to the electrophoretic mobility μ of the copolymer through eq S40[9]:

$$C = \frac{\alpha\mu}{\mu(\alpha-1)+ \mu_0} \quad \text{S40}$$

where α is a rescaling factor, and μ_o is the electrophoretic mobility of the charged homopolymer. α depends on the chemical nature of both homopolymers, on the background electrolyte, and on the temperature[10]. Combining eq S40 with eq 9 leads to:

$$W(C) = W(\mu)\frac{[\mu(\alpha-1)+ \mu_0]^2}{\alpha\mu_0} \quad \text{S41}$$

Any error in the determination of the rescaling factor α would thus result in an error in the calculated composition distribution, *W*(*C*).

Determining alpha

For a block copolymer consisting of one charged block and one neutral block the number of effective monomer units can be related to its electrophoretic mobility in the following equation[11]:

$$\mu = \mu_0 \frac{n_c}{n_c + \alpha n_u} \quad \text{S42}$$

Where n_c is the number of charged monomer units in the copolymer and n_u is the number of uncharged monomer units in the copolymer.

Eq S42 can be rearranged into eq S43 so that a plot of μ_0/μ - 1 vs n_u/n_c will yield α as the slope.

$$\frac{\mu_0}{\mu} - 1 = \alpha \frac{n_u}{n_c} \quad \text{S43}$$

Since synthetic block copolymers contain a distribution of n_u and n_c values, which then produce multiple μ values, careful selection of n_u and n_c values is required to accurately represent the sample. The values for n_u and n_c were calculated from the theoretical M_n of the block copolymer (previously listed in [12] as well as in the caption of Figure 7).

Table S8. Dispersity of P(AA-*b*-AM) samples

Sample	PAA2KPAM10K		PAA2KPAM10K	
	A is μ	*A* is *C*	*A* is μ	*A* is *C*
D(*W*(*A*),1,0)	1.12	1.19	1.12	1.25
D(*W*(*A*),2,0)	1.10	1.16	1.08	1.15
D(*W*(*A*),3,0)	1.08	1.36	1.05	1.10
SD (x10^{-9})	4.46[a]	0.090	6.56[a]	0.178

[a] the standard deviation is given in $m^2V^1s^{-1}$

References

(1) Zabisky, R. C. M.; Chan, W. M.; Gloor, P. E.; Hamielec, A. E. *Polymer* **1992**, *33*, 2243-2262.

(2) Hamielec, A. E.; Ouano, A. C. *J. Liq. Chromatogr.* **1978**, *1*, 111-120.

(3) Gaborieau, M.; Gilbert, R. G.; Gray-Weale, A.; Hernandez, J. M.; Castignolles, P. *Macromol. Theory Simul.* **2007**, *16*, 13-28.

(4) Maniego, A. R.; Ang, D.; Guillaneuf, Y.; Lefay, C.; Gigmes, D.; Aldrich-Wright, J. R.; Gaborieau, M.; Castignolles, P. *Anal. Bioanal. Chem.* **2013**, *405*, 9009-9020.

(5) Oliver, J. D.; Gaborieau, M.; Hilder, E. F.; Castignolles, P. *J. Chromatogr. A* **2013**, *1291*, 179-186.

(6) Oliver, J. D.; Sutton, A. T.; Karu, N.; Phillips, M.; Markham, J.; Peiris, P.; Hilder, E. F.; Castignolles, P. *Biotechnol. Appl. Biochem.* **2015**, *62*, 329-342.

(7) Domard, A. *Carbohydr. Polym.* **2011**, *84*, 696-703.

(8) Mnatsakanyan, M.; Thevarajah, J. J.; Roi, R. S.; Lauto, A.; Gaborieau, M.; Castignolles, P. *Anal. Bioanal. Chem.* **2013**, *405*, 6873-6877.

(9) Vreeland, W. N.; Desruisseaux, C.; Karger, A. E.; Drouin, G.; Slater, G. W.; Barron, A. E. *Anal. Chem.* **2001**, *73*, 1795-1803.

(10) Nedelcu, S.; Slater, G. W. *Electrophoresis* **2005**, *26*, 4003-4015.

(11) Vreeland, W. N.; Desruisseaux, C.; Karger, A. E.; Drouin, G.; Slater, G. W.; Barron, A. E. *Anal. Chem.* **2001**, *73*, 1795-1803.

(12) Sutton, A. T.; Read, E.; Maniego, A. R.; Thevarajah, J. J.; Marty, J. D.; Destarac, M.; Gaborieau, M.; Castignolles, P. *J. Chromatogr. A* **2014**, *1372*, 187-195.

International Journal of Biological Macromolecules 95 (2017) 40–48

Contents lists available at ScienceDirect

International Journal of Biological Macromolecules

journal homepage: www.elsevier.com/locate/ijbiomac

Determination of the distributions of degrees of acetylation of chitosan

Joel Jerushan Thevarajah[a,b], Matthew Paul Van Leeuwen[a,c], Herve Cottet[d], Patrice Castignolles[b,*], Marianne Gaborieau[a,b]

[a] Western Sydney University, Molecular Medicine Research Group (MMRG), Parramatta Campus, Locked Bag 1797, Penrith 2751, Australia
[b] Western Sydney University, Australian Centre for Research on Separation Science (ACROSS), School of Science and Health, Parramatta Campus, Locked Bag 1797, Penrith 2751, Australia
[c] Western Sydney University, School of Medicine, Parramatta Campus, Locked Bag 1797, Penrith 2751, Australia
[d] Institut des Biomolécules Max Mousseron IBMM, UMR 5247, CNRS, Universiét de Montpellier, Ecole Nationale Supérieure de Chimie de Montpellier, Place Eugène Bataillon, CC 1706, 34095 Montpellier Cedex 5, France

ARTICLE INFO

Article history:
Received 13 August 2016
Received in revised form 6 October 2016
Accepted 17 October 2016
Available online 19 October 2016

Keywords:
Chitosan
Distribution of degrees of acetylation
Capillary electrophoresis

ABSTRACT

Chitosan is often characterized by its average degree of acetylation. To increase chitosan's use in various industries, a more thorough characterization is necessary as the acetylation of chitosan affects properties such as dissolution and mechanical properties of chitosan films. Despite the poor solubility of chitosan, free solution capillary electrophoresis (CE) allows a robust separation of chitosan by the degree of acetylation. The distribution of degrees of acetylation of various chitosan samples was characterized through their distributions of electrophoretic mobilities. These distributions can be obtained easily and with high precision. The heterogeneity of the chitosan chains in terms of acetylation was characterized through the dispersity of the electrophoretic mobility distributions obtained. The relationship between the number-average degree of acetylation obtained by solid-state NMR spectroscopy and the weight-average electrophoretic mobilities was established. The distribution of degrees of acetylation was determined using capillary electrophoresis in the critical conditions (CE-CC).

1. Introduction

Chitosan is a polysaccharide derived from the *N*-deacetylation of chitin. Chitin is an abundant polysaccharide and it naturally occurs in the shells of arthropods such as shrimps, crabs and the cell walls of yeasts [1]. The molecular structure of the polysaccharide chitosan includes varying proportions of D-glucosamine and *N*-acetyl-D-glucosamine units (Fig. 1). Chitosan has several desirable properties that allowed it to become a significant area of research: it is biocompatible, biodegradable, antimicrobial and antifungal [2,3]. In characterizing chitosan samples, a properly established structure-property relationship is required to assist in tailoring individual samples for specific uses [4,5]. Therefore, accurately characterizing the supramolecular structure of chitosan is essential to understanding its properties. However, due to an incomplete understanding of chitosan's complex structure, several limitations exist in its characterization.

The degree of acetylation (*DA*) is defined as the fraction of *N*-acetyl-D-glucosamine units. The distributions of *DA*s correspond to the relative amount of chitosan macromolecules having a given *DA* plotted against *DA*. The existence of this distribution means that chitosan chains having different degrees of acetylation are present in a given sample. Although it has been well documented that a distribution of *DA*s exists (not all chitosan chains have the same *DA*), this is often overlooked [6,7]. Due to its natural origin and the variation in processing conditions, chitosan can have broad distributions of *DA*s. The existence and importance of the distributions of the *DA*s has been revealed through a coupling of size-exclusion chromatography (SEC) separation with ^{1}H NMR spectroscopy detection; however, the distributions still have not been determined [6]. SEC [8], gradient SEC [9] and gradient liquid adsorption chromatography [10] have been used to determine chemical composition against molar mass (named "chemical composition distribution"), as well as distributions of composition in some cases [10,11], for various copolymers, but not for chitosan. In addition, the

* Corresponding author.
E-mail addresses: joel.thevarajah@westernsydney.edu.au (J.J. Thevarajah), m.vanleeuwen@westernsydney.edu.au (M.P. Van Leeuwen), herve.cottet@umontpellier.fr (H. Cottet), p.castignolles@westernsydney.edu.au (P. Castignolles), m.gaborieau@westernsydney.edu.au (M. Gaborieau).

http://dx.doi.org/10.1016/j.ijbiomac.2016.10.056
0141-8130/

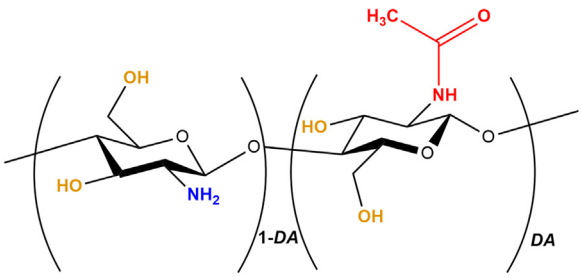

Fig. 1. Chemical structure of chitosan (of degree of acetylation *DA*) and of chitin (for *DA* = 1).

distribution of compositions (or distribution of *DA*s for chitosan) have never been determined. The presence of a distribution of *DA*s can be attributed to the production of chitosan from chitin. Chitin exists in 3 forms, α, β and γ [12]. The α and β forms vary in reactivity due to their structure. The α form is strongly stabilized by intra- and inter-sheet hydrogen bonds conversely to the β form which does not exhibit hydrogen bonding between successive chains. This results in β chitin being more soluble [13] as well as reactive [14]; however, the α form is more industrially available due to its natural abundance. Thus, heterogeneity is influenced by the structure of the chitin used in the production of chitosan.

The treatment of chitin to produce chitosan can also be a homogeneous or a heterogeneous process. The heterogeneous method was shown to be more effective in the deacetylation and is therefore more researched and used. A study in the heterogeneous deacetylation of both α and β chitin showed that in the deacetylation process two domains of deacetylation existed. There was also differences between α and β chitin which could be attributed to the structure of the α form preventing the accessibility of certain sites [15]. It was also identified that homogeneous deacetylation would increase the chance of a random distribution whereas heterogeneous deacetylation could cause blocks of acetylated/deacetylated units [16]. Block deacetylation is then attributed to the starting materials crystallinity in which the more amorphous region had the reactive acetylated sites more readily available and allowed a random distribution of acetylation [15].

Methods used to characterize chitosan by its average degree of acetylation/deacetylation previously include FTIR [17], Raman [18] and NMR spectroscopy [7,19–21]. To determine the distribution of *DA*s, we require a method to identify the average degree of acetylation and a separation technique to identify the distribution of *DA*s. The most widely used method to separate polymers, especially polysaccharides, is size-exclusion chromatography (SEC) [22]. SEC separates polymers by their size (hydrodynamic volume) [23]. For chitosan this depends on both the molar mass and the degree of acetylation. Further, SEC analysis of chitosan has been plagued with aggregation [19]. Separation by composition is possible using liquid chromatography in the critical conditions [24] however, this can be extremely tedious and problematic [25] and is quasi-exclusively applied to organic systems, and not aqueous systems as used for chitosan. For this reason we propose to use free solution capillary electrophoresis (CE) for the analysis of chitosan by its degree of acetylation and its distributions [26,27].

CE has been proven to effectively separate the polysaccharide pectin by composition. Several studies reported the separation of pectin by its degree of substitution (*DS*, which may include esterification) [28]. Other research involved the use of capillary electrophoresis to determine the *DS* of caboxymethylcellulose [29]. Further, CE was proven to be a robust, reproducible method in the detection of impurities in the negatively charged biomolecule heparin [30]. The conditions of separation fall above the Manning condensation; however, separation is still possible although with a low selectivity. The separation of heparin is therefore very similar to that of chitosan. The ability to separate polymers by their composition independently from their molar mass is what differentiates CE from the aforementioned methods and makes it particularly appropriate for our study. It has been proven in the study of polylysine in which the electrophoretic mobility did not vary for a degree of polymerization above 4 [31]. This method is described as "in the critical conditions" (not referring to the separation mechanism but to the absence of separation by molar mass) and has been reviewed recently [26]. CE has also previously been used in chitosan analysis including both native [7,32] and modified chitosan [33].

To allow meaningful distributions to be obtained, the raw data, UV absorption against migration time, first needs to be converted into a distribution of electrophoretic mobilities, [34] and finally into chemical composition distributions. Different expressions of the dispersity of this distribution have recently been developed [27]. The dispersities determined from these different expressions are compared in this work in the case of chitosan. Analysis of the distributions of electrophoretic mobilities of cationic copolymers reveals information regarding their heterogeneity of composition. Understanding the heterogeneity of composition allows for property-structure relationships to be established. Expressions for the composition distributions were also established and tested for some block copolymers [27]. In this study, composition distributions for chitosan (under the form of distribution of *DA*s), or any statistical copolymer, are obtained for the first time.

2. Experimental section

2.1. Materials

Chitosan powders were purchased from Sigma-Aldrich, Castle Hill, Australia and from AK Biotech LTD, Jinan, China (Table S1). Samples were prepared at 1 g L^{-1}. Orthophosphoric acid (85%) and boric acid were purchased from BDH AnalR, Merck Pty Ltd. Acetic acid (AcOH, glacial, 99%) and hydrochloric acid (32%) were purchased from Unilab. Poly(diallyldimethyl ammonium chloride) (PDADMAC 20% in H_2O), alginic acid sodium salt, poly(allylamine hydrochloride) (PAlAm), sodium hydroxide pellets, lithium hydroxide, sodium chloride, hexaamminecobalt(III) chloride (≥99.5%), dimethyl sulfoxide (DMSO, ≥99.5%) and adamantane (99%) were purchased from Sigma-Aldrich. Sodium dihydrogen orthophosphate was purchased from Univar. Three ^{13}C singly labeled alanines were purchased from Cambridge Isotope Laboratories. All water used in this study was of Milli-Q quality. Sodium borate buffer (75 mM) was prepared from 0.5 M boric acid in Milli-Q water, titrated to pH 9.20 with 10 M sodium hydroxide, and diluted with Milli-Q water. Sodium phosphate buffer (100 mM) was prepared from 0.5 M sodium dihydrogen phosphate, titrated with phosphoric acid, and diluted with Milli-Q water. Lithium phosphate buffer (100 mM) was prepared from 85% orthophosphoric acid, titrated to pH 2 with 10 M LiOH and diluted with Milli-Q water. Lithium phosphate, sodium borate and sodium phosphate buffers were sonicated for 5 min and filtered with a Millex GP polyethersulfone (PES) syringe filter (0.22 μm) before use.

2.2. Methods

2.2.1. Capillary electrophoresis

Free solution capillary electrophoresis (CE) was carried out using an Agilent 7100 CE (Agilent Technologies, Waldbronn, Germany) instrument equipped with a diode array detector, contactless conductivity detector (TraceDeC, Innovative Sensor Technologies GmbH, Austria) and external circulating bath with MX temperature controller (Polyscience, USA). Polyimide-coated

fused silica high sensitivity (HS) capillaries (50 μm internal diameter, bubble factor 3) were purchased from Agilent (Australia). Fused silica capillaries used for multilayer PDADMAC and alginate coatings with 50 μm internal diameter were purchased from Polymicro (USA). The HS capillary (112.5 cm total length, 104 cm effective length) was initially pretreated by flushing for 10 min with 1 M NaOH, then 5 min each with 0.1 M NaOH, Milli-Q water, and sodium borate, respectively at the start of a series of separations. The NaOH 1 M was prepared less than 24 h before use. In conditions of sodium borate (75 mM, pH 9.3) an oligoacrylate with a known separation [35] and a broad range of electrophoretic mobilities was injected to validate the capillary and the instrument before each session. After the standard separation and before the series of chitosan separations, the sodium borate was removed with a rinse method which included flushes for 5 min with 1 M NaOH, 0.1 M NaOH, and Milli-Q water, respectively, then a 10 min with 50 mM HCl and finally 5 min with either sodium or lithium phosphate. Before each injection the capillary was rinsed with HCl (50 mM) and the background electrolyte (either sodium or lithium phosphate, 100 mM, pH 2) for 5 min each. Separation was obtained by applying 30 kV and 50 mbar pressure at 55 °C.

The fused silica capillary used for multilayer coatings was first treated for 45 min with 1 M NaOH and rinsed for 5 min with Milli-Q water. The coating process adapted from literature [36] included 45 min flushes with 2% w/v PDADMAC in H_2O, then with 1% w/v alginate in H_2O and finally 2% w/v PDADMAC in H_2O. Following the coating process, the capillary was rinsed for 5 min with Milli-Q water and preconditioned before each injection for 10 min with 0.1 M NaOH and for 10 min with sodium phosphate (10 mM, pH 3). The separation was obtained by applying −30 kV at 25 °C. The detection was set at 195 nm with a bandwidth of 10 nm.

2.2.2. Solid-State NMR spectroscopy

Solid-state ^{1}H and ^{13}C NMR spectra were recorded on a Bruker Avance DPX 200 spectrometer operating at Larmor frequencies of 200 MHz and 50 MHz, respectively. A commercial double resonance probe supporting zirconia MAS rotors with a 4 mm outer diameter and a 3 mm inner diameter was used, and samples were spun at 10 kHz at the magic angle. ^{1}H NMR spectra were recorded using a 5.73 μs 90° pulse, a 3 s repetition delay and at least 64 scans. ^{13}C CP-MAS NMR experiments were adapted from published quantitative measurements [19]. They were recorded with a 1 ms contact time and a 4 s repetition delay, and 21,586 to 104,924 scans. For ^{1}H experiments the 90° pulse was optimized using adamantane and power levels for the ^{13}C CP-MAS experiments were optimized using a mixture of three ^{13}C singly labeled alanines. The ^{1}H and ^{13}C chemical shifts scales were externally referenced using adamantane by setting the CH resonance to 1.64 and 38.48 ppm, respectively [37]. The degree of acetylation was measured through Eq. (1) [20]:

$$DA_n^{SSNMR}(\%) = \frac{I_{CH_3}}{(I_1 + I_2 + I_3 + I_4 + I_5 + I_6)/6} \quad (1)$$

where I_{CH3} is the integral of the methyl group of the acetyl group and I_1 to I_6 are the integrals of the signals assigned to the chitosan backbone.

3. Results and discussions

3.1. Chitosan dissolution

Analyzing a fully dissolved sample of chitosan in solution allows a complete characterization; however, obtaining a true solution of chitosan is quite difficult. In a previous study [19] the dissolution of chitosan was analyzed in a range of conditions with CE including the use of deuterated and aqueous solvents. Our new methodology to determine the distribution of electrophoretic mobilities and their dispersity [27] was applied to monitoring chitosan dissolution in aqueous solvents [19]. This allows further characterization of the dissolution. Initial CE separations of chitosan were based on apparent electrophoretic mobility [7]. Pressure-assisted capillary electrophoresis (PACE) was used to analyze chitosan samples to obtain more precise electrophoretic mobility values [19]. This was necessary as deacetylation during the dissolution process is suspected and it could be detected only with sufficient precision in the measurement of electrophoretic mobility. PACE allowed the detection of both an internal standard and an electroosmotic flow marker (a neutral marker). It was noted previously that the weight-average electrophoretic mobility did not significantly vary with time of dissolution apart from the first 5 h in which incomplete dissolution led to high variations in electrophoretic mobility due to aggregation. In this work, the dispersity of the electrophoretic mobility distributions obtained were calculated and on a 15 h time scale exhibited similar behaviors for the different samples with the exception of LowMW1. MedMW samples were seen to have a similar dispersity over the period of dissolution with a slight increase in dispersity after the first 5 h suggesting that there was not a significant bias in dissolution (Fig. 2). The LowMW1 sample exhibited a very different dispersity with a large increase in dispersity after the initial 5 h. This suggests a bias in the dissolution with certain polymer chains with similar compositions dissolving first followed by the rest of the polymer chains. Therefore it is important to study the distributions of composition for chitosan as the *DA* may play a more important role than molar mass in the dissolution [27].

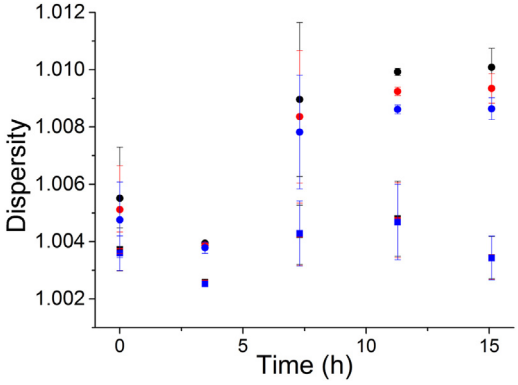

Fig. 2. Dispersity $D(W(\mu),1,0)$ (black), $D(W(\mu),2,0)$ (red) and $D(W(\mu),3,0)$ (blue) of chitosan MedMW1 (squares) and LowMW1 (circles) during kinetic measurement of dissolution in 50 mM HCl in H_2O using CE-CC with the carousel kept at 60 °C. See Supporting information Eqs. S1–S3 for dispersity calculations [27]. (For interpretation of the references to colour in this figure legend, the reader is referred to the web version of this article.)

The kinetics of dissolution of MedMW in 50 mM HCl in H_2O was also compared to that in 50 mM DCl in D_2O (Fig. S1). No significant variation of dispersities of the $W(\mu)$ was observed. Following the dissolution study [19] 50 mM HCl at 60 °C for 2 h was chosen in this work as the dissolution conditions for the range of commercially available chitosan samples with different viscosities, degrees of acetylation (supplied and measured), molar masses and suppliers. This was to ensure minimal deacetylation during the dissolution.

3.2. Separation

3.2.1. Adsorption onto the capillary surface

It is important to optimize the conditions of separation to prevent unwanted broadening especially in the analysis of distributions. A factor that may negatively affect CE-CC separations is the adsorption of the polymer onto the surface of the capillary. To prevent adsorption a number of steps were taken including an increased cassette temperature and a lower pH buffer [19].

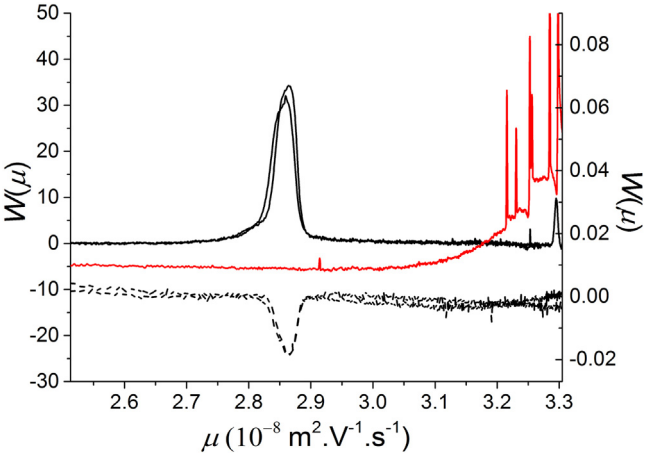

Fig. 3. Electropherogram of PAlAm (black lines) and chitosan (red line) separated in a PDADMAC/alginate/PDADMAC coated capillary (50 cm total length) in LiPB10 at −30 kV with UV (solid line – left y axis) and contactless capacitively-coupled conductivity (dashed line – right y axis) detections. μ is the electrophoretic mobility and $W(\mu)$ is the weight fraction of polyelectrolyte chains with a given electrophoretic mobility calculated as the absorbance ($S(t)$) multiplied by the migration time. (For interpretation of the references to colour in this figure legend, the reader is referred to the web version of this article.)

Multilayer coatings have been previously used to prevent the adsorption of proteins and plasma [36]. A cationic/anionic multilayer coating of PDADMAC and alginate was successfully tested with a model polyamine sample of poly(allylamine hydrochloride) (PAlAm). PAlAm was separated successfully (Fig. 3) in lithium phosphate 10 mM at pH 3 (LiPB10). A lower concentration of lithium phosphate buffer was used to prevent interaction with the multilayer coating. Detection of PAlAm was with UV at 195 nm as well as with a conductivity detector. The separation was also tested with sodium phosphate 10 mM at pH 3 (NaPB10); however, low sensitivity was experienced (Fig. S2). In the separation of chitosan with this coating, no chitosan peak was detected, assumingly because chitosan strongly adsorbs onto the coating, the signals detected at very high electrophoretic mobilities may correspond to either coating displaced by the chitosan or chitosan aggregates. It is assumed that chitosan has a higher affinity at pH 2 with alginate than PAlAm or PDADMAC. This prevented further use of the coating for chitosan characterization.

Although the multilayer coating was unable to be used to analyze chitosan, it has successfully been used in the separation of another cationic polymer. The methodology developed below could thus apply to a number of cationic polymers, even if they adsorbed onto standard fused silica capillaries.

3.2.2. Selectivity

To enhance the selectivity of the separation of chitosan in CE-CC compared to previous results [7,19] various parameters were tested. This included the use of the surfactant Brij™ 35 as a complexation reagent to adjust the selectivity [38]. However, chitosan did not dissolve in the presence of Brij™ 35 and remained as particulates. Brij™ 35 also caused the precipitation of chitosan in solution, which prevented its analysis using CE (the use of an anionic surfactant would lead to water-insoluble complexes [39] and this was not attempted). Different counter-ions for the background electrolyte were also compared.

Chitosan was separated in sodium phosphate and lithium phosphate and the resulting electropherograms were analyzed (Section 3.3). It was noted that chitosan was separated with a greater selectivity in lithium phosphate compared to sodium phosphate. The range of electrophoretic mobilities and dispersity values were determined as 3.0–4.8 (10^{-8} m^2 V^{-1} s^{-1}) and 1.000–1.006 in sodium phosphate, as well as 2.7–4.8 (10^{-8} m^2 V^{-1} s^{-1}) and 1.000 to 1.008 in lithium phosphate.

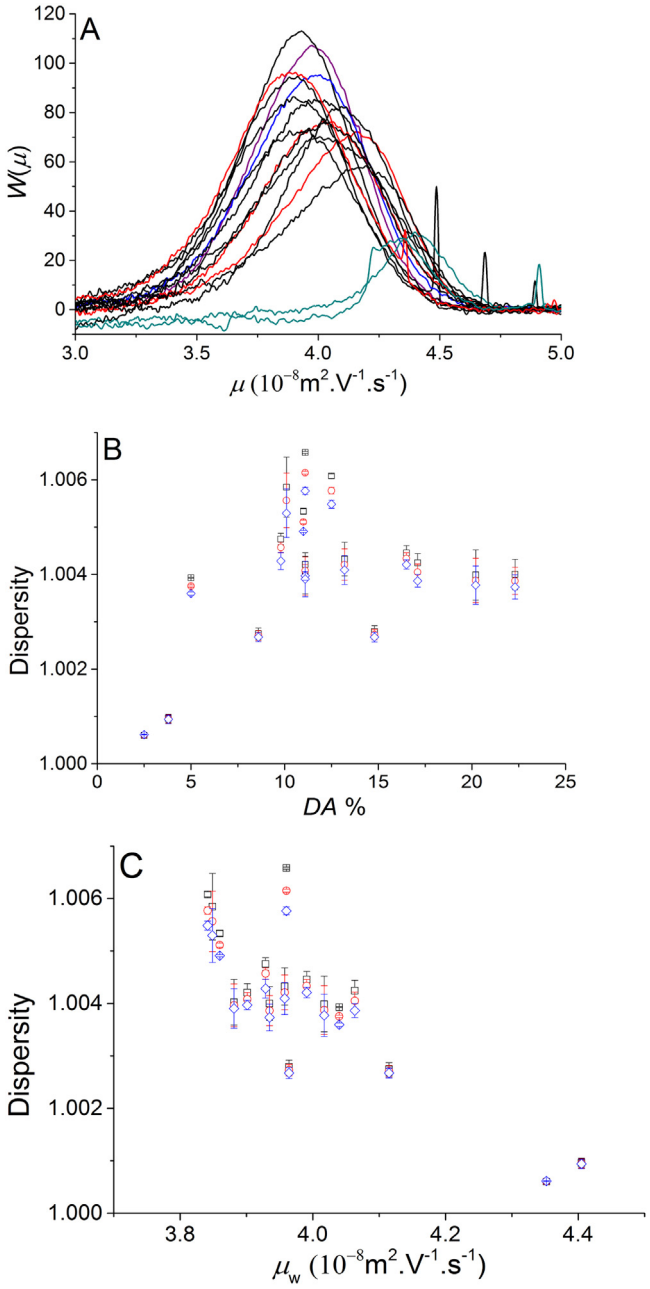

Fig. 4. A. Distribution of electrophoretic mobilities, $W(\mu)$, of chitosan separated with PACE using NaPB100 for samples with an average *DA* (measured by SSNMR) below 5% (green lines), between 5% and 10% (blue line), between 10% and 15% (red lines), between 15% and 20% (black lines) and above 20% (purple line). Dispersity values (see Supporting information for expressions) for chitosan samples as $D(W(\mu),1,0)$ (black squares), $D(W(\mu),2,0)$ (red circles) and $D(W(\mu),3,0)$ (blue diamonds) against their (B) number-average degree of acetylation or (C) weight-average electrophoretic mobility (μ_w). See Supporting information Eqs. S1–S3 for dispersity calculations [27]. (For interpretation of the references to colour in this figure legend, the reader is referred to the web version of this article.)

3.3. Electrophoretic mobility distributions

3.3.1. Chitosan in sodium phosphate

Appropriate treatment of the raw electropherograms [34] allowed meaningful mobility distributions to be obtained (Fig. 4A). The different chitosan samples were each seen to have a broad

range of distributions of electrophoretic mobilities. The dispersity of the mobility distributions was calculated based on a ratio of moments [27] and plotted against the average *DA* measured by solid-state NMR spectroscopy (Fig. 4B). The dispersity was also plotted against the weight-average mobility (Fig. 4C). The general trend seen is that samples with a low average *DA* have a lower dispersity. This is expected as the heterogeneity of the composition at low *DA* is likely lower since negative *DA* values are physically impossible. The dispersity is seen to first increase and then decrease as the average *DA* increases. This trend is dissimilar to that which is seen for the dispersity against the weight-average electrophoretic mobility. As the weight-average electrophoretic mobility of the chitosan samples increases, their dispersity decreases.

3.3.2. Chitosan in lithium phosphate

In an effort to improve the selectivity of the chitosan separation, migration was also undertaken using LiPB100 as the background electrolyte (Fig. 5A). Lithium has a mobility (3.9×10^{-8} $m^2 V^{-1} s^{-1}$) more similar to that of chitosan than sodium (5.2×10^{-8} $m^2 V^{-1} s^{-1}$) [40]. This prevents the occurrence of electrodispersion which may cause unwanted focusing and reduce selectivity further.

The distributions and dispersity values obtained of chitosan in LiPB100 showed similar trends to that in NaPB100. However, a greater repeatability was noted in the dispersity values of each of the samples.

Determining the dispersity of the electrophoretic mobility distributions is useful especially in the case of complex polyelectrolytes for which obtaining a correlation between the parameter of interest and mobility is challenging. Comparison of the dispersity values obtained from electrophoretic mobility distributions allows a direct qualitative comparison of the heterogeneity of the samples with respect to each other.

3.4. Composition distributions

3.4.1. Correlation between mobility and composition

To obtain composition distributions from electrophoretic mobility distributions a correlation is required between mobility and composition. Initial calibration curves which included all the chitosan samples used the average *DA* measured with solid-state NMR spectroscopy plotted against the weight-average electrophoretic mobility (Fig. S3). The *DA* values were measured using solid-state NMR spectroscopy as it was proven that analyzing the *DA* by solution-state NMR spectroscopy was inaccurate due to poor dissolution or to deacetylation in the most commonly used solvents [19]. The initial calibration curves seemed to show 2 separate populations with a very low correlation. However, calibration curves, especially in the case of molar mass distributions, are generally made with narrow standards and the chitosan samples analyzed do not fit this criterion due to their heterogeneities of composition. Therefore to obtain a calibration curve samples were removed based on their dispersity value (below 1.0036 for LiPB100 ($r^2 > 0.75$) and 1.0040 for NaPB100 ($r^2 > 0.55$) until a correlation was obtained with a reasonable number of samples. This was undertaken for samples separated both in NaPB100 and LiPB100. Using the least disperse samples for the calibration curve various fits including linear, polynomial, inverse and log functions were tested for the chitosan samples separated in NaPB100 (Fig. S4-7). All of the trends suffered from low correlation and the linear, inverse and log functions resulted in distributions containing populations with negative *DA* values. As the *DA* cannot physically fall below 0, the fit should rather be performed with a mathematical function which is defined only between 0 and 1 (as is the *DA*). The Bradley

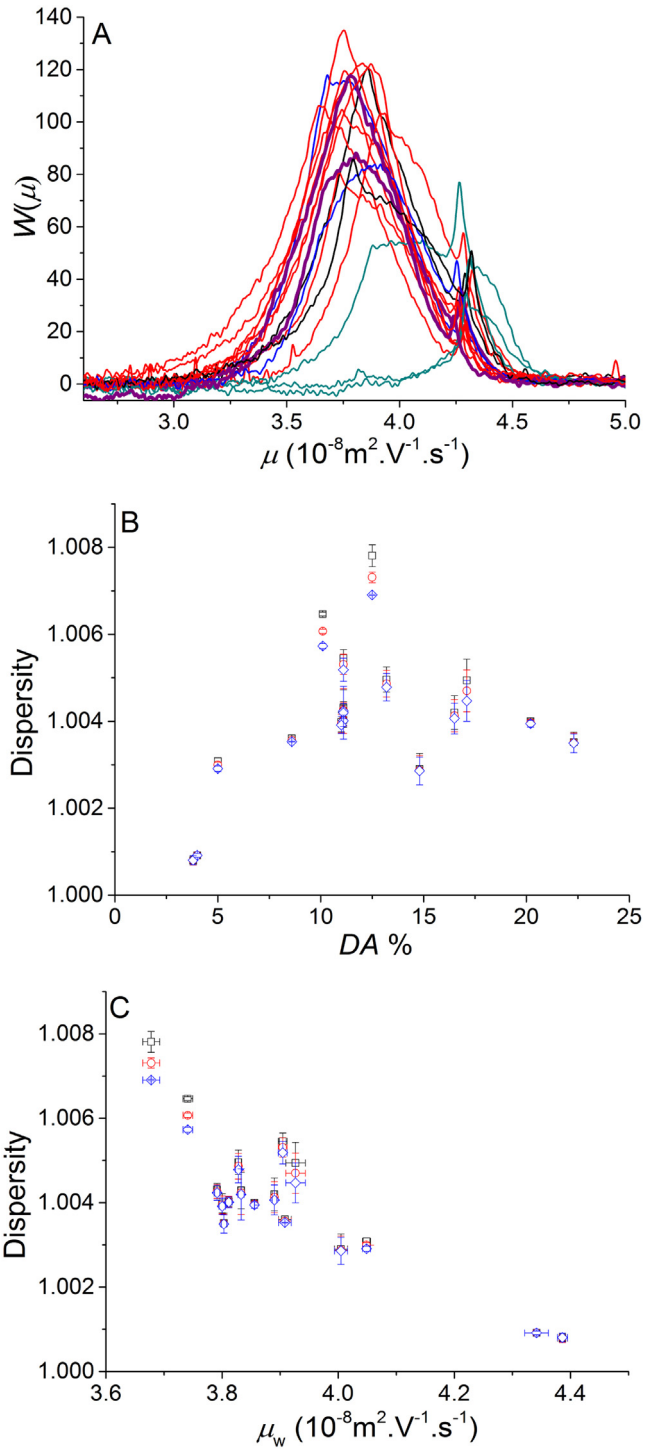

Fig. 5. A. Distributions of electrophoretic mobilities, $W(\mu)$, of chitosan separated with PACE using LiPB100 with samples with an average *DA* below 5% (green lines), between 5% and 10% (blue line), between 10% and 15% (red lines), between 15% and 20% (black lines) and above 20% (purple line). Dispersity values for chitosan samples as $D(W(\mu),1,0)$ (black squares), $D(W(\mu),2,0)$ (red circles) and $D(W(\mu),3,0)$ (blue diamonds) against their (B) number-average degree of acetylation or (C) weight-average electrophoretic mobility. See Supporting information Eqs S1–S3 for dispersity calculations [27]. (For interpretation of the references to colour in this figure legend, the reader is referred to the web version of this article.)

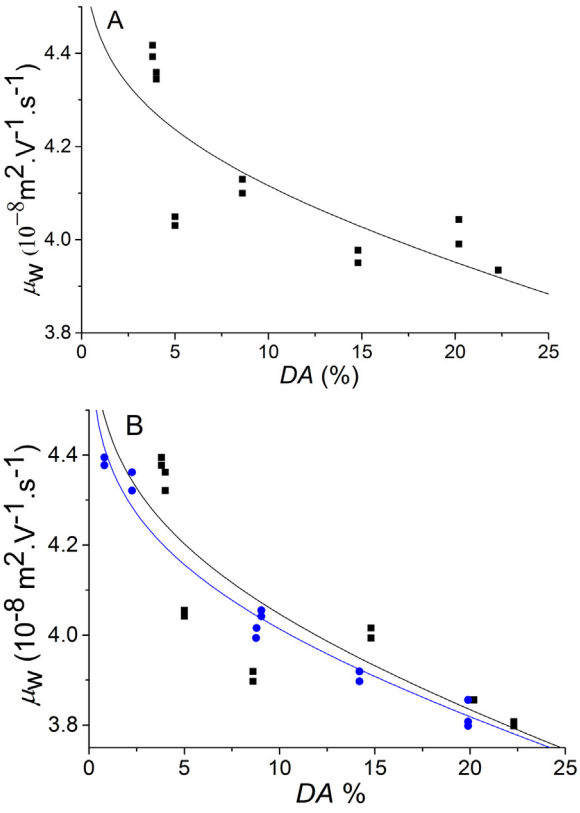

Fig. 6. Calibration curve of the weight-average electrophoretic mobility as a function of *DA* for chitosan with a Bradley function fit in A. NaPB100 ($a = 4.58 \times 10^{-9}$, $b = 3447.2$, $r^2 = 0.62$) B. LiPB100 first (black line) ($a = 5.44 \times 10^{-9}$, $b = 693.77$, $r^2 = 0.70$) and second iteration (blue line) ($a = 5.93 \times 10^{-9}$, $b = 399.21$, $r^2 = 0.97$). The electrophoretic mobilities were measured in duplicates; both duplicates are shown on the graph and included in the fit (see Section 3.4.2). (For interpretation of the references to colour in this figure legend, the reader is referred to the web version of this article.)

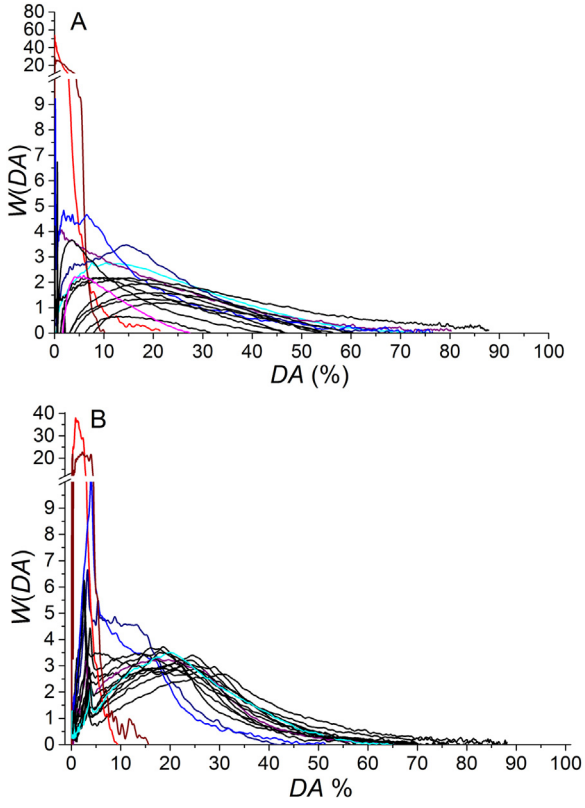

Fig. 7. Composition distributions of chitosan samples separated in A. NaPB100 and B. LiPB100.

function (double logarithmic reciprocal function) was thus tested and deemed the most appropriate fit (Eq. (2) and Fig. 6).

$$\mu = a \times \ln(-b \times \ln(DA)) \quad (2)$$

Low correlations could be explained by a number of reasons. First the use of the Bradley fit is empirical (like that of the polynomial fit used for molar mass determination by SEC) but not based on a theory predicting the relation between μ and *DA*. Second, heterogeneity of the composition of chitosan is not just due to differences in average *DA* but may also be in the form of blocks of deacetylated groups. This would influence the separation as for the chitosan sample to be in the critical conditions for capillary electrophoresis the charges should be evenly distributed along the polymer chain. If there are blocks of charged species the chitosan chains may behave as a block copolymer [41] rather than a statistical copolymer. In this case the separation (electrophoretic mobility) is influenced by both the mobility of the charged species and the hydrodynamic friction of the uncharged species. Without an appropriate correction factor the occurrence of this bias cannot be accounted for. One reason for block deacetylation is the semi-crystalline structure of the precursor of chitosan, chitin [42]. To check if the occurrence of 2 populations was due to block deacetylation XRD measurements were undertaken. Crystallinity from the precursor chitin would likely play a role in the block deacetylation. However no significant difference was noted between the samples which exhibited diffractograms typical of amorphous chitosan samples [43] (Fig. S8). This suggests that no long range order is present in the chitosan samples; however, the occurrence of short chain blocks is still possible and would influence the mobility. Further reasons of a low correlation may include the dissolution and the treatment of chitin to chitosan. The dissolution of the sample plays an important role in the meaningful characterization of the sample as a whole and bias in dissolution would prevent an accurate correlation between the accurate *DA* measured in solid-state NMR spectroscopy and the distributions of mobility. Although the problem of dissolution was not overcome and requires further investigation, composition distributions were obtained with the best current dissolution.

3.4.2. Calculation of composition distributions

Using the calibration curve the electrophoretic mobility distributions were transformed to composition distributions using the following equations:

$$DA = exp\left(-\frac{exp\left(\frac{\mu}{a}\right)}{b}\right) \quad (3)$$

$$W(DA) = W(\mu) \times \frac{-a}{DA \times \ln(DA)} \quad (4)$$

The composition distributions of the chitosan samples used in calibration curves were obtained (Fig. 7). This is the first time composition distributions of chitosan are presented in the literature. The composition distributions reveal information on the amount of chains with a specific composition in the sample. The dispersities of the composition distributions were observed to be larger than those seen for electrophoretic mobility distributions (Fig. 8). There is no expectation of the dispersities values for these two different types of distributions to be similar. However, larger variations in dispersity values of the composition distributions were seen between replicates. The dispersity values of the composition distributions are less repeatable than the ones of the electrophoretic mobility distributions; however, the variations were still small (e.g.

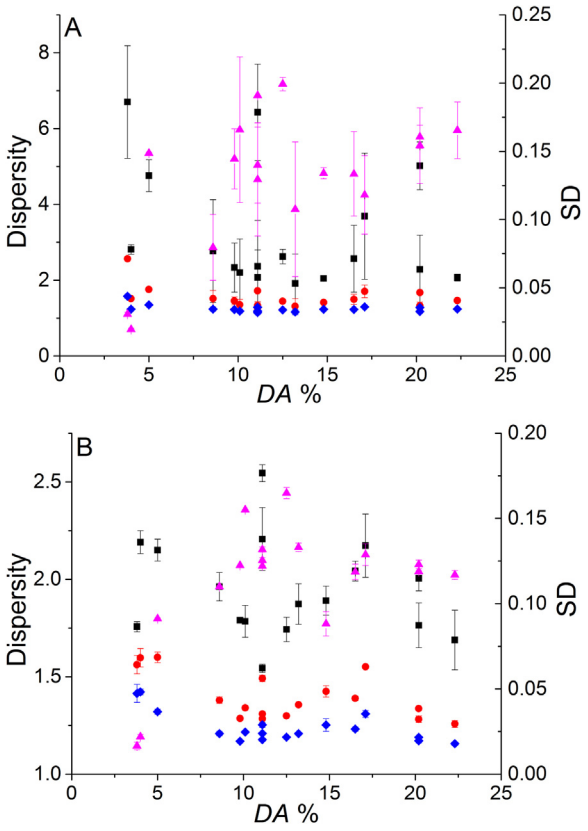

Fig. 8. Dispersity of composition distributions as $D(W(DA),1,0)$ (black squares), $D(W(DA),2,0)$ (red circles), $D(W(DA),3,0)$ (blue diamonds) and standard deviation (pink triangles) for chitosan samples separated in A) NaPB100 and B) LiPB100. See Supporting information Eqs. S1–S8 for dispersity calculations [27]. (For interpretation of the references to colour in this figure legend, the reader is referred to the web version of this article.)

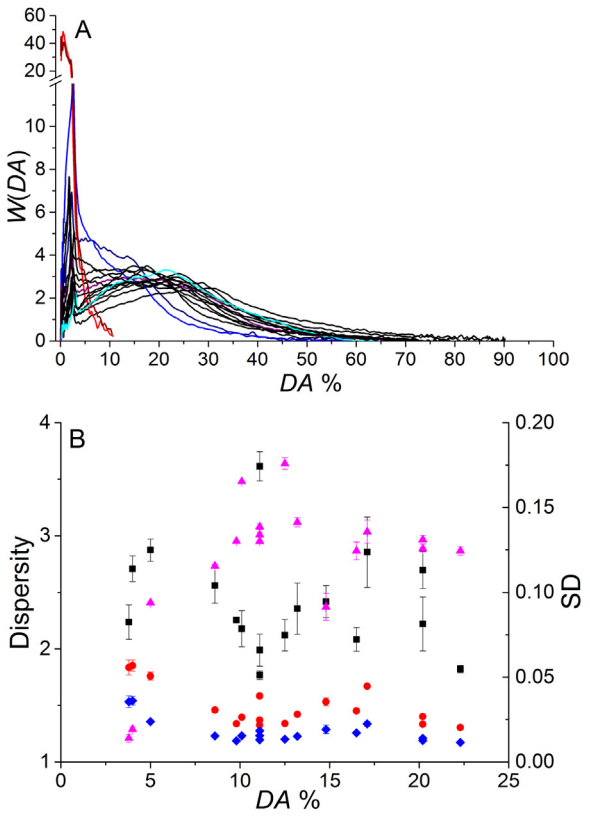

Fig. 9. A. Composition distributions and B. Dispersity of composition distributions as $D(W(DA),1,0)$ (black squares), $D(W(DA),2,0)$ (red circles), $D(W(DA),3,0)$ (blue diamonds) and standard deviation (pink triangles) for chitosan samples separated in LiPB100 and treated with the 2nd iteration. See Supporting information Eqs. S1–S8 for dispersity calculations [27]. (For interpretation of the references to colour in this figure legend, the reader is referred to the web version of this article.)

in comparison to the 2000% variation for M_n and M_w determined in a round-robin test for poly(acrylic acid) using SEC [44]). The dispersity values were calculated for composition distributions for the first time. The dispersity values for $D(W(\mu),1,0)$ were determined to be larger than those for $D(W(\mu),2,0)$ and $D(W(\mu),3,0)$. A different trend of the dispersity values was seen compared to those calculated from the electrophoretic mobility distributions. This is likely due to the lower selectivity in terms of μ at low *DA* compared to intermediate *DA* (the calibration curve has a higher slope at low *DA* than intermediate *DA*). The conversion from $W(\mu)$ to $W(DA)$ thus corrects an artefact in a similar fashion as the conversion from SEC chromatograms to molar mass distributions corrects for an artefact when the SEC calibration is not linear in the region of interest [45]. Standard deviation values of $W(DA)$ showed a trend similar to that obtained with the dispersities of $W(\mu)$. The dispersity of $W(DA)$ and its standard deviation thus give different information on the composition and its heterogeneity. They may relate to different functional properties. The standard deviation values are corresponding to the visual comparison of the $W(DA)$: the distributions at the lowest *DA*s appear sharper. It is to note that the translation of the $W(DA)$ at higher *DA* (+0.05) led to a decrease of the dispersity values from around 2 (Fig. 7) to 1.0001. The dispersity values are thus giving an interesting perspective on the $W(DA)$ that visual observation of the distributions in this work could not provide. Properties (such as some mechanical properties) affected by both the magnitude of *DA* and the width of the distribution of *DA*s might relate to $D(W(DA),1,0)$, $D(W(DA),2,0)$ or $D(W(DA),3,0)$. Properties affected primarily by the width of the distribution of *DA*s, rather than the magnitude of *DA* (such as adhesive vs cohesive failure in adhesives) might relate to standard deviation.

Using the composition distributions obtained (Fig. 7B) a second iteration of the *DA* versus electrophoretic mobility calibration curve was determined for the chitosan samples separated in LiPB100. There is no reason for the average *DA* determined by NMR spectroscopy to correspond to μ_w. To obtain the second iteration the average *DA* values determined from the solid-state NMR measurements were thus replaced with those determined at the peak apex of the relevant composition distributions. This was re-plotted against the weight-average electrophoretic mobilities obtained by CE (Fig. 6B). The correlation improved compared to the initial calibration curve. This was not the case for the chitosan samples separated in NaPB100 (Fig. S9). Therefore, composition distributions were calculated for the chitosan samples using the 2nd iteration of the calibration curve only in LiPB100. Further the dispersity values of the composition distributions were plotted against the *DA* obtained by solid-state NMR spectroscopy (Fig. 9B). The composition distributions exhibited minimal changes, although slightly more tailing may be noticed. The trend of the dispersity values is similar to that before the iteration. Once again the standard deviation supports the visual observation for the composition distributions; however, the corresponding values are higher in the re-treated composition distributions. The dispersity values are constant throughout the whole range of samples. Therefore a quantitative analysis of the composition distributions is possible using the standard deviation which discriminates the different chitosan in this work and potentially the dispersities for other samples.

4. Conclusions

In this study distributions of electrophoretic mobilities and of compositions were obtained for a range of chitosan samples and their dispersity values were determined. Multilayer coatings were tested to prevent adsorption and a cationic polymer, poly(allylamine hydrochloride) was separated successfully. The selectivity of the chitosan separation was improved with the use of lithium as the counter-ion. The distribution of electrophoretic mobilities, $W(\mu)$, and its dispersity can be used for a quick and precise characterization of the heterogeneity of *DA* of chitosan (or the heterogeneity of composition of any statistical copolymer where at least one monomer unit is charged). The application of this methodology to the monitoring of the dissolution of chitosan confirmed that the *DA* can influence the dissolution of chitosan. Strategies to obtain the distribution of *DA*s, $W(DA)$, have been proposed and tested as well. The determination of $W(DA)$ requires establishing a correlation between the *DA* of several chitosan samples and their electrophoretic mobility. The usual mathematical functions (linear, polynomial) used to produce calibration curves (in SEC) did not provide any correlation. Bradley functions did provide some correlation between the weight-average electrophoretic mobility and the *DA* (composition) of chitosan samples which allowed composition distributions to be obtained for the first time. Standards with low dispersity of the distribution of *DA*s do not exist. The quality of the calibration can thus be rather improved by using an iteration process (in which the peak apex from the composition distributions is used as an improved *DA* value). For the specific example of chitosan, the standard deviation and dispersity were valuable in numerically representing the heterogeneity of the composition distributions and give different perspectives. This methodology can be applied to any charged copolymer such as heparin, carboxymethylcelluloses and pectins and would truly be advantageous. Separations by composition with a high selectivity would allow a strong correlation between mobility and composition. Further work may also involve improving the selectivity specifically in the separation of chitosan. This would result in a greater precision and potentially greater accuracy in the resulting composition distributions. In conclusion, the calculation of composition distributions provides an improved characterization which influences the possible modification or functionalization of copolymers, quality control of the synthesis and a step closer towards understanding structure-property relationships of complex polymers, which has already been identified as crucial. For example the *DA* has been shown to influence significant properties such as bioadhesion [5], dissolution [19] and biodegradability [46,47]. The functional characterization of chitosan and its derivatives is nowadays one of the most productive research areas [3].

Acknowledgments

J.J.T. thanks Leena Thevarajah for assistance with data treatment, Aidan Grosas for discussions, Alison Maniego and Melissa Meinel for assistance in the lab. J.J.T. also thanks the Australian Government for an Endeavour Research fellowship to travel to the University of Montpellier, Montpellier, France. The authors thank Timothy Murphy and Richard Wuhrer from the Advanced Materials Characterisation Facility (AMCF) at Western Sydney University for discussions and instrumentation training/assistance.

Appendix A. Supplementary data

Supplementary data associated with this article can be found, in the online version, at http://dx.doi.org/10.1016/j.ijbiomac.2016.10.056.

References

[1] M. Rinaudo, Chitin and chitosan: properties and applications, Prog. Polym. Sci. 31 (2006) 603–632.
[2] A. Domard, A perspective on 30 years research on chitin and chitosan, Carbohydr. Polym. 84 (2011) 696–703.
[3] S.K. Shukla, A.K. Mishra, O.A. Arotiba, B.B. Mamba, Chitosan-based nanomaterials: a state-of-the-art review, Int. J. Biol. Macromol. 59 (2013) 46–58.
[4] M.J. Barton, J.W. Morley, D.A. Mahns, D. Mawad, R. Wuhrer, D. Fania, S.J. Frost, C. Loebbe, A. Lauto, Tissue repair strength using chitosan adhesives with different physical-chemical characteristics, J. Biophoton. 7 (2014) 948–955.
[5] B. Menchicchi, J.P. Fuenzalida, K.B. Bobbili, A. Hensel, M.J. Swamy, F.M. Goycoolea, Structure of chitosan determines its interactions with mucin, Biomacromolecules 15 (2014) 3550–3558.
[6] S. Nguyen, S. Hisiger, M. Jolicoeur, F.M. Winnik, M.D. Buschmann, Fractionation and characterization of chitosan by analytical SEC and H-1 NMR after semi-preparative SEC, Carbohydr. Polym. 75 (2009) 636–645.
[7] M. Mnatsakanyan, J.J. Thevarajah, R.S. Roi, A. Lauto, M. Gaborieau, P. Castignolles, Separation of chitosan by degree of acetylation using simple free solution capillary electrophoresis, Anal. Bioanal. Chem. 405 (2013) 6873–6877.
[8] I.A.H. Ahmad, A.M. Striegel, Determining the absolute chemical-heterogeneity-corrected molar mass averages, distribution, and solution conformation of random copolymers, Anal. Bioanal. Chem. 396 (2010) 1589–1598.
[9] H. Maier, F. Malz, W. Radke, Characterization of the chemical composition distribution of poly(*n*-butyl acrylate-stat-acrylic acid)s, Macromol. Chem. Phys. 216 (2015) 228–234.
[10] M. Shakun, T. Heinze, W. Radke, Determination of the DS distribution of non-degraded sodium carboxymethyl cellulose by gradient chromatography, Carbohydr. Polym. 98 (2013) 943–950.
[11] M. Shakun, T. Heinze, W. Radke, Characterization of sodium carboxymethyl cellulose by comprehensive two-dimensional liquid chromatography, Carbohydr. Polym. 130 (2015) 77–86.
[12] M.K. Jang, B.G. Kong, Y.I. Jeong, C.H. Lee, J.W. Nah, Physicochemical characterization of alpha-chitin beta-chitin, and gamma-chitin separated from natural resources, J. Polym. Sci. Pol. Chem. 42 (2004) 3423–3432.
[13] T. Sannan, K. Kurita, Y. Iwakura, Studies on chitin, 2. Effect of deactylation on solubility, Makromol. Chem. Macromol. Chem. Phys. 177 (1976) 3589–3600.
[14] K. Kurita, S. Ishii, K. Tomita, S.I. Nishimura, K. Shimoda, Reactivity characteristics of squid beta-chitin as compared with those of shrimp chitin: high potentials of squid chitin as a starting material for facile chemical modifications, J. Polym. Sci. A: Polym. Chem. 32 (1994) 1027–1032.
[15] G. Lamarque, C. Viton, A. Domard, Comparative study of the first heterogeneous deacetylation of alpha- and beta-chitins in a multistep process, Biomacromolecules 5 (2004) 992–1001.
[16] K. Kurita, T. Sannan, Y. Iwakura, Studies on Chitin, 4. Evidence for formation of block and random copolymers of N-Acetyl-D-glucosamine and D-glucosamine by Hetero- and Homogenous Hydrolyses, Macromol. Chem. Phys. 178 (1977) 3197–3202.
[17] M.R. Kasaai, Various methods for determination of the degree of *N*-acetylation of chitin and chitosan: a review, J. Agric. Food Chem. 57 (2009) 1667–1676.
[18] A. Zajac, J. Hanuza, M. Wandas, L. Dyminska, Determination of *N*-acetylation degree in chitosan using Raman spectroscopy, Spectrochim. Acta A: Mol. Biomol. Spectrosc. 134 (2015) 114–120.
[19] J.J. Thevarajah, J.C. Bulanadi, M. Wagner, M. Gaborieau, P. Castignolles, Towards a less biased dissolution of chitosan, Anal. Chim. Acta 935 (2016) 258–268.
[20] M.H. Ottoy, K.M. Varum, O. Smidsrod, Compositional heterogeneity of heterogeneously deacetylated chitosans, Carbohydr. Polym. 29 (1996) 17–24.
[21] L. Heux, J. Brugnerotto, J. Desbrieres, M.F. Versali, M. Rinaudo, Solid state NMR for determination of degree of acetylation of chitin and chitosan, Biomacromolecules 1 (2000) 746–751.
[22] M. Gaborieau, P. Castignolles, Size-exclusion chromatography (SEC) of branched polymers and polysaccharides, Anal. Bioanal. Chem. 399 (2011) 1413–1423.
[23] Z. Grubisic, P. Rempp, H. Benoit, A universal calibration for gel permeation chromatography, J. Polym. Sci. B: Polym. Phys. 34 (1996) 1707–1713, Reprinted from Polymer Letters, vol 5, pg 753–759, 1967.
[24] Y. Brun, P. Foster, Characterization of synthetic copolymers by interaction polymer chromatography: separation by microstructure, J. Sep. Sci. 33 (2010) 3501–3510.
[25] A. Favier, C. Petit, E. Beaudoin, D. Bertin, Liquid chromatography at the critical adsorption point (LC-CAP) of high molecular weight polystyrene: pushing back the limits of reduced sample recovery, E Polym. 9 (2009) 15.
[26] J.J. Thevarajah, M. Gaborieau, P. Castignolles, Separation and characterization of synthetic polyelectrolytes and polysaccharides with capillary electrophoresis, Adv. Chem. 2014 (2014), Article ID 798403.
[27] J.J. Thevarajah, A.T. Sutton, A.R. Maniego, E.G. Whitty, S. Harrisson, H. Cottet, P. Castignolles, M. Gaborieau, Quantifying the heterogeneity of chemical structures in complex charged polymers through the dispersity of their distributions of electrophoretic mobilities or of compositions, Anal. Chem. 88 (2016) 1674–1681.
[28] S.E. Guillotin, E.J. Bakx, P. Boulenguer, H.A. Schols, A.G.J. Voragen, Determination of the degree of substitution, degree of amidation and degree

of blockiness of commercial pectins by using capillary electrophoresis, Food Hydrocoll. 21 (2007) 444–451.
[29] K.A. Oudhoff, F.A. Ab Buijtenhuijs, P.H. Wijnen, P.J. Schoenmakers, W.T. Kok, Determination of the degree of substitution and its distribution of carboxymethylcelluloses by capillary zone electrophoresis, Carbohydr. Res. 339 (2004) 1917–1924.
[30] T. Wielgos, K. Havel, N. Ivanova, R. Weinberger, Determination of impurities in heparin by capillary electrophoresis using high molarity phosphate buffers, J. Pharm. Biomed. Anal. 49 (2009) 319–326.
[31] H.F. Wu, S.A. Allison, C. Perrin, H. Cottet, Modeling the electrophoresis of highly charged peptides: application to oligolysines, J. Sep. Sci. 35 (2012) 556–562.
[32] C.H. Wu, C.Y. Kao, S.Y. Tseng, K.C. Chen, S.F. Chen, Determination of the degree of deacetylation of chitosan by capillary zone electrophoresis, Carbohydr. Polym. 111 (2014) 236–244.
[33] C. Lefay, Y. Guillaneuf, G. Moreira, J.J. Thevarajah, P. Castignolles, F. Ziarelli, E. Bloch, M. Major, L. Charles, M. Gaborieau, D. Bertin, D. Gigmes, Heterogeneous modification of chitosan via nitroxide-mediated polymerization, Polym. Chem. 4 (2013) 322–328.
[34] J. Chamieh, M. Martin, H. Cottet, Quantitative analysis in capillary electrophoresis: transformation of raw electropherograms into continuous distributions, Anal. Chem. 87 (2015) 1050–1057.
[35] M. Gaborieau, T. Causon, Y. Guillaneuf, E.F. Hilder, P. Castignolles, Molecular weight and tacticty of oligoacrylates by capillary electrophoresis—mass spectrometry, Aus. J. Chem. 63 (2010) 1219–1226.
[36] H. Katayama, Y. Ishihama, N. Asakawa, Stable cationic capillary coating with successive multiple ionic polymer layers for capillary electrophoresis, Anal. Chem. 70 (1998) 5272–5277.
[37] C.R. Morcombe, K.W. Zilm, Chemical shift referencing in MAS solid state NMR, J. Magn. Reson. 162 (2003) 479–486.
[38] M.T. Bowser, E.D. Sternberg, D.D.Y. Chen, Development and application of a nonaqueous capillary electrophoresis system for the analysis of porphyrins and their oligomers, Anal. Biochem. 241 (1996) 143–150.
[39] L. Chiappisi, M. Gradzielski, Co-assembly in chitosan-surfactant mixtures: thermodynamics, structures, interfacial properties and applications, Adv. Colloid Interface Sci. 220 (2015) 92–107.
[40] J. Wu, K. Gerstandt, H. Zhang, J. Liu, B.J. Hinds, Electrophoretically induced aqueous flow through single-walled carbon nanotube membranes, Nat. Nano 7 (2012) 133–139.
[41] A.T. Sutton, E. Read, A.R. Maniego, J. Thevarajah, J.D. Marty, M. Destarac, M. Gaborieau, P. Castignolles, Purity of double hydrophilic block copolymers revealed by capillary electrophoresis in the critical conditions, J. Chromatogr. A 1372 (2014) 187–195.
[42] C.K.S. Pillai, W. Paul, C.P. Sharma, Chitin and chitosan polymers: chemistry, solubility and fiber formation, Prog. Polym. Sci. 34 (2009) 641–678.
[43] C. Gartner, B.L. Lopez, L. Sierra, R. Graf, H.W. Spiess, M. Gaborieau, Interplay between structure and dynamics in chitosan films investigated with solid-State NMR, dynamic mechanical analysis, and X-ray diffraction, Biomacromolecules 12 (2011) 1380–1386.
[44] D. Berek, Size exclusion chromatography—a blessing and a curse of science and technology of synthetic polymers, J. Sep. Sci. 33 (2010) 315–335.
[45] M. Gaborieau, R.G. Gilbert, A. Gray-Weale, J.M. Hernandez, P. Castignolles, Theory of size exclusion chromatography (SEC) of complex branched polymers, Macromol. Theory Simul. 16 (2007) 13–28.
[46] Y. Shigemasa, K. Saito, H. Sashiwa, H. Saimoto, Enzymatic degradation of chitins and partially deacetylated chitins, Int. J. Biol. Macromol. 16 (1994) 43–49.
[47] S. Aiba, Studies on chitosan 4. Lysozyme hydrolysis of partially *N*-acetylated chitosans, Int. J. Biol. Macromol. 14 (1992) 225–228.

Supporting Information For

Determination of the Distribution of Degrees of Acetylation of Chitosan

Joel Jerushan Thevarajah[a,b], Matthew Paul Van Leeuwen[a,c], Herve Cottet[d], Patrice Castignolles[b*], Marianne Gaborieau[a,b]

[a] Western Sydney University, Molecular Medicine Research Group (MMRG), Parramatta campus, Locked bag 1797, Penrith 2751, Australia, joel.thevarajah@westernsydney.edu.au, m.gaborieau@westernsydney.edu.au

[b] Western Sydney University, Australian Centre for Research on Separation Sciences (ACROSS), School of Science and Health, Parramatta campus, Locked bag 1797, Penrith 2751, Australia, p.castignolles@westernsydney.edu.au

[c] Western Sydney University, School of Medicine, Parramatta campus, Locked bag 1797, Penrith 2751, Australia, m.vanleeuwen@westernsydney.edu.au

[d] Institut des Biomolécules Max Mousseron (IBMM, UMR 5247 CNRS-Université de Montpellier-Ecole Nationale Supérieure de Chimie de Montpellier), Place Eugène Bataillon CC 1706, 34095 Montpellier Cedex 5, France, herve.cottet@umontpellier.fr

* Corresponding author: p.castignolles@westernsydney.edu.au, tel: +61 2 9685 9970, fax: +61 2 9685 9915

Chitosan samples and supplier information

A number of chitosan samples were analyzed. The samples were commercially available from different suppliers.

Table S1: Information of chitosan samples studied in the manuscript provided by supplier and measured. *DA* is the degree of acetylation in % of monomer units (DA_{supp} was given by the supplier, DA_{SSNMR} was measured by solid-state NMR spectroscopy). The viscosity in cps was given by the supplier in the following conditions: [A] at 20°C; [B] at 1% in 1% AcOH; [C] at 1 % in 1 % AcOH, at 20 °C, according to DIN 45, 100S-1; [D] at 20°C, [B] at 1% in 1% AcOH.

Sample	*Supplier*	*Catalog number*	*Lot*	DA_{supp}	DA_{SSNMR}	*Viscosity*
HighMW1	Sigma-Aldrich	419419	MKBD7240V	22	11.1	1218 [B]
HighMW2	Sigma-Aldrich	419419	12913CJ	24	11.0	1540 [B]
MedMW2	Sigma-Aldrich	448877	03318AJ	20	20.2	590 [B]
MedMW3	Sigma-Aldrich	448877	MKBF1336V	20	13.2	503 [B]
MedMW1	Sigma-Aldrich	448877	MKBH1108V	24	22.3	563 [B]
MedMW4	Sigma-Aldrich	448877	09303PE	25	11.1	453 [B]
LowMW2	Sigma-Aldrich	448869	06714DJ	8.9	5	238 [B]
LowMW1	Sigma-Aldrich	448869	MKBG3334V	3.9	17.1	35 [B]
Sig	Sigma-Aldrich	C3646	120M0028V	12	9.8	
Fluk	Sigma-Aldrich (Fluka)	28191	440698/1	not indicated	8.6	337 [C]
AKbioV1	AK Biotech Ltd		090426V1	13.8	10.1	30 [A]
AKbioV2	AK Biotech Ltd		090423V2	14	16.5	320 [A]
AKbioV3	AK Biotech Ltd		090426V3	14	14.8	570 [A]
AKbioD1	AK Biotech Ltd		090422D1	13.9	12.5	35 [A]
AKbioD2	AK Biotech Ltd		090422D2	9.8	11.1	55 [A]
AKbioD3	AK Biotech Ltd		090422D3	4.4	3.8	55 [A]
chitAL	[1]			2.5	4.0	unknown

Dispersity of the electrophoretic mobility distributions and of the composition distributions (distributions of DAs)

The expressions of dispersity for electrophoretic mobility distributions and composition distributions have recently been established [2]. The expressions are analogous to the calculation of dispersity of molar mass distributions by a ratio of moments. The discrete expressions used to calculate the dispersity are as below:

$$D(W(\mu),1,0) = \frac{[\sum_z W(\mu_z)\mu_z\,(\mu_{z+1}-\mu_z)][\sum_z W(\mu_z)\mu_z{}^{-1}(\mu_{z+1}-\mu_z)]}{[\sum_z W(\mu_z)\,(\mu_{z+1}-\mu_z)]^2} \quad \text{(S1)}$$

$$D(W(\mu),2,0) = \frac{[\sum_z W(\mu_z)\,\mu_z{}^2(\mu_{z+1}-\mu_z)][\sum_z W(\mu_z)\,(\mu_{z+1}-\mu_z)]}{[\sum_z W(\mu_z)\,\mu_z(\mu_{z+1}-\mu_z)]^2} \quad \text{(S2)}$$

$$D(W(\mu),3,0) = \frac{[\sum_z W(\mu_z)\,\mu_z{}^3(\mu_{z+1}-\mu_z)][\sum_z W(\mu_z)\,\mu_z(\mu_{z+1}-\mu_z)]}{[\sum_z W(\mu_z)\,\mu_z{}^2(\mu_{z+1}-\mu_z)]^2} \quad \text{(S3)}$$

$$D(W(DA)1,0) \quad = \frac{[\sum_z W(DA_z)\,DA_z\,(DA_{z+1}-DA_z)][\sum_z W(DA_z)\,DA_z^{-1}\,(DA_{z+1}-DA_z)]}{[\sum_z W(DA_z)\,(DA_{z+1}-DA_z)]^2} \quad \text{(S4)}$$

$$D(W(DA),2,0) = \frac{[\sum_z W(DA_z)\,DA_z{}^2(DA_{z+1}-DA_z)][\sum_z W(DA_z)\,(DA_{z+1}-DA_z)]}{[\sum_z W(DA_z)\,DA_z(DA_{z+1}-DA_z)]^2} \quad \text{(S5)}$$

$$D(W(DA),3,0) = \frac{[\sum_z W(DA_z)\,DA_z{}^3(DA_{z+1}-DA_z)][\sum_z W(DA_z)DA_z\,(DA_{z+1}-DA_z)]}{[\sum_z W(DA_z)\,DA_z{}^2(DA_{z+1}-DA_z)]^2} \quad \text{(S6)}$$

$$D_\sigma = \left[\frac{[\sum_z W(\mu_z)\,(\mu_z-\mu_\mathrm{w})^2(\mu_{z+1}-\mu_z)}{[\sum_z W(\mu_z)\,(\mu_{z+1}-\mu_z)]}\right]^{0.5} \quad \text{(S7)}$$

$$D(W(DA),\sigma,DA_\mathrm{W}) = \left[\frac{[\sum_z W(DA_z)\,(DA_z-DA_\mathrm{w})^2(DA_{z+1}-DA_z)]}{[\sum_z W(DA_z)(DA_{z+1}-DA_z)]}\right]^{0.5} \quad \text{(S8)}$$

Kinetics of chitosan dissolution

Pressure assisted capillary electrophoresis (PACE) measurements of the dissolution of MewMW1 in either 50 mM HCl or 50 mM DCl in D_2O were undertaken with the carousel set to 60 °C.

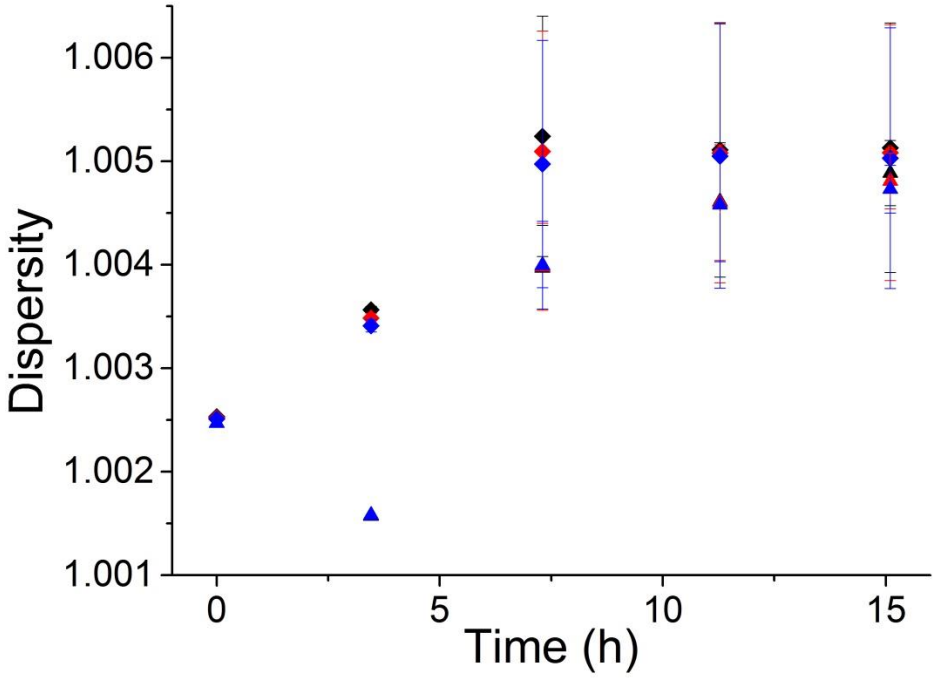

Figure S1: Dispersity of electrophoretic mobility distributions $D(W(\mu),1,0)$ (black), $D(W(\mu),2,0)$ (red), $D(W(\mu),3,0)$ (blue) of chitosan MedMW1 dissolved in 50 mM HCl in H_2O (diamonds) and 50 mM DCl in D_2O (triangles) during kinetic measurement using CE-CC with the carousel kept at 60 °C

Separation of PAlAm

Separation of the cationic polymer poly(allylamine hydrochloride) was possible using a PDADMAC/alginate mulilayer coated capillary. The separation was undertaken using NaPB10 at pH 3. It was detected using both UV absorbance and conductivity.

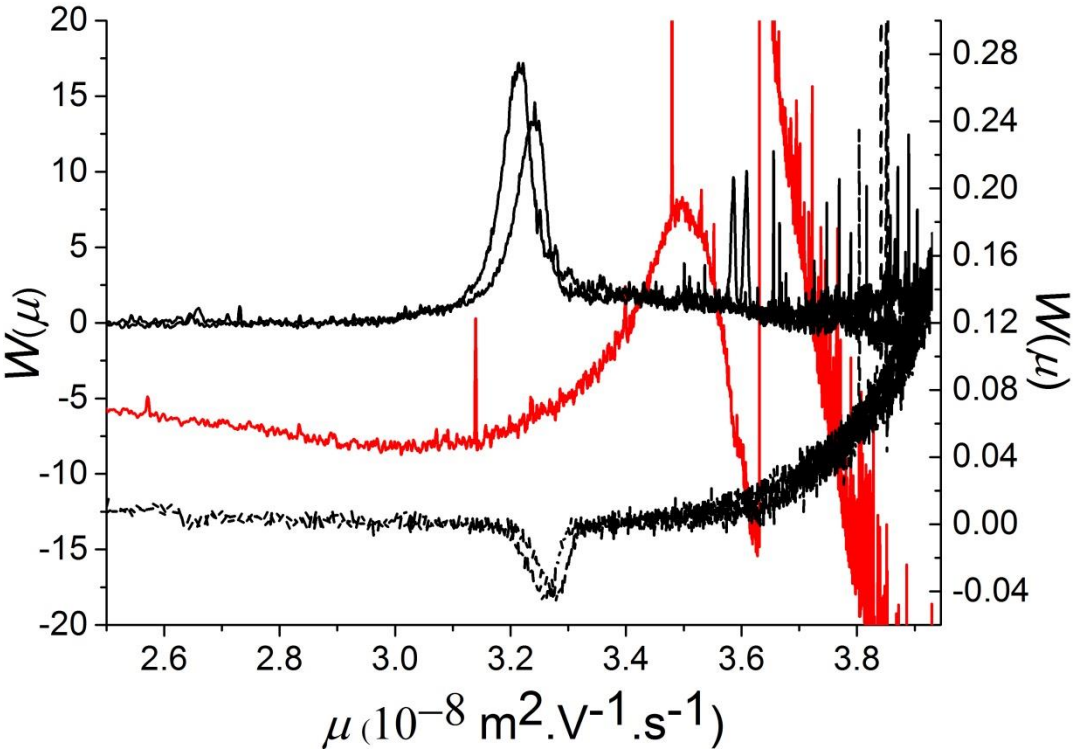

Figure S2: Electropherogram of PAlAm (black lines) and chitosan (red line) separated in a PDADMAC/alginate multilayer coated capillary in NaPB10, detected with UV (solid line – left y axis) or conductivity (dashed line – right y axis).

Correlation of electrophoretic mobility and composition

The weight-average electrophoretic mobility of the complete range of chitosan samples separated in NaPB100 and LiPB100 were plotted against their average *DA* measured by solid-state NMR spectroscopy.

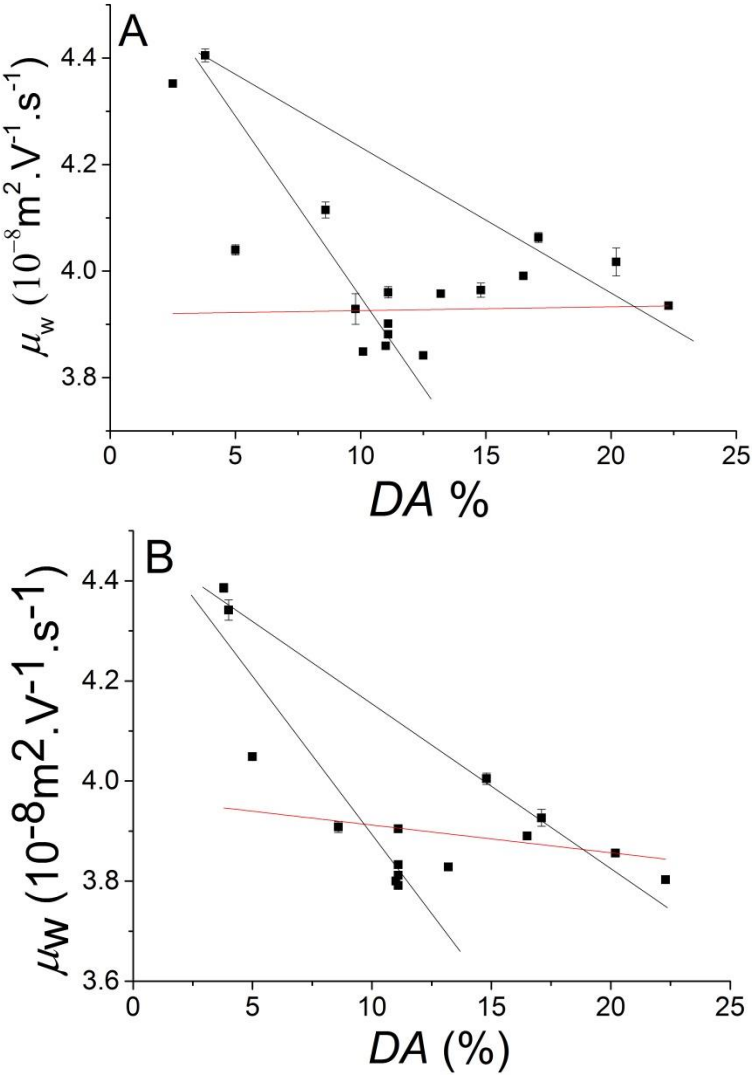

Figure S3 A. Calibration curve of the weight-average electrophoretic mobility (μ_w) of chitosan samples separated in A. NaPB100 and B. LiPB100. Red line represents linear fit and black lines represent possible population fits

Chitosan samples were removed in initial calibration curves based on their dispersity. This was to allow the calibration to curve mimic those made with "narrow" standards. Various fits were tested including linear, polynomial, inverse and log functions.

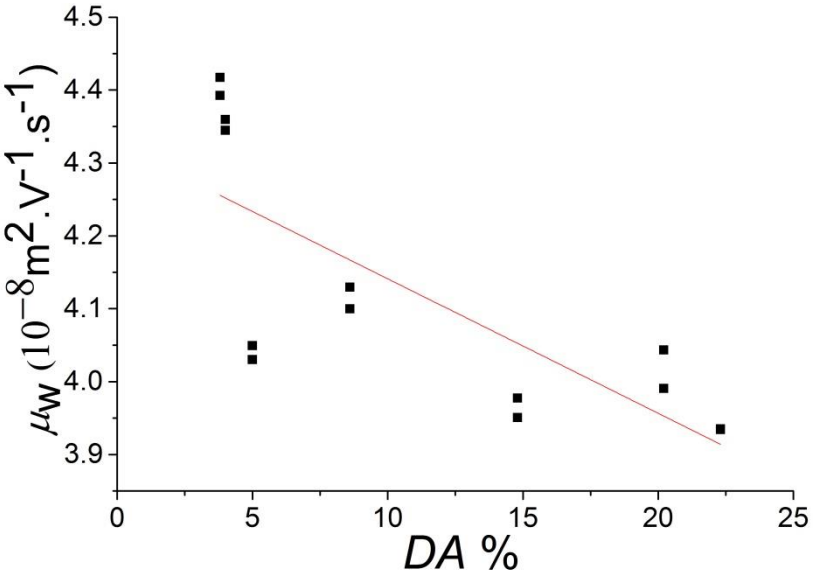

Figure S4: Calibration curve of weight-average electrophoretic mobility in NaPB100 as a function of DA for chitosan with a linear fit (red line) ($r^2 = 0.56$)

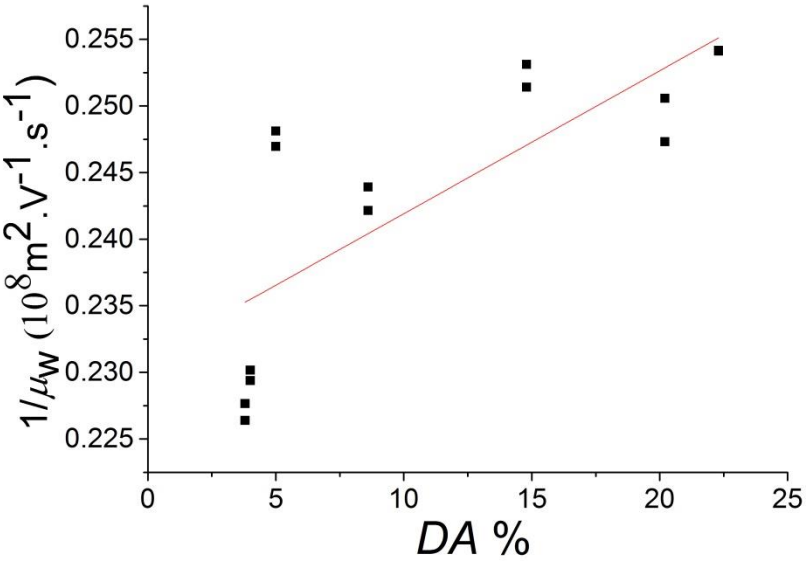

Figure S5: Calibration curve of the inverse function of weight-average electrophoretic mobility in NaPB100 as a function of DA for chitosan with a linear fit (red line) ($r^2 = 0.57$)

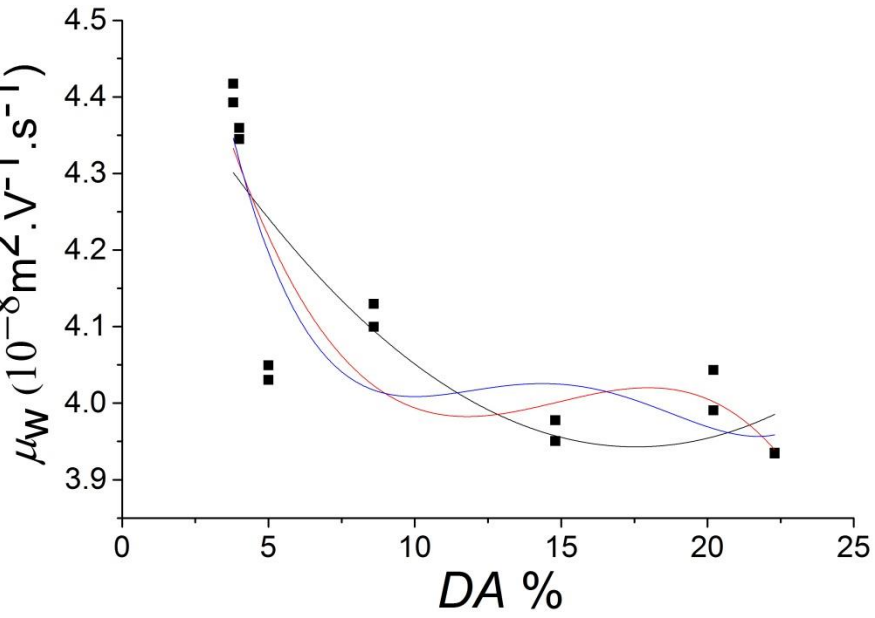

Figure S6: Calibration curve of weight-average electrophoretic mobility in NaPB100 as a function of DA for chitosan with order 2 (black line), 3 (red line) and 4 (blue line) polynomial fit.

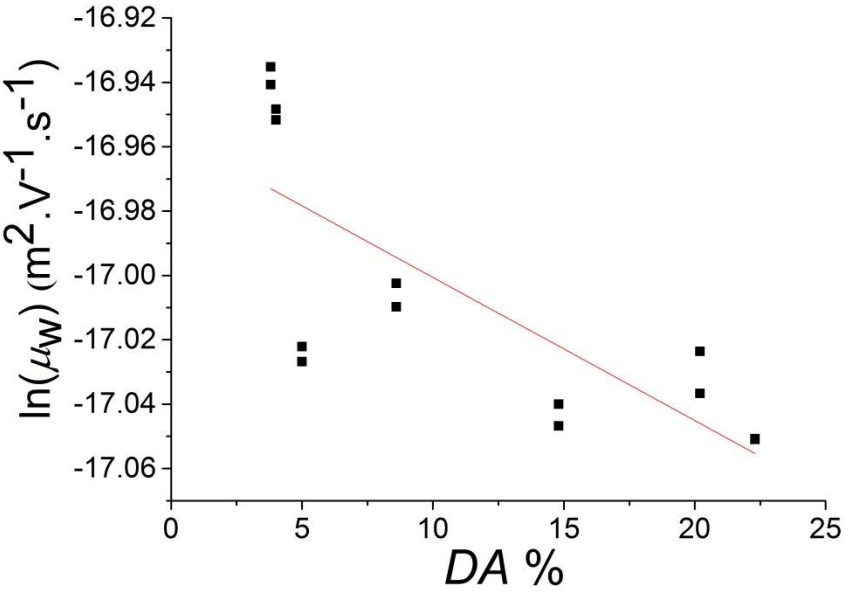

Figure S7: Calibration curve of the log function of weight-average electrophoretic mobility in NaPB100 as a function of DA for chitosan with a linear fit (red line) ($r^2 = 0.56$)

X-ray diffraction of chitosan

Chitosan samples were measured with a Bruker D8 Advance Powder Diffractometer (XRD). Incident radiation was Cu Kα II with detection by a Bruker Lynx eye silicon drift detector. Samples were placed on a sample holder in powder form and levelled to a thin, flat layer.

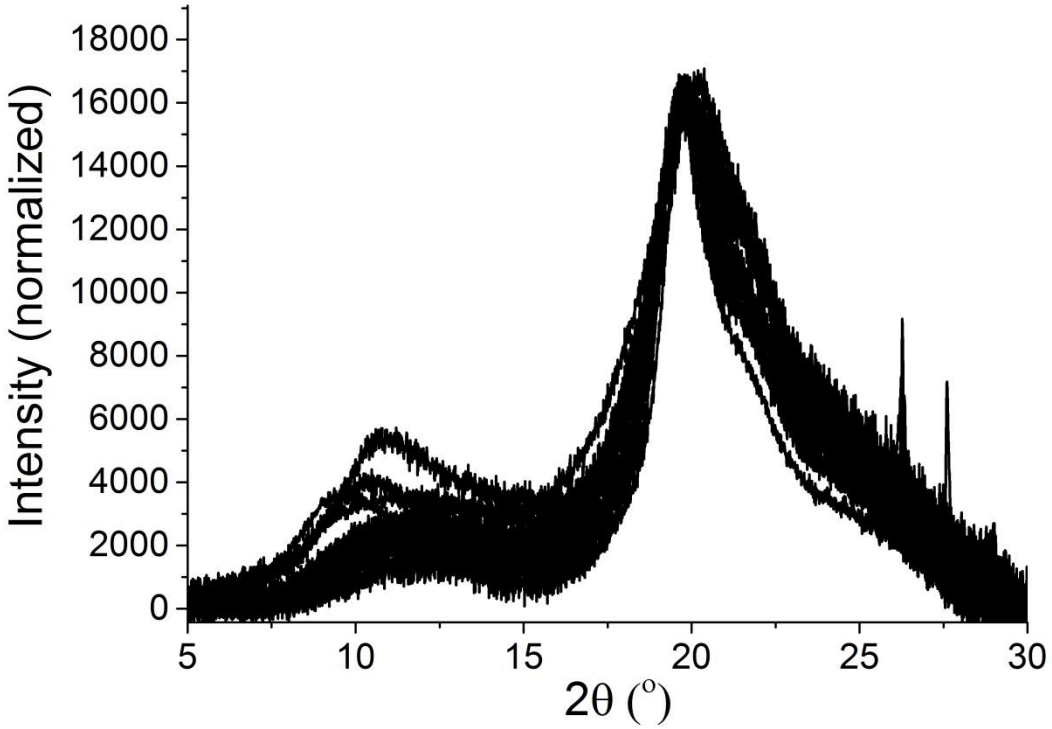

Figure S8: X-ray diffractograms of various chitosan samples normalized by the peak maximum between 18 and 22°.

Composition Distributions

Using the initial composition distributions, the average *DA* at the peak apex could be determined. A second iteration of the calibration was calculated. For chitosan samples separated in NaPB100, the correlation between the *DA* from the peak apex and the weight-average electrophoretic mobility did not improve as seen below. Therefore composition distributions were not calculated.

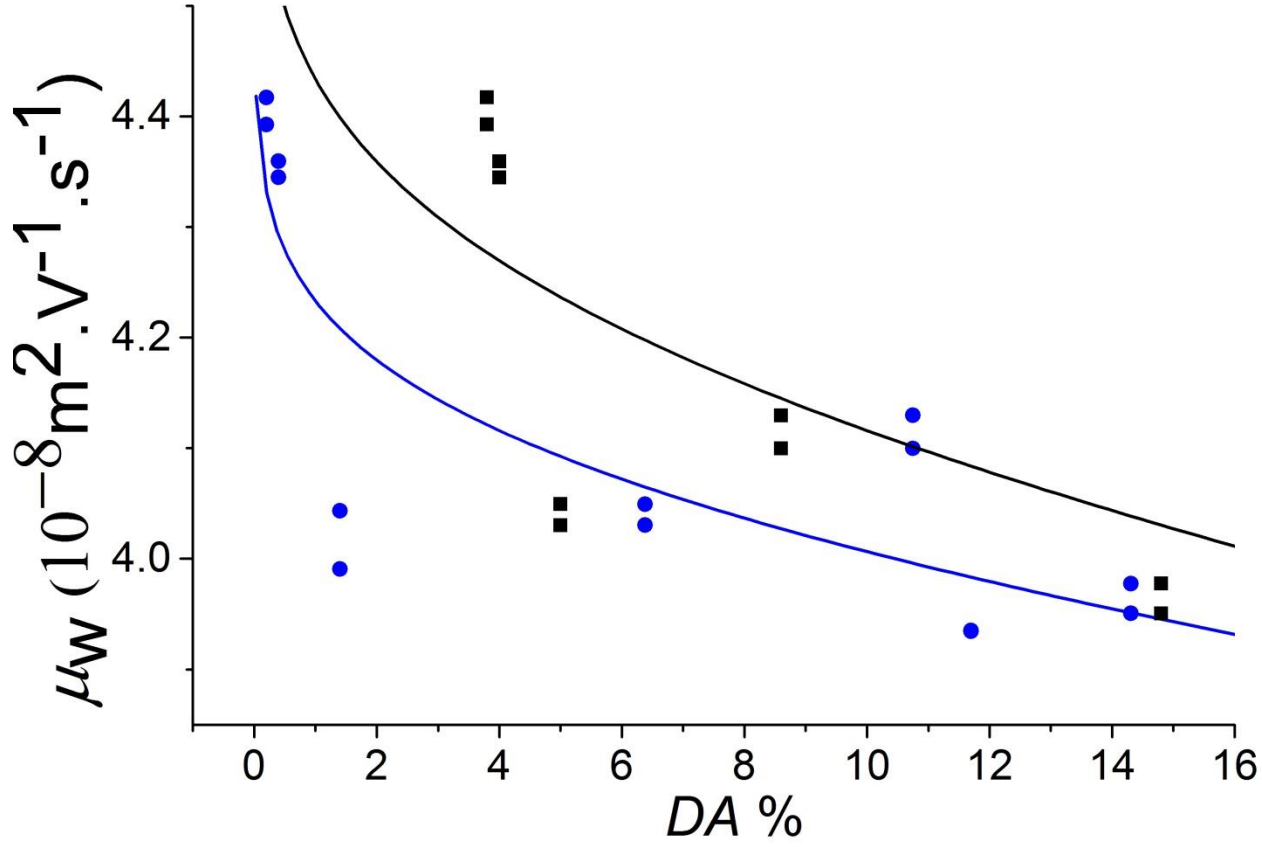

Figure S9: Calibration curve with a Bradley function fit of the weight-average electrophoretic mobility in NaPB100 as a function of *DA* from the solid-state NMR spectroscopy measurements (black) or the peak apex of the composition distributions (blue).

References

[1] M. Mnatsakanyan, J.J. Thevarajah, R.S. Roi, A. Lauto, M. Gaborieau, P. Castignolles, Separation of chitosan by degree of acetylation using simple free solution capillary electrophoresis, Anal. Bioanal. Chem. 405 (2013) 6873-6877.

[2] J.J. Thevarajah, A.T. Sutton, A.R. Maniego, E.G. Whitty, S. Harrisson, H. Cottet, P. Castignolles, M. Gaborieau, Quantifying the Heterogeneity of Chemical Structures in Complex Charged Polymers through the Dispersity of Their Distributions of Electrophoretic Mobilities or of Compositions, Anal. Chem. 88 (2016) 1674-1681.

Video Article

Capillary Electrophoresis to Monitor Peptide Grafting onto Chitosan Films in Real Time

Joel J. Thevarajah[1,2,3], Michael D. O'Connor[1,4], Patrice Castignolles[2,3], Marianne Gaborieau[1,2,3]

[1]Molecular Medicine Research Group, Western Sydney University

[2]Australian Centre for Research on Separation Science, Western Sydney University

[3]School of Science and Health, Western Sydney University

[4]School of Medicine, Western Sydney University

Correspondence to: Marianne Gaborieau at m.gaborieau@westernsydney.edu.au

URL: http://www.jove.com/video/54549
DOI: doi:10.3791/54549

Keywords: Chemistry, Issue 116, capillary electrophoresis, reaction monitoring, real time, grafting, peptide, chitosan, films, epithelial cells, solid-state nuclear magnetic resonance (NMR) spectroscopy

Date Published: 10/26/2016

Citation: Thevarajah, J.J., O'Connor, M.D., Castignolles, P., Gaborieau, M. Capillary Electrophoresis to Monitor Peptide Grafting onto Chitosan Films in Real Time. *J. Vis. Exp.* (116), e54549, doi:10.3791/54549 (2016).

Abstract

Free-solution capillary electrophoresis (CE) separates analytes, generally charged compounds in solution through the application of an electric field. Compared to other analytical separation techniques, such as chromatography, CE is cheap, robust and effectively requires no sample preparation (for a number of complex natural matrices or polymeric samples). CE is fast and can be used to follow the evolution of mixtures in real time (*e.g.*, chemical reaction kinetics), as the signals observed for the separated compounds are directly proportional to their quantity in solution.

Here, the efficiency of CE is demonstrated for monitoring the covalent grafting of peptides onto chitosan films for subsequent biomedical applications. Chitosan's antimicrobial and biocompatible properties make it an attractive material for biomedical applications such as cell growth substrates. Covalently grafting the peptide RGDS (arginine - glycine - aspartic acid - serine) onto the surface of chitosan films aims at improving cell attachment. Historically, chromatography and amino acid analysis have been used to provide a direct measurement of the amount of grafted peptide. However, the fast separation and absence of sample preparation provided by CE enables equally accurate yet real-time monitoring of the peptide grafting process. CE is able to separate and quantify the different components of the reaction mixture: the (non-grafted) peptide and the chemical coupling agents. In this way the use of CE results in improved films for downstream applications.

The chitosan films were characterized through solid-state NMR (nuclear magnetic resonance) spectroscopy. This technique is more time-consuming and cannot be applied in real time, but yields a direct measurement of the peptide and thus validates the CE technique.

Video Link

The video component of this article can be found at http://www.jove.com/video/54549/

Introduction

Free solution capillary electrophoresis (CE) is a technique that separates compounds in solutions based on their charge-to-friction ratio[1,2]. Charge-to-size ratio is often mentioned in the literature, but this simplification does not apply to polyelectrolytes, including polypeptides in this work, and was also shown not to be appropriate for small organic molecules[3]. CE differs from other separation techniques in that it does not have a stationary phase, only a background electrolyte (usually a buffer). This allows the technique to be robust in its ability to analyze a large range of samples with complex matrices[4] such as plant fibers[5], fermentation brews[6] grafting onto synthetic polymers[7], food samples[8], and hardly soluble peptides[9] without tedious sample preparation and purification. This is especially significant for complex polyelectrolytes which have dissolution issues (such as chitosan[10] and gellan gum[11]) and therefore exist as aggregated or precipitated in solution and have been successfully analyzed without sample filtration. Further, the analysis of sugars in breakfast cereals involved injecting samples with particles of breakfast cereal samples precipitated in water[8]. This also extends to the analysis of branched polyelectrolytes or copolymers[12,13]. Extensive work has also been completed in the development of CE techniques specifically for the analysis of proteins for proteomics[14], chiral separation of natural or synthetic peptides[15] and microchip separations of proteins and peptides[16]. Since the separation and analysis take place in a capillary, only small volumes of sample and solvents are used which enables CE to have a lower running cost than other separation techniques including chromatography[5,6,17]. Since the separation by CE is fast, it allows the monitoring of reaction kinetics. This was demonstrated in the case of the grafting of peptides onto chitosan films for improved cell adhesion[18].

Chitosan is a polysaccharide derived from the *N*-deacetylation of chitin. Chitosan films can be used for various biomedical applications such as bioadhesives[19] and cell growth substrates[18,20], due to chitosan's biocompatibility[21]. Cell attachment to specific extracellular matrix proteins, such as fibronectin, collagens and laminin, is directly linked to the survival of the cells[22]. Notably, different cell types often require attachment to different extracellular matrix proteins for survival and proper function. Cell attachment to chitosan films was shown to be enhanced through

the grafting of fibronectin[23]; however, preparation, purification and grafting of such large proteins is not economically viable. Alternately a range of small peptides have been shown to be able to mimic the properties of large extracellular matrix proteins. For example, peptides such as the fibronectin mimetics RGD (arginine - glycine - aspartic acid) and RGDS (arginine - glycine - aspartic acid - serine) have been used to facilitate and increase cell attachment[24]. Covalent grafting of RGDS onto chitosan films resulted in improved cell attachment for cells known to attach to fibronectin *in vivo*[18]. Substituting larger proteins likes fibronectin with smaller peptides that have the same functionality provides a significant cost reduction.

Here, peptide grafting to chitosan was performed as previously published[18]. As previously demonstrated, this approach provides simple and efficient grafting by using the coupling agents EDC-HCl (1-ethyl-3-(3-dimethylaminopropyl)carbodiimide) and NHS (*N*-hydroxysuccinimide) to functionalize the carboxylic acid of the RGDS to be grafted onto the chitosan film. Two advantages of this grafting method are that it does not require any modification of the chitosan or of the peptide, and it is undertaken in aqueous medium to maximize compatibility with future cell culture applications[18,20]. As the coupling agents and the peptide can be charged, CE is a suitable method for the analysis of the reaction kinetics. Importantly, analysis of the reaction kinetics via CE enables real-time monitoring of the grafting reaction, and thus enables both optimizing and quantifying the degree of grafting.

While it is not routinely necessary, the results of the CE analysis can be validated off-line by a direct measurement of the peptide grafting onto the chitosan films using solid-state NMR (nuclear magnetic resonance) spectroscopy[25,26] to demonstrate the covalent grafting of the peptide onto the film[18]. However, compared with solid-state NMR spectroscopy, the real-time analysis provided by CE enables the quantification of the peptide consumption in real time and thus the ability to assess the kinetics of the reaction.

The above mentioned method is simple and allows the real-time analysis of peptide grafting onto chitosan films with indirect quantification of the extent of the grafting. The demonstrated method can be extended to the real time quantitative assessment of different chemical reactions as long as the reactants or the products to be analyzed can be charged.

Protocol

1. Preparation of Chitosan Films

1. Weigh out 2 g of glacial acetic acid, complete to 100 ml with ultrapure water.
2. Weigh out 1.7 g of chitosan powder, add 100 ml of the 2% m/m acetic acid aqueous solution. Stir for 5 days with stirring bar and magnetic stirring plate at room temperature either covered with aluminum foil or in the dark.
3. Centrifuge the chitosan dispersion at 1,076 x g at 23 °C for 1 hr. Collect the supernatant with a syringe and discard the precipitate.
4. For each film, aliquot 10 ml of the chitosan suspension into a 9 cm plastic Petri dish at room temperature. Leave the films covered to dry for at least 7 days.
5. Using scissors cut the dry films into 1 x 1 cm squares. Note: The experiment can be paused at this stage.

2. Preparation of Phosphate-buffered Saline (PBS)

1. Weigh out 8 g sodium chloride, 0.2 g potassium chloride, 1.44 g disodium hydrogen phosphate and 0.24 g potassium dihydrogen phosphate.
2. Dissolve these weighed out chemicals in 800 ml of ultrapure water and titrate the solution with concentrated hydrochloric acid to pH 7.4. Note: The experiment can be paused at this stage.

3. Preparation of 75 mM Sodium Borate Buffer at pH 9.2

1. Weigh out 3.0915 g of boric acid. Dissolve it in 75 ml of ultrapure water.
2. Titrate the boric acid solution to a pH of 9.2 with a sodium hydroxide solution at a concentration of 10 M or higher.
   Caution: Concentrated sodium hydroxide solutions are corrosive and should be handled with gloves.
3. Complete with ultrapure water to obtain 100 ml of solution. This yields a 500 mM sodium borate buffer at pH 9.2.
4. Dilute the 500 mM sodium borate buffer with ultrapure water to 75 mM sodium borate buffer. Note: The experiment can be paused at this stage.

4. Preparation of Chitosan Films for the Grafting Reaction

1. Rinse 10 square chitosan films (1 x 1 cm) in 5 ml of PBS for 2 hr in a Petri dish at room temperature.
2. During this time, prepare and validate the capillary electrophoresis instrument (step 5).

5. Preparation and Validation of the Capillary Electrophoresis Instrument

1. Prepare a 43.5 cm bare fused silica capillary with an internal diameter of 50 µm (43.5 cm is the total length, the effective length to the detection window is typically 35 cm) by weakening the polymer outer coating of the capillary at the set length with a blunt utensil then snapping the capillary.
   1. Create a window for the capillary by using a lighter to burn the polymer coating at 8.5 cm from the inlet and after it cools wipe it clean with ethanol. Burn the coating of the capillary at each end for a few millimeters with a lighter, and after it cools wipe it clean with ethanol.

2. Place capillary inside detection window and install it in the capillary cassette by placing it at equal lengths in the inlet and outlet and winding it around the spindles of the cassette. Then install the cassette in the capillary electrophoresis instrument.

2. Set the parameters of the method for each separation. In the software menu select "method" then "edit the entire method". Set the temperature, time, voltage, and vials used for the separation (for example 25 °C, 10 min, 30 kV).
    1. In the pre-conditioning section, set the consecutive flushes: 10 min with 1 M sodium hydroxide (in water), 5 min with 0.1 M sodium hydroxide (in water), 5 min with ultrapure water and 5 min with 75 mM sodium borate buffer at pH 9.2 for the first method of a series of analyses.
    2. For the subsequent methods, set the set the consecutive flushes in the pre-conditioning section: 1 min with 1 M sodium hydroxide (in water), 5 min with 75 mM sodium borate buffer at pH 9.2.
    3. In the injection section, set parameters for a hydrodynamic injection with 30 mbar pressure for 10 sec for all methods. In the separation section, set the separation conditions to 30 kV at 25 °C for 9 min for all methods.
    NOTE: Consult user manual of specific CE instrument as procedure for operating the CE instrument may vary between manufacturers. Prepare the 1 M sodium hydroxide solution on the day.

3. Inject and separate a neutral internal standard (10 µl of 10% v/v dimethylsulfoxide (DMSO), in water diluted into 450 µl of 75 mM sodium borate buffer). Then inject and separate in the same way an oligoacrylate standard (dissolved in ultrapure water at 10 $g \cdot L^{-1}$; see List of Materials) to check the validity of the capillary. Pause the sequence here until the grafting reaction is ready to start.

6. Grafting of RGDS onto Chitosan Film

1. Weigh out the peptide (1 mg RGDS) and the coupling agents (3 mg EDC-HCl and 2 mg NHS).
2. 2 hr after the start of the chitosan film soaking in PBS, dissolve the peptide and the coupling agents in 5 ml of PBS.
    1. Take a 50 µl aliquot of this solution. Add 2 µl of 10% v/v DMSO in water as an internal neutral standard to the aliquot. Analyze the aliquot with CE (see step 7).

3. Remove the 5 ml of PBS used to rinse the chitosan films from the Petri dish. Add the 5 ml solution of peptide and coupling agents to the Petri dish containing the chitosan films.
4. Cover the Petri dish with paraffin film and place it on an orbital shaker at room temperature. Take 50 µl aliquots of reaction media at set times.
NOTE: The total analysis time with CE is 15 min, thus an aliquot can be taken every 15 min (or every 30 min if two reactions are monitored in parallel, *etc.*).
    1. Add 2 µl of 10% v/v DMSO in water as an internal neutral standard to each aliquot.
    NOTE: Aliquots should be analyzed with CE as soon as they are taken (see step 7).

5. After 4 hr of shaking and aliquot removal, remove the Petri dish from the shaker. Remove the reaction medium from the Petri dish. Add 5 ml of PBS to rinse the chitosan films.
6. Remove the PBS from the Petri dish, rinse the chitosan film with ultrapure water and allow them to dry overnight. Remove the ultrapure water and store the films at -20 °C in a plastic Petri dish.

7. Monitoring of Grafting Reaction Using CE

1. Inject and separate aliquots of reaction media immediately after removal from the Petri dish using the analysis conditions as in section 5.2.
2. Upon completion of the separations rinse the capillary with ultrapure water for 10 min. Dry it through a flush with an empty vial (air) for 10 min.
NOTE: The experiment can be paused at this stage.

8. Data Treatment for CE

1. Check the validity of each separation, by checking that both the current during the separation and the migration time of the electroosmotic mobility marker (DMSO in this case) are similar to the ones observed for the oligoacrylate standard separation.
NOTE: Up to 10-15% variation is acceptable from the expected current value of about 50 µA and migration time value of 1.3 min (electrophoretic mobility values should be used instead of migration times if a higher repeatability is required).
2. For each successful separation, export the raw data from the capillary electrophoresis software by selecting a specific data set, right clicking on export and selecting an appropriate signal.
3. Convert the raw data recorded by the CE (presented as UV absorbance as a function of migration time). Convert the X-axis (migration time t_m) into an electrophoretic mobility μ following Equation 1:

$$\mu_{ep} = \frac{L_d \cdot L_t}{V} \cdot \left(\frac{1}{t_m} - \frac{1}{t_{eo}}\right) \quad (1)$$

where L_d is the length to the detector, L_t is the total length of the capillary, V is the voltage, and t_{eo} is the migration time of a neutral specie (the DMSO internal standard in this case)[27].
Convert the Y-axis of the raw data (absorbance in a.u.) to a distribution of electrophoretic mobilities $W(\mu)$ following Equation 2:[28]

$$W(\mu) = t_m * absorbance \quad (2)$$

9. Additional Characterization of Peptide-grafted Films[18]

1. Insert peptide-grafted chitosan films, rolled around themselves, in a 4 mm solid-state NMR rotor. Fill the rotor with phosphate-buffered saline to swell the films, and close the rotor. Wait for a few hours.
2. Analyze the film with ^{13}C NMR spectroscopy[18].

Representative Results

CE is well suited to monitoring the grafting of peptides (*e.g.*, RGDS) onto chitosan films. Suitable coupling agents include EDC-HCl and NHS which activate the peptide to be grafted onto the chitosan (**Figure 1**). CE is able to separate the different molecules of interest from the reaction medium. To assign the peaks on the electropherogram, pure RGDS, EDC-HCl and NHS were dissolved, injected and separated separately. After the peak assignment, the reaction medium was injected and the various reactants were identified (**Figure 2**). EDC-HCl reacted into a side product EDH-HCl (3-(((ethylamino)(hydroxy)methylene)amino)-*N*,*N*-dimethylpropan-1-amine). Dimethyl sulfoxide (DMSO) is used as an internal standard for the CE separations. Chitosan is present in the grafting experiment in the form of insoluble films and is thus not injected or observed in CE. Note that for all raw data, the recorded migration time axis is converted into an electrophoretic mobility axis (Equation 1) and the UV absorbance axis into a distribution of electrophoretic mobilities $W(\mu)$ (Equation 2).

As the aliquots are taken from the reaction medium they are placed into the CE instrument and injected. The extent of the reaction is monitored through the decrease of the peak associated with RGDS (**Figure 3**). It can also be seen that the EDC-HCl peak decreases while the EDH-HCl peak increases over time. It is important to note that there is no signal that can be assigned to a product from a side reaction of the peptide, thus it is assumed that the RGDS being removed from the reaction medium is being grafted onto the chitosan film. Overlaid electropherograms (**Figure 3A**) allow the quantification of peptide consumption from the start to the end of the reaction. It is to be noted that although the kinetics was initially measured for 18 hr (**Figure 3B**), 4 hr was deemed sufficient for the reaction to proceed to its maximal extent. To allow quantification an optimal injection volume is required to ensure the signal-to-noise ratio is high enough while preventing overloading (**Figure 4A**) and in the case of RGDS, injections were required to be completed in real time to prevent polycondensation (**Figure 4B**).

The CE-based technique described here to analyze peptide grafting to chitosan films is fast and simple; however, it does not quantify the grafting process directly. NMR spectroscopy is used to demonstrate the grafting; this measurement cannot be done in real time (it typically takes several hours) and needs to be completed post-reaction. The qualitative comparison of the chitosan films before and after grafting shows the successful grafting of the peptides through the appearance of a signal at 70 ppm in the grafted films corresponding to the amide bond between the chitosan and the peptide (**Figure 5**).

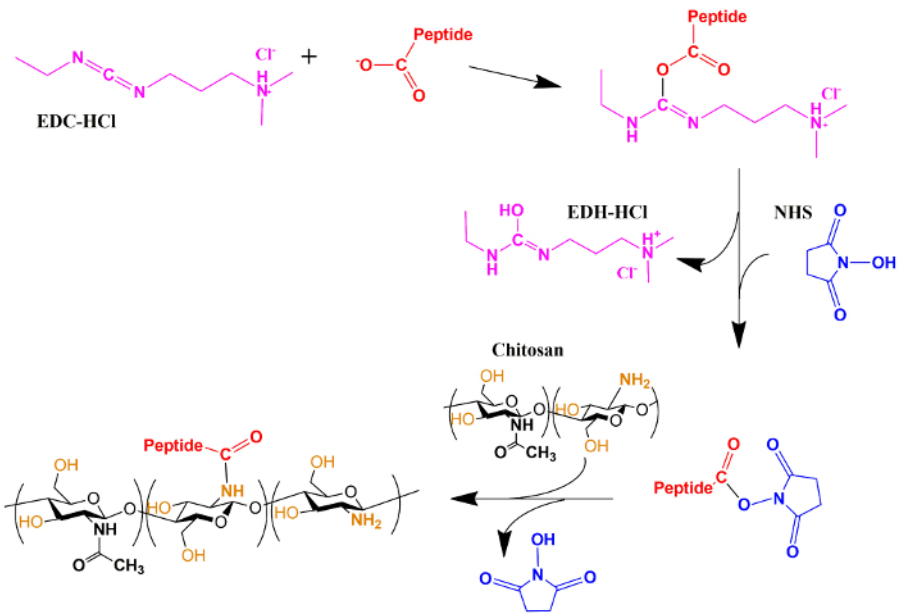

Figure 1. Scheme of the grafting reaction. Chemical reaction scheme showing the activation by EDC-HCl and NHS of the carboxylic acid functional group of RGDS followed by its grafting onto the chitosan's film surface. Please click here to view a larger version of this figure.

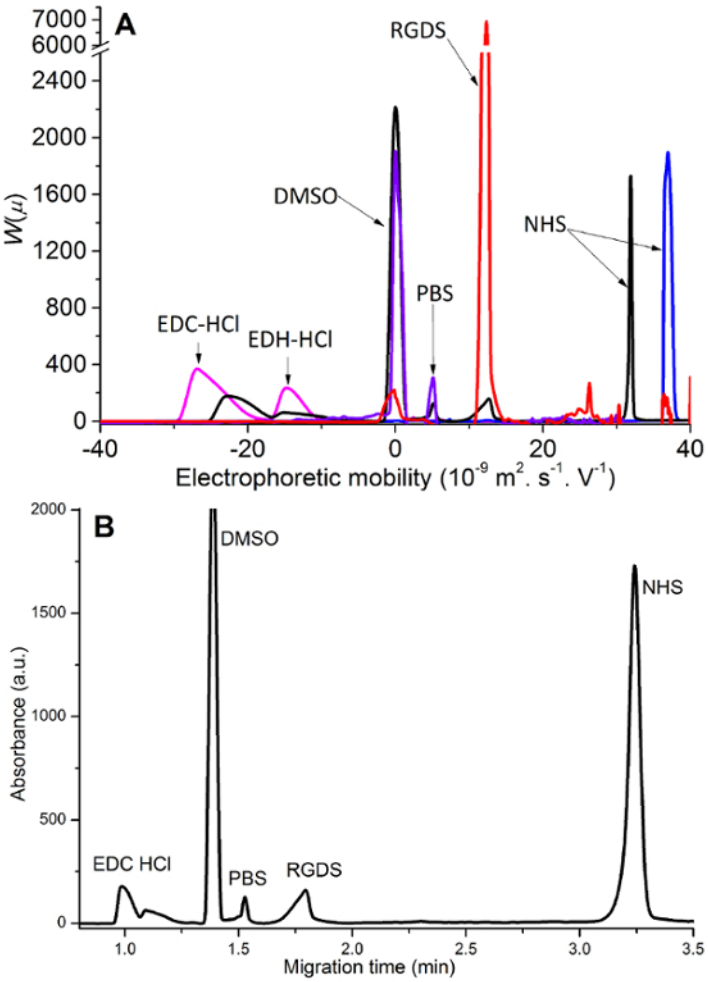

Figure 2. Peak assignment of the species present in the reaction medium. A. Separation and peak assignment for solutions of partially hydrolyzed EDC-HCl (pink), RGDS (red), NHS (blue), as well as for PBS (purple) and the reaction medium (black). **B.** Electropherograms of reaction media (black) presented as a function of migration time (electrophoretic mobility should be used to overcome poor repeatability in migration times). Please click here to view a larger version of this figure.

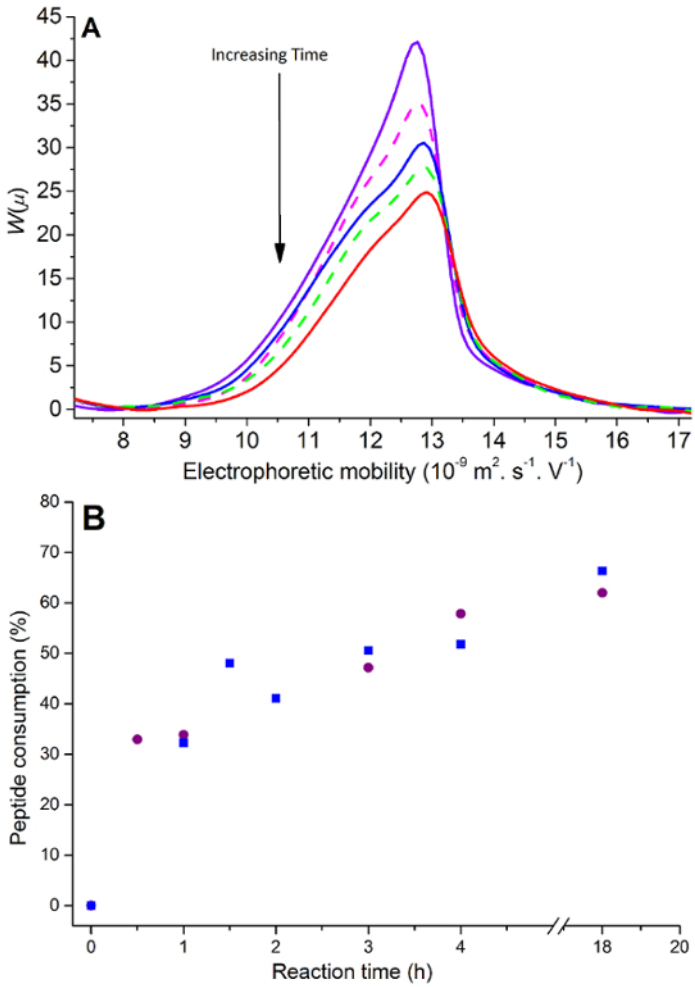

Figure 3. CE monitoring of RGDS consumption. (**A**) Overlaid peptide peaks at reaction time 30 min (purple solid line), 60 min (magenta dash line), 90 min (blue solid line), 120 min (green dash line), 150 min (red solid line) and (**B**) kinetics of grafting completed over 18 hr in replicates (square and circle). Please click here to view a larger version of this figure.

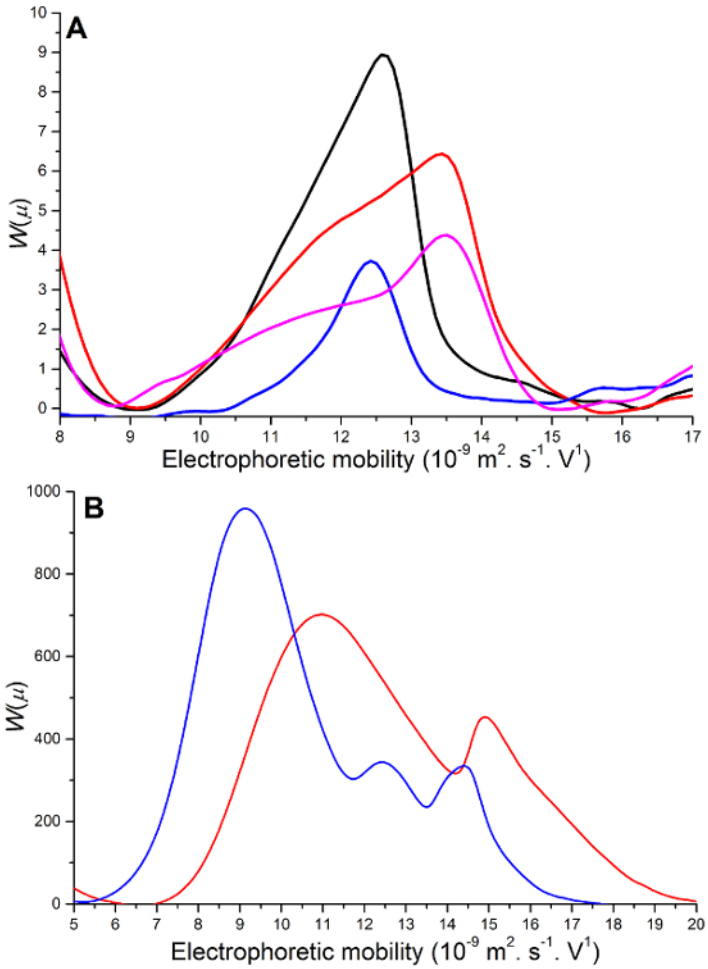

Figure 4. Overlaid peptide peaks in reaction media showing suboptimal results. (**A**) Varying (hydrodynamic) injection times: 5 sec (blue line), 10 sec (black line), 20 sec (red line) and 30 sec (magenta line). (**B**) Reaction media left in a CE vial for an extended period of time before injection: 30 min (red line) and 90 min (blue line). Please click here to view a larger version of this figure.

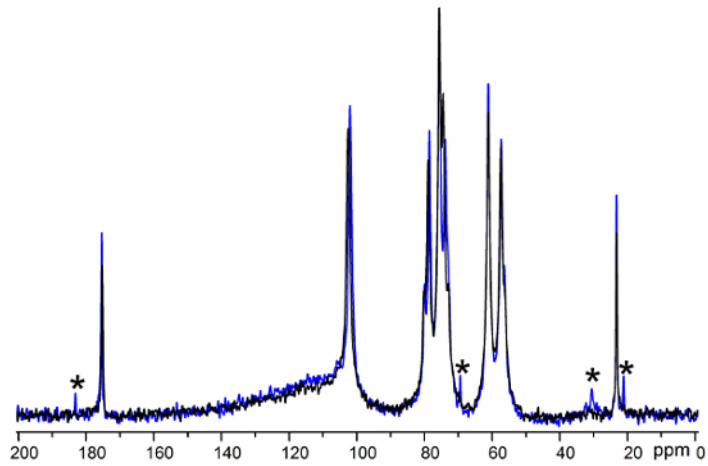

Figure 5. ^{13}C swollen-state NMR spectra of chitosan films. Comparison of the films before (black line) and after (blue line) peptide grafting. Signals present only in the spectrum recorded after grafting are indicated by asterisks. Please click here to view a larger version of this figure.

Discussion

The simplicity of the protocol described here makes it ideally suited to widespread application. However, particular attention needs to be paid to of the following key steps.

Proper CE instrument preparation

It is important to separate a known standard immediately prior to the separation of unknown samples (as well as at the end of a series of separations) to check the validity of the capillary and instrument on the day. This standard can be an oligoacrylate[27] or any sample known to give multiple peaks over a wide range of migration times. Monitoring the current during all separations and analyzing the migration of a neutral marker in each separation are key steps to identify issues. An unstable current or large variations (more than 10-15%) in the plateau value of the current may be due to inconsistency in the buffer (pH or concentration). If it is followed by a delayed migration time of the neutral maker it may also be due to the capillary not being sufficiently clean. Routine checks of the pH of the buffer and an extra flush of the capillary for 10 min with 1 M sodium hydroxide (freshly prepared) can be used to prevent/amend this problem. During the experiment, extra cleaning steps can be employed to ensure an optimal separation, typically including or lengthening a flush with concentrated aqueous sodium hydroxide to regenerate the fuse silica capillary surface.

Proper data treatment

At the conclusion of the experiment, appropriate treatment of the raw data is essential when comparing results. This involves the conversion of the X and Y-axis obtained from the CE instrument (step 8.3). The migration times determined in CE have a relatively poor repeatability and we recommend using electrophoretic mobilities instead, leading to a much better repeatability. The significance of correctly treating data has been shown previously with the separation and characterization of chitosan[10], poly(acrylic acid)[29], block copolymers[13] and the detection of sugars in breakfast cereals[8] through smaller standard deviations (RSD) observed between experiments for mobilities than for migration times. Further, CE has been shown to be more robust than HPLC in the separation of monosaccharides in complex matrices[5]. Other steps of optimization may include adjusting the injection volume (time of injection) to allow separation with good sensitivity without causing overloading which would prevent quantification. An injection time of 10 sec is deemed optimal at 30 mbar (**Figure 4B**): a shorter injection time leads to a reduced sensitivity while longer injection times lead to a peak shape distortion indicative of capillary overloading.

Importance of real-time monitoring

A critical strength of this CE-based method is the ability to monitor reactions in real time. This requires optimal CE conditions for detection and separation of the relevant reactant(s) and/or product(s). Furthermore, for the analysis of chemical reactions an appropriate time zero must be taken as a benchmark of the reaction; this typically consists in the separation of the measured out reactants just prior to the reaction starting. This can be done for example before one particular reactant is introduced, before the temperature is increased, or before UV irradiation is started to trigger the reaction.

In the case of the grafting of the peptide RGDS (onto chitosan or onto another substrate), the peptide is able to react with itself to produce linear oligomers or branched structures through polycondensation[18]. This is because RGDS contains both amine and carboxylic acid functional groups. These peptide oligomers do not have the same electrophoretic mobility as the initial peptide RGDS and therefore may cause an inaccurate quantification, through for example co-migration with other species. It is therefore important to ensure that aliquots of the reaction medium are injected and separated within a few minutes of being taken from the reaction medium (**Figure 4B**).

Proper preparation of the chitosan films

When specifically dealing with chitosan films there are a number of steps to adhere to. During the production of the chitosan films, the films need to be left to dry for at least 7 days (preferably more). If this is not completed, when the films are placed in PBS buffer to rinse they will dissolve rather than form a swollen film which then prevents the next steps. Additionally, it is important to neutralize the film prior to the grafting reaction to remove any remaining acetic acid which may leach out of the film and compete with the peptide for the grafting reaction[18]. This can be done through soaking in dilute aqueous sodium hydroxide or in PBS. The pH of the buffer used as solvent for the grafting reaction is also critical: if it is too acidic the films will partially or completely dissolve. During the grafting reaction it is important that the film is able to have maximum contact with the reaction solution. Therefore, the Petri dish containing the films and the reaction mixture are placed on a shaker. It is also imperative to prevent the evaporation of the reaction mixture to prevent uncontrolled concentration variations resulting in inaccurate quantifications; the use of paraffin film to cover the Petri dish was effective to prevent it.

The main limitation of the CE technique is that individually it is not able to confirm the grafting process. In the context of the chemical grafting process mentioned above, the quantification of the peptide grafting is indirect. This can be overcome with the use of a complementary technique such as solid-state NMR spectroscopy as previously mentioned. Other limitations of the CE technique include that it requires the compound of interest to be charged. Therefore neutral species will migrate at the same time. In certain cases this can be overcome if the compound of interest complexes with borate. Finally if the compound of interest does not contain chromophores detection other than UV such as conductivity may need to be used. This requires the additional purchase of a conductivity detector which requires optimization.

Advantages of analyzing peptide grafting via CE vs other analytical methods

The CE method has several advantages over alternative indirect methods including high performance liquid chromatography (HPLC), amino acid analysis (AAA) and the direct method of NMR spectroscopy. Compared to AAA it is a high-throughput, robust method which allows it to analyze complex samples efficiently without tedious sample preparation. This is advantageous especially in the analysis of chemical reactions in real time. HPLC has been used previously for peptide grafting analysis[30], however it was deemed only semi-quantitative. CE has a lower running cost

than HPLC and does not require sample filtration prior to analysis, minimizing the risk of sample loss[5]. Although ^{13}C NMR spectroscopy is able to directly measure the product of interest, it is a costly technique and is unable to measure it in real time.

The protocol descripted here provides a rapid, efficient, inexpensive and reliable method for optimizing peptide grafting to chitosan film. This new approach thus provides significant advantages for tailoring the cell attachment properties of chitosan films compared to traditionally used methods such as chromatography and AAA. This CE method can be used to monitor a number of other chemical reactions in real time, typically reactions occurring on the timeframe of several hr, for which the reactants/products of interest can be charged. In this case, it is however important to note that the CE method should be optimized prior to the analysis of a different chemical reaction to allow a successful analysis. This includes the analysis of the pure reactants and products prior to the reaction to allow them to be identified and ensure that they can be detected and separated, as well as to ensure that no contaminants may prevent quantification. The separation may be improved and the total analysis time changed by varying the capillary length, buffer composition and voltage, and potentially using a capillary with coated walls. The detection may be improved by modifying the conditions in which the sample is injected to favor the charged reactants or by injecting a larger amount of the sample into the capillary. Further, other detectors apart from UV detection can be employed including fluorescence, contactless conductivity detectors or the CE can be coupled to a mass spectrometer. The ability to monitor reactions in real time enables the grafting reaction to be performed directly in a CE vial if the substrate is in solution and is able to be analyzed by CE. This can take place directly inside the CE instrument, as we recently performed it for grafting of aminoantipyrine on poly(acrylic acid)[7] Additionally, the approach is not limited to grafting reactions but can be extended to monitor various other chemical reactions. Further, the monitoring of the reactions allows optimization of the reaction and may also be used to validate the product of the reaction. As long as the compound of interest can be dissolved and charged, the CE method allows fast, cheap and robust separation, detection and quantification.

Disclosures

The authors declare that they have no competing financial interests.

Acknowledgements

MG, MO'C and PC thank the Molecular Medicine Research Group at WSU for Research Seed Funding, as well as Michele Mason (WSU), Richard Wuhrer (Advanced Materials Characterisation Facility, AMCF, WSU) and Hervé Cottet (Montpellier) for discussions.

References

1. Muthukumar, M. Theory of electrophoretic mobility of a polyelectrolyte in semidilute solutions of neutral polymers. *Electrophoresis.* **17**, 1167-1172 (1996).
2. Barrat, J. L., & Joanny, J. F. in *Advances in Chemical Physics, Vol Xciv* Vol. 94 *Advances in Chemical Physics.* 1-66 John Wiley & Sons Inc, (1996).
3. Fu, S. L., & Lucy, C. A. Prediction of electrophoretic mobilities. 1. Monoamines. *Anal. Chem.* **70**, 173-181 (1998).
4. Harvey, D. *Modern Analytical Chemistry.* McGraw Hill, (2000).
5. Oliver, J. D., Gaborieau, M., Hilder, E. F., & Castignolles, P. Simple and robust determination of monosaccharides in plant fibers in complex mixtures by capillary electrophoresis and high performance liquid chromatography. *J. Chromatogr. A* **1291**, 179-186 (2013).
6. Oliver, J. D., Sutton, A. T., Karu, N., Phillips, M., Markham, J., Peiris, P., Hilder, E. F., & Castignolles, P. Simple and robust monitoring of ethanol fermentations by capillary electrophoresis. *Biotechnology and Applied Biochemistry.* **62**, 329-342 (2015).
7. Thevarajah, J. J., Sutton, A. T., Maniego, A. R., Whitty, E. G., Harrisson, S., Cottet, H., Castignolles, P., & Gaborieau, M. Quantifying the Heterogeneity of Chemical Structures in Complex Charged Polymers through the Dispersity of Their Distributions of Electrophoretic Mobilities or of Compositions. *Anal. Chem.* **88**, 1674-1681 (2016).
8. Toutounji, M. R., Van Leeuwen, M. P., Oliver, J. D., Shrestha, A. K., Castignolles, P., & Gaborieau, M. Quantification of sugars in breakfast cereals using capillary electrophoresis. *Carbohydr. Res.* **408**, 134-141 (2015).
9. Miramon, H., Cavelier, F., Martinez, J., & Cottet, H. Highly Resolutive Separations of Hardly Soluble Synthetic Polypeptides by Capillary Electrophoresis. *Anal. Chem.* **82**, 394-399 (2010).
10. Mnatsakanyan, M., Thevarajah, J. J., Roi, R. S., Lauto, A., Gaborieau, M., & Castignolles, P. Separation of chitosan by degree of acetylation using simple free solution capillary electrophoresis. *Anal. Bioanal. Chem.* **405**, 6873-6877 (2013).
11. Taylor, D. L., Ferris, C. J., Maniego, A. R., Castignolles, P., in het Panhuis, M., & Gaborieau, M. Characterization of Gellan Gum by Capillary Electrophoresis. *Australian Journal of Chemistry.* **65**, 1156-1164 (2012).
12. Thevarajah, J. J., Gaborieau, M., & Castignolles, P. Separation and characterization of synthetic polyelectrolytes and polysaccharides with capillary electrophoresis. *Adv. Chem.* **2014**, 798503 (2014).
13. Sutton, A. T., Read, E., Maniego, A. R., Thevarajah, J., Marty, J.-D., Destarac, M., Gaborieau, M., & Castignolles, P. Purity of double hydrophilic block copolymers revealed by capillary electrophoresis in the critical conditions. *J. Chromatogr. A.* **1372**, 187-195 (2014).
14. Righetti, P. G., Sebastiano, R., & Citterio, A. Capillary electrophoresis and isoelectric focusing in peptide and protein analysis. *Proteomics.* **13**, 325-340 (2013).
15. Ali, I., Al-Othman, Z. A., Al-Warthan, A., Asnin, L., & Chudinov, A. Advances in chiral separations of small peptides by capillary electrophoresis and chromatography. *J. Sep. Sci.* **37**, 2447-2466 (2014).
16. Kasicka, V. Recent developments in capillary and microchip electroseparations of peptides (2011-2013). *Electrophoresis.* **35**, 69-95 (2014).
17. JoVE Science Education Database. Capillary Electrophoresis (CE). *Essentials of Analytical Chemistry.* JoVE Cambridge, MA (2016).
18. Taylor, D. L., Thevarajah, J. J., Narayan, D. K., Murphy, P., Mangala, M. M., Lim, S., Wuhrer, R., Lefay, C., O'Connor, M. D., Gaborieau, M., & Castignolles, P. Real-time monitoring of peptide grafting onto chitosan films using capillary electrophoresis. *Anal. Bioanal. Chem.* **407**, 2543-2555 (2015).
19. Rinaudo, M. Chitin and chitosan: Properties and applications. *Prog. Polym. Sci.* **31**, 603-632 (2006).

20. Li, Z., Leung, M., Hopper, R., Ellenbogen, R., & Zhang, M. Feeder-free self-renewal of human embryonic stem cells in 3D porous natural polymer scaffolds. *Biomaterials.* **31**, 404-412 (2010).
21. Domard, A. A perspective on 30 years research on chitin and chitosan. *Carbohydr. Polym.* **84**, 696-703 (2011).
22. Shekaran, A., & Garcia, A. J. Nanoscale engineering of extracellular matrix-mimetic bioadhesive surfaces and implants for tissue engineering. *Biochim. Biophys. Acta Gen. Subj.* **1810**, 350-360 (2011).
23. Custodio, C. A., Alves, C. M., Reis, R. L., & Mano, J. F. Immobilization of fibronectin in chitosan substrates improves cell adhesion and proliferation. *J. Tissue Eng. Regen. Med.* **4**, 316-323 (2010).
24. Boateng, S. Y., Lateef, S. S., Mosley, W., Hartman, T. J., Hanley, L., & Russell, B. RGD and YIGSR synthetic peptides facilitate cellular adhesion identical to that of laminin and fibronectin but alter the physiology of neonatal cardiac myocytes. *Am. J. Physiol. Cell Physiol.* **288**, C30-38 (2005).
25. Lefay, C., Guillaneuf, Y., Moreira, G., Thevarajah, J. J., Castignolles, P., Ziarelli, F., Bloch, E., Major, M., Charles, L., Gaborieau, M., Bertin, D., & Gigmes, D. Heterogeneous modification of chitosan via nitroxide-mediated polymerization. *Polym. Chem.* **4**, 322-328 (2013).
26. Gartner, C., Lopez, B. L., Sierra, L., Graf, R., Spiess, H. W., & Gaborieau, M. Interplay between Structure and Dynamics in Chitosan Films Investigated with Solid-State NMR, Dynamic Mechanical Analysis, and X-ray Diffraction. *Biomacromolecules.* **12**, 1380-1386 (2011).
27. Castignolles, P., Gaborieau, M., Hilder, E. F., Sprong, E., Ferguson, C. J., & Gilbert, R. G. High resolution separation of oligo(acrylic acid) by capillary zone electrophoresis. *Macromol. Rapid Commun.* **27**, 42-46 (2006).
28. Chamieh, J., Martin, M., & Cottet, H. Quantitative Analysis in Capillary Electrophoresis: Transformation of Raw Electropherograms into Continuous Distributions. *Anal. Chem.* **87**, 1050-1057 (2015).
29. Maniego, A. R., Ang, D., Guillaneuf, Y., Lefay, C., Gigmes, D., Aldrich-Wright, J. R., Gaborieau, M., & Castignolles, P. Separation of poly(acrylic acid) salts according to topology using capillary electrophoresis in the critical conditions. *Anal. Bioanal. Chem.* **405**, 9009-9020 (2013).
30. Chung, T. W., Lu, Y. F., Wang, S. S., Lin, Y. S., & Chu, S. H. Growth of human endothelial cells on photochemically grafted Gly-Arg-Gly-Asp (GRGD) chitosans. *Biomaterials.* **23**, 4803-4809 (2002).

Materials List for:

Capillary Electrophoresis to Monitor Peptide Grafting onto Chitosan Films in Real Time

Joel J. Thevarajah[1,2,3], Michael D. O'Connor[1,4], Patrice Castignolles[2,3], Marianne Gaborieau[1,2,3]

[1]Molecular Medicine Research Group, Western Sydney University

[2]Australian Centre for Research on Separation Science, Western Sydney University

[3]School of Science and Health, Western Sydney University

[4]School of Medicine, Western Sydney University

Correspondence to: Marianne Gaborieau at m.gaborieau@westernsydney.edu.au

URL: http://www.jove.com/video/54549
DOI: doi:10.3791/54549

Materials

Name	Company	Catalog Number	Comments
Water	Millipore		All water used in the experiment has to be of Milli-Q quality
Chitosan powder (medium molecular weight)	Sigma-Aldrich	448877	lot MKBH1108V was used. Significant batch-to-batch variations occur with natural products such as polysaccharides
Acetic acid - Unilab	Ajax Finechem	2-2.5L GL	laboratory reagent
Dimethylsulfoxide	Sigma-Aldrich	D4540	laboratory reagent, slightly hazardous to skin, hazardous if ingested
Sodium hydroxide	Sigma-Aldrich	221465	laboratory reagent, corrosive
1-ethyl-3-(3-dimethylaminopropyl)carbodiimide	Sigma-Aldrich	D80002	Irritant to skin
N-hydroxysuccinimide	Sigma-Aldrich	130672	Irritant to skin
Sodium chloride	Ajax Finechem	466-500G	laboratory reagent
Potassium chloride - Univar	Ajax Finechem	384-500G	analytical reagent, slight skin irritant
Disodium hydrogen phosphate - Unilab	Ajax Finechem	1234-500G	laboratory reagent, slight skin irritant
Potassium dihydrogen phosphate - Univar	Ajax Finechem	4745-500G	analytical reagent, slight skin irritant
Oligoacrylate standard	custom made		See reference for synthetic protocol: Castignolles, P.; Gaborieau, M.; Hilder, E. F.; Sprong, E.; Ferguson, C. J.; Gilbert, R. G. *Macromol. Rapid Commun.* 2006, **27**, 42-46
Boric acid	BDH AnalR, Merck Pty Ltd	10058	Corrosive
Hydrochloric acid - Unilab	Ajax Finechem	A1367-2.5L	laboratory reagent, corrosivie
Fused silica tubing	Polymicro (Molex)	TSP050375	Flexible fused silica capillary tubing with standard polyimide coating, 50 µm internal diameter, 363 µm outer diameter
Agilent 7100 CE	Agilent Technologies	G7100CE	Capillary electrophoresis instrument
Orbital shaker	IKA	KS260	
Electronic balance	Mettler Toledo	MS204S	
Milli-Q Synthesis	Millipore	ZMQS5VF01	Ultrapure water filtration system

Parafilm	Labtek	PM966	Parrafin wax